Ex Tenebris Lux: Illuminating Reactive Oxygen and Nitrogen Species with Small Molecule Probes

Maidileyvis C. Cabello,[a,∫] Gen Chen,[a,∫] Michael J. Melville,[b,∫] Rokia Osman,[a,∫] G. Dinesh Kumar,[b] Dylan W. Domaille,[b,*] Alexander R. Lippert[a,*]

[a] Department of Chemistry, Southern Methodist University, Dallas TX 75275-0314, United States
[b] Department of Chemistry, Colorado School of Mines, Golden CO 80401, United States
* E-mail: alippert@smu.edu
* E-mail: ddomaille@mines.edu

[∫] These authors contributed equally.

Abstract

Reactive oxygen and nitrogen species are small reactive molecules derived from elements in the air – oxygen and nitrogen. They are produced in biological systems to mediate fundamental aspects of cellular signaling but must be very tightly balanced to prevent indiscriminate damage to biological molecules. Small molecule probes can transmute the specific nature of each reactive oxygen and nitrogen species into an observable luminescent signal (or even an acoustic wave) to offer sensitive and selective imaging in living cells and whole animals. This Review focuses specifically on small molecule probes for superoxide, hydrogen peroxide, hypochlorite, nitric oxide, and peroxynitrite that provide a luminescent or photoacoustic signal. Important background information on general photophysical phenomena, common probe designs, mechanisms, and imaging modalities will be provided, and then probes for each analyte will be thoroughly evaluated. A discussion of the successes of the field will be presented, followed by recommendations for improvement and a future outlook of emerging trends. Our objectives are to provide an informative, useful, and thorough field guide to small molecule probes for reactive oxygen and nitrogen species as well as important context to compare the ecosystem of chemistries and molecular scaffolds that has manifested within the field.

Table of Contents

1. Introduction

Reactive oxygen and nitrogen species are a family of small reactive molecules that typically originate from oxygen (O_2) and/or nitric oxide (NO). While O_2 can be considered an ROS in its own right, it also serves as the originator of a host of other reactive derivatives, including superoxide (O_2^{-}), hydrogen peroxide (H_2O_2), alkyl peroxides (ROOH), hydroxyl radical ($HO^{\bullet}$), hypochlorite (HOCl), hypobromite (HOBr), singlet oxygen ($^1O_2$), ozone (O_3), high oxidation state metal oxo species, and carbonate radical ($CO_3^{-\bullet}$).[1–4] Similarly, nitric oxide (NO) is a ubiquitous signaling molecule, but its reactive radical nature also leads to the generation of damaging

reactive nitrogen species (RNS).[5] Common RNS include peroxynitrite ($ONOO^-$), nitrogen dioxide radical (NO_2), nitrite (NO_2^-), nitrate (NO_3^-), nitroxyl (HNO), *S*-nitroso compounds, *N*-nitroso compounds, and others.[6] In addition to these species, there also are a number of reactive sulfur species, including hydrogen sulfide, persulfides, polysulfides, *S*-nitroso compounds, sulfenic acids, sulfinic acids, HSNO, and others,[7,8] as well as an emerging area of reactive carbon species that includes carbon monoxide, formaldehyde, formic acid, and others.[9]

Over the past several decades, increasing evidence has revealed that living systems can harness reactive species for diverse roles in biology, ranging from acting as signaling molecules to mediating pathologies associated with disease.[1–3,6] For instance, oxygen is the terminal electron acceptor of in aerobic organisms.[10] However, this reactive molecule can serve as the starting material for the library of ROS described above. The generation and decomposition of ROS must be carefully regulated to avoid damaging proteins, nucleic acids, lipids, and other cellular components.[11]. Owing to their reactivity, reactive species typically control signaling through direct non-enzymatic reaction with protein side chains.[12] Because they are small and diffusible, reactive species are capable of traversing the crowded intracellular and extracellular environment. Their limited lifetimes dictate how far a particular ROS/RNS can diffuse before reacting, enforcing a restricted signaling range for each reactive oxygen or nitrogen species. As our understanding of reactive oxygen and nitrogen species has increased, it has become clear that each species has its own specific chemistry and biology, and the specific roles of each must be independently defined in biological systems.[13]

The unique signaling properties of reactive oxygen and nitrogen species are also what make them difficult to study with specificity and sensitivity in biological systems.[14] Because they are reactive, they are transient and require immediate capture as they are produced or one must rely on indirect measurements of either biologically modified substrates or their penultimate decomposition products. The latter method is complicated by multiple paths to generating the same decomposition products and the loss of significant spatial and temporal resolution in the measurement. Reactive oxygen and nitrogen species also tend to have very low steady state concentrations (~nM), although higher and lower concentrations can occur under specific conditions. Nevertheless, detection methods require good analytical sensitivity.[12] Finally, selectively detecting a single reactive oxygen or nitrogen species is challenging because of similar reactivities and properties, so clever and carefully designed strategies must be developed. A recent panel has provided important guidelines and best-practices for measuring reactive oxygen species in biological systems.[14]

Luminescent probes are small molecules, proteins, or nanostructures that display a modulation in photon emission upon interaction with an analyte.[15] Early work in this area was pioneered by Roger Tsien with his development of small molecule fluorescent calcium probes and genetically engineered fluorescence proteins.[16,17] Luminescent probes are attractive because they can be designed to have a very selective and sensitive optical response compatible with live cell microscopy and whole animal imaging.[15,18,19] For metal ions, an approach where the analyte reversibly binds to the probe has been a preferred strategy, allowing for quantification using ratiometric imaging.[20,21] Although some binding-based strategies have been adopted for developing luminescence probes for reactive oxygen and nitrogen species, reaction-based or activity-based strategies have dominated.[15,19,22] These approaches rely on a chemical reaction with the reactive oxygen or nitrogen species and the probe that alters the luminescence properties when converting the probe from its starting form to its final form. This framework was adopted in early redox probes where a reduced fluorophore could be oxidized by reactive oxygen species to

provide a fluorescence turn-on response, and tuning reactions to be ever more selective and sensitive is the predominant strategy discussed in the context of this review.[23–25]

This review article aims to provide a thorough description of the field of luminescent probes for reactive oxygen and nitrogen species. While many reviews have been written in this area,[19,26–31] we aim to provide the reader with an unprecedentedly comprehensive evaluation of small molecule probes for reactive oxygen and nitrogen species as well as ample background on photophysical properties and analytical mechanisms/modalities to provide an invaluable reference for established practitioners and entrants into the field. We will begin with an overview of the photophysical properties and background information on the modalities and sensing strategies often used in the design of small molecule probes. This will be followed by a thorough summary of luminescent probes for reactive oxygen and nitrogen species organized by analyte and sensing trigger, including a brief biological background and survey of alternative detection methods for each analyte. The emerging field of photoacoustic imaging will also be included;[32–35] although not strictly a luminescence mode of detection, photoacoustic techniques are often coupled with fluorescence imaging and comprise an important class of small molecule imaging probes. The field is vast, so the scope of the review article will be limited to reactive oxygen and nitrogen analytes that are generally accepted to have a physiological role. This will include superoxide, hydrogen peroxide, hypochlorite, nitric oxide, and peroxynitrite. There are many luminescence probe designs for nitroxyl,[36–43] singlet oxygen, [44–47] triplet oxygen and hypoxia,[48–52] hydroxyl radical,[53–55] nitrogen dioxide radical,[56,57] and others, but unfortunately these will not be able to be covered in detail. We also will not discuss the literature surrounding luminescence probes for reactive sulfur species[58–64] or reactive carbon species[65,66] but note that there are many other review articles engulfing targeted aspects of reactive sulfur, oxygen, and nitrogen species are available.[19,22,27–68] Additionally, we will limit our discussion to small molecule designs and will not comprehensively cover protein-based designs, nanostructures, or other non-small molecule approaches.[69–71]

We anticipate this review will provide a valuable reference to explore the diverse ecosystem of small molecule probes for reactive oxygen and nitrogen species. Comprehensive tables of probes are provided and organized according to analyte within the manuscript. These contain key information including absorption and emission wavelengths, applications, references, and other important properties. We note that we have adhered to the naming of probes that were used in each reference, so there are multiple entries with names like “**Probe 1**” or “**Compound 1**”. We strongly advise researchers to give probes unique names as it becomes quite confusing when comparing probes from different studies if they are simply given a generic label (e.g. **1** or **Probe**). Nonetheless, the tables (sorted by analyte and year) provide key information including analyte, trigger, wavelengths, and references that should make each probe easily identifiable. An example figure for each major trigger is provided. Red color highlights the parts of each molecule that react with the analyte and what functional groups are formed in each product. We also note that the reported excitation and emission wavelengths are reported as either the absorbance / emission maxima or as the wavelengths used in the imaging experiments to best match how they are reported in each reviewed manuscript. In general, this review article focuses on reactivity and sensing strategies and tries to bring a cohesive understanding of the different approaches. Finally, we will conclude with our impressions of current trends in the field, unsolved challenges, and a future outlook.

2. Photophysical mechanisms

2.1 Jablonski diagram

The Jablonksi diagram[72–74] is used to understand photophysical processes and will be the framework with which we describe the fundamental mechanisms of operation of small molecule luminescent probes for reactive oxygen and nitrogen species. Typically, the Jablonski diagram will represent the S_0, S_1, and T_1 states as Morse potentials with vibrational states drawn in for each electronic state. The energy surface of a molecule is more complex than a simple Morse potential for a single bond, but this representation provides an easy-to-follow diagram of how light interacts with matter (Figure 1).

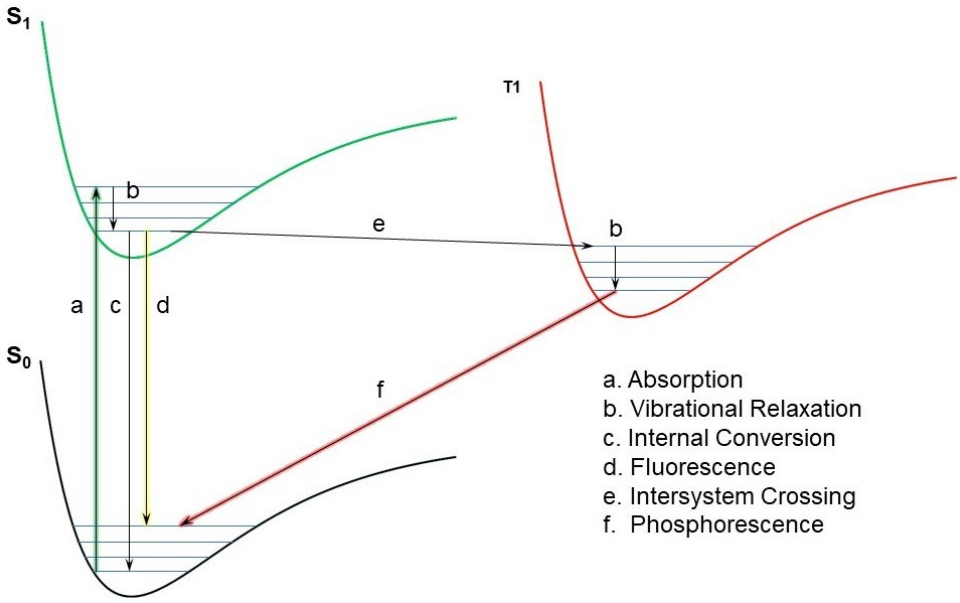

Figure 1. Jablonski diagram showing common photophysical processes. a. Absorption, b. Vibrational Relaxation, c. Internal Conversion, d. Fluorescence, e. Intersystem Crossing, f. Phosphorescence.

2.1.1 Absorption

Absorption is the first step for most luminescence probes, with the notable exception of chemiluminescence and bioluminescence. According to the Stark-Einstein law, if the energy of light exactly matches the energy gap between two energy levels of a molecule, the molecule will absorb the energy of the photon by exciting an electron from the lower energy state to the higher energy state. In most cases, photophysical and photochemical processes occur from the first excited electronic state (either S_1 or T_1). Excitation to higher electronic excited states (S_2, S_3, etc.) is possible, but relaxation to the first excited state S_1 is very fast, a phenomenon generally referred to as Kasha's rule. The rate of absorption is very fast (~10^{14} – 10^{16} s^{-1}), and specifically faster than nuclear motions and most other photophysical processes. Empirically, absorption is governed by Beer's law (Equation 1), which states that the optical density (OD), defined as the logarithm of the ratio of the light intensity that enters the sample and the light intensity that exits the sample is equal to the extinction coefficient, ε, a constant for a given molecule at a given wavelength, the path length, b, or distance of the solution that the light travels through, and the concentration of the sample c:

$$OD = \log[I_0/I] = A = \varepsilon bc \quad (1)$$

Electronic transitions can be described by the lower energy singly occupied orbital, X, the higher energy singly occupied orbital, Y, and whether the molecule is in a singlet state (electrons have opposite spins) or a triplet excited state (electrons have the same spin), using a super-script, ^{Z}. The formal notation is $^Z(X,Y)$. For many fluorescent probes the initial absorption provides a $^1(n,\pi^*)$

or $^1(\pi,\pi^*)$ excited state resulting from excitation of an electron from a non-bonding orbital (lone pair) or π orbital to the π^* antibonding orbital.

2.1.2 Vibrational relaxation and internal conversion

While absorption usually (but not always) occurs from the ground vibrational state of the ground electronic state, it often excites the electron to a range of vibrational states of the excited electronic state. In the cases in which excitation advances an electron into an excited vibrational state, there is a rapid, non-radiative process of vibrational relaxation down to the ground vibrational state of the excited electronic excited state. This process usually occurs with a rate of $10^{11} – 10^{12}$ s^{-1}, a timescale that is slower than absorption, but still faster than most other photophysical processes. From this ground vibrational state of the electronic excited state, relaxation back to the ground electronic state can occur with photon emission (radiative decay) or without (non-radiative decay) photon emission. In the case that return to the ground state occurs without photon emission, this process is called internal conversion, and the energy is released as heat, a process that is harnessed in the development of photoacoustic probes. Internal conversion can have many mechanisms, some of which are non-productive photochemical reactions.

2.1.3 Fluorescence

Fluorescence is the process of relaxation from the singlet excited state (S_1) to the ground electronic state (S_0) with the emission of a photon. This type of radiative decay typically occurs with rates from $10^5 – 10^8$ s^{-1}. The intensity of fluorescence emission is related to the absorption, A, of the sample and the quantum yield of fluorescence, Φ_{fl}. In general, quantum yield is the ratio of the number of molecules that do a certain photophysical or photochemical process divided by the total number of photons absorbed. Fluorescence spectra can be acquired either as an excitation spectrum or as an emission spectrum, with both being standard components for characterizing fluorescent probes. In an excitation spectrum, one wavelength of light is observed (with its bandwidth determined by the slit size), while the excitation wavelengths are scanned to provide a spectrum based on the excitation wavelength. In an emission spectrum, emission intensity at a single excitation wavelength is measured while scanning through emission wavelengths. In many cases, the excitation spectrum matches the absorption spectrum and is a mirror image of the emission spectrum, but there are exceptions. Because vibrational relaxation to the ground vibrational state of the excited electronic state is faster than fluorescence, emission spectra are often red shifted to lower energy wavelengths versus the excitation spectrum and this is called a Stokes shift. Large Stokes shifts are advantageous for fluorescence microscopy because a better separation between the excitation and emission wavelengths reduces background from overlap between the excitation and emission channels.

2.1.4 Intersystem crossing and phosphorescence

Intersystem crossing refers to the interconversion between two electronic states with different spin states. This is the process that converts an S_1 singlet state into a T_1 triple state. It is a “forbidden” process that has a relatively slow rate because the conversion from a singlet to a triplet requires a spin flip. In order to increase the rate of intersystem crossing, there must be a coupling between the change in the spin quantum number and the orbital quantum number, which is called spin-orbit coupling. One common strategy to achieve spin-orbit coupling and high rates of intersystem crossing includes the heavy atom effect, where atoms in the 3rd or higher numbered rows on the periodic table are added to the molecule. Another strategy is to couple a change in spin with a change in orbital, converting $^1(n,\pi^*)$ to $^3(\pi,\pi^*)$, for example. This is a common mechanism in carbonyl triplet sensitizers. Phosphorescence is the relaxation from T_1 to S_0 with the emission of a photon. Just like the S_1 to T_1 conversion, this is a “forbidden” and therefore slow process, with rates on the order $10^2 – 10^3$ s^{-1} for relaxation from $^3(n,\pi^*)$ state and 10^{-1} to 10 s^{-1} for relaxation

from $^3(\pi,\pi^*)$ states. Importantly, the T_1 state can be quenched by molecular oxygen, which has a triplet ground state. For this reason, molecules that display phosphorescence can be used as luminescent probes for oxygen sensing.[50,51,75]

2.2 Bimolecular/Intramolecular photophysical processes

2.2.1 Photoinduced electron transfer (PeT)

Photoinduced electron transfer (PeT or PET)[76–79] involves the transfer of an electron between an excited state and a ground state of neighboring molecular structures. In the context of luminescent probe design, the two structures are usually covalently tethered together, and the PeT process leads to quenching of fluorescence with the generation of a charge-separated radical anion and radical cation. Generally, there are two different modes of PeT that are used in probe design, one abbreviated a-PeT, which involves electron transfer from the ground state highest occupied molecular orbital (HOMO) to the lower energy singly occupied orbital of the excited state of the acceptor (Figure 2A), and d-PeT, which involves electron transfer from the higher energy singly occupied orbital of the excited state donor to the ground-state lowest unoccupied molecular orbital (LUMO) of the acceptor (Figure 2B). Generally, the probe design involves tethering a fluorophore to a functional group that will experience a shift in the energy levels of the localized HOMO and LUMO upon interacting with an analyte (Figure 2). For a turn-on probe, PeT quenching should be efficient before interacting with the analyte, but after reacting with the analyte, the energy levels are shifted such that PeT is no longer a competitive process with fluorescence. PeT quenching serves as a mechanism for metal cation probes based on binding in a way that reduces PeT quenching, often by binding to a lone pair on the chelating group and lowering the energy levels of the HOMO and LUMO of an aromatic amine to move it outside of the range for PeT quenching.[20,21] Another strategy that is common for luminescence probes for reactive oxygen and nitrogen species involves a chemical transformation upon reacting with an analyte to alter the HOMO/LUMO levels and eliminate PeT.

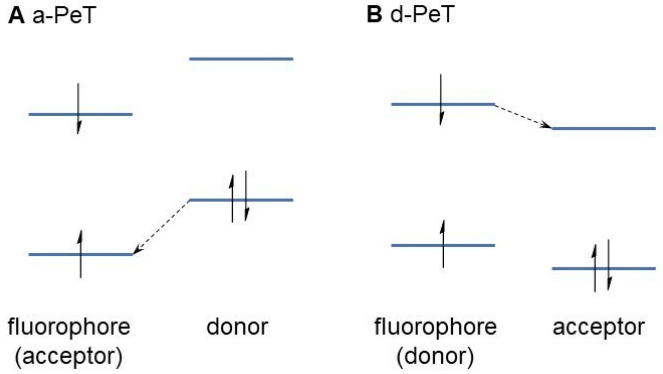

Figure 2. Photophysical mechanism of photoinduced electron transfer (PeT). (A) In a-PeT, the excited state fluorophore acts as an electron acceptor for a nearby donor. (B) In d-PeT, the excited state fluorophore acts as an electron donor for a nearby acceptor.

2.2.2 Resonance energy transfer processes

Energy transfer processes, particularly the Förster Resonance Energy Transfer (FRET) mechanism have been exceptionally useful in small molecule luminescence probe design by enabling modulation of emission/excitation wavelengths as a mechanism for analyte sensing, and to provide a ratiometric response.[80–83] FRET involves non-radiative energy transfer from a donor group to an acceptor group based on dipolar interactions between fluorophores (Figure 3). Generally, efficient FRET depends on (1) the distance between the donor and acceptor (typically between 1 and 10 nm in small molecule intramolecular systems), (2) the overlap integral between the donor emission and acceptor excitation spectra, (3) the relative orientation of the two fluorophores to optimize dipole-dipole coupling. There are several ways that probes can be

designed using a FRET technique. One method is to have a chemical group that reacts with an analyte to make it a better or worse FRET acceptor, thereby changing the FRET efficiency in the presence of an analyte. A second method is to have a linker that cleaves the connection between a FRET donor and FRET acceptor, thereby turning off FRET. A third method is to have the distance change between the FRET donor and acceptor upon interacting with an analyte. One useful property of FRET-based probes is that emission can usually be observed from both the donor and acceptor and the ratio of these emission wavelengths will change after reaction with an analyte to provide a ratiometric response that can be useful for quantification. Förster Resonance Energy Transfer has also been used in the context of chemiluminescence and bioluminescence where the excited state is accessed during a chemical reaction. Although these are still Förster Resonance Energy Transfer processes, they are sometimes referred to as chemiluminescence resonance energy transfer (CRET) and bioluminescence resonance energy transfer (BRET). These strategies have been used to develop ratiometric chemiluminescence probes as well as dark photodynamic therapy agents via energy transfer to a triplet sensitizer to produce singlet oxygen without the need for an excitation source. [50,84,85] Other types of energy transfer include through-bond energy transfer (TBET), which has a reduced need for spectral overlap and radiative energy transfer, and has been used in some interesting cases of chemiluminescence.[86]

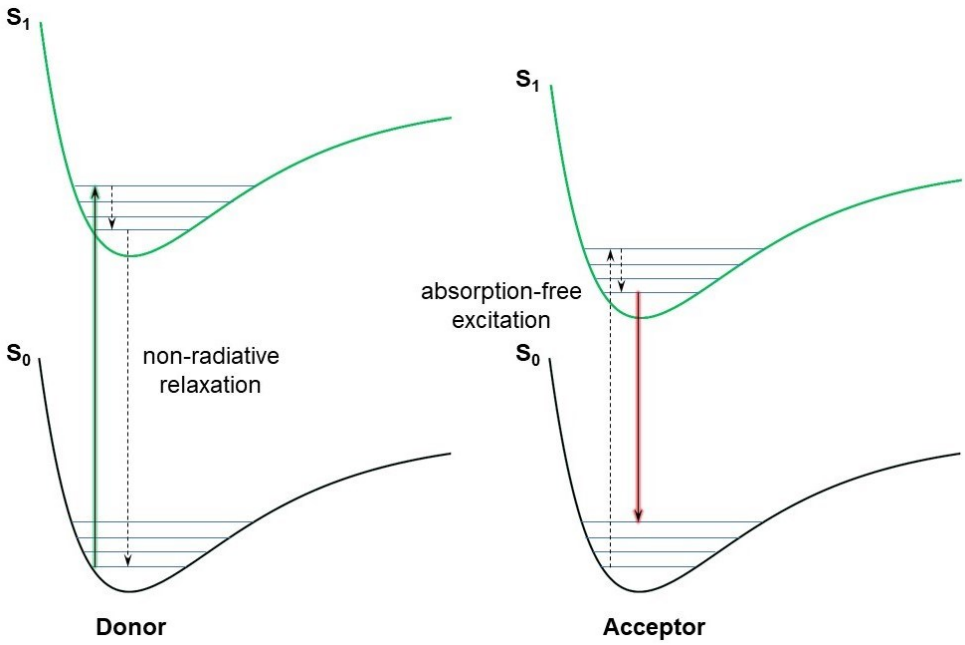

Figure 3. Förster resonance energy transfer (FRET) occurs when an excited state donor non-radiatively relaxes to the ground state while a nearby acceptor with spectral overlap is non-abortively excited to the excited state.

2.3 Intramolecular charge transfer

Intramolecular or internal charge transfer (ICT) refers to the formation of a charge-transfer species following photon absorption, excitation from the ground state to the excited state, and electron transfer from a donor group to an acceptor group.[87] This phenomenon is most commonly observed in “push-pull” conjugated systems where an electron donating group is linked to an electron withdrawing group by a series of conjugated atoms.[88] Generally, molecules that undergo ICT will have different geometries in their ground and excited state and will display solvatochromatism due to the differences in polarity between the ground and the excited state. Because of the differences in the ground state and excited state geometries, a fluorophore will often undergo a bond rotation in the excited state giving rise to what has been called twisted-ICT. This is an important consideration in fluorophore design and a strategy of tethering rotatable bonds to make them rigid has been used to improve fluorophore properties.[89,90] For probe design,

chemical reactions with analytes can change the probe's structure from a structure that does not undergo significant ICT to one that displays high ITC, often by converting a weakly donating donor group into a more strongly donating donor group. Many ICT probes display a change in emission wavelength after reacting with an analyte, making this a photophysical mechanism useful in the development of ratiometric probes.

2.4 Excited state intramolecular proton transfer (ESIPT)

Excited state intramolecular proton transfer (ESIPT)[91] is a process by which a rapid proton transfer occurs in the excited state and has been used in the design of numerous luminescent probes. The process is thought to proceed via four states (Figure 4). Absorption of a photon occurs in the S_0 state of an enol, which excites it to the S_1 state. This S_1 state is usually more acidic due to increased polarization of the excited state. The increased acidity combined with geometrical preorganization leads to a very fast rate of proton transfer ($k_{ESIPT} \sim 10^{12}$ s^{-1}) that can compete with the rate of fluorescence emission ($k_{fluor} \sim 10^{9}$ s^{-1}) and yield the ketone form in the excited S_1 state. Emission from the ketone S_1 state yields the ketone S_0 state that can then tautomerize back to the ground state enol form. Molecules that undergo ESIPT processes usually have large Stokes shifts and probes can readily be designed to toggle between ESIPT "active" and ESIPT "inactive" forms that have a shift in the emission wavelength, making this photophysical process useful for developing ratiometric probes. Protic solvents can interfere with ESIPT through competitive hydrogen bonding, therefore a hydrophobic environment (either by using organic solvents or surfactants) is often needed. Common strategies to develop probes that use an ESIPT mechanism will include structures where cation binding interferes with the ESIPT process or using caged phenols that can be decaged by analytes including reactive oxygen, sulfur, and nitrogen species to "turn-on" ESIPT.

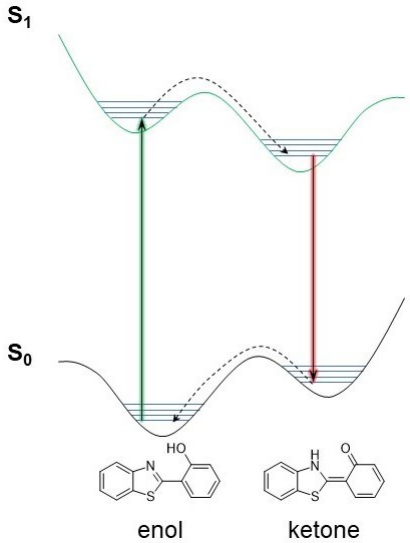

Figure 4. Excited state intramolecular proton transfer (ESIPT) occurs when a proton transfer is rapid in the excited state leading to emission from a tautomeric species that re-isomerizes in the ground state.

2.5 Aggregation-induced emission

Aggregation-induced emission (AIE)[92,93] is a phenomena that some molecules exhibit in which luminescence emission is quenched when the molecules are dispersed in solution, but become highly emissive when they form aggregates. Often, the mechanism of increased emission is due to the restriction of intramolecular motions, including bond rotations and vibrations, upon aggregating. Probe designs have been characterized into three types.[94] Type 1 probes interact

with biomolecules through electrostatic forces, leading to aggregation. [95] For example, a positively charged probe can bind to the negative charges of a heparin macromolecule to induce aggregation and increase luminescence emission.[96] Type 2 probes use targeted host-guest interactions to induce aggregation. Type 3 designs use a reaction-based trigger to induce aggregation and is the most amenable to developing luminescent probes for reactive oxygen and nitrogen species.

2.6 Chemiluminescence

Chemiluminescence is the emission of light from an excited state formed during a chemical reaction without the need for photon absorption.[97] This usually occurs when S_0 and S_1 are close in energy, often near the transition state of an exothermic reaction. Crossover can occur either into the S_1 or T_1 state and light emission occurs via fluorescence or phosphorescence. Chemiluminescence techniques are advantageous because no external light source is needed. This dramatically reduces background by eliminating autofluorescence and attenuating light scattering, providing increases in sensitivity for diagnostic protocols, cellular assays, and whole animal imaging.[12,68,98–100] A wide scope of chemiluminescent reactions have been used for developing optical analytical tools including luminol oxidation,[101–103] peroxyoxalate chemiluminescence,[104,105] luciferin analogues,[106,107] ozone-based chemiluminescence,[108] and triggered decomposition of 1,2-dioxetanes.[12,68,98–100] In recent years, triggered decomposition of sterically stabilized 1,2-dioxetanes has been particularly fruitful by virtue of being able to switch on chemiluminescence through conversion of a phenyl ether into a phenolate that can undergo electron transfer to an appended 1,2-dioxetane in the first step of a chemically initiated electron exchange luminescence (CIEEL) mechanism.[98–100] This enables the design of probes for a wide swath of analytes by using reactive triggers that release a phenolate.[109] When the chemiluminescence reaction is mediated by an enzyme, this is referred to as bioluminescence,[97] and the caging of luciferins has become a versatile strategy to generate bioluminescence-based probes for reactive oxygen and nitrogen species.[110]

3. Mechanisms and modalities

3.1 Mechanisms

3.1.1 Organelle-targeting

While most probes can be used for single cell resolution when combined with luminescence microscopy techniques, the distinct chemical microenvironments of subcellular organelles enable specific targeting and subcellular resolution.[111] Directing small molecule probes and other chemical tools to different organelles requires molecular designs that target a unique physiochemical or biochemical characteristic of the organelle. Over the past several decades, small and easily installed motifs have been identified that direct fluorophores (and other molecular cargo) to specific subcellular destinations, including mitochondria, endoplasmic reticulum (ER), lysosomes, Golgi, nucleus, and plasma membrane. Additionally, several strategies for genetic targeting have been developed. Here, we summarize the most used motifs and identify the precise molecular features that direct functionality to an organelle.

Mitochondria targeting strategies

The mitochondria generate adenosine triphosphate (ATP) via a proton motive force, in which protons are pumped against a concentration gradient from the matrix to the intermembrane space.[112,113] As the protons flow back down the concentration gradient into the matrix, their movement drives ATP synthase activity. Molecular oxygen is reduced to H_2O in this overall transformation, and because of the abundance of redox chemistry in the mitochondria, it is a major source of ROS/RNS. The actively maintained proton gradient causes the mitochondrial matrix to be slightly basic (pH 7.6–8.3) and cationic substrates will accumulate in the matrix.

However, to pass through the mitochondrial membrane, the compound must also have a lipophilic component. Thus, lipophilic cations are good choices to selectively drive the accumulation of a compound into the mitochondria. Several specific targeting motifs have been developed, including triphenyl phosphonium salts, pyridinium salts, and indolium groups.[114] The installation of triphenylphosphonium salts is typically achieved by alkylating a substrate with triphenylphosphine, while pyridinium salts are typically synthesized by first installing the pyridine and then alkylating it. Notably, fluorescent rhodamine derivatives, which meet both the cationic and lipophilicity requirements, tend to accumulate in the mitochondria, making them a useful example of a fluorescent scaffold with specific subcellular localization. There are also mitochondria penetrating peptides consisting of arginine and/or lysine-rich motifs that can be appended to probes to endow them with positive charge for mitochondrial localization.[114]

Lysosome targeting strategies

The lysosome is an acidic vacuole (pH 4.5–5.0) that breaks down biological macromolecules (e.g., lipids, carbohydrates, proteins, and nucleic acids); repairs cell membranes; and protects against invading pathogens.[115] Owing to its role in cellular defense, it is an important organelle to study in the context of ROS/RNS. Amines with pKa ~8 and other pH-activatable groups are common targeting groups because they become protonated and charged in the acidic lysosome, preventing their diffusion back into the cytosol.[116] Common lysosome targeting functionality thus include morpholine, dimethylamino, and semithiocarbazides. These can be easily installed through simple alkylation reactions.

Endoplasmic reticulum and Golgi apparatus targeting strategies

The endoplasmic reticulum (ER) is a complex folded organelle studded with ribosomes and is important in protein synthesis.[117] Closely associated with the ER is the Golgi apparatus, which further processes proteins, including posttranslational modifications and sorting them for distribution to different parts of the cell.[118] Several chemical functional groups have been found to localize probes to the endoplasmic reticulum and Golgi apparatus including phenyl sulfonamides, ceramides, and sphingomyelins.[119] Specific targeting groups for the ER include sulfonamides, especially *p*-toluenesulfonamide, as well as sulfonylurea-based drugs, such as glibenclamide. Installation of *p*-toluenesulfonamide is synthetically straightforward, as it can be linked to a chemical cargo via its sulfonamide nitrogen atom. A few small molecule targeting motifs for the Golgi apparatus exist. Cysteine-modified and sulfonamide fluorophores have been shown to localize to the Golgi.[120–122] Moreover, ceramide-modified fluorophores are metabolically incorporated into the Golgi and can also be used to label this organelle.[119] Some peptide sequences are also known to deliver molecular cargo to the endoplasmic reticulum and Golgi apparatus.[123] Natural products like rapamycin and brefeldin A can also target the endoplasmic reticulum and Golgi apparatus, but since they have intrinsic biological activity, they are not favored as a method for targeting probes. DNA-based targeting has been exploited for multiple organelles including the trans-Golgi network.[124]

Nucleus targeting strategies

It is challenging to deliver molecular cargo to the nucleus because of the nuclear membrane is highly restrictive.[111] Nevertheless, planar, cationic hydrophobic small molecule fluorophores can penetrate the nuclear membrane and bind to DNA by targeting the minor grooves of DNA or using DNA intercalators, effectively labeling the nucleus. For instance, DAPI and Hoechst stain bind to DNA in the nucleus. These compounds both have a planar, aromatic architecture with a slight curvature that fits within the minor groove of DNA. Conjugating these common nuclear stains to molecular cargo can be a successful strategy to drive nucleus-specific labeling or delivery of chemical probes. Nuclear localization peptide sequences can also be used to deliver cargo to the nucleus of cells.

Genetic targeting strategies

A number of genetic techniques involving the use of self-labeling proteins (SLP) are now available where a small protein enzyme that catalyzes a self-labeling covalent bond formation with a distinct chemical handle can be genetically linked to a protein of interest.[125] Synthesizing a probe that has this specific chemical handle can then be covalently linked to the protein, allowing versatile control of probe localization. Examples include the SNAP-tag,[126] CLIP tag,[127] and HaloTag.[128] The SNAP-tag uses the enzyme O^6-alkylguanine-DNA alkyl transferase (hAGT), which is a human DNA repair protein that catalyzes the substitution of one of its cysteine residues with an alkyl group on an O^6-benzylguanine derivative. The protein hAGT can be fused to a protein of interest, while the O^6-benzylguanine can be appended to a small molecule tag to provide an effective and selective method to label proteins with a wide range of fluorophores and other types of small molecules.[126] An orthogonal self-labeling protein / synthetic handle pair was developed and called a CLIP-tag that uses another AGT self-labeling protein optimized to use O^2-benzylcytosine as a substrate and can be used simultaneously with the SNAP-tag.[127] The HaloTag is a haloalkane dehalogenase enzyme that catalyzes the self-labeling of a chloroalkane tag that can be appended to small molecules.[128] Each of these have been shown to be versatile and have been applied for the detection of specific reactive oxygen and nitrogen species with organelle-level specificity.[129–131]

Targeting strategies for other organelles

Several other organelle structures have been targeted. The plasma membrane can be targeted by appending a hydrophobic membrane anchoring group such as long alkyl chains that insert and anchor small molecules into the hydrophobic membrane.[132,133] Hepatocytes and the liver have been targeted by appending β-galactose units that can carry a molecular cargo into hepatocytes via receptor mediated endocytosis.[134] Microtubules have been targeted using docetaxel,[135,136] and a range of chemical strategies have also been used to target lipid droplets,[137–139] cell surface receptors,[140,141] and amyloids/protein aggregates.[142–146]

3.1.2 Dual-analyte probes

Reactive oxygen and nitrogen species are often generated co-localized in time and space, making simultaneous measurements of multiple species challenging. Using multiple probes that are selective for different species is a potential solution that has been implemented,[147] but non-uniform uptake, localization, and retention can complicate interpretation of such experiments. For these reasons there has been significant effort aimed at developing dual (or more) analyte responsive probes.[148,149] When a single molecular probe responds to two or more analytes to give one or more optical signals as a response, these can in essence serve as molecular logic gates, for example, an “AND” gate requires both analytes to react to give a signal, while an “OR” gate requires at least one of two analytes to be present. Many dual responsive probes have been developed for reactive nitrogen and oxygen species and other analytes.

3.1.3 Quantification, reversible probes, analyte replacement

Binding-based fluorescent probes can quantitatively image real-time fluxes of ions due to fast reversible binding of the analytes to the probe coupled with a ratiometric response.[15,18,19] A prime example is using fluorescent calcium probes for imaging neuronal firing.[150] Most reaction-based probes, however, typically cannot measure fluxes of analytes due to the irreversible nature of the reaction-based sensing strategy. There have been some efforts to address this by developing probes that have a reversible ratiometric response, with perhaps the most notable example being for the quantitative imaging of glutathione using a reversible 1,4-addition reaction.[151–153] Other efforts have been aimed towards dual-analyte probes where one analyte provides an optical

response that is reversed by a second analyte. An example of this are sulfite/hydrogen peroxide probes that typically display a shift in emission wavelength upon conjugate addition with sulfite and recovery with hydrogen peroxide-mediated elimination of the sulfate group.[154–156] Chemiluminescence and bioluminescence detection methods are inherently reversible since photon flux ceases once the analyte has been consumed. Quantification of reactive oxygen and nitrogen species with a fast reversible ratiometric probe faces steep challenges by the low concentrations of these analytes that require significant time integration to build up an observable signal. Recently, a kinetics-based approach has been developed whereby the kinetics of a probe's response is carefully measured and the knowledge of the rate constants is used to back-calculate the concentration of the analyte to provide real-time quantification of reactive oxygen and nitrogen species and enzymes.[42,49,157] Another challenge is that the analyte is usually consumed by the probe and in some cases this may perturb the inherent biology of the system. Analyte replacement strategies have been developed where the analyte is regenerated after reacting with the probe by various mechanisms (essentially making the probe response catalytic in the analyte).[158,159] This can also amplify signal by enabling the analyte to turn-over the probe response. In general, precise quantification of reactive oxygen and nitrogen species remains an unsolved challenge.

3.2 Cellular measurements and imaging

3.2.1 Multiwell plate readers and flow cytometry

Multiwell plate readers have reached an elevated degree of sophistication and are capable of high-throughput kinetics and endpoint reads using absorbance, fluorescence, luminescence, and other techniques. These simple fluorescence or luminescence measurements are often a workhorse for biological laboratories. Additionally, many modern plate readers are capable of high-throughput fluorescence microscopy in living cells. Flow cytometry and cell-sorting methods operate by sorting cells and acquiring single cell fluorescence measurements. It provides detailed cellularly resolved data that can provide important insight into heterogeneous cell populations. Much of probe development has focused on using the probes in conjunction with advanced imaging techniques, but validation in widely accessible multiwell plate readers and flow cytometers could go a long way to encourage adoption of probes amongst biological researchers.

3.2.2 Single-photon microscopy

Regardless of the sophistication of the optical setup and excitation source, the general principles of fluorescence microscopy remain the same.[160] A sample is illuminated with an excitation wavelength to excite a fluorophore in the sample. This may be a fluorophore introduced into a fixed sample (e.g., fluorescent antibody), it may be an analyte-responsive fluorophore in a live sample (e.g., H_2O_2-responsive probe), or it may be a native fluorophore (e.g., flavin adenine dinucleotide). Upon relaxation and emission of a photon, the emitted photons are collected through appropriate optical filters into a camera to provide an image of the specimen. Several different flavors of fluorescence microscopy are commonly used in research laboratories, including epifluorescence microscopy, one-photon and two-photon confocal microscopy, laser sheet microscopy, and super-resolution microscopy. Below, we briefly describe the utility of each type of microscopy, balancing the information provided against logistical challenges of availability, simplicity, and cost.

3.2.3 Epifluorescence microscopy

Epifluorescence microscopy uses a wide-field excitation source, in which the entire sample is illuminated with a broad excitation light.[161] Common sources of excitation include tungsten-halogen, mercury and xenon arc, metal halide, and light emitting diodes (LEDs). The broad excitation light is passed through a filter cube to leave only the desired excitation wavelength. For instance, a filter with the designation 575/50 indicates that 575 nm is the central wavelength that

is allowed through with a spectral width of 50 nm. Thus, excitation light of 550–600 nm will pass through. The excitation wavelengths illuminate and excite the fluorophores in the sample, which emit fluorescence at a longer wavelength owing to the fluorophore Stokes shift. The emitted fluorescence is then collected by the objective lens and passed through an emission filter to remove any stray excitation light. The fluorescence is then typically directed to a camera detector to provide the fluorescence image. A major benefit of this type of microscopy is its relatively low-cost compared to laser excitation systems. Several turn-key all-in-one systems are now available, making these a compelling option for workhorse tissue-culture facility analysis, though higher-resolution single-cell imaging is possible with more advanced systems. Thick samples, such as tissue samples, are challenging to image with epifluorescence microscopy. This is because fluorophores from above and below the plane of the sample of interest will be stimulated, and the out-of-focus light will blur the image.

3.2.4 Confocal fluorescence microscopy

Confocal fluorescence microscopy is a technique that uses a focused diffraction-limited point source of light and carefully aligned pinholes to reject out-of-plane light, thereby enhancing resolution and enabling 3D reconstructions of thick samples.[162] In single-photon confocal microscopy, the fluorophore is excited upon absorption of a single-photon, whereas two-photon excitation sources deliver two lower-energy photons in rapid succession to access the excited state. This technique is advantageous because it allows for deeper imaging of thick biological samples compared to conventional microscopy techniques. However, because the probability of two photons arriving at the same time and location is very low, this process only occurs within a small volume, which enables high-resolution imaging in three dimensions. Some drawbacks exist. For instance, a laser capable of delivering two longer wavelength photons in rapid succession is more expensive than single-photon excitation sources. Additionally, only a subset of fluorophores is suitable for two-photon microscopy, as they require a suitable two-photon cross-section—that is, the ability to absorb two photons simultaneously to access their excited state— which can limit the range of biological questions that can be addressed. Nevertheless, after the fluorophore is excited, it relaxes to its ground state with emission of a longer wavelength photon, which is detected by a detector, most commonly a photomultiplier tube (PMT).

Several flavors of laser confocal microscopy exist. The most common is laser scanning confocal microscopy (LSCM). In LSCM, the sample is irradiated with a focused laser beam and scanned across the sample. A pinhole rejects out-of-focus light, and the emitted photons are detected at each point, which allows for a three-dimensional image of the sample to be constructed. Though LSCM is the most commonly used technique, the image acquisition can be slow, which subjects the sample to long periods of illumination, increasing the possibility of photodamage. An alternative to LSCM is spinning disc confocal microscopy. In spinning disc confocal microscopy, hundreds of pinholes decorate a disc, which rotates at high speeds. As the pinholes scan across the sample, the whole sample is imaged, significantly reducing image acquisition time, limiting photodamage, and enabling rapid and dynamic processes to be captured.

3.2.5 Light sheet microscopy

Light sheet microscopy is a relatively new technique that combines the benefits of both confocal and epifluorescence microscopy.[163] A thin sheet of light is used to illuminate a single plane of the sample, while cameras collect tens to thousands of images each second. The low photobleaching and low phototoxicity enables long-term imaging of large biological specimens, making this an ideal technique for imaging embryo development, 3D cell culture samples, and organoids. This technique provides a high-resolution, three-dimensional image with minimal out-of-focus fluorescence and background noise and is ideal for thick samples but requires specialized equipment and has a correspondingly high entry cost.

3.2.6 Super resolution microscopy

Stimulated emission depletion (STED) microscopy

Stimulated emission depletion (STED) microscopy is a multi-wavelength optical technique to achieve super resolution images (60–80 nm).[164] A focused laser beam excites fluorescent molecules in a small region of the sample. A second laser beam, which is shaped like a doughnut, irradiates the fluorophores with a wavelength in the emission spectrum. With a high enough intensity, this second laser source forces the excited fluorophores to relax with emission of a photon equal to that of the excitation source in a process called "stimulated emission" leaving only active fluorophores in the center of the doughnut. This effectively reduces the illumination region. By scanning the doughnut-shaped beam across the sample, high-resolution images can be obtained. There are now turnkey STED systems available, which makes this a powerful technique, even for novice users.

Structured illumination microscopy (SIM)

Upon recognizing that the diffraction limit holds only if certain assumptions are made, including that the sample is uniformly illuminated, Gustafsson showed that modulating the sample illumination improved lateral resolution beyond the classical diffraction limit.[165] Calling the technique "structured illumination microscopy" (SIM), Gustafsson used a structured pattern from a coherent light to illuminate the sample. By analyzing the pattern of the fluorescence emission from multiple images of the sample, super-resolution images are obtained. Using this technique, a two-fold improvement in resolution can be obtained (~ 120 nm). Typically, samples that are appropriate for confocal microscopy are suitable for SIM, and the availability of turnkey systems, complete with reconstruction software, makes this one of the most accessible super-resolution imaging techniques.

Single molecule localization microscopy (SMLM)

Single molecule localization microscopy (SMLM) comprises a family of techniques that use computationally localized fluorescent molecules from diffraction-limited image sequences to generate super-resolution images.[166–168] Two of the most often used methods are photoactivated localization microscopy (PALM) and stochastic optical reconstruction microscopy (STORM), which uses the stochastic blinking behavior of individual fluorescent molecules to localize their positions with high precision. Both approaches require unique fluorophores that have both a 'dark' state (non-emissive) and 'bright' state (emissive). Photoactivatable fluorescent proteins, photoactivatable and spontaneous blinking small molecule fluorophores, and quantum dots, with intrinsic 'blinking' are often used.[169] A large series of images are acquired, and because only a small subset of fluorophores are emissive at any given time, single emitters can be visualized. If the diffraction limited spot is coming from a single molecule, then the point-spread function of the light can be analyzed, and the fluorophore can be localized beyond the diffraction limit with 20 nm resolutions often achieved. By analyzing the positions of many individual fluorophores over time, a high-resolution image can be reconstructed. Since its development in 2006, significant advances have occurred, enabling 3-dimensional imaging, live-cell imaging, and multi-color imaging.[166,167]

3.2.7 Two-photon microscopy

Two-photon microscopy relies on a two-photon absorption process where the chromophore absorbs two long wavelength photons instead of one higher energy (shorter wavelength) photon.[170] For this process to be effective, the chromophore must have what is referred to as a "high two-photon cross section", an indicator of its efficiency to undergo two-photon absorption. Many useful two-photon fluorophores are known and can be adapted to develop two-photon fluorescent probes for reactive oxygen and nitrogen species.[171] Two-photon microscopy has many

benefits including less photodamage, deeper imaging depth for thick samples (e.g., brain slices), improved resolution because of low probability of two photons being successfully absorbed. It is particularly useful for imaging deeper into tissue and acquiring high resolution and 3D-images. One salient application is calcium imaging in behaving mice, a critical tool for understanding synaptic neuronal communication.[150] Some of the challenges associated with two-photon microscopy include limited fluorophore selection and more complex (and expensive) instrumentation, including a pulsed laser to deliver two photons at a timescale appropriate for two-photon absorption.

3.2.8 Time-gated microscopy

Time-gated microscopy is a fluorescence microscopy technique that uses time-resolved detection to separate fluorescence signals from background autofluorescence or scattered excitation light.[172] This is achieved by delaying the detection of fluorescence emission until after the excitation light and any short-lived background fluorescence has decayed. Time-gated microscopy has several benefits, including improved contrast, improved resolution, and high versatility. The improved contrast and resolution results by removing autofluorescence and scattered excitation light, which can improve the signal-to-noise ratio and enable better visualization of the target fluorescence signal. By removing background fluorescence, time-gated microscopy can improve resolution by reducing the contribution of out-of-focus fluorescence and enhancing the localization of fluorescent structures. However, there are also some drawbacks to time-gated microscopy, including longer acquisition times, and the need for a long-lived emissive state, which typically requires emission from a lanthanide complex (e.g., Tb^{3+}, Eu^{3+}, or Yb^{3+}).

3.3 Whole animal imaging

While whole animal preclinical and clinical imaging can be accomplished using computed tomography (CT), magnetic resonance imaging (MRI), and positron emission tomography (PET)/ single-photon emission computerized tomography (SPECT), and ultrasound, these techniques typically require specialized instrumentation and expertise that can be challenging to implement and reduce throughput for preclinical imaging experiments.[173–177] Additionally, techniques to measure specific reactive oxygen and nitrogen species are rare using these types of imaging technologies. In comparison, optical methods offer the potential for low cost and high throughput molecular imaging, but deep tissue whole animal optical imaging must overcome challenges with tissue absorption, light scattering, and autofluorescence, as well as navigating tissue heterogeneity and non-linear relationships in signal intensity. This section will discuss three methods used to overcome these challenges: NIR fluorescence imaging, chemiluminescence/bioluminescence imaging, and photoacoustic imaging.

3.3.1 Near-infrared fluorescence imaging

A significant amount of effort has been made towards developing luminescent probes that have emission in the near-infrared (NIR) window with wavelengths between 650 nm and 1700 nm.[178,179] This NIR window has been further categorized into the NIR I window (650 nm – 900 nm), NIR IIa (1300 nm – 1400 nm), and NIR IIb (1400 nm – 1700 nm). Having luminescence probes that emit in the NIR region of the electromagnetic spectrum is advantageous versus visible emission because there is reduced absorbance, fluorescence, and scattering by biological molecules in this region.[178,179] This can be readily appreciated by observing the autofluorescence of a vivisected mouse using green, red, or NIR filters sets (Figure 5), where autofluorescence is highly attenuated and difficult to observe when using the NIR filter set, highlighting the dramatic advantages of decreased background autofluorescence in NIR fluorescence imaging.

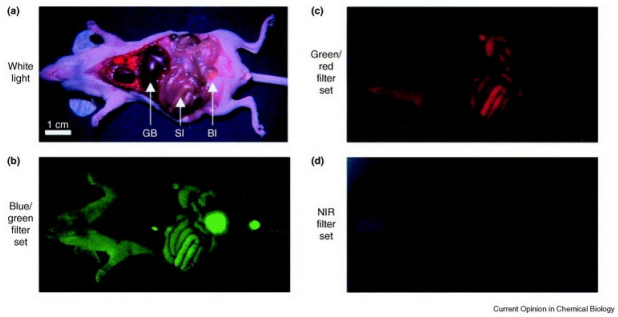

Figure 5. Comparison of autofluorescence images using green, red, or NIR filter sets. This image was published in Current Opinion of Chemical Biology, Vol 7, John V. Frangioni, In vivo near-infrared fluorescence imaging, Page 627, Copyright Elsevier (2003).[178]

An early NIR fluorophore that was developed was indocyanine green (ICG), which has been approved for clinical use.[180] There is now a large set of fluorophores and luminophores available that have emission in the NIR I region,[181–184] including cyanine dyes, silicon, phosphorous, and sulfur rhodamines, hemicyanine dyes, porphyrin complexes, iridium complexes, as well as fluorescent proteins, quantum dots, and other structures. There has also been significant work to develop chemiluminescent and bioluminescent molecules that emit in the NIR I wavelength, with many options existing.[32,100] The NIR II region, also referred to as short-wave infrared (SWIR), spans from 1000 nm – 1700 nm and while there is slightly more absorption in this region, there is exponentially less light scattering and autofluorescence, leading to overall reduced interference from the optical properties of biological tissue.[185,186] Fluorophores emitting in the NIR I region can be characterized using similar instrumentation as typical visible wavelength fluorophores, but specialized detectors (InGaAs, for example) are needed for characterizing emitters in the NIR IIa and NIR IIb region. These types of detectors and cameras usually need to be cooled to −190 °C using liquid nitrogen. There is now a growing family of fluorophores, carbon nanotubes, and quantum dots that emit in the NIR II region. Examples of chemiluminescent or bioluminescent emission in the NIR II region are rare, but some have been reported.[187]

3.3.2 Chemiluminescence/Bioluminescence imaging

As discussed in more detail above, chemiluminescence and bioluminescence arise from the emission of light during a chemical reaction/biological process, without the absorption of a photon.[97] The major benefit for whole animal imaging is that the external light source can be completely removed which drastically reduces autofluorescence and light scattering enabling imaging deep into tissue in living whole animal imaging experiments. This also has the potential advantage of simplified instrumentation as optical filters can also be removed; practically, however, the same instruments that are used for chemiluminescence/bioluminescence imaging are also used for near-infrared fluorescence imaging. Bioluminescence imaging is commonly used to track gene expression and signaling, tracking the growth of tumors, and some caged luciferin probes have been developed for molecular imaging of reactive oxygen and nitrogen species.[188] Bioluminescence typically requires genetic modification to endow organisms with the ability to express the luciferase enzyme, although some interesting exceptions have been used for endogenous bioluminescence imaging.[189] There has been a recent surge in the development of non-enzymatic chemiluminescence probes, particularly 1,2-dioxetanes, which offer the advantages for low background *in vivo* imaging without the need for genetic modification and additional versatility in probe design.[12,68,98–100]

3.3.3 Photoacoustic imaging

Photoacoustic or optoacoustic imaging merges the advantages of NIR optical imaging with ultrasound imaging.[190–192] It works through stimulating a biological sample with repeated non-ionizing laser pulses that can be absorbed by endogenous or exogenous chromophores. When this energy is thermally released by non-radiative mechanisms, it will cause pressure waves in the tissue that can be detected using ultrasound imaging techniques.[191] This gives the advantages NIR illumination, including its biocompatibility and depth penetration as well as the high resolution and reduced light scattering granted by ultrasound imaging. Although photoacoustic imaging does not strictly depend on luminescence emission, we include photoacoustic probes in this review because it is an important imaging modality emerging for detecting ROS/RNS and it is often used in combination with luminescence imaging. The instrumentation for photoacoustic imaging requires NIR light excitation via a short-pulse laser system and a wideband ultrasonic transducer for imaging, with many such systems that are commercially available. Photoacoustic imaging requires a chromophore, which can either be from endogenous or exogenous source. Imaging endogenous hemoglobin and oxyhemoglobin is a useful technique to image oxygenation in blood vessels *in vivo*, and other endogenous chromophores like DNA/RNA, melanin, lipids, and water are capable of being imaged.[191] Exogenous agents have also been developed from small molecule chromophores and nanoparticles. Generally, exogenous chromophores should have a high extinction between 680 nm and 950 nm to maximize light absorption from commercially available instrumentation and low fluorescence quantum yields to maximize non-radiative heat dissipative processes.[192] Due to the advantages of this modality, the development of photoacoustic probes for reactive oxygen and nitrogen species is rapidly gaining popularity.

4. Luminescent probes for reactive oxygen species

4.1 Superoxide

4.1.1 Superoxide in health and disease

Oxygen is fundamental to animal life as the key mediator of cellular respiration but is also a source of all other reactive oxygen and nitrogen species. Oxygen has a high reduction potential, but due to its triplet ground state, displays slow kinetics when reacting with closed-shell molecules. These properties make it useful as an energy source for ATP generation in the mitochondrial electron transport chain.[193] In addition to cellular respiration, oxygen is also important for its interactions with numerous proteins and enzymes. Oxygen binds to hemoglobin, which transports it throughout the body. Oxygen is an important co-factor in enzymes including oxidases,[194] where it acts as an electron acceptor, and in oxygenases that catalyze reactions to incorporate oxygen into substrates.[195] Given its importance and the fine line between its physiological functions and the production of reactive oxygen species, oxygen levels must be tightly regulated. Hypoxia Inducible Factor (HIF) proteins are critical oxygen sensing proteins that regulate genetic transcription to account for variation in oxygen levels.[196] Hypoxia response is particularly important in cancer where rapidly growing tumors will often have a hypoxic core due to incomplete vascularization. This hypoxic condition can cause cells to change their metabolism, become more aggressive, and metastasize.[197]

Superoxide (O_2^-) is a diatomic radical anion produced from the one electron reduction of molecular oxygen. Its conjugate acid, the peroxyl radical, has a pK_a of 4.8, making the anion the predominant form under physiological conditions. Superoxide behaves as both an oxidant and reductant with redox potentials of +0.93V for the O_2^-, $2H^+/H_2O_2$ redox couple and −0.35V for the O_2/O_2^- redox couple.[198,199] In many cases, superoxide is the first reactive oxygen species generated in biological systems and can be produced in the mitochondrial electron transport chain (ETC),[193] by NADPH oxidase (NOX) enzymes,[200] and by other enzymatic and non-enzymatic processes. In the mitochondrial ETC, the major source of superoxide production occurs in the NADH-ubiquinone oxidoreductase Complex I, particularly in situations where the mitochondria

are not generating ATP and/or when there is a high NADH/NAD^+ ratio. Mitochondrial superoxide production is in many cases detrimental because it leads to the production of more highly reactive oxygen species that can indiscriminately damage biological molecules. On the other hand, superoxide can be generated purposefully for healthy biological functions by proteins like the NADPH oxidase (NOX) family of enzymes – for example, by NOX2 in leukocytes and phagocytic cells as a precursor to highly reactive oxygen species to kill invading pathogens.[201] Additionally, NOX enzymes can generate superoxide to control signaling and cell proliferation,[202,202] usually through dismutation to hydrogen peroxide, which then signals through the oxidation of thiols to disulfides to alter protein structure and function. On the other hand, evidence is beginning to emerge that superoxide can react directly with metalloproteins to mediate signaling.[203] Other enzymes that produce superoxide include xanthine oxidase which is excreted in milk. This enzyme catalyzes the oxidation of xanthine or hypoxanthine to uric acid with the conversion of oxygen to superoxide. Xanthine oxidase is a useful tool for the controlled enzymatic generation of superoxide in model systems.[204,205]

Superoxide undergoes spontaneous dismutation to form hydrogen peroxide and oxygen, but there are a series of superoxide dismutase (SOD) enzymes that catalyze this reaction at rate of 10^9 M^{-1} s^{-1}, highlighting the immense importance of controlling the formation of this initiatory reactive oxygen species.[206] There are three SOD enzymes. SOD1 is a Cu/Zn SOD that is found in the cytoplasm, nucleus, and mitochondria. SOD2 is a MnSOD enzyme located in the mitochondrial matrix. SOD3, also called EC-SOD, is an SOD enzyme that is found in the extracellular matrix. Generally, these superoxide dismutase enzymes share a similar mechanism that consists of an initial reduction of the metal center in the enzyme by superoxide to generate molecular oxygen, followed by reaction with a second equivalent of superoxide to reoxidize the metal and generate hydrogen peroxide. Superoxide also reacts with other metals found in biological systems. Iron-sulfur clusters react with superoxide with rate constants on the order of 10^6 M^{-1} s^{-1}, [207] by oxidizing the iron-sulfur cluster and causing it to break apart, ultimately releasing iron and H_2O_2.[207] Superoxide also reacts with enzymes such as *e. coli* acotinase at a rate of 10^9 M^{-1} s^{-1},[208] as well as cytochrome c, myeloperoxidase, and other iron or copper containing proteins. Being a ground state doublet with an unpaired electron, superoxide readily reacts with other radical species.[209] Superoxide can react with phenoxy radicals derived from tyrosine to generate tyrosine hydroperoxides, as well as other biological radicals derived from vitamin E or tryptophan. An important radical reaction of superoxide is its reaction with nitric oxide to form peroxynitrite, which proceeds with fast kinetics and a rate constant of 10^{10} M^{-1} s^{-1}.[210,211] As discussed below, peroxynitrite has potent two-electron reactivity and will also decompose to highly reactive radical species like hydroxyl radical, carbonate radical, and nitrogen dioxide radical.[212] Superoxide has fast rates of reaction with ascorbate,[213] but its direct reaction with biological thiols and glutathione is relatively slow at rates of $10^2 - 10^3$ M^{-1} s^{-1}.[214]

4.1.2 Classical detection techniques for superoxide

Given its initiatory role to produce reactive oxygen species, much effort has been spent to develop techniques to detect superoxide in biological systems. Other non-luminescent techniques for the detection of superoxide include monitoring oxygen consumption by electrochemical or other means,[215] monitoring a change in the absorbance of cytochrome c when it is reduced by superoxide,[201] nitroblue tetrazolium and water soluble derivatives,[216,217] superoxide selective electrodes,[218] iron release from acotinase, and electron paramagnetic resonance spectroscopy using spin traps to trap and stabilize the superoxide radical.[219] It is worthy to note that practical development of superoxide detection methods requires reliable and controlled sources of superoxide. It can be supplied as a stable salt potassium superoxide (KO_2), which can be made as saturated solutions in DMSO, the xanthine/xanthine oxidase enzymatic system,[204,205] and

various donor compounds that can generate superoxide usually via reduction of oxygen and redox cycling.[220]

4.1.3 Superoxide probes by trigger

Luminescent probes for superoxide have been made that take advantage of superoxide's natural reactivity and include strategies based on oxidative triggers (Table 1, Sections 1–9), nucleophilic triggers (Table 1, Sections 10–13), combined oxidative and nucleophilic approaches (Table 1, Section 14), and reductive triggers (Table 1, Section 15).

Luminol/L-012 (Table 1, Section 1)

One of the earliest luminescent probes for superoxide detection was luminol, a phthalic hydrazide that undergoes a chemiluminescence reaction upon oxidation. It was first convincingly used for detection of cellular superoxide by Allen and Loose in 1976 in a cell suspension of macrophages undergoing phagocytosis in which luminol provided a superoxide dismutase inhibitable chemiluminescence signal (Figure 6).[101] A new derivative of luminol, L-012, was developed by Nishinaka in 1993 and displayed better water solubility, enhanced chemiluminescence, less redox cycling, and superoxide dismutase-dependent signal from EoL-1 cells.[221,] However, L-012 has since been studied in more detail. Daiber in 2004 demonstrated that L-012 also has a chemiluminescence response to peroxynitrite.[102,205] In 2013, detailed mechanistic work was performed by Zielonka and Kalyanaraman showing that L-012 does not react directly with superoxide but instead more highly reactive radical species like hydroxyl radical and nitrogen dioxide radical.[103] Interestingly, the superoxide dismutase dependence of the signal originated from superoxide that was being generated during the reaction as an important reactive intermediate. Scavenging of the formed superoxide halts the progress of the chemiluminescence mechanism, attenuating response and explaining the superoxide dismutase dependence. These observations teach that caution and careful controls should be put in place when using luminol and its derivatives for the detection and imaging of superoxide. Table 1, Section 1 summarizes these and any other examples of probes using luminol triggers.

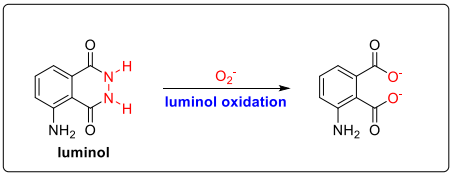

Figure 6. The chemiluminescent probe **luminol** as an example of luminol oxidation trigger for O_2^- detection.[101]

Lucigenin and other acridinium salts (Table 1, Section 2)

Lucigenin (10,10'-dimethyl-9,9'-biacridinium dinitrate) is an acridinium salt that reacts with superoxide to produce chemiluminescence emission centered at 503 nm,[222] and can be used to monitor superoxide production in macrophages.[223] The dinitrate salt is not cell-permeable, so it works best when monitoring superoxide production after being internalized into phagosomes via phagocytosis. However, in 2013, Kobayashi developed the cell permeable derivate **MMT** where the nitrates were replaced by monomethyl terephthalate anions that form a charge transfer complex, allowing the probe to be taken up across the cellular membrane.[224] The cell permeable **MMT** was used to image superoxide production in PMA-activated and apoptotic neutrophils. Another example that used acridinium salts relied on PeT quenching of a porphyrin fluorophore by appended acridinium salts in the probe **Acr^+-H_2P-Acr^+** (λ_{ex} = 512 nm, λ_{em} = 651 nm) developed by Crossley and Fukuzumi in 2011.[225] Reduction of the acridinium groups by superoxide reduces PeT quenching and increases fluorescence, providing potential opportunities for biological sensing. Some concerns have been raised about using lucigenin to monitor superoxide because

it can undergo redox cycling;[226] however, others have shown that this can be avoided by using lower concentrations of lucigenin when monitoring superoxide production.[227] Table 1, Section 2 summarizes these and any other examples of probes containing this trigger.

Cypridina *luciferin and coelenterazine analogues (Table 1, Section 3)*

In 1980, Goto and Takagi reported a *Cypridina* luciferin analogue (**CLA**) that could detect superoxide generated in a xanthine/xanthine oxidase superoxide generating system via chemiluminescence emission that was inhibited by addition of superoxide dismutase (Figure 7).[106] A number of analogues have been developed including methoxy,[228,229] naphthyl,[230] and indole derivatives.[230] Lucas reported in 1992 that the structurally related molecule coelenterazine could be used to measure superoxide in neutrophils (Figure 8).[231] Alkylated coelenterazine derivatives were reported to have improved superoxide dismutase chemiluminescence inhibition properties by Shimomure in 1997[232] and in more recent years, Pinto da Silva has investigated a number of fluorinated derivatives of coelenterazine not only for their chemiluminescent superoxide detection properties but also for their photodynamic therapy capabilities.[233–236] In an interesting 2016 study, Contag showed that coelenterazine could be used for whole animal *in vivo* imaging of superoxide in the pancreas of diabetic mice.[189] Covalent attachment of *Cypridina* luciferin analogues to high performing fluorescent scaffolds have been a fruitful strategy to red-shift the chemiluminescence emission wavelengths, beginning with Goto's disclosure of a fluorescein-conjugated derivative **FCLA** in 1991.[237] Since then a number of energy transfer constructs have been developed including cyclodextrin linked fluorescein and rhodamine conjugates developed by Teranishi,[238,239] a BODIPY-linked coelenterazine with emission at 545 nm developed by Saito,[240] and an indocyanine conjugate **MCLA-800** with near-infrared emission centered at 795 nm developed by Teranishi that was used for whole animal *in vivo* imaging in rat models of inflammation.[241,242] Table 1, Section 3 summarizes these and any other examples of probes containing this trigger.

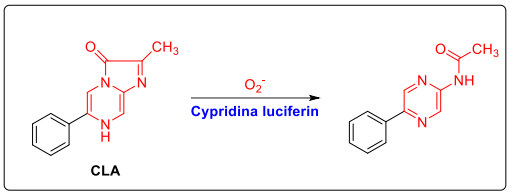

Figure 7. The chemiluminescent probe **CLA** as an example of *Cypridina* luciferin trigger for O_2^- detection.[106]

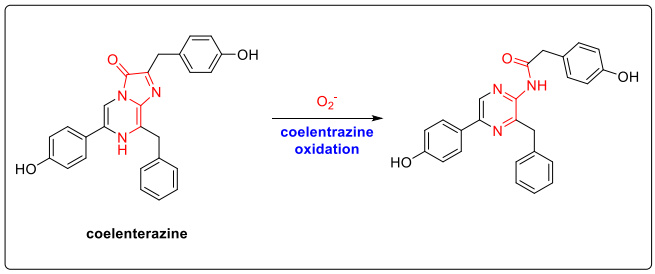

Figure 8. The chemiluminescent probe **coelenterazine** as an example of coelenterazine oxidation trigger for O_2^- detection.[231]

Hydroethidine (Table 1, Section 4)

Hydroethidine is a diaminodihydrophenanthridine with a C–H bond that can be readily oxidized by superoxide to form a fluorescent compound (λ_{ex} = 470 nm, λ_{em} = 590 nm) and was first persuasively demonstrated by Miller in 1996 to be able to measure superoxide in rat hippocampal neurons treated with NMDA or FCCP (Figure 9).[243] **Hydroethidine** and a phosphonium-based mitochondrial targeted derivative that is commercially available as **MitoSOX Red** are common

reagents for the detection of superoxide.[244] It was believed that hydroethidine was selectively oxidized to the fluorescence product ethidium; however, in 2003 Kalyanaraman demonstrated that the reaction product from hydroethidine and superoxide was actually a product distinct from hydroethidine,[245] later characterized by HPLC to be 2-hydroxy ethidine.[246] The same group showed that while it was not a perfectly reliable imaging probe for superoxide using fluorescence imaging, it could garner useful information about superoxide production when used in conjunction with HPLC separation.[247,248] An analogue of hydroethidine was developed by Kalyanaraman that incorporated a three carbon spacer and a positively charged ammonium functionality that was able to prevent the probe from entering the cell and provide a measure of extracellular superoxide.[249] A radiolabeled derivative for PET imaging was reported by Mach in 2014,[250] and another interesting derivative was developed by Murphy and Hartley in 2017 which added an oxidizable C–D bond in place of a C–H bond to enhance selectivity for superoxide, a triphenylphosphonium unit to target the mitochondria, and neopentyl groups to mitigate DNA intercalation.[251] This probe was called **MitoNeoD** (λ_{ex} = 544 nm, λ_{em} = 605 nm) and was used to measure mitochondrial superoxide production in cells and mouse models *in vivo*. Table 1, Section 4 summarizes these and other examples of probes containing this trigger.

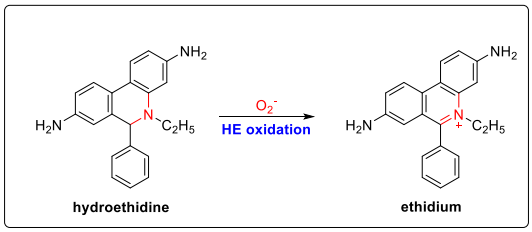

Figure 9. The fluorescent probe **hydroethidine** as an example of hydroethidine (HE) oxidation trigger for O_2^- detection.[243]

Hydrocyanines and hydrocoumarins (Table 1, Section 5)

In 2009, Murthy developed a class of fluorescent probes called hydrocyanines for the selective detection and imaging of superoxide and hydroxyl radical.[252] Cyanine dyes can be synthetically reduced with $NaBH_4$ to form non-fluorescent hydrocyanines, which selectively undergo oxidation of the C–H bond upon reaction with superoxide or hydroxyl radical to reform the fluorescence product. A series of hydrocyanine probes were developed with emissions between 560 nm to 830 nm. The probe **hydro-Cy3** (λ_{ex} = 535 nm, λ_{em} = 560 nm) was used to image angiotensin-stimulated ROS production in rat aortic smooth muscle (RASM) cells and mouse aorta *ex vivo* in mice treated with LPS (Figure 10). The deeper NIR probe **hydro-Cy7** (λ_{ex} = 735 nm, λ_{em} = 760 nm) was used in whole animal imaging of the mouse intraperitoneal cavity *in vivo* upon LPS stimulation. Later, Murthy utilized a hydroindocyanine, **H-800CW** (λ_{ex} = 774 nm, λ_{em} = 789 nm), for *in vivo* imaging of retinal oxidative stress.[253] A clever strategy used caged hydrocyanines to offer an opportunity to generate dual responsive probes in an approach pioneered by Chen starting in 2015 with the development of the dual superoxide/polysulfide probe **HCy-FN** (λ_{ex} = 775 nm, λ_{em} = 794 nm) using a hydrocyanine caged with a polysulfide sensitive trigger.[254] **HCy-FN** was used to image superoxide and polysulfides in PMA/LPS stimulated RAW 264.7 macrophages and mice. Similar strategies with other polysulfide triggers[255,256] or dual probes for mercury using appropriately caged-hydrocyanines have also been reported.[257] More recently, in 2021, Xing used a strategy that linked a hydrocyanine that oxidizes to a fluorescent cyanine form with superoxide and another cyanine dye that photoblues upon truncation reaction with peroxynitrite to make a dual superoxide/peroxynitrite probe **HCy5-Cy7** (λ_{ex} = 620 nm / 740 nm, λ_{em} = 660 nm / 800 nm).[258] Another C–H oxidation strategy was developed by Wen and Cui in 2020, but used dihydrocoumarin probe **1** or **R1** (λ_{ex} = 371 nm, λ_{em} = 468 nm) instead of hydrocyanine (Figure

11).[259] The oxidation was shown to be selective for superoxide and the same group performed a very useful and rare comparison to other triggers for superoxide detection.[260] Table 1, Section 5 summarizes these and any other examples of probes containing this trigger.

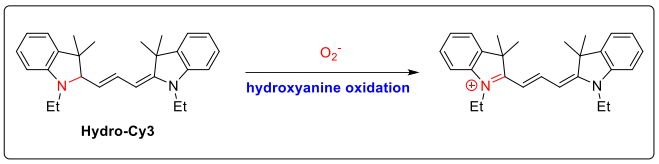

Figure 10. The fluorescent probe **Hydro-Cy3** as an example of hydrocyanine oxidation trigger for O_2^- detection.[252]

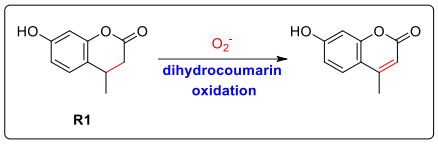

Figure 11. The fluorescent probe **R1** as an example of dihydrocoumarin trigger for O_2^- detection.[259]

Benzothiazoline oxidation (Table 1, Section 6)

In another manifestation of a C–H oxidation-based fluorescent superoxide probe, Tang showed in 2004 that the oxidation of a benzothiazoline to the aromatic benzothiazole could be used as a superoxide-selective trigger by developing a probe **H. Py. Bzt.** that forms a fluorescent 2-pyridyl-thiazole as a fluorescence product (λ_{ex} = 377 nm, λ_{em} = 528 nm), and was used with flow injection spectrometry to monitor superoxide production (Figure 12).[261] Later, in 2007, Tang showed that a *bis*-benzothiazoline probe **DBZTC** linked through a cyclohexene linker provided red-shifted excitation and emission wavelengths (λ_{ex} = 485 nm, λ_{em} = 559 nm) capable of live-cell imaging of superoxide production in PMA stimulated RAW 264.7 macrophages.[262] Tang and others went on to report a series of two-photon probes,[263–265] some of which could be that could be targeted to the mitochondria[263] or endoplasmic reticulum.[264] Table 1, Section 6 summarizes these and any other examples of probes containing this trigger.

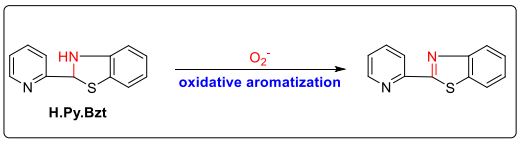

Figure 12. The fluorescent probe **H.Py.Bzt** as an example of benzothiazoline trigger for O_2^- detection.[261]

Catechol oxidation (Table 1, Section 7)

Tang introduced a new trigger for superoxide detection based on the oxidation of a catechol to a benzoquinone by showing that the probe **TCA**, a *bis*-caffeic acid derivatized tripolycyanamide scaffold, could operate as a fluorescent probe for superoxide imaging (λ_{ex} = 491 nm, λ_{em} = 515 nm) (Figure 13).[266] The trigger has useful properties in that it is reversible upon the product benzoquinone reacting with glutathione to reform the catechol, as well as being able to be excited by two-photon absorption at 800 nm. **TCA** was successfully used to image superoxide in HL-7702 cells, HepG2 cells, and *in vivo* in both zebrafish and mice. In 2018, Sun developed a near-infrared probe I**R-747-SAPH** using catechol oxidation to modulate photoinduced electron transfer quenching of an appended cyanine fluorophore (λ_{ex} = 690 nm, λ_{em} = 747 nm).[267] The catechol trigger endows the probe with reversibility upon reaction with glutathione and **IR-747-SAPH** was used for imaging superoxide production during ischemia/reperfusion in an *in vivo* mouse model. The trigger has proven to be translatable to other scaffolds and modalities including ratiometric imaging,[268] two-photon imaging probes,[269–272] NIR probes,[273] as well as for the development of

probes targeted to the mitochondria,[268] endoplasmic reticulum,[274] and Golgi apparatus.[272] The catechol oxidation trigger has also been coupled with pH[270] and $ONOO^-$[271] sensing moieties to generate dual responsive probes. Deeper mechanistic studies could help illuminate the details of its reactivity with superoxide. Table 1, Section 7 summarizes these and any other examples of probes containing this trigger.

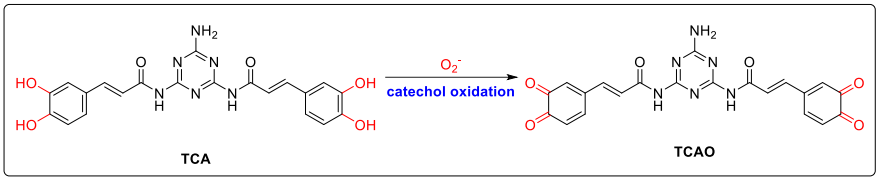

Figure 13. The fluorescent probe **TCA** as an example of catechol oxidation trigger for O_2^- detection.[266]

Sulfide and selenide oxidation (Table 1, Section 8)

Churchill discovered that certain sulfides could be used as selective fluorescent probes for superoxide in 2013.[275] A thiofuran with two pyridyl sulfide groups attached to a BODIPY scaffold was shown to not only provide a luminescence response upon Hg^{2+} binding, but also a turn-on response upon oxidation with superoxide (λ_{ex} = 506 nm, λ_{em} = 524 nm). Although the exact product with superoxide was unable to be identified, the sulfoxide and sulfone products were, curiously enough, able to be ruled out. In 2014, Churchill continued exploring chalcogens for superoxide sensing with the report of a diselenide *bis*-BODIPY probe that could be oxidized by superoxide to form the diselenide dioxide with increased fluorescence emission due to reduced PeT quenching (λ_{ex} = 504 nm, λ_{em} = 514 nm) (Figure 14).[276] The diselenide dioxide could be reduced by glutathione, making the probe a reversible superoxide sensor that could be used to image superoxide generated in MCF-7 cells treated with PMA. Manjare published a series of selenium-based superoxide sensors beginning in 2019 with a phenylselenide linked to a BODIPY dimer to give a fluorescence response from superoxide (λ_{ex} = 505 nm, λ_{em} = 526 nm) and fluorescence images in MCF-7 cells.[277] These studies were followed by the same group reporting a diselenide *mono*-BODIPY (λ_{ex} = 506 nm, λ_{em} = 521 nm),[278] a tetraphenyl BODIPY selenide derivative (λ_{ex} = 573 nm, λ_{em} = 608 nm),[279] and a pair of coumarin derivatives (λ_{ex} = 388 nm, λ_{em} = 469 nm and λ_{ex} = 380 nm, λ_{em} = 458 nm).[280] The coumarin derivatives are of note because the authors provide evidence for a selenium dioxide product as confirmed by NMR and mass spectrometry. The rich redox chemistry of chalcogens has been used to probe several reactive oxygen and nitrogen species and careful consideration of the selectivity for each unique chalcogen-based probe should be a prerequisite for any biological study. Table 1, Section 8 summarizes these and any other examples of probes containing this trigger.

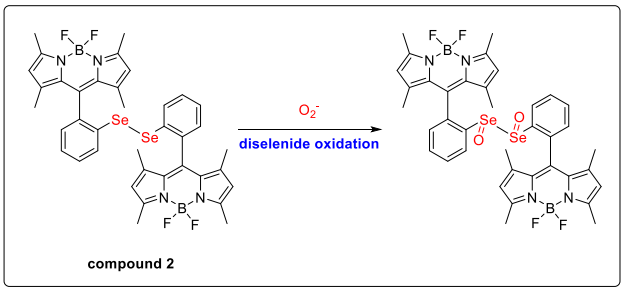

Figure 14. The fluorescent probe **compound 2** as an example of diselenide oxidation trigger for O_2^- detection.[276]

Other oxidative triggers (Table 1, Section 9)

There is an assortment of other oxidative triggers for superoxide detection that have been reported but remain relatively unexplored. Ohyashiki reported in 1999 that exposure to superoxide

causes quenching of the fluorescence of 1,3-diphenylisobenzofuran **DPBF** (λ_{ex} = 410 nm, λ_{em} = 477 nm), which was exploited to detect superoxide generation in a phospholipid liposomal membrane.[281] A study by Gao in 2009 indicated that an *ortho*-imino phenol could react with superoxide via a hydrogen atom abstraction/one-electron oxidation, followed by reaction with peroxide to yield a nitroxyl with a fluorescence signal at λ_{ex} = 294 nm and λ_{em} = 355 nm (Figure 15).[282] In 2010, Payrastre and Hoffman showed that streptocyanines, arylated derivatives of cyanines, are selectively bleached by superoxide, enabling a method for fluorescence monitoring.[283] In 2013, Li developed an ionic liquid probe **ImS-FILA** (λ_{ex} = 373 nm, λ_{em} = 422 nm) in which two imidazolium units were covalently linked to an anthracene (Figure 16). Superoxide induced oxidative decomposition of the imidazolium groups with a quenching of fluorescence.[284] In 2019, Ma and Lei presented a study showing that the oxidation of Hantzsch esters (Figure 17) and boronates (Figure 18) could be used as triggers for superoxide, developing a series of probes with emission wavelengths ranging from 463 nm to 597 nm, and demonstrated that these probes could be used for imaging superoxide in live HeLa cells.[285] Another example of using boronates for imaging superoxide in the mitochondria was reported in 2022;[286] however it should be noted that in these cases a negative control with superoxide dismutase was not performed, so a complete understanding of reactivity with other ROS remains to be elucidated. Table 1, Section 9 summarizes these and any other examples of probes containing this trigger.

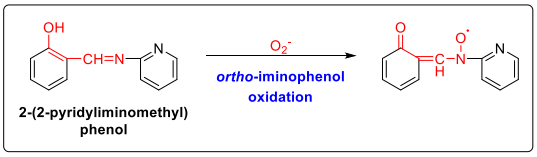

Figure 15. The fluorescent probe **2-(2-pyridyliminomethyl) phenol** as an example of *ortho*-imino phenol trigger for $O_2^{\cdot-}$ detection.[282]

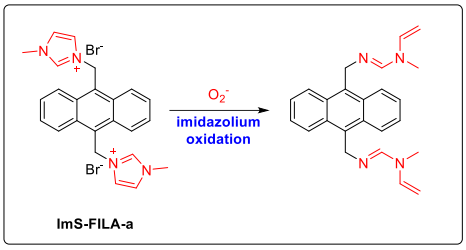

Figure 16. The fluorescent probe **Ims-FILA-a** as an example of imidazolium oxidation trigger for $O_2^{\cdot-}$ detection.[284]

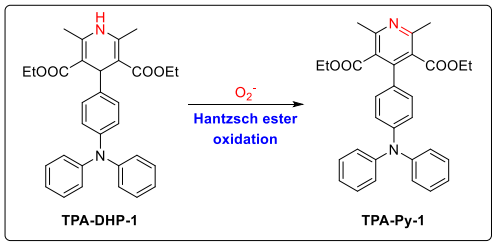

Figure 17. The fluorescent probe **TPA-DHP-1** as an example of Hantzsch ester oxidation trigger for $O_2^{\cdot-}$ detection.[285]

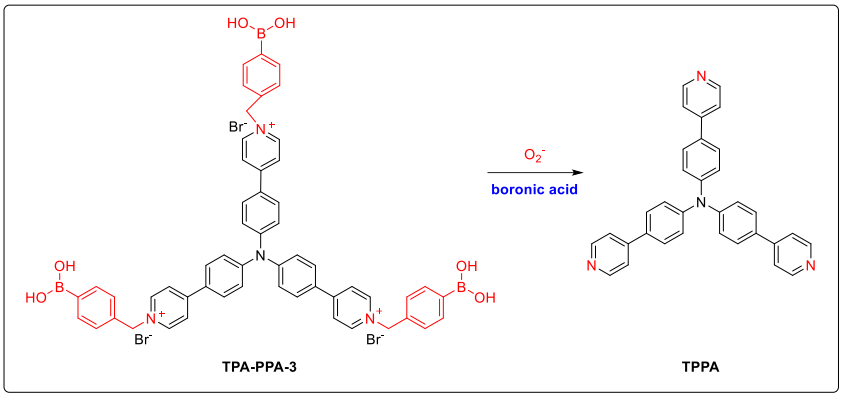

Figure 18. The fluorescent probe **TPA-PPA-3** as an example of boronic acid trigger for O_2^- detection.[285]

Sulfonyl group cleavage (Table 1, Section 10)
Oxidative mechanisms for the detection of superoxide face inherent challenges regarding selectivity versus other reactive oxygen species. A non-redox mechanism based on the nucleophilicity of superoxide was proposed by Maeda in 2005 to address this with the development of a probe based on fluorescein *bis* protected with a 2,6-dinitrosulfonyl group (Figure 19).[287] The idea was that using a nucleophilic mechanism as opposed to a redox mechanism should garner better selectivity versus other reactive oxygen species by exploiting a different mode of reactivity. Various probe structures including the dichloro, difluoro, and unsubstituted fluorescein were investigated, and it was found that the protected tetrafluorofluorescein derivative gave the best selectivity versus glutathione, a key competitive nucleophile in the cell. The probe was used for the spectroscopic detection of superoxide production in neutrophils. Two years later in 2007, Maeda reported that using a different protecting group, a 2-nitro-4,5-dimethoxy sulfonyl group, increased performance and reduced the glutathione reactivity of the resultant probe **BESSo** and its acetoxymethyl ester derivative **BESSo-AM** (λ_{ex} = ~488 nm, λ_{em} = ~520 nm), enabling its use for imaging superoxide in human Jurkat T cells.[288]

In 2015, Yang realized that a trifluoromethylsulfonyl (triflate) protecting group provided excellent selectivity for superoxide and developed a series of probes based on triflate protection of fluorescein, **HKSOX-1**, **HKSOX-1r** for cellular retention, and **HKSOX-1m** for mitochondrial targeting (λ_{ex} = 509 nm, λ_{em} = 534 nm) (Figure 20).[289] These probes were used to image superoxide in HCT116 colon cancer cells, BV-2 microglial cells, RAW 264.7 macrophages, and zebrafish *in vivo*. Perhaps due to the synthetic accessibility of this trigger and release of a phenol moiety that is easy to incorporate into fluorescent scaffolds, it has been widely adopted with many examples of two-photon imaging probes,[134,290–297] ratiometric fluorescence probes,[292–294,298] near-infrared fluorescence probes[120,134,297,299–303] and probes targeted to the endoplasmic reticulum,[294,304,305] lysosomes,[295] hepatocytes,[134,306] mitochondria,[297] Golgi apparatus,[120,121] as well as probes applied for bacterial imaging.[307] Interestingly, moving from a triflate to a triflimide retains the superoxide sensitivity and selectivity as was demonstrated by Yu and Chen in 2018 in their design of a triflimide protected cyanine probe **Mito-Cy-Tfs** (Figure 21).[308] This probe is ratiometric, near infrared, and mitochondrial targeted (λ_{ex} = 600 nm / 730 nm, λ_{em} = 742 nm / 790 nm), and was used for imaging superoxide in cells and in *in vivo* mouse models.

Photoacoustic probes were recently developed in 2022 by Zhao and Liang who targeted mitochondria using a triflimide protected cyanine dye called **APSA** that gave a good photoacoustic signal when excited at 690 nm and a fluorescence signal when excited at 745 nm, enabling *in vivo* photoacoustic imaging of superoxide.[297] In 2023, Yuan, Gao, and Su reported a hepatocyte targeted NIR fluorescence/photoacoustic probe that used a cholic acid targeting group and triflate

trigger attached to a hemicyanine dye named **hCy-Tf-CA**.[306] This probes gives a photoacoustic signal when excited at 680 nm or 710 nm and can also be used for NIR fluorescence with λ_{ex} = 675 nm and λ_{em} = 760 nm. It was applied for fluorescence imaging in cells as well as in dual mode NIR fluorescence/photoacoustic whole animal imaging of superoxide in acute inflammatory liver injury and autoimmune hepatitis. An interesting use of the triflate trigger was reported by Zhang in 2018 where a *bis*-triflate fluorescein was radiolabeled with radioactive iodine for dual SPECT/fluorescence imaging of superoxide produced during inflammation in an *in vivo* mouse model.[309]

In 2019, Pu reported the first 1,2-dioxetane based chemiluminescent probes for superoxide **MRP$_D$** that linked a triflate-caged spiroadamantane 1,2-dioxetane with emission at λ_{em} = 540 nm for superoxide detection to a cyanine dye for NIR fluorescence, and a renal clearable cyclodextrin to optimize pharmacokinetics.[310] Interestingly, no energy transfer from the dioxetane to the cyanine was observed, so the NIR fluorescence could be used as a superoxide independent signal for tracking the probe. The same year, Pu reported another triflate caged 1,2-dioxetane linked to a hemicyanine dye with a caspase cleavable unit named **CFR** for multimodal imaging of superoxide and caspase in cells and animal models.[311] Reaction with superoxide increased emission at 540 nm, again indicating inefficient energy transfer to the hemicyanine dye which allowed for allowing multianalyte imaging. The next year in 2020, Pu reported a triflate protected 1,2-dioxetane with a dicyanochromone displaying near-infrared chemiluminescence emission at 700 nm named **NCR1**, which was used for NIR fluorescence imaging in cells (λ_{ex} = 535 nm, λ_{em} = 700 nm) and whole animal chemiluminescence imaging in mouse models.[312] Other examples of triflate caged 1,2-dioxetane probes for superoxide include the acrylic ester 1,2-dioxetane reported by Gao & Yuan,[313] and a series of nanoparticle-based approaches reported by Huang[314] and Sun and Jiang.[315] In 2018, Lee reported a related *bis*-sulfinate caged fluorescein **SoDA-1** (λ_{ex} = 480 nm, λ_{em} = 512 nm) for imaging superoxide to visualize avian influenza virus infection (Figure 22).[316] Sulfonyl cleavage, sulfinate cleavage, and triflate/triflimide cleavage, in particular have become a widely used triggers for developing luminescence probes for superoxide imaging. Table 1, Section 10 summarizes these and any other examples of probes containing this trigger.

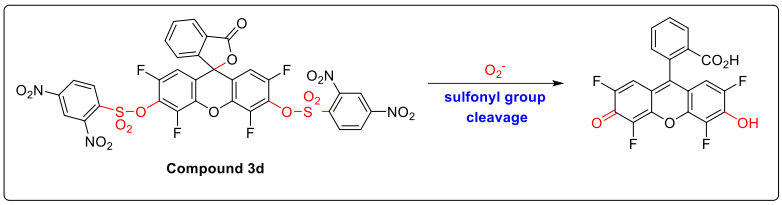

Figure 19. The fluorescent probe **Compound 3d** as an example of sulfonyl group cleavage trigger for O_2^- detection.[287]

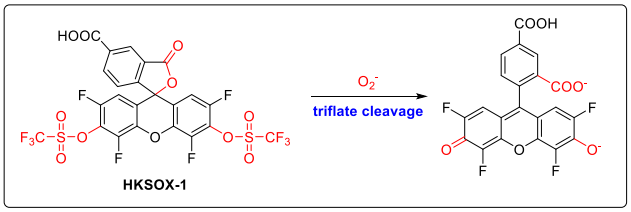

Figure 20. The fluorescent probe **HKSOK-1** as an example of triflate cleavage trigger for O_2^- detection.[289]

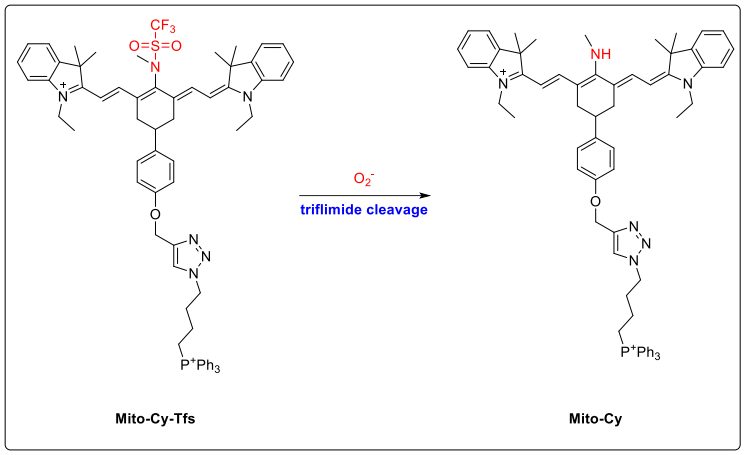

Figure 21. The fluorescent probe **Mito-Cy-Tfs** as an example of triflimide cleavage trigger for O_2^- detection.[308]

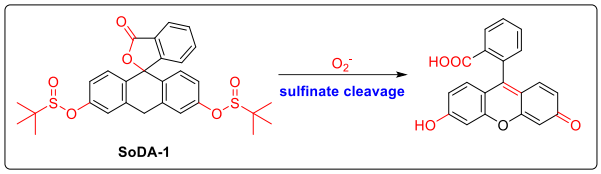

Figure 22. The fluorescent probe **SoDA-1** as an example of sulfinate cleavage trigger for O_2^- detection.[316]

Phosphinate cleavage (Table 1, Section 11)

In 2007, Tang described 3',6'-bis(diphenylphosphinyl)fluorescein – **PF-1** (λ_{ex} = 490 nm, λ_{em} = 530 nm)[317] and 4′,9′-bis(diphenylphosphinyl)naphthofluorescein – **PNF-1** (λ_{ex} = 602 nm, λ_{em} = 662 nm),[318] the first fluorescent probes for superoxide based on cleavage of a phosphinate group (Figure 23). These probes displayed good selectivity for superoxide and were able to be used for imaging superoxide production in living macrophage cells. Like sulfonyl group cleavage, this strategy has also been widely adopted with numerous examples of two-photon,[319,320] NIR,[310,318,321–323] ratiometric,[324–327] and mitochondrial targeted[325,326,328–330] probes. A phosphinate-caged luciferin was developed in 2018 by Xu and Lu, which was used for bioluminescence detection of superoxide in Huh7 cells.[331] In 2014, Churchill used a related strategy but with a phosphonate ester formed after reaction with and detection of chlorophosphate nerve agents by fluorescence quenching, which was reversed with superoxide cleavage of the phosphonate ester (Figure 24).[332] Kim and Yoon reported a probe **TPP** using a phosphinothioate trigger in 2019 that releases a 5-(dimethylamino)naphthalene-1-thiol (λ_{ex} = 345 nm, λ_{em} = 470 nm) after selective reaction with superoxide.[333] This probe could be used in two-photon microscopy with excitation at 740 nm to enable live cell imaging PMA stimulated superoxide production in RAW 264.7 macrophages. It would be interesting to see detailed mechanistic and/or theoretical studies to elucidate why the related sulfonyl cleavage and phosphinate cleavage triggers yield such high selectivity for superoxide detection versus other nucleophiles and reactive oxygen species. Table 1, Section 11 summarizes these and any other examples of probes containing this trigger.

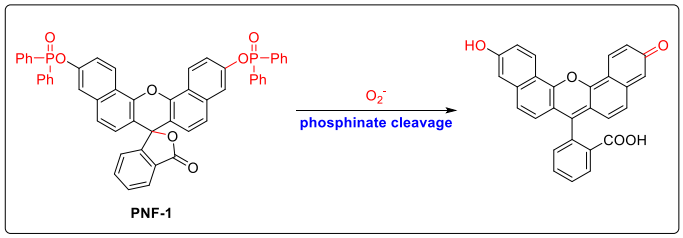

Figure 23. The fluorescent probe **PNF-1** as an example of phosphinate cleavage trigger for O_2^- detection.[318]

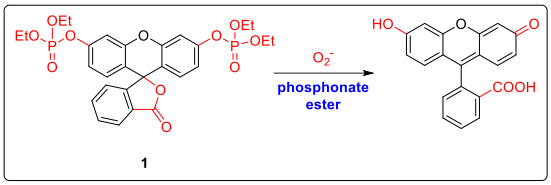

Figure 24. The fluorescent probe **1** as an example of phosphonate ester cleavage trigger for O_2^- detection.[332]

Nitrophenyl ester and ether cleavage (Table 1, Section 12)

Nitrophenyl groups are oftentimes sufficiently electrophilic that they can be cleaved by the nucleophilicity of superoxide. In 2013, Churchill reported a *bis*-3,5-dinitrobenzoate derivative of fluorescein and showed that it provided a fluorescence turn-on in response to superoxide (Figure 25).[334] While selective versus other ROS, glutathione can also give a signal from this probe making it an "OR" molecular logic gate that was used for fluorescence imaging in SH-SY5Y cells. In the same year, Churchill studied a *para*-nitrophenyl ether as a superoxide trigger to release a ESIPT fluorophore (λ_{ex} = 310 nm, λ_{em} = 460 nm), displaying a 90 nm red-shift from the starting probe (Figure 26).[335] This study is of interest because a direct comparison was made between the phosphinate and *para*-nitrophenyl ether triggers, showing that the phosphinate was more selective. Table 1, Section 12 summarizes these and any other examples of probes containing this trigger.

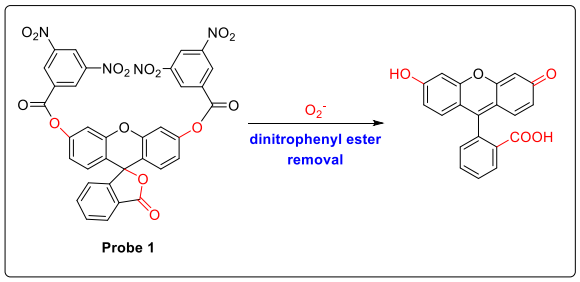

Figure 25. The fluorescent **Probe 1** as an example of dinitrophenyl ester removal trigger for O_2^- detection.[334]

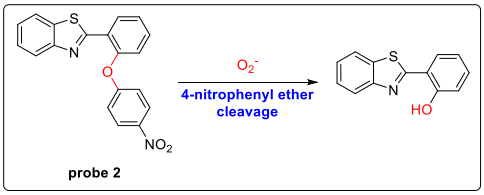

Figure 26. The fluorescent **Probe 2** as an example of 4-nitrophenyl ether cleavage trigger for O_2^- detection.[335]

Other nucleophilic triggers (Table 1, Section 13)

Several other nucleophilic triggers for fluorescence superoxide probes have been reported. Abramson reported in 2005 that 4-chloro-7-nitrobenzo-2-oxa-1,3-diazole (**NBD-Cl**) can react with superoxide via nucleophilic aromatic substitution of the chlorine atom to form a fluorescence product (λ_{ex} = 470 nm, λ_{em} = 550 nm) to monitor enzymatic superoxide production.[287] Recently, Ma reported that pyridinium cleavage could also be used as a superoxide trigger.[336] Finally, an interesting strategy was developed by Banala in 2019 showed that the reversible binding of superoxide to metallophorphyrins, porphyrins, and oxoporphyrins could be used for photoacoustic superoxide imaging with excitations between 740 nm to 760 nm for different structures as

demonstrated in *ex vivo* chicken muscle tissue (Figure 27).[337] Table 1, Section 13 summarizes these and any other examples of probes containing this trigger.

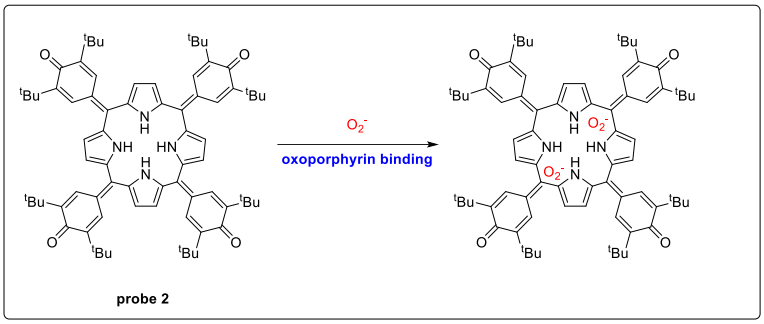

Figure 27. The fluorescent **probe 2** as an example of oxoporphyrin binding trigger for O_2^- detection.[337]

Combined oxidative and nucleophilic triggers (Table 1, Section 14)

Combining both the oxidative and nucleophilicity reactivities of superoxide can offer improved opportunities for selectivity. Au-Yeung reported in 2017 a copper(II) chelated tris(2-picolyl)amine ligand substituted with a hydroxylmethyl group that could be attached to several fluorophore scaffolds via an ether linkage as a selective superoxide probe that combines its oxidative potential and nucleophilicity.[338] Mechanistically, superoxide first binds to the copper(II) center, and then the bound superoxide oxidatively cleaves the adjacent ether bond to release a fluorophore, a strategy inspired by copper oxygenases.[339] This trigger was used to develop three probes, **SOP-blue** using a ratiometric coumarin scaffold (λ_{ex} = 325 nm, λ_{em} = 385 nm / 485 nm), **SOP-cyan** using a thiazonyl coumarin (λ_{ex} = 455 nm, λ_{em} = 488 nm), and **SOP-orange** using a resorufin scaffold (λ_{ex} = 570 nm, λ_{em} = 585 nm), with **SOP-cyan** being successfully used for live cell imaging in HEK293T cells. In 2020, Au-Yeung expanded this strategy to a hydroxymethyl fluorescein scaffold **SOP-green** (λ_{ex} = 470 nm, λ_{em} = 510 nm) (Figure 28), and synthesized a lysosome targeted probe **Lyso-SOP-green** that was used to image LPS-stimulated superoxide production in RAW 264.7 macrophages.[340] Another example of this type of combined approach was reported by Churchill in 2018, where it was demonstrated that a hemicyanine dye **HemiSe** could undergo 1,4-addition with superoxide, followed by H-atom abstraction to form the peroxide and provide a blue-shifted fluorescence response (λ_{ex} = 360 nm, λ_{em} = 439 nm) (Figure 29).[341] The probe was used to image superoxide in PMA/taxol treated RAW 264.7 macrophages. Interestingly, the probe **HemiSe** contains a phenyl selenide that was not oxidized by superoxide indicating that this reactivity can be nuanced and should be carefully considered in probe design. Table 1, Section 14 summarizes these and any other examples of probes containing this type of trigger.

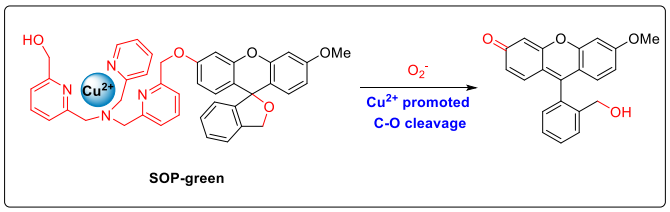

Figure 28. The fluorescent probe **SOP-green** as an example of Cu^{2+} promoted C-O cleavage trigger for O_2^- detection.[338]

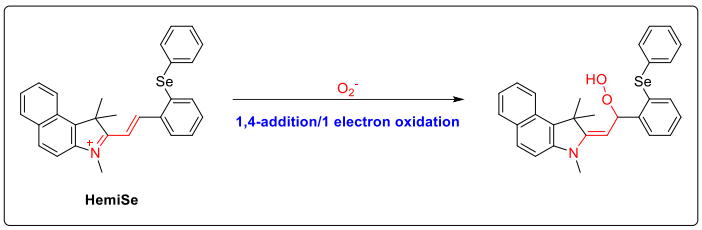

Figure 29. The fluorescent probe **HemiSe** as an example of 1,4-addition trigger for O_2^- detection.[341]

Reductive Triggers (Table 1, Section 15)

Although less common, there is a selection of probes that operate at least in part by superoxide's ability to act as a reductant. In 2010, Wang reported a pyrene fluorophore covalently bonded to a stable perchlorotrityl radical that could be reduced by superoxide to form a triphenyl methane and molecular oxygen.[342] This yielded a decrease in the EPR signal with a concomitant increase in fluorescence response (λ_{ex} = 346 nm, λ_{em} = 397 nm). This approach is related to a fluorescent spin trap **HO-1889NH** designed by Hideg in 2002 (Figure 30).[343] The sensing unit is a secondary amine flanked by four methyl groups that can react with superoxide or singlet oxygen to quench fluorescence (λ_{ex} = 330 nm, λ_{em} = 550 nm), and was used to look at ROS produced in spinach leaves exposed to UV light. A more recent approach was developed by Wang and Li in 2023, where they designed a probe based on the reaction of superoxide with a tetrazine sensing moiety (Figure 31).[344] The mechanism commenced with initial one-electron reduction of the tetrazole, followed by radical recombination with another equivalent of superoxide, cyclization, and loss of nitrogen. This strategy was used to make a series of probes **Tz1-9** and used to image superoxide in myocardial ischemia/reperfusion. Table 1, Section 15 summarizes these and any other examples of probes containing reductant-based trigger.

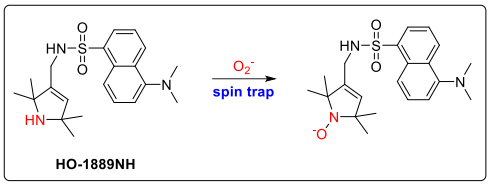

Figure 30. The fluorescent probe **HO-1889NH** as an example of spin trap trigger for O_2^- detection.[343]

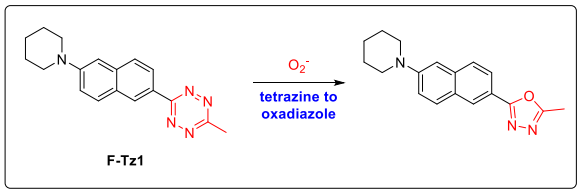

Figure 31. The fluorescent probe **F-Tz1** as an example of tetrazine to oxadiazole trigger for O_2^- detection.[344]
of tetrazine to oxadiazole trigger for O_2^- detection.[344]

4.1.4 Concluding remarks for superoxide probes

Superoxide is, in most cases, the initial reactive oxygen species formed that leads to the production of other ROS involved in both signaling and stress. Classic chemiluminescence probes including **luminol/L-012**,[101,103,205,221,229] **CLA**,[106] and **coelenterazine**[232] are commercially available and can be used, but the ROS selectivity and susceptibility to autooxidation can potentially complicate experiments. **Hydroethidine** and the commercially available **MitoSOX Red** still hold an important place for superoxide measurements,[243,244] but we note that the reaction products should be considered carefully and combination with HPLC can give more reliable results.[247,248] For oxidative probes, hydrocyanines[252,253] and catechol oxidations[266,267] have garnered the most

interest although hydroxyl radical reactivity should be remembered in the case of hydrocyanines and it would be informative to have better mechanistic understanding of catechol oxidation, especially given reports of hydrogen peroxide reactivity of this functional group.[345,346] Triflate deprotection has emerged as a dominate strategy for nucleophilic based probes,[289–293] likely due to their synthetic ease, but again it would build confidence to understand why these are selective versus other ROS and nucleophiles. Finally, the combined approach that mimics copper oxygenase enzymes reported by Au-Yeung is innovative and effective because it takes advantage of multiple aspects of superoxide reactivity.[338, 340]

4.2 Hydrogen peroxide

4.2.1 Hydrogen peroxide in health and disease

Hydrogen peroxide, a reduced form of oxygen with the formal addition of two electrons and two protons, plays important roles in healthy physiology and pathological disease states.[1,347,348] Its chemistry is dominated by two-electron mechanisms.[349] With a two-electron redox potential E'_0 of 1.23V, it is thermodynamically more oxidizing than other reactive oxygen species (ROS) like hypochlorous acid or peroxynitrite. However, a high activation barrier generally makes oxidation by hydrogen peroxide relatively slow and kinetically controlled with most biological molecules. It is also a weak one-electron oxidant with an E'_0 of 0.32V, but if it does get reduced by one electron, it forms hydroxyl radical, which is an exceptionally strong and fast oxidizing species with an E'_0 of 2.31V. The pK_a of hydrogen peroxide is 11.6, so it is predominantly in the neutral form under physiological conditions. The polarizability of the oxygen-oxygen bond makes it a good electrophile, the α-effect of vicinal lone pairs makes it a good nucleophile, and it is prone to homolytic cleavage to form hydroxyl radical under certain photolytic or radiolytic conditions. Hydrogen peroxide reacts with many biological molecules. Reactions with thiols are relatively slow but can be dramatically enhanced in the protein environment such as in proteins like peroxiredoxins. The initial product in the reaction with thiols is usually a sulfenic acid, which can rapidly form intermolecular and intramolecular disulfide bonds to modulate protein function. Sulfenamide, sulfinic acid, and sulfonic acid modifications can also occur.[348] Selenocysteine residues react rapidly with hydrogen peroxide such as in the protein glutathione reductase. Hydrogen peroxide can also react with α-ketoacids like pyruvate,[349] a strategy which has been used to develop hyperpolarized ^{13}C MRI probes.[350] Transition metals are important sites for hydrogen peroxide reactivity, and can either lead to more highly reactive species or safely decompose hydrogen peroxide.[349] Fenton chemistry with Fe(III) or Cu(II) is an important pathway for the formation of the highly reactive species hydroxyl radical, which can be detrimental physiologically, but has also been harnessed for chemodynamic therapy.[351] Heme peroxidases like myeloperoxidase, eosinophil peroxidase, and lactoperoxidase react with hydrogen peroxide with very high rate constants (10^7 to 10^8 M^{-1} s^{-1}) to generate more reactive oxygen species during host defense against pathogens by the immune system. Several families of antioxidant proteins, including catalase, glutathione reductase, and peroxiredoxins safely decompose hydrogen peroxide, eliminating its ability to transform into damaging reactive oxygen species. Models of the reactivity and diffusivity of hydrogen peroxide in a cellular context have led to estimates of hydrogen peroxide having a lifetime on the millisecond time scale allowing it to diffuse approximately 1 μm from the site of generation.[352]

The sources for the production of hydrogen peroxide can vary according to organelle and context.[1,347] In the mitochondria, the electron transport chain proceeds through a series of protein complexes (I–IV) to create a proton gradient for ATP synthesis.[353] While tightly regulated, it is estimated that 0.1%–2% of the electrons in the ETC are transferred to O_2 from some of these complexes, believed to predominately be from Complex I and Complex III, to generate superoxide, which can spontaneously dismutate or enzymatically be dismutated by superoxide

dismutase to form hydrogen peroxide. Hydrogen peroxide can also be formed in the plasma membrane by NADPH oxidase (NOX) enzymes, again through initial superoxide generation followed by spontaneous or enzymatic dismutation.[200,347] These enzymes are responsible for ROS production during phagocytosis as well as for generating hydrogen peroxide at the extracellular membrane for signaling purposes. In the endoplasmic reticulum, hydrogen peroxide is generated as a byproduct of protein folding.[1,347] Disulfide formation during protein folding in the endoplasmic reticulum is mediated by the protein Ero1, which oxidizes protein disulfide isomerase (PDI) using oxygen as the oxidant, producing one equivalent of hydrogen peroxide for each disulfide bond that is formed. Hydrogen peroxide has been studied for its role in numerous physiological processes including the immune response,[354] growth and proliferation,[202] wound healing,[355] transcription factor regulation,[356] epigenetics,[357] and circadian rhythms.[348,358] Additionally, misregulation of hydrogen peroxide has been implicated in many diseases including type 2 diabetes and insulin resistance, cancer, ischemia reperfusion injury, neurodegeneration and many others.[348]

4.2.2 Classical detection techniques for hydrogen peroxide

In addition to colorimetric methods,[359] early fluorescent approaches for detecting hydrogen peroxide include using reduced dihydroxanthenes that are oxidized into a fluorescent form in a process that can be mediated by hydrogen peroxide (Table 2, Section 1). These types of early probes comprise dihydrofluorescein, dihydrodichlorofluorescein including *bis*-acetate derivatives (Figure 32), and dihydrorhodamine 123.[23,24] A similar strategy has been used with a dihydrophenoxazine derivative in the commonly used assay Amplex Red (Figure 33).[25] While these luminescence strategies have certainly been useful, it is known that the oxidation of these probes by hydrogen peroxide depends on the presence of a peroxidase enzyme,[360] and cross-reactivity with other reactive oxygen and nitrogen species can occur.[23,361] Luminol and derivatives have been used in conjunction with peroxidases for chemiluminescent detection of hydrogen peroxide,[362] but this system can potentially respond with a variety of reactive oxygen and nitrogen species including peroxynitrite.[103] Nevertheless, there have been interesting recent reports of chemiluminescent probes operating via covalent attachment of luminol to metal complexes[363,364] or incorporation into polymers.[365] Acridinium salts have been shown to generate chemiluminescence upon reaction with hydrogen peroxide through the decomposition of a dioxetanone intermediate,[366–370] and this chemistry has been used to detect nucleic acids in addition to peroxide.[371] Peroxyoxalate chemiluminescence, similar chemistry as used in commercial glow sticks, has also been used for hydrogen peroxide detection with high selectivity due to the mechanism involving acyl substitution at the vicinal diester of an oxalate.[372] This chemiluminescent approach has been capitalized for smartphone detection of hydrogen peroxide[373] and has been used to measure this reactive oxygen species in the exhaled breath condensate of asthma patients.[105] Furthermore, Murthy showed that with proper formulation, peroxyoxalate chemistry could be used to image hydrogen peroxide,[374] an approach that has been advanced for near-infrared *in vivo* imaging.[375,376] Finally, the genetically encoded probe HyPer is a very useful tool for hydrogen peroxide detection and imaging, however, protein-based fluorescent probes are beyond the scope of this review.[377,378] Table 2, Section 1 summarizes these and any other examples of probes using these types of classical detection techniques.

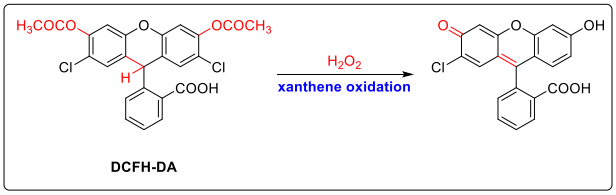

Figure 32. The fluorescent probe **DCFH-DA** as an example of xanthene oxidation trigger for H_2O_2 detection.[23,24]

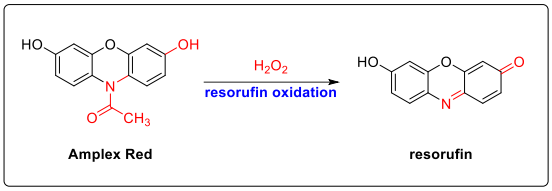

Figure 33. The fluorescent probe **Amplex Red** as an example of resorufin oxidation trigger for H_2O_2 detection.[25]

4.2.3 Hydrogen peroxide probes by trigger

Phosphine oxidation (Table 2, Section 2)

An early strategy to develop reaction-based fluorescent probes for hydrogen peroxide and hydroperoxides relied on the oxidation of phosphines to phosphine oxides. In 1987, Meguro reported diphenyl-1-pyrenylphosphine (**DPPP**, Figure 34) as part of a series of triaryl phosphine derivatives also including 1-naphthyldiphenylphosphine (**NDPP**), 9-anthryldiphenylphosphine (**ADPP**), and triphenylphosphine (**TPP**) that were demonstrated to be oxidized by hydroperoxides to the respective phosphine oxides with an increase in blue fluorescence emission.[379] Noguchi showed in 2000 that **DPPP** reacts with H_2O_2, but more rapidly with methyl linoleate hydroperoxide to give an increase in fluorescence (λ_{ex} = 351 nm, λ_{em} = 380 nm) upon formation of the phosphine oxide, likely due to reduced PeT quenching.[380] **DPPP** was used to image lipid peroxidation in polymorphonuclear leukocytes treated with methyl linoleate hydroperoxide. In 2005, Onoda developed a diphenyl *N*-acetyl benzofuran phosphine probe (λ_{ex} = 360 nm, λ_{em} = 492 nm) that responded to cumene hydroperoxide, but its reactivity with hydrogen peroxide was not determined.[381] In the same year, Imato designed the probe **DPPEA-HC**, a diphenylphosphine linked to a coumarin that did give an increase in fluorescence in response to hydrogen peroxide (λ_{ex} = 396 nm, λ_{em} = 449 nm) that was selective versus other ROS with some cross reactivity observed with nitric oxide.[382] **Spy-HP**, consisting of a triphenylphosphine unit linked to a tetracarbonyl bisimide, was a probe created in 2006 by Soh and Imato that displayed a fluorescence response when reacting with *m*-CPBA or cumene hydroperoxide (λ_{ex} = 524 nm, λ_{em} = 535 nm), but in this case the reactivity with hydrogen peroxide was not tested.[383] A mitochondrial targeted version of **DPPP**, **MitoDPPP** (λ_{ex} = 350 nm, λ_{em} = 380 nm) was disclosed by Shioji in 2010.[384] It was shown that **MitoDPPP**, a diphenylpyrenylphosphine for peroxide detection linked to a triphenyl phosphonium for mitochondrial targeting, reacts with H_2O_2, cumene hydroperoxide, *tert*-butyl hydroperoxide, and methyl linoleate hydroperoxide, and was used to image *tert*-butyl hydroperoxide in HepG2 cells. In 2022, Wang and Chen developed a NIR emissive probe consisting of a diphenylphosphine trigger linked to a cyanine dye, **CyNOH2** (λ_{ex} = 605 nm, λ_{em} = 750 nm).[385] It was shown to be selective for H_2O_2, but cross reactivity with NO, superoxide, hydroxyl radical, and singlet oxygen was observed. The probe was used to detect increases in H_2O_2 in response to bisphenol A treatment of living LO2 cells, zebrafish, and mice via whole animal imaging. As seen from these studies, phosphine triggers are not perfectly selective for hydrogen peroxide, but can be useful for imaging hydrogen peroxide and other alkyl peroxides when high selectivity is not needed. Table 2, Section 2 summarizes these and any other examples of probes containing this trigger.

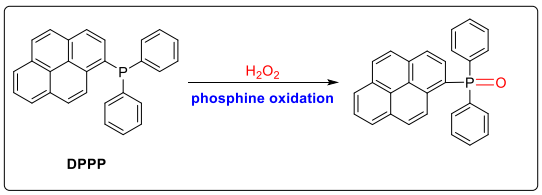

Figure 34. The fluorescent probe **DPPP** as an example of phosphine oxidation trigger for H_2O_2 detection.[379]

Boronate oxidation (Table 2, Section 3)

As opposed to phosphine oxidation, oxidation of an aryl boronate or boronic acid to a phenol is selective for hydrogen peroxide versus other types of alkyl hydroperoxides. In 2003, Lo demonstrated that a boronate could be used as a reaction-based trigger for the detection of hydrogen peroxide by linking a 2,3-butanediol protected aryl boronate to a coumarin fluorophore that produced a fluorescence signal (λ_{ex} = 355 nm, λ_{em} = 460 nm) upon reaction with hydrogen peroxide.[386] In 2004, Chang reported a green-emitting probe **PF1** (Figure 35) that consisted of a bis(pinacolato)boronate protected fluorescein that was non-fluorescent until reaction with hydrogen peroxide induced oxidation of the boronate to form fluorescein (λ_{ex} = 450 nm, λ_{em} = ~510 nm).[387] This study was important because it showed a clear selectivity for hydrogen peroxide versus alkyl peroxides like *tert*-butyl hydroperoxide and was the first study that demonstrated imaging of hydrogen peroxide in living cells using a boronate-based fluorescent probe. This was shortly after followed by an expanded study by Chang in 2005 that included deeper characterization of **PF1**, as well as the blue-shifted probe **PX1** (λ_{ex} = 350 nm, λ_{em} = 450 nm), based on a boronate-caged xanthone scaffold and the red-shifted probe **PR1** (λ_{ex} = 530 nm, λ_{em} = 580 nm), based on a resorufin scaffold.[388] These probes generally showed selectivity for hydrogen peroxide with some cross reactivity observed with NO and NO^+. They were all validated for live cell hydrogen peroxide imaging in HEK cells, and **PF1** was also used to image hydrogen peroxide in primary hippocampal neurons. Chang reported the first ratiometric boronate-based hydrogen peroxide probe in 2006 with **RPF1** (λ_{ex} = 420 nm, λ_{em} = 517 nm / 464 nm) using a FRET approach that linked a diethyl coumarin to a *bis*-boronate caged fluorescein scaffold reminiscent of **PF1**, and this probe was able to detect hydrogen peroxide in isolated mitochondria.[389] In 2008, Chang developed the first ratiometric fluorescent boronate-based probe for live cell imaging **PL1** (λ_{ex} = 410 nm, λ_{em} = 540 nm / 475 nm) based on a boronate-caged lucifer yellow fluorophore that had modulated ICT properties after oxidation of the boronate to the phenol.[390] This probe could also be excited by two-photon absorption using 800 nm light, enabling ratiometric two-photon microscopy imaging of hydrogen peroxide produced in PMA stimulated macrophages. Since this time a large number of boronate-based ratiometric fluorescent probes have been reported,[391–446] as well as boronate probes for two-photon imaging.[391,392,401,412,415,420,431,433,434,445,447–461] Another important advance was made by the Chang group in 2007, with the Tokyo Green-based **PG1** (λ_{ex} = 460 nm, λ_{em} = 510 nm) and resorufin-based **PC1** (λ_{ex} = 480 nm, λ_{em} = 584 nm) boronate probes.[462] These probes were shown selective for hydrogen peroxide, with some cross reactivity observed for nitric oxide and hypochlorite. Importantly, **PG1** was used as a first demonstration of live cell imaging of cellularly produced hydrogen peroxide in A431 cells stimulated with EGF, which has become a benchmark validation for fluorescent hydrogen peroxide probes.

Chang also pioneered organelle-targeted boronate based fluorescent probes in 2008 with the disclosure of **MitoPY1**, a boronate-caged rhodol with a triphenylphosphonium group to target the probe to the mitochondria which was able to achieve fluorescence imaging (λ_{ex} = 510 nm, λ_{em} = 528 nm) of hydrogen peroxide in the mitochondria of live cells.[463] In 2010, Chang also reported a SNAP-tag approach as a versatile method to target multiple organelles. Peroxygreen derivatives were labeled with two different substrates for the *O*-alkylguanine-DNA alkyltransferase (AGT) protein to generate the **SNAP-PG** fluorescence probes **SPG1** and **SPG2** (λ_{ex} = 465 nm, λ_{em} = 515 nm).[129] The AGT protein can be fused to a protein of interest and, depending on which protein it is fused to, enable organelle-targeted imaging in the endoplasmic reticulum, mitochondria, nucleus, and membrane of live HEK293T cells. Many strategies have been developed to generate boronate-based fluorescence probes targeted to mitochondria,[392,400,409,417,425,436,441,446,450,455,457,458,461,464–477] endoplasmic reticulum,[465] nucleus,[399,478] lysosome,[448,461,479–486] amyloids/protein aggregates,[142–146] integrin receptors,[140] targeting with

biotin,[487,459] lipid droplets,[137–139] microtubules,[136] estrogen beta receptor,[141] and the Golgi apparatus.[122] The first NIR boronate fluorescent probe was reported by Chang in 2008 as a *bis*-boronate caged naphthofluorescein **NPF1** (λ_{ex} = 598 nm, λ_{em} = 660 nm), which was used to monitor hydrogen peroxide production using flow cytometry in RAW 264.7 macrophages.[488] In 2011, Shabat reported the first *in vivo* NIR fluorescence imaging using a boronate-caged Cy7 fluorophore (λ_{ex} = 590 nm, λ_{em} = 715 nm) and used this to image an intramuscular injection of hydrogen peroxide in a live mouse.[489] A very large number of NIR I boronate probes for hydrogen peroxide with peak emissions above 650 nm have since been reported.[139,141,142,144,402–405,411,416,417,419,422,438,439,442,446,451,455,461,471–473,484,487,489–522]

Chang developed the bioluminescent probe **PCL-1** in 2010, consisting of a boronate-caged luciferin connected by a self-immolative linker.[523] **PCL-1** was used to measure hydrogen peroxide formed in paraquat stimulated LNCaP-luc cells and testosterone-induced hydrogen peroxide formation in an *in vivo* LNCaP-luc tumor xenograft mouse model. ATP is a substrate for the luciferin/luciferase which could potentially cause a perturbation of signal when there are significant fluxes in ATP. In order to solve this problem, Heffern designed a bioluminescent hydrogen peroxide probe **bor-DTZ** in 2022 that was formed from a boronate-caged diphenylterazine that is a substrate for the Nanoluciferase (Nanoluc) enzyme.[524] **bor-DTZ** was used to measure hydrogen peroxide in paraquat treated MDA-MB-231 cells expressing this Nanoluc enzyme. Boronate-caged 1,2-dioxetanes were reported by Turan in 2017, who developed a boronate-caged phenol with a self-immolative linker designed to release two chemiluminescent spiroadamantane 1,2-dioxetanes (Schaap's dioxetane) per equivalent of hydrogen peroxide to give an emission at 466 nm in 90% DMSO.[525] Also in 2017, Shabat reported 1,2-dioxetanes with simple acrylonitrile, acrylate, or acrylamide substitutions with improved chemiluminescence emissions in aqueous systems.[526] In this study, a boronate-based probe for hydrogen peroxide was reported with an acrylic acid substitution that displayed an emission at 520 nm when treated with hydrogen peroxide in aqueous buffer containing 10% DMSO. The same probe was later used by Caliceti in 2020 for chemiluminescence detection of hydrogen peroxide in Caco-2, HaCaT, and HUVEC cells.[527] Shabat also showed that appending a dicyanochromone to the 1,2-dioxetane can extend chemiluminescence emission into the NIR with a peak at 690 nm, and this probe was used to image hydrogen peroxide production in LPS stimulated mice in 2017.[496] In 2019, the same researcher expanded a strategy using a boronate-caged 1,2-dioxetane that releases methanol after reacting with hydrogen peroxide that could be used to regenerate hydrogen peroxide with the addition of an alcohol oxidase for a chain reaction amplification of the chemiluminescence signal.[528]

Recently, imaging in the NIR II spectrum and photoacoustic imaging probes with deeper imaging depth, less light scattering, and higher resolution have begun to emerge. In 2021, Lei and Zhang designed and studied the NIR II boronate-caged imaging probe **PN910** using a boronate-caged merocyanine fluorophore named **Chrodol-3** (λ_{ex} = 870 nm, λ_{em} = 910 nm).[529] The probe was shown to react with both hydrogen peroxide and peroxynitrite and was used for NIR II fluorescence imaging of hydrogen peroxide in LPS-treated mice and in a colitis model. In 2022, Xiong reported a boronate-caged polymethine dye with NIR II emission **IR-990** (λ_{ex} = 790 nm, λ_{em} = 990 nm).[530] This probe was used for imaging hydrogen peroxide in LPS stimulated HeLa cells, APAP treated HepG2 cells, and an *in vivo* mouse model of liver injury. Zeng and Wu developed a boronate-caged benzoindolium heptamethine cyanine probe **BHC-Lut** for NIR II fluorescence (λ_{ex} = 830 nm, λ_{em} = 930 nm) and photoacoustic imaging, with co-release of an antioxidant luteolin in a mouse liver injury model.[531] In 2019, Bohndiek reported a boronate-caged heptamethine carbocyanine, **JW41**, with NIR fluorescence (λ_{ex} = 790 nm, λ_{em} = 825 nm) and photoacoustic imaging using excitation at 800 nm of MDA-MB-231 tumors in mice.[499] In 2021, Chan described

the boronate-caged and sulfur substituted hemicyanine fluorophore **PA-HD-H_2O_2**, as part of a general strategy using this new fluorophore (λ_{ex} = 745 nm, λ_{em} = 765 nm).[507] This probe was used for fluorescence imaging in Neuroscreen-1 cells and photoacoustic imaging with a maximum photoacoustic excitation at 735 nm for imaging hydrogen peroxide in an *in vivo* Alzheimer's mouse model and wild type mice. Clearly, boronates are choice triggers for the design of small molecule hydrogen peroxide probes, likely due to their selectivity versus alkyl peroxides and other RNS/ROS, ease of synthesis, and large numbers of luminogenic scaffolds that are accessible with the release of a phenol from the boronate cage. Cross reactivity has been observed versus peroxynitrite, hypochlorite, and some other species, so it is important to use the appropriate controls including nitric oxide inhibition in biological experiments. Table 2, Section 3 summarizes these and any other examples of probes containing this trigger.

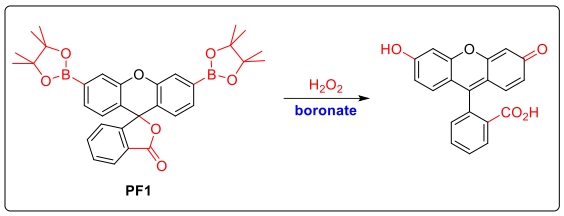

Figure 35. The fluorescent probe **PF1** as an example of boronate trigger for H_2O_2 detection.[387]

Sulfonyl cleavage (Table 2, Section 4)

Probe triggers that operate through oxidative mechanisms are at inherent risk for cross-reactivity versus other reactive oxygen species. In 2004, Maeda aimed to address this by developing the deprotection of a sulfonyl group as a non-oxidative mechanism for detecting H_2O_2 (Figure 36). A series of acetylated and non-acetylated fluorescein, dichlorofluorescein, and difluoroflorescein derivatives were investigated using the fluorescence emission at λ_{ex} = 485 nm, λ_{em} = 530 nm.[532] These were caged by a pentafluorobenzenesulfonyl protecting group and the rates of deprotection of the fluorescein, dichlorofluorescein, and difluorofluorescein derivatives were measured as 2.7, 23, and 25 x10^2 M^{-1} s^{-1}, respectively, following expected trends based on the strength of the electron withdrawing groups. The deprotection was shown to be selective (with some observed cross reactivity with nitric oxide) and these probes were used to image hydrogen peroxide production in *Chlamydomonas reinhardtii* algae stimulated with Cu^{2+}, paraquat, or methylene blue in the light and dark. In 2005, Tang reported two other sulfonyl protected fluorophores, the *bis*-toluenesulfonyl protected naphthofluorescein **NFDS-1** (λ_{ex} = 602 nm, λ_{em} = 662 nm) and perfluorooctanesulfonyl naphthofluorescein **NFDS-2** (λ_{ex} = n.r., λ_{em} = 692 nm) with NIR emission.[533] Although **NFDS-2** proved to be unstable, **NFDS-1** was shown to be selective (although some cross-reactivity with alkyl hydroperoxides and hypochlorite was observed) and was used to image hydrogen peroxide in PMA-treated peritoneal macrophages. Tang also reported *bis*-toluenesulfonyl fluorescein **FS-1** (λ_{ex} = 491 nm, λ_{em} = 515 nm), and the dichlorofluorescein derivative **FS-2** (λ_{ex} = 493 nm, λ_{em} = 520 nm) in 2009.[19] **FS-1** was shown to be capable of imaging hydrogen peroxide in PMA-treated peritoneal macrophages.[534] Two ratiometric probes were reported in 2019. Xiao described a fluorophore hybrid between coumarin and fluorescein fluorophores caged by a pentafluorobenzenesulfonyl group to make the ratiometric probe **JNY-1**, which displayed a shift from a coumarin-like emission to a fluorescein-like emission upon treatment with hydrogen peroxide (λ_{ex} = 380 nm, λ_{em} = 440 nm / 540 nm), and was used to image exogenous hydrogen peroxide in HepG2 cells.[535] In the same year, Chen and Yu reported a near-infrared ratiometric probe using a pentafluorobenzenesulfonyl-caged ketocyanine fluorophore **Cy-PFS**, which showed a ratiometric shift from the near-infrared (λ_{ex} = 730 nm, λ_{em} = 836 nm) to red (λ_{ex} = 560 nm, λ_{em} = 635 nm) upon reacting with hydrogen peroxide.[536] This probe was used to image EGF-stimulated hydrogen peroxide production in

A431 and HT22 cells. Finally, there was a more recent report by Wang in 2021 of a pentafluorobenzenesulfonyl spirolactam rhodol **GW-1**, which served as a dual hydrogen peroxide/H^+ probe (λ_{ex} = 475 nm, λ_{em} = 549 nm) based on sulfonyl cleavage and acid-mediated spirolactam ring opening.[537] These studies show that the desulfonylation trigger can be used as a non-oxidative mechanism for hydrogen peroxide detection. Use and development of new probes using this trigger should carefully consider selectivity versus hydrolysis and other nucleophilic species given their ubiquity in biological systems. Table 2, Section 4 summarizes these and any other examples of probes containing this trigger.

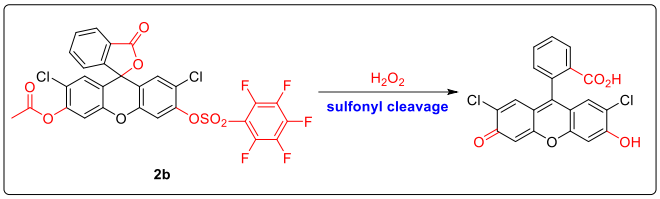

Figure 36. The fluorescent probe **2b** as an example of sulfonyl cleavage trigger for H_2O_2 detection.[532]

Benzil/α-ketoketone Baeyer-Villager oxidation (Table 2, Section 5)

In 2011, Nagano discovered that the Baeyer-Villager oxidation of a *para*-nitro benzil fluorescein derivate **NBzF** (λ_{ex} = 495 nm, λ_{em} = 519 nm) and its diacetylated derivative **NBzFDA** gave a selective fluorescence response to hydrogen peroxide based on a modulation of PeT quenching when converting from the benzil to the carboxylic acid product.[538] Unsubstituted benzil and benzils substituted with Br, OMe, CN, and NO_2 substituents were investigated, with the CN and NO_2 substituents giving the best response in agreement with their Hammett parameter trends. The probe was shown to be selective for hydrogen peroxide, although some cross-reactivity with peroxynitrite and *tert*-butyl hydroperoxide were observed. The diacetylated **NBzFDA** was capable of imaging cellular generated hydrogen peroxide in RAW 264.7 macrophages stimulated with PMA and in A431 cells stimulated with EGF. Sumimoto designed a SNAP-tag derivative of **NBzF** in 2014 called **NBzF-BG** (Figure 37) and the fluorophore-protein conjugate was termed **SNAP-NBzF** (λ_{ex} = 500 nm, λ_{em} = 525 nm).[130] By labeling the fusion protein with AlexaFluor 560, a ratiometric signal could be generated and the probe could be targeted to the extracellular membrane to image extracellular hydrogen peroxide in HEK cells and phagocytosed beads in RAW 264.7 macrophages. A two-photon benzil-based fluorescence probe was reported by Liu and Bai in 2015 that consisted of a benzil-modified coumarin (λ_{ex} = 380 nm, λ_{em} = 505 nm) and could be excited at 760 nm for two-photon microscopy imaging of hydrogen peroxide in SMMC-7721 liver cells.[539] Several BODIPY benzil derivates have been developed. In 2018, Sun reported a benzil *meta* to a BODIPY fluorophore (λ_{ex} = 498 nm, λ_{em} = 508 nm) for vapor phase hydrogen peroxide detection,[540] while Heng reported a benzil *para* to the BODIPY (λ_{ex} = 470 nm, λ_{em} = 510 nm) for imaging in denuded bovine oocytes in the same year.[541] More recently in 2022, Xu, Gong, Liu, and Duan reported the probe **BPHP** (λ_{ex} = 475 nm, λ_{em} = 508 nm) containing a benzil BODIPY linked to a biotin targeting group that was used to image hydrogen peroxide in biotin receptor overexpressing HeLa, A549, and MCF-7 cells, but not in RAW 264.7 that under express the biotin receptor. This probe was also used to compare tumor tissue to liver tissue, showing increased hydrogen peroxide in the tumor tissue. Table 2, Section 5 summarizes these and any other examples of probes containing this trigger.

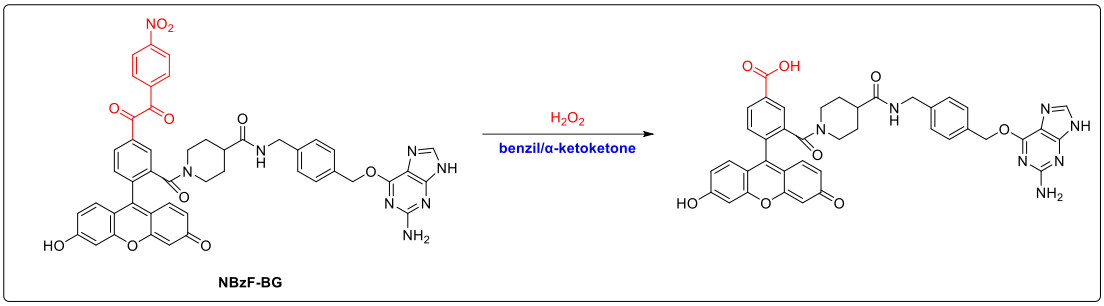

Figure 37. The fluorescent probe **NBzF-BG** as an example of benzil/α-ketoketone trigger for H_2O_2 detection.[130]

α-Ketoamide oxidation (Table 2, Section 6)

A trigger related to the benzil trigger is the α-ketoamide trigger first reported for hydrogen peroxide detection by Wang and Tang in 2016.[542] The probe **Mito-NIRHP** is a *para*-nitro-α-ketoamide caged hemicyanine dye that gives an increase in NIR fluorescence (λ_{ex} = 670 nm, λ_{em} = 704 nm) upon reaction with hydrogen peroxide (Figure 38).[542] The probe was reported as being selective for hydrogen peroxide, although it should be noted that the α-ketoamide trigger has also been used for the detection of peroxynitrite.[543] **Mito-NIRHP** displays mitochondrial localization and was used to image PMA-stimulated hydrogen peroxide production in HepG2 cells. In 2017, Zeng and Wu reported a probe based on linking an α-ketoamide trigger to an extended naphthalimide scaffold **NPs-A**, which was inserted into a lipid bilayer to make a nanoprobe with a ratiometric response (λ_{ex} = 483 nm, λ_{em} = 516 nm / 595 nm).[544] This probe was used to image hydrogen peroxide in L929, RAW 264.7, and in APAP treated zebrafish. Zhang, Jing, and Zhang developed an endoplasmic reticulum targeted probe **α-Naph** formed using an α-ketoamide protected naphthalimide scaffold with a ratiometric response (λ_{ex} = 395 nm, λ_{em} = 465 nm / 540 nm) that was used to image hydrogen peroxide in PMA and tunicamycin induced ER stress in HeLa cells.[545] In 2019, Hu designed and synthesized the NIR probe **Cy-H_2O_2** that used an α-ketoamide linked to a cyanine fluorophore and gave an increase in NIR fluorescence (λ_{ex} = 730 nm, λ_{em} = 790 nm) due to reduced PeT quenching.[22] **Cy-H_2O_2** was used to image PMA-stimulated hydrogen peroxide production in HeLa cells and APAP-treated zebrafish.[546] In 2020, Hu reported **RhB-NIR**, an α-ketoamide-caged rhodamine scaffold that showed an increase in large Stokes shift emission (λ_{ex} = 590 nm, λ_{em} = 730 nm) and was used to image hydrogen peroxide in PMA stimulated cells with mitochondrial localization.[547] Zeng, Wu, and Zhao developed a NIR II and photoacoustic imaging agent for hydrogen peroxide named **BTPE-NO_2** in 2021.[548] They used an α-ketoamide linked to a benzothiadiazole appended with AIE fluorophores that was formulated in an amphiphilic polymer Pluronic F127. The probe displayed an increase in NIR II emission (λ_{ex} = 808 nm, λ_{em} = 938 nm) and photoacoustic signal (λ_{ex} = 680 nm) in response to hydrogen peroxide and was used for NIR II and photoacoustic imaging in mice injected with cyclophosphamide to induce cystitis, a trazadone liver injury model, and a liver ischemia-reperfusion injury model. Shen and Rao reported the probe **Mito-H_2O_2** (λ_{ex} = 670 nm, λ_{em} = 702 nm) in 2022 consisting of an α-ketoamide linked to a hemicyanine fluorophore through a self-immolative linker, displaying an increase in NIR fluorescence selective for hydrogen peroxide (but with a hint of peroxynitrite reactivity) and was used to image PMA-stimulated HeLa cells and mice injected with hydrogen peroxide.[549] α-Ketoamides and α-ketoketones have been investigated for both hydrogen peroxide and peroxynitrite imaging so careful study and consideration should be given when using these types of probes to discriminate between these species. Table 2, Section 6 summarizes these and any other examples of probes containing this trigger.

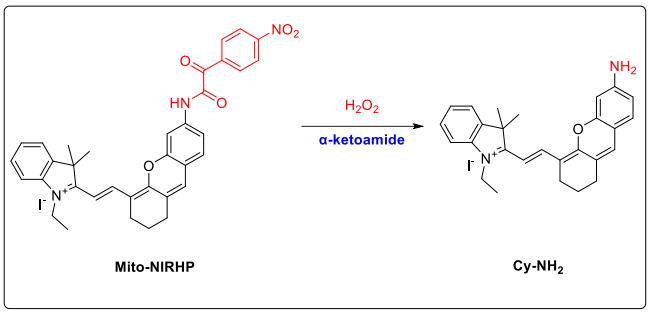

Figure 38. The fluorescent probe **Mito-NIRHP** as an example of α-ketoamide trigger for H_2O_2 detection.[542]

Iron-mediated triggers (Table 2, Section 7)

In 2011, Hitomi reported the probe **MBFh1** (λ_{ex} = 570 nm, λ_{em} = 590 nm), which consisted of an iron(III) complex linked to a reduced resorufin scaffold through an amide linkage (Figure 39).[550] Hydrogen peroxide reacts with the iron center to form highly reactive species to release oxidized resorufin in an intramolecular fashion. The probe design was advanced by the same group in 2013 in the form of **MBFh2** (λ_{ex} = 530 nm, λ_{em} = 590 nm), which used a modified ligand and connected resorufin through a three carbon chain that eliminates after hydrogen peroxide reacts with the iron to cleave the ligand in a similar mechanism as an MAO probe reported by Chang.[551,552] The probe was shown to be selective for hydrogen peroxide (although hydroxyl radical was not evaluated) and it was used to image exogenous hydrogen peroxide added to HeLa cells and hydrogen peroxide produced in EGF stimulated A431 cells. Hitomi expanded this to a fluorescein scaffold in 2014 with the probe **MBFh3** (λ_{ex} = 450 nm, λ_{em} = 517 nm), again connecting through a 3-carbon linker to release fluorescein for use in imaging hydrogen peroxide in HeLa cells and EGF stimulated A431.[553] You and Nam studied a *bis*-iron chelated dichlorofluorescein derivative **ZP1Fe$_2$** (an iron-chelated derivative of the zinc probe **Zinpyr-1**) in 2012 that underwent oxidative *N*-dealkylation of the ligand causing an increase in fluorescence (λ_{ex} = 507 nm, λ_{em} = 528 nm).[554] The probe was selective for H_2O_2, but some reactivity with hydroxyl radical was observed and some variability with other ROS was seen. The probe displayed lysosome localization and was used to image hydrogen peroxide in HeLa cells. Another example of using iron to detect hydrogen peroxide was reported by Qu and Liu in 2014 using a styryl cyanine chelated to Fe(II) which displayed a quenching in fluorescence (λ_{ex} = 369 nm, λ_{em} = 540 nm) upon hydrogen peroxide oxidation to Fe(III).[555] Table 2, Section 7 summarizes these and any other examples of probes containing this trigger.

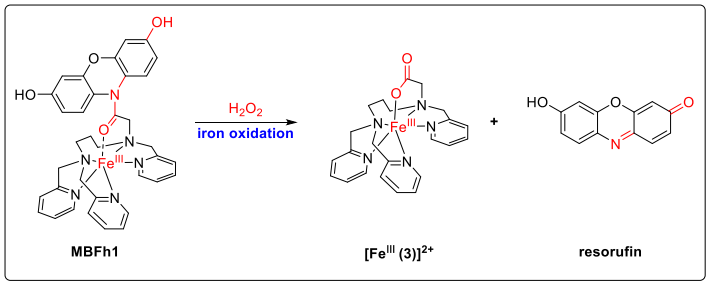

Figure 39. The fluorescent probe **MBFh1** as an example of iron oxidation trigger for H_2O_2 detection.[550]

Chalcogen oxidation (Table 2, Section 8)

Chalcogens can be oxidized by ROS and have been used in different contexts to probe multiple ROS including hydrogen peroxide. In 2007, Chang reported a reversible xanthene oxidation coupled to a disulfide/dithiol redox pair by linking a naphthyldisulfide to a xanthene core forming the probe **RF1** (λ_{ex} = 495 nm, λ_{em} = 503 nm) as well as the cell-trappable version **RF1-AM**.[556] The

disulfide/dithiol redox couple could be oxidized by reaction with hydrogen peroxide and other reactive oxygen species and reductions were demonstrated using TCEP in cuvette studies and were mediated by thiols inside the cell to achieve reversible imaging of reactive oxygen species in HEK cells. In 2013, Tang reported that linking the antioxidant ebselen to a heptamethine scaffold provided the NIR fluorescence probe **Cy-O-Eb** (λ_{ex} = 768 nm, λ_{em} = 794 nm) (Figure 40).[557] Ebselen is a cyclic compound containing an amide nitrogen-selenium bond that in this study was proposed to be reduced by glutathione to cleave the Se-N bond and provide the free selenol to quench the appended fluorophore. Reoxidation to ebselen selectively by hydrogen peroxide restores fluorescence and this probe was used for reversible hydrogen peroxide imaging in HepG2 cells and for imaging hydrogen peroxide in the wound margins of zebrafish. The next year, Li and Yu reported the probe **D-HMSe**, which linked ebselen to a benzimidazole fluorophore (λ_{ex} = 330 nm, λ_{em} = 476 nm).[558] The selenium of ebselen was proposed to be oxidized to the selenium oxide to provide a selective turn-on response. Recently, in 2023, Zhang reported the probe **NapEb** that appended ebselen to a naphthalimide fluorophore for a glutathione-reversible increase in fluorescence upon treatment with hydrogen peroxide (λ_{ex} = 350 nm, λ_{em} = 455 nm).[559] Interestingly, the authors proposed and provided mass spectrometry evidence for the ring-opened selenic acid as the fluorescent oxidized product. The three ebselen-based probe studies proposed three different oxidation mechanisms, suggesting that this chemistry is likely to be complicated and nuanced. A recent, mechanistically interesting example of a selenium-based probe was reported by Koide in 2020, where an allylic selenide linked to a hydroxymethyl fluorescein underwent a hydrogen peroxide-mediated Mislow-Evans rearrangement and ether cleavage with an increase in fluorescence (Figure 41).[560] Hydrogen peroxide oxidized the selenide to the selenium oxide, followed by a [2,3]-sigmatropic rearrangement and cleavage of a hydroxymethyl fluorescein. The probe was used to image hydrogen peroxide in ionomycin-treated endothelial cells and wound healing in zebrafish. Sulfides have also been used as triggers for hydrogen peroxide detection. In 2016, Muthusubramanian developed a boranil linked to an alkyl phenyl sulfide to make **SB-1** (λ_{ex} = 370 nm, λ_{em} = 503 nm), or to a diaryl sulfide to make **SB-2** (λ_{ex} = 370 nm, λ_{em} = 510 nm).[561] Mass spectrometry evidence supported the formation of a sulfoxide product selective for hydrogen peroxide, and the probe was used for imaging hydrogen peroxide added to HeLa cells. Griesback studied a series of dialkyl sulfide triggers linked to phthalimide fluorophores in 2017 and showed that although these fluorescent probes reacted with hydrogen peroxide, they reacted more rapidly and efficiently with singlet oxygen, suggesting that the electronic environment (alkyl versus aryl) around the sulfide may play an important role in the selectivity of the sulfide trigger.[562] In 2018, Xu reported an alkyl phenyl sulfide linked to a phenoxazium fluorophore that resulted in reduced PeT quenching upon oxidation of the sulfide to the sulfoxide resulting in an increase in near-infrared emission (λ_{ex} = 590 nm, λ_{em} = 676 nm).[563] The probe localized in lysosomes and was used to image hydrogen peroxide added to HeLa cells. Lastly, a single report of a tellurium-based probe was disclosed by Choi in 2014 that consisted of a diketopyrrolopyrrole-tellurophene conjugate that underwent oxidization at the tellurium atom with hydrogen peroxide to give a reversible and selective increase in fluorescence emission (λ_{ex} = 500 nm, λ_{em} = 579 nm) (Figure 42).[564] Chalcogens, with their rich redox chemistry, hold a special position for the design of detection strategies for reactive oxygen and nitrogen species. Careful studies of their reactivity and selectivity could yield useful insights into advancing their use as luminescent probes. Table 2, Section 8 summarizes these and any other examples of probes containing this trigger.

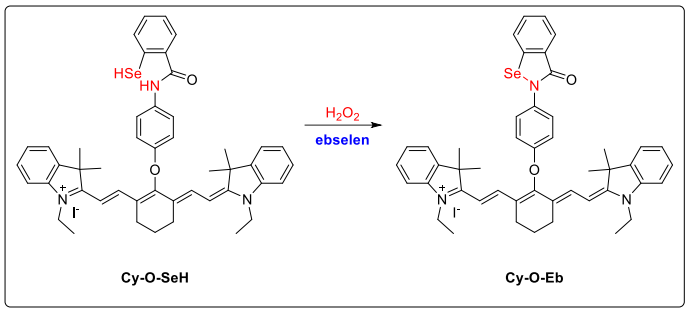

Figure 40. The fluorescent probe **Cy-O-Eb** as an example of ebselen trigger for H_2O_2 detection.[557]

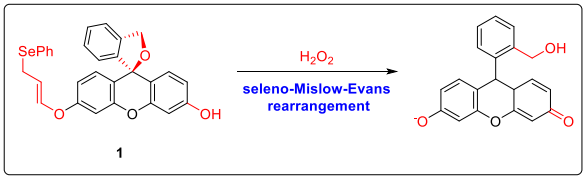

Figure 41. The fluorescent probe **1** as an example of seleno-Mislow-Evans rearrangement trigger for H_2O_2 detection.[560]

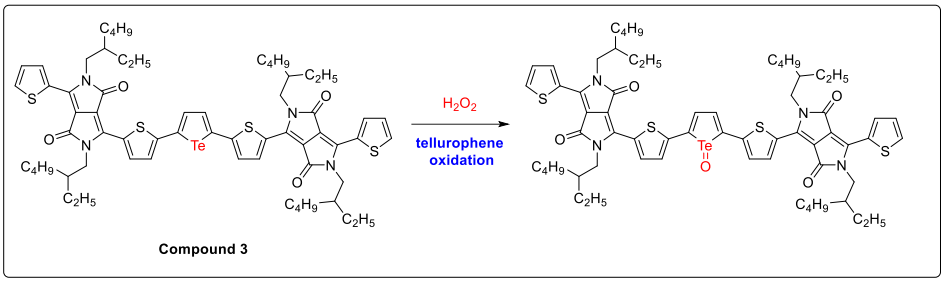

Figure 42. The fluorescent probe **Compound 3** as an example of tellurophene oxidation trigger for H_2O_2 detection.[564]

Sulfate elimination (Table 2, Section 9)

An interesting approach for a system that can reversibly monitor bisulfite/hydrogen peroxide cycles was initially developed by Sun and Wang in 2016 and consisted of an active methylene unit linked to a fluorophore (Figure 43).[154] This probe **HBT-Cy** was designed using a benzothiazole-functionalized cyanine fluorophore that displayed fluorescence (λ_{ex} = 390 nm, λ_{em} = 590 nm) that is blue-shifted after conjugate addition of bisulfite (λ_{ex} = 390 nm, λ_{em} = 450 nm), followed by recovery of the red-shifted emission upon a proposed hydrogen peroxide mediated elimination of the formed sulfate. Although the mechanism of the hydrogen peroxide mediated elimination is not entirely clear, it was shown that it was partially selective for hydrogen peroxide with some cross-reactivity observed for *tert*-butyl hydroperoxide, hypochlorite, hydroxyl radical, and alkoxy radicals. **HBT-Cy** was used for reversible bisulfite/hydrogen peroxide imaging in MCF-7 cells. In 2017, Yin reported a naphthopyran-benzothiazolium conjugate (λ_{ex} = 400 nm, λ_{em} = 630 nm) that gave a similar blue-shift upon bisulfite addition (λ_{ex} = 390 nm, λ_{em} = 520 nm) that was recoverable with hydrogen peroxide.[155] In 2019, another active methylene-fluorophore scaffold was designed and studied by Yin that was quenched by bisulfite and showed a turn-on response (λ_{ex} = 570 nm, λ_{em} = 660 nm) to hydrogen peroxide with mitochondrial localization in HeLa, HepG2, and *in vivo* mouse models.[156] A similar mitochondrial targeting approach was also adopted by Hu in 2021 with the probe **NBD** (λ_{ex} = 550 nm, λ_{em} = 618 nm).[565] Qi, in 2019 reported a cyclometalated iridium complex that showed reversible bisulfite/hydrogen peroxide sensing in a similar fashion.[566] Meng, Wang, and Zang developed the probe **NI** in 2021, consisting of a naphthalimide connected to an active methylene unit that goes from a red-shifted fluorescence

(λ_{ex} = 500 nm, λ_{em} = 580 nm) to a blue-shifted fluorescence (λ_{ex} = 430 nm, λ_{em} = 510 nm) upon reaction with bisulfite, followed by recovery of the red-shifted fluorescence with hydrogen peroxide as shown in HeLa cells and in mice *in vivo*.[567] Wang and Hu observed a slightly different type of reactivity in their probe **BN-DUAL** in 2022, where an initial conjugate addition to a dicyano active methylene unit quenches fluorescence (λ_{ex} = 545 nm, λ_{em} = 595 nm), and subsequent reaction with hydrogen peroxide cleaves the C-C bond to form an aldehyde with a yellow emission (λ_{ex} = 430 nm, λ_{em} = 508 nm), and was used for sequential imaging of bisulfite and hydrogen peroxide in SKBR cells and mice.[568] In 2023, Sun and Tang reported two probes, **TPE-y**, an AIE scaffold linked to a benzothiazole that showed reversible bisulfite/peroxide sensing in food samples with a reversible modulation of fluorescence (λ_{ex} = 390 nm, λ_{em} = 614 nm) with bisulfite quenching of fluorescence and peroxide recovery,[569] and then **DCA-Bba** (λ_{ex} = 600 nm, λ_{em} = 685 nm), a benzopyran-barbiturate conjugate that showed quenched fluorescence with bisulfite that was restored with hydrogen peroxide and used for detection of bisulfite in food samples and reversible imaging in MCF-7 cells.[570] The reversible nature of this trigger could be of interest in certain systems where the interplay of bisulfite and hydrogen peroxide is important. The mechanism of bisulfite elimination should be studied in more detail to elucidate the role that hydrogen peroxide plays to further understand the sensing capabilities of this class of triggers. Table 2, Section 9 summarizes these and any other examples of probes containing this trigger.

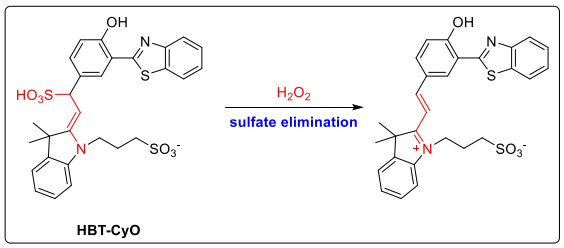

Figure 43. The fluorescent probe **HBT-CyO** as an example of sulfate elimination trigger for H_2O_2 detection.[154]

Catechol oxidation (Table 2, Section 10)

In 2012, Han designed and developed the probe **DA-Cy** using a catechol trigger linked to a cyanine fluorophore that, upon reaction with hydrogen peroxide, oxidized the catechol to the *ortho*-quinone with a reduction in PeT quenching fluorescence (λ_{ex} = 630 nm, λ_{em} = 755 nm) (Figure 44).[345] The response was shown to be selective for hydrogen peroxide and hydroxyl radical and was reversible with glutathione which can re-reduce the *ortho*-quinone to the catechol. **DA-Cy** was used for imaging hydrogen peroxide added to HL-7702 and rat hippocampal neurons. Kaur and Kumar also reported the probe **LyNC** (λ_{ex} = 450 nm, λ_{em} = 537 nm) in 2017, consisting of a catechol linked to a naphthalimide scaffold with a catechol trigger and an appended morpholine group for lysosome targeting. Imaging was performed in LPS-treated C6 and BV-2 cells. The selectivity and response for these probes for hydrogen peroxide versus superoxide is striking given the large volume of literature for the catechol trigger being selective for superoxide.[266,268–272] Table 2, Section 10 summarizes these and any other examples of probes containing this trigger.

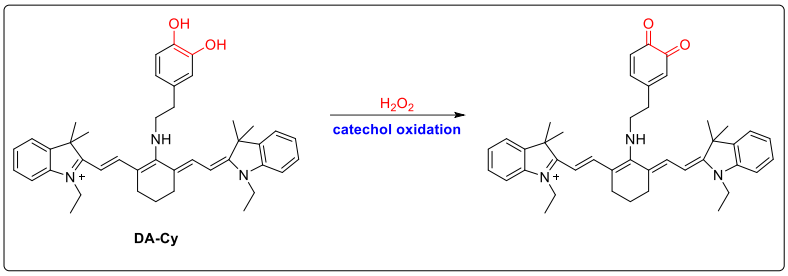

Figure 44. The fluorescent probe **DA-Cy** as an example of catechol oxidation trigger for H_2O_2 detection.[345]

Payne/Dakin reaction (Table 2, Section 11)

In 2017, Yang from the University of Hong Kong reported the Payne/Dakin reaction that uses hydrogen peroxide to convert an *ortho*-hydroxybenzaldehyde into a catechol as a trigger for hydrogen peroxide detection (Figure 45).[571] This trigger was linked through a self-immolative linker to a rhodamine scaffold to form **HKPerox-1** (λ_{ex} = 520 nm, λ_{em} = 543 nm) or a rhodol scaffold to form **HKPerox-2** (λ_{ex} = 480 nm, λ_{em} = 527 nm). Operation of probes using the Payne/Dakin trigger requires the addition of CCl_3CN, which was shown to be non-toxic in mammalian cell culture, enabling imaging of hydrogen peroxide in PMA-treated RAW 264.7 macrophages. Mechanistically, hydrogen peroxide nucleophilically attacks the nitrile carbon of CCl_3CN to form a peroxytrichloroacetimidic acid (the Payne reaction), which adds to the aldehyde to induce a 1,2-aryl shift and eliminate trichloroacetamide, forming the phenol after formate hydrolysis (the Dakin reaction). Yang collaborated with Shabat in 2020 to develop a chemiluminescent 1,2-dioxetane probe for hydrogen peroxide **H_2O_2-CL-510** with chemiluminescence emission at 510 nm that was used to image hydrogen peroxide in As_2O_3 treated THP-1 cells and ischemia-reperfusion in rat brain.[572] In 2020, Yang further developed two new Payne/Dakin-based probes, **HKPerox-Red** (λ_{ex} = 565 nm, λ_{em} = 602 nm) using a resorufin scaffold that was used to image hydrogen peroxide in PMA-treated RAW 264.7 and rotenone treated zebrafish, and the ratiometric probe **HK-Ratio** (λ_{ex} = 410 nm, λ_{em} = 475 nm / 540 nm) using a naphthalimide scaffold that was could monitor As_2O_3 triggered peroxide production in leukemia cells and serum starved RAW 264.7 macrophages.[573] In 2021, Yang from Northwest University, Xi'an developed a coumarin-based probe **Cou-CHO** (λ_{ex} = 391 nm, λ_{em} = 502 nm) that uses a Payne/Dakin trigger to image PMA-stimulated hydrogen peroxide production in HepG2 cells.[574] While the need for the addition of CCl_3CN for probe operation is a potential complication, this additive has been shown to be non-toxic for cell studies and this mechanistically interesting trigger remains relatively unexplored. Table 2, Section 11 summarizes these and any other examples of probes containing this trigger.

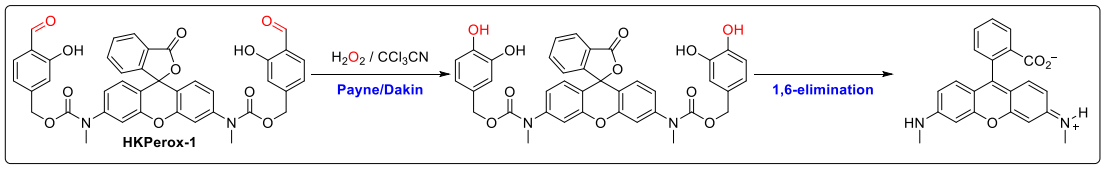

Figure 45. The fluorescent probe **HKPerox-1** as an example of Payne/Dakin trigger for H_2O_2 detection.[571]

Carbonyl group perhydrolysis (Table 2, Section 12)

In 2002, Maeda studied a series of ester-protected resorufin probes that showed selective hydrogen peroxide-mediated perhydrolysis and provided a fluorescence signal above background hydrolysis with water (Figure 46).[575] Resorufin probes with the oxygen atom protected as an acetyl (**AR**), *tert*-butyl (**TBAR**), isobutyryl (**IBR**), cyclohexanecarbonyl (**CHR**), or pivaloyl (**PVR**) ester were all examined with **PVR** giving the best signal versus background hydrolysis. In 2013, Churchill used a *bis*-thiocarbamate-caged fluorescein that first reacted with Hg^{2+} to form a

carbamate, and then perhydrolyzed with hydrogen peroxide, making an AND logic gate for Hg^{2+} and hydrogen peroxide with a fluorescence increase (λ_{ex} = 480 nm, λ_{em} = 527 nm) that was used for imaging Hg^{2+} and hydrogen peroxide added to HeLa cells.[576] Zhang reported the probe **ACF** (λ_{ex} = 490 nm, λ_{em} = ~520 nm) in 2016 consisting of a 2-(azidomethyl)benzoyl acid protecting group on dichlorofluorescein showing selective hydrogen peroxide imaging in HeLa cells.[577] Other examples include an ester-protected rhodol derivative **ACR** (λ_{ex} = 470 nm, λ_{em} = 560 nm) designed by Zhan in 2017 and an ethyl ester coumarin derivative (λ_{ex} = 390 nm, λ_{em} = 505 nm) reported by Zeng in 2021.[578] Wang and Liu developed a duo of coumarin probes connected to a 1-fluoro-4-nitrobenzene linked to the coumarin through an ester without a carbon spacer **FAA-MC-OH** or with a 1-carbon spacer **FBA-MC-OH** that both showed an increase in emission upon reaction with hydrogen peroxide (λ_{ex} = 309 nm, λ_{em} = 505 nm).[579] The mechanism involved nucleophilic aromatic substitution of the fluorine atom with peroxide, followed by intramolecular ring closure and ester cleavage. **FBA-MC-OH** was shown to have a faster response to hydrogen peroxide and while it was selective, cross reactivity with hydrogen sulfide and hydrogen persulfide was observed. Recently in 2023, Yang developed the probe **YQ-2**, which is an acetate-protected dicyano fluorophore that undergoes a fluorescence increase upon perhydrolysis with hydrogen peroxide and was used to image peroxide in HeLa cells.[580] Table 2, Section 12 summarizes these and any other examples of probes containing this trigger.

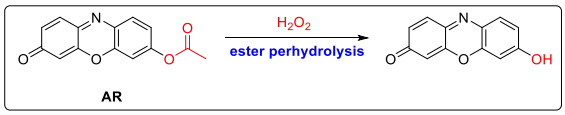

Figure 46. The fluorescent probe **AR** as an example of ester perhydrolysis trigger for H_2O_2 detection.[575]

Lanthanide binding (Table 2, Section 13)

There are examples of using a lanthanide complex as a luminophore in combination with other peroxide triggers,[581,582] but hydrogen peroxide binding to lanthanide centers has also been used as a mechanism to modulate luminescence. Wolfbeis initially studied the hydrogen-binding complex **Eu(tc)** in 2002[583] with a full account in 2005,[584] consisting of an Eu^{3+}-tetracyclin compound that forms a peroxide-bound complex upon interaction with hydrogen peroxide, modulating lanthanide-based luminescence (λ_{ex} = 405 nm, λ_{em} = 616 nm) for measuring glucose oxidase enzyme activity. In 2014, Another example of a lanthanide-binding trigger was investigated by Zuchner, who reported a terbium phthalate complex that showed quenched luminescence (λ_{ex} = 285 nm, λ_{em} = 545 nm) upon complexing hydrogen peroxide.[585] An advantage of lanthanide-based luminescence is that these molecules display long-lived luminescence lifetimes due to spin forbidden relaxation processes. If combined with a time-gated delay between excitation and emission, autofluorescence can completely decay to enable low background time-gated detection and imaging of hydrogen peroxide in cellular systems.[172,581,582] Table 2, Section 13 summarizes these and any other examples of probes containing this trigger.

Oxonium oxidation/cleavage (Table 2, Section 14)

Conversion of an oxonium moiety into a carboxylic acid with C–O and C–C bond cleavage was reported as a fluorescence trigger for hydrogen peroxide imaging by Lin in 2016 (Figure 47).[586] The probe **BC** was formed from a benzopyrylium coumarin that yielded a ratiometric fluorescence response (λ_{ex} = 410 nm, λ_{em} = 472 nm / 693 nm) upon selective reaction with hydrogen peroxide to form a coumarin carboxylate, with some cross reactivity observed with peroxynitrite and hypochlorite. The ratiometric emission could also be excited with two-photon excitation at 760 nm and was used to image PMA-stimulated macrophages and zebrafish. In 2020, Li and Li developed a second example of this trigger in the form of the probe **GCP**, a coumarin-pyran-based fluorophore that reacted with hydrogen peroxide to cleave the oxonium and form a coumarin

carboxylate.[587] The probe was armed with a galactose group for hepatocyte targeting and provided a ratiometric fluorescence response (λ_{ex} = 410 nm, λ_{em} = 482 nm / 706 nm) that was used to image PMA and APAP-stimulated HepG2 cells, as well as hydrogen peroxide, PMA, and APAP treated zebrafish. Table 2, Section 14 summarizes these and any other examples of probes containing this trigger.

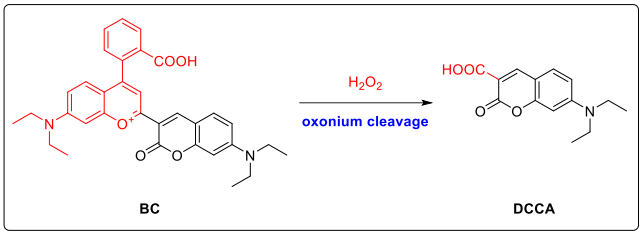

Figure 47. The fluorescent probe **BC** as an example of oxonium cleavage trigger for H_2O_2 detection.[586]

Aromatic amine oxidation (Table 2, Section 15)

Oxidation reactions involving aromatic amines/anilines have been used as triggers to monitor hydrogen peroxide production. Duerkop and Wolfbeis in 2011 reported the fluorescence sensor **HP Green** consisting of a *p*-anisidine aromatic amine sensing unit connected to a naphthalimide scaffold (Figure 48).[588] Oxidation of *p*-anisdine with hydrogen peroxide resulted in reduced PeT quenching of fluorescence (λ_{ex} = 444 nm, λ_{em} = 534 nm) in a reaction that was enhanced with horseradish peroxidase and used to measure glucose based on glucose oxidase activity. Also in 2011, Ye and Yuan reported a 3,4-diaminophenyl ether linked to a terbium complex that reacted with hydrogen peroxide and horseradish peroxidase to provide an increase in long-lived lanthanide luminescence (λ_{ex} = 315 nm, λ_{em} = 542 nm) and was used for time-resolved imaging of oligosaccharide stimulated hydrogen peroxide production in tobacco leaves.[582] In 2021, Meng reported **TPE-TAF**, a *bis*-phenylene diamine modified AIE fluorophore that responds to hydrogen peroxide/horseradish peroxidase with an increase in fluorescence (λ_{ex} = 320 nm, λ_{em} = 450 nm) with the proposed mechanism being enzyme-catalyzed cross-linking of the diamine units.[589] Lastly, Zhang and You reported a series of dialkyl amines connected to an AIE fluorophore in 2022, including **2E2F** (Figure 49), that undergo hydrogen peroxide mediated oxidation to the *N*-oxide with a quench of fluorescence (λ_{ex} = 360 nm, λ_{em} = 475 nm),[590] and these probes were used to image oxidative stress in apple cells and tobacco leaves. Table 2, Section 15 summarizes these and any other examples of probes containing this trigger.

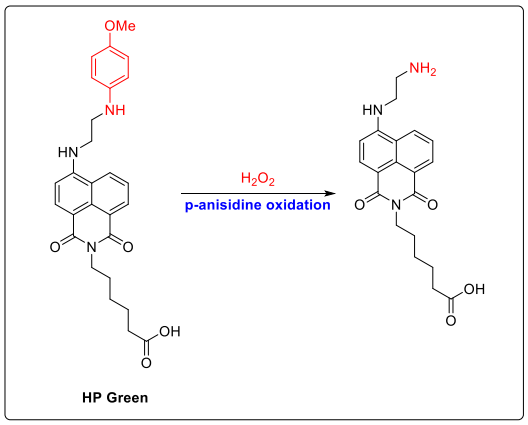

Figure 48. The fluorescent probe **HP Green** as an example of *p*-anisidine oxidation trigger for H_2O_2 detection.[588]

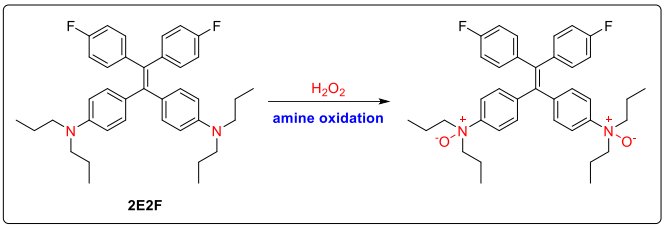

Figure 49. The fluorescent probe **2E2F** as an example of amine oxidation trigger for H_2O_2 detection.[590]

Other triggers (Table 2, Section 16)

There are several other triggers that have been explored for the luminescence detection of hydrogen peroxide. Nakahara showed in 2008 that fluorescein hydrazide underwent an oxidation reaction with hydrogen peroxide (that was enhanced by Co^{2+}) and induced an increase in fluorescence emission (λ_{ex} = 494 nm, λ_{em} = 527 nm).[591] Kumar developed a zinc chelated pyridyl imine linked to a naphthalimide that yielded a fluorescence response to hydrogen peroxide (λ_{ex} = 360 nm, λ_{em} = 550 nm), as well as responses to Zn^{2+} and pyrophosphate enabling the construction of a multi-analyte logic gate circuit.[592] In 2017, Stains invented an innovative strategy for fluorescence detection of hydrogen peroxide by synthesizing pro-xanthene fluorophores where the central atom acts as a trigger, consisting of either a central borinic acid (**RF_{620}**) or a silanediol (**SiOH2R**) (Figure 50), both of which were shown to react with hydrogen peroxide to insert an oxygen into the scaffold and form a rhodamine fluorophore.[593] These were shown to be selective for hydrogen peroxide versus other ROS and provided a ratiometric response for **RF_{620}** (λ_{ex} = 620 nm / 550 nm, λ_{em} = 636 nm / 570 nm) and **SiOH2R** (λ_{ex} = 663 nm / 550 nm, λ_{em} = 681 nm / 570 nm) that was used to image hydrogen peroxide in PMA, EGF, or serum-starvation stimulated HeLa cells. Cui and Wang also designed a trigger using the central xanthene atom by caging a central phosphinate with a boronate to make the NIR probe **PRB2-H_2O_2** (λ_{ex} = 672 nm, λ_{em} = 695 nm), used for imaging rotenone-treated HepG2 cells and mice.[497] Lou and Xia reported an oxidative tyrosine crosslinking strategy in 2018 where a bis-tyrosine modified AIE fluorophore **TT** was shown to be crosslinked upon reaction with hydrogen peroxide and myeloperoxidase to induce aggregation and turn-on aggregation induced fluorescence (λ_{ex} = 320 nm, λ_{em} = ~460 nm).[594] **TT** was selective for hydrogen peroxide and used to image PMA-treated RAW 264.7 macrophages and RAW 264.7/HLF cell co-cultures. In 2018, Lin reported an interesting click/detect strategy where a tetrazole modified BODIPY first underwent photoclick reaction with a fumarate to form a quenched pyrazoline, followed by hydrogen peroxide mediated oxidation to the pyrazole with recovery of fluorescence (λ_{ex} = 480 nm, λ_{em} = 509 nm).[135] The probe was used to image hydrogen peroxide in HeLa cells first incubated with a fumarate modified docetaxel to target microtubules, followed by addition of hydrogen peroxide. An interesting chemiluminescence reaction with hydrogen peroxide was reported by Zhu and Liu in 2022, where they identified and studied *tetra*-bromoquinone (**TBBQ**) as the bioluminescent substrate of the acorn worm.[595] They showed that hydrogen peroxide underwent a nucleophilic substitution with two of the bromine atoms on the quinone to form a dioxetane intermediate that decomposed with chemiluminescence emission at 515 nm (Figure 51). Chen, Raay, and Manderville in 2022 showed the probe **ACou-Ind**, a coumarin group attached to an indolenium with an ethylene linker, could undergo conjugate addition with hydrogen peroxide. This was followed by epoxide formation to give a ratiometric response to hydrogen peroxide (λ_{ex} = 395 nm, λ_{em} = 475 nm / 650 nm), and was used to image hydrogen peroxide in zebrafish.[596] Finally, Li and Zhou reported in 2023 that the probe **TBBP-Pro** consisting of a 4-(1-cyanovinyl)-pyridinium can be cleaved to an aldehyde in an oxidative cleavage reaction with an epoxide intermediate to give an increase in fluorescence upon 458 nm excitation (λ_{ex} = 458 nm, λ_{em} = 617 nm).[597] **TBBP-Pro** was shown to be mitochondrial targeted and was used to image PMA-stimulated zebrafish and mice treated with dextran sulfate sodium

to induce ulcerative colitis. Table 2, Section 16 summarizes these and any other examples of probes with other triggers.

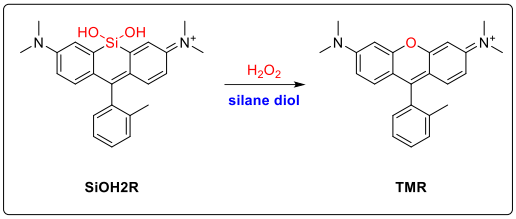

Figure 50. The fluorescent probe **SiOH2R** as an example of silane diol trigger for H_2O_2 detection.[593]

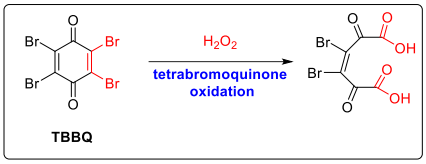

Figure 51. The fluorescent probe **TBBQ** as an example of tetrabromoquinone oxidation trigger for H_2O_2 detection.[595]

4.2.4 Concluding remarks for hydrogen peroxide probes

Hydrogen peroxide has perhaps the best standing amongst reactive oxygen species as an important signaling molecule due to its temperate rate of reactivity that enables selective reaction-based signaling. Two general strategies have been used to design luminescent probes for hydrogen peroxide that rely on either its oxidative or nucleophilic reactivity. Oxidation-based probes generally need careful consideration of selectivity versus other ROS. Probes that operate via two-electron oxidation mechanisms should be examined judiciously in comparison to peroxynitrite and hypochlorite, while probes that operate by one-electron oxidations may suffer cross-reactivity with superoxide, hydroxyl radical, and other free radical species. Boronate-based probes have been a very popular choice for luminescent probes that operate by a two-electron oxidation mechanism,[386–390] and these should be used in combination with careful controls to rule out reaction with peroxynitrite, namely inhibiting production or direct scavenging of NO, a precursor to peroxynitrite. Hypochlorite can also be generated in many of the same biological scenarios as hydrogen peroxide, so cross-reactivity with this species should be examined in any given experiment. Other two-electron oxidation luminescent probe mechanisms such as those operating in α-keto compounds[538–541] and the Payne/Dakin-based probes[571–574] show promise and should also be similarly investigated for their cross-reactivity with peroxynitrite and hypochlorite. Luminescence probes that operate via a nucleophilic-displacement mechanism (sulfonyl cleavage, perhydrolysis, etc.)[532,575] must compete with background hydrolysis and reaction with abundant cellular nucleophiles like amines and thiols, which can be even more nucleophilic in a protein environment. These factors should be controlled for as best as possible. Classic commercially available probes like **DCFH** and **DCFH-DA** and **Amplex Red** are still in use, but as discussed above, they do not have ideal selectivity for hydrogen peroxide and/or require peroxidase activity to generate signal. Several boronate-based probes are commercially available with **PY1** and **PO1** being good options to use in cellular experiments to monitor hydrogen peroxide production when used in combination with the appropriate controls.[147]

4.3 Hypochlorite

4.3.1 Hypochlorite in health and disease

Hypochlorite ($^{-}$OCl) and hypochlorous acid (HOCl) are two protonation states of the reactive oxygen species (ROS) most often associated with the roles it plays as a powerful microbiocidal oxidizing agent.[598] Hypochlorous acid is generated through enzymatic reactions in living

organisms, primarily by myeloperoxidase (MPO) found in white blood cells, which is especially abundant in neutrophils.[599,600] This heme protein catalyzes the reaction between hydrogen peroxide (H_2O_2) and chloride ions (Cl^-), resulting in the formation of HOCl. The primary function of MPO-generated HOCl is to eliminate microorganisms, contributing to the body's immune response. While HOCl is widely recognized for its biocidal properties during the immune response, overproduction of HOCl contributes to the progression of a range of inflammatory diseases, such as atherosclerosis, ischemia-reperfusion injury, and cancer.

Owing to its p*K*a value of 7.5, HOCl exists in roughly equal concentrations with hypochlorite (^-OCl) at physiological pH. Unlike hydrogen peroxide, which is relatively unreactive with biomolecules in the absence of enzymes, hypochlorous acid rapidly reacts with biomolecules, including DNA, RNA, proteins, carbohydrates, and lipids.[601] Its rapid rate of reaction with biomolecules is one of the major reasons why it is such an effective biocidal agent. HOCl exhibits diverse reactivity with biomolecules, including with amino side chains, (e.g., lysine and histidine), sulfides (methionine), and thiols (cysteine), as well as nucleic acids and lipids. Thiols and sulfides react the most rapidly with HOCl ($k_2 \sim 10^7\ M^{-1}s^{-1}$). Thiols, especially cysteine and glutathione, react rapidly with HOCl to form the corresponding sulfenyl chloride. This highly reactive intermediate undergoes several different fates. Reaction with water gives sulfenic acid, which can be further oxidized to its corresponding sulfinic acid. Alternatively, a second thiol can react with the sulfenyl chloride to give a disulfide, which can be further oxidized to a thiosulfinate. The reaction of HOCl with sulfides gives the corresponding sulfoxide, which can be enzymatically reduced back to methionine. The reversible oxidation of methionine is an important signaling motif for the activation of redox-responsive transcription factors.

The reaction between HOCl and amines yields *N*-chloramines, which can, in turn, undergo secondary reactions, including chlorine transfer reactions. *N*-chlorination reactions occur quickly ($k_2 \sim 10^5\ M^{-1}s^{-1}$), with rate constants second only to thiols and sulfide reactivity. Given the abundance of amines in biological systems, *N*-chlorination is one of the most important routes of HOCl reactivity. HOCl commonly reacts with the α-amino group of free amino acids, the γ-amino group of lysine side chains and the imidazole side chain of histidine, yielding *N*-chlorohistidine. Other nitrogen atoms are also targeted, including the guanidinium of arginine and backbone amides to form the corresponding *N*-chloramides, though these rate constants are ~100,000 times slower ($k_2 \sim 10^0\ M^{-1}s^{-1}$) than the reaction of HOCl with primary amines. Recent evidence indicates *N*-chlorination can convert blood plasma proteins to holdases and prevent protein aggregation, suggesting the use of *N*-chlorination as a potential reversible signaling motif in biology. Nucleobases, nucleosides, nucleotides, and nucleic acids are also common sites of reactivity, with *N*-chlorination happening faster at heterocyclic amines than exocyclic amines, potentially influencing genetic material stability.

4.3.2 Classical detection techniques for hypochlorite

Since the mid-2000s, HOCl detection has been dominated by luminescent probes as described in the sections below. However, prior to the widespread adoption of this technology, other methods have been employed, primarily focused on the detection of reaction products between HOCl and biological substrates.[602] For instance, detection of the oxidation byproducts of HOCl provides an indirect method of assay HOCl presence. Because myeloperoxidase is released extracellularly from monocytes, elevated levels of oxidized amino acids, including 3,4-dihydroxyphenylalanine have been isolated from human atherosclerotic lesions compared to healthy arterial tissue.[603] Though HOCl oxidizes substrates rapidly, it also is able to chlorinate substrates, which allows for more rigorous connection between HOCl and biological activity. Chloramines form most rapidly; however, they are unstable and are challenging to detect/isolate.

Lipid chlorohydrins, in which formal addition of HOCl addition across a double-bond also provides insight into past presence of HOCl.[604] Chlorinated aromatic rings, such as chlorotyrosine derivatives[605] and 5-chlorocytosine as well as glutathione sulfonamide, are especially useful biomarkers for HOCl because they are stable enough for isolation and quantification. These metabolites can be separated by HPLC and detected with electrochemical means or GC/MS.[606] The characteristic fragmentation pattern of chlorine-containing substrates in GC/MS is particularly helpful to identify chlorinated biomarkers. An advantage to this approach is that the chlorinated substrates can be quantified; however, these techniques provide poor temporal information as to when the HOCl was generated. Antibodies for chlorotyrosine are also available, enabling the spatial distribution of chlorinated biomarkers to be determined by immunohistochemistry/immunofluorescence. Because this analysis must be done on fixed cells, this approach provides limited temporal information.

4.3.3 Hypochlorite probes by trigger

Dearylation (Table 3, Section 1)

In 2003, Nagano developed the first selective probe for hypochlorous acid, a significant achievement in the field of reactive oxygen species (ROS) detection (Figure 52).[607] This report not only opened the door for hypochlorous acid-specific probes but also laid the groundwork for creating other probes targeting reactive oxygen species such as hydrogen peroxide, peroxynitrite, and superoxide. An *O*-dearylation reaction was used to impart selectivity for HOCl over other ROS. Previously, the authors had observed that aryloxyphenols undergo *O*-dearylation by specific ROS, including hydroxyl radical, peroxynitrite, and HOCl, while remaining unreactive towards others.[608] Inspired by this, they incorporated an *O*-dearylation mechanism into a fluorescent scaffold, resulting in a turn-on probe for hypochlorous acid. Out of several tested derivatives, aminophenol dearylation offered the highest selectivity. The aminophenol-derived fluorescein, known as **APF**, showed the highest relative reactivity with hypochlorite, although it also displayed some reactivity towards hydroxyl radical and peroxynitrite. However, this early probe effectively discriminated against singlet oxygen, superoxide, hydrogen peroxide, nitric oxide, and alkoxy radical, which previous probes had been unable to do. **APF** was demonstrated to be effective in detecting endogenously produced HOCl in PMA-stimulated neutrophils. Overall, this study not only pioneered the development of reactivity-based fluorescent probes but also established a comprehensive framework for their design, synthesis, selectivity testing, and biological imaging.

Four years later, the Libby group employed an aminophenyl ether dearylation strategy to develop a near-infrared (NIR) analog for the fluorescent detection of $^{-}$OCl.[609] The longer emission wavelength enhances its suitability for bioimaging due to reduced tissue absorption. This sulfonaphthol fluorescein derivative, named **SNAPF**, was synthesized with the expectation that the aminophenyl ether trigger would provide high selectivity for hypochlorite over other reactive oxygen species while exhibiting a longer emission wavelength. Synthesis and characterization of **SNAPF** supported this hypothesis. **SNAPF** displays an absorption maximum at 614 nm and an emission maximum at 676 nm. Compared to the original **APF** compound, **SNAPF**'s emission is red shifted by approximately 150 nm. Like **APF**, **SNAPF** exhibits excellent discrimination for $^{-}$OCl over hydroxyl radical, H_2O_2, NO, ROO$^{\bullet}$, and O_2^{-}. **SNAPF** was used to detect HOCl generated from stimulated human neutrophils, as well as hypochlorous acid in human atherosclerotic plaque. This demonstration showcased the modular nature of the aminophenyl ether dearylation trigger and its high selectivity for hypochlorous acid and hypochlorite over other reactive oxygen species.

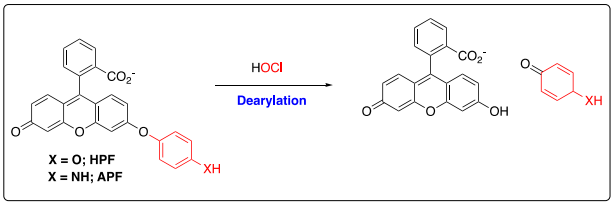

Figure 52. The fluorescent probes **HPF** and **APF** as examples of the dearylation trigger for HOCl detection.[607]

One drawback of fluorescent probes is their short fluorescence lifetime of the excited singlet state, which can be problematic in bioimaging. This is because autofluorescence from native cellular components may interfere with the fluorescent signal emitted by the probe. To address this issue, Yuan and coworkers developed an aminophenyl ether dearylation strategy to prompt emission from lanthanide complexes.[610] The long-lived luminescence of lanthanides enables the use of time-gated measurement techniques to avoid interference from autofluorescence. The emission collection occurs after a brief delay, allowing autofluorescence signals to decay while preserving the long-lived luminescence for collection. The authors modified the classical aminophenyl ether trigger with an *ortho*-nitro group. Oxidation led to dearylation resulting in an enhanced lanthanide complex emission. The biological applicability of this probe was demonstrated in HeLa cells treated with hypochlorous acid and in macrophages after incubation with LPS and IFN-γ. Importantly, the steady-state luminescence signal was abolished when myeloperoxidase was inhibited, lending evidence that the optical signal was specific for HOCl over other ROS/RNS. Subsequent work by the same group showcased the versatility of the *ortho*-nitroaminophenylether trigger with the successful inclusion in a ruthenium complex.[611] Nabeshima and co-workers also showed it could be used to trigger a HOCl-specific increase in luminescence from an iridium complex.[612]This trigger has also been applied in a cyanine-based probe for near-infrared imaging of hypoxic stress in zebrafish and mice.[613]

The sensitivity of HOCl-triggered dearylation trigger to small molecular changes was elegantly demonstrated by Zhao and associates.[614] The authors examined an *N*-dearylation from a BODIPY scaffold using 4-hydroxyaniline. They found that a minor alteration—changing a hydroxyl group to a methoxy group—shifted the selectivity of the probe from peroxynitrite to hypochlorous acid. The resulting methoxy derivative, named **BMI-NI**, exhibited excellent selectivity for hypochlorous acid over alkoxy radical, hydrogen peroxide, nitric oxide, superoxide, and hydroxyl radical. It also remained unresponsive to various thiol-containing compounds, such as cysteine, homocysteine, glutathione, and hydrogen sulfide. Critically, **BMI-NI** did not react to peroxynitrite. However, when the methoxy group was converted back to a hydroxyl group, the probe became selective for peroxynitrite over HOCl. Imaging experiments conducted in stimulated RAW 264.7 macrophages showcased **BMI-NI**'s capability to image endogenously produced hypochlorous acid. When myeloperoxidase was inhibited using 4-aminobenzoic acid hydrazide (4-ABAH), the fluorescence increase was abolished, confirming the probe's selectivity for HOCl in cellular systems.

Two-photon imaging is a technique that enables the use of long-wavelength excitation to prompt shorter-wavelength fluorescence emission. This approach offers a strategy to avoid excitation of native cellular chromophores. The incorporation of an aminophenol ether trigger into a benzothiazole dearylation probe delivers a two-photon probe for imaging endogenous HOCl.[615] Another probe with the advantages of both two-photon excitation and near-infrared emission was developed based on the Nile red scaffold but with an aminophenyl ether trigger to prompt a fluorescence turn-on. Known as **NiI-ClO**, this probe emits at 650 nm and has been successfully used to image hypochlorous acid in HeLa cells, RAW 264.7 macrophages, and in tissue imaging experiments.[616] A separate effort yielded a lysosomal-targeted 2-photon probes for HOCl with a 13 nM detection limit.[617]

Zhang and co-workers used a naphthalene scaffold to develop a hepatoma specific fluorescent probe for hypochlorous acid.[618] This probe featured an aminophenol ether trigger and a triazole linked galactose moiety as a hepatoma targeting unit. It was used to detect endogenous hypochlorous acid in HepG2 cells. Like other aminophenyl ether-based probes, the galactose-modified naphthalimide shows single analyte reactivity with HOCl. Because of the galactose targeting moiety the probe was internalized by HepG2 cells because they overexpress ASPG-R, which specifically recognizes galactose. This probe was also tested in MGC 803 cells, A549 cells, and SH SY5Y cells but only the HepG2 cells showed a signal from the galactose functionalized probe. A control probe without a galactose moiety showed similar uptake across the four cell lines confirming that galactose was the key motif necessary for efficient HepG2 uptake.

Organelle directed probes provide a powerful tool to image subcellularly resolved HOCl. A report from Yuan and co-workers, building off their previously described luminescent complexes, showed that a europium complex could be directed to the mitochondria with a triphenylphosphonium group, and dearylation of a *p*-nitrophenylthioether with HOCl could be used to detect mitochondrial HOCl in cells and of exogenously applied HOCl in zebrafish.[619] A rhodol-based probe for hypochlorous acid was reported by the Yang group using a dichlorohydroxy phenyl ether trigger that could be directed to the mitochondria and engineered to have increased cellular retention.[620] These probes were used to image hypochlorous acid in a middle cerebral artery occlusion model. A naphthalimide-based probe featuring a methyl sulfonamide group as an endoplasmic reticulum targeting group and an aminophenyl ether trigger to confer HOCl selectivity can track image HOCl in the endoplasmic reticulum of HeLa cells.[621] Table 3, Section 1 summarizes these and any other examples of probes containing this trigger.

Thioether oxidation / spirocyclic ring-opening (Table 3, Section 2)
In 2007, Nagano and coworkers introduced an new strategy to link HOCl to an increase in fluorescence (Figure 53).[622] This innovative probe, named **HySOx**, utilizes a thioether group, which not only maintains the spirocyclized non-fluorescent form but also acts as the center for the redox reaction. In the presence of HOCl, the oxidation of the thiol to a sulfonate triggers a ring-opening process, converting the non-fluorescent dihydrofuran form of rhodamine to its quinoid form. **HySOx** shows excellent selectivity for hypochlorous acid over a library of other ROS, including $HO^{\bullet}$, $ONOO^{-}$, $NO^{\bullet}$, O_2^{-}, and H_2O_2. **HySOx** was effectively utilized to visualize phagocytosis by porcine neutrophils. A separate study in 2015 revealed that inclusion of a triphenylphosphonium on this platform could monitor hypochlorous acid in the mitochondria of macrophages during bacterial infection.[623] Expanding on their earlier work in 2007, the Nagano group developed a long-wavelength analog based on a Si-rhodamine platform. This new analog, named **MMSiR**, emits at 670 nm, which is more than 200 nm red-shifted from the original **HySOx** rhodamine.[624] Owing to this advancement, **MMSiR** was capable of *in vivo* imaging of HOCl in a mouse peritonitis model. The Si-rhodamine platform has also been used to develop a photoacoustic probe (**PA-MMSiNQ**) to track HOCl photoacoustically in a mouse subcutis model.[625] Another contribution to long-wavelength HOCl imaging tools was made by the McCarroll group who reported a Si-fluorescein based analog called **Hypo-SiF**.[626] Utilizing the thiospirocyclization trigger, this emits a red fluorescence at 606 nm upon oxidation with HOCl and exhibits both colorimetric and fluorescence responses. Interestingly, when exposed to excess hypochlorous acid, **Hypo-SiF** displayed the emergence of a new emission band resulting from chlorination of the xanthene ring. **Hypo-SiF** was used to monitor myeloperoxidase activity. A twist on this approach is to couple spirothioether oxidation to a β-elimination. Because this mechanism relies on a bond-breaking process, the authors merged it into a FRET scaffold, in which oxidation liberated a fluorescein donor from its rhodamine acceptor, resulting in a ratiometric

chemodosimeter for HOCl.[627] Table 3, Section 2 summarizes these and any other examples of probes containing this trigger.

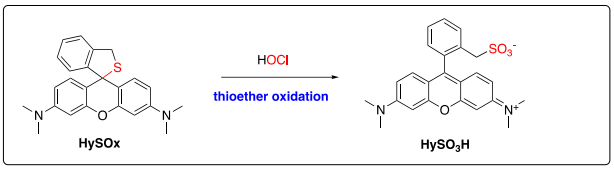

Figure 53. The fluorescent probe **HySOx** as an example of a thioether oxidation / spirocyclic ring-opening trigger for HOCl detection.[622]

Dimethylthiocarbamate (DMTC) cleavage (Table 3, Section 3)
The dimethylthiocarbamate (DMTC) trigger has been rapidly adopted in the generation of novel HOCl-specific probes because of its high selectivity and ease of synthetic incorporation. First reported in 2016, the Tang group utilized this switch to modify a naphthalimide scaffold, resulting in **NDMTC** (Figure 54).[628] In the presence of HOCl, the DMTC undergoes oxidation and hydrolysis, releasing a hydroxy naphthalimide, leading to a large increase in fluorescence. The DMTC-based probe is highly selective for HOCl over more than 20 common ROS and RNS, metal ions, anions, and amino acids. In PMA-activated macrophages, **NDMTC** was used in one- and two-photon fluorescence imaging experiments. Pre-treatment of the macrophages with the MPO inhibitor, 4-aminobenzoic acid hydrazide, led to a suppression of the fluorescence increase, indicating that the observed fluorescence increase was HOCl-dependent. This trigger has subsequently been merged into coumarin platforms[629] biscoumarin scaffolds[630], rhodol scaffolds[631], fluorescein[631], and BODIPY.[632]

The small size of the dimethylthiocarbamate group allows it to be merged with many different fluorescent scaffolds while also permitting additional subcellular targeting functionality to be installed. **Mito-Q** is a dimethylthiocarbamate-based HOCl probe that localizes to the mitochondria because of its positively charged lipophilic cation scaffold.[633] When oxidized by HOCl, it undergoes a 1,6-elimination to prompt a fluorescence increase at 590 nm. Co-localization studies revealed high localization in the mitochondria. Because the positive charge is eliminated upon reaction with HOCl, it ensures the probe first localizes to the mitochondria to detect mitochondrial HOCl acid rather than reacting with cytosolic HOCl and then localizing to the mitochondria.

HOCl-responsive endoplasmic reticulum targeted probes have also been reported with the dimethylthiocarbamate trigger. The same naphthalimide ER-targeted probe was reported by two groups: first by the Lin group in 2019[634] and then by the Zhang group in 2020.[635] This probe features a naphthalimide scaffold with a dimethylthiocarbamate trigger and an ethylsulfonamide linked through the imide functionality. Like other dimethylthiocarbamate-based probes, this probe features high selectivity for HOCl over other common cellular analytes is capable of imaging HOCl in zebrafish and EC1 cells. A recent paper described the use of a phenylsulfonamide-functionalized naphthalimide probe with a dimethylthiocarbamate trigger to image HOCl associated with the Golgi in HeLa cells.[636]

An especially clear demonstration of the modularity of the dithiocarbamate motif was reported by the Guo group.[637] A palette of different probes that span the emission range from 454–630 nm was synthesized. Remarkably, one derivative (**C7**) responded with a turn-on response to basal nanomolar concentrations of HOCl and a ratiometric response at high concentrations of HOCl. The authors proposed a phenol deprotonation that interrupted the ESIPT process was responsible for the dual-concentration range response. The probes were used to track HOCl in HepG2 cells, *C. elegans* and whole animal models. The dimethylthiocarbamate motif has also been combined

in NIR scaffolds, including dicyanopyran motifs for imaging HeLa cells, a DDAO scaffold for imaging cells, zebrafish, and live animals, and a cyanine-based probe has been used for imaging a mouse model of acute lung injury (ALI), which revealed an increase in HOCl as the severity of ALI increased. The ease of synthetic installation of the DMTC and its high specificity for HOCl makes it a popular motif for organelle-targeted,[634,638] two-photon,[630,639,640] NIR,[632,641–643] and bioluminescent scaffolds.[644] Table 3, Section 3 summarizes these and any other examples of probes containing this trigger.

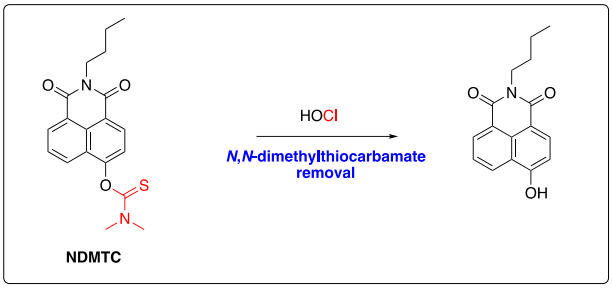

Figure 54. The fluorescent probe **NDMTC** as an example of an *N,N*-dimethylthiocarbamate removal trigger for HOCl detection.[628]

Chalcogen oxidation (Table 3, Section 4)

Early studies of *S*-oxidation by Churchill and co-workers established that thiophene oxidation could modulate the photophysical properties of BODIPY complexes.[645] However, the first example of sulfide oxidation to detect HOCl was reported by Kim and coworkers in 2011 (Figure 55).[646] The authors reasoned that the oxidation of thioethers into sulfoxides could be triggered by hypochlorous acid, and this chemical change could be linked to modulating the optical properties of fluorescent scaffolds. A BODIPY core modified with methylthioether groups delivered a hypochlorous acid-based probe, **2** (Figure 55). In aqueous solution **2** displays an absorption maximum at 519 nm and an emission maximum at 650 nanometers. Oxidation of the electron-rich methyl thioether groups significantly increased the quantum yield (Φ = 0.82) and blue-shifts the emission spectrum to 525 nm. **2** has good selectivity for hypochlorite over other common ROS. Imaging experiments in RAW 264.7 macrophages demonstrated that **2** could detect exogenously added hypochlorite and endogenously produced HOCl triggered with LPS and PMA stimulation. Inhibition of myeloperoxidase decreased the fluorescent signal confirming that the fluorescence increase was a result of an increase in intracellular hypochlorous acid. The use of sulfide oxidation as first described by Kim and coworkers has been extensively employed in the development of organelle targeted probes near IR probes and multi analyte probes. For instance, a PET-based probe using an acridine orange fluorophore was reported two years later. Sulfide oxidation abolishes PET quenching prompting an increase in 540 nm fluorescent submission. Like previous authors, this group reported their probe could detect endogenously produced hypochlorous acid in RAW 264.7 macrophages with LPS and PMA stimulation.[647] A near IR cyanine 7 derivative with 789 nm emission has also been described. This probe can detect mitochondrial hypochlorous acid as well as quantitatively monitoring myeloperoxidase activity. A naphthalimide-based probe with a methyl ethyl ether trigger and a morpholino functionality enabled the detection of lysosomal hypochlorous acid.[648] **PT-1** is another naphthalimide-based lysosomal probe that relies on a PET quenching mechanism.[649] **PT-1** is capable of detecting endogenously produced HOCl in LPS and PMA-activated macrophages. To expand the sulfide to sulfoxide switch to live animal studies, the Zhang group developed **PQI**, a phenothiazine-quinolinium platform that relies on sulfide oxidation to abolish PET quenching. This probe features a large Stokes shift. Excitation at 460 nm prompts emission at 588 nm across physiologically a

relevant pH range. The authors report excellent selectivity for **PQI** for HOCl excellent over common reactive oxygen species, anions, metal ions, and thiols.[650]

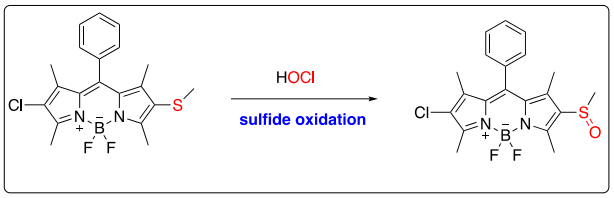

Figure 55. A thioether-modified BODIPY fluorescent probe as an example of a sulfide oxidation trigger for HOCl detection.[646]

The sulfide oxidation trigger integrates well with organelle-targeted hypochlorous acid probes. To date, HOCl detection with organelle targeted probes has been reported for mitochondria,[651–655] and lysosomes.[656,657] Common directing motifs such as triphenylphosphonium groups have been used to deliver mitochondrial specific to track mitochondrial HOCl in HeLa cells and macrophages.[658] Two sulfonamide-derivative naphthalimides were reported to localize to the endoplasmic reticulum and enable monitoring HOCl in the ER. Sulfonamide derivatized probes localize to the endoplasmic reticulum and detect hypochlorous acid using the sulfide to sulfoxide switch.[659] Morpholine derivatized probes preferentially localize to lysosomes enabling the detection of lysosomal hypochlorous acid.[660] However, both are turn-off probes, which limits their utility. Lysosomal targeted probes that rely on a morpholine subcellular directing group have also shown utility with the sulfide oxidation switch to detect lysosomal HOCl in macrophages and zebrafish.[657]

The chalcogens sulfur and selenium share similar chemical properties, and this similarity has been explored by using a selenide to selenoxide oxidation switch. A PET-based BODIPY probe (**HCSe**) using a diphenylselenide oxidation was report by Liu and coworkers in 2013 (Figure 56),[661] the same year they reported a similar structure that used a sulfide oxidation switch.[662] Like sulfide oxidation, selenide oxidation is, in some cases, highly selective for HOCl over other common ROS and RNS. Notably, the selenoxide could be converted back to the non-fluorescent selenide with glutathione, an abundant thiol-based tripeptide in the cytosol, showing that the probe can be cycled between its oxidized fluorescent form and reduced non-fluorescent form. Fluorescence imaging of RAW 264.7 cells showed that the response to HOCl and glutathione persisted in live cells. Endogenous HOCl was also detected in PMA-activated macrophages. Like sulfide-based switches, selenide-based probes have also been directed to lysosomes[663] and mitochondria.[664] This design logic has also been extended to tellurium-based probes, with a near IR aza-BODIPY-based that emits at 738 nm, and a BODIPY analog, based on the work of Liu and Wu, that uses a diphenyltelluride PET switch to modulate BODIPY fluorescence (Figure 57).[665] Selenide oxidation can also be coupled to more complex chemical changes. For instance, oxidation followed by elimination of the resulting selenoxide, a twist on the classic α-selenation reaction, has been used to trigger production of a highly fluorescent coumarin derivative.[666] Notably, in synthetic conditions, H_2O_2 and peroxyacids are used to effect the selenoxide elimination; however, the selenoxide trigger shows high selectivity for HOCl over other oxidants. This approach has also been merged into a two-photon scaffold to visualize HOCl in live cells and animals.[667]

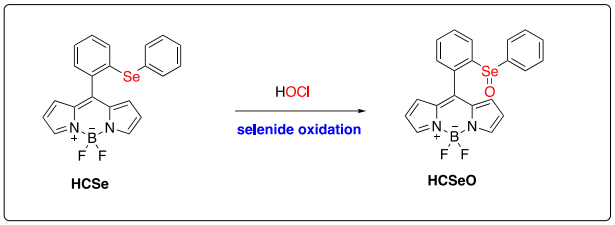

Figure 56. The fluorescent probe **HCSe** as an example of a selenide oxidation trigger for HOCl detection.[661]

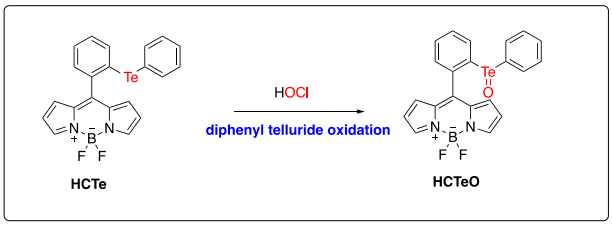

Figure 57. The fluorescent probe **HCTe** as an example of a diphenyl telluride oxidation trigger for HOCl detection.[665]

The HOCl-mediated deprotection of S,O and S,S ketals is another trigger that affords selective detection of HOCl when merged with an appropriate fluorophore. An early demonstration by Hwang and coworkers showed that a pyrene-based probe with a 6-membered dithiolane was selectively converted to its corresponding aldehyde with selectivity for HOCl over other ROS including H_2O_2, *tert*-butyl hydrogen peroxide, peracetic acid, and superoxide (Figure 58). The probe was also selective against all physiologically relevant alkali, alkali earth cations, anions, and common transition and heavy metals. However, these studies were performed in mixed organic/aqueous buffer at pH 5, which does not closely approximate common physiological conditions.[668]

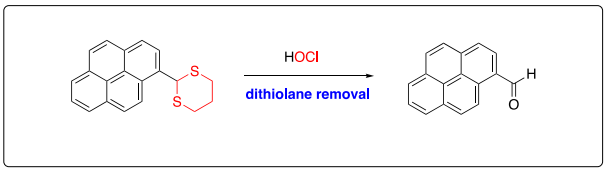

Figure 58. Hwang's probe as an example of dithiolane removal for HOCl detection.[668]

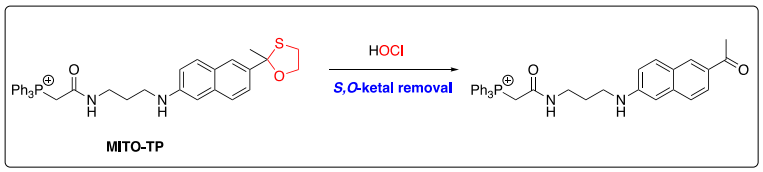

Figure 59. MITO-TP as an example of *S,O*-ketal removal for HOCl detection.[669]

Four years later, a paper by Yuan and co-workers showed that *S,O*-ketals were selective motifs for HOCl imaging (Figure 59).[669] In this report, **TP-HOCl1** and mitochondrial and lysosomal targeted 2-photon probes (**MITO-TP** and **LYSO-TP**, respectively) were made with an *S,O*-ketal trigger. Acedan was chosen as the two-photon fluorophore. The authors reasoned that including the ketal would alter the push-pull ability of the fluorophore and yield a fluorescence turn-on upon HOCl-mediated conversion to the ketone. Selectivity for HOCl was excellent, with no response observed for hydrogen peroxide, hydroxyl radical, *tert*-butyl hydrogen peroxide, *tert*-butyl hydroxyl

radical, nitric oxide, superoxide, and peroxynitrite. The improved sensitivity and selectivity over the dithiolane analogs were proposed to be a result of having only a single sulfur atom needed for oxidative removal. Co-localization studies confirmed that the triphenyl phosphonium-modified probe was directed to the mitochondria while the morpholine-modified probe was directed toward the lysosome. Endogenous HOCl imaging was accomplished in RAW 264.7 macrophages with PMA stimulation and in tissue samples from LPS-treated mice. This comprehensive report firmly established the *S,O*-ketal as a selective and sensitive motif for HOCl detection, with subsequent reports showing that it can be incorporated into an acetyl-benzocoumarin two-photon dye for ratiometric HOCl imaging[670] and as a way to monitor redox-cycling with HOCl and Cys/HCy in SKVO-3 cells.[671] *S,O*-acetals are also effective HOCl-detecting motifs, with Liu and coworkers showing that their reported probe **HPBD** can be used to detect exogenous and endogenous HOCl [672] and with Mao and co-workers showing that the *S,O*-acetal can be used to deliver a two-photon ratiometric probe **QClO** that can image HOCl generated during the wound healing process.[673] Table 3, Section 4 summarizes these and any other examples of probes containing chalcogen-based trigger.

Nitrogen atom oxidation (Table 3, Sections 5, 9, and 11)

A variety of C=N bonds are used for the detection of hypochlorous acid. These include oxime, hydrazone, and imine bonds. HOCl is able to oxidize these moieties, which can be coupled to electronic changes in a fluorophore to give rise to a different emission profile. Dibenzoylhydrazine is known to undergo hypochlorite-dependent oxidation to dibenzoyl diimide, which further decomposes to the corresponding carboxylic acid. This reaction has been used extensively to ring open spirocyclized compounds and deliver conjugated fluorescent products. An early example of this strategy was reported by Chan and co-workers (Figure 60).[674] The authors reasoned that this reaction could be coupled to a ring-opening process to give rise to a fluorescent rhodamine derivative. Their design was validated experimentally with a rhodamine-based dibenzyolhydrazine that responds to HOCl with an increase in fluorescence intensity at 578 nm, consistent with the ring opening mechanism. Though no cell studies were conducted, this initial design would serve as the basis for more than a dozen related probes. Lysosomal probes directed with morpholine groups,[675,676] ER directed probes with sulfonamide groups,[677,678] and mitochondrial-directed probes.[679]

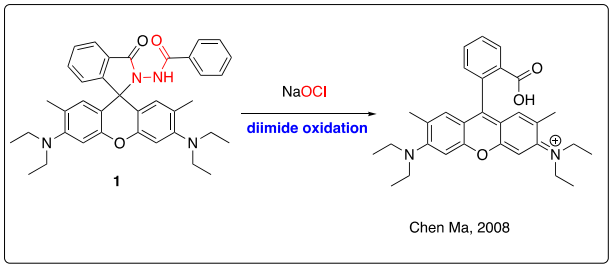

Figure 60. A rhodamine-based fluorescent probe as an example of a diacylhydrazide oxidation trigger for HOCl detection.[674]

A similar probe with a hydroxamic acid moiety shows improved selectivity for HOCl over other ROS (Figure 61).[680] This probe was used to image NaOCl in A549 cell and in zebrafish. Because this detection motif results in a bond breaking event, it can be used in FRET probes as shown by Jia and coworkers. In this approach a dansyl probe was linked to a rhodamine via a diimide bond. Upon HOCl oxidation, the dansyl probe cleaves from the rhodamine, abolishing the FRET signal.[681] Instead of linking the FRET pair through the dynamic bond, Xiao and coworkers used a coumarin fluorophore coupled to a rhodamine that was modified with the diimide.[682] In the absence of oxidation, only emission from the coumarin was observed. Upon oxidation with

hypochlorite, energy transfer from the coumarin gave rise to a rhodamine emission.[682] Several reports have shown that oximes also undergo HOCl-mediated oxidation. When the oxime is derived from hydroxylamine, upon oxidation, the oxime is converted to a strongly electron-withdrawing cyano group, which can substantially change the emission profile. In some cases, the product is an aldehyde instead.[683]

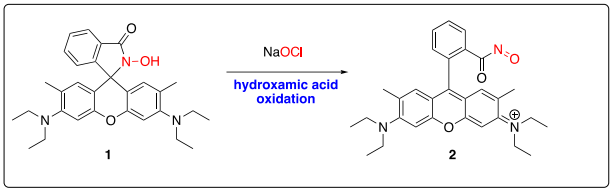

Figure 61. A rhodamine fluorescent probe as an example of a hydroxamic acid oxidation trigger for HOCl detection.[680]

Imine, oxime, and hydrazone-based probes for HOCl have been extensively reported. The common molecular feature is a C=N bond, traditionally formed via condensation of an amine-based nucleophile and a carbonyl group, either an aldehyde or ketone. Varying the specific functionality on the amine nucleophile has a strong effect on the stability of the conjugate to hydrolysis. As a general rule, oximes have the lowest rate of hydrolysis, followed by hydrazones, and imines have the fastest rate of hydrolysis. This is a key consideration when designing molecular probes that operate in aqueous conditions, as it is important to distinguish between hydrolysis-based mechanisms, often accelerated at lower pH conditions such as those found in lysosomes, and a true HOCl-mediated response.

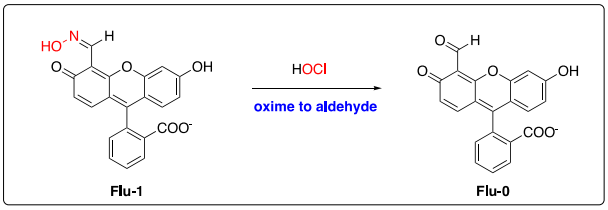

Figure 62. Flu-1 as an example of an oxime to aldehyde conversion for detecting HOCl.[684]

An early example coupled the conversion of a fluorescein oxime derived from hydroxylamine to HOCl-triggered turn-on of fluorescence. The design of **Flu-1** relies on HOCl-mediated removal of C=N isomerization in the oxime (Figure 62).[684] Traditionally, non-radiative decay occurs through this molecular motion, quenching the fluorescence of a compound. Reaction with HOCl liberates hydroxylamine and converts the oxime to an aldehyde, which abolishes this route of quenching and restores fluorescence. **Flu-1** shows good selective for $^{-}$OCl over other anions, but it was not tested against other common ROS/RNS except for H_2O_2. Nevertheless, this early probe was an important example of using loss of C=N isomerization to prompt a fluorescence turn-on, and its utility was demonstrated for detecting $^{-}$OCl in live HeLa cells. The conversion of oximes to aldehydes and/or acids has also been reported by a number of other groups, including coumarin scaffolds,[685,686] hydroxynaphthalene scaffolds[687], and NIR variants.[688]

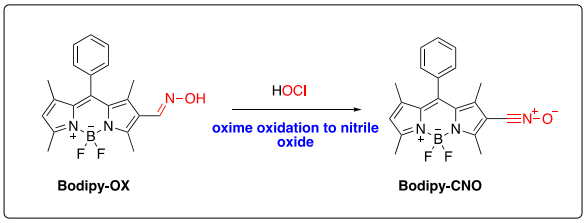

Figure 63. Bodipy-OX as an example of oxime oxidation to a nitrile oxide for detecting HOCl.[689]

An interesting extension of this work was reported by Emrullahoğlu, in which a BODIPY oxime (**Bodipy-Ox**) was shown to undergo HOCl-mediated oxidation to a nitrile oxide (Figure 63).[689] The nitrile oxide product was confirmed by isolating and characterizing it, eliminating the possibility that the HOCl-produced product was the corresponding aldehyde or acid. This is in contrast with an almost contemporaneous report of **BOD-OXIME**[690] and a later report of a lysosomal probe[691] that were proposed to yield an aldehyde product upon HOCl-mediated fluorescence turn-on. Other nitrile oxide probes have been reported, including a carbazole-pyridinium push-pull system,[692] a long-wavelength BODIPY variant for ratiometric mapping,[693] benzothiazole based systems,[694] a rhodamine derivative,[695] and multi-oxime scaffolds.[696]

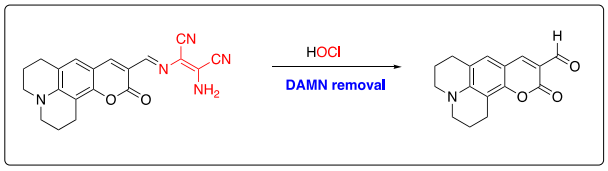

Figure 64. Yuan's probe as an example of detecting HOCl with a DAMN trigger.[697]

Diaminomalonitrile (DAMN)-based triggers are a common motif in HOCl probes. An early report from Yuan and co-workers drew analogy to dinitrophenylhydrazones and proposed that a C=N linked group with strong electron-withdrawing groups may offer selective reaction with HOCl (Figure 64).[697] Indeed, this was the case, with Yuan's probe responding rapidly to HOCl with a fluorescence turn-on via modulation of internal charge transfer (ICT). Isolation of the fluorescence product revealed that it was an aldehyde **7** from which Yuan's probe was synthesized. This initial probe boasts several useful features, including a high selectivity, rapid reaction with HOCl, and a ratiometric output that makes it useful for imaging NaOCl in MCF-7 cells.

The DAMN imine trigger has been rapidly adopted owing to its good performance and ease of synthesis. A double-DAMN carbazole scaffold was also identified to give the corresponding dialdehyde as a product.[698] Like other C=N condensation-based probes, DAMN-based probes have been constructed from coumarin,[699] though this probe was proposed to cyclize to a substituted imidazole upon reaction with HOCl; a biphenyl scaffold;[700] an anthracene scaffold with ~3 nM detection limit;[701] and a BODIPY-based probe reminiscent of several oxime-based probes mentioned earlier.[702] Table 3, Sections 5, 9, and 11 summarize these and any other examples of probes using nitrogen atom oxidation triggers.

Thiosemicarbazide oxidation (Table 3, Section 6)
Thiosemicarbazide oxidation offers high selectivity for HOCl over other ROS but results in a cyclic oxadiazole product instead of a bond breaking event. This trigger has been used extensively in the development of ratiometric, organelle targeted, and near IR probes. First reported by Yuan and co-workers, the cyclization of thiosemicarbazide to an oxadiazole was selective for HOCl over

H_2O_2, O_2^-, CH_3COOOH, and various metal ions, anions, and biomolecules (Figure 65).[703] Their initial report included a ratiometric analog, featuring a coumarin and rhodamine cassette, and its utility was demonstrated by imaging exogenously added NaOCl in Bel 7702 cells and endogenously produced HOCl in stimulated RAW macrophages. A single-wavelength turn-on probe was reported soon after by Zuo and co-workers, which has also been used to image endogenously produced HOCl in macrophages.[704] Because the cyclization product is an aromatic heterocycle, its production can be used to extend the conjugation of a fluorophore system and afford a through-bond energy transfer cassette. Zhang and co-workers used this strategy to deliver a ratiometric probe. Successful production of the oxadiazole extended the conjugation, yielding a ratiometric probe that could be used to image HOCl in activated macrophages.[705] Table 3, Section 6 summarizes these and any other examples of probes containing this trigger.

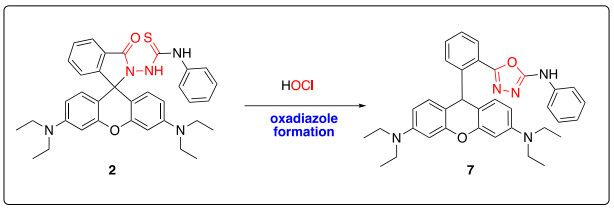

Figure 65. A rhodamine-based fluorescent probe as an example of an oxadiazole formation trigger for HOCl detection.[703]

Hydrazone oxidation (Table 3, Section 7)

Hydrazone oxidation has also been reported to couple HOCl oxidation to an optical change. This reaction can lead to a difference in emission wavelength because of a loss of conjugation or a fluorescence turn on because of energy loss through the hydrazone C=N bond. In some cases, an aldehyde is the reported product. However, it is always important to distinguish between hydrolysis and HOCl-mediated transformations in triggers with potentially labile C=N bonds. This is especially important in acidic locales, such as lysosomes, where the acidic environment can promote hydrolysis. Nevertheless this mechanism has been used for HOCl detection in a number probes, including conversion of a BODIPY dihydrazone into its corresponding aldehyde (Figure 66).[706] Other probes, including some that trigger release of a conjugate moiety, have also been reported. For instance, Ding and co-workers reported a ratiometric variant to image HOCl in bacteria, eukaryotic cells, and zebrafish by employing a thiophene hydrazone trigger[707] while merging a benzothiazole hydrazone to a coumarin scaffold enabled HOCl visualization in mung beans and live cells.[708] The hydrazone functionality is versatile and easily installed through a condensation with formyl-functionalized fluorophore. For instance, a condensation between *p*-sulfonylhydrazide and a formyl-derivatized coumarin delivers a sulfonylhydrazone probe in a simple two-step preparation that reacts selectively with HOCl over other ROS.[709] An alternative to this approach, reported the Guo group, is to use a motif that extends the conjugation upon reaction with HOCl. In this case, an oxidative cyclization between a hydrazone pyridine results in a triazolopyridine product to yield bright fluorophores with good discrimination among common cellular ROS and metal ions (Figure 67).[710] This trigger has also been converted into a mitochondrial directed probe by the same group.[711] Table 3, Section 7 summarizes these and any other examples of probes containing this trigger.

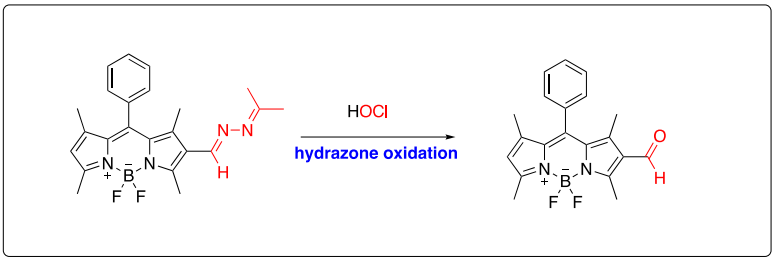

Figure 66. A BODIPY-based fluorescent probe as an example of a hydrazone oxidation trigger for HOCl detection.[706]

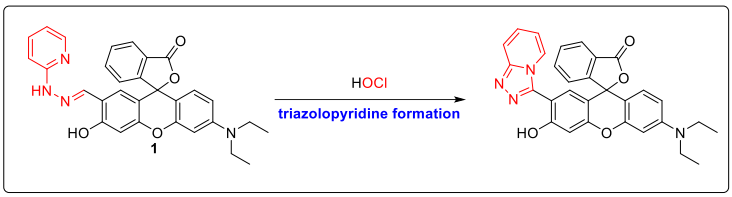

Figure 67. The rhodol-based fluorescent probe **1** as an example of a triazolopyridine formation trigger for HOCl detection.[710]

C=C oxidation (Table 3, Section 8)

Oxidative cleavage of alkenes is a commonly used detection motif in HOCl-probes, with more than 70 distinct HOCl-probes using this approach. Generally, these probes employ an electron-deficient alkene, such as a dicyano alkene, which undergoes oxidative cleavage to the corresponding carbonyl compound in a reaction analogous to ozonolysis. In some cases, the epoxide product is proposed to form; however, in living cells, this compound likely undergoes reaction with endogenous nucleophiles. An early report used an alkene-linked ferrocene to quench the fluorescence of anthracene. Upon HOCl-mediated cleavage, the quenching was relieved, and the anthracene fluorescence was restored.[712]

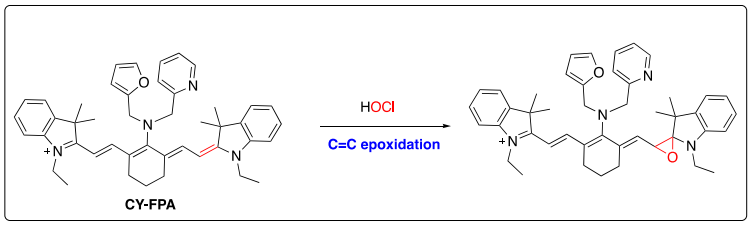

Figure 68. Probe **CY-FPA** as an example of alkene epoxidation for the detecting of HOCl.[713]

The extended conjugation of cyanine dyes makes them a natural fit for HOCl-detection using alkene reactivity. Indeed, a cyanine scaffold initially functionalized with a chloride was unreactive to HOCl; however, modifying it with an amine gave **CY-FPA**, which had an appropriate electron-richness to unlock its reactivity to HOCl (Figure 68).[713] The reaction with HOCl was proposed to proceed through an epoxide intermediate that ultimately decomposes into other products. Because the reaction cleaves off a dimethylindole portion of the parent probe, the absorption wavelength changes from 710 nm to 520 nm with a concomitant decrease in its emission intensity.

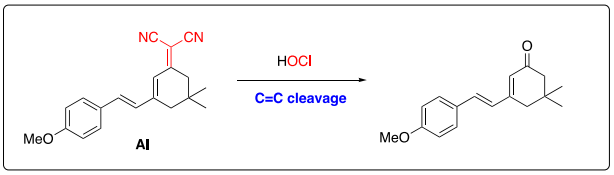

Figure 69. AI as an example of alkene oxidative cleavage for HOCl detection.[714]

Because C=C oxidation strategies effectively shorten conjugation and result in a shift in optical properties, it is an ideal approach to develop ratiometric probes. Lou and co-workers showed that a Cy7 scaffold (**Cy7-NR**) oxidizes to an epoxide with a concomitant shift in fluorescence emission, enabling ratiometric imaging.[715] The indole functionality of cyanine dyes offers another position to tune the behavior of the probe. Zhang reported **ClO1**, which enabled HOCl imaging in A549 cells and in *ex vivo* samples from LPS-treated mice. Unlike **CY-FPA**, **ClO1** shows a ratiometric response, rather than a fluorescence turn-off, upon the proposed epoxidation of the cyanine scaffold.[716] Xiao and co-workers showed that a phenothiazine scaffold with a triphenylphosphonium mitochondrial targeting group and a dicyano alkene (**PMN-TPP**) undergoes HOCl-mediated cleavage to the corresponding aldehyde, resulting in a shift of its emission wavelength from 644 nm to 522 nm in 99.5% aqueous solution and 1% v/v Triton surfactant. Co-localization studies confirmed its mitochondrial localization and live-cell imaging showed it could detect HOCl from PMA-stimulated macrophages and in live animals.[717] Other ratiometric fluorophores have also been reported, including ones based on AIE[718] and on the oxidative cleavage of an anisaldehyde/dicyanoisophorone probe to enable selective ratiometric imaging of HOCl in live HeLa cells (Figure 69).[714] Owing to the oxidative cleavage, dual-fluorophore cassettes work well when linked through an alkene. Kang and co-workers used this strategy to link a coumarin and BODIPY through an alkene that is cleaved by HOCl via a purported epoxide intermediate. With excitation at 450 nm, the fluorescence intensity at 660 nm decreased with an increase in fluorescence at 510 nm, corresponding to the effectively cleaved product. This probe was used to image exogenous HOCl in HeLa cells and endogenous HOCl in a mouse model of arthritis.[719] Park and co-workers used a similar strategy with a BODIPY conjugated to a 2-dicyanomethylene-3-cyano-2,5-dihydrofuran (DCDHF) group.[720]

Subcellular probes that utilize an alkene cleavage motif have also been reported. Indolium groups are effective at targeting probes to the mitochondrial.[721] For instance, a mitochondrial-directed probe using a cationic indolium group linked to an HPQ fluorophore delivers a ratiometric response upon HOCl-mediated cleavage.[722] A similar design, using an indolium linked to a coumarin also shows a strong ratiometric response to HOCl in the NIR region.[723] *N*-alkylated pyridiniums are also effective targeting groups.[724] To target probes to the lysosome, protonatable groups are effective. A diethylaniline directs **BDHA** to the lysosome while also reporting viscosity and serving as a turn-off probe for HOCl.[725] Table 3, Section 8 summarizes these and any other examples of probes containing this trigger.

4.3.3 Concluding remarks for hypochlorite probes

Hypochlorite is well-known as a key ROS in the immune response, responsible for destroying invading pathogens. Its broad oxidative reactivity with endogenous amino acids and thiol-containing biomolecules makes it challenging to detect with kinetically competitive fluorescent probes. Nevertheless, a variety of different probes can be modularly incorporated into different fluorescent, luminescent, two-photon, NIR, and organelle-targeted probes. Though boronic acid-based probes have been reported for HOCl (Table 3, Section 10),[726] their reaction with more abundant H_2O_2 and faster reaction with $ONOO^-$ is a persistent cause of concern about their

chemoselectivity. Hydrazone-[706] and oxime-based probes[727] have been reported to give several different reaction products with HOCl; however, both have been reported to deliver aldehyde products. As noted above, it is prudent to be wary of oxidative triggers that form identical products upon simple hydrolysis, especially when endogenous ligands may catalyze transimination reactions. Dimethylthiocarbamate moieties are especially selective and give a clear and consistent product upon reaction with HOCl.[628] The cyclization of thiosemicarbazides gives similarly unique oxadiazole cyclization products with the added benefit of extending conjugation to yield ratiometric analogs.[703] These existing probes provide a broad foundation on which to design next-generation probes, with color-coded outputs for multiple ROS built into a single probe.

5. Luminescent probes for reactive nitrogen species

5.1 Nitric oxide

5.1.1 Nitric oxide in health and disease

Nitric oxide is a diatomic radical species that was long known as a toxic gas[728] but surprised the scientific community when it was discovered to be the long-sought endothelial derived relaxation factor (EDRF), the discovery of which was awarded the Nobel prize in 1998.[729] Nitric oxide is a reactive free radical species that undergoes autooxidation with triplet oxygen to form nitrogen dioxide radical ($NO_2^{\bullet}$) with a large rate constant, but in a termolecular process that requires two equivalents of nitric oxide, making the rate steeply dependent on concentration.[5] Combination of NO with $NO_2^{\bullet}$ yields dinitrogen trioxide (N_2O_3), a potent electrophilic nitrosating agent that can react with thiol groups to form *S*-nitroso compounds. NO also reacts rapidly with superoxide (O_2^{-}) to form peroxynitrite ($ONOO^{-}$) that can directly mediate two-electron oxidations and induce tyrosine nitration via its radical decomposition products including $NO_2^{\bullet}$. Nitric oxide has high binding affinity to the iron in heme, and this chemistry mediates what is referred to as its canonical signaling pathway with soluble guanylyl cyclase.

Nitric oxide is produced enzymatically from nitric oxide synthases, with three main isoforms in mammalian systems: neuronal nitric oxide synthase (NOS-1 or nNOS), inducible nitric oxide synthase (NOS-2 or iNOS), and endothelial nitric oxide synthase (NOS-3 or eNOS). It can also be generated from nitrate ingested in the diet via reduction to nitrite by the microbiome, followed by enzymatic reduction of nitrite to form nitric oxide.[730] The canonical signaling pathway for nitric oxide in the vasculature refers to its production in endothelial cells by eNOS, where it can diffuse to the smooth muscle cell layer to induce relaxation. Nitric oxide binds to the heme in soluble guanylyl cyclase to activate cyclic guanosine monophosphate (cGMP) production that ultimately leads to smooth muscle relaxation.[731] This molecule can also signal via formation *S*-nitrosocysteine residues and other types of *S*-nitroso compounds to alter protein function,[732] formation of nitrate and nitrite,[733] and through downstream reactive nitrogen species like peroxynitrite and nitrogen dioxide radical.[734] Nitric oxide plays ubiquitous and important roles in human physiology, especially in the cardiovascular system, as it regulates blood pressure, mediates angiogenesis, and other effects.[735] Nitric oxide is a key molecule in the phagocytic immune response, where it can combine with reactive oxygen species to form an arsenal of oxidative and nitrosative species to kill invading pathogens, as well as modulate the immune response through other signaling mechanisms.[736] It can act as a neuronal messenger in the brain, mediating crucial functions in neuropathic pain and migraine headaches.[737] Furthermore, it has an important role in cancer,[738] the gastrointestinal tract,[739] and is even involved in the relationship between psychosocial stress and respiratory infection.[740]

5.1.2 Classical detection techniques for nitric oxide

There are several non-luminescent probe strategies for detecting nitric oxide including nitrite detection using the Griess assay, ozone-based chemiluminescence, electron paramagnetic

resonance spectroscopy (EPR), and electrochemical techniques. The Griess assay[741] colorimetrically detects nitrite as an end-product of nitric oxide decomposition. The chemistry of the technique relies on the acidification of nitrite to form a nitrosating species that can convert sulfanilamide into a diazonium salt. The diazonium salt in turn reacts with *N*-naphthyl-ethylenediamine to form a highly colored azo dye with an increase in absorbance at 540 nm. The Griess assay can be extended to include nitrate, another potential product of nitric oxide decomposition by first reducing nitrate to nitrite using a nitrate reductase enzyme. The advantages of the Griess assay are that it is well validated, reliable, and not as dependent on the timing of the measurement because it is measuring a stable decomposition product. Some of its disadvantages are that it is indirect and is incompatible with live-cell imaging, an important premise for the development of luminescent probes. Another well-established method is ozone-based chemiluminescence.[108] Ozone reacts with NO to form nitrogen dioxide radical ($NO_2^{\bullet}$) in the excited state, which emits light in a chemiluminescent reaction. Commercial instrumentation has been developed to use this technique for detecting NO in a range of biological samples. This method is advantageous because it provides a more direct measurement of NO, has high sensitivity, and can be adapted to measure *S*-nitroso compounds and other nitric oxide stores. Its disadvantages include the required generation of toxic ozone gas, special instrumentation, the necessity to release NO from internal stores, and its incompatibility with live cell imaging. Electron spin paramagnetic resonance (EPR) spectroscopy[742] measures free radical species based on the electronic spin state. While in principle it can detect nitric oxide without a label, NO has low abundance and a broad signal in the liquid state of biological systems, so it practically requires a spin trap. These spin traps are small molecules that react with nitric oxide to form a stable radical and include nitronyl nitroxides, iron dithiocarbamates, hemoglobin, and other types of probes. As discussed below, some spin traps have been adapted to provide a modulation in luminescent properties to act as luminescent probes for nitric oxide. EPR has several advantages. It is only sensitive to paramagnetic species, allowing better selectivity and signal to background. It also reports on the nitrogen isotope so can be used in labeling experiments to track down sources of nitric oxide generation. Lastly, it can detect other NO-derived paramagnetic biomolecules. The disadvantages include expensive instrumentation and the need for specialized technical expertise. Finally, nitric oxide can be measured using electrochemical techniques.[743] Electrochemical methods detect NO based on its oxidation or reduction potentials, which have the advantages of being direct, real-time, and label-free with disadvantages including biofouling and interferences from other reducible or oxidizable biological molecules.

5.1.3 Nitric oxide probes by trigger

Nitrosation triggers

Nitrosation of amines by nitrosating species generated from NO and O_2 (most likely N_2O_3) are a leading strategy for developing small molecule nitric oxide probes and we classify these into four types of *N*-nitrosation triggers as summarized in Scheme 1. *N*-Nitrosation type 1 triggers use an *ortho*-phenylenediamine starting material that is converted into a triazole product, type 2 triggers convert a 3-dimethylaminophenyl group into a fluorescent azo dye, type 3 triggers react with primary aromatic amines to form deamination or phenol products, and type 4 triggers convert secondary amines into stable *N*-nitroso compounds. These triggers and probes that use them are described in more detail in the sections below.

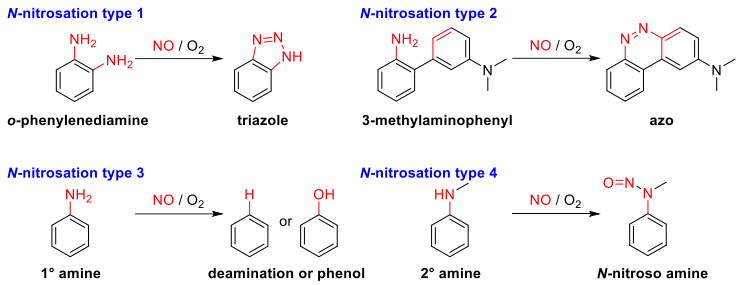

Scheme 1. *N*-Nitrosation trigger types.

N-Nitrosation type 1 (Table 4, Section 1)

2,3-diaminonaphthalene (**DAN**) (λ_{ex} = 365 nm, λ_{em} = 415 nm) was used as a fluorometric reagent in the 1970's for detecting nitrite[744] and nitrate[745] based on *N*-nitrosation of one of the amines of a phenylenediamine motif followed by triazole formation, a process which we herein term as an *N*-nitrosation Type 1 detection mechanism. This *ortho*-phenylenediamine motif of **DAN** was later shown by Miles and Wink in 1996 to be useful for measuring nitric oxide based on the oxygen-dependent formation of the nitrosating species dinitrogen trioxide (N_2O_3) from nitric oxide, which can perform the *N*-nitrosation type 1 chemistry.[746] In 1997, Nagano developed a derivative of **DAN** that was more cell permeable **DAN 1-EE** and used it as an early example of imaging nitric oxide in living rat aortic smooth muscle cells.[747] Shortly after, the same research group developed the widely used diaminofluorescein derivatives **DAF**, **DAF-2**, **DAF-2 DA**, and **DAF-2 FM** (λ_{ex} = 495 nm, λ_{em} = 515 nm) that relied on the modulation of photoinduced electron transfer (PeT) quenching upon conversion of the *ortho*-phenylenediamine group into a triazole (Figure 70). **DAF-2 DA** was used to image nitric oxide production in rat aortic smooth muscle cells.[748–750] This probe has since been extensively used for different applications[751–753] and is commercially available from a number of sources. The same *N*-nitrosation type 1 trigger was extended to diaminorhodamine **DAR** probes (λ_{ex} = 560 nm, λ_{em} = 575 nm) by Nagano in 2001, and the cell permeable probe **DAR 4M AM** was utilized to image nitric oxide in bovine aortic endothelial cells using fluorescence microscopy.[754]

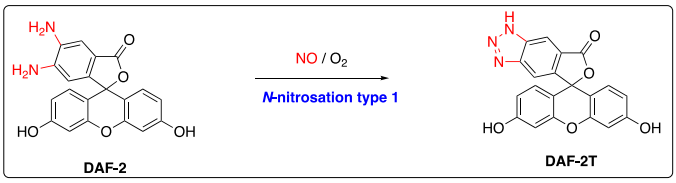

Figure 70. The fluorescent probe **DAF-2** as an example of *N*-nitrosation type 1 trigger for NO detection.[748]

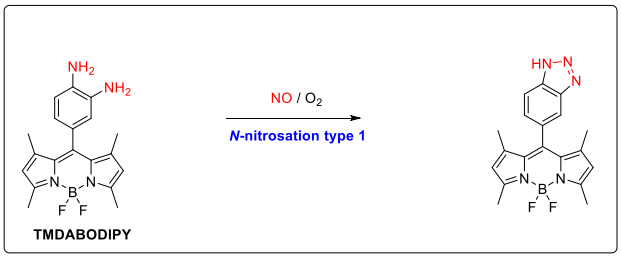

Figure 71. The fluorescent probe **TMDABODIPY** as an example of an *N*-nitrosation type 1 trigger for NO detection.[755]

A diamino BODIPY scaffold **TMDABODIPY** (λ_{ex} = 500 nm, λ_{em} = 510 nm) with an *ortho*-phenylenediamine *N*-nitrosation type 1 trigger was reported in 2003 by Zhang (Figure 71),[755] with a number of BODIPY derivatives reported by Nagano and Zhang between 2003 and 2007,[756–764]

as well as a far-red BODIPY derivative reported by Zhang in 2013,[765] a water soluble BODIPY reported by Liu in 2013,[766] and many others.[767–776] Nagano developed the first NIR nitric oxide probe in 2005 by appending an *ortho*-phenylenediamine *N*-nitrosation type 1 trigger to a cyanine scaffold **DAC-S**, which underwent reduced PeT quenching to increase fluorescence (λ_{ex} = 750 nm, λ_{em} = 785 nm) after reacting with nitric oxide, and was used to image NO generated by a NOC-13 nitric oxide donor in an *ex vivo* rat kidney model.[777] Many examples of NIR nitric oxide probes using this trigger have since been developed.[778–783] In 2008, Zeng and Xu described a modified application of the *N*-nitrosation type 1 trigger that couples triazole formation with the spirocyclic ring opening of a spirolactam rhodamine (Figure 72) to provide a turn-on fluorescence response (λ_{ex} = 554 nm, λ_{em} = 574 nm).[784]

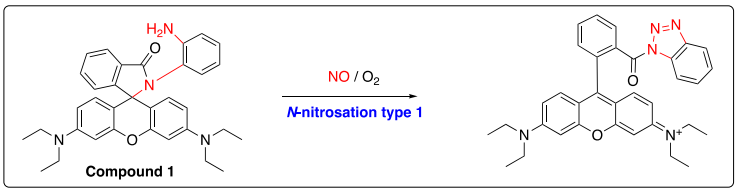

Figure 72. The fluorescent probe **Compound 1** as an example of a spirolactam ring opening modification of the *N*-nitrosation type 1 trigger for NO detection.[784]

Lin reported **Cou-Rho-NO** (λ_{ex} = 410 nm, λ_{em} = 473 nm / 583 nm), the first *N*-nitrosation type 1 ratiometric probe for nitric oxide in 2011, which used a FRET approach by linking a coumarin to a spirolactam rhodamine that could undergo the spiro ring opening mechanism upon triazole formation.[785] This probe was used to image nitric oxide generated in LPS/IFN-γ stimulated RAW 264.7 macrophages. Jin and Dai used a similar FRET-based approach in 2013 with a spirolactam rhodamine, but linking to a BODIPY fluorophore as part of the FRET pair instead of a coumarin (λ_{ex} = 488 nm, λ_{em} = 510 nm / 590 nm).[786] Many other ratiometric *N*-nitrosation type 1 probes are now available in the literature.[124,776,781,786–793] Kim and Cho developed the two-photon nitric oxide probe **ANO-1** in 2012 that used a high two-photon cross section fluorophore 2-acetyl-6-dialkylaminonaphthalene (acedan) linked to an *ortho*-phenylenediamine *N*-nitrosation type 1 trigger that underwent reduced PeT quenching upon triazole formation causing an increase in fluorescence emission (λ_{ex} = 370 nm, λ_{em} = 502 nm).[794] **ANO-1** could be employed for two-photon microscopy imaging (750 nm excitation) in LPS/IFN-γ treated RAW 264.7 and NMDA treated rat hippocampal slices. There is now a wide scope of other two-photon probes for nitric oxide using the *N*-nitrosation type 1 trigger.[795–802]

Many organelle-targeted probes have been developed using the *N*-nitrosation type 1 trigger. In 2012, Xiao and Jin developed a lysosome-targeted probe **LYSO-NINO** (λ_{ex} = 440 nm, λ_{em} = 530 nm) by appending a morpholine targeting group to a naphthalimide scaffold with the *N*-nitrosation type 1 trigger, and used it to image nitric oxide in stimulated RAW 264.7 macrophages.[795] In 2013, Jin reported a triphenylphosphonium-appended mitochondrial targeted probe **Mito-Rho-NO** using an *N*-nitrosation trigger (λ_{ex} = 559 nm, λ_{em} = 585 nm) and this probe was used to image nitric oxide in the mitochondria of RAW 264.7 and MCF-7 cells.[803] Hu and Yang developed a HaloTag approach to organelle targeting in 2015, where they designed and synthesized the alkyl halide modified **DAF**, **HTDAF-2DA** (λ_{ex} = 488 nm, λ_{ex} = 512 nm), and showed that by appropriate expression of the HaloTag fusion protein, localization to the cytosol, nucleus, plasma membrane, and mitochondria could be accomplished in HeLa, MCF-7, or RAW 264.7 macrophages.[131] A similar approach using a SNAP tag has also been reported.[804] In 2020, Krishnan harnessed DNA for nitric oxide detection and developed targeted probes by linking a diaminorhodamine (λ_{ex} = 550 nm, λ_{ex} = 575 nm) to DNA sequences that target the plasma membrane **NOckout^{PM}** (with an

Alexa 488 fluorophore as a reference signal for ratiometric imaging) or trans-Golgi network **NOckout^{TGN}** (using Alexa 647 as a reference fluorophore for ratiometric imaging). This probe series was used to image nitric oxide simultaneously in multiple organelles in T-47D cells,[124] and additional **NOckout** constructs were later used to image NO in live brains.[805] Zhang and Xiao reported an interesting click chemistry approach for organelle targeting in 2022 by linking a spirolactam rhodamine diamine to a tetrazine unit to make the probe **TMR-Tz-NO** (λ_{ex} = 555 nm, λ_{ex} = 585 nm).[806] The probe could be modified via a tetrazine/cyclooctyne click reaction with chemical handles to target the mitochondria (triphenylphosphonium), lysosomes (morpholine), and the plasma membrane (tetra-acetylated *d*-mannosamine), and this strategy was used to image LPS treated RAW 264.7, HeLa cells, and zebrafish.[806] Many other probes have been developed to target the mitochondria,[807,798] lysosomes,[808–810] endoplasmic reticulum,[799] hepatocytes,[811] plasma membrane,[133] nucleus,[791] and Golgi apparatus.[812]

Urano reported the bioluminescent nitric oxide probe **DAL** in 2015 using a bioluminescent enzyme-induced electron transfer (BioLeT) strategy by linking an *ortho*-phenylenediamine-modified luciferin that remained a substrate for luciferase but was quenched by the appended *ortho*-phenylenediamine.[813] An increase in bioluminescence emission at 600 nm could be obtained upon NO-mediated conversion to the triazole in an *N*-nitrosation type 1 mechanism. This probe was used for *in vivo* imaging in a luc-Tg rat treated with NOC7. In 2022, Chan described another bioluminescence probe shifted into the NIR regime **BL$_{660}$-NO** using the luciferin analogue AkaLumine with a modified *ortho*-phenylenediamine linked via an amide linkage.[814] In an interesting modification of the *N*-nitrosation type 1 mechanism designed to release a carboxylic acid, NO-induced triazole formation followed by hydrolysis (Figure 73) yielded the free luciferin with 660 nm NIR emission and was used to image NO generated in A549-Luc2 lung tumors *in vivo*.

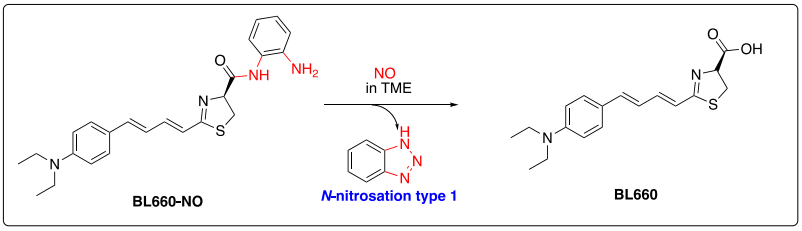

Figure 73. The fluorescent probe **BL660-NO** as an example of a triazole hydrolysis *N*-nitrosation type 1 trigger for NO detection.[814]

Several photoacoustic nitric oxide probes have been reported. Yuan and Zhang disclosed the photoacoustic probe **PS** in 2018 consisting of a thiadiazole with an *ortho*-phenylenediamine *N*-nitrosation type 1 trigger that induces a red-shift after triazole formation with the optimal photoacoustic excitation shifting from 368 nm to 568 nm. **PS** was used for photoacoustic imaging of nitric oxide in LPS-treated mice.[815] In 2023, Chen, He, and Liu developed a blood-brain barrier permeable photoacoustic *N*-nitrosation type 1 BODIPY probe that shifts the photoacoustic excitation maximum from 790 nm to 690 nm upon nitric oxide mediated triazole formation and the probe was used for ratiometric photoacoustic imaging in a Parkinson's disease mouse brain.[776] Chan and Scott developed another photoacoustic probe in 2023 based on a short-wave infrared (SWIR) xanthene fluorophore appended with amino thiofuran groups to extend conjugation and red-shift emission.[816] This probe **SCR-NO** undergoes spirocylic ring opening and hydrolysis upon NO-mediated triazole formation to provide a turn-off photoacoustic response at 895 nm. **SCR-NO** was formulated into nanoparticles with IR-1061 for ratiometric imaging of nitric oxide in a mouse model of drug induced liver injury. The *N*-nitrosation type 1 strategy has been used in many other fluorogenic designs, including acridine,[817,818] naphthalimide,[808–821] luminescent ruthenium,

[768,822–824] iridium,[825,801] europium,[826,827] and terbium[809] complexes, spirobifluorene,[828] dibenzoxanthenium,[829] silicon rhodamine,[780–782] and thiadiazole, [783,810,815,830] among others. It has also been used in several multi-analyte probe approaches.[831–834] While this *N*-nitrosation type 1 trigger for nitric oxide detection was among the earliest developed triggers, it still remains among the most popular approaches for imaging nitric oxide in living cells. Table 4, Section 1 summarizes these and any other examples of probes containing this trigger.

N-Nitrosation type 2 (Table 4, Section 2)

While the *N*-nitrosation type 1 conversion of an *ortho*-phenylenediamine motif into an aryl triazole has been extensively utilized, there is documented cross-reactivity with biomolecules like dehydroascorbic acid that must be carefully considered when using probes that rely on *ortho*-phenylenediamine nitrosation.[835,836] In order to address this short coming, Anslyn and Shear developed a trigger based on *N*-nitrosation of an aniline unit followed by electrophilic aromatic substitution of a 3-dimethylaminophenyl group to form a fluorescent azo fluorophore, which we here refer to as an *N*-nitrosation type 2 trigger,[837] and is also generally referred to as a covalent assembly approach. The probe **NO_{550}** (λ_{ex} = 470 nm, λ_{em} = 550 nm) was the first to use this *N*-nitrosation type 2 trigger (Figure 74) and overcomes dehydroascorbic acid cross-reactivity by having just one amine. It was used for imaging neonatal spinal astrocytes treated with IFN-γ and IL-1β, and was later validated in primary vascular endothelial cells, fibroblasts, and stem cell-derived endothelial cells.[214] A scalable synthesis of **NO_{550}** has been reported.[215] In 2014, Guo showed how this 2-amino-3'-dimethylaminobiphenyl *N*-nitrosation type 2 trigger could be generalized by appending the trigger to a BODIPY fluorophore and showing that PeT quenching could be effectively modulated to increase fluorescence emission (λ_{ex} = 480 nm, λ_{em} = 518 nm) after reacting with nitric oxide.[838] The probe was used to image nitric oxide in DEA NONOate treated HL-7702 cells. Zhang showed in 2017 that this approach could be extended to ratiometric, two-photon, and mitochondrial-targeted imaging by synthesizing the probe **Mito-N**, an amino naphthalimide with an appended 2-amino-3'-dimethylaminobiphenyl *N*-nitrosation type 2 trigger that resulted in a shift in the fluorescence emission maximum (λ_{ex} = 500 nm, λ_{em} = 540 nm / 595 nm) for ratiometric imaging.[788] **Mito-N** was used to image nitric oxide in RAW 264.7 cells supplemented with L-arginine and treated with IFN-γ and LPS, as well as for *in vivo* imaging in LPS treated mice. Zhou and Song developed the probe **NO-QA5** (λ_{ex} = 432 nm, λ_{em} = 540 nm) in 2017, based on appending a 3-dimethylaminophenyl group to a 5-aminoquinoline. This probe has a high two-photon cross section with excitation at 760 nm and was used to image nitric oxide in stimulated RAW 264.7 macrophages and in mouse liver slices treated with the nitric oxide donor SNP.[839] In 2020, Song designed a similar quinoline scaffold bit with the amine at the 6-position of the quinoline and the 3-dimethylaminophenyl group at the 5-position, which granted the probe **RatioTr** a ratiometric response when reacting with nitric oxide (λ_{ex} = 345 nm / 428 nm, λ_{em} = 440 nm / 538 nm) with a single excitation at 370 nm used for ratiometric spectroscopy and imaging (λ_{ex} = 370 nm, λ_{em} = 424 nm / 530 nm) in stimulated RAW 264.7 macrophages.[840] In 2020, Shear, Anslyn, and Yang reported derivatives of **NO_{550}**, **NO_{530}** (λ_{ex} = 445 nm, λ_{em} = 530 nm) with one of the amines tied back in a six-membered ring, and **NO_{562}** (λ_{ex} = 470 nm, λ_{em} = 562 nm) with both amines tied back into six-membered rings.[841] These probes were all validated in stimulated RAW 264.7 macrophages. In 2022, Luo and Yang developed the probe **NOP3** (λ_{ex} = 450 nm, λ_{em} = 530 nm) which combines the *N*-nitrosation type 1 and type 2 triggers and they showed that the type 2 trigger displayed faster kinetics.[842] **NOP3** exhibited lysosome localization and was used to image nitric oxide in LPS-treated RAW 264.7. Recently in 2023, Zheng reported the probe **MTNO** (λ_{ex} = 344 nm, λ_{em} = 457 nm) which used a naphthalimide scaffold and triphenylphosphonium group to image mitochondrial localized nitric oxide in stimulated RAW 264.7 and in two-photon microscopy imaging of liver slices treated with sodium nitroprusside using 760 nm two-photon excitation.[843] Although the selectivity versus dehydroascorbic acid should be a clear advantage, the number of

probes being developed that use the *N*-nitrosation type 2 trigger is smaller than those being developed with the type 1 trigger. We believe this is likely due to the type 2 trigger being more synthetically difficult as well as design challenges to develop probes that will be able to modulate luminescence output based on this *N*-nitrosation type 2 trigger. Table 4, Section 2 summarizes these and any other examples of probes containing this trigger.

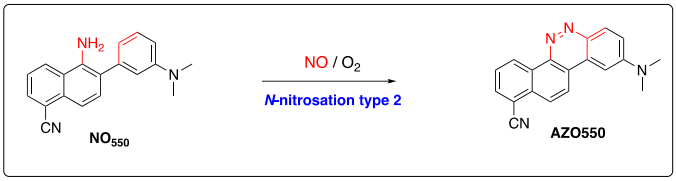

Figure 74. The fluorescent probe **NO$_{550}$** as an example of *N*-nitrosation type 2 trigger for NO detection.[837,844,845]

N-Nitrosation type 3 (Table 4, Section 3)

Another class of *N*-nitrosation triggers aimed at eliminating interference from dehydroascorbic acid involves the nitrosation of a single primary amine followed by deamination (Figure 75) or hydrolysis (Figures 76). In 2012, Wang showed that the probe **FA-OMe** consisting of the methyl ester of 5-aminofluorescein underwent deamination upon reaction with nitric oxide with a concomitant increase in fluorescence emission (Figure 75).[846] The proposed mechanism proceeded first by nitrosation of an aromatic amine with N_2O_3 (formed from NO and O_2), followed by nucleophilic substitution of nitrite to release NO^-, a second N_2O_3-mediated *N*-nitrosation step, rearrangement, and finally decomposition to N_2, NO_3 radical, and an aryl radical that abstracts a hydrogen from solvent. **FA-OMe** displayed a selective fluorescence increase (λ_{ex} = 460 nm, λ_{em} = 524 nm) upon reaction with nitric oxide and was used to image nitric oxide production in LPS-stimulated macrophages. In 2014, Ramaih also reported using a monoamine trigger (Figure 76).[847] However this group showed that reaction with nitric oxide yielded a phenol product proposed to form as the result of hydrolysis of a diazonium salt generated from reaction of the monoamine with N_2O_3. The probe itself was a bis-azido-BODIPY that first reacts with hydrogen sulfide to form the *bis*-aromatic amines, followed by the *N*-Nitrosation type 3 hydrolysis reaction with nitric oxide to form the *bis*-phenol with an increase in fluorescence (λ_{ex} = 740 nm, λ_{em} = 815 nm).

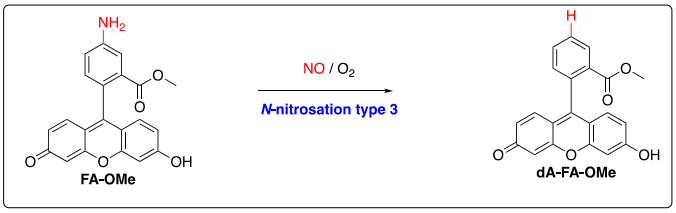

Figure 75. The fluorescent probe **FA-OMe** as an example of *N*-nitrosation Type 3 deamination trigger for NO detection.[846]

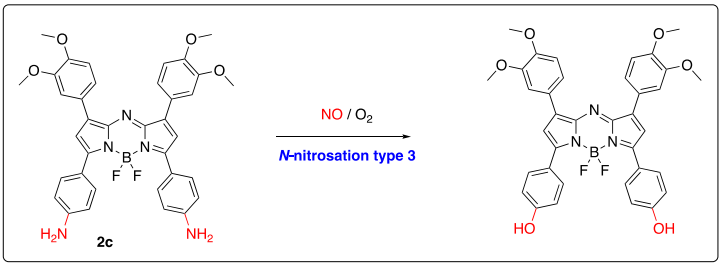

Figure 76. The fluorescent probe **2c** as an example of *N*-nitrosation type 3 hydrolysis trigger for NO detection.[847]

Hu and Liu reported a second example of a subsequent hydrogen sulfide/NO probe in 2018 that employed an azide to monoamine hydrogen sulfide trigger followed by reaction of the monoamine with NO through a proposed *N*-nitrosation type 3 deamination mechanism.[848] They showed that 5-azido fluorescein first reacted with hydrogen sulfide to turn off fluorescence followed by reaction to nitric oxide to give the *N*-nitrosation type 3 deamination product with an increase in fluorescence (λ_{ex} = 465 nm, λ_{em} = 526 nm). The probe was validated for cellular microscopy imaging in PC12 cells sequentially treated with NaSH and SNP. Luis and Galindo developed an *ortho*-hydroxyaminobenzene trigger in 2014, which they linked to a triaryl pyrylium scaffold and identified the deamination product with excess nitric oxide as confirmed by single crystal x-ray crystallography.[849] Reaction with nitric oxide gave an increase in fluorescence (λ_{ex} = 470 nm, λ_{em} = 550 nm), and the probe was used to image nitric oxide in RAW 264.7 macrophages using L-NMMA inhibition as a negative control. In 2021, Galindo reported an improved structure **mtNOpy** (λ_{ex} = 480 nm, λ_{em} = 585 nm), using an *ortho*-methoxyamine trigger and demonstrated that the pyrylium scaffold granted mitochondrial localization for imaging LPS-treated RAW 264.7, as well as capability for monitoring NO production in leukocytes and neutrophils using flow cytometry.[850] Guo designed and synthesized a series of monoamine probes in 2017, including **MA** (λ_{ex} = 475 nm, λ_{em} = 519 nm) based on a BODIPY scaffold and **NIR-MA** (λ_{ex} = 750 nm, λ_{em} = 794 nm) based on a cyanine scaffold.[1730] They provided mass spectrometry confirmation of the deamination product and proposed a mechanism in which the NO-mediated formation of a diazonium salt reacts with another equivalent of nitric oxide to form the aryl radical and NO^+. Both probes were used to image NO in LPS-treated macrophages and **NIR-MA** was used for whole animal *in vivo* imaging in NOC-9 treated mice. A short time later, Cheng, Li, and Liu reported the probe **ENNH$_2$** which operates via deamination of a naphthalimide scaffold providing a ratiometric response (λ_{ex} = 460 nm, λ_{em} = 530 nm / 605 nm) and was used for imaging nitric oxide in LPS treated RAW 264.7 macrophages and zebrafish.[792] Lastly, Guo developed the *para*-methoxyphenylamine trigger/BODIPY scaffold probe **BDP3** (λ_{ex} = 648 nm, λ_{em} = 668 nm) in 2023.[851] This probe was validated by measuring nitric oxide production in IL-4 or LPS/IFN-γ treated macrophages and characterization of RAW 264.7 macrophages polarized into M1 or M2 phenotypes. Additionally, **BDP3** was used to investigate reprogramming of tumor associated macrophages by immunotherapeutic drugs *in vivo*. While the *N*-nitrosation Type 3 trigger has found application with several scaffolds, there are differing reports which make it difficult to predict which product (deamination versus hydrolysis) will be preferentially formed. Table 4, Section 3 summarizes these and any other examples of probes containing this trigger.

N-Nitrosation type 4 (Table 4, Section 4)

As opposed to primary amines, secondary amines undergo *N*-nitrosation to form a stable *N*-nitroso product. In 2016, Guo first showed that the stable *N*-nitrosation of a secondary amine could be used as a NO-detection trigger by linking a benzylphenyl amine to a BODIPY scaffold which underwent reduced PeT quenching and an increase in fluorescence (λ_{ex} = 490 nm, λ_{em} = 518 nm) upon NO-mediated formation of the *N*-nitroso compound (Figure 77).[852] The probe was

shown to be selective for nitric oxide versus dehydroascorbic acid and other species, with a slight increase in signal observed upon reaction with peroxynitrite. The stable *N*-nitroso product was observed by mass spectrometry. The probe could be attached to a triphenylphosphonium unit for mitochondrial targeting and was used to image nitric oxide production in L-arginine supplemented, LPS/IFN-γ treated RAW 264.7, as well as in an oxygen-glucose deprivation (OGD) ischemic model in EA.hy926 cells. In 2017, Liu used a secondary methylaniline trigger linked to a silicon rhodamine scaffold to make the two-photon (λ_{ex} = 820 nm) and near-infrared fluorescence probe **SIRNO** (λ_{ex} = 653 nm, λ_{em} = 670 nm) that operated via reduced PeT quenching upon formation of the *N*-nitroso product.[853] **SIRNO** was used to image nitric oxide in L-arginine supplemented, LPS/IFN-γ treated RAW 264.7 tumor xenograft slices from mice using c-PTIO as a negative control. Ali reported a series of probe that use this *N*-nitrosation type 4 trigger starting in 2018 with the ratiometric probe **PyDA-NP** (λ_{ex} = 390 nm, λ_{em} = 445 nm / 523 nm) using a pyrene scaffold and secondary amine,[854] followed by the probe **PQPY** with emission at 505 nm that interestingly used *N*-nitrosation of an imidazole unit as a trigger,[855] and finally the probe **HqEN$_{480}$** (λ_{ex} = 390 nm, λ_{em} = 480 nm) which demonstrated that *N*-nitrosation of a secondary *amide* on a quinoline fluorophore could also be used as a trigger for imaging nitric oxide in HepG2 cells.[856] A study by Chan in 2018 aimed at developing a photoacoustic probe for nitric oxide imaging was particularly informative because it directly compared *N*-nitrosation type 1, type 3, and type 4 triggers and demonstrated that the type 4 trigger was optimal because it resulted in faster kinetics, a simplified reaction mechanism, and was synthetically more accessible.[790] The probe **APNO-5** that used this trigger with an *ortho*-methoxy aniline on an extended BODIPY scaffold showed an absorption blue-shift from 764 nm to 673 nm upon reaction with nitric oxide and was used for ratiometric photoacoustic imaging with 680 nm and 770 nm excitation. It was selective for nitric oxide although some cross-reactivity with peroxynitrite was observed. The probe **APNO-5** was also utilized for photoacoustic imaging of nitric oxide in LPS stimulated mice. Chan later optimized this scaffold to develop the probe **SR-APNO-3** in 2020.[857] In 2019, Guo synthesized a *para*-methoxy secondary amine linked to a BODIPY scaffold and observed a robust response (λ_{ex} = 485 nm, λ_{em} = 518 nm) for nitric oxide via *N*-nitrosation, but response was also observed for peroxynitrite.[858] The product from reaction with peroxynitrite was identified as an *ortho*-iminoquinone, providing a plausible explanation for some of the peroxynitrite cross reactivity seen with some of the other reported probes. The probe contained a triphenylphosphonium moiety for mitochondrial targeting and was used to study NO communication in co-cultures of macrophages and SKOV-3 cancer cells. Zeng and Wu reported the NIRII/photoacoustic probe **QY-N** (λ_{ex} = 808 nm, λ_{em} = 935 nm) in 2021 consisting of a secondary amine *N*-nitrosation type 4 trigger on a fluorophore comprised of a *bis*-methoxyphenyl-amine-dihydroxanthene donor and quinolinium acceptor.[859] Photoacoustic imaging with excitation at 780 nm was performed for imaging NO in liver injury induced by herbal medicine. Chan developed a NIR-II excitable photoacoustic probe **APNO-1080**, which could be used for photoacoustic imaging in *in vivo* breast and liver cancer models using 1080 nm excitation.[860] There are other examples of NIR,[861,862,863] two-photon,[862] ratiometric, [793,864] lipid droplet targeted,[862,865] lysosome targeted,[866,867] and dual-analyte probes[793,868–870] using this *N*-nitrosation type 4 trigger. This trigger is gaining increasing attention due to its simplified reaction mechanism and synthetic ease, but the cross-reactivity with peroxynitrite should be investigated more deeply. Table 4, Section 4 summarizes these and any other examples of probes containing this trigger.

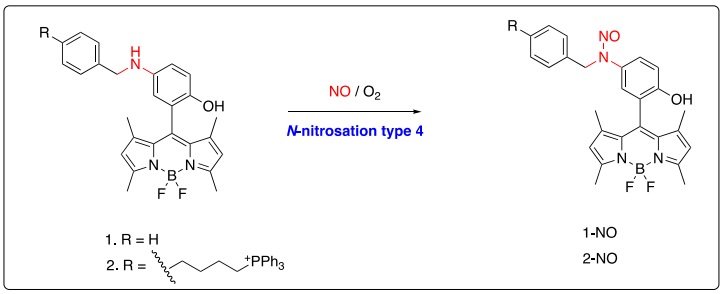

Figure 77. The fluorescent probes **1** and **2** as examples of *N*-nitrosation type 4 triggers for NO detection.[852]

Other nitrosation-based triggers (Table 4, Section 5)

Other types of triggers have been developed that rely on the nitrosative abilities of nitric oxide in the presence of oxygen. In 1998, Sasamoto investigated the use of **rhodamine hydrazide** for detecting nitrite and nitric oxide by showing that acidic nitrite or NOC-7 react with **rhodium hydrazide** to form a fluorescent product (λ_{ex} = 561 nm, λ_{em} = 581 nm).[871] The proposed mechanism involved *N*-nitrosation of the terminal hydrazide nitrogen, followed by a Curtius rearrangement, presumably from an acyl azide. The amine product was detected by mass spectrometry. In 2011, Wang proposed a different mechanism for nitric oxide detection with **rhodium hydrazide** involving the hydrolysis of an acyl azide intermediate.[872] A related approach was reported by Song in 2019 using a BODIPY with a hydrazine appended to the *meso* position, **8-HB**, that was converted to a diazonium salt upon reaction with nitric oxide (Figure 78).[873] Nitrogen evolution and hydride abstraction provided the unsubstituted fluorescent BODIPY product (λ_{ex} = 505 nm, λ_{em} = 512 nm), which was used to image L-arginine supplemented, LPS/IFN-γ stimulated RAW 264.7.

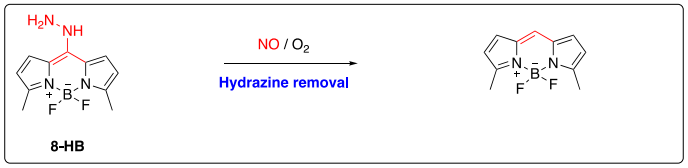

Figure 78. The fluorescent probe **8-HB** as an example of hydrazine removal trigger for NO detection.[873]

In 2021, Zang and Lin reported a reversible *S*-nitrosation based probe consisting of a diethylamino coumarin (λ_{ex} = 418 nm, λ_{em} = 477 nm) or julolidine coumarin (λ_{ex} = 447 nm, λ_{em} = 490 nm) linked to a cysteine methyl ester (Figure 79).[874] *S*-nitrosation results in a quenching of the fluorescence, which can be restored by glutathione mediated reduction of the *S*-nitroso to the thiol. These probes were used to image nitric oxide in L-arginine, LPS/IFN-γ stimulated RAW 264.7 macrophages and HUVEC cells treated with the eNOS activator A23187.

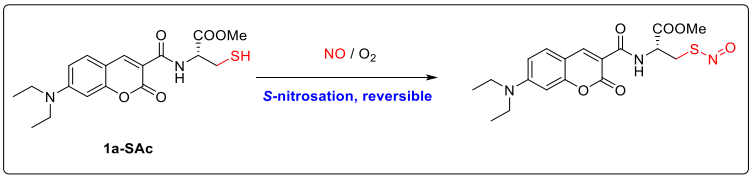

Figure 79. The fluorescent probe **1a-SAc** as an example of *S*-nitrosation, reversible trigger for NO detection.[874]

In 2023, Gandhi and Swamy evaluated a strategy using spirolactam ring opening of an *ortho*-amino sulfide upon *N*-nitrosation or *S*-nitrosation followed by benzothiadiazine formation and

hydrolysis, giving an increase in fluorescence (λ_{ex} = 560 nm, λ_{em} = 580 nm) that was used to image nitric oxide in DEA NONOate treated lung epithelial cells (Figure 80).[875]

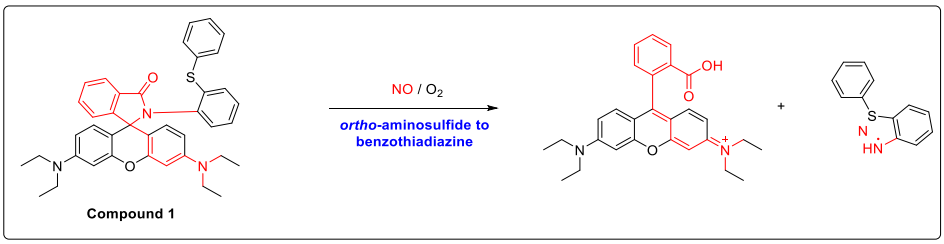

Figure 80. The fluorescent probe **Compound 1** as an example of *ortho*-aminosulfide to benzothiadiazine trigger for NO detection.[875]

In the same year, Guo reported an *ortho*-amino phenylimine with the imine carbon being at the *meso* position of a xanthene fluorophore (Figure 81).[876] Triazole formation upon reaction with nitric oxide converts the structure from a bent to a planar form, resulting in an increase in fluorescence. This design was installed onto a NIRII silicon rhodamine scaffold to make the probe **SiRhd-7** (λ_{ex} = 800 nm, λ_{em} = 1050 nm), which could also be used for photoacoustic imaging with 800 nm excitation and showed a photothermal effect with 808 nm excitation. The probe was formulated into liposomes and used for NIRII imaging of nitric oxide in LPS treated RAW 264.7 macrophages and mice as well as in the brains of Alzheimer's disease model mice.

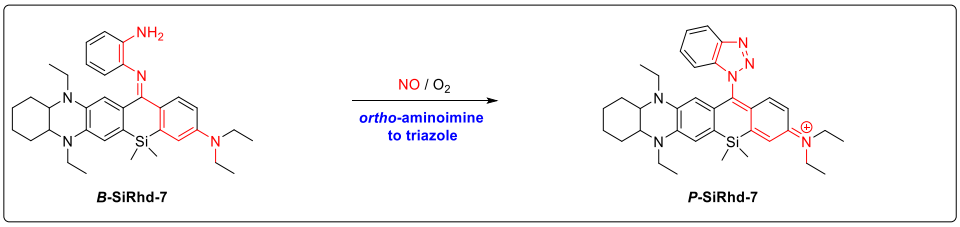

Figure 81. The fluorescent probe ***B*-SiRhd-7** as an example of *ortho*-aminoimine to triazole trigger for NO detection.[876]

As can be seen, the nitrosative potential of nitric oxide has been harnessed in numerous creative designs to generate a large library of nitrosative probes. One drawback, however, is that oxygen is required to generate the putative nitrosative species N_2O_3 so in reality these probes are likely N_2O_3 probes or probes for other nitrosative species and do not directly react with nitric oxide. Table 4, Section 5 summarizes these and any other examples of probes containing nitrosation triggers.

Metal-based nitric oxide detection (Table 4, Section 6)

The reaction of nitric oxide with transition metal centers has been used as a strategy to circumvent the oxygen dependence of nitrosation-based probes for the direct detection of nitric oxide. In 1998, Katayama reported an early transition metal-based approach for nitric oxide detection using a biomimetic iron(II) quinoline complex that showed quenching of the quinoline florescence (λ_{ex} = 366 nm, λ_{em} = 460 nm) upon reacting with nitric oxide.[877] Katayama continued along this vein in 2001 and developed a dithiocarboxysarcosine iron(II) complex bound to a acridine-linked TEMPO ligand (Figure 82).[878] Binding of nitric oxide to the iron center releases the acridine and the uncaged nitroxide radical quenches fluorescence (λ_{ex} = 361 nm, λ_{em} = 438 nm).

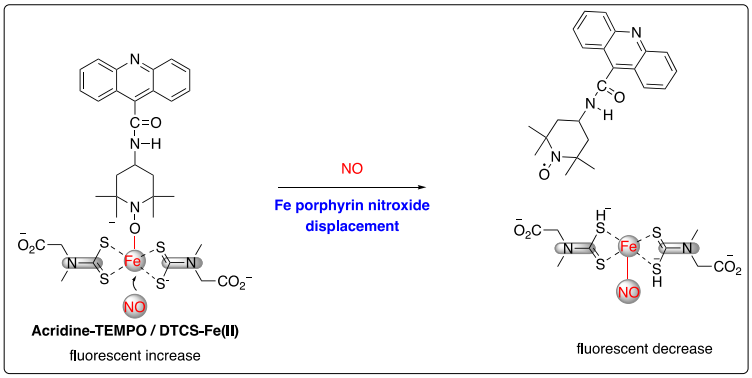

Figure 82. The fluorescent probe **Acridine-TEMPO / DTCS-Fe(II)** as an example of Fe porphyrin nitroxide displacement trigger for NO detection.[878]

In 2002, Soh used a nitroxide PROXYL ligand linked to fluorescamine fluorophore and an iron (II) complexed to a cyclam-coumarin ligand.[879] Upon binding to nitric oxide, the nitroxide ligand is released with a ratiometric change in the fluorescence output that increased at 410 nm and decreased at 470 nm (λ_{ex} = 360 nm, λ_{em} = 410 nm / 470 nm). Between 2000 and 2004, Lippard reported a series of cobalt, rhodium, ruthenium, iron, and copper complexes with fluorescent ligands that responded to NO through NO binding to the metal center to displace the ligand and provide an increase in fluorescence.[880–884] However, a breakthrough came in 2005 when Lippard demonstrated a new strategy based on NO-mediated metal reduction using a bis-dansylaminomethyl pyridine ligand bound to copper(II) with quenched fluorescence that was increased upon reaction with nitric oxide to reduce copper(II) to copper (I) (λ_{ex} = 342 nm, λ_{em} = ~560 nm),[885] with a similar approach being explored across a range of dansyl and anthracene based ligands.[886] Importantly, this approach does not depend on the presence of oxygen to form the nitrosating N_2O_3 species, allowing direct detection of nitric oxide. In 2006, Lippard reported the fluorescein-based probe **CuFL** series containing aminoquinoline ligands that provided a fluorescence increase (λ_{ex} = 503 nm, λ_{em} = 520 nm) upon treatment with NO to reduce copper(II) to copper (I) in aqueous pH 7 buffer (Figure 83).[887] The mechanism was studied in detail and revealed that nitric oxide reacted with a deprotonated nitrogen atom on the ligand with electron transfer from the ligand to the metal to form the *N*-nitrosated ligand and reduced copper (I).[163] The derivative **CuFL1** was used to image estradiol induced nitric oxide formation in SK-N-SH cells.[888,889]

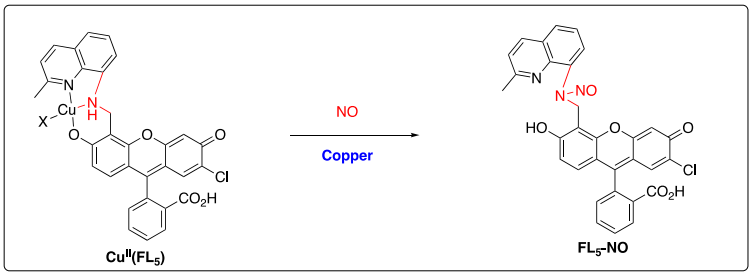

Figure 83. The fluorescent probe **Cu^{II}(FL$_5$)** as an example of copper trigger for NO detection.[887–889]

In 2010, Lippard reported cell-trappable derivatives of **CuFL**, including the derivatives **CuFL1E** and **CuFL^{Dex}** containing a single ester and a cyclodextrin, respectively.[890] Both were used to image nitric oxide production in LPS/IFN-γ treated RAW 264.7. While selective for nitric oxide, some cross-reactivity with nitrite was observed. In a separate 2010 study, Lippard developed another cell trappable probe **Cu$_2$(FL2E)** containing two aminoquinoline ligands with two esters for enhanced trappability.[891] The probe was selective for nitric oxide, but cross-reactivity with

hydrogen peroxide and peroxynitrite was observed. **Cu_2(FL2E)** was used to image nitric oxide in SK-N-SH cells and mouse olfactory bulb slices[892] and in explanted murine carotid arteries using two-photon imaging.[893] In 2008, Zhang reported a napthylimidazole copper(II) complex called **MNIP-Cu** (λ_{ex} = 360 nm, λ_{em} = 492 nm) which was used to image nitric oxide in LPS activated RAW 264.7 macrophages and liver slices of mice who had experienced liver injury.[894] In another example of a copper-based probe, Duan developed the probe **CuRBT** in 2011, which consisted of a rhodamine fluorophore with a tripodal amine ligand that underwent amide nitrosation, reduction of copper (II) to copper (I), and spirolactam ring opening to provide an increase in fluorescence (λ_{ex} = 510 nm, λ_{em} = 580 nm) that was used to image NO treated MCF-7 cells.[895] The same researcher also reported the rhodamine spirolactam ring opening copper(II) probes **RB-Py** (λ_{ex} = 550 nm, λ_{em} = 580 nm) and **RB-TP** (λ_{ex} = 540 nm, λ_{em} = 580 nm) in 2013 that formed *N*-nitroso hydrazide products (Figure 84).[896] A similar copper(II)-assisted spirolactam ring opening was reported using a sulfonamide ligand by Patra in 2019.[897]

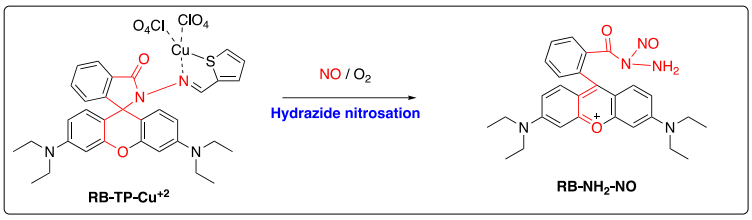

Figure 84. The fluorescent probe **RB-TP-Cu^{+2}** as an example of a copper-dependent hydrazide nitrosation trigger for NO detection.[896]

Lippard expanded the use of copper reduction to the far-red with a series of seminaphthofluor scaffolds appended with aminoquinoline ligands, **CuSNFL1** (λ_{ex} = 527 nm, λ_{em} = 548 nm), **CuSNFL1^{Br}** (λ_{ex} = 540 nm, λ_{em} = 615 nm), **CuSNFL1E** (λ_{ex} = 527 nm, λ_{em} = 549 nm), **CuSNFL1E^{Br}** (λ_{ex} = 536 nm, λ_{em} = 615 nm).[898] While cross-reactivity with nitrite was again observed, these probes were successfully used to image LPS/IFN-γ treated RAW 264.7. A series of copper-based probes were also reported in 2013, **CuBRNO1-3** (λ_{ex} = 563 nm or 570 nm, λ_{em} = 623 nm or 625 nm) based on a benzoresorufin fluorophore and aminoquinoline or aminopyridine ligands.[899] These probes reacted with both NO and HNO and were used to image HeLa and RAW 264.7 cells treated with the HNO donor Angeli's salt. A similar cross reactivity between NO and HNO using a copper based trigger was observed by Ali in 2019 during testing of the probe **[(PIP)Cu(II)(Cl)]** (λ_{ex} = 407 nm, λ_{em} = 560 nm), which could be used to image DEA NONOate or Angeli's salt in A549 cells as well as nitric oxide production in LPS/IFN-γ treated RAW 264.7.[900] A FRET-based ratiometric strategy was developed by Lippard in 2017 using the probe **Cu(FL3A-Ppz-CC)** (λ_{ex} = 400 nm, λ_{em} = 450 nm / 519 nm) consisting of a coumarin linked to a copper(II)-bound fluorescein-aminoquinoline, which was used to image DEA NONOate in A549 cells.[901] Copper(II) reduction for nitric oxide detection has been further investigated in the context of a wide variety of ligands and fluorophores. Duan and Qian investigated using naphthalimide scaffolds for copper-based NO detection;[902,903] Mondal, Chellapa, and Ali investigated the a range of ligand and small fluorophore combinations including the dansyl fluorophore,[904–907] Chellapa reported a rhodamine 6G scaffold,[908] Costero has disclosed a BODIPY scaffold,[909] Woscholski and Vilar used a nitrobenzoxadiazole fluorophore,[910] and Schiesser reported using coumarin scaffolds.[911,912] This trigger has also been used in non-mammalian organisms including plants[913] and the bacterial *Pseudomonas aeruginosa* biofilms.[911] Finally, in 2020, Costero developed an interesting metal-based strategy that relies on the nitric oxide mediated reduction of copper (II) to copper (I) and then using the copper (I) to catalyze a click reaction to induce aggregation in an alkyne-containing AIE fluorophore for an increase in fluorescence emission (λ_{ex} = 330 nm, λ_{em} = ~500 nm) (Figure 85).[914]

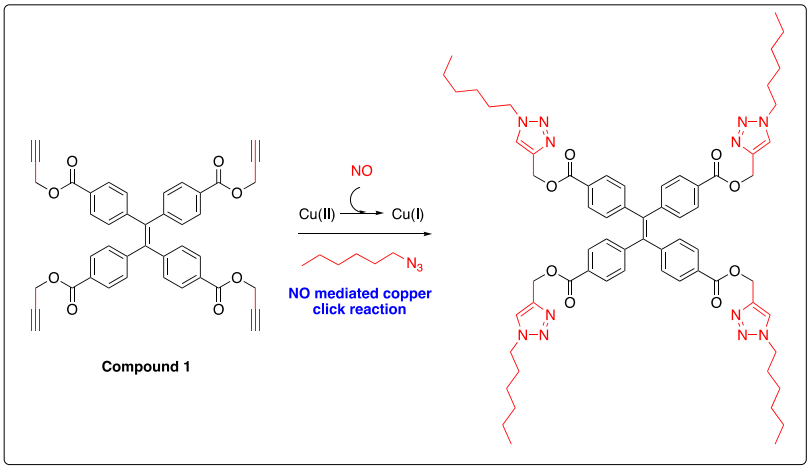

Figure 85. The fluorescent probe **Compound 1** as an example of NO mediated copper click rx trigger for NO detection.[914]

Metal-based approaches offer a potential strategy for direct nitric oxide detection and have been successfully used with a number of fluorophores and ligand strategies. However, cross-reactivity with other species like nitrite and HNO has been observed so these types of potential interferents should be carefully considered when adopting metal-based strategies for NO detection. Table 4, Section 6 summarizes these and any other examples of probes containing this trigger.

Fluorescent cheletropic traps and spin traps (Table 4, Section 7)

Spin traps that react with and stabilize free radical species have been an important tool for studying nitric oxide using EPR spectroscopy.[742] Spin trapping agents that have a modulation in their luminescence response after reacting with nitric oxide can also provide a means for optical detection. In 1997, Korth and Sustmann developed a cheletropic trap for nitric oxide based on the cheletropic addition of nitric oxide to a cyclic *ortho*-quinodimethane derivative to form a nitroxide, which subsequently reacted to form fluorescent non-radical products (λ_{ex} = 315 nm, λ_{em} = 380 nm).[915] Sustmann continued this work and reported cell-trappable derivatives containing acetoxymethyl esters showing increases in emission upon reaction with nitric oxide at λ_{ex} = 320 nm, λ_{em} = 380 nm (Figure 86)[916] and at λ_{ex} = 380 nm, λ_{em} = 460 nm,[917] as well as using a pyrene-based fluorophore (λ_{ex} = 350 nm, λ_{em} = 380 nm),[918] all of which could be used to measure nitric oxide production in LPS-stimulated rat alveolar macrophages.

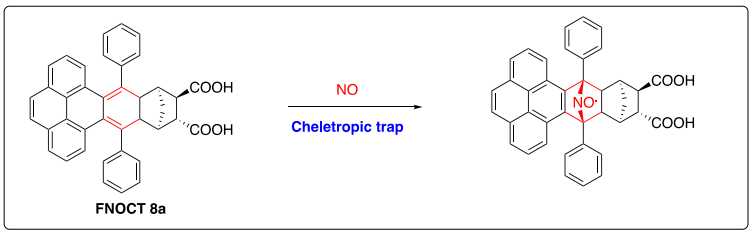

Figure 86. The fluorescent probe **FNOCT 8a** as an example of cheletropic trap trigger for NO detection.[916]

In 2011, He and Duan reported an interesting spin-trap based approach where the spin trap PTIO was encapsulated in a metal-organic tetrahedron cage with fluorescent triarylamine ligands and cerium metal coordination sites.[919] PTIO quenched the fluorescence of the triarylamine ligands, but fluorescence was recovered (λ_{ex} = 350 nm, λ_{ex} = 470 nm) upon PTIO reacting with nitric oxide and this creative design was used to image nitric oxide donated by sodium nitroprusside in living

MCF-7 cells. Table 4, Section 7 summarizes these and any other examples of probes containing this trigger.

Other Triggers (Table 4, Section 8)
Several other triggers have been developed and used for luminescent nitric oxide probes. Although also used for detecting other ROS and RNS, the selenolactone trigger was shown by Ma in 2011 to be able to detect nitric oxide by selenium atom nitrosation coupled with selenolactone ring opening to give rhodamine B after hydrolysis or the diselenide as the final fluorescent product (λ_{ex} = 560 nm, λ_{em} = 580 nm) and was used to image nitric oxide in NOC-5 treated HeLa cells (Figure 87).[920] In 2023, Jiao used a selenolactone trigger installed on a near-infrared Changsha fluorophore **CS-Se** (λ_{ex} = 680 nm, λ_{em} = 780 nm) to image nitric oxide in NOC 5 treated Cal-27 cells.[921]

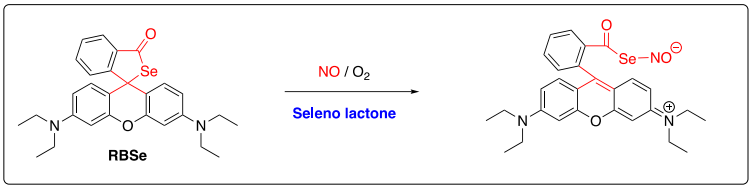

Figure 87. The fluorescent probe **RBSe** as an example of seleno lactone trigger for NO detection.[920]

Dihydropyridine oxidation has been used for detecting nitric oxide, as well as other ROS, including superoxide. In 2014, Li, He, and Gong developed a dihydropyridine trigger linked to a coumarin scaffold that showed reduced PeT quenching (λ_{ex} = 334 nm, λ_{em} = 450 nm) upon NO-mediated oxidation of the dihydropyridine to a pyridine and was used to image nitric oxide in LPS-treated RAW 264.7.[922] A water-soluble coumarin derivative was reported in 2016,[923] and a derivative with the dihydropyridine at an isomeric position on the coumarin was reported in 2020.[924] In 2016, Mahapatra used a dihydropyridine trigger on a pyrene fluorophore to make the ratiometric probe **Py-NO** (λ_{ex} = 346 nm, λ_{ex} = 393 nm / 439 nm) and on a triaryl amine fluorophore to make the ratiometric probe **TPA-NO** (λ_{ex} = 308 nm, λ_{ex} = 416 nm / 520 nm), which were used to image NO in Vero 76 cells (Figure 88).[925] In this study, they proposed a mechanism involving H-atom abstraction by nitric oxide, followed by *N*-nitrosation, and elimination of HNO to form the pyridine. In 2017, Li and Zhang used a fluorescein linked to a quenching group via a dihydropyridine linker in their probe **DHFPQ**.[926] NO-mediated oxidation to the dihydropyridine to the pyridine induced cleavage of the linker and quencher likely via a 1,6-elimination to increase fluorescence (λ_{ex} = 490 nm, λ_{em} = 525 nm) and the probe was used to image LPS-treated RAW 264.7 and nitric oxide in the hind leg of a mouse injected with Freund's adjuvant to induce inflammation. Lin and He reported the probe **Mito-DHP** (λ_{ex} = 470 nm, λ_{em} = 525 nm) in 2018 which consisted of a dihydropyridine trigger and triphenylphosphonium mitochondrial targeting group on a BODIPY scaffold that was used to image NO-treated HepG2 cells.[927]

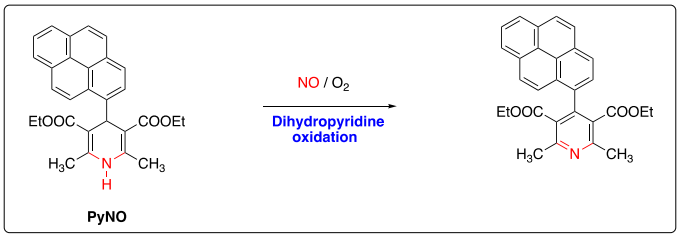

Figure 88. The fluorescent probe **PyNO** as an example of dihydropyridine oxidation trigger for NO detection.[925]

Ali developed a thiosemicarbazide trigger in 2017 that is converted to an oxadiazole via *S*-nitrosation followed by elimination of HSNO (Figure 89).[928] This trigger was mounted onto a quinoline fluorophore to make the fluorescence probe **QT$_{490}$** (λ_{ex} = 380 nm, λ_{em} = 490 nm) capable of imaging nitric oxide in LPS/IFN-γ treated RAW 264.7. This thiosemicarbazide trigger has also been installed on coumarin[929] and naphthalimide[930] scaffolds for nitric oxide imaging.

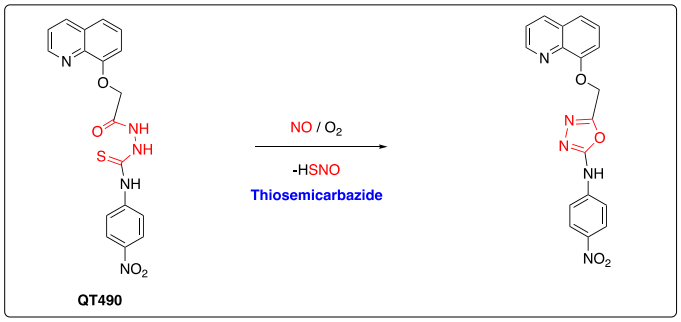

Figure 89. The fluorescent probe **QT$_{490}$** as an example of thiosemicarbazide trigger for NO detection.[928]

Ali also reported a series of probes using the conversion of an acyl hydrazine to a 1,3,4-oxatriazole on a quinoline (λ_{ex} = 380 nm, λ_{em} = 490 nm) (Figure 90)[931] or benzocoumarin (λ_{ex} = 410 nm, λ_{em} = 470 nm)[932] fluorophore for imaging LPS/IFN-γ treated RAW 264.7 macrophages.

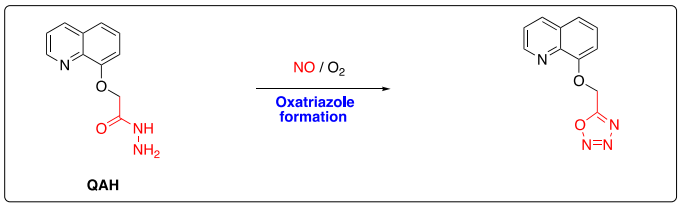

Figure 90. The fluorescent probe **QAH** as an example of oxatriazole formation trigger for NO detection.[931]

In 2022, Jenni, Renault, and Romieu described a covalent assembly approach for nitric oxide detection based on the NO-mediated conversion of a diaryl ether to form a phenoxazine with an increase in fluorescence emission (λ_{ex} = 685 nm, λ_{em} = 730 nm) (Figure 91).[933] Finally in 2023, Wu developed an alkene nitration of a dicyanostyryl pyran as a strategy for nitric oxide detection in the lysosome localizing probe **LysoNO-DCM** (λ_{ex} = 450 nm, λ_{em} = 633 nm) used to image nitric oxide in LPS treated RAW264.7 and zebrafish (Figure 92).[934] Table 4, Section 8 summarizes these and any other triggers for nitric oxide probes.

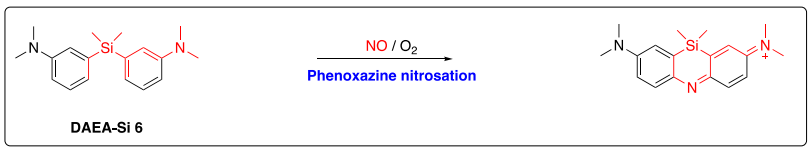

Figure 91. The fluorescent probe **DAEA-Si 6** as an example of phenoxazine covalent assembly trigger for NO detection.[933]

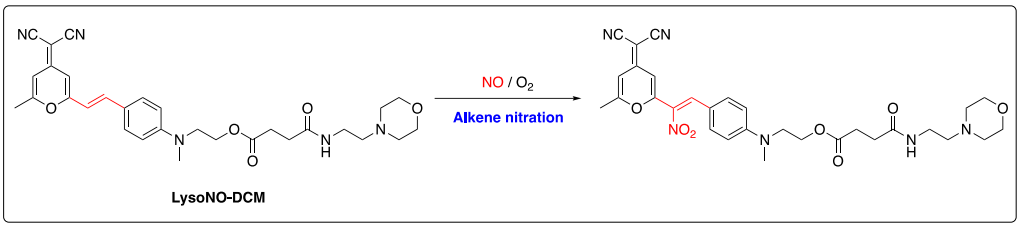

Figure 92. The fluorescent probe **LysoNO-DCM** as an example of alkene nitration trigger for NO detection.[934]

5.1.4 Concluding remarks for nitric oxide probes

Nitric oxide holds a venerable position in the family of reactive oxygen, nitrogen, and sulfur species as it was the first molecule to convince a skeptical scientific community that such toxic and reactive species could be critical to healthy physiological function. While Griess assays and ozone-based chemiluminescence are traditional core techniques for its measurement in biological systems, optical probes open opportunities to study nitric oxide in living cells and animals. Nitrosation of amines is by far the most common optical probe strategy, with *N*-nitrosation type 1 (*ortho*-phenylenediamine to triazole triggers)[750] dominating and *N*-nitrosation type 4 (forming stable *N*-nitroso adducts from secondary amines)[852] receiving increasing attention. Probes that operate via *N*-nitrosation strategies are commercially available from several companies, especially **DAF** and **DAR** derivatives, making them an easy option when looking for an NO probe to use in a biological experiment. However, the oxygen dependence and dehydroascorbate cross-reactivity of these *N*-nitrosation probes needs to be considered carefully, and a user should understand that they are really looking at nitrosation, likely by the NO product N_2O_3. Probes that yield an optical response directly from reaction with nitric oxide, like metal-based probes and spin traps, can overcome some of these challenges, although there are more limited commercially available options. The copper-based probes derived from Lippard's **CuFL** are the most used probes in this class.[887,890] Cross reactions between nitrite, HNO, and thiols should be kept in mind when using metal-based probes and using multiple probes that operate by disparate mechanisms can lead to increased confidence in the reliability of a measurement. Interesting designs for bioluminescence, photoacoustic, and SWIR are emerging, and it is expected that in the future well-validated luminescence probe tools will be available for measuring and imaging nitric oxide in a wide variety of biological contexts.

5.2 Peroxynitrite

5.2.1 Peroxynitrite in health and disease

It was not until nitric oxide (NO) was identified as the endothelium-derived relaxing factor (EDRF) that peroxynitrite ($ONOO^-$) and its conjugate acid, peroxynitrous acid (ONOOH), were recognized as potential biological oxidants. In 1990, Beckman showed that $ONOO^-$ formation occurs in biological systems through a diffusion-limited combination reaction between NO and superoxide, with a rate constant of 10^9 M^{-1} s^{-1}.[935] Once formed, $ONOO^-$ has a biological half-life of 5–20 ms, during which time it can diffuse 1–2 cell lengths from its formation site before degradation.[936] Despite its short lifespan, $ONOO^-$ has significant implications as both an oxidant and a nucleophile *in vivo*. As an oxidant, the redox potentials for the $ONOO^-/NO_2^\bullet$ and $ONOO^-/NO_2^-$ pairs have been measured at 1.4 and 1.2 V, respectively, at pH 7.[937] This suggests $ONOO^-$ is a strong one- and two-electron oxidant *in vivo*, with direct implications in mammalian metabolism. For example, in the citric acid cycle, $ONOO^-$ is implicated in the disassembly of [4Fe-4S] cluster-containing enzymes. The release of iron into the mitochondrial matrix can cause additional oxidative damage. Moreover, $ONOO^-$ can react with Complexes I and II of the electron transport chain and ATPase. Reaction with these components irreversibly knocks out protein function, disrupting cell homeostasis. Unable to function, the cell undergoes apoptosis, generating reactive species such as superoxide, which can produce more $ONOO^-$.[938,939]

While $ONOO^-$ production can adversely affect health, its production is essential to immune system function, acting as a cytotoxic effector of invading pathogens.[938] More concerning is the overproduction of $ONOO^-$ associated with specific disease states such as atherosclerosis, chronic arthritis, inflammatory bowel disease, cancer, and neurodegenerative diseases such as Alzheimer's. Determining the relative abundance of $ONOO^-$ *in vivo* may offer insight into disease progression. Thus, for the past three decades, the development of detection methods for $ONOO^-$ has been of great interest to scientists, though it has been difficult due to the species' short lifespan and high reactivity.

6.2.2 Classical detection techniques for peroxynitrite

As a nucleophile, a prominent biological reaction is between $ONOO^-$ and carbon dioxide (CO_2) to form nitrosoperoxocarboxylate ($ONOOCO_2^-$). $ONOOCO_2^-$ quickly undergoes homolysis to form carbonate radical ($CO_3^{\bullet-}$) and nitrogen dioxide radical ($NO_2^{\bullet}$). Another mechanism by which $ONOO^-$ degrades into secondary oxidants is through the reaction with transition metals of metalloproteins, to generate $NO_2^{\bullet}$. Additionally, ONOOH can directly undergo homolytic cleavage to generate hydroxyl radical ($^{\bullet}OH$) and $NO_2^{\bullet}$, though this is considered a minor pathway.[938] The indirect generation of secondary radicals by $ONOO^-$ and ONOOH underpins tyrosine nitration, a biomarker long used as an indicator of $ONOO^-$ generation *in vivo*. Since 1998, various methods have been developed to detect 3-nitrotyrosine including EPR spectroscopy, immunohistochemical assays, and LC-MS-MS.[940–943] Nitration of tyrosine residues has the potential to knockout enzyme function. An example of this, with significant implications, is the nitration of Tyr34 of the enzyme Mn-superoxide dismutase (Mn-SOD). Knockout of Mn-SOD function can directly promote further generation $ONOO^-$ *in vivo*, potentially creating a feedback loop.[939]

6.2.2 Peroxynitrite probes by trigger

Early probes (Table 5, Section 1)

The earliest use of a fluorescent probe for $ONOO^-$ was reported in 1994. The group demonstrated that dihydrorhodamine was oxidized to rhodamine 123, with low micromolar concentrations of $ONOO^-$.[944] The reaction is not inhibited by hydroxyl radical scavengers such as mannitol and dimethyl sulfoxide, nor by SOD. Only thiol-based scavengers and urate competitively inhibited the reaction.[944] Over the next decade, only two other probes were used for $ONOO^-$ detection. In 2002, Roychowdhury *et al.* showed that 4,5-diaminofluorescein diacetate (**DAF-2**), a probe initially used to detect nitric oxide, could react faster with $ONOO^-$ under the same cellular conditions. The group conceded, however, that 2,7-dihydrodichlorofluorescein diacetate (**DCFH-DA**) was slightly more sensitive *in vivo* and gave a more robust response to $ONOO^-$, making it a better option for imaging studies.[945] The DCF scaffold is widely used today in numerous fluorescent probes. Complexity in these early probes was minimal, consisting of pro-fluorophore scaffolds that undergo oxidization to re-establish conjugation and turn-on fluorescence. In 2006, Ueno *et al.* developed a series of probes called **NiSPY**. These BODIPY-based probes exploited the nitrosative potential of $ONOO^-$ that had been observed in tyrosine nitration. In the **NiSPY** series, fluorescence was quenched via an a-PET process, which could be disrupted upon radical nitrosation by $ONOO^-$ of a benzene moiety attached to the BODIPY scaffold. Since NO seldom performs aromatic nitrosation, this probe proved selective for high-energy $ONOO^-$.[946] While this study represents a seminal advance for peroxynitrite fluorescent probes, this nitration trigger has not been widely adopted likely because, under physiological conditions, the radical mechanism of $ONOO^-$ nitration is complex and, in some cases, leads to low chemical yields. Table 5, Section 1 summarizes these and other early probes for peroxynitrite.

Trifluoromethyl ketones (TFMK) (Table 5, Section 2)

In 2006, Yang *et al*. reported **HKGreen-1**, a probe that exploits the nucleophilic nature of $ONOO^-$. The group employed a DCFH scaffold substituted with an anisole-derived trifluoromethyl ketone (TFMK) trigger (Figure 93). In a manner analogous to Oxone™ ($KHSO_5$), $ONOO^-$ reacts with the strongly activated ketone to form a dioxirane intermediate. This reactive intermediate then oxidizes the anisole unit, initiating hydrolytic *O*-dearylation and opening the spirocycle to give the fluorescent DCF product. In its activated form, **HKGreen-1** exhibited a 7- to 8-fold fluorescent enhancement at 521 nm when treated with 15 equivalents of $ONOO^-$, with a quantum yield of 0.46. Additionally, selectivity studies showed only a 3-fold enhancement with hydroxyl radical, a 1-fold enhancement by H_2O_2, and no reaction with HOCl over 1 hour.[947] In subsequent work, Yang and colleagues developed **HKGreen-2** and **HKGreen-3** utilizing this same trigger, which focused on improving its dynamic range and sensitivity.[948,949]

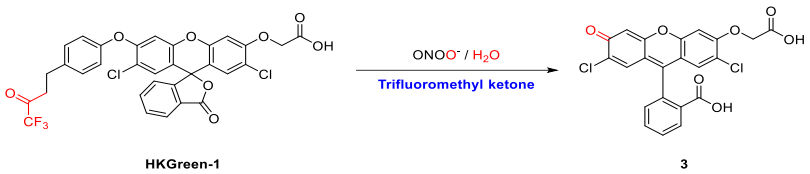

Figure 93. The fluorescent probe **HKGreen-1** as an example of trifluoromethyl ketone trigger for $ONOO^-$ detection.[947]

In an exciting application, Zhang *et al*. used a hemicyanine scaffold elaborated with a TFMK trigger.[950] In addition, a sulfonic acid group was included to aid in solubility. Upon reaction with $ONOO^-$, the probe emits at 712 nm with a 59-fold turn-on in fluorescence intensity. In addition, the hemicyanine fluorophore allowed the authors to perform photoacoustic (PA) imaging. This type of imaging is beneficial for animal studies because it offers a higher depth of tissue penetration, up to 5 cm. They utilized PA for imaging tumors in mice, where they could detect a PA signal around 680 nm when excited by a laser at the same wavelength. In addition to this, the authors determined a LOD of 53 nM for the probe and a rate constant of 1.49×10^3 $M^{-1}s^{-1}$ with $ONOO^-$. However, the authors did not provide a rate constant for reaction with other analytes. Instead, they performed a separate selectivity study, measuring the response to different analytes over 3 minutes. Another instance of the TFMK trigger in the literature was when Huang *et al.* built it onto a cyanine scaffold.[951] Overall, the studies described here have shown that the TFMK trigger has a low detection limit and can be applied to several different fluorescent scaffolds. Importantly, this trigger served as an inspiration for developing more complex carbonyl-based $ONOO^-$ probes. Table 5, Section 2 summarizes these and any other examples of probes containing this trigger.

Isatins and α-ketoamides (Table 5, Section 3)

Other carbonyl-based reactive motifs have shown selectivity for $ONOO^-$ over other ROS and RNS. In 2014, Lippert discovered that isatin, a small α-ketolactam, reacted rapidly and selectively with peroxynitrite to form a fluorescent anthranilic acid product.[952] The rate constant of the reaction of isatin with peroxynitrite was measured using a competition kinetics assay and later confirmed by stopped-flow fluorescence[157] to react with a second order rate constant of ~3×10^4 M^{-1} s^{-1}. In comparison, hydrogen peroxide reacts approximately 10,000,000 times slower with a rate constant of 3×10^{-3} M^{-1} s^{-1}, clearly demonstrating the selectivity of the trigger for hydrogen peroxide. In this study, a 5-fluoroisatin was used as an ^{19}F NMR probe to detect peroxynitrite produced in LPS stimulated A549 cells. In 2018, the same grouped used isatin as a reaction-based trigger for the chemiluminescent probe **PNCL** (Figure 94).[953] This was accomplished by tethering isatin via an ether linkage to a 1,2-dioxetane scaffold, yielding the probe **PNCL**. $ONOO^-$ mediates rapid ring opening of the α-ketolactam in **PNCL** to form an anthranilic acid intermediate that is followed by a slower 1,6-elimination to provide a rapidly responding and convenient

chemiluminescence signal with long-lived glow kinetics and green emission at 525 nm. **PNCL** boasts a detection limit of 6 nM towards $ONOO^-$ with a chemiluminescent output that was used to monitor $ONOO^-$ production in RAW 264.7 macrophages stimulated with LPS/IFN-γ as confirmed by MnTMPyP peroxynitrite scavenging and inhibition of nitric oxide synthase. **PNCL** was later used by Haimovitz-Friedman in 2019 to investigate the production of peroxynitrite in prostate cancer cells undergoing radiation therapy and showed that sildenafil could protect cells exposed to radiation by reducing peroxynitrite production.[954] In 2022, Lippert developed a kinetics-based approach as an innovative method for the real-time quantification of peroxynitrite fluxes using a deep understanding of reaction kinetics and the fluorescence response from isatin.[157] Rate constants between isatin and peroxynitrite were measured using stopped-flow fluorescence and an equation was derived using the kinetics information to convert the fluorescence response in arbitrary units into precise concentrations of peroxynitrite being generated from donor compounds like SIN-1 and Angeli's salt in a rare example of quantification of peroxynitrite using optical techniques. After the report of **PNCL**, isatin has been used as a trigger in several other small molecule probes throughout the years.[955–959]

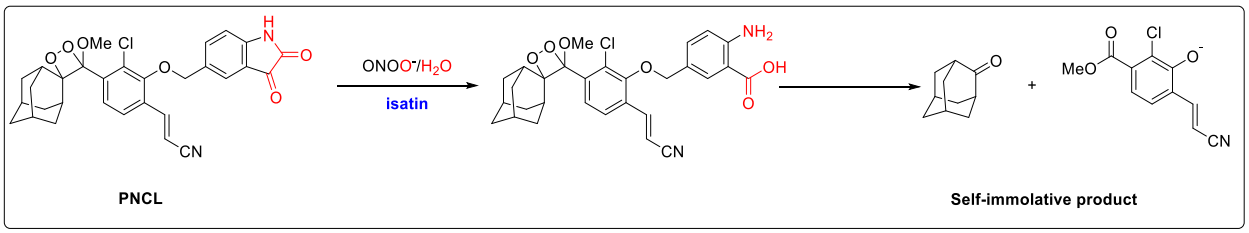

Figure 94. The chemiluminescent probe **PNCL** as an example of an isatin trigger for $ONOO^-$ detection.[953]

Acyclic α-ketoamides have also been used for peroxynitrite detection. Cheng *et al.* utilized a *para*-nitrophenyl α-ketoamides trigger in **Rhod-ONOO⁻** (Figure 95), a probe designed to investigate the drug-induced hepatotoxicity pathway. **Rhod-ONOO⁻** has a low detection limit of 43 nM and can operate in a two-photon imaging mode with two-photon excitation at 800 nm with emission at 558 nm.[543] Applying this probe to HepG2 cells, the group demonstrated that cells treated with 0–500 μM of acetaminophen (APAP) produced $ONOO^-$ in a concentration-dependent matter, consistent with previous reports in the literature. It should be noted that this α-ketoamide trigger has well-documented reactivity with hydrogen peroxide and there have been many examples of fluorescent probes for hydrogen peroxide that use the same trigger.[542–549] Detailed kinetic studies as have been performed for the isatin trigger could help shed light on the precise reactivity of acyclic α-ketoamides. Nonetheless, α-ketoamides have been used to investigate several diseases such as (DILI),[960–962] ischemic stroke,[956] sepsis-induced acute lung injury,[963] and Parkinson's disease.[964]

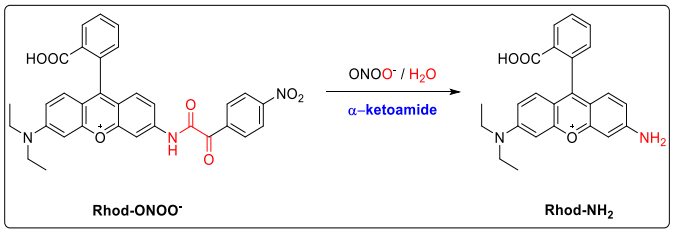

Figure 95. The fluorescent probe **Rhod-ONOO⁻** as an example of an α-ketoamide trigger for $ONOO^-$ detection.[543]

In general probes using the isatin and α-ketoamide trigger have low background fluorescence in cell imaging, owing to the combined effects of ICT and d-PeT imparted by α-ketoamides.[965] Mechanistically, $ONOO^-$ is believed to initiate an oxidative decarbonylation of the α-ketoamide, ultimately leading to the formation of a carboxylic acid and an aromatic amine. While the precise

mechanism has not been elucidated, similar chemistry has been studied in reactions between peroxynitrite and carbon dioxide as well as other carbonyl species.[966,967] These studies suggest a single electron decomposition of the initial adduct formed from nucleophilic addition of peroxynitrite with the carbonyl species. On the other hand, free radical scavengers had no effect in some cases,[953] suggesting that other mechanisms may be at play. Table 5, Section 3 summarizes these and any other examples of probes containing these triggers.

C=C bridge cleavage (Table 5, Section 4)

The nucleophilicity of $ONOO^-$ can also be exploited to cleave electron-deficient C=C double bonds and alter the conjugation of a system. Thus, these probes typically act through ICT and FRET mechanisms. The product distribution for these probes can vary depending on the overall assembly. In 2014, Hou *et al.* reported **C-Py-1**, a probe built off a coumarin scaffold conjugated to pyridinium, which disrupts the ICT process (Figure 96). The primary product of the reaction forms when $ONOO^-$ attacks the methine bridge connecting the coumarin and pyridinium. After this, NO_2^- is released, and an epoxide intermediate is formed, which continues to react and ultimately leaves a formyl group on both probe components. With ICT reestablished, the probe exhibits a colorimetric change from pink to yellow and a fluorescent response at 493 nm when excited at 365 nm. The intensity increase was 25-fold with $ONOO^-$ and 2–3-fold when exposed to S^{2-} and cysteine. More importantly, there was minimal response to H_2O_2 and HOCl, and low cytotoxicity was observed.[968]

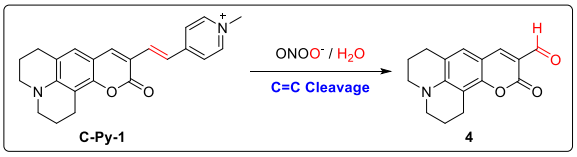

Figure 96. The fluorescent probe **C-Py-1** as an example of an C=C cleavage trigger for $ONOO^-$ detection.[968]

Zhou and colleagues employed a coumarin-indolium-derived scaffold to create **CHCN**, a probe that displays a sizeable ratiometric shift upon $ONOO^-$ reaction. This reaction is initiated when $ONOO^-$ attacks the C=N π^* of the indolium moiety. From here, rearrangement and hydrolysis of the methine bridge releases oxindole and formylated coumarin as the major products. This cleavage of this extended π-system resulted in a shift from 635 nm to 515 nm with 475 nm excitation. Moreover, they noted a 474-fold enhancement in fluorescent intensity ratio towards $ONOO^-$ compared to the less than 10-fold enhancement observed for other analytes under the same conditions. Their cell studies on RAW 264.7 cells also gave comparable results, with a blue shift only noticeable in cells undergoing a phagocytotic immune response.[969] These two studies demonstrate the ability to tune the selectivity of the C=C trigger to be more selective for $ONOO^-$. In addition, the trigger has proven versatile in various applications, such as subcellular localization. In 2018, Guo *et al.* made a lysosome targeting probe that could detect $ONOO^-$ and changes in lysosomal viscosity due to the TICT process in the unreacted probe.[970] Zhan *et al.* and Wang *et al.* created probes that could target mitochondria and the endoplasmic reticulum, respectively, to study idiopathic pulmonary fibrosis (IPF). In addition to the targeting functionality, these probes were both two-photon excitable, essential when working with dense lung tissues.[971,972] Finally, Feng *et al.* made a Golgi apparatus targeting probe to study DILI.[973] Table 5, Section 4 summarizes these and any other examples of probes containing these types of triggers.

Benzopyrylium ring opening (Table 5, Section 5)

The benzopyrylium-trigger, like the C=C bridge, relies on an electron-deficient π-bond as a recognition site for $ONOO^-$, and this trigger mechanism is the basis of two important ratiometric probes. Cheng and colleagues sought to design a FRET-based two-photon probe for imaging intracellular $ONOO^-$ with high sensitivity and selectivity. The group evaluated 19 different structures for their reactivity and fluorescent properties to do this. They identified two primary fluorophores—benzopyrylium and coumarin—as the primary scaffold and linked them through a piperazine unit. This resulted in the development of a mitochondria-targeted probe, **MITO-CC** (Figure 97). **MITO-CC** has a detection limit of 11.30 nM, giving a 5.8-fold enhancement in fluorescence ratio (F_{478}/F_{654}) with excitation at 420 nm in HepG2 and RAW 264.7 cells. It is important to note that HOCl gave a roughly 1.5-2-fold enhancement in these same studies. The group also demonstrated the probe's two-photon imaging ability by imaging inflamed hepatic tissue in mice.[974]

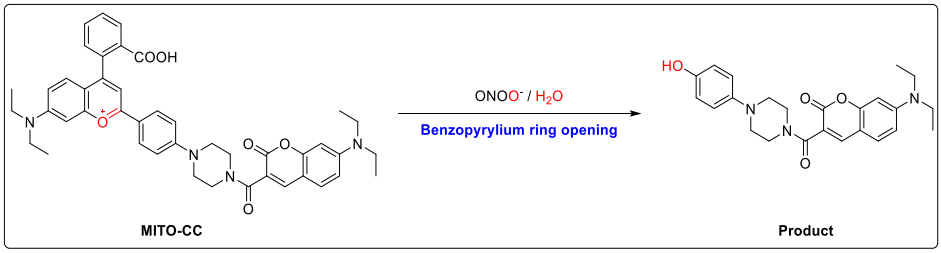

Figure 97. The fluorescent probe **MITO-CC** as an example of a benzopyrylium ring opening trigger for $ONOO^-$ detection.[974]

Inspired by the work of Cheng, Jiang *et al.* designed a probe that improved on the desirable features already present in **MITO-CC** by utilizing a similar scaffold. In **Gal-NIR**, the coumarin and benzopyrylium units are directly bound to each other, eliminating the piperazine spacer. Instead, the benzoic acid unit of the benzopyrylium was functionalized with galactose to incorporate hepatocyte-specific targeting. As a result of these modifications, the group showcased a probe with impressive fluorescent properties. **Gal-NIR** demonstrated a blue shift from 720 nm to 500 nm in cells treated with APAP with a 72-fold fluorescent enhancement. This huge fluorescence shift enhanced the signal-to-background ratio, increasing sensitivity in detecting $ONOO^-$. Similar APAP studies were performed in mice, showing that the probe was almost entirely localized in the liver, making this probe a valuable tool for understanding drug-induced hepatotoxicity better.[975] The benzopyrylium trigger has also been used to investigate DILI,[976–978] rheumatoid arthritis (RA),[979,980] and to monitor $ONOO^-$ and GSH redox cycles. However, the trigger is not exceptionally selective for $ONOO^-$ over other analytes. Table 5, Section 5 summarizes these and any other examples of probes containing this trigger.

Arylboronate oxidation (Table 5, Section 6)

Arylboronate triggers are the most widely used motif applied in the detection of H_2O_2, HOCl, and $ONOO^-$. Studies by Sikora *et al.* established that some arylboronates can react with $ONOO^-$ with a rate constant of 10^6 $M^{-1}s^{-1}$, which is 200 times faster than the reaction with HOCl, and 1 million times faster than with H_2O_2.[981] Later work by Zielonka *et al.* also confirmed that $ONOO^-$ did not generate 100% phenolic product like HOCl and H_2O_2 did. Instead, 15–20% of the products formed were radical-derived, which is advantageous in confirming the detected species.[982] Zielonka *et al.* created coumarin-7-boronic acid (**CBA**) and coumarin-7-pinacol boronate (**CBE**), the first arylboronate-based probes used to react with $ONOO^-$ (Figure 98). The group also demonstrated that even under conditions where HOCl and H_2O_2 are present, arylboronates preferentially respond with $ONOO^-$.[983] **CBA** is an important demonstration of employing arylboronate triggers

for sensing $ONOO^-$ and benefits from detailed kinetic studies to gain deep understanding of the probe's selectivity.

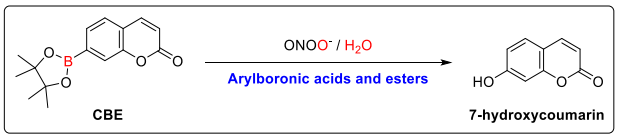

Figure 98. The fluorescent probe **CBE** as an example of a boronic acid trigger for $ONOO^-$ detection.[983]

Building off work from Zielonka, Shu *et al*. designed **MBTBE**, a probe consisting of a benzothiazolium fluorophore and phenylboronic ester trigger, with a detection limit of 16 nM $ONOO^-$. Upon oxidation of the boronate ester to the phenolate, the probe exhibits a yellow fluorescence at 569 nm. **MBTBE** was used to image HeLa cells. In these studies, the group showed that the probe localizes mitochondria and that H_2S is an effective scavenger of $ONOO^-$. This corroborates previous findings showing that patients with Alzheimer's disease exhibit lower levels of H_2S in the brain and elevated levels of $ONOO^-$.[984]

Arylboronates are frequently employed as a trigger to initiate reaction cascades as well. An example of this is **DDAO-PN**, designed by Wang *et al.* This probe features an acridine scaffold functionalized with an arylboronate ester trigger. The probe was built to avoid non-specific oxidation by $ONOO^-$, which could destroy fluorescence while maintaining a high selectivity for the analyte and a robust fluorescent response. The cascade starts with the oxidative conversion of the boronate moiety to phenolate. Following this, a 1,6-elimination ensues, cleaving the aryl ether bond between the trigger and fluorophore, triggering a fluorescent response at 657 nm. The probe shows an 84-fold fluorescence enhancement after 30 seconds *in vitro*. For comparison, the probe only showed a 7.5-fold fluorescence enhancement over 30 minutes when exposed to H_2O_2 under the same conditions. In cell studies, a 68-fold enhancement was observed upon exposure to LPS, as well as a 4- to 8-fold fluorescence enhancement in an inflamed mouse model.[985]

A handful of probes have incorporated an additional reaction into this cascade by including an acrylonitrile or malonitrile group *ortho* to where the 1,6-elimination terminates. Following the termination to phenolate, a further reaction occurs with the nitrile group, causing an iminocoumarin to form.[986–989] Most recently, Sang *et al*. reported **CNN2-B**, a "dual-lock" probe explicitly designed for imaging atherosclerotic plaques. The probe boasts a low LOD towards $ONOO^-$ of 1.33 nM, with a fluorescent response at 486 nm. Moreover, **CNN2-B** changes its distribution before and after oxidation. Before reaction with $ONOO^-$, **CNN2-B** localizes in the mitochondria of A549 and RAW 264.7 cells. Upon reaction of the probe with $ONOO^-$ to generate **CNN2**, not only was there a fluorescent enhancement factor (F/F_0) of 365, but **CNN2** relocated into lipid droplets. In addition, selectivity studies performed over 250 minutes demonstrated that the probe had a 3-fold lower response to H_2O_2 and HOCl than $ONOO^-$.[989] With a strong fluorescent response, high selectivity, sensitivity, and ability to specifically detect atherosclerotic plaques, **CNN2-B** is a valuable tool for studying atherosclerotic-related diseases. The tunability and versatility of arylboronates have made them a prevalent choice of trigger for fluorescent $ONOO^-$ probes. Researchers have exploited this trigger in a variety of ways, such as in AND-logic gates,[990,991] $ONOO^-$-mediated drug release,[992] in the study of a plethora of other disease states,[993–1006] and some emerging probes have tried to push the selectivity further.[1007] Table 5, Section 6 summarizes these and any other examples of probes containing this trigger.

Diphenyl phosphinate (Table 5, Section 7)

Diphenyl phosphinates (DPP) are a relatively new trigger mechanism applied to sensing $ONOO^-$ in biological systems. Mulay *et al.* were the first to utilize this trigger on a chromene scaffold (Figure 99).[1008] The response mechanism of the trigger to $ONOO^-$ was first corroborated by Huihui *et al.* in 2021 and has been employed in probes in ways analogous to arylboronates. $ONOO^-$ attacks at π^* of the P=O bond, and subsequent electron rearrangement causes the release of the phosphinate moiety, forming a phenolate on the scaffold.[1009] The formation of phenolate can be the end product or coupled to a 1,6-elimination to form iminocoumarins, much like with the arylboronate trigger.[1009,1010]

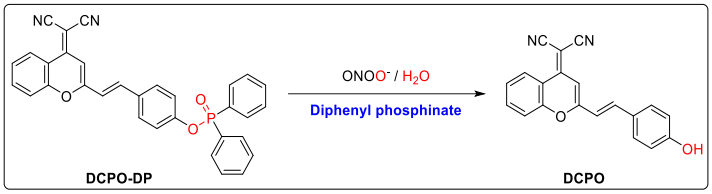

Figure 99. The fluorescent probe **DCPO-DP** as an example of a diphenyl phosphinate trigger for $ONOO^-$ detection.[1008]

In 2018, Yongquan Wu and colleagues were the first to use the diphenyl phosphinate moiety in an ICT-based probe. Their probe, **NOF2**, consisted of a xanthene scaffold functionalized with the diphenyl phosphinate moiety through a benzene spacer. Their primary motivation behind the probe was to reduce background autofluorescence by moving the operational wavelengths of the probe further into the infrared region. NIR operation is a desirable feature for probes because it helps boost the signal-to-noise ratio (SNR) in vivo, and the lower energy light helps avoid cell damage. Before its reaction with $ONOO^-$ reaction, **NOF2** exhibits a strong absorbance band centered at 556 nm. Following the reaction, this absorption band redshifts to 670 nm, and fluorescent is enhanced 10-fold at 742 nm, well into the NIR region. In RAW 264.7 cell studies, this response remained strong with a 6-fold enhancement at 742 nm. However, no measurable response was observed in cells treated with HOCl and H_2O_2 over 30 and 10 minutes, respectively. To further demonstrate the probe's utility *in vivo*, they performed a study on inflamed mice, showing the increased SNR and improved sensitivity of 400 nM. Since **NOF2**, many improvements have been made to the sensitivity of the DPP moiety, making it a popular trigger.[1010–1017] Moreover, the trigger has also been used in the design of colorimetric probes,[1011,1012] dual-analyte sensors,[1018–1020] and to study the pathology of $ONOO^-$ in disease.[1001,1016,1021,1022] One avenue that has not been investigated is the kinetics of the reaction of various analytes with this trigger moiety. Such studies would give significant credence to its use as an $ONOO^-$ detection strategy, especially given that this trigger has also been extensively used for the detection of superoxide.[317–331] Table 5, Section 7 summarizes these and any other examples of probes containing this trigger.

The triggers discussed thus far have relied on the nucleophilicity or "pro-oxidant" behavior of $ONOO^-$. These comprise the bulk of the trigger mechanism employed for $ONOO^-$ detection in luminescent probes. Currently, three additional trigger moieties are believed to rely on the direct oxidative potential of $ONOO^-$ and ONOOH. These include aryl chalcogenides, hydrazide spirocycles, and *p*-aminophenols.

Aryl chalcogenides (Table 5, Section 8)
As soft bases with high-lying HOMOs, late chalcogens are excellent fluorescence quenchers via a PET process. It is speculated the high-lying HOMO may also underpin the response mechanism of chalcogenides towards $ONOO^-$.[1023] The high energy lone-pair of the chalcogen reacts with the σ^* of the O—O bond on ONOO/ONOOH, removing O or OH and releasing NO_2^-. Next, a simple

electron rearrangement transforms the chalcogenide into a chalcogenoxide, lowering the energy and blocking the PET process. In 2011, Yu and Li *et al*. built an aryl selenide trigger onto a cyanine scaffold (Figure 100). This scaffold benefited significantly from a NIR excitation and emission wavelength of 758 nm and 775 nm, respectively. Thus, it could avoid autofluorescence problems typically arising from probes operating in the lower wavelength region. Upon conversion of selenide to selenoxide by 10 μM $ONOO^-$, a 23.3-fold fluorescent increase was observed over 60 minutes under physiological conditions. The group also employed other analytes to gauge the reactivity of the probe. Of these analytes, a treatment with 100 μM nitric oxide, 200 μM H_2O_2, and 200 μM hydroxyl radical were the only ones to give a fluorescent response. While there was a response during this time, it was 10-fold lower than what was observed with $ONOO^-$ at a much lower concentration. Using RAW 264.7 cells, the group was also able to monitor the redox cycle of the probe with oxidation by $ONOO^-$ and selenoxide reduction with GSH through several cycles.[1024] The group expanded on this work using tellurium in 2013 with **Cy-NTe**, and the same concept has been employed with sulfur; however, it is essential to note that sulfides are much more prone to HOCl oxidation.[1025–1028] Overall, the selenide motif is the primary variant used.[1029–1031]

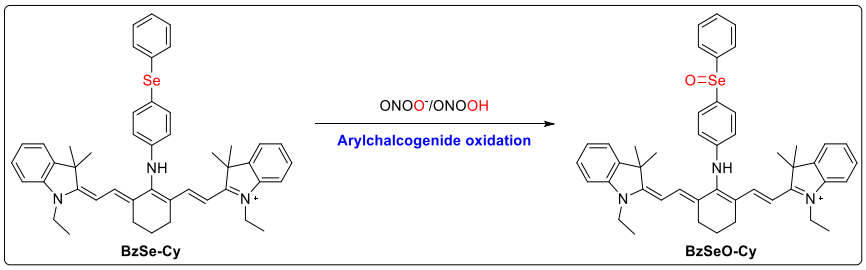

Figure 100. The fluorescent probe **BzSe-Cy** as an example of a arylchalcogenide trigger for $ONOO^-$ detection.[1024]

The primary advantage seen with the chalcogenide trigger is the lower background fluorescence observed in the various probes. While these triggers may react preferentially with $ONOO^-$ over other ROS and RNS, they can still act as strong nucleophiles and ligands. In a much more complex biological environment, these triggers could readily coordinate with metal centers and facilitate the oxidation of various biomolecules. Table 5, Section 8 summarizes these and any other examples of probes containing these types of triggers.

p-Phenols and p-aminophenols (Table 5, Section 9)

The *p*-aminophenol moiety was derived from previous work by the Nagano group, incorporating a *p*-hydroxy anisole moiety onto a xanthene scaffold. The two probes, **APF** and **HPF**, came out of this study as tools for the detection of HOCl, $ONOO^-$, and hydroxyl radical and are commercially available today, although they must be used with the understanding that they do not perfectly discriminate between these three species.[1032–1034] The Yang group was the first to improve on this trigger with **HKGreen-4** (Figure 102), which incorporated a *p*-hydroxyaniline trigger onto a rhodamine scaffold, showing enhanced selectivity for $ONOO^-$.[1035] The mechanism by which this trigger responds to $ONOO^-$ remains somewhat elusive, with a consensus of a “two-electron” oxidation facilitated by $ONOO^-$.

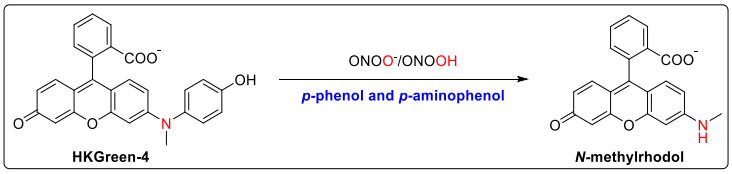

Figure 101. The fluorescent probe **HKGreen-4** as an example of a *p*-aminophenol trigger for $ONOO^-$ detection.[1035]

Li and Tao *et al.* sought to design a probe for utilization in imaging brain vasculature with high temporal and spatial resolution. Their probe, **NP3**, is built on a benzothiazole scaffold linked to a hydroxyphenyl group. This scaffold expresses intense fluorescence at 470 nm, owing to the ESIPT process between the hydroxyl and nitrogen of thiazole. This process was interrupted by installing *N*-methyl-*p*-hydroxyaniline at the hydroxyl group, quenching the fluorescence of the probe. The probe also benefited from being two-photon excitable, which, as mentioned previously, minimizes cell damage during imaging. Preliminary characterization demonstrated that **NP3** is highly sensitive towards $ONOO^-$ (LOD = 5 nM) while retaining significant selectivity in a 30-minute selectivity study over HOCl, H_2O_2, and hydroxyl radical. Even when applied to a much more complex environment in cells and animals, **NP3** demonstrated additional valuable characteristics. For one, it was virtually non-cytotoxic towards endothelial cells up to 100 μM, which is a much higher concentration than what would be used in practice. Moreover, **NP3** was introduced to mice intravenously through the tail. Following a brief incubation period, a neurovascular brain injury was simulated using both Rose bengal to induce an occlusion and laser irradiation to induce microvessel rupture. A fluorescent response was detected in both cases in 10–30 seconds. Other than showing the ability of **NP3** to selectively detect $ONOO^-$ in a brain injury model, these experiments also showed **NP3**'s ability to cross the blood-brain barrier.[1036] **NP3** was only the second $ONOO^-$ probe to utilize the *p*-aminophenol moiety and yet demonstrated profound efficacy in neurovascular imaging. Subsequent publications have also applied this trigger to monitor drug-induced liver injury and Parkinson's disease progression utilizing different fluorescent scaffolds.[1037–1039] Additionally, subcellular targeting functionality has been incorporated into several probes using this trigger.[1040–1045] Table 5, Section 9 summarizes these and any other examples of probes containing these types of triggers.

Hydrazide spirocycles (Table 5, Section 10)

Ambikapathi and colleagues were the first to employ the hydrazide trigger in 2013 in their Rhodamine B phenyl hydrazide (**RBPH**) design (Figure 102). Their early experiments arrived at a detection limit of 1.4 nM and showed minimal reaction with other common analytes.[1046] The mechanism of detection of hydrazide consists of two components: oxidation of the hydrazide followed by hydrolysis to form a carboxylic acid and reestablish aromaticity in the primary scaffold.[1023] This trigger moiety benefits from fluorescence not just being quenched but completely turned off due to lack of π-conjugation, eliminating background fluorescence.

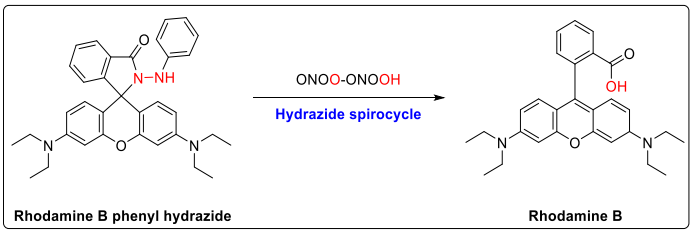

Figure 102. The fluorescent probe **Rhodamine B phenyl hydrazide** as an example of a hydrazide spirocycle trigger for $ONOO^-$ detection.[1046]

Chen *et al.* sought to design a ratiometric probe for quantitative analysis of arginine metabolism in macrophages. Specifically, they wanted to look at M1 and M2 macrophages, which are implicated in the progression and regression of atherosclerosis, respectively. By studying these macrophages in atherosclerotic mice, they hoped to draw a link between the prevalence of $ONOO^-$ and arginase 1 activity. They built their probe, **P2**, on a Rhodamine B hydrazide scaffold as the energy acceptor and tethered this to a quinoline derivative as the energy donor. Before

$ONOO^-$ exposure, the probe can be excited at both 405 nm and 800 nm and emit at 474 nm. After reaction with 10 μM $ONOO^-$, the aromaticity of the rhodamine scaffold was re-established, allowing energy transfer from the quinoline and shifting emission to 575 nm, with a fluorescent enhancement ratio of 0.23 to 63. Other analytes gave a minuscule fluorescent increase, which was deemed negligible during the time frame of the experiment. Applying this probe to living cells and mice, they were able to draw an inverse relationship between $ONOO^-$ production and arginase 1. During the progression of atherosclerosis, they noted the accumulation of M1 macrophage, which primarily expresses iNOS, and an increase in $ONOO^-$ production as well as down-regulation of arginase 1. Conversely, during regression, the M2 macrophage phenotype emerged, which expresses arginase 1 more than iNOS, which caused a decrease in $ONOO^-$ production. The rationale for this observation is that arginase 1 competes with iNOS for L-arginine. Thus, when it is upregulated, more arginine can convert into L-ornithine instead of nitric oxide. This provides substantial evidence to the idea that arginase is a significant regulator of $ONOO^-$ *in vivo*. **P2** is an impressive deployment of the hydrazide moiety and may be a powerful tool in the investigation of inflammatory diseases.[1047] This is among the most impressive applications of the hydrazide spirocycle trigger, though it has also been used to target specific organelles and track various diseases, including mitophagy specifically.[1048–1054] This probe offers a best-case scenario for imaging experiments because fluorescence is almost entirely off until a reaction occurs. Table 5, Section 10 summarizes these and any other examples of probes containing this trigger.

N-oxidation (Table 5, Section 11)

This next trigger has taken on a range of different forms, but ultimately exploits the oxidative power of $ONOO^-$ against electron rich amino groups. Regardless of probe, the *N*-oxidation mechanism begins with oxidative addition to an amino group. For example, the probe **SiRTA** (Figure 103) created by Miao and colleagues in 2018 uses this approach. **SiRTA** was built using an Si-rhodamine scaffold functionalized with methoxyaniline. In the probe methoxyaniline both quenches fluorescence through a PeT mechanism and acts as the trigger. The response mechanism is proposed to consist of three parts: oxidation of aniline, hydrolysis, and electrophilic nitrosation. Upon nitrosation, the PeT process is disrupted triggering a fluorescent response at 680 nm under 650 nm excitation. **SiRTA** boasts an exceptional detection limit of 3.0 nM with peak intensity being reached within 20 seconds of $ONOO^-$ exposure. **SiRTA** was used by the group to study ischemia-reperfusion in EA.hy926 endothelial cells as well as diabetic nephropathy in the pancreatic β-cells of diabetic rats.[1055] Owing to the NIR spectral properties of **SiRTA** the probe proved effective in live cell imaging and showed reasonable selectivity for $ONOO^-$. The authors cite their previous work utilizing an identical trigger applied to a BODIPY scaffold, in which the only product obtained was an *N*-oxide product.[1041] Other author's also report *N*-oxide as the major product of oxidative addition in their probes.[1056–1058] **SiRTA** is thus unique in its major product distribution. The authors associate this alternative product with improved activation energy owing to the Si-rhodamine scaffold.[1055] While for these probes *N*-nitroso or *N*-oxide are the final products, for others, this may just be the first step in a larger cascade.

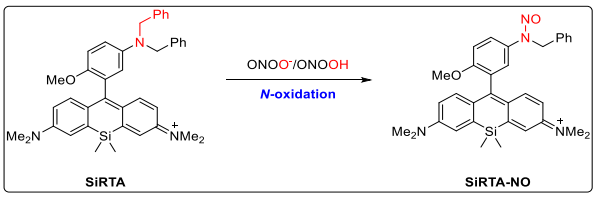

Figure 103. The fluorescent probe **SiRTA** as an example of *N*-oxidation for $ONOO^-$ detection.[1055]

A "π-extending" cascade to "turn-on" or change fluorescence is another strategy to detect $ONOO^-$.[944,1059] Of these probes **PN_{600}** (Figure 104), developed by Quanjuan Zhang and colleagues, is worth highlighting for its peculiarity. **PN_{600}** is built using a coumarin scaffold, substituted with a primary amine such that resorufin is obtained following an *N*-oxidation-initiated cascade. Upon initial exposure to $ONOO^-$ **PN_{600}** is cyclized to intermediate, **1**. This causes a bathochromic shift in both excitation and emission wavelength from 355 to 475 and 525 to 585, respectively. With continued exposure to $ONOO^-$, **1** is then oxidized again to **2**, a resorufin derivative. In this final form excitation wavelength is shifted to 576 nm and emission to 595 nm. Mechanistically **PN_{600}** is impressive, but what is more is its ability to differentiate between HOCl and $ONOO^-$. The authors found that **1** could be obtained by reaction with both species. However, further oxidation to **2** could only be accomplished by $ONOO^-$ even upon addition of 30 equivalents of HOCl. Furthermore, **PN_{600}** showed minimal response towards other competing analytes and was successfully applied to the imaging of human glioma cells.[1060] Other applications of this *N*-oxidation and aromatization scheme are much simpler, involving the oxidation of dihydro-rhodamines or Si-rhodamines. Currently it is proposed that an amino group is activated to an *N*-hydroxyl by $ONOO^-$ which acts as a leaving group for subsequent elimination, which reestablishes fluorescence.[1054,1056–1059] Table 5, Section 11 summarizes these and any other examples of probes containing these types of triggers.

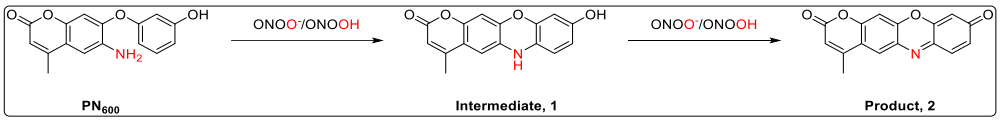

Figure 104. The fluorescent probe **PN_{600}** as an example of *N*-oxidation for $ONOO^-$ detection.[1060]

C=N bond cleavage (Table 5, Section 12)

The C=N trigger moiety is not as often used in the field of reactive species probes but is worth mentioning for its unique quenching mechanism. Under aqueous conditions, the C=N isomerization promotes nonradiative decay excited states, consequently blocking fluorescence. Prior to its adoption as a reactive species probe, it was most frequently used to detect metal ions through a complex mechanism which blocks isomerization.[1065] In 2018, Shen *et al.* adopted the trigger to detect peroxynitrite in their probe **BTP** (Figure 105). Beyond $ONOO^-$ acting as a nucleophile, the exact mechanism of reaction with the C=N trigger has not been confirmed. In the case of **BTP**, the C=N bond of a hydrazonylpyridine moiety is hydrolyzed to an aldehyde, which in turn re-establishes fluorescence. **BTP** responded to $ONOO^-$ in 60 seconds producing a 40-fold increase in fluorescence at 524 nm under 433 nm excitation. In addition, **BTP** had a detection limit of 58 nM, minimal response towards competing analytes, and was successfully used in HeLa cells.[1066] The C=N trigger has only been used in a handful of other $ONOO^-$ probes. Work by Wang *et al.,* and Wang *et al.,* demonstrated the AIE mechanism resulting from the C=N bond, which can be exploited for the dual detection of viscosity much like the C=C trigger.[1067,1068] Meanwhile, Liu *et al.* designed the probe **L-1** which displayed innate mitochondria targeting ability.[1069] All of these probes benefit from a simple design applicable to any fluorescent scaffold, as well as nanomolar detection limits for $ONOO^-$. With that said, the trigger has likely not been widely adopted because of their interaction with metal ions *in vivo* which could result in false positives. Moreover, the typical response time is around a minute for these probes, which is much slower than probes utilizing other triggers. Table 5, Section 12 summarizes these and any other examples of probes containing these types of triggers.

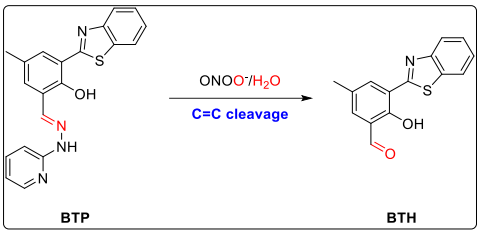

Figure 105. The fluorescent probe **BTP** as an example of *C=N cleavage* for $ONOO^-$ detection.[1066]

Other triggers (Table 5, Section 13)

There are a handful of other triggers which have been employed over the years. In 2019, Xie et al reported a series of probes called **FPP-Blue, Green, Yellow,** and **Red** by applying an aryl formamide trigger onto a range of commercially available fluorescent scaffolds. In response to $ONOO^-$, these probes undergo deformylation to liberate CO_2 and a primary amine, which activates fluorescence. This work demonstrated a facile, versatile, and efficient method of achieving a $ONOO^-$ probes with good selectivity.[1070] Mechanistically similar probes also used aryl formates and triflates,[312] aryl amides,[1071] and aryl esters.[1072–1074]

There are a few other probes that exploit the reactivity of carbonyl species. For example, Yang *et al*. and Sun *et al.* designed two diketone probes that are reminiscent of α-ketoamides, and exploit the nucleophilicity of $ONOO^-$.[1075,1076] In 2021 and 2022, Xie *et al.* designed two probes **BTNPO** and **NATP,** which used an oxindole trigger for detection through a joint decarbonylation and decarboxylation mechanism. The group used these probes to image amyloid-β plaques using two-photon imaging. With these probes, they were able to show that $ONOO^-$ production and Aβ aggregation mutually exacerbate one another.[1077,1078]

Deprotonation is an obscure mechanism that has been used in a few probes to primarily sense changes in $ONOO^-$ concentration.[1079] This mechanism has also been combined with silyl-ether bond cleavage for two probes by Lu *et al*. and Zhuo *et al.*. These groups combined these triggers to design concentration dependent ratiometric probes, which operated through a combined effort of ESIPT, TBET, and ICT mechanisms.[1080,1081] This deprotonation method can also be seen in the iridium based probe by Wu and Liao *et al*., which used a hydroquinone trigger to monitor $ONOO^-$ and GSH redox cycles.[1082] Another less common trigger is 1,4-oxazepine that was used by Zhang and Xu *et al.*in their probe **ON-RB**.[1083] Table 5, Section 13 summarizes these and examples of probes that operate by other types of triggers not covered in the other sections.

6.2.4 Concluding remarks for peroxynitrite probes

Several trigger mechanisms have been employed in the design of reaction-based probes for peroxynitrite ($ONOO^-$). Many of the same moieties used for selective $ONOO^-$ detection are similarly employed for hydrogen peroxide (H_2O_2), hypochlorous acid (HOCl), and superoxide (O_2^-) detection. This includes boronate esters,[1084] electron deficient C=C bonds,[969,1085] phosphinate esters, and late chalcogen-based triggers.[1024–1026,1086,1087] This can be problematic because of the comparable and higher abundance of HOCl and H_2O_2, respectively, in biological systems compared to peroxynitrite.[1088–1090] Thus, it should be best practice to include kinetic data when reporting $ONOO^-$ probes. This allows one to compare reaction rates of different analytes which gives a sense of the timeframe in which a fluorescent response indicates the presence of $ONOO^-$ specifically. With that said, kinetic experiments involving $ONOO^-$ are challenging to perform because of their short lifetime under physiological conditions, which necessitates specialized equipment, such as stopped-flow spectrometers, for accurate measurements. Due to this barrier, most probes reported in the literature lack kinetic data on the reaction with $ONOO^-$ versus other

analytes. We do note here, however, that competition kinetics studies can be performed using the known reaction rate with glutathione,[952] and these have been benchmarked versus stopped-flow experiments to show they give similar results.[953] This does not diminish the efforts put towards the design of $ONOO^-$ probes over the years, but rather, this means claims of selectivity should be caveated. Most probes we will discuss will employ simple selectivity studies where a probe's response to different analytes over a given time frame is measured. These experiments are run anywhere from five minutes to sixty minutes. In general, it is best practice to let these experiments run for as long as possible, and preferably to determine rate constants, to give more support to claims of selectivity.

7. Discussion

In the previous sections, we have given a thorough overview of the strategies used to develop small molecule probes for reactive oxygen and nitrogen species, including trigger types, molecular scaffolds, imaging modalities, and biological experiments/questions that can be addressed using these tools. In this section, the authors will provide their insights as to what the field is doing well and what could be improved.

What is the field doing well? First, the field of luminescent probes for reactive oxygen and nitrogen species provides an excellent training ground for young scientists. Successful probe development requires a wide range and depth of technical skills including multi-step organic synthesis, advanced spectroscopic characterization techniques, analytical expertise, cell biology, biochemistry, and kinetics. In some cases, students will learn to operate advanced imaging instrumentation and learn to work safely and ethically with live animal models. Second, the field has generated a sea of new knowledge around luminophore design. An enormous library of molecular structures has been investigated with characterization of emission/excitation wavelengths and quantum yields. Interesting photophysical processes, including FRET, ICT, PeT, ESIPT, and others can now be masterfully harnessed to design molecular systems with predictable and tunable photophysical properties. Additionally, these luminescent molecules have been characterized in cellular and animal models and extensive information regarding their toxicity, uptake, subcellular localization, and pharmacokinetics are now known in the literature. Chemical studies of luminescent probes for reactive oxygen and nitrogen species have revealed new understanding on the reactivity of these species with a wide range of functional groups that can be used not only as reaction-based triggers, but in other types of chemical processes. The selectivity of the probes provides useful data and the information gained from probes that have less than perfect selectivity is often more useful than probes that are presented as 100% selective. The probes' operation in cellular systems also gives information on the biorthogonality of these functional groups. Lastly, the field has generated new knowledge on the roles of reactive oxygen and nitrogen species in biological systems, and while there are significant caveats concerning selectivity and sensitivity, there are certain model systems that have been reproduced in numerous labs with different probes that give a high degree of confidence in the production of reactive oxygen and nitrogen species in these model systems. More broadly, the knowledge gained in luminescent probe design can be extended to many other fields, including 3D printing, 2D and 3D optical displays, photoactivatable materials, photothermal agents, and light harvesting for energy applications.[1091–1095]

What can be improved? As has been outlined in previous reviews,[1096] the field would be well-served by more rigorous and standardized analytical practices. First and foremost, detailed methods for all experiments should be included in a publication, including *in vitro* characterization of response and selectivity, details for cellular imaging experiments, and protocols for animal imaging. Limits of detection should be determined using the $3\sigma/k$ method, where the standard deviation of a blank/vehicle control sample is rigorously determined with at least 3 completely

independent experiments. The calibration curve should be constructed within the range of the limit of detection, and it should be determined as 3 times the standard deviation of the blank divided by the slope of this linear curve. In general, each measurement should be the average of 3 independent experiments, and this is particularly important for cellular and animal studies where there can often be large variability between experiments. The number and type of replicates should be clearly indicated in the figure caption and methods section. Methods for quantification of images in cellular experiments should be clearly described to ensure reproducibility. Additionally, reporting on the stability of a given probe when stored as aliquots or in an organic solvent/buffer aids in reproducibility. The core design principle of most luminescent probes is the reaction-based trigger. Determining rate constants and showing full kinetic traces in selectivity studies would drastically improve our understanding of how each probe reacts and what is being measured in each biological experiment. Physical organic mechanistic studies are very rarely performed during probe design, but these could shine considerable light on the function of a given probe. We believe that following these recommendations will lead to more robust probe designs for better interlab reproducibility and adoption by non-experts.

8. Conclusions and future directions

The field of small molecule probes for reactive oxygen and nitrogen species is vast, even when limiting the scope of analytes. In most cases, the best results in using a newly developed probe are obtained when they are used in the same hands as those who developed them. Use by non-chemist biologists is still relatively limited for several reasons. Many of the advanced luminescent probes for reactive oxygen and nitrogen species are synthetically challenging to obtain and not commercially available. Additionally, the stability of the probes can be uncertain (and are rarely measured, as discussed above) and proper use may require advanced instrumentation and protocols. Hence, biological investigations with these probes usually occur in the lab of the developers or require active collaborations to be established to navigate these issues. Following some of the recommendations above may render some of the probes more commercially viable for non-expert use. Another critical need in the field is the ability to quantify reactive oxygen and nitrogen species using luminescence probes. Most methods to date provide relative measurements to show that more or less of the reactive oxygen or nitrogen species is present in each biological environment compared to another. Specific quantification of reactive oxygen or nitrogen species concentrations could provide critical insight into their roles. For reversible probes, ratiometric approaches could be calibrated to give a good quantitative estimate and this has been achieved for a protein-based probe HyPer,[1097] but designing probes that provide a high enough signal when the reaction is reversible is a considerable challenge. End-point dosimetry is possible, although this loses much of the spatial and temporal resolution that luminescent probes boast as an advantage. Recent kinetics-based approaches have been shown to be capable of real-time quantification of fluxes of reactive nitrogen and oxygen species,[42,49,157] but only semi-quantitative methods have been achieved *in vivo*.[42,49] Developing these types of methods require very careful, robust, and reproducible methods – researchers need to be very transparent, with all assumptions clearly stated as these are being developed.

Where is the field going? Thorough review of the literature has revealed several emerging trends in the field of luminescent probes for reactive oxygen and nitrogen species. First, new imaging modalities are emerging that are well suited for the types of luminescent probe design discussed in this review. Chemiluminescence and bioluminescence offer exciting opportunities for low background imaging and the demonstrations that sterically stabilized 1,2-dioxetanes could be used for *in vivo* imaging of reactive species has led to an explosion of interest in this area.[98–100] Related to this is an emerging area of “afterglow” imaging, where a 1,2-dioxetane is generated *in situ* from photochemical generation of singlet oxygen, which reacts with an alkene precursor to generate a short-lived chemiluminescence emission that can be imaged after all other

luminescence background has decayed.[1098] Photoacoustic imaging boasts considerable gains in imaging depth and resolution and many new probes for use with this modality are appearing,[192] as well as designs for pure ultrasound imaging.[1099] Imaging in the NIR-II region of the spectrum reduces light scattering and the development of molecules with emission in this region have significant fundamental and practical applications.[185] The field of sensing multiple analytes with a single probe as a sort of logic gate is gaining significant traction[148] and even the beginnings of complex circuitry are appearing where a single or multiple probes perform rudimentary computations based on the analytes that are present. Finally, although the scope of this review was limited to small molecules, there are wide areas of active research into supramolecular and nanoparticle approaches that are being explored to generate different types of molecular device architectures.[1100]

As can be seen from the volume of this review, the field of small molecule probes for reactive oxygen and nitrogen species is thriving across the world, illuminating and revealing how the air we breathe is transmuted and harnessed by the miraculous powers of the cell.

Table 1. Small molecule probes for superoxide

Probe	Type[a]	λ_{ex}[b]	λ_{em}[b]	Application	Trigger/Comments	Ref	Year
Section 1 - Luminol/L-012							
luminol	CL	-	424	phagocytes	luminol oxidation	[101]	1976
luminol	CL	-	424	sea urchin eggs	luminol oxidation	[229]	1989
L-012	CL	-	450	EoL-1, leukocytes, aortic rings, hyperlipidemic rabbits	luminol oxidation	[103,221, 205,1101 ,1102]	1993
Section 2 - Lucinogen and other acridinium salts							
lucigenin	CL	-	503	neutrophil leukocytes	acridinium	[222]	1986
ACR^+-H_2P-ACR^+	F	512	651	buffer	acridinium	[216]	2011
MMT	FCL	n.r.	430/ 500	neutrophils, NIH 3T3	acridinium, mitochondria	[224]	2013
Section 3 - Cypridina luciferin and coelenterazine analogues							
CLA	CL	-	400	buffer	*Cypridina* luciferin	[106]	1980
ICLA	CL	-	n.r.	organic	*Cypridina* luciferin	[230]	1992
NCLA	CL	-	n.r.	organic	*Cypridina* luciferin	[230]	1992
Compound 4	CL	-	521	buffer	*Cypridina* luciferin	[238]	2004
Compound 5	CL	-	521	buffer	*Cypridina* luciferin	[238]	2004
Compound 6	CL	-	521	buffer	*Cypridina* luciferin	[238]	2004
Compound 7	CL	-	460	buffer	*Cypridina* luciferin	[238]	2004
Compound 3	CL	-	610	buffer	*Cypridina* luciferin	[239]	2006
Compound 4	CL	-	610	buffer	*Cypridina* luciferin	[239]	2006
Compound 1	CL	-	545	buffer	*Cypridina* luciferin	[240]	2010
TPE-CLA	CLF	350	500	RAW 264.7, HL7702, mouse in vivo	*Cypridina* luciferin	[1103]	2017
MCLA-800	CL	-	800	neutrophils, rat in vivo/ ex vivo	*Cypridina* luciferin	[241,242]	2021
MCLA	CL	-	460	buffer, sea urchin eggs	*Cypridina* luciferin	[6,228,229,237]	1988
Compound 3	CL	-	462	buffer	coelenterazine	[232]	1997
Compound 9	CL	-	462	buffer	coelenterazine	[232]	1997
Compound16	CL	-	462	buffer	coelenterazine	[232]	1997
Br-Cla	CL	-	480	buffer	coelenterazine	[233]	2019
Br2-Cla	CL	-	445	buffer	coelenterazine	[235]	2022
MeOBrCla	CL	-	450	buffer	coelenterazine	[234]	2022
FBr-Cla	CL	-	425	buffer	coelenterazine	[236]	2023
coelentrazine	FCL	430	520	mouse in vivo	coelentrazine	[189]	2016
Section 4 - Hydroethidine							
HEt	F	470	590	hippocampal neurons, rat ex vivo	hydroethidine	[243]	1996

MitoNeoD	F	544	605	C2C12, HEK293T, mouse ex vivo	hydroethidinium, mitochondria	[251]	2017
MitoSox Red	F	470	579	oligodendrocytes	hydroethidium	[244]	2006
[^{18}F]12	F	480	595	EMT6, mouse in vivo	hydroethidium, PET tracer	[250]	2014
Section 5 - Hydrocyanines and hydrocoumarins							
Hydro-Cy3	F	535	560	RASM, mouse ex vivo	hydrocyanine oxidation	[252]	2009
Hydro-Cy5	F	635	660	buffer	hydrocyanine oxidation	[252]	2009
Hydro-Cy7	F	735	760	mouse in vivo	hydrocyanine oxidation	[252]	2009
Hydro-ICG	F	750	830	buffer	hydrocyanine oxidation	[252]	2009
Hydro-IR-676	F	675	693	buffer	hydrocyanine oxidation	[252]	2009
Hydro-IR-783	F	765	800	buffer	hydrocyanine oxidation	[252]	2009
H-800CW	F	774	789	mouse in vivo, rat in vivo	hydrocyanine oxidation	[253]	2015
HCy−SeH	F	755	800	HEK 293, mouse in vivo/ex vivo	hydrocyanine oxidation, dual with Hg^{2+}	[257]	2018
HCy-ONO	F	765	785	SH-SY5Y	hydrocyanine oxidation, dual with polysulfides	[256]	2019
HCy5-Cy7	F	620/ 740	660/ 800	RAW 264.7, mouse in vivo	hydrocyanine oxidation, dual with $ONOO^-$ and ClO^-	[258]	2021
HCy-FN	F	775	794	RAW 264.7, mouse in vivo	hydrocyanine oxidation, dual with persulfides, mitochondria	[254]	2015
Hcy-Biot	F	730	780	HeLa, mouse in vivo	hydrocyanine oxidation, dual with polysulfides, biotin-targeted	[255]	2016
Hcy-Mito	F	730	780	RAW 264.7, HUVEC, mouse in vivo	hydrocyanine oxidation, dual with polysulfides, mitochondria	[255]	2016
MitoHCy5	F	620	645	BPAEC	hydrocyanine oxidation, mitochondria	[1104]	2023
Ra	F	330	476	buffer	dihydrochromone oxidation	[260]	2021
Rb	F	330	450	buffer	dihydrochromone oxidation	[260]	2021
Rc	F	348	482	buffer	dihydrochromone oxidation	[260]	2021
Probe 1	F	371	468	buffer	dihydrocoumarin oxidation	[259]	2020
Probe 3	F	371	468	buffer	dihydrocoumarin oxidation	[259]	2020
R1	F	330	450	buffer	dihydrocoumarin oxidation	[260]	2021
R2	F	346	446	buffer	dihydrocoumarin oxidation	[260]	2021
R3	F	390	476	buffer	dihydrocoumarin oxidation	[260]	2021
Section 6 - Benzothiazoline oxidation							
H. Py. Bzt	F	377	528	buffer	benzothiazoline	[261]	2004
DBZTC	F	485	559	RAW 264.7	benzothiazoline	[262]	2007
HQ	F2P	430/ 820	548	RAW 264.7, zebrafish, mouse in vivo	benzothiazoline	[1105]	2017
NS-O	FR2P	400/ 800	531	HeLa, mouse ex vivo, zebrafish	benzothiazoline	[265]	2018
ER-BZT	F2P	360/ 700	450	HepG2, mouse ex vivo	benzothiazoline, endoplasmic reticulum	[264]	2017
MF-DBZH	F2P	483/ 800	512	HepG2, HeLa, mouse ex vivo	benzothiazoline, mitochondria	[263]	2013
Section 7 - Catechol oxidation							
PY-CA	F2P	400/ 800	520	4T1, *C. elegans*, mouse in vivo	catechol oxidation	[1106]	2015
IR-747-SAPH	F	690	747	HepG2, mouse in vivo	catechol oxidation	[267]	2018
Myricetin	FR	407	545	HeLa, mouse in vivo	catechol oxidation	[1107]	2019
DPC	F	370	480	HL-7702, mouse in vivo/ex vivo	catechol oxidation	[1108]	2023
Per *qdOH*	F	700	750	B16, RAW 264.7, *T. pallidum*, mouse in vivo	catechol oxidation	[273]	2023
TCA	F2P	491/ 800	515	HL-7702, HepG2, zebrafish, mouse in vivo	catechol oxidation, reversible with GSH	[266]	2013
ER-NAPC	FR	400	545	H9c2, mouse ex vivo	catechol oxidation, endoplasmic reticulum	[274]	2018
CCA	F2P	370/ 800	490	hepatocytes, mouse ex vivo	catechol oxidation, Golgi apparatus	[272]	2019
CST	FR2P	400/ 800	450/ 590	HL7702, mouse in vivo	catechol oxidation, mitochondria	[268]	2019
CyCA	F2P	380/ 800	470	hepatocytes, mouse ex vivo	catechol oxidation, dual with $ONOO^-$	[271]	2019
CFT	F2P	400/ 800	450	4T1	catechol oxidation, dual with pH	[270]	2017

NpRbH	F2P	400/ 780	596	RAW 264.7, rat ex vivo	catechol oxidation, reversible with GSH	[269]	2016
Section 8 - Sulfide and selenide oxidation							
TBT	F	333	387	buffer	sulfhydryl oxidation	[1109]	2010
Probe 3	F	506	524	buffer	sulfide oxidation	[275]	2013
Probe 4	F	506	524	buffer	sulfide oxidation	[275]	2013
Compound 2	F	504	514	MCF-7, ADR	diselenide oxidation, reversible with thiols	[276]	2014
HCy-SH	FR	634	777	HEK 293, mouse in vivo/ex vivo	thiol oxidation, dual with Hg^{2+}	[1110]	2019
Probe 4	F	505	526	MCF-7	selenide oxidation	[277]	2019
Probe 3	F	506	521	MCF-7	cyclic diselenide	[278]	2020
Probe 3	F	573	608	buffer	selenide oxidation	[279]	2022
Probe 4	F	388	469	buffer	selenide oxidation, reversible with thiols	[280]	2022
Probe 5	F	380	458	buffer	selenide oxidation, reversible with thiols	[280]	2022
Probe	F	352	511	A549, MCF-7	diselenide oxidation	[1111]	2023
Section 9 - Other oxidative triggers							
DPBF	F	410	477	buffer	benzofuran quenching	[281]	1999
2-(2-pyridyliminomethyl)phenol	F	294	355	buffer	*ortho*-imino phenol	[282]	2009
9Cl(NEt_2)$_2$	F	728	-	buffer	streptocyanine bleaching	[283]	2010
ImS-FILA	F	373	422	buffer	imidazolium oxidation	[284]	2013
TPA-DHP-1	F	313	463	HeLa	Hantzsch ester oxidation	[285]	2019
TPA-DHP-2	F	346	470	buffer	Hantzsch ester oxidation	[285]	2019
TPA-DHP-3	F	357	560	buffer	Hantzsch ester oxidation	[285]	2019
N1	F	340	480	buffer	boronate	[260]	2021
N2	F	340	468	buffer	boronate	[260]	2021
TPA-PPA-1	F	432	546	buffer	boronic acid	[285]	2019
TPA-PPA-2	F	437	598	buffer	boronic acid	[285]	2019
TPA-PPA-3	F	451	597	HeLa	boronic acid	[285]	2019
Mito-YX	F	494	565	MCF-7, RAW 264.7, mouse ex vivo	boronic acid	[286]	2022
Section 10 - Sulfonyl group cleavage							
Compound 3d	F	485	515	neutrophils	sulfonyl cleavage	[1112]	2005
BESSo-AM	F	~488	~520	neutrophils, Jurkat T	sulfonyl cleavage	[288]	2007
Probe 1	F	494	520	RAW 264.7	sulfonyl cleavage	[1113]	2015
MLS-1	F	494	520	RAW 264.7	sulfonyl cleavage, mitochondria	[1113]	2015
SoDA-1	F	480	512	MDCK	sulfinate cleavage	[316]	2018
Probe 1	F	492	513	HepG2, zebrafish	sulfonyl cleavage, mitochondria, lysosome	[1114]	2018
BSR6	F	535	580	HeLa, Bv2, mouse in vivo	sulfonyl cleavage	[1115]	2021
N3	F	330	450	buffer	sulfonyl cleavage	[260]	2021
N4	F	348	450	buffer	sulfonyl cleavage	[260]	2021
NAP-SCM	F	390	454	RAW 264.7, zebrafish	sulfonyl cleavage	[1116]	2021
MC-O-TBS	F2P	538/ 800	557	HepG2, mouse ex vivo	sulfonyl cleavage	[1117]	2023
HKSOX-1	F	509	534	RAW 264.7, THP-1	triflate cleavage	[289]	2015
Probe 1	F2P	365/ 720	500	RAW 264.7, mouse ex vivo	triflate cleavage	[290]	2017
NIR-O_2^-	F	660/ 800	719	HK-2, mouse in vivo/ex vivo, HepG2	triflate cleavage	[291]	2018
HMBT-LW	F	310	378/ 483	buffer	triflate cleavage	[298]	2019
MRP_D	CL	-	540	mouse in vivo/ex vivo	triflate cleavage	[310]	2019
TFR-O	FR2P	370/ 740	425/ 550	RAW 264.7, mouse ex vivo	triflate cleavage	[292]	2019
NCR1	FCL	535	700	HK2, mouse in vivo/ex vivo	triflate cleavage	[312]	2020
TP-Tfs	FR2P	400/ 470	520/ 580	A549, SH-SY5Y, mouse in vivo	triflate cleavage	[293]	2020
DLS4	F	600	660	HeLa, RAW 264.7, H9c2	triflate cleavage	[300]	2021
IFP-O2	F	500	645	Cal-27	triflate cleavage	[299]	2021
LW-OTf	FR	675	710	HL-7702, mouse in vivo/ex vivo	triflate cleavage	[301]	2021

CLO	CL	-	540	HepG2, RAW 264.7, mouse in vivo	triflate cleavage	313	2022
TCF-OTf	F	560	606	*P. aeruginosa, S. aureus, E. coli, E. faecalis*	triflate cleavage	307	2022
ADN1	CL	-	620	mouse in vivo	triflate cleavage	314	2023
ADN2	CL	-	800	mouse in vivo	triflate cleavage	314	2023
BZT	F	460	541	HeLa	triflate cleavage	1118	2023
CT-CF_3	F	500	665	PC12, BV-2, mouse in vivo	triflate cleavage	303	2023
NIR-FP	F	490	650	PC-12, mouse in vivo/ex vivo	triflate cleavage	302	2023
Peptide-CL	CL	-	510	neutrophils, HEK 293, mouse in vivo	triflate cleavage	315	2023
$^{125/131}$I-PISO	F	495	515	buffer, SPECT/CT in vivo	triflate cleavage, radioiodinated for SPECT/CT	309	2018
Naph-$O_2^{\cdot-}$	F2P	450/ 800	554	mouse ex vivo, HepG2	triflate cleavage, mitochondria	291	2018
ER-NFTTA-Eu^{3+}/Tb^{3+}	L	330	610	HepG2, mouse in vivo/ex vivo	triflate cleavage, endoplasmic reticulum	304	2019
HKSOX-1r	F	509	534	HCT116, BV-2, RAW 264.7, THP-1, zebrafish	triflate cleavage, cell-trappable	289	2015
CFR	CL	-	540	AML-12, mouse in vivo	triflate cleavage, dual with caspase-3	311	2019
ADR	CL	-	520	mouse in vivo	triflate cleavage, dual with *N*-acetyl-beta-D-glucosaminidase	1119	2019
ER-NFTTA-Tb^{3+}	L	330	540	HepG2, mouse in vivo/ex vivo	triflate cleavage, endoplasmic reticulum	304	2019
TPER-$O2^{\bullet-}$	F2P	450	554	HepG2, mouse ex vivo	triflate cleavage, endoplasmic reticulum	294	2020
ER-Rs	F2P	500/ 800	558	HeLa, RAW 264.7, zebrafish, mouse ex vivo	triflate cleavage, endoplasmic reticulum	296	2021
ER-Tf	FR	405	462	HeLa	triflate cleavage, endoplasmic reticulum	305	2023
Gol_{ROS}	F	719	740	HL-7702, mouse in vivo	triflate cleavage, golgi	120	2022
Gol-Cou-$O_2^{\bullet-}$	F	356	460	HepG2, H9c2, zebrafish	triflate cleavage, Golgi apparatus	121	2023
AP	FPAR	745/ 815	850	L02, HEK 293, mouse in vivo	triflate cleavage, hepatocytes	134	2022
hCy-Tf-CA	FPA	710	740	HepG2, mouse in vivo	triflate cleavage, hepatocytes	306	2023
Lyso-MHC	F2P	450/ 730	556	HeLa, zebrafish, mouse ex vivo	triflate cleavage, lysosome	295	2021
HKSOX-1m	F	509	534	RAW 264.7, THP-1	triflate cleavage, mitochondria	289	2015
Mito-Cy-Tfs	FR	600/ 730	742/ 790	RH-35, mouse in vivo	triflimide cleavage, mitochondria	308	2018
APSA	FPA	690/ 845	748	HL-7702, mouse in vivo	triflimide cleavage, mitochondria	297	2022

Section 11 - Phosphinate cleavage

PF1	F	490	530	macrophages	phosphinate cleavage	317	2007
PNF-1	F	602	662	RAW 264.7	phosphinate cleavage	318	2007
Probe 1	FR	310	370/ 460	buffer	phosphinate cleavage	335	2013
Probe 1	FR	390	525/ 615	HepG2	phosphinate cleavage	324	2017
BDP	FR	500	716	HepG2	phosphinate cleavage	321	2018
phosphinate-luciferin	BL	-	530	Huh7	phosphinate cleavage	331	2018
MRP1	F	675	760	mouse in vivo/ex vivo	phosphinate cleavage	310	2019
RDX	F2P	580/ 800	638	HeLa, RAW 264.7, mouse in vivo/ex vivo	phosphinate cleavage	319	2021
BODIPY-T	F	480	530	RAW 264.7	phosphinate cleavage	1120	2022
NR1	F	590	650	4T1, HeLa	phosphinate cleavage	322	2022
MB-SO	F	635	690	HT-22, mouse in vivo	phosphinate cleavage	323	2023
NA-T	FR	415	475/ 540	HepG2, *Daphnia magna*	phosphinate cleavage, mitochondria	325	2018
DPP-S	FR	490	545/ 652	MCF-7, RAW 264.7, mouse in vivo	phosphinate cleavage, mitochondria	327	2019
PBD-B	FR	410	475/ 540	HepG2, mouse in vivo	phosphinate cleavage, mitochondria	326	2019
PF-MitoSOX Green	F	488	515	H9C2, *C. elegans*	phosphinate cleavage, mitochondria	328	2019

V-OS	F2P	377/ 890	530	HepG2, mouse in vivo	phosphinate cleavage, dual with viscosity	320	2023
DMPS-O	F	418	635	MCF-7, HepG2	phosphinate cleavage, mitochondria	329	2021
DTPB	FR	405	587	MCF-7	phosphinate cleavage, mitochondria, dual with viscosity	330	2023
TPP	F2P	345/ 740	470	RAW 264.7, rat ex vivo	phosphinothioate cleavage	333	2019
Probe 1	F	490	511	buffer	phosphite cleavage, reversible with nerve agents	332	2014
CyR	F	675	704	HepG2, zebrafish, mouse in vivo	phospinate cleavage	1121	2016
Section 12 - Nitrophenyl and ether cleavage							
Probe 1	F	490	522	SH-SY5Y	dinitrophenyl ester removal	334	2013
Probe 2	FR	310	370/ 460	buffer	4-nitrophenyl ether cleavage	335	2013
Section 13 - Other nucleophilic triggers							
NBD-Cl	F	470	550	buffer	nucleophilic aromatic substitution	287	2005
TPA-Pyr-Thiourea	F	430	525/ 580	HeLa	pyridinium cleavage, mitochondria	336	2020
Probe 2	PA	750	PA	chicken ex vivo	oxoporphyrin binding	337	2019
2-SAP	F	295	360	buffer	Schiff base	1122	2011
Section 14 - Combined oxidative and nucleophilic triggers							
SOP-blue	FR	325	385/ 485	buffer	Cu^{2+} promoted C-O cleavage	338	2017
SOP-cyan	F	455	488	HEK293T, HeLa, A431	Cu^{2+} promoted C-O cleavage	338	2017
SOP-orange	F	570	585	buffer	Cu^{2+} promoted C-O cleavage	338	2017
SOP-green	F	470	510	HeLa, HEK293T	Cu^{2+} promoted C-O cleavage	340	2020
Lyso-SOP-green	F	470	510	RAW 264.7	Cu^{2+} promoted C-O cleavage, lysosome	340	2020
HemiSe	F	360	439	RAW 264.7	1,4-addition/1-electron oxidation	341	2018
Section 15 - Reductive triggers							
HO-1889NH	F	330	550	spinach leaves	spin trap	343	2002
Compound 15	F	330/ 346	377/ 397	buffer	trityl radical, dual EPR	342	2010
Compound 7	F	330/ 346	377/ 397	buffer	trityl radical, dual EPR	342	2010
Compound 8	F	330/ 346	377/ 397	buffer	trityl radical, dual EPR	342	2010
F-Tz1	F	323	470	HepG2	tetrazine to oxadiazole	344	2023
F-Tz2	F	334	460	HepG2	tetrazine to oxadiazole	344	2023
F-Tz3	F	350	530	HepG2	tetrazine to oxadiazole	344	2023
F-Tz4	F	385	510	HepG2, H9C2, mouse ex vivo	tetrazine to oxadiazole	344	2023
F-Tz5	F	346	445	HepG2	tetrazine to oxadiazole	344	2023
F-Tz6	F	450	505	HepG2	tetrazine to oxadiazole	344	2023
F-Tz7	F	445	540	HepG2	tetrazine to oxadiazole	344	2023
F-Tz8	F	566	585	HepG2	tetrazine to oxadiazole	344	2023
F-Tz9	F	474	600	HepG2	tetrazine to oxadiazole	344	2023

[a] F = fluorescence, R = ratiometric, 2P = two-photon, L= luminescence, CL = chemiluminescence, BL = bioluminescence, PA = photoacoustic. [b] Wavelengths given in nanometers.

Table 2. Small molecule probes for hydrogen peroxide

Probe	Type[a]	λ_{ex}[b]	λ_{em}[b]	Application	Trigger/Comments	Ref	Year
Section 1 – Classical detection methods (xanthene oxidation, luminol, and peroxyoxalate)							
DCFH-DA	F	504	523	leukocytes, HUVEC	xanthene oxidation	24	1965
Amplex Red	F	563	587	neutrophils	resorufin oxidation	25	1997
$[Ru(bpy)_2(lumino\ l\text{-}bpy)](PF6)_2$	LCL	450	645	buffer	luminol	363	2015
P-HP	F2P	478/ 850	645	mouse liver ex vivo	luminol	364	2017
PO-Tz1	CL	-	480	organic	peroxyoxalate	1123	2019
PO-Tz2	CL	-	525	organic	peroxyoxalate	1123	2019
NIR-II CLS	CL	-	935	mouse in vivo	peroxyoxalate	376	2020

m-carboxy luminol	CL	-	424	buffer	luminol oxidation	[1124]	2021
NIR-Cl-NP	CL	-	755	mouse in vivo	peroxyoxalate	[375]	2022
Section 2 - Phosphine oxidation							
DPPP	F	351	380	PMN	phosphine oxidation	[379, 380]	1987
Probe 2	F	458	520	organic	phosphine oxidation	[1125]	2003
Probe 1	F	360	492	organic	phosphine oxidation	[381]	2005
DPPEA-HC	F	396	449	buffer	phosphine oxidation	[382]	2005
Spy-HP	F	524	535	buffer	phosphine oxidation	[383]	2006
DPPEA-BODIPY	F	502	515	buffer	phosphine oxidation	[1126]	2009
MitoDPPP	F	350	380	HepG2	phosphine, mitochondria	[384]	2010
Cy-NOH2	FR	605	750	L02, zebrafish, mouse in vivo	phosphine oxidation	[385]	2022
Section 3 - Boronate oxidation							
Probe 1b	F	355	460	buffer	boronate	[386]	2003
PF1	F	450	~510	HEK, rat hippocampal neurons	boronate	[387, 388]	2004
PR1	F	530	580	HEK	boronate	[388]	2005
PX1	F	350	450	HEK	boronate	[388]	2005
RPF1	FR	420	517/ 464	mitochondria	boronate	[389]	2006
PG1	F	460	510	HEK 293, A431	boronate	[462]	2007
PC1	F	480	584	HEK 293	boronate	[462]	2007
PL1	FR2P	410/ 800	540/ 475	RAW 264.7	boronate	[390]	2008
MitoPY1	F	510	528	HeLa	boronate, mitochondria	[463]	2008
NPF1	F	598	660	RAW 264.7	boronate	[488]	2008
Probe 1	F	332	454	buffer	boronate	[1127]	2008
SNAP-PG1	F	465	515	HEK 293T	boronate, SNAP tag	[129]	2010
SNAP-PG2	F	465	515	HEK 293T	boronate, SNAP tag	[129]	2010
PF2	F	475	511	A431, RAW 264.7	boronate	[147]	2010
PF3	F	492	515	A431, RAW 264.7	boronate	[147]	2010
PE1	F	491	514	A431, RAW 264.7	boronate	[147]	2010
PY1	F	519	548	A431, RAW 264.7	boronate	[147]	2010
PO1	F	540	565	A431, RAW 264.7	boronate	[147]	2010
PCL-1	BL	-	530	LNCaP-luc, mouse in vivo	boronate	[523]	2010
TPR1	L	280	545	buffer	boronate, time gated	[581]	2010
TPR2	L	280	545	RAW 264.7	boronic acid, time-gated	[581]	2010
RS-BE	F	550	580	SH-SY5Y	boronate, with Fe^{2+} and Cu^{2+}	[1128]	2010
Probe 1	F	400	475	buffer	boronate	[1129]	2010
Probe 4	F	370	450	buffer	boronic acid	[1130]	2010
PY1-ME	F	515	540	HEK 293, HT29	boronate	[1131]	2010
PN1	F2PR	370/ 358/ 750	450/ 500	RAW 264.7, rat hippocampal ex vivo	boronate	[391]	2011
NucPE1	F	505	530	HEK 293, HeLa, *C. elegans*	boronate, nucleus	[478]	2011
probe 4	F	590	720	mouse in vivo	boronate	[489]	2011
***p*-NPBA**	F	294	405	buffer	boronic acid	[1132]	2011
SHP-Mito	F2PR	383	470/ 545	RAW 264.7, rat hippocampal ex vivo	boronate, mitochondria	[392]	2012
probe 3	FR	400	484/ 566	PC3	boronate	[393]	2012
DQHP	FR	405	480/ 542	buffer	boronate	[394]	2012
FP-H_2O_2-NO	F	400	460	HeLa, RAW 264.7	boronate, dual with NO	[831]	2012
FloB-SI	F	495	520	HeLa	boronate, dual with Fe^{3+} and Cu^{2+}	[1133]	2012
Probe 1	FR	380	410/ 542	RAW 264.7	boronate	[395]	2013
Probe 1A	FR	375	420/ 510	buffer	boronate	[396]	2013
Probe 1C	FR	375	480/ 570	buffer	boronate	[396]	2013
SHP-Mito	F2P	342/ 740	470	HeLa, rat hippocampal ex vivo	boronate	[447]	2013
D-BBO	F	341	405/ 510	buffer, surfactant	boronate	[1134]	2013
2a	F	450	560	buffer	boronate	[1135]	2013

2b	F	450	560	buffer	boronate	[1135]	2013
3a	F	450	560	buffer	boronic acid	[1135]	2013
3b	F	450	560	buffer	boronic acid	[1135]	2013
Probe 1	F	290	410	buffer	boronate, dual with fructose	[1136]	2013
Probe 2	F	370	410	buffer	boronate, dual with fructose	[1136]	2013
C6NIB	F	450	~550	buffer, vapor	boronate	[1137]	2013
FBBBE	F	494	521	RAW 264.7, mouse brain ex vivo	boronate	[1138]	2013
1a	FR	361	415/ 527	buffer	boronic acid	[397]	2014
1b	FR	379	408/ 600	buffer	boronic acid	[397]	2014
1c	FR	366	415/ 527	HeLa, Jurkat	boronic acid	[397]	2014
1d	FR	361	408/ 600	buffer	boronic acid	[397]	2014
Probe 1	FR	372/ 453	446/ 546	RAW 264.7	boronate	[398]	2014
NP1	FR	354/ 446	403/ 555	HeLa, RAW 264.7, A431, rat hippocampal ex vivo	boronate	[399]	2014
pep-NP1	FR	353	403/ 551	HeLa	boronic acid, nuclear	[399]	2014
Compound 1	F	365	510	buffer	boronate	[1139]	2014
Probe 4	F	480	520	HepG2, LO2, angelfish	boronate	[1140]	2014
Probe 3	BL	-	525	ES-2-luc, mouse in vivo	boronic acid	[1141]	2014
Compound 1	F	503	485	buffer	boronate	[1142]	2014
BCQ	F	350	454	buffer	boronate, prochelator	[1143]	2014
pep3-NP1	F	455	555/ 646	HeLa	boronic acid, mitochondria	[400]	2015
Probe 1	F	405	528	HeLa, RAW 264.7	boronate, lysosome	[479]	2015
Probe 1	F	560	670	HeLa	boronic acid	[491]	2015
DCM-B1	F	560	700	buffer	boronate	[492]	2015
DCM-B2	F	560	700	MCF-7, mouse in vivo	boronate	[492]	2015
Compound 2	F	445	556	buffer	boronate	[1144]	2015
Probe 1	F	400	460	HEK293	boronate	[1145]	2015
EEPF1	F	450	520	spermatozoa	boronate	[1146]	2015
P1	F	360	515	buffer, milk	boronic acid	[1147]	2015
TPE-BO	F	400	500	RAW 264.7	boronate	[1148]	2015
CRANAD-88	F	630	730	brain homogenate, mouse in vivo	boronate, Aβ-responsive	[142]	2016
NPP	F2PR	430/ 740/ 810	460/ 540	RAW 264.7	boronic acid	[401]	2016
azaBDPBA	F	655	682/ 724	HeLa	boronic acid	[402]	2016
CSBOH	FR	560/ 670	650/ 720	HeLa, RAW 264.7, mouse in vivo	boronate, alkaline conditions	[403]	2016
BNBI	FR	480/ 555	590/ 690	buffer	boronate	[404]	2016
Cy-B	FR	554/ 685	709	MCF-7, mouse in vivo	boronate	[405]	2016
Lyso-HP	F2P	474/ 780	550	HeLa, RAW 264.7, rat liver ex vivo	boronate, lysosome	[448]	2016
B(OH)$_2$-QPD	F2P	365/ 730	525	HeLa, RAW 264.7	boronic acid	[449]	2016
CBZ-H$_2$O$_2$	F2P	350/ 720	430	HeLa, rat ex vivo	boronate, mitochondria	[450]	2016
M-H$_2$O$_2$	F	530	558	HepG2, macrophages, zebrafish	boronate, mitochondria	[464]	2016
ER-H$_2$O$_2$	F	400	458/ 558	HepG2, 4T1	boronate, endoplasmic reticulum	[465]	2016
MI-H$_2$O$_2$	F	525	555	HepG2, 4T1	boronic acid, mitochondria	[465]	2016
Mito-H$_2$O$_2$	F	376	527	HeLa	boronate, mitochondria	[466]	2016
HP-L1	F	520	584	HeLa	boronate, lysosome, pH-switchable	[480]	2016
QCy-BA	F	400	680	HeLa, MRC5	boronic acid	[493]	2016
DH-1	F	560	700	MCF-7, mouse in vivo	boronate	[494]	2016
OTB	F	366	466	vapor	boronate	[1149]	2016
OTBPA	F	365	445	vapor	boronate	[1149]	2016

FLB$_2$SSCou	F	408	525	HeLa	boronate, dual with thiols	[1150]	2016
TPE-HPro	F	373	540	buffer	boronate	[1151]	2016
NBCD	F	530	590	HeLa	boronate	[1152]	2016
TPE-TLE	FR	380	435/ 550	RAW 264.7, HepG2	boronate	[406]	2017
CNP	FR	420	485/ 558	HeLa	boronate	[407]	2017
TPNR-H_2O_2	F2P	560/ 860	699	MCF-7, RAW 264.7	boronate	[451]	2017
Probe 1	F2P	360/ 740	505	HeLa	boronate	[452]	2017
HPQ-H.	F2P	405/ 720	~480	HeLa, mouse muscle ex vivo	boronate, ESIPT	[453]	2017
CAI	F	405	575	RAW 264.7	boronate, mitochondria	[467]	2017
Lyso-B-L1	F	570	606	HeLa	boronate, lysosome, pH activatable	[481]	2017
ztl-4	F	~420	~490	SH-SY5Y	boronate, lysosome	[482]	2017
pep4-NP1	F	450	663	HeLa, RAW 264.7	boronic acid, dual with caspase 3	[495]	2017
Probe 2a	CL	-	690	mouse in vivo	boronate	[496]	2017
Probe 1	CL	-	~460	buffer	boronate	[525]	2017
Probe 7	CL	-	540	buffer	boronate	[526]	2017
PAM-BN-PB	F	410	480	HeLa, mouse in vivo	boronate	[1153]	2017
HPQB	F	333	495	C666-1	boronate	[1154]	2017
Mito-VH	F	400	510	HeLa, RAW 264.7	boronate, dual with viscosity	[1155]	2017
AVPM	F	448	596	organic	boronate	[1156]	2017
P1	FR	343	408/ 546	buffer	boronate	[1157]	2017
P2	F	329	512	buffer	boronate	[1157]	2017
FD-1	F	480	615	buffer	boronate	[1158]	2017
FD-2	F	480	615	U87, mouse ex vivo	boronate	[1158]	2017
Py-Boe	F	385	485	RAW 264.7	boronate	[1159]	2017
RF620	FR	550/ 620	570/ 636	HeLa	borinate	[593,1160]	2017
PEP-Npb1-Cy3	F	425	567	SKOV-3	boronic acid, integrin receptor targeted	[140]	2018
Mito-HP	FR	391	543	HeLa	boronate, mitochondria	[408]	2018
Compound 1	FR	500	535/ 640	HeLa, NRK	boronate, mitochondria	[409]	2018
Probe 3	FR	365	450/ 543	HeLa	boronate	[410]	2018
AB-1	FR	535	620/ 660	HeLa, mouse in vivo	boronate	[411]	2018
FB	F2PR	405/ 800	485/ 585	VSMC, zebrafish	boronate, releases CO	[412]	2018
CNBE	FR	410	480/ 551	HeLa, zebrafish	boronate	[413]	2018
HCyHP	FR	524	599	HeLa	boronate	[414]	2018
SHP-Cyto	FR2P	371/ 750	455/ 528	HeLa, rat ex vivo	boronate	[415]	2018
HBTPB	FR	373	539/ 669	A549	boronate	[416]	2018
HKB	FR	440	594/ 666	HeLa	boronate, mitochondria	[417]	2018
TX-HP	F2P	450/ 800	512	HeLa, RAW 264.7, mouse liver ex vivo	boronate	[454]	2018
Probe 1a	F	550	604	HeLa, Ges-1	boronate, mitochondria	[468]	2018
PRB2-H_2O_2	F	672	695	HepG2, mouse in vivo	boronate	[497]	2018
PB1	F	470	510	bovine oocytes	boronate	[541]	2018
TCF-PB	F	560	605	A549	boronate	[1161]	2018
Probe 1	F	368	580	4T1	boronate	[1162]	2018
RhoB	FR	580	638	HeLa, mouse live ex vivo, mouse in vivo	boronate	[1163]	2018
FE-H_2O_2	F	365	512	RAW 264.7	boronate, electrochemical	[1164]	2018
BNBD	F	465	535	A549	boronic acid	[1165]	2018
BQA-GGFF	FR	406	490	HeLa, HepG2, MCF-7, PANC-1, HUVEC	boronic acid	[1166]	2018
Probe 1	F	480	619	HeLa	boronate	[1167]	2018
Peroxymycin-1	F	488	496	A431, MDA-MB-231, MDA-MB-468, MCF-7, MCF-10A, HS 578T, HS578Bst	boronate, puromycin staining	[1168, 1169]	2018

NIR-HP1	FR	395	500/650	HeLa, zebrafish, Drosophila	boronate	[418]	2019
Cy-ArB	FR	605/780	758/806	HepG2, mouse in vivo	boronate	[419]	2019
FH$_2$O$_2$	FR2P	324/358	484/562	BV-2, rat brain ex vivo	boronate	[420]	2019
probe 1	FR	375/430	535/640	HeLa	boronate	[421]	2019
Probe	FR	450	550/672	RAW 264.7, MCF7, MDA-MB-231	boronic acid, dual with MMP2	[422]	2019
TP-NIR-H$_2$O$_2$	F2P	585/800	665	HeLa, mouse liver ex vivo	boronic acid, mitochondria	[455]	2019
AzuFluor 483-Bpin	F2P	350/800	483	RAW 264.7, rat hippocampal ex vivo	boronate	[456]	2019
Mito-NP	F	463	553	HeLa, A549	boronate, mitochondria	[469]	2019
BP$_5$-NB-OB	FR	650/695	700/720	A549, mouse in vivo	boronate, biotin targeted	[487]	2019
NDCM-HP	F	550	676	Hela, MCF-7	boronate	[498]	2019
JW41	FPA	730/790	825	MDA-MB-231, MCF-7, mouse in vivo	boronate	[499]	2019
NRBE	FR	585	670	BEL-7402	boronate	[500]	2019
Probe 1	FR	670	708	HepG2, mouse in vivo	boronate	[501]	2019
Probe 1	CL	-	499	buffer	boronate	[528]	2019
Probe 2	CL	-	499	buffer	boronate	[528]	2019
Mito-FBN	F	470	528	KB	boronate	[1170]	2019
DCM-B	F	557	688	HepG2	boronate	[1171]	2019
PB1	FR	540	640	HepG2, Drosophila ex vivo	boronate	[1172]	2019
TPYS	FR	420	590	HeLa	boronate	[1173]	2019
PHS1	FR	390	460	HT-29, HeLa, zebrafish	boronate, dual with H_2S	[1174]	2019
BBD	F	401	512	HeLa	boronate	[1175]	2019
TPECNPB	F	450	625	MCF-7	boronic acid, lipid droplet, PDT	[137]	2020
probe 1a	FR	365	458/510	HeLa	boronic acid	[423]	2020
JNH-1	FR	380	455/540	HGC-27	boronate	[424]	2020
Mito-HT	FR	395	493/562	CHO-K1	boronate, mitochondria	[425]	2020
Py-VPB	FR	380	480/600	HeLa, RAW 264.7	boronate	[426]	2020
Ir-BE	F	365	490/550	buffer, river water	boronate	[427]	2020
HDP-1	FR	420	485/618	HDP-1	boronate	[428]	2020
CSU1	FR	376/440	409/640	MCF-7	boronate, dual with HOCl	[429]	2020
TCAB	FR	325	413/486	HeLa, zebrafish	boronate, dual with H_2S	[430]	2020
TFP	FR2P	380/710	470	neurons, zebrafish	boronate, mitochondria	[457]	2020
Pyp-B	F2P	437/800	625	A549, zebrafish	boronate, mitochondria	[458]	2020
QVD-B	FR	405	580	HepG2	boronate, mitochondria, super resolution	[470]	2020
Mito-NIRHV	FR	440	700	HeLa, mouse in vivo	boronate, mitochondria, dual with viscosity	[471]	2020
HCy-BOH	FPA	679	706	HeLa, RAW 264.7, mouse in vivo	boronic acid	[472]	2020
TPP-HCy-BOH	FPA	690	716	HeLa, RAW 264.7, mouse in vivo	boronic acid, mitochondria	[472]	2020
PRB	F	450	550	HeLa	boronate, dual with thiols	[483]	2020
PMB	F	450	565	HeLa	boronate, lysosome	[483]	2020
DCP-BA	FR	546	680	HeLa	boronic acid	[502]	2020
PCN-BP	FR	470	680	RAW 264.7	boronate	[503]	2020
NIR-pH-H$_2$O$_2$	F	560	680	MCF-7, mouse in vivo	boronic acid, dual with pH	[504]	2020
Compound 1	CL	-	540	Cco-2, HaCat, HUVEC	boronate	[527]	2020
DCX-B	F	590	748	HCT116, HepG2, mouse in vivo	boronate	[1176]	2020
CBH	F	488	530	HeLa, zebrafish, *C. elegans*	boronate	[1177]	2020
PT1	F	595	610	buffer	boronate	[1178]	2020
BPN-TOB	FR	365	471	MGC-803, RAW 264.7, zebrafish	boronate	[1179]	2020

RAH225	F	330	452	buffer	boronate	[1180]	2020
RAH2115	F	560	585	HeLa	boronate	[1180]	2020
HF-6	FR	451	526	SH-SY5Y	boronate, dual with formaldehyde	[1181]	2020
HP	FR	396	566	HepG2	boronate	[1182]	2020
Geisha-1	F	450	550	HeLa, mouse liver ex vivo	boronate, dual with HOCl	[1183]	2020
MT-PY1	F	488	540	HeLa, A431	boronate, microtubule targeting	[136]	2021
CyBP-600	F	355	530	GL261	boronate, dual with protein aggregates	[143]	2021
BtBC-H_2O_2	FR2P	380/ 480/ 850	520/ 610	HeLa, HT29, A549, HepG2, mouse ex vivo	boronate	[431]	2021
TPP-Tba	FR	405	460/ 614	HeLa, 3T3, mouse ex vivo	boronate, dual with viscosity	[432]	2021
PyBC590	FR2P	427/ 519 /880	593/ 642	HeLa, mouse ex vivo	boronate	[433]	2021
NAB-BE	FR2P	340/ 745	512	RAW 264.7	boronate	[434]	2021
NAB-BA	FR2P	340/ 745	512	RAW 264.7	boronic acid	[434]	2021
QVB-B	FR	405	464/ 580	HepG2	boronate	[435]	2021
HQPQ-B	FR	450	575/ 670	HeLa	boronate, mitochondria	[436]	2021
NPDIN	FR	380/ 405	398/ 554	A549, LoVo, HT29, Caco-2	boronate	[437]	2021
BT-HP	F2P	450/ 780	550	HeLa, tumor ex vivo	boronate, biotin tagged	[459]	2021
Mito-Bor	F	700	730	A549, PC9, IMR90, MRC-5, mouse in vivo	boronate, mitochondria	[473]	2021
Py-SiRh-HP	F	655	680	HeLa, mouse in vivo	boronic acid, lysosome	[484]	2021
NPT-H_2O_2	FR	375/ 450	425/ 550	HeLa, mouse ex vivo	boronic acid, lysosome	[485]	2021
ADM	F2P	450	667	H9C2	boronate, dual with viscosity, COS release	[505]	2021
MTR-HH	F	701	724	HeLa, RAW 264.7, mouse in vivo	boronate	[506]	2021
PA-HD-H_2O_2	FPA	745	765	NeuroScreen-1, mouse in vivo	boronate	[507]	2021
CX-B-DF	FR	550	695	HCT116, mouse in vivo	boronate, drug release	[508]	2021
BOD-H_2O_2	F	695	725	HeLa	boronate	[509]	2021
QX-B	FR	725	772	HeLa, HCT116, AT1, zebrafish, mouse in vivo	boronate	[510]	2021
FP-BDP4	F	615	720	RAW 264.7, mouse in vivo	boronic acid	[511]	2021
DX-B-DA	FR	670	705	mouse in vivo	boronate, drug release	[512]	2021
PN910	FR	870	910	mouse in vivo	boronate	[529]	2021
Hcy-OB	F	400	550	HeLa, mouse in vivo	boronate, dual with SO_2	[1184]	2021
Probe 19	F	454	511	HeLa	boronate	[1185]	2021
XH-2	F	570	638	HepG2	boronate	[1186]	2021
BC-OB	F	475	495	RAW264.7	boronate	[1187]	2021
PG1-FM	F	488	525	HeLa, A431, RAW 264.7, microglia-neuron coculture	boronate, tandem activity based	[1188]	2021
Cy-Hy	BL	-	489	MDA-MB-231	boronate	[1189]	2021
BTFMB	FR	380	542	HepG2	boronate	[1190]	2021
CMB	FR	405	450	MCF-7, zebrafish	boronate	[1191]	2021
BCO	F	440	547	A549, mouse ex vivo	boronate	[1192]	2021
N-Py-BO	F	480	650	RAW 264.7	boronate	[1193]	2021
Probe 4	F	405	450	COS7	borinic acid	[1194]	2021
NATPA	FR	365	550	HepG2, L-02	boronate, dual with polarity, lipid droplet	[138]	2022
R-MA-SLM	FR	490	574/ 661	N2a, N2aSW, mouse in vivo/ex vivo	boronate, AB targeted	[144]	2022
CBD	F	514	635	SH-SY5Y, mouse ex vivo	boronate, dual with AB fibrils and viscosity, mitochondria	[145]	2022
NCR	FR	410/ 590	522/ 670	HeLa	boronic acid	[438]	2022
HBQ-B	FR	422	538/ 656	MCF-7, HeLa, RAW 264.7, zebrafish	boronate	[439]	2022
THMP	FR	500	540/ 610	HepG2, mouse in vivo	boronate	[440]	2022
HBQ-L	FR	405	508/	A549, zebrafish, mouse in vivo	boronate, mitochondria	[441]	2022

QM-R	FR	460/620	642 555/720	HepG2	boronate	[442]	2022
Probe 1	FR	360	450/605	HepG2, zebrafish, mouse ex vivo	boronate, dual with HOCl	[443]	2022
CI-Bz-B	F2P	330/735	481	RAW 264.7	boronic acid, responds to $ONOO^-$	[460]	2022
LY-H_2O_2	F2P	370/800	445	PC12, mouse in vivo	boronate, lysosome	[461]	2022
MI-H_2O_2	F	610	670	PC12, mouse in vivo	boronate, mitochondria	[461]	2022
JQ-1	F	524	572	HeLa, zebrafish	boronate, mitochondria	[474]	2022
TMN-H_2O_2	F	480	660	HepG2, zebrafish, mouse in vivo	boronate	[513]	2022
DCM-HNU	F	453	658	HeLa, zebrafish	boronate	[514]	2022
HD-BPin	FR	660	704	A549	boronate, dual with $ONOO^-$	[515]	2022
DBIS	FR	670	708	mouse in vivo	boronate	[516]	2022
MB-m-borate	F	665	684	A375, PIG1, HepG2, LO2, mouse in vivo	boronate, dual with tyrosinase	[517]	2022
BC-B	F	550	672	HeLa	boronate	[518]	2022
bor-DTZ	BL	-	500	MDA-MB-231	boronate	[524]	2022
IR-990	FR	790	990	HeLa, HepG2, mouse in vivo	boronate	[530]	2022
BHC-Lut	FPA	830	930	mouse in vivo	boronate, drug-release	[531]	2022
NH-MT	F	460	550	HepG2, RAW 264.7, HUVEC, MGC803, zebrafish	boronic acid	[1195]	2022
CDM-C	FR	430	617	HUVEC, HeLa, zebrafish	boronate	[1196]	2022
QM-RSH	FR	460	700	HepG2, zebrafish	boronate, dual with H_2S	[1197]	2022
BHA-B	FR	370	595	HeLa, zebrafish	boronate, acetyl assisted	[1198]	2022
TZ-BO	F	350	545	HeLa	boronate	[1199]	2022
BBS	F	394	464	MCF-7	boronate	[1200]	2022
Probe-1	FR	365	405/550	MCF-7	boronate	[1201]	2022
HP-H_2O_2	FR	800	937	mouse in vivo	boronic acid	[1202]	2022
Probe 1	F	400	483	HeLa, HepG	boronate	[1203]	2022
Probe 2	FR	500	650	HeLa	boronate	[1204]	2022
QX9A-H_2O_2	F	450	540	HeLa	boronate	[1205]	2022
8-quinoline boronic acid	F	370	515	buffer	boronic acid, Al assisted	[1206]	2022
Golnap-H_2O_2	F	405	520	HeLa, zebrafish	boronate, H_2S release, Golgi	[122]	2023
DPP-BPYS	F	504	684	MCF-7, ZJU0430, HeLa, mouse in vivo	boronate, singlet oxygen generation, lipid droplet targeted	[139]	2023
P1	F	410	653	DU-145	boronate, estrogen receptor-beta targeted	[141]	2023
P2	F	413	655	DU-145, mouse in vivo	boronate, estrogen receptor-beta targeted	[141]	2023
VBD	F	522	590	PC12, mouse ex vivo	boronate, dual with AB aggregates	[146]	2023
Probe 1	FR	405	468/542	MCF-7	boronic acid	[444]	2023
GT-H_2O_2	FR2P	360/760	420/505	HeLa, HU-EVC, zebrafish	boronate	[445]	2023
DFB-1	FR	470/590	560/680	A549, HepG2	boronate, mitochondria	[446]	2023
HTQ-R	F	400	620	HeLa, mouse in vivo	boronate, mitochondria	[475]	2023
HCyB	F	525	556	RAW 264.7, WS1, MDA-MB-231, THP-1	boronate, mitochondria	[476]	2023
TP/TPP-NB	F	402	530	HeLa	boronate, clickable mitochondria localization	[477]	2023
Probe 1	F	340	473	A549	boronate, lysosome	[486]	2023
AAE-COU-TCF	FR	590	675	HeLa, mouse in vivo	boronate, dual with SO_2	[519]	2023
BOD-BH-OS	F	640	745	HeLa, HEK293	boronate, dual with H_2S	[520]	2023
LTA	F	550	645	HeLa, zebrafish	boronate	[521]	2023
LTQ	F	550	670	buffer	boronate	[521]	2023
YFE-1	F	474	655	HeLa, rice roots	boronic acid	[522]	2023
Probe 1	F	372	451	RAW 264.7, SW480	boronate	[1207]	2023
YSXH	F	415	455	A549	boronic acid	[1208]	2023
BI	F	333	470	HeLa, zebrafish	boronate, dual with SO_2	[1209]	2023
BBI	F	333	470	HeLa, zebrafish	boronate, dual with SO_2	[1209]	2023
BZT-TPA	F	350	575	HeLa	boronate	[1210]	2023
FDOCL-N-Na	F	460	548	COS-1, HUVEC, HeLa, Huh-7, QBC939, A549, ID8, *C. elegans*	boronate, dual with HOCl	[1211]	2023

Section 4 – Sulfonyl cleavage							
2a	F	485	530	*Chlamydomonas reinhardtii*	sulfonate cleavage	[532]	2004
2b	F	485	530	*Chlamydomonas reinhardtii*	sulfonate cleavage	[532]	2004
2c	F	485	530	*Chlamydomonas reinhardtii*	sulfonate cleavage	[532]	2004
NFDS-1	F	602	662	peritoneal macrophages	sulfonate cleavage	[533]	2005
NFDS-2	F	n.r.	692	buffer	sulfonate cleavage	[533]	2005
FS-1	F	491	515	peritoneal macrophages	sulfonate cleavage	[534]	2009
FS-2	F	493	520	peritoneal macrophages	sulfonate cleavage	[534]	2009
JNY-1	FR	380	440/ 540	HepG2	perfluorosulfate ester	[535]	2019
Cy-PFS	FR	560/ 730	635/ 836	HL7702, A431, HT22, mouse in vivo	perfluorosulfate ester	[536]	2019
GW-1	F	475	549	buffer	aryl sulfonate cleavage, dual with pH	[537]	2021
Section 5 -Benzil/α-ketoketone Baeyer-Villager oxidation							
Compound 4	F	493	518	buffer	benzil	[538]	2011
NBzFDA	F	495	519	RAW 264.7, A431	benzil	[538]	2011
NBzF-BG	F	505	525	HEK 293T, RAW 264.7	benzil, SNAP tag	[130]	2014
Probe 1	F2P	380/ 760	505	MKN-45, SMMC-7721	benzil	[539]	2015
***p*-NBBD**	F	498	508	buffer	benzil	[540]	2018
***m*-NBBD**	F	498	508	HeLa	benzil	[540]	2018
NbzB	F	470	510	bovine oocytes	benzil	[541]	2018
BBHP	F	475	508	HeLa, MCF-7, RAW 264.7, mouse ex vivo	benzil, biotin targeted	[1212]	2022
Section 6 - α-Ketoamide oxidation							
Mito-NIRHP	FR	670	704	HepG2, mouse in vivo/ex vivo	α-ketoamide	[542]	2016
NPs-A	FR	483	516/ 595	L929, RAW 264.7, zebrafish	α-ketoamide	[544]	2017
α-Naph	FR	395	465/ 540	HeLa	α-ketoamide, endoplasmic reticulum	[545]	2017
Cy-H_2O_2	F	730	790	HeLa, zebrafish	α-ketoamide	[546]	2019
DCHP	F	487	653	A549, SMMC-7721, HeLa, MCF-7, 4T1, HL-7702, Hi-5, *C. elegans*, zebrafish	α-ketoamide	[1213]	2019
RhB-NIR	F	590	730	HeLa	α-ketoamide, mitochondria	[547]	2020
BTPE-NO_2@F127	FRPA	808	938	RAW 264.7, mouse in vivo	α-ketoamide	[548]	2021
Mito-H2O2	F	670	702	HeLa, mouse in vivo	α-ketoamide, mitochondria	[549]	2022
Section 7 – Iron-mediated triggers							
MBFh1	F	570	590	buffer	iron	[550]	2011
ZP1Fe_2	F	507	528	HeLa	iron, lysosome	[554]	2012
MBFh2	F	530	590	HeLa, A431	iron	[551]	2013
MBFh3	F	450	517	HeLa, A431	iron	[553]	2014
Probe 1 / Fe^{2+}	F	369	540	zebrafish, DU145	iron	[555]	2015
Section 8 – Chalcogen oxidation							
RF1	F	495	503	HEK	xanthene oxidation, reversible	[556]	2007
Compound 2	F	543	592	neuroblastoma cells	sulfide oxidation	[1214]	2012
Cy-O-Eb	F	768	794	HepG2, zebrafish	ebselen, reversible with GSH, mitochondria	[557]	2013
D-HMSe	F	330	476	buffer	selenium oxidation	[558]	2014
Compound 3	F	500	579	buffer	tellurophene oxidation	[564]	2014
SB-1	F	370	503	HeLa	sulfide oxidation	[561]	2016
SB-2	F	370	510	HeLa	sulfide oxidation	[561]	2016
Probe 1a	F	340	502	buffer	sulfide oxidation	[562]	2017
Probe 2	F	338	425	buffer	sulfide oxidation	[562]	2017
Probe 2	F	590	676	HeLa	sulfide oxidation, lysosome	[563]	2018
BODIPY–Se	FR	460	504	MCF-7, HepG2, zebrafish	selenide oxidation, lysosome	[1215]	2019
Probe 1	F	490	~515	HeLa, zebrafish	seleno-Mislow-Evans rearrangement	[560]	2020

Pyrimidine-Se	F	390	469	buffer	selenide oxidation, reversible with GSH	[1216]	2022
MNG	FR	398	533	MCF7	selenide oxidation, reversible with GSH	[1217]	2022
NapEb	F	350	455	MCF-7	selenium-nitrogen, reversible with GSH	[559]	2023
Section 9 – Sulfate elimination							
HBT-Cy	F	390	450/ 590	MCF-7	sulfate elimination, reversible with bisulfite	[154]	2016
Probe 1	F	400	520/ 630	MCF-7, zebrafish	sulfate elimination, reversible with bisulfite	[155]	2017
Probe 1	F	570	660	HeLa, HepG2, mouse in vivo	sulfate elimination, reversible with bisulfite	[156]	2019
Probe 1	L	350	595	HeLa	sulfate elimination, reversible with bisulfite	[566]	2019
NBD	FR	550	618	HepG2	sulfate elimination, reversible with SO_2, mitochondria	[565]	2021
NI	FR	430/ 500	510/ 580	HeLa, zebrafish, mouse in vivo	sulfate elimination, reversible with bisulfite	[567]	2021
BN-DUAL	F	430	508	SKBR-3, mouse in vivo	sulfate elimination, reversible with SO_2	[568]	2022
TPE-y	F	390	614	MCF-7	sulfate elimination, reversible with bisulfite	[569]	2023
DCA-Bba	FR	600	685	MCF-7	sulfate elimination, reversible with SO_2	[570]	2023
Section 10 – Catechol oxidation							
DA–Cy	F	630	755	HL-7702, rat hippocampal ex vivo	catechol oxidation	[345]	2012
LyNC	F	450	537	C6, BV-2, rat hippocampal ex vivo	catechol oxidation, lysosome	[346]	2017
Section 11 – Payne/Dakin reaction							
HKPerox-1	F	520	543	RAW 264.7	Payne/Dakin	[571]	2018
HKPerox-2	F	480	527	RAW 264.7	Payne/Dakin	[571]	2018
H_2O_2-CL-510	CL	-	510	THP-1, mouse in vivo	Payne/Dakin	[572]	2020
HKPerox-Red	F	565	602	RAW 264.7, zebrafish	Payne/Dakin	[573]	2020
HKPerox-Ratio	FR	410	475/ 540	RAW 264.7	Payne/Dakin	[573]	2020
Cou-CHO	F	391	502	HepG2	Payne/Dakin	[574]	2021
Section 12 – Carbonyl group perhydrolysis							
AR	F	572	589	buffer	ester perhydrolysis	[575]	2002
PVR	F	572	589	buffer	ester perhydrolysis	[575]	2002
IVR	F	572	589	buffer	ester perhydrolysis	[575]	2002
TBAR	F	572	589	buffer	ester perhydrolysis	[575]	2002
IBR	F	572	589	buffer	ester perhydrolysis	[575]	2002
CHR	F	572	589	buffer	ester perhydrolysis	[575]	2002
ADR	F	572	589	buffer	ester perhydrolysis	[575]	2002
BR	F	572	589	buffer	ester perhydrolysis	[575]	2002
MOBR	F	572	589	buffer	ester perhydrolysis	[575]	2002
FUR	F	572	589	buffer	ester perhydrolysis	[575]	2002
Compound 1	F	490	~520	SH-SY5Y	carbamate removal, Hg^{2+} assisted	[576]	2013
ACF	F	450	527	HeLa	perhydrolysis	[577]	2016
ACR	F	470	560	HeLa	ester removal	[1218]	2017
DCM-AC	F	560	704	HepG2, mouse in vivo/ex vivo	acetate removal	[1219]	2019
HAA	FR	550	700	HepG2	acetate hydrolysis	[1220]	2020
Probe 1	F	309	505	RAW 264.7, zebrafish	ester removal	[578]	2021
YQ-2	F	550	678	HeLa	acetate removal	[1221]	2022
FAA-MC-OH	FR	325	440	buffer	nucleophilic aromatic substitution/acyl substitution	[579]	2021
Rhodol-OAc	F	500	560	A549	acetate removal, mitochondria	[1222]	2022
YQ-2	F	550	678	HeLa	acetate removal	[580]	2023
Compound 3a	F	430	617	milk, HepG2, zebrafish	acetate removal	[1223]	2023
Compound 3c	F	590	657	milk	acetate removal	[1223]	2023
Section 13 – Lanthanide binding							
Eu(tc)	L	405	616	buffer	europium binding	[583]	2002
Eu_3Tc	L	400	616	buffer	europium binding	[584]	2005

Tb^{3+}/PA	L	285	545	buffer	terbium binding	[585]	2014
Section 14 – Oxonium oxidation/cleavage							
BC	FR2P	410/ 760	472/ 693	RAW 264.7, zebrafish	oxonium cleavage	[586]	2016
GCP	FR	410	482/ 706	HepG2, HCT116, HeLa, MCF-7, zebrafish	oxonium cleavage, hepatocyte	[587]	2020
Section 15 – Aromatic amine oxidation							
HP Green	F	444	534	buffer	*p*-anisidine oxidation/cleavage	[588]	2011
BMTA-Tb^{3+}	L	315	542	tobacco leaf epidermal tissues	diamino phenyl ether cleavage	[582]	2011
TPE-TAF	FR	320	450	buffer	*ortho*-phenylenediamine oxidation	[589]	2021
2E2F	F	360	475	apple cells, tobacco leaf	amine oxidation, reversible with reductase	[590]	2022
Section 16 – Other triggers							
DTMC	CL	-	448	alkaline buffer	triazine oxidation	[1224]	2001
FH	F	494	527	buffer	hydrazide oxidation	[591]	2008
KBI	CL	-	545	HL-60	luciferin oxidation	[1225]	2009
3-Zn^{2+}	FR	360	510/ 550	PC3	zinc complex, dual with Zn and PPi	[592]	2013
SiOH2R	FR	550/ 663	570/ 681	HeLa	silane diol	[593]	2017
DPBF	F	410	450	aqueous	oxanthrone	[1226]	2017
2-pyr	F	480	509	HeLa	pyrazoline oxidation, photoclick reaction activation	[135]	2018
TT	FR	320	~460	RAW 264.7	tyrosine crosslinking	[594]	2018
GC-2	F	370	485	HepG2, mouse ex vivo	enamine removal	[1227]	2018
RH-1	FR	342	425	U251	chromone oxidation	[1228]	2019
CA/Co(II)	CL	-	550	buffer	dioxetane formation	[1229]	2020
BODIPY 2	FR	480	506/ 540	RAW 264.7	malononitrile oxidation	[1230]	2021
TBBQ	CL	-	425	buffer	tetrabromoquinone oxidations	[595]	2022
ACou-Ind	FR	395	475/ 650	zebrafish	alkene epoxidation	[596]	2022
TBBP-Pro	F	458	617	HepG2	oxidative cleavage of alkene, mitochondria	[597]	2023
LC-1250 NP	FR	808	1150/ 1250	Hepa1-6, mouse in vivo/ex vivo	spirocyclization	[1231]	2023

[a] F = fluorescence, R = ratiometric, 2P = two-photon, L= luminescence, CL = chemiluminescence, BL = bioluminescence, PA = photoacoustic. [b] Wavelengths given in nanometers.

Table 3. Small molecule probes for hypochlorite

Probe	Type[a]	λ_{ex} [b]	λ_{em} [b]	Application	Trigger/Comments	Ref	Year
Section 1 - Dearylation							
APF	F	490	515	PMA activated neutrophils	*O*-dearylation	607	2003
SNAPF	F	614	676	atherosclerosis associated macrophages	*O*-dearylation	609	2007
ANMTTA-Eu3+	L	330	610	HeLa, RAW 264.7	*O*-dearylation	610	2012
ANMTTA-Tb3+	L	330	540	HeLa, RAW 264.7	*O*-dearylation	610	2012
[Ru(bpy)2(AN-bpy)]2+	F	456	612	HeLa	*O*-dearylation	611	2014
Ir-ANMM	F	400	620	HeLa	*O*-dearylation	612	2014
3	F	410	465	HeLa	*O*-dearylation	1232	2015
BMAni	F	488	528	RAW 264.7	*N*-dearylation	614	2016
Np-ClO	F	372	508	HeLa cells	*O*-dearylation	615	2016
HKOCl-3	F	490	527	RAW 264.7, BV-2 mouse microglia, THP-1, zebrafish	*O*-dearylation	1233	2016
Gal-NPA	F	455	558	HepG2, MGC803, A549, SHSY5Y, hepatoma targeting	*O*-dearylation	618	2018
1	F	458	515	RAW 264.7	*O*-dearylation, spirolactam	1234	2018
Cy-HOCl	F	543	625	LO2, zebrafish, mouse	*O*-dearylation	613	2019
PAPE-HA	F	468	557	RAW 264.7, zebrafish	*O*-dearylation	1235	2019
HCA-Green	F2P	450/ 810	556	HeLa	*N*-dearylation	1236	2019
Nil-ClO	F2P	560/ 800	650	HeLa, RAW 264.7, rat liver tissue; mouse	*O*-dearylation	616	2020
HKOCl-4	F	530	557	RAW 264.7, rat brain, stroke model	*O*-dearylation, mitochondria	620	2020
ER-NPA	F2P	450/ 800	550	HeLa, zebrafish,	*O*-dearylation, endoplasmic reticulum	621	2020
Ru-AN-Gd	P	450	610	RAW 264.7, mouse, MRI	*O*-dearylation, lysosomal	1237	2020
NB4OH	F	468	540	RAW 264.7, HeLa	*p*-hydroxyaniline, endoplasmic reticulum	1238	2020
HNPE	F	460	550	RAW 264.7, zebrafish	*N*-dearylation	1239	2020
Lyso-PHE	F	468	560	RAW 264.7, HeLa	*O*-dearylation, lysosomal	1240	2021
BTH	F	468	553	HeLa	*O*-dearylation	1241	2022
Section 2 - Sulfur oxidation / spirocyclic ring opening							
HySOx	F	550	569	Neutrophils	spirothioether ring opening	622	2007
CMTH	FR	400	518/ 430	Human neutrophils; kidney sections from mice	thiospirolactam opening	1242	2010
MMSiR	F	652	670	Neutrophils; mice	thiospirolactone	624	2011
R19-S	F	515	550	Human PMNs, *Drosophila melanogaster*	spirocyclic ring opening	1243	2011
thiocoumarin probe 3	F	414	465	CH_3CN and acetate buffer	thione to lactone	1244	2012
Hypo-SiF	FR	570	586/ 475	buffer	spirothioether ring opening	626	2013
3	F	650	753	RAW 264.7, mice	spirothiolactone ring opening	1245	2013
RSTPP	F	553	580	RAW 264.7	thiolactone ring opening	623	2015
RGNH	F	500	550	RAW 264.7	spirocyclic ring opening, hydrazide	1246	2015
NIR-1	FR	650	707/ 486	HeLa, RAW 264.7	thiolactone to carboxylic acid	1247	2015
R19S	F	515	545	Mouse neutrophils, Drosophila	thiolactone ring opening	1248	2016
BRT	FR	525	540/ 580	RAW 264.7	spirocyclic ring opening, thioacyl hydrazide	1249	2016
STBR	FR	370	514/ 595	*E. coli*	spirocyclic ring opening, dual with Hg	1250	2016
CR-ClO	F	510	578	HeLa	thiolactone oxidation; ring opening	1251	2017
R19-S	F	515	550	Neutrophils, reactive halogen species	spirothioether ring opening	1252	2018
RPC-1	F2P	545/ 750	580	RAW 264.7, mouse liver cells, DILI	spirothioester ring opening, dual with H_{2S}	1253	2018
PA-MMSiNQ	PA	671	PA	Mouse in vivo	cyclic sulfide to SO_3	625	2019
HN2-TP	F2P	590/ 800	630	HeLa	thiospirolactam opening	1254	2019
Lyso-SiR-2S	F	616	677	HK-2, HeLa, RAW 264.7, mouse	spirodithiolactone ring opening, lysosomal	1255	2019

CR-HA	FR2P	563/800	580/471	HeLa, RAW 264.7 zebrafish	spironolamide ring opening	[1256]	2019
DQF-S	F	580	650	MCF-7, HeLa, RAW 264.7	spirothiolactone ring opening	[1257]	2020
SRh	F	525	582	HK2	thione to dihydrothioazole	[1258]	2020
MMBR	FR	530	575/646	RAW 264.7, MCF-7, zebrafish	spirothioether ring opening	[1259]	2021
Fcoum-S	FR	435	526/602	HeLa	thiolacone to lactone	[1260]	2022

Section 3 – Dimethylthiocarbamate (DMTC) removal

NDMTC	F	410	547	RAW 264.7, MCF-10, HepG2	DMTC cleavage, mitochondrial	[628]	2016
BCTP	F2P	460/800	540	RAW 264.7	DMTC cleavage	[630]	2018
BODIPY-DMTC	F	498	516	MCF-7, RAW 264.7, zebrafish	DMTC cleavage	[638]	2018
TP-HA	F2P	780	515	RAW 264.7, HeLa	DMTC cleavage	[640]	2018
Probe 1	BL	-	560	ES-2, mice	DMTC cleavage	[644]	2018
DAME	F	370	453	PC12, homemade test papers	DMTC cleavage	[1261]	2018
QYMTC	F	580	700	RAW 264.7	DMTC cleavage	[1262]	2018
QEMTC	F	630	720	RAW 264.7	DMTC cleavage	[1262]	2018
TCHC	F	370	455	RAW 264.7	DMTC cleavage	[1263]	2018
TCRH	F	480	550	RAW 264.7	DMTC cleavage, lysosomal	[1264]	2018
TCBT-OME	F	310	472	HeLa	DMTC cleavage	[1265]	2018
TCFL	F	470	515	RAW 264.7	DMTC cleavage	[631]	2019
ER-NTE	F	460	555	HepG2, zebrafish	DMTC cleavage, endoplasmic reticulum	[634]	2019
TPFR	F2P	550/800	603	RAW 264.7, MGC803, A549, HepG2, MCF-7	DMTC cleavage	[639]	2019
DCPO-DMTC	F	545	685	RAW 264.7	DMTC cleavage	[641]	2019
LSS-HA	F	400	505	RAW264.7, zebrafish	DMTC cleavage	[1266]	2019
C7	FR	460	468/630	HepG2, *C. elegans,* mouse	DMTC cleavage	[1267]	2019
RHSNO	F	405	590	MCF-7	DMTC cleavage, diacylhydrazide spirolactam opening	[1268]	2019
RF1	F	550	586	HeLa, RAW 264.7	DMTC cleavage	[1269]	2019
DCM-OCl	F	560	652	HeLa	DMTC cleavage	[1270]	2019
R1	F	450	550	EC1	DMTC cleavage, endoplasmic reticulum	[635]	2020
DDAO-ClO	F	605	658	HeLa, MCF-7, zebrafish	DMTC cleavage	[1271]	2020
BCy-HOCl	F	500	630	A549, mouse, acute lung injury	DMTC cleavage	[1272]	2020
NDS	F	420	525	HeLa	DMTC cleavage, lysosomal	[1273]	2020
DM-BDP-OCl	F	465	614	RAW 264.7, HeLa	DMTC cleavage	[1274]	2020
CS	F	345	451	HeLa	DMTC cleavage, lysosomal	[1275]	2020
DCOH-FR-OCl	FR	479	522/637	RAW 264.7	DMTC cleavage	[1276]	2020
Geisha-1	F	400	452	HeLa, mouse liver tissue	DMTC cleavage, boronic acid for H_2O_2	[1277]	2020
CDCl-HClO	F	510	700	HeLa, zebrafish, mouse	DMTC cleavage	[643]	2021
CDCl-HClO	F	510	700	HeLa, zebrafish, mouse	DMTC cleavage	[643]	2021
CyClOP	F	685	725	RAW 264.7, mouse	DMTC cleavage	[1278]	2021
CX-MTC	FR	390	525/665	PC12, zebrafish, mouse	DMTC cleavage	[1279]	2021
BM-HA	F	440	490	HeLa, zebrafish	DMTC cleavage	[1280]	2021
BM-HA	F	440	490	HeLa, zebrafish	DMTC cleavage	[1280]	2021
HDI-HClO	F	440	520	HeLa, RAW 264.7	DMTC cleavage	[1281]	2021
NFL-S	F	708	732	RAW 264.7, mouse	DMTC cleavage	[1282]	2021
RESClO	F	580	590	RAW 264.7, mouse	DMTC cleavage	[1283]	2021
KSQT	F	467	589	HepG2, zebrafish	DMTC cleavage	[1284]	2021
QM-ClO	F	430	620	MCF-7	DMTC cleavage	[1285]	2021
BBD	F	567	623	HeLa, zebrafish, mouse	DMTC cleavage, mitochondrial	[1286]	2021
HCy-HClO	F	475	585	HeLa, RAW 264.7	DMTC cleavage, mitochondrial	[1287]	2021
BDP-R-ClO	F	560	661	RAW 264.7, HepG2, mouse	DMTC cleavage	[632]	2022
Mito-QL	F	387	590	RAW 264.7, HepG2	DMTC cleavage, quinoline release, mitochondrial	[633]	2022
TCF-ClO	F	475	635	HeLa	DMTC cleavage	[642]	2022
TPAQ-ClO	F	450	560	HeLa	DMTC cleavage, mitochondrial	[1288]	2022
Compound 1	FR	397	480/550	HeLa	DMTC cleavage	[1289]8/15/	2022

						2024 4:18 :00 PM	
DFSN	F	432	535	RAW 264.7, HeLa, HepG2, zebrafish	DMTC cleavage	[1290]	2022
MEBTA-Cl	F	440	548	A549, HepG2, MCF-7, zebrafish	DMTC cleavage	[1291]	2022
DCM-DMTC	F	540	699	HeLa, lung tissue, asthmatic mice	DMTC cleavage	[1292]	2022
D-HBT	F	520	700	MCF-7	DMTC cleavage	[1293]	2022
HDCX-HClO	F	590	750	RAW 264.7, zebrafish	DMTC cleavage	[1294]	2022
HCTP-NTC	F	520	615	RAW 264.7	DMTC cleavage	[1295]	2022
BNA-HClO	F	384	510	HeLa	DMTC cleavage	[1296]	2022
HTCP	F	391/ 502	615	RAW 264.7	DMTC cleavage	[1297]	2022
Bp-S	F	495	508	RAW 264.7, HeLa	DMTC cleavage	[1298]	2022
1	F	302	502	PC-12	DMTC cleavage	[1299]	2022
HD-Br-1	F	650	710	MCF-7, tissue, superresolution	DMTC cleavage	[1300]	2022
THPIC	F2P	370/ 720	501	H9C2	DMTC, lysosomal	[1301]	2022
Section 4 - Chalcogen oxidation							
methylthio-BODIPY 2	F	519	525	RAW 264.7	sulfide oxidation	[646]	2011
HCS	F	505	516	RAW 264.7	sulfide oxidation	[1302]	2013
3	F	542	560	SH-SY5Y	sulfide oxidation	[1303]	2013
[Ru(bpy)$_3^{2+}$]PTZ	F	450	610	mouse in vivo	sulfide oxidation	[1304]	2014
PTZ-Cy2	F	450	605	mouse in vivo	sulfide oxidation, reversible with H_2S	[1304]	2014
Ptz-AO	F	475	540	INS-1 β-islet cells	sulfide oxidation	[647]	2016
Cy7-NphS	F	750	789	HL-60	sulfide oxidation, mitochondrial	[1305]	2016
Cy7-NphS	F	752	789	HL-60	sulfide oxidation	[1305]	2016
HES-BODIPY	FR	480	562/ 532	RAW 264.7	sulfide oxidation	[1306]	2016
L1 (Lyso)	F2P	405/ 800	505	MCF-7, 4T1	sulfide oxidation	[1307]	2017
PT-1 (Lyso)	F	460	540	L929 cells	sulfide oxidation	[1308]	2017
PQI	F	460	588	MCF-7, mice, zebrafish	sulfide oxidation	[650]	2018
PTZ-TDPP	FR	365	420/ 615	RAW 264.7	sulfide oxidation, mitochondrial	[658]	2018
PZ-HA	F	450	605	HeLa, Zebrafish	sulfide oxidation	[1309]	2018
L	F	600	672	L929	sulfide oxidation, mitochondrial	[1310]	2018
EtS-DMAB	F	440	610	RAW 264.7	sulfide oxidation	[1311]	2018
PT1	FR	423	446/ 622	RAW 264.7, zebrafish	sulfide oxidation	[1312]	2018
PT2	FR	468	516/ 665	RAW 264.7, zebrafish	sulfide oxidation	[1312]	2018
Dcp-EPtz	F	475	617	RAW 264.7, L929	sulfide oxidation	[1313]	2018
HCP	F	590	610	RAW 264.7	sulfide oxidation	[1314]	2018
PTZ-BT	F	484	642	HepG2	sulfide oxidation	[1315]	2018
NHS-ER	F2P	405/ 800	502	RAW 264.7, HeLa	sulfide oxidation, endoplasmic reticulum targeted	[659]	2019
S-BODIPY	FR	540	587/ 619	HeLa, zebrafish, mouse	sulfide oxidation	[1316]	2019
FPT	FR	380	524/ 586	HeLa, Zebrafish	sulfide oxidation	[1317]	2019
Probe 1	F	400	520	HeLa	sulfide oxidation, GSH & HOCl redox cycle	[1318]	2019
Probe 1	F	480	561	HeLa	sulfide oxidation	[1319]	2019
TJ2	FR	500/ 600	594/ 730	L929, RAW 264.7	sulfide oxidation, lysosomal	[1320]	2019
PI	F	486	620	RAW 264.7, zebrafish	sulfide oxidation	[1321]	2019
NS-ClO	F2P	360/ 800	450	RAW 264.7, HeLa, zebrafish	sulfide oxidation	[1322]	2019
NPG-1	F	488	510	HepG2, A549, HeLa, SGC7901	sulfide oxidation, hepatocyte targeting	[1323]	2019
NPG-2	F	488	510	HepG2, A549, HeLa, SGC7901	sulfide oxidation, hepatocyte targeting	[1323]	2019
BSi-1	FD	405	500	RAW 264.7, HeLa, zebrafish	sulfide oxidation, GSH & HOCl redox cycle	[1324]	2019

TPA-ClO	FR2P	365/ 720	497/ 437	HeLa	sulfide oxidation	[1325]	2019
TpyZnS	F	380	525	HeLa	sulfide oxidation	[1326]	2019
FSQTZ	F	345	513	PC12	sulfide oxidation	[1327]	2019
Avyl-BODIPY-PTZ	F	370	599/ 660	HepG2	sulfide oxidation	[1328]	2019
MXS	F	530	654	HeLa	sulfide oxidation, mitochondrial	[655]	2020
JX-1	F2P	365/ 800	509	HeLa, zebrafish	sulfide oxidation, endoplasmic reticulum targeted	[660]	2020
PTZ-Et	FR	396	534/ 626	RAW 264.7	sulfide oxidation	[1329]	2020
BSP	F	530	579	RAW 264.7	sulfide oxidation	[1330]	2020
CSU1	FR	376	409/ 520	MCF-7	sulfide oxidation, dual with H_2O_2	[1331]	2020
PDC	F	400	503	RAW 264.7, mouse, osteoarthritis	sulfide oxidation	[1332]	2020
Lyso-PTB	FR	320	418/ 520	HUVEC, zebrafish	sulfide oxidation, lysosomal	[1332]	2020
BTMSP	FR	365	450/ 580	HepG2	sulfide oxidation	[1333]	2020
Han-HClO-H_2S	FR	440	520/ 640	MCF-7	sulfide oxidation, dual with H_2S	[1334]	2020
Pl-Py	F	500	515	HeLa	sulfide oxidation, mitochondrial	[1335]	2020
Hy-2	F	436	526	HepG2, RAW 264.7, rat	sulfide oxidation and elimination	[1336]	2020
PTZ-HClO	FR	460	535/ 670	HeLa, zebrafish	sulfide oxidation	[1337]	2020
PBC	F	385	520	MCF-7	sulfide oxidation	[1338]	2020
PTC	F	520	627	HeLa, RAW 264.7, zebrafish	sulfide oxidation, mitochondrial	[652]	2021
AS-ClO	F	383	520	A549, MOVAS, RAW 264.7	sulfide oxidation, mitochondrial	[653]	2021
Cou-Lyso	FR	440	535/ 610	RAW 264.7, zebrafish	sulfide oxidation	[656]	2021
NUU-1	F	365	503	SH-SY5Y, mouse PD model, *Drosophila*	sulfide oxidation, C-C cleavage	[1339]	2021
1	FR	380	630/ 500	RAW 264.7	sulfide oxidation	[1340]	2021
CVS	F	596	638	HepG2	sulfide oxidation, mitochondrial	[1341]	2021
TPRS-HOCl	FR2P	350/ 800	490/ 595	RAW 264.7, A549; mouse	sulfide oxidation, lysosomal	[1342]	2021
PTZ-TPP	F	380	610	INS-1 b-islet	sulfide oxidation and C=C cleavage	[1343]	2021
PHPQ	FR	405	437/ 535	RAW 264.7, zebrafish	sulfide oxidation	[1344]	2021
PTMQ	F	460	577	HeLa	sulfide oxidation, also detects N_2H_4	[1345]	2021
FP	F	330	376	HeLa	sulfide oxidation	[1346]	2021
PTZ-2Cy	FR	325	600/ 488	L929	sulfide oxidation, C=C cleavage	[1347]	2021
PBC1	F	380	485	HeLa, zebrafish	sulfide oxidation, also detects SO_2	[1348]	2021
PPS	F	430	580	HeLa, RAW 264.7, mouse in vivo	sulfide oxidation	[1349]	2022
PM-S	F	375	490	HepG2	sulfide oxidation, mitochondrial	[651]	2022
PTZ-H	FR	400	640/ 520	RAW 264.7, zebrafish	sulfide oxidation	[1350]	2022
BPPy	F	420	562	Diabetic HLE	sulfide oxidation	[1351]	2022
NAP-RS	FR	405	638/ 452	HeLa	sulfide oxidation, lysosomal	[1352]	2022
PTBI	F	465	590	HeLa, HepG2	sulfide oxidation, also detects SO_2, mitochondrial	[1353]	2022
DP	F	480	608	HeLa, mice	sulfide oxidation, also detects SO_2	[1354]	2022
PBN-1	FR	390	495/ 550	HepG2, zebrafish	sulfide oxidation	[1355]	2022
HBA	F	420	456	HeLa	sulfide oxidation	[1356]	2022
BPQO	F	420	610	HepG2	sulfide oxidation	[1357]	2022
iSHERLOCK	FR	561	600/ 670	RAW 264.7	sulfide oxidation in lipid droplets	[1358]	2022
TMDC	F	396	717	H_2O:DMF	sulfide oxidation	[1359]	2022
Probe 1	FR	440	500/ 605	HepG2, zebrafish, alcoholic liver injury in mice	sulfide oxidation, also detects H_2O_2 via boronate oxidation	[1360]	2022
PNIS	F2P	325/ 700	447	HeLa, RAW 264.7	sulfone removal, mitochondrial	[1361]	2016

B-Ts	F	470	508	HeLa, RAW 264.7	sulfonyl hydrazone to aldehyde	[1362]	2017
Probe 1	F	355	444	SW480	sulfonyl hydrazone	[709]	2020
1	FR	412	542/ 488	U-373MG	sulfonyl-semicarbazide	[1363]	2020
QBH	F	395	520	RAMOS	sulfonyl hydrazone	[1364]	2020
Ir-Ts	L	360	574	HeLa	sulfonyl hydrazone	[1365]	2020
NH	FR	434	643/ 517	HUVEC, A549	sulfide oxidation, also detects NQO1	[1366]	2022
ClO-1	F	450	635	RAW 264.7, MCF-7	sulphur oxidation to sulfoxide	[1367]	2022
HCTe	F	480	531	RAW 264.7	telluride to telluroxide	[665]	2015
5	F	498	515	RAW 264.7	tellenide oxidation	[1368]	2019
Probe 1	F	340	457	buffer	S,S acetal	[668]	2011
TP-HOCl	F2P	375/ 800	500	HeLa, macrophages	S,O ketal deprotection	[669]	2015
HPBD	F	455	585	HeLa, RAW 264.7	S,O ketal removal	[672]	2016
rTP-HOCl 1	FR2P	460/ 900	598/ 633	HeLa	S,O ketal to ketone	[1369]	2017
OPV-MEP	F2P	400/ 740	534	BV-2 Cells	S,O acetal	[1370]	2017
Probe 1	FR	368	464/ 546	HeLa	S,S acetal to CHO	[1371]	2017
CMOS	FD	405	480	SKVO-3	S,O ketal to ketone	[671]	2018
QClO	FR2P	414/ 820	562/ 492	HeLa, mouse, wound healing	S,O-acetal	[673]	2018
LH	F	440	520	MACF7	S,S acetal deprotection	[1372]	2018
TQC-HClO	FR2P	476/ 800	650/ 583	HeLa, zebrafish	S,O ketal	[1373]	2020
LG-1	F	395	520	RAW 264.7	S,O-acetal	[1374]	2020
LG-3	F	395	520	RAW 264.7	S,O-acetal, dual with $ONOO^-$	[1374]	2020
DQ-HOCl	F	395	533	W138, B16F10, RAW 264.7	S,O acetal	[1375]	2020
MCL	FR	358	525/ 465	HeLa	S,O acetal	[1376]	2020
Cou-HOCl	F	410	510	HeLa, A549, HepG2,	S,O ketal	[1377]	2021
P-Hc	FR	346	550/ 461	serum	S,O acetal to aldehyde	[1378]	2022
YT	FR	400	590/ 640	SMMC-7721, zebrafish	S,S acetal	[1379]	2022
CM1	F	405	480	NIH-3T3, HL-60, RAW 264.7	selenoxide elimination	[666]	2013
CM2	F	405	468	buffer	selenoxide elimination	[666]	2013
HCSe	F	510	526	RAW 264.7	selenide oxidation	[1380]	2013
MPhSe-BOD	F	500	510	RAW 264.7	selenide oxidation, reversible with H_2S	[1381]	2013
SeCy7	F	690	786	mouse	selenide to selenoxide	[1382]	2014
Lyso-NI-Se	F	430	530	RAW 264.7	selenide to selenoxide, lysosomal	[663]	2015
FO-PSe	F2P	415/ 800	520	RAW 264.7, zebrafish, mice	selenide oxidation, reversible with GSH	[1383]	2015
1	F	492	507	RAW 264.7	selenide to selenoxide	[1384]	2016
2	F	511	526	RAW 264.7	selenide to selenoxide	[1384]	2016
Nap-Se	FD	410	540	RAW 264.7	selenide oxidation, HOCl & GSH redox cycle, mitochondrial	[664]	2018
Coum-Se	FR2P	475/ 800	618/ 495	RAW 264.7, mouse	selenide, coumarin formation	[667]	2018
BSez-Et	F	532	548	buffer	selenide oxidation, mitochondrial	[1385]	2019
BSe-Bz	F	530	545	RAW 264.7	selenide oxidation, mitochondrial	[1385]	2019
BSe-Ph	F	532	550	Buffer	selenide oxidation, mitochondrial	[1385]	2019
Fl-Se	F	~490	517	HL-60	selenide oxidation, reversible with GSH	[1386]	2020
BOPHY-SePh	F	452	482	MCF-7	selenide oxidation	[1387]	2021
Fluo-Se	F	494	528	L929	selenide oxidation	[1388]	2021
PzSe	F	500	600	HeLa, PC-12, RAW 264.7	selenide oxidation, reversible with H_2S	[1389]	2021
Boppy-SePh	F	413	437	HeLa	selenide oxidation	[1390]	2022
TRA	F	520	562	*E. coli*	thioamide opening	[1391]	2014
CM2	F	417	485	SHSY5Y, Mouse	thioamide to amide	[1392]	2019
MBTC	F	620	690	RAW 264.7	thiocarbamate cleavage	[1393]	2018
1	F	435	552	HeLa, RAW 264.7	thioester to ester	[1394]	2018

CARSH	FR	350	580/490	RAW 264.7	thiohydrazide	[1395]	2016
Fcoum-S	FR	435	526/602	RAW 264.7, zebrafish	thiophene acylhydrazone	[707]	2021
TF	F	495	520	HeLa	thiophene hydrazone to CHO	[1396]	2016
PCTP	F	415	638/514	HEK293; zebrafish	thiophene oxidation	[1397]	2020
NTPC	F	453	536/622	HeLa	thiophene oxidation	[1398]	2020
TCS	F	380	435	MCF-7	thiophene oxidation	[1399]	2021
CZCN-O	F	405	486	HeLa	desulfurization	[1400]	2020
PDI-S	F	493	564	A549, RAW 264.7	desulfurization	[1401]	2022
PZ-Py	F	400	562	HeLa, RAW 264.7, mouse	sulfide oxidation, mitochondria	[1402]	2015
6	F	630	738	RAW 264.7	diphenyltelluride oxidation	[1403]	2021
AETU-HOCl	FR	380	533/473	RAW 264.7	thiourea cyclization	[1404]	2016
FDOCl-20	F	620	686	HepG2, RAW 264.7, mouse	thiourea	[1405]	2020
BR-1	F	610	669	RAW 264.7, HL-60	thiourea	[1406]	2020
5	F	363	488	PC-12	thiourea cyclization, mitochondrial	[1407]	2021
ASiP_HOCl	FR	504	717/642	RAW264.7, mouse,	thiourea cyclization	[1408]	2021
Probe 1	FR	380	484/533	PC-12	thiourea cyclization, endoplasmic reticulum targeted	[1409]	2020
Probe 1	FR	380	476/533	HepG2	thiourea cyclization, lysosomal	[1410]	2019
PIPT	FR	365	505/430	Human lung adenocarcinoma	thiourea to C-H	[1411]	2014
TPFP	F2P	430/800	538	HeLa	thiourea to urea, lysosomal	[1412]	2018
SPF-S	FD2P	370/800	429	A549	thiourea to urea	[1413]	2018
TPE-M	F	350	492	HeLa	thiourea to urea, AIE	[1414]	2022
Section 5 - Nitrogen atom oxidation							
DNS-RBPH	F	370	501	HeLa cells	hydrazide oxidation	[681]	2011
Rhodamine B hydrazide	F	500	550	A549	hydrazide spirolactam	[1415]	2011
Probe 1	F	500	550	A549, RAW 264.7	hydrazide spirolactam	[1415]	2011
Probe 2	F	500	550	buffer	hydrazide spirolactam	[1415]	2011
RGPH	F	500	550	A549 cells	hydrazide oxidation	[1416]	2016
LR1	F	560	582	RAW 264.7	hydrazide spirolactam, lysosomal	[1417]	2018
RIM	FR	370	585/465	RAW 264.7	hydrazide spirolactam, lysosomal	[1418]	2018
FHP	F	325	518	buffer	acylhydrazone spirolactam	[1419]	2012
RG6H	F	505	548	water	acylhydrazide spirolactam	[1420]	2012
NMICl	F	318	397	HepG2	acylhydrazide-imide to nitroso	[1421]	2015
RBT	F	550	575	RAW 264.7	acylhydrazide to COOH	[1422]	2015
FHZ	F	490	520	HeLa, RAW 264.7, zebrafish	acylhydrazide ring opening, dual with hydroxyl radical	[1423]	2016
PIPH	F	330	415	HeLa	acylhydrazide to acid	[1424]	2017
TPAD	F	375	523	A549	acylhydrazone cleavage to CHO	[1425]	2018
N1-N6	F	505	563	HepG2, zebrafish	acylhydrazone pyridine to triazolopyridine	[710]	2020
CMSH	FR	365	470/532	*E. coli*, MRC-5, zebrafish	acylhydrazone	[1426]	2020
PTC	F	385	450	A549, HeLa	acylhydrazone	[1427]	2020
LH-1	F	415	488	HeLa, RAW 264.7, zebrafish	acylhydrazide	[1428]	2020
FCZ	F	470	530	RAW 264.7, zebrafish	acylhydrazone	[1429]	2020
Ir-Iso	L	344	592	4T1	acylhydrazone, mitochondrial	[1288]	2020
FCJD	F	506	530	RAW 264.7, HeLa, zebrafish, mice	acylhydrazone spirolactam	[1430]	2021
Probe 3	F	440	500	HepG2	acylhydrazone	[1431]	2021
TPB-NO_2	F	330	469	mouse, LM-3	acyl hydrazone spirolactam,dual with $ONOO^-$	[1432]	2021
6	F	515	556	HepG2, zebrafish	acylhydrazone spirolactam	[1433]	2022
Lyso-NIR-HClO	F	620	680	HeLa, RAW 264.7, zebrafish	4-nitrobenzenesulfonylhydrazide	[1434]	2022
CoPh-ClO	F2P	420/	505	HeLa, RAW 264.7, zebrafish	4-nitrobenzenesulfonylhydrazide	[1434]	2022

		740					
Ir-1	F	370	615	buffer	aldoxime	[727]	2009
1	F	339	458	buffer	oxime oxidation; turn-off	[1435]	2010
Flu-1	F	365	530	HeLa	aldoxime	[684]	2011
MitoClO	F	488	529	MCF-7	aldoxime oxidation, mitochondrial	[1436]	2013
Bodipy-OX	F	470	529	MCF10A	aldoxime to nitrile oxide	[689]	2013
BOD-OXIME	F			RAW 264.7	aldoxime oxidation	[690]	2013
NACl	F	370	510	RAW 264.7	aldoxime to CHO	[1437]	2016
HCH	F2P	422/ 860	546	CHO	aldoxime to nitrile oxide, mitochondrial	[692]	2016
1	F	350	540	HeLa	aldoxime to nitrile oxide	[694]	2018
Probe 1	F	358	460	RAW 264.7	aldoxime to CHO	[685]	2018
BTN	FR2P	366/ 588	660/ 440	A549	aldoxime to nitrile oxide	[696]	2018
D1	F	415	575	HeLa and zebrafish	aldoxime to CHO	[687]	2019
MN-BODIPY	FR	420	530/ 558	MCF-7	aldoxime to CHO, lysosomal	[691]	2019
Aza-BODIPY-CNOH	F	631	667	RAW 264.7	aldoxime oxidation	[1438]	2019
1	F	397	465/ 506	A549, MCF-7	aldoxime oxidation	[686]	2019
Ir-CLFLPLIM	CFP	730	564/ 570	LM-3, mouse	aldoxime to acid	[1439]	2020
Ir1	F	271	562	buffer	aldoxime to acid	[1440]	2020
Ir2	F	292	578	RAW 264.7, A549	aldoxime to acid	[1440]	2020
OFN	FR	340	515/ 575	RAW 264.7	oxime to aldehyde	[1441]	2020
HE	F	473	610	HepG2	oxime	[1442]	2020
PyOX	F	633	680	RAW 264.7, A549, COS-7, HepG2, T98G, BEAS-2B, HUCEC, mouse	aldoxime oxidation	[695]	2021
SWJT-1	F	520	676	HeLa; mouse	aldoxime	[688]	2021
BD-NOH	FR	600	670/ 645	HeLa	aldoxime to nitrile oxide	[693]	2022
ATHO	F	365	453	HeLa, zebrafish	oxime	[1443]	2022
DV26	F	520	625	HepG2	amino oxidation, azo compound formation	[1444]	2014
probe	F	325	518	HepG2	aniline oxidation	[1445]	2014
BRClO	FR	480	585/ 505	MCF-7	pyrrole NH oxidation	[1446]	2015
Ir-dmn	F2P	402/ 750	590	HeLa, RAW 264.7	imine to COOH, mitochondrial	[1447]	2015
2	F	430	526	HepG2	NH_2 to nitroso	[1448]	2016
DMD	FR	485	635/ 521	A549, colorimetric	NH_2 to nitroso	[1449]	2018
QBN	F	365	464	HeLa, RAW 264.7	NH_2 to nitroso	[1450]	2021
FN-2	F	490	529	HeLa	aminonaphthalene removal	[1451]	2017
Dye 1	F	360	425	HeLa, make-shift test papers	indole N-H to N-O	[1452]	2018
LV-2(H)	FD	560	650	HeLa	amino to imine, NAD(P)H & HOCl redox cycle	[1453]	2018
NBD-NH_2	F	465	549	HeLa	amine to nitroso	[1454]	2018
Probe 1	F	479	553	HeLa	amine to imine	[1455]	2018
NB-OCl	F	600	672	HeLa	NH_2 to nitroso	[1456]	2018
1	F	580	630	PC12	amine to nitroso	[1457]	2019
DN	F	365	435	HeLa, RAW 264.7	imine oxidation	[1458]	2019
BK	F	350	455	zebrafish	imine cleavage	[1459]	2020
Lyso-NA	F2P	432/ 860	540	RAW 264.7, mouse	aminophenol, lysosomal	[617]	2020
XS-1	F	580	626	HepG2	aniline oxidation to nitroso	[1460]	2020
CVA	F	580	627	Eca 109	aniline oxidation to nitroso	[1461]	2020
HCA-Green	F2P	450/ 810	556	HEK293T	imidazole hydrazone	[1462]	2022
Probe	F	447	550	water samples, RAW 264.7, zebrafish	aminonaphthalimide oxidation	[1463]	2022
Luminol	CL	-	425	neutrophils, *Crassoostrea virginica,* PMN leukocytes	luminol oxidation	[1464] [1465] [1466]	1995
1	F	520	578	buffer	diacylhydrazide ring opening	[674]	2008
Probe 1	F	515	580	buffer	diacylhydrazine spirolactam	[1467]	2011
RHQ	F	530	580	PBMCs	diacylhydrazide spirolactam	[1468]	2014

Probe 1	FR	410	470/580	RAW 264.7	diacylhydrazide cleavage, ring opening	682	2014
Rh-TPP	F	540	577	HeLa, mouse in vivo	diacylhydrazide, mitochondria	1469	2014
Rh-Py	F	540	575	HeLa, mouse in vivo	diacylhydrazide, mitochondria	1469	2014
RHHP	F	520	580	HeLa	diacylhydrazide spirolactam	1470	2014
Lyso-HA	FR	365	450/585	HeLa, A549, RAW 264.7	diacylhydrazide cleavage, ring opening, lysosomal	1471	2016
RHQ	F	520	580	leukocytes monocytes, neutrophils from diabetic subjects	diacylhydrazide spirolactam	1472	2016
Ir-Fc	F	450	600	Mouse liver	diacylhydrazide ferrocene	1473	2016
RBP	F	540	583	L929, mice	diacylhydrazide to COOH	1474	2016
FL-HA	FR	380/530	455/584	HeLa, RAW 264.7	diacylhydrazide	1475	2017
Ir-Fc	L2P	850	600	HepG2, zebrafish, mouse	diacylhydrazide to COOH	1476	2017
1	F	480	542	HeLa	diacylhydrazide spirolactam	1477	2017
BiTClO	F	560	575	HEK293, RAW 264.7, HeLa	diacylhydrazide, mitochondria	1478	2017
IRP (mito)	FR	370	467/575	RAW 264.7	diacylhydrazide to acid	1479	2017
RIL	FR	360	588/463	RAW 264.7	diacylhydrazide spirolactam opening, lysosomal	1480	2018
RPM	FR	400	587/462	RAW 264.7	diacylhydrazide spirolactam opening	1481	2018
L	F	565	576	HeLa	diacylhydrazide spirolactam opening	1482	2018
Cou-dhz-Ph-NO_2	F	430	478	MDA-MB-231, RAW 264.7, neutrophils, liver	diacylhydrazide	1483	2018
FLNC	FR	517	535/474	buffer	diacylhydrazide spirolactam opening	1484	2018
Rh-ClO	F	556	578	HeLa	diacylhydrazide spirolactam opening, mitochondrial	1485	2018
Lyso-HA-HS	FD	550	580	HeLa	diacylhydrazide spirolactam opening, dual with H_2S, lysosomal	676	2019
TR-OCl	FR	326	589/477	RAW 264.7, B16F10 and WI38	diacylhydrazide spirolactam opening	1486	2019
RC	FR	420	590/480	HeLa, tap water	diacylhydrazide spirolactam opening	1487	2019
RL1	F	568	592	HeLa	diacylhydrazide spirolactam opening, lysosomal	1488	2019
IRh-Ly	FR	370	589/462	RAW 264.7	diacylhydrazide spirolactam opening, lysosomal	1267	2019
Mito-TP-ClO	F2P	605/820	650	HeLa, RAW 264.7, mouse	diacylhydrazide spirolactam opening	1458	2019
FD-301	F	620	686	HL-60, mouse	diacylhydrazine	1489	2020
Mito-P-OCl	FR2P	573/800	595/453	BV-2, HepG2, hypoxic ischaemia, mouse brain	diacylhydrazine, mitochondrial	1427	2020
ZED	F	543	580	MCF-7	diacylhydrazine, mitochondrial, dual with Cys/HCy	1490	2020
Rd1	F	530	585	A549, mouse liver tissue, RAW 264.7, zebrafish	diacylhydrazine, mitochondrial	1491	2020
Fl-Mito	F	580	637	RAW 264.7, mouse	diacylhydrazine, mitochondrial	1492	2021
RHE	FR	560	515/585	HepG2	diacylhydrazone spirolactam, endoplasmic reticulum	678	2022
RIC	F	543	580	MCF-7	diacylhydrazide to acid, mitochondrial	679	2022
WD-HOCl	F	597	682	BV-2	diacylhydrazide pyridinium, mitochondria	1493	2022
TJM	F	585	730	HeLa, zebrafish, mice	diacylhydrazide	1494	2022
RSHClO	FR	405	558/464	B16	diacylhydrazide, dual with biothiols	1495	2022
RhNp-ClO-ONOO	F	420	574	RAW 264.7, rat, muscle tissue	diacylhydrazide oxidation, dual with $ONOO^-$	1496	2022
1b	FR	540/464	505/585	A549 cells; zebrafish	hydroxamic acid ring opening	680	2008
RMClO-1	FR	405	570/481	buffer	diacylhydrazide to COOH, mitochondrial	1497	2015
RMClO-2	FR	405	570/476	A549, HeLa, HEK293, RAW 264.7	diacylhydrazide to COOH, mitochondrial	1497	2015

PL-HA	F	480	525	RAW 264.7, HeLa	photolysis at 365 nm, diacylhydrazide spirolactam opening, lysosomal	675	2018
HOCMem	F	460	520	HepG2, near-membrane tracking	photolysis at 365 nm, diacylhydrazide spirolactam	1498	2018
NM1	F	505	580	HepG2, zebrafish	pyridine hydrazone to triazaolopyridine, mitochondrial	711	2020
DV26	F	520	625	HepG2	azo formation	1444	2014
HBP	F	480	508	RAW 264.7	triazole formation	661	2015
Ruazo	F	465	600	Mouse in vivo	triazole formation from ortho amino azo	1499	2016
Probe 1	F	480	537	HeLa cells	TEMPO oxidation	1500	2016
NAP-OH	F	475	530	HeLa, RAW 264.7	TEMPO oxidation	1501	2021
RHN	F	500	550	HeLa	phenylazo cleavage, mitochondrial; turn off	1502	2022
CAN	FR	380	510/ 440	A549, RAW 264.7	diamine oxidation	1503	2020
HSiO3	F	700	760	RAW 264.7, mouse	Si-oxazine oxidation	1504	2020
TPP	F	400	544	MG63, MC3T3	pyridinium oxidation	1505	2021
Section 6 – Thiosemicarbazide							
2	FR	414	473/ 594	Bel 7702, RAW 264.7	thiosemicarbazide	703	2012
Probe 1b	FR	414	594/ 473	Bel 7702, RAW 264.7	thiosemicarbazide	703	2012
Probe 2	F	569	590	buffer	thiosemicarbazide	703	2012
1	F	365	556	RAW 264.7	thiosemicarbazide	704	2012
Naph-Rh	FR	350	440/ 585	RAW 264.7	thiosemicarbazide	705	2015
NR	FR	405	532/ 582	RAW 264.7	thiosemicarbazide	1506	2017
NCS-BOD-OCH3	FR2P	530/ 656	595/ 665	A357	thiosemicarbazide to oxadiazole	1507	2017
DICX(Lyso)	FR	410	480/ 580	RAW 264.7	thiosemicarbazide to oxadiazole	1508	2017
RHSDN	FR2P	406/ 800	530/ 590	A549, MCF-7 Cells	thiosemicarbazide to oxadiazole, ring opening	1509	2017
RHClO-1	FR	410	575/ 473	RAW 264.7	thiosemicarbazide spirolactam opening	1510	2018
RHClO-2	FR	325	585/ 460	RAW264.7	thiosemicarbazide spirolactam opening	1510	2018
2	FR	475	612/ 570	HeLa	thiosemicarbazide spirolactam opening	1511	2018
1	F	370	457	RAW 264.7	thiosemicarbazide cleavage	1512	2018
Lyso-NIR-HClO	F	620	680	HeLa, mouse	acylthiosemicarbazide spirolactam opening, lysosomal	1513	2019
CR-Ly	FR	420	582/ 479	RAW 264.7	acylthiosemicarbazide spirolactam opening, lysosomal	1514	2019
ACO and CETC	F	380	478	HepG2	thiosemicarbazide and coumarin cleavage	1515	2019
PR-HOCl	F	710	730	RAW 264.7, mouse	acylthiosemicarbazide to oxadiazole	1516	2020
TPE-RNS	FR	405	590/ 480	RAW 264.7, HeLa, MCF-7	acylthiosemicarbazide to oxadiazole	1517	2020
M1	FR	420	580/ 534	EC109	acylthiosemicarbazide to oxadiazole	1518	2020
Lyso-TP-HClO	F2P	622/ 820	655	RAW 264.7, mouse	acylthiosemicarbazide to oxadiazole, lysosomal	1519	2021
TB	F	400	500	onion cells, zebrafish	thiosemicarbazide, also detects Hg(II)	1520	2021
Lyso-R-HClO	F	568	590	HeLa, RAW 264.7, bacteria infected macrophage	thiosemicarbazide	1521	2022
Probe 1	F	414	523	HeLa	thiosemicarbazide	1522	2022
Section 7 - Hydrazone Oxidation							
1b	F	510	542	*Rhodobacter ferroxidans*	hydrazone spirolactam	1523	2013
1	F	490	524	MG-63	hydrazone dimer to fluorescein release	1524	2014

2	F	490	528	MG-63	hydrazone dimer to fluorescein release	1524	2014
1	F	517	533	MG-63	hydrazone to fluorescein release	1524	2014
BODH	F	480	508	RAW 264.7	dihydrazone	706	2015
Probe 1	F	494	521	MCF-7	hydrazone to aldehyde	1525	2015
1	F	355	383	HeLa	hydrazone oxidation	1526	2015
INCN	F	375	480	RAW 264.7	hydrazone to acid	1527	2016
YDN	F	485	516	HeLa, mice	hydrazone oxidation	1528	2016
Probe 1	F	490	535	L929 Cells, MG-63	hydrazone oxidation/ring opening	1529	2017
Lyso-1	F	500	563	L929 cells	hydrazone oxidation/ring opening	1530	2017
NPPTA-Eu^{3+}	L	330	610	RAW 264.7, *Daphnia magna*	dinitrophenylhydrazone oxidation	1531	2017
HBM	F	420	528	RAMOS	hydrazone to CHO		2018
HBI-Cl	F	328	455	HeLa, MCF-7	hydrazone cleavage	1532	2018
F-BH	F	323	523	HeLa, naked eye detection	hydrazone cleavage and spirolactam opening	1533	2018
NNH	FR2P	445/ 800	440/ 525	RAW264.7, mouse, DILI	hydrazone to nitrile	1534	2018
DNPH-NA	F	430	518	HeLa, J774A.1, zebrafish	hydrazone oxidation	1535	2018
Probe 1	F	470	515	HepG2	hydrazone to CHO	1536	2018
6G-ClO	F	533	556	HUVEC	cyclic hydrazone to CHO	1537	2019
L1	F	350	550	HeLa	hydrazone cleavage	1538	2019
L2	FR	350	430/ 540	HeLaC	hydrazone cleavage	1538	2019
HBT-HBZ	FR	400	470/ 572	HeLa	benzothiazole hydrazone cyclization	1539	2020
R	F	354	463	RAW 264.7	toluenesulfonylhydrazone, dual wih Co(II)	1540	2020
CM-hbt	FR	395	478/ 528	RAW 264.7, mung beans	benzothiazole hydrazone	708	2021
HClO-ER	F2P	500/ 800	556	HeLa, RAW 264.7, mouse,	hydrazone spirolactam, endoplasmic reticulum targeted	1541	2021
TPB-NO_2	F	330	469	HeLa, zebrafish	hydrazone	1542	2021
Probe 1	F	550	705	HepG2	hydrazone carbamate, dual with Zn	1543	2022
BTN-Fu	F	360	465	zebrafish	bis-acylhydrazone	1544	2021
LL3	F	430	490	HeLa	hydrazone cleavage	1545	2022
NQ	FR	320	551/ 479	HeLa	FRET hydrazone cleavage	1546	2022
Probe 1	F	400	475	HeLa	hydrazone cleavage, ER targeted	1547	2022
Section 8 - C=C bond oxidation							
9-AEF	F	360	441	HeLa cells	C=C oxidation	712	2010
1	FR	465	629/ 520	RAW 264.7	C=C cleavage	720	2013
Cy7-NR	FR	540	566/ 780	HeLa cells	C=C epoxidation	715	2013
CY-FPA	F	710	774	A549	C=C epoxidation	713	2014
CMCY	FR	460	480/ 631	HeLa	C=C cleavage	1548	2014
PMN-TPP	FR	410	640/ 522	RAW 264.7	C=C oxidation	717	2015
Probe 1	F	373	468	HepG2	C=C epoxidation	1549	2015
CYDEA	F	685	771	MCF-7	C=C epoxidation	1550	2016
Compound 1	FR	430	620/ 515	HepG2	C=C cleavage	1551	2016
Compound 2	FR	430	630/ 515	buffer	C=C cleavage	1551	2016
WCN	F	530	560	HeLa, mouse in vivo	C=C oxidation	1552	2016
HPQ-Cy2	FR	365	575/ 435	A375	C=C cleavage, mitochondrial	722	2016
BDP-CY	F	505	510	MCF-7	C=C oxidation, dual with viscosity	1553	2016
CMBI	FR	390	475/ 658	HeLa	C=C oxidation, mitochondrial	723	2016
CYDEA	F	685	771	MCF-7	C=C epoxidation	1550	2016

BFClO	FR	480/635	713/511	MCF-7	C=C cleavage	[1554]	2017
DFP	FD	360	490	HeLa	C=C cleavage, SO_2 addition	[1555]	2017
Probe 1	FR	398	615/460	HeLa	C=C cleavage, mitochondria	[1556]	2017
CPBT (mito)	FR	405	480/580	RAW 264.7	C=C oxidation	[1557]	2017
MPIBA	FR	380	500/625	HeLa	C=C oxidation	[1558]	2017
DNB	FR2P	460/420	600/525	HeLa, RAW 264.7	C=C oxidation, SO_2 detection, mitochondrial	[1559]	2017
P	FR	488	480/612	HeLa, zebrafish	C=C cleavage	[1560]	2018
BIP	FR	380	455/632	HeLa	C=C cleavage, mitochondrial	[721]	2018
Probe 1	FR	450	510/660	HeLa, mouse, RA	C=C cleavage	[719]	2018
XWJ	FR	370	550/670	RAW 264.7	C=C cleavage	[1561]	2018
ClO1	FR	650–550	600/750	A549, mouse lung	C=C epoxidation	[716]	2018
Zcp-Me	FR	420	486/609	RAW 264.7	C=C epoxidation	[1562]	2018
FL	F	490	530	HeLa	C=C cleavage	[1563]	2018
ZBM-H	FR	405	512/653	RAW 264.7	C=C cleavage	[1564]	2018
NPA-CN	FR2P	400/760	449/583	HepG2, zebrafish	C=C cleavage, logic gate of ClO^-, OH^- and H_2O	[1565]	2018
TPP-TCF	F	488	660	HeLa, mouse	C=C cleavage	[1566]	2018
CBP	R	410	456/662	HeLa	C=C cleavage	[1567]	2018
FL-CyN	FR2P	460/800	630/754	zebrafish, MCF-7	C=C cleavage	[1568]	2018
PI	F	440	551	HeLa, zebrafish, mouse	C=C cleavage	[1569]	2019
ICC	FR	530	486/685	HepG2	C=C cleavage	[1570]	2019
BODIPY-P	FR	500	567/629	L929	C=C cleavage	[1571]	2019
ZBM-H	F	555	653	A549	C=C cleavage, endoplasmic reticulum targeted	[1572]	2019
NClO	FR	450	520/615	HeLa, zebrafish	C=C cleavage	[1573]	2019
MTPA-Cy	F2P	365/538/730	514	HeLa	C=C cleavage, mitochondrial	[1574]	2019
DMI	F	395	622	A549	C=C cleavage, mitochondrial	[1575]	2019
XHZ	FR	410	470/672	RAW 264.7	C=C cleavage; neutral lipid droplet	[1576]	2019
CMM	F	360	459	MDA-MB-231	C=C cleavage	[1577]	2019
SB2	FR	573	590/657	RAW 264.7	C=C oxidation to epoxide	[1578]	2019
1	F	530	567	Eca109	C=C cleavage	[1579]	2019
ZOC	FR	420	478/610	RAW 264.7	C=C cleavage	[1458]	2019
PPC	F	420	462/629	RAW 264.7	C=C cleavage	[1580]	2019
Py-Pd	F	373	469	HeLa, zebrafish	C=C cleavage	[1581]	2019
Probe 1	FR	561	608/735	HepG2	C=C oxidation	[1582]	2019
COTN	F	405	520	RAW 264.7, mouse	C=C cleavage	[1583]	2020
HOTN	F	405	535				
NSSN	FR	450	670/540	HeLa, mouse, dual mode	C=C oxidation, mitochondrial	[1584]	2020
Ql	F	390	520	HeLa, mouse in vivo	C=C cleavage	[1585]	2020
1	F	420	490	HepG2, *Arabidopsis thaliana*	C=C oxidation	[1586]	2020
DL	FR	410	496/713	HeLa	C=C to halohydrin	[1587]	2020
AI	FR	370	495/570	HeLa, mouse	C=C oxidation to ketone	[714]	2020

S-ClO	F	360	475	RAW 264.7, mouse, patient samples	C=C oxidation	[1588]	2020
1	F	465	520	HeLa	C=C oxidation, lysosomal	[1589]	2020
Cy7-Nil	FR	580/ 700/ 520	650/ 780/ 560	HeLa	C=C oxidation	[1590]	2020
DCC	FR	488	420/ 570	HeLa, zebrafish, *Arabidopsis thaliana*	C=C cleavage	[1591]	2020
NEC-TBA	F	480	648	HeLa, zebrafish	C=C cleavage	[1592]	2020
TPE-TBA	F	455	678	HeLa, zebrafish	C=C cleavage	[1592]	2020
HN-ClO	F	430	560	HepG2, zebrafish, mouse	C=C cleavage	[1593]	2021
JBD	F	400	607	HeLa	C=C oxidation	[1594]	2021
TBDP	F	400	599	HeLa, RAW 264.7	C=C oxidation	[1595]	2021
TBDT	F	466	617	HeLa, RAW 264.7	C=C oxidation	[1595]	2021
RSS-HClO	F	410	490	KYSE-30; MCF-7	C=C oxidation, also responds to Cys/Hcy	[1596]	2021
1	FR	365	482/ 567	HepG2	C=C oxidation	[718]	2021
SE	F	510	522	HeLa, RAW 264.7, zebrafish	C=C oxidation	[1597]	2021
Probe C	F	~335	493	RAW 264.7	C=C oxidation	[1598]	2021
Probe D	F	~364	530	RAW 264.7	C=C oxidation	[1598]	2021
Probe 2	F	375	520	HeLa, zebrafish	C=C oxidation	[1599]	2021
DBTM	F	469	650	L929	C=C cleavage	[1600]	2021
NIR-ClO	F	680	740	RAW 264.7, mouse, OA	C=C cleavage, mitochondrial	[1601]	2022
BL	F	375	450	RAW 264.7	C=C oxidation to ketone	[1602]	2022
Probe 1	F	450	640	HeLa, zebrafish	C=C chlorination, lysosomal	[1603]	2022
ADP-TCF	F	643	670	RAW 264.7	C=C cleavage	[1604]	2022
3	F	700	643	RAW 264.7	C=C oxidation	[1604]	2022
BIDID	FR	400	501/ 641	HeLa	C=C oxidation	[1605]	2022
BACN	F	400	606	HeLa	C=C oxidation	[1606]	2022
Probe	F	450	540	RAW 264.7, zebrafish	C=C oxidation	[1607]	2022
MYQ	FR	410	580/ 480	HeLa	C=C oxidation	[1608]	2022
DTC	F	375	452	buffer	C=C oxidation	[1609]	2022
BDHA	F	442	626	HeLa; zebrafish	C=C oxidation	[725]	2022
SFQ	FR	469	489/ 613	HepG2	C=C oxidation	[1610]	2022
C3H	FR	330	480/ 750	HepG2; mice	C=C oxidation, mitochondrial	[1611]	2022
T	F	335 504	430 715	HeLa	C=C oxidation	[1612]	2022
Probe 1	F	400	525	HeLa	C=C oxidation	[1613]	2022
NRH-O	FR	442	500/ 710	L01, 293T	C=C cleavage, mitochondrial	[1614]	2022
Section 9 - C=N bond cleavage							
HS1	F	344	454	RAW264.7	C=N-OH oxidation to cyano	[1615]	2014
TAM	FR	430	485/ 630	PBMCs	C=N cyano oxidation to aldehyde	[1616]	2015
Bodipy-Hy	F	465	510	PC12	C=N hydrazone cleavage	[1617]	2015
BDP-OX	FR	488	589/ 538	A549	C=NOH oxidation	[1618]	2017
1	F	340	410	HeLa	C=N cyano oxidation to aldehyde	[1619]	2017
HQMN	FR	370	468/ 572	monocytes, diabetes	C=N cleavage	[1620]	2018
AB	F	490	648	RAW 264.7	C=N cleavage	[1621]	2018
C-DAN	F	452	475	A549, zebrafish	C=N cleavage to aldehyde	[1622]	2020
Ir-CHO	F	430	625	Water samples	C=N to aldehyde	[1623]	2022
Section 10 - Boronates							
FBS	F	498	523	intestinal epithelia of *Drosophila*	boronate, spirothioether opening	[726]	2013
Z2	F	484	600	buffer	boronic acid	[1624]	2013
TCF-OCl	F	560	610	RAW 264.7	boronate	[1625]	2015
BTCBA	F	450	515	HeLa	boronic acid	[1626]	2016

2	F	495	515	HepG2	boronic acid, mitochondrial	1627	2017
NIAD-4	FR	482	640/ 565	mouse brain homogenate, phantom imaging	boronate	1628	2018
TPM	FR	416	468/ 600	RAW 264.7, HeLa	boronic acid, mitochondrial	1629	2019
DPH-BP	F	374	452/ 536	HeLa	boronate	1630	2019
Probe 1	FR	490	652/ 582	RAW264.7, HepG2, zebrafish	boronic acid	1631	2020
BEDB	F	540	575	RAW 264.7, MCF-7, zebrafish; liver tissue	boronic acid, also detects SO_3^{2-}	1632	2022
DAB	F	495	660	A549, Zebrafish	boronic acid	1633	2022

Section 11- 2,3-Diaminomaleonitrile (DAMN) imine

1b	FR	540/ 464	505/ 585	MCF-7	DAMN imine	697	2011
CDH	FR	316	376/ 456	buffer	DAMN imine	698	2013
Probe 1	FR2P	360/ 740	435/ 440	RAW 264, exo or endo	DAMN imine	1634	2018
ADT-MAM	F	420	500	HeLa, A549, colorimetric	DAMN imine to CHO	1635	2018
Probe 1	FR	415	515/ 640	HepG2	DAMN imine to CHO	1636	2018
RO610	F	535	577	A549, mouse,	DAMN imine to CHO	1637	2018
HCCN	F	436	541	HepG2	DAMN imine to CHO	1638	2018
Probe 1	F	365	495	A549	DAMN imine cyclization	699	2018
PDAM-Me and PDAM-Lyso	FR	410	470/ 620	RAW264.7, zebrafish	DAMN imine to COOH, lysosomal	1639	2019
1	FR	325	500/ 607	RAMOS	DAMN imine cleavage	700	2019
Probe 1	F	365	432	HeLa, RAW 264.7	DAMN imine to NO_2	701	2019
Probe 1	F	380	462/ 582	HeLa	DAMN imine to CHO	1640	2019
M-TPEP-CN	F	370	534	PC12	DAMN imine	1641	2020
A-DM	FR2P	425/ 720	525/ 625	RAW 264.7	DAMN imine	1642	2020
NIB-M	F	365	440	RAW 264.7	DAMN imine	1643	2020
probe P	F	361	480	DLD-1	DAMN imine, also detects ^{-}CN	1644	2020
BTD-1	F	396	448	HeLa, macrophage, zebrafish	DAMN imine, mitochondrial	1645	2020
2TD	F	350	423	HeLa	DAMN cleavage to aldehyde	1646	2020
Mul-NIRIr	F2P	380/ 800	663	RAW264.7, LM-3, mouse	DAMN imine, mitochondrial	1647	2021
TPB-CN	F	350	440	HeLa, mouse	DAMN imine	1648	2021
Lyso-VH	FD	475	580	A549, ALI	DAMN imine, viscosity, lysosomal	1649	2022
BODIPY-DAMN	F	490	511	B16-F10, SH-Sy5Y, zebrafish	DAMN imine	1676	2022

Section 12 -Phenol oxidation

HKOCl-1	F	520	541	RAW 264.7	phenol oxidation	702	2008
PMOPP	F	320	388	buffer	phenol oxidation	1651	2011
FCN1	F	415	485	buffer	phenol oxidation	1652	2012
FCN2	F	415	485	NIH 3T3; zebrafish	phenol oxidation	1652	2012
FCN3	F	415	485	buffer	phenol oxidation	1652	2012
Probe 1	F	496	517	RAW 264.7	catechol oxidation, ring opening	1653	2014
HKOCl-2a	F	523	545	buffer	phenol oxidation	1654	2014
HKOCl-2b	F	523	545	RAW 264.7, THP-1	phenol oxidation	1654	2014
HKOCl-2c	F	523	545	buffer	phenol oxidation	1654	2014
1	F	420	544	HepG2	phenol oxidation	1655	2014
NBD-DOP	F	470	540	HeLa Cells	dopamine oxidation	1656	2017
SF-1	F	550	586	macrophage	catechol oxidation, lysosomal, Golgi	1657	2018
BHC	F	394	510	HeLa	phenol oxidation	1658	2019
2a	FR	339	489/ 413	HeLa	phenol oxidation	1659	2019
2b	FR	316	537/ 406	HeLa	phenol oxidation	1659	2019
2c	FR	323	435/ 387	HeLa	phenol oxidation	1659	2019
L1	F	395	483	RAW 264.7	phenol oxidation	1660	2019

MB-DOPA	F	620	683	HeLa	catechol oxidation decarboxylation	[1661]	2019
Probe 1	F	420	525	HepG2	phenol oxidation	[1662]	2020
HBTC	FR	406	620/ 506	MDA-MB-231	phenol oxidation, viscosity	[1663]	2020
HQ	F	450	550	zebrafish, mouse	phenol oxidation	[1664]	2021
RFP-Ptz	F	460	610	SGC-7901	phenol oxidation, O-Cl formation	[1665]	2021
HOCl-CL-510	CL	-	500	RAW 264.7, mice (LPS) and arthritic model	phenol oxidation/dearylation	[1666]	2022
HE	F	473	610	rat macrophages	aromatization	[1667]	1995
2,7-DCHF-DA	F	501	521	rat macrophages; neutrophils	aromatization	[1153]	1995
DHR 123	F	501	528	rat macrophages; neutrophils	aromatization	[1153]	1995
HE	F	473	610	rat macrophages; neutrophils	aromatization	[1153]	1995
RB-thiazole	F	560	590	L929 cells	benzothiazole ring opening	[1670]	2013
SA-thiazole	F	402	462	L929 cells	benzothiazole, mitochondrial	[1670]	2013
DPNO	FR	305	354/ 430	buffer	diaminonapthalene oxidation	[1671]	2013
AC-ClO	F	480	576	RAW 264.7	diaminonapthalene oxidation	[1672]	2015
Ru-1	F	365	587	HEK293T	C-H hydroxylation	[1673]	2019
ZPAC	FR	410	472/ 600	RAW 264.7	methylene oxidation	[1674]	2019
TPP-AN	FR	370	414/ 620	HeLa	*N*-benzylpyridinium cleavage, mitochondrial; viscosity	[1675]	2022

Section 13 – Other triggers

Pholasin	CL	-	480	Pholas dactylus	luciferin based	[1676]	2000
1	F	488	525	MCF-7	alcohol oxidation	[1302]	2013
Probe 1	F	414	523	A549 cells	alcohol oxidation	[1677]	2017
CB	F	430	590	PMN neutrophils	glycol oxidation	[1678]	2022
[Ru(bpy)2(DNCA -bpy)]	F	470	626	RAW 264.7	dinitroamide lysis	[1679]	2013
[Ru(bpy)2(DNPS -bpy)]	F	456	626	HeLa, RAW 264.7	dinitrothioether lysis	[1680]	2013
Mito-NPSTTA-Eu^{3+}	L	488	610	HepG2, RAW264.7, zebrafish	nitrophenol lysis	[1681]	2017
MB-Rs	F	620	685	RAW 264.7, PC-12, mice	amide lysis	[1682]	2022
REClO-6	F	568	590	HeLa, zebrafish, mouse arthritis, solid tumor	amide lysis	[1683]	2022
7	F	323	463	HepG2	coumarin ring opening	[1684]	2016
4	F	287	377	buffer	coumarin ring opening	[1684]	2016
1b	FR	380	460/ 523	HEK293T	coumarin ring opening	[1685]	2019
BCO	F	257/ 383	430	HepG2	coumarin ring opening	[1538]	2019
BETC	F	270/ 373	438	HepG2	coumarin ring opening	[1538]	2019
CCO	F	410	530	HEK293T	coumarin ring opening	[1686]	2019
EDPC	F	380	475	HEK293T	coumarin ring-opening	[1687]	2019
BAC	F	412	480	HEK293T, HeLa	coumarin ring opening	[1688]	2020
TCAB	F	418	480	HEK293T, HeLa	coumarin ring opening, mitochondrial	[1688]	2020
Ir-1	F	370	615	HepG2	acrylate ester hydrolysis	[1580]	2019
Lyso-BHHBCB-Eu^{3+}	L	328	607	HepG2, RAW 264.7	β-diketonate oxidation, Eu^{3+} ejection, lysosomal	[1689]	2017
Mito-BHHBCB-Eu^{3+}	L	333	607	HepG2, RAW 264.7	β-diketonate oxidation, Eu^{3+} ejection, lysosomal	[1689]	2017
Eu(Lyso-CDHH)$_3$(DPBT)	L	400	610	RAW 264.7	β-diketonate oxidation, Eu^{3+} ejection, lysosomal	[1690]	2020
Eu(L)$_3$(DPBT)	L	400	607	RAW 264.7, HeLa, mouse	β-diketonate oxidation, Eu^{3+} ejection, mitochondrial	[1691]	2020
4	FR2P	326/ 720	450/ 361	RAW 264.7, rat, ERT	NHC borane	[1692]	2018
1·BH3	F2P	350/ 710	374/ 477	RAW 264.7	NHC Borane	[1693]	2018
FDOCl-1	F	664	686	RAW 264.7, mouse, arthritis model	deformylation	[1694]	2018
FH-HA	F	555	580	RAW 264.7, HeLa, A549, HepG2, zebrafish	deformylation	[1695]	2019
FDOCl	F	488	535	HL-60	deformylation & deamidation	[1696]	2019
G1 and G2	F	610	669	HL-60, HeLa, mouse, psoriasis	deformylation	[1697]	2022

1	F	289	484	RAW 264.7	aldehyde oxidation	[1698]	2018
2	F	418	512	RAW 264.7	aldehyde oxidation	[1698]	2018
L1 and L2	F	300	400	MCF-7	aldehyde oxidation	[1699]	2020
MTRN	F	561	616	Cos-7, HL-7702, RWPE-1, HeLa, MCF-7, and HepG2	pyrrole oxidation	[1700]	2018
RT-1	F	550	587	RAW 264.7, HeLa	carbonodithioate	[1701]	2019
Cy-HR	F	635	706	RAW 264.7, zebrafish	O-Cl formation	[1702]	2019
PBAS	F	400	570	A549	O-Cl formation	[1703]	2019
RFP-Ptz	F	460	610	HeLa, RAW 264.7, mouse	O-Cl formation	[1704]	2021
BP	F	546	564	RAW 264.7	phosphine oxidation	[1705]	2021
BR-O	F	610	670	RAW 264.7, HL-60	urea	[1706]	2020
MB-NAP-N_3	F	620	686	HeLa, RAW 264.7, zebrafish	urea, also detects H_2S	[1707]	2021
NHF	F	664	700	HepG2, HeLa, A549, GES-1; zebrafish, mouse	urea, hepatocyte targeting	[1708]	2021
MB-N-NAP	F	620	690	HepG2, Hep3B, Huh7	urea, also detects H_2S	[1709]	2021
MCB	F	620	464/ 700	MCF-7, RAW 264.7, zebrafish	urea cleavage & aminophenol oxidation	[1710]	2022
T	F	460	561	MCF-7, *Arabidopsis thaliana*	nitrone oxidation	[1711]	2021
3	F	475	512	RAW 264.7	triazolopyridine	[1712]	2022
2	F	475	512	RAW 264.7	triazolopyridine	[1712]	2022
CB2-H	FD	631	468	HeLa, zebrafish	*o*-chlorination for HOCl, dual with $ONOO^-$	[1713]	2022

[a] F = fluorescence, R = ratiometric, 2P = two-photon, L= luminescence, CL = chemiluminescence, BL = bioluminescence, PA = photoacoustic. [b] Wavelengths given in nanometers.

Table 4. Small molecule probes for nitric oxide

Probe	Type[a]	λ_{ex}[b]	λ_{em}[b]	Application	Trigger/Comments	Ref	Year
Section 1 – N-Nitrosation type 1 triggers							
DAN	F	365	415	rat neutrophils	*N*-nitrosation type 1	[746]	1996
DAN-1	F	360	447	buffer	*N*-nitrosation type 1	[747]	1997
DAF-2	F	490	515	buffer	*N*-nitrosation type 1	[748]	1998
DAF-2 DA	F	490	515	rat aortic smooth muscle cell	*N*-nitrosation type 1	[748]	1998
DAA	F	488	580	rat eyes, hippocampal neurons, RAW 264.7	*N*-nitrosation type 1	[1714–1718]	1998
DAF-FM	F	490	515	rat bladder smooth muscle cells	*N*-nitrosation type 1	[750]	2000
DAR-4M AM	F	560	575	bovine aortic endothelial cells	*N*-nitrosation type 1	[754]	2001
12	F	360	450	buffer	*N*-nitrosation type 1	[1719]	2001
TMDABODIPY	F	500	510	buffer	*N*-nitrosation type 1	[755]	2003
DAMBO	F	496	505	buffer	*N*-nitrosation type 1	[755, 756]	2004
DAMBO-P^H	F	519	535	buffer	*N*-nitrosation type 1	[756, 757]	2004
DABODIPY	F	500	510	buffer	*N*-nitrosation type 1	[758]	2004
TMAPABODIPY	F	500	510	buffer	*N*-nitrosation type 1	[759]	2005
DAC-S	F	750	785	rat kidney ex vivo	*N*-nitrosation type 1	[777]	2005
TMDABODIPY	F	498	507	human serum, rat tissue	*N*-nitrosation type 1	[760, 761]	2006
DAMBOO	F	497	510	buffer	*N*-nitrosation type 1	[762, 763]	2006
DAMBO -CO_2Et	F	500	510	PC12	*N*-nitrosation type 1	[764]	2006
Compound 1	F	554	574	buffer	*N*-nitrosation type 1	[784]	2008
VDABA	F	354	479	RAW 264.7	*N*-nitrosation type 1	[817]	2008
$[Ru(bpy)_2(dabpy)]^{2+}$	L	455	616	mouse macrophage, gardenia, rabbit blood	*N*-nitrosation type 1	[822, 823]	2010
EDADO	F	339	443	organic	N-nitrosation type 1	[828]	2011
Cou-Rho-NO	FR	410	473/ 583	RAW 264.7	*N*-nitrosation type 1	[785]	2011
ANO1	F2P	370/ 750	502	RAW 264.7, rat hippocampal ex vivo	*N*-nitrosation type 1	[794]	2012
[Ru(MAA-phen)3]2+	L	468	598	buffer	*N*-nitrosation type 1	[824]	2013
DAN	F	370	454	HT-29	*N*-nitrosation type 1	[819]	2013
BRP-NO	FR	488	510/ 590	MCF-7	*N*-nitrosation type 1	[786]	2013
DANPBO-H	F	621	631	ECV-304, RAW 264.7, mouse ex vivo, rice (HPLC)	*N*-nitrosation type 1	[765]	2013
A	F	539	570	RAW 264.7, ARPE-19	*N*-nitrosation type 1	[766]	2013

BOPB	F	622	643	RAW 264.7, onion	*N*-nitrosation type 1	[767]	2013
***o*-MOPB**	F	552	590	RAW 264.7	*N*-nitrosation type 1	[1720]	2013
***p*-MOPB**	F	582	620	RAW 264.7	*N*-nitrosation type 1	[1720]	2013
DAP-LT1	F	720	790	buffer	*N*-nitrosation type 1	[778]	2013
DABPA	F	279	361	PC12	*N*-nitrosation type 1	[818]	2014
ADNO	F2P	405/820	546	NIH 3T3	*N*-nitrosation type 1	[796]	2014
DANPBO-H	F	621	631	ECV304, mouse ex vivo, rice	*N*-nitrosation type 1	[769]	2014
DANPBO-M	F	609	619	ECV304, mouse ex vivo, rice	*N*-nitrosation type 1	[769]	2014
QNO	F2P	408/810	535	RAW 264.7, rat brain ex vivo	*N*-nitrosation type 1	[797]	2014
NPA	F	400	490	buffer	*N*-nitrosation type 1	[820]	2015
TMDSDAB	F	500	512	RAW 264.7	*N*-nitrosation type 1	[770]	2015
DAL	BL	-	600	HEK293, mouse in vivo	*N*-nitrosation type 1	[813]	2015
1a	F	612	681	HeLa	*N*-nitrosation type 1	[829]	2015
1b	F	683	750	HeLa	*N*-nitrosation type 1	[1721]	2015
Ir-Mito-NO	L2P	335/730	576	HeLa	*N*-nitrosation type 1, mitochondria	[798]	2015
NRNO	F2P	585/820	650	HeLa, RAW 264.7, mouse ex vivo	*N*-nitrosation type 1	[779]	2016
SiRB-NO	F	667	680	HepG2	*N*-nitrosation type 1	[780]	2016
TMR-NO-BG	F	535	566	COS-7	*N*-nitrosation type 1	[804]	2016
OPD-FF	F	275	367	HepG2 (spectroscopy)	*N*-nitrosation type 1	[1722]	2016
deOxy-DALSiR	F	645	680	HeLa, RAW 264.7, pancreatic B-cells, EA.hy926, mouse in vivo	*N*-nitrosation type 1	[782]	2017
p-MOPB DSDMHDAB	F	582/515	620/529	Plasma membrane in RAW 264.7, ECV-304	*N*-nitrosation type 1	[132]	2017
Probe 1	F	470	532	HepG2	*N*-nitrosation type 1	[773]	2018
APNO-1	PAR	731/676	PA	buffer	*N*-nitrosation type 1	[790]	2018
ROPD	F	505	581	L929, HeLa, RAW 264.7	*N*-nitrosation type 1	[1723]	2018
PS	FPA	532/405	550	RAW 264.7, mouse in vivo	*N*-nitrosation type 1	[815]	2018
Iridium (III) probe 1	L	355	608	HeLa	*N*-nitrosation type 1	[825]	2018
Compound 1	F	505	528	RAW 264.7	*N*-nitrosation type 1	[774]	2019
BTNH	F	525	620	HEPG2, SH-SY5Y, Drosophilia brain ex vivo	*N*-nitrosation type 1	[830]	2019
Ir-BPDA	L2P	405/730	587	RAW 264.7, zebrafish	*N*-nitrosation type 1	[801]	2019
TTNO	F2P	590/840	658	HeLa, mouse liver ex vivo	*N*-nitrosation type 1	[802]	2019
LS-NO	F	650	760/804	RAW 264.7, HCC1299, mouse vivo and ex vivo	*N*-nitrosation type 1	[783]	2021
ZJL-3	F	600	637	RAW 264.7, C. elegans	*N*-nitrosation type 1	[1724]	2021
13	F	447	564	Jurkat	*N*-nitrosation type 1	[1725]	2021
Compound 1	F	354	464	buffer	*N*-nitrosation type 1	[1726]	2022
Compound 2	F	354	456	RAW 264.7	*N*-nitrosation type 1	[1726]	2022
Compound 3	F	354	464	RAW 264.7	*N*-nitrosation type 1	[1726]	2022
Compound 4	F	354	456	buffer	*N*-nitrosation type 1	[1726]	2022
BL_{660}-NO	BL	-	660	A549-Luc2, mouse in vivo	*N*-nitrosation type 1	[814]	2022
PA_{NO} 1	PAR	628/725	PA	mouse in vivo	*N*-nitrosation type 1	[776]	2023
PA_{NO} 2	PAR	705/785	PA	mouse in vivo	*N*-nitrosation type 1	[776]	2023
PA_{NO} 3	PAR	705/785	PA	mouse in vivo	*N*-nitrosation type 1	[776]	2023
SCR-NO	FPA	895	PA	mouse in vivo/ex vivo	*N*-nitrosation type 1	[816]	2023
NOP3	F	450	540	HeLa, RAW 264.7	*N*-nitrosation type 1 and 2	[842]	2022
DAN-1 EE	F	365	440	rat aortic smooth muscle cells	*N*-nitrosation type 1, cell-permeable	[747]	1997
DATTA-Eu^{3+}	L	326	612	onion	*N*-nitrosation type 1, time-gated	[826]	2011
MATTA-Eu3+	L	321	610	PC-12	*N*-nitrosation type 1, time-gated	[827]	2012
LYSO-NINO	F2P	440/840	530	MCF-7, RAW 64.7	*N*-nitrosation type 1, lysosome	[795]	2012
FP-NO	F	550	580	HeLa, RAW 264.7	*N*-nitrosation type 1, dual with H_2O_2	[831]	2012

[Ru(bpy)$_2$(DA-Phen)]$^{2+}$	F	448	613	tobacco, onion	*N*-nitrosation type 1, electrochemiluminescence	768	2013
Mito-Rh-NO	F	559	585	MCF-7, RAW 264.7	*N*-nitrosation type 1, mitochondria	803	2013
probe 1	F	570	616	B16	*N*-nitrosation type 1, mitochondria	807	2014
LysoNO-Naph	F	368	454	CHO	*N*-nitrosation type 1, lysosome	808	2016
Lyso-SiRB-NO	F	667	680	HepG2, LO2	*N*-nitrosation type 1, lysosome	780	2016
TMR-NO-SNAP	F	535	564	COS-7	*N*-nitrosation type 1, SNAP Tag	804	2016
DSDMHDAB	F	515	529	RAW 264.7	*N*-nitrosation type 1, membrane	771	2016
LyNPNO	F	450	541	C6, rat hippocampal ex vivo	*N*-nitrosation type 1, lysosome	821	2016
SiRD	R	680	710	HeLa, MT	*N*-nitrosation type 1, mitochondria	781	2017
TRP-NO	L	330	580	HepG2, *D. magna*	*N*-nitrosation type 1, lysosome	809	2017
ER-Nap-NO	F2P	440/ 820	538	HeLa, mouse ex vivo	*N*-nitrosation type 1, ER targeted	799	2018
MBTD	R	421/ 488	550/ 625	RAW 264.7, mouse ex vivo	*N*-nitrosation type 1, lysosome	810	2018
Gal-RhB	F	550	580	HepG2, HeLa, L929, A2780, zebrafish	*N*-nitrosation type 1, hepatocyte	811	2018
Mem-NO	F2P	810	538	HUVEC, PC12, mouse brain ex vivo	*N*-nitrosation type 1, membrane targeted	133	2018
S1/Int-1	F	510	527	A549	*N*-nitrosation type 1, SERS imaging	772	2018
Mito-1	F	485	518	HeLa, RAW 264.7, SKOV-3	*N*-nitrosation type 1, mitochondria	858	2019
NOckout^{PM}	FR	488/ 550	520/ 575	T-47D	*N*-nitrosation type 1, DNA-based	124	2020
NOckout^{TGN}	FR	550/ 650	575/ 665	T-47D	*N*-nitrosation type 1, DNA-based	124	2020
NOckout^{fn}	FR	550/ 650	575/ 665	primary microglia, alveolar macrophages, zebrafish	*N*-nitrosation type 1, DNA based	805	2020
PYSNO	F	402	581	SH-SY5Y, RAW 264.7, mouse heart ex vivo, mouse in vivo	*N*-nitrosation type 1, lysosome	1727	2020
Lyso-TP-NO	F2P	435/ 840	539	BV2, mouse ex vivo	*N*-nitrosation type 1, lysosome	866	2020
Compound 1	F	532	565	HUVEC, zebrafish	*N*-nitrosation type 1, dual with GSH	833	2021
HNB	F	530	555	HeLa, HepG2, A549	*N*-nitrosation type 1, hepatocyte/lipid droplets	865	2021
Hoe–Rh-NO	FR	405	463/ 603	HeLa, macrophages, zebrafish	*N*-nitrosation type 1, nucleus	791	2022
Golgi-NO	F	560	589	SH-SY5Y, HEPG2	*N*-nitrosation type 1, Golgi	812	2022
1	F	660	685	H9C2, mouse in vivo, ex vivo	*N*-nitrosation type 1, dual with GSH	834	2022
BQ	F	405	565	RAW 264.7	*N*-nitrosation type 1, dual with Cu^{2+}	863	2023
BDP	FR	590	625/ 715	HeLa, mouse in vivo/ex vivo	*N*-nitrosation type 1, dual with viscosity	793	2023
Probe 5	F	510	516	HeLa	*N*-nitrosation type 1, lipid droplet	775	2023
TMR-Tz-NO	F	555	585	HeLa, RAW 264.7, zebrafish	*N*-nitrosation type 1, click rx for organelle targeting	806	2022
Naph–RhB	F	550	570	L929	*N*-nitrosation type 1, dual with H_2S	832	2015
1	FR	420	470/ 560	HeLa	*N*-nitrosation type 1, ESIPT	789	2018
HTDAF-2DA	F	488	512	HeLa, RAW 264.7	*N*-nitrosation type 1, Halo tag	131	2015
A6	F	355	492	HeLa	*N*-nitrosation type 1, hypoxia activated, photolytic drug release	1728	2018
1-NO	FR	420	505/ 580	HeLa, RAW 264.7	*N*-nitrosation type 1, TBET	787	2018

Section 2 – N-Nitrosation type 2							
NO550	F	470	550	neonatal spinal astrocytes, PC-12, human microvascular endothelial cells	*N*-nitrosation type 2	837	2010
probe 1	F	480	518	HL-7702	*N*-nitrosation type 2	838	2014
NO-QA5	F2P	432/ 760	540	RAW 264.7, mouse liver ex vivo	*N*-nitrosation type 2	839	2017
Mito-N	FR2P	500/ 900	540/ 595	RAW 264.7, mouse in vivo	*N*-nitrosation type 2, mitochondrial	788	2017
RatioTr	FR	370	424/ 530	RAW 264.7	*N*-nitrosation type 2	840	2020
NO530	F	445	530	NIH3T3, RAW 264.7	*N*-nitrosation type 2	841	2020
NO562	F	470	562	NIH3T3, RAW 264.7	*N*-nitrosation type 2	841	2020
MTNO	F	350	457	HeLa, RAW 264.7, mouse ex vivo	*N*-nitrosation type 2, mitochondria	843	2023
Section 3 - N-Nitrosation type 3							
Reduced fluoresceinamine	F	450	522	buffer	*N*-nitrosation type 3, xanthene oxidation	1729	2010
FA-OMe	F	460	524	RAW 264.7	*N*-nitrosation type 3	846	2012
2c	F	470	550	RAW 264.7	*N*-nitrosation type 3	849	2014
3b	F	740	815	1M HCl	*N*-nitrosation type 3, H_2S activated	847	2014
MA	F	475	519	HeLa, RAW 264.7	*N*-nitrosation type 3	1730	2017
NIR-MA	F	750	794	HeLa, RAW 264.7, mouse in vivo	*N*-nitrosation type 3	1730	2017
1-H_2S	F	465	526	PC12	*N*-nitrosation type 3, H_2S activated	848	2018
APNO-2	PAR	735/ 676	PA	buffer	*N*-nitrosation type 3	790	2018
APNO-3	PAR	679/ 678	PA	buffer	*N*-nitrosation type 3	790	2018
mtNOpy	F	480	585	HT29, RAW 264.7, whole blood	*N*-nitrosation type 3, mitochondria-targeted	850	2021
$ENNH_2$	FR	460	530/ 605	RAW 264.7, zebrafish	*N*-nitrosation type 3	792	2022
BDP-3	F	648	668	4T1, RAW 264.7, mouse in vivo	*N*-nitrosation type 3	851	2023
Section 4 – N-Nitrosation type 4							
Probe 1	F	490	518	HeLa, RAW 264.7, EA.hy926	*N*-nitrosation type 4	852	2016
SiRNO	F2P	645/ 820	672	HeLa, RAW 264.7, mouse ex vivo	*N*-nitrosation type 4	853	2017
L3	F	510	587	HepG2, zebrafish	*N*-nitrosation type 4	1731	2018
PyDA-NP	FR	390	445/ 523	organic	*N*-nitrosation type 4	854	2018
PQPY	F	400	505	HepG2 cells	*N*-nitrosation type 4	855	2018
APNO-4	PAR	764/ 678	PA	buffer	*N*-nitrosation type 4	790	2018
APNO-5	PAR	764/ 673	PA	mouse in vivo	*N*-nitrosation type 4	790	2018
HqEN480	F	390	480	HepG2	*N*-nitrosation type 4	856	2019
Cy7-MA	F	760	800	HeLa, mouse in vivo	*N*-nitrosation type 4	861	2019
1	F	485	518	HeLa, RAW 264.7, SKOV-3	*N*-nitrosation type 4	858	2019
TAN	F2P	488/ 790	638	HeLa, mouse ex vivo	*N*-nitrosation type 4	862	2020
SR-APNO-3	PA	790/ 704	PA	RAW 264.7, 4T1, mouse in vivo	*N*-nitrosation type 4	857	2020
RBA	F	530	585	HeLa, RAW 264.7	*N*-nitrosation type 4	1732	2020
Rh-NO-1	F	530	600	HeLa	*N*-nitrosation type 4	1733	2020
QY-N	FPA	808	935	mouse in vivo	*N*-nitrosation type 4	859	2021
AC-SA	FR	475	525/ 625	RAW 264.7, zebrafish	*N*-nitrosation type 4	864	2021
APNO-1080	PA	1080	PA	mouse in vivo	*N*-nitrosation type 4	860	2021
QY-NO	FPA	780	935	mouse in vivo	*N*-nitrosation type 4	859	2021
Probe 2	F	490	518	HeLa, RAW 264.7, EA.hy926	*N*-nitrosation type 4, mitochondria	852	2016
LJ–Zn2+	F	295	365	buffer	*N*-nitrosation type 4, dual with Zn	868	2021
QBN	F	365	512	HeLa, RAW 264.7	*N*-nitrosation type 4, dual with HOCl	869	2021

BOD-NH-SC	F	570	645	HEPG2, colonic smooth muscle	N-nitrosation type 4, dual with H_2S	870	2022
BML	F	530	590	HeLa, PC-3, MCF-7, HepG2, zebrafish	*N*-nitrosation type 4, lysosome	867	2023
Section 5 - Other nitrosation triggers							
RBH	F	561	581	RAW 264.7	hydrazide nitrosation	871, 872	1998
8-HB	F	505	512	HEPG2, RAW 264.7	hydrazine removal	873	2019
1a-SAc	F	418	477	HeLa, HUVEC, Raw 264.7	*S*-nitrosation, reversible	874	2021
2a-SAc	F	447	490	HeLa, HUVEC, Raw 264.7	*S*-nitrosation, reversible	874	2021
Compound 1	F	560	580	lung epithelial cells	*o*-aminosulfide	875	2023
***B*-SiRhd-7**	FPA	808	1050	mouse in vivo	*o*-aminoimine	876	2023
Section 6 - Metal-based nitric oxide triggers							
compound (1)	F	366	460	buffer	iron	877	1998
Compound 1	F	350	505	organic	cobalt	880	2000
Compound 12	F	350	505	organic	cobalt	881	2000
Acridine-TEMPO/ DTCS-Fe(II)	F	361	438	buffer	Fe-nitroxide displacement	878	2001
Mmc-cyclam	FR	360	410/ 470	buffer	Fe-nitroxide displacement	879	2002
Compound 4 and 1	F	365	~560	organic	Dirhodium binding	882	2004
Compound 2	F	350	~505	organic	cobalt	883	2004
Compound 1	F	350	~505	organic	iron	883	2004
Ru(TPP)(CO)(Ds-im)	F	368	550	organic	ruthenium	884	2004
[Cu(Ds-AMP)2	F	342	~560	buffer	copper	885	2005
Complex 7	F	342	550	buffer	copper	886	2006
Complex 8	F	342	550	buffer	copper	886	2006
Complex 10	F	342	550	buffer	copper	886	2006
CuFL	F	503	520	SK-N-SH, RAW 264.7	copper	887	2006
MNIP–Cu	F	360	492	RAW 264.7, mouse liver ex vivo	copper	894	2008
Cu_2FL2E	F2P	496 /800	526	RAW 264.7, SK-N-SH, mouse ex vivo	copper	891–892, 893	2010
$CuFL1_5$	F	499	520	buffer	copper	890	2010
CuFL1A	F	499	520	buffer	copper	890	2010
CuFL1E	F	500	520	RAW 264.7	copper	890	2010
$CuFL^{Dex}$	F	500	520	RAW 264.7	copper	890	2010
Cu_2FL2	F	494	526	buffer	copper	891	2010
Cu_2FL2A	F	496	526	buffer	copper	891	2010
CuRBT	F	510	580	MCF-7	copper	895	2011
CuSNFL1	F	527	548	RAW 264.7	copper	898	2011
CuSNFLE	F	527	549	RAW 264.7	copper	898	2011
$CuSNFL1^{Br}$	F	540	615	RAW 264.7	copper	898	2011
$CuSNFL1E^{Br}$	F	536	615	RAW 264.7	copper	898	2011
Complex 1	F	342	560	buffer	copper	904	2011
Complex 4	F	350	~540	organic	copper	905	2011
CuQNE	F	466	530	MCF-7	copper	902	2012
Cu^{2+}[FS]	F	350	430	buffer	copper	903	2012
complex 1	F	340	~525	buffer	copper	906	2012
RB-TP	F	540	580	HeLa	copper	896	2013
RB-Py	F	550	580	HeLa	copper	896	2013
CuBRNO1	F	570	623	HeLa, RAW 264.7	copper, dual with HNO	899	2013
CuBRNO2	F	570	623	buffer	copper, dual with HNO	899	2013
CuBRNO3	F	563	625	HeLa, RAW 264.7	copper, dual with HNO	899	2013
Complex 3	F	342	~530	buffer	copper	907	2013
RDN–Cu	F	480	548	MCF-7, RAW 264.7	copper	908	2014
Cu(bpq)(OAc)(H_2 O)	F	400	515	organic	copper	1734	2014
Cu (NSQ)2	F	370	500	organic	copper	1686	2014
FI-Cu^{2+}	F	465	518	RAW 264.7	copper	1735	2014
QHYN•Cu(II)	FR	325	434	organic	copper	1736	2014
$[Cu^{II}(L2)Cl]^+$	F	345	532	HeLa	copper	1737	2014
1-Cu^{II}	F	501	521	RAW 264.7	copper	909	2015
Cu(II) complex 7	F	440	580	MCF-7	copper	910	2016
16a	F	405	445	*P. aeruginosa*	copper	911, 912	2016

MNIP-Cu	F	330-385	420-500	plants	copper	[913]	2016
Cu(FL3A-Ppz-CC)	FR	400	450/519	A549	copper	[901]	2017
RPD-Cu^{2+}	F	560	580	HeLa	copper	[897]	2019
PIP(Cu^{II})Cl	F	407	560	A549, RAW 264.7	copper	[900]	2019
Compound 1	F	330	~500	buffer	NO mediated copper click reaction	[914]	2020
Ru-NO	L	450	615	THP1 monocytes, macrophages, mouse in vivo/ex vivo, plasma, human plasma	ruthenium	[1738]	2022
Section 7 - Fluorescent cheletropic traps and spin traps							
1a	F	315	380	buffer	cheletropic trap	[915]	1997
4d	F	380	460	rat alveolar macrophages	cheletropic trap	[917]	1999
15	F	320	380	rat alveolar macrophages	cheletropic trap	[916]	2006
FNOCT 8a	F	350	380	rat alveolar macrophages	cheletropic trap	[918]	2010
Compound 1	F	350	470	MCF-7	c-PTIO spin trap in cage	[919]	2011
Section 8 - Other triggers							
RBSe	F	560	580	HeLa	selenolactone	[920]	2011
Probe 1	F	334	450	RAW 264.7	dihydropyridine	[922]	2014
DHPS	F	324	400	RAW 264.7	dihydropyridine	[923]	2016
PyNO	FR	346	393/439	Vero 76	dihydropyridine	[925]	2016
TPANO	FR	308	416/502	Vero 76	dihydropyridine	[925]	2016
DHP-1	F	323	392	RAW264.7	dihydropyridine	[1739]	2016
DHPFQ	F	490	525	RAW 264.7, mouse in vivo	dihydropyridine	[926]	2017
QT_{490}	F	380	490	Raw 264.7	thiosemicarbazide	[928]	2017
XNO1	F2P	405/820	590	BSH-SY5Y, zebrafish	imine hydrolysis	[800]	2018
Mito-DHP	FR	470	525	HepG2, RAW 264.7	dihydropyridine, mitochondria	[927]	2018
QAH	F	380	490	A549, RAW 264.7	oxatriazole formation	[931]	2018
FP-NO	F	436	475	MCF-7, J774A.1, zebrafish	thiosemicarbazide	[929]	2019
DHP-4	F	365	423	RAW264.7	dihydropyridine	[924]	2020
BCM	F	410	470	A375, RAW 264.7	oxatriazole formation	[932]	2020
1	F	450	550	HeLa	thiosemicarbazide, dual with viscosity	[930]	2021
Mi-NO	FR	410/510	581/594	HeLa, zebrafish	pyrazole formation, mitochondria	[1740]	2021
4	F	685	730	buffer	phenoxazine formation	[933]	2022
DPAC-$(peg)_4$-memantine	F	360	480	BV2, HT22	phenazine formation, AD theranostic	[1741]	2022
CS-Se	F	680	780	Cal-27, saliva	selenolactone	[921]	2023
LysoNO-DCM	F	450	633	RAW 264.7, zebrafish	alkene nitration, lysosome	[934]	2023

[a] F = fluorescence, R = ratiometric, 2P = two-photon, L= luminescence, CL = chemiluminescence, BL = bioluminescence, PA = photoacoustic. [b] Wavelengths given in nanometers.

Table 5. Small molecule probes for peroxynitrite

Probe	Type[a]	λ_{ex}[b]	λ_{em}[b]	Application	Trigger/Comments	Ref	Year
Section 1 - Early probes							
DCFH-DA	F	504	523	leukocytes, HUVEC	xanthene oxidation	[24]	1965
Luminol	CL	-	425	buffer	luminol oxidation	[1742–1744]	1999–2000
DHR 123	F	500	536	buffer	xanthene oxidation	[944]	1994
DAF-2	F	488	515	mouse glial cultures	*ortho*-phenylenediamine	[24,945,1745–1748]	2002
NiSPY-1,2,3	F	505	525	HeLa	aromatic nitrosation	[946]	2006
Section 2 - Trifluoromethyl ketones (TFMK)							
HKGreen-1	F	490	521	neuronal cells	trifluoromethylketone	[947]	2006
HKGreen-2	F	520	539	J774.1 macrophage	trifluoromethylketone	[948]	2009
HKGreen-3	F	520	535	RAW 264.7	trifluoromethylketone, *N*-dearylation	[949]	2010
$CySO_3CF_3$	FPA	675/680	712	RAW264.7, mouse	trifluoromethylketone	[950]	2018

Mito-NA	FR	390	450/ 550	HeLa, RAW264.7	trifluoromethyl cinnamic acid, mitochondrial	[1749]	2021
Cy-CF3	F	500/ 800	630	L02, zebrafish, mouse, kinetic, hypoxia	trifluoromethylketone	[951]	2022
Section 3 - Isatins and α-ketoamides							
Isatin	F	312	405	buffer	isatin	[157, 952]	2014
Rhod-ONOO	F	500	558	HepG2, DILI	α-ketoamide, mitochondrial	[543]	2017
Naph-ONOO	F	459	546	HepG2, DILI	α-ketoamide	[543]	2017
TP-KA	F2P	430	560	HepG2, mouse, DILI	α-ketoamide	[960]	2017
PNCL	CL	-	525	RAW264.7	isatin	[953]	2018
TPNIR-FP	F2P	570/ 800	630	H9c2, mouse	α-ketoamide, mitochondrial	[1750]	2018
BP-PN	BL	-	500-700	MDA-MB-231, mouse	α-ketoamide	[1751]	2018
NIR-ONOO$^-$	F	660	703	HepG2, mouse, DILI	α-ketoamide	[1752]	2019
DCM-KA	F	480	630	J774A.1	α-ketoamide	[1753]	2019
Rd-PN2	F2P	500/ 820	557	RAW264.7, zebrafish, mouse, stroke imaging	isatin	[956]	2020
LSDQ-ONOO	F	580	660	HepG2, mouse, DILI	α-ketoamide	[962]	2020
DHQ-Rd-PN	F2P	560/ 820	653	HeLa, zebrafish, mouse	α-ketoamide	[1754]	2020
DCI-NPG-ONOO	F	460	660	HeLa, RAW264.7, zebrafish, mouse	α-ketoamide	[1755]	2020
TCFISA	F	525	606	RAW264.7	α-ketoamide	[1756]	2020
IC-ONOO	F	400	560	MCF-7, mouse	α-ketoamide	[1757]	2020
RF-IT-OC	F	525	590	HepG2, mouse	isatin	[957]	2022
FC-ONOO	F	405	490	A549, mouse, sepsis induced lung injury	α-ketoamide	[963]	2022
CMONOO1	F	380	488	RAW264.7, mouse	α-ketoamide	[1758]	2022
CMONOO2	F	400	510	RAW264.7, mouse	α-ketoamide	[1758]	2022
RFAc	F	525	590	HepG2, RAW264.7, mouse, DFT	α-ketoamide	[1759]	2022
BDP-PN	F	465	613	HepG2, mouse	isatin	[1887]	2022
HJ-ONOO-P3	F	582	719	PC12, BV-2, mouse	isatin	[958]	2023
Rd700-PN	F	570	702	4T1, mouse	isatin	[959]	2023
DFlu	F2P	350/ 760	490	SH-SY5Y, zebrafish, PD	α-ketoamide	[964]	2023
Section 4 - C=C bond cleavage							
C11-BODIPY	FR	488	595/ 520	rat-1 fibroblasts	C=C bond cleavage	[1763]	2002
C-Py-1,2	F	365	493	RAW264.7	C=C bond cleavage	[968]	2014
CHCN	FR	475	635/ 515	WI38 VA13, RAW264.7	C=C bond cleavage	[969]	2015
PNCy3Cy5	FR	530	660/ 560	RAW264.7	C=C bond cleavage, mitochondrial	[1764]	2016
HMBT-Py	FR	400	645/ 545	A549, HeLa	C=C bond cleavage	[1765]	2016
F482	R	480	606/ 510	RAW264.7, THP-1, mouse	C=C bond cleavage	[1766]	2017
Cy7-PEI-UCNP	F	980	800	HeLa, mouse	C=C bond cleavage	[1767]	2017
Lyso-NA	F	440	510	RAW264.7	C=C bond cleavage, lysosomal	[970]	2018
N-CBT	F	405	518	HeLa	C=C bond cleavage	[1768]	2018
Cy-Net$_2$	FR	710/ 360	742/ 487	HepG2, mouse	C=C bond cleavage, mitochondrial	[1769]	2018
TP-1Bz	FR2P	880	650	HepG2, RAW264.7	C=C bond cleavage, dual with viscosity, mitochondrial	[1770]	2018
NP560	F	375	583/ 475	EA.hy926	C=C bond cleavage	[1771]	2018
rTPONOO-1	FR2P	375/ 800	718/ 535	A549, RAW264.7, mouse, pulmonary fibrosis	C=C bond cleavage, mitochondrial	[971]	2019
Mito-WQPhOH	FR	540	645/ 575	RAW264.7	C=C bond cleavage, mitochondrial	[1045]	2019
Cy-SN	F	630	650	RAW264.7	C=C bond cleavage	[1772]	2019
Cy-NH$_2$	FR	680/ 360	708/ 460	HepG2, RAW264.7	C=C bond cleavage, mitochondrial	[1773]	2019
TPE-COU	F2P	390/ 780	525	H9C2, estrogen protection	C=C bond cleavage	[1774]	2019

BPVI	FR	635	702/ 522	A549	C=C bond cleavage	[1775]	2019
CyCA	FR2P	640/ 800	660/ 470	HL-7702, mouse	C=C bond cleavage	[1776]	2019
SiRho-HD	FRPA	635	750/ 680	HK-2, mouse, AKI	C=C bond cleavage, mitochondrial	[1777]	2020
Ratio-A	FR	480/ 600	700/ 564	RAW264.7, mouse, RA	C=C bond cleavage	[1778]	2020
Ratio-B	FR	680/ 414	808/ 564	buffer	C=C bond cleavage	[1778]	2020
DCCM	FR	390	535/ 390	HeLa	C=C bond cleavage	[1779]	2020
LW-OTf	F2P	720	466	HL7702, mouse, DILI	C=C bond cleavage, dual with O_2^-	[301]	2021
BMP	F2P	427	515	HeLa	C=C bond cleavage, lysosomal	[1780]	2021
BC-PN-2	FR	450	630/ 520	HepG2, MCF-7	C=C bond cleavage, mitochondrial	[1825, 1826]	2021
RN-NA	F	420	710/ 525	HepG2, zebrafish	C=C bond cleavage, lysosomal	[1783]	2021
NRF/Cy-O	FR	365	720/ 462	HepG2, mouse, DFT	C=C bond cleavage	[1784]	2021
DMANI	FR	346/ 529	444/ 692	HepG2	C=C bond cleavage, mitochondrial	[1785]	2021
HD-BPin	F	360	460	A549	C=C bond cleavage, dual with H_2O_2	[515]	2022
TP^{ER}-ONOO	F2P	360/ 800	460	HL-7702	C=C, endoplasmic reticulum targeted	[972]	2022
MG-ONOO	FR	410	650/ 477	HeLa, mouse, DILI	C=C bond cleavage	[973]	2022
TPPT	F	488	670	RAW264.7, zebrafish, mouse	C=C bond cleavage, mitochondrial	[1786]	2022
CQ	F	590	505	HeLa, RAW264.7, mouse	C=C bond cleavage, dual with viscosity	[1787]	2022
WND-1	FR	420	634/ 527	HeLa, zebrafish	C=C bond cleavage, endoplasmic reticulum targeted	[1788]	2022
NTG	F	450	530	MCF-10A. HL-60, RAW264.7	C=C bond cleavage, logic gate	[1789]	2022
MCSA	F	488	635	HeLa, RAW264.7, PC12, zebrafish	C=C bond cleavage, Mitochondrial, endoplasmic reticulum targeted	[1790]	2022
MXMP	FR	435	530/ 660	HeLa	C=C bond cleavage, mitochondrial	[1791]	2022
SX-1	F	360	456	HeLa	C=C bond cleavage	[1792]	2022
COU-Mito	F	450	500	HepG2	C=C bond cleavage, dual with SO_2	[1793]	2022
Mito-ONOO	FR2P	416/ 810	495/ 621	BV-2	C=C bond cleavage	[1794]	2022
Lyso-Cy	F	390	505	RAW264.7, mouse	C=C bond cleavage	[1795]	2022
SQDC	F	630	685	HepG2	C=C bond cleavage, mitochondrial	[1796]	2023
MITO-HC-TZ	F	560	620/ 760	HepG2	C=C bond cleavage, mitochondrial	[1797]	2023
Mito-VO	F	370	470	HeLa, HL-7702, mouse, DILI	C=C bond cleavage	[1798]	2023
B-Ch	FR	545/ 425	480/ 580	HeLa	C=C bond cleavage	[1799]	2023
COUS	FR	400	723/ 484	HepG2	C=C bond cleavage, mitochondrial	[1800]	2023
TR-ONOO	F	390	490	HeLa	C=C bond cleavage	[1801]	2023
FLSP	F	480	535	HepG2, zebrafish, mouse	C=C bond cleavage, spiropyran	[1802]	2023
HPDQ	F	380	445	A549, mouse	C=C bond cleavage	[1803]	2023
ZQNQ	F	425	548	U87MG, A549, HeLa, HepG2, MCF-7, mouse	C=C bond cleavage	[1804]	2023
NFP-ONOO	F	488	654	HK-2, mouse	C=C bond cleavage	[1805]	2023
DCO-POT	F	500	670	SH-SY4Y	C=C bond cleavage	[1806]	2023
DCVP-NO_2	FR	510	538/ 640	HepG2	C=C bond cleavage	[1807]	2023
Ru-Mit	F	332	610	HepG2	C=C cleavage, Ruthenium	[1808]	2023
Section 5 - Benzopyrylium ring opening							
MITO-CC	R2P	420/ 800	651/ 473	HepG2, RAW264.7, mouse	benzopyrylium, mitochondrial	[974]	2017

Gal-NIR	FR	440	720/500	HepG2, mouse, DILI	benzopyrylium	[975]	2019
BCB & BCN	F	400	520	PC-12, HepG2, mouse	C-C cleavage	[1809]	2019
RTFP	FR	405	703/469	HepG2, L02, mouse, DILI	benzopyrylium	[977]	2020
AHMC	FR	405	626/462	RAW264.7, L02, DILI	benzopyrylium mitochondrial	[976]	2021
MULTI-ONOO	FR	410	468/526/706	RAW264.7, rat, arthritis	benzopyrylium	[979]	2022
CSU-FT	F	405	468/573/706	RAW264.7, mouse, arthritis	benzopyrylium	[980]	2022
Mito-CM-CD	FR	410	480/640	HepG2	benzopyrylium, dual with GSH, mitochondrial	[1810]	2022
NIR-GYf	F	489	577	HepG2, A375	benzopyrylium	[1811]	2022
TPE-ONOO	F	400	500	MCF-7	benzopyrylium	[1812]	2022
5	F	560-584	575-628	HepG2, mouse, DILI	benzopyrylium, mitochondrial	[978]	2023
Section 6 - Aryl boronate oxidation							
CBE/CBA	F	332	470	buffer	boronic acid oxidation, boronate oxidation	[983]	2010
P2	FR	440	580/480	RAW264.7	boronate oxidation, aminocoumarin formation	[986]	2014
1	F	430	540	J774A.1	boronate oxidation	[1813]	2014
1	F	436	486	RAW264.7	boronate oxidation, aminocoumarin formation	[988]	2015
1	F	472	522	RAW264.7, Eq.hy926	boronate oxidation, aminocoumarin formation	[987]	2016
Fl-B	F	492	515	J774A.1	boronate oxidation	[1814]	2016
3	F	400	460	HeLa, RAW264.7	boronate oxidation	[1815]	2016
FBBE	F	495	518	EAhy.926	boronate oxidation	[1816]	2016
4-MBH	F	322	450	RAW264.7, zebrafish	boronate oxidation	[1817]	2017
TCFB1	F	560	606	RAW264.7, HepG2, A549, HeLa	boronate oxidation, mitochondrial	[1818]	2017
TCFB2	F	560	606	RAW264.7, HepG2, A549, HeLa	boronate oxidation, mitochondrial	[1818]	2017
KB7	F	480	610	HepG2	boronic acid oxidation	[1819]	2017
GSH-PF3	F	488	530-590	RAW264.7	boronate oxidation	[991]	2018
ABT	FR	317	405/483	buffer	boronate oxidation	[1820]	2018
3-HF-OMe	FR	365	425/530	transgenic mice studies	boronate oxidation	[1821]	2018
Py-PhB	FR	354	430/598	MCF-7, DFT	boronate oxidation	[1822]	2018
1	F2P	450/500	550	SH-SY5Y, NMDA receptors neuronal cells	boronic acid oxidation	[1823]	2018
PR1	F	550	590	J774.2	boronate oxidation	[1824]	2018
Probe N	F	405	452	HeLa	boronate oxidation	[1825]	2018
ABAH-LW	FR	370	405/481	HeLa	boronate oxidation, endoplasmic reticulum	[1826–1828]	2018
RFR-PN	FR	480	590/630	RAW264.7	boronate oxidation	[1829]	2018
CC-RNS	F	345	460	HeLa	boronate oxidation, drug release	[992]	2019
CI-RNS	F	345	460	HeLa	boronate oxidation, drug release	[992]	2019
IRBTP-B	F	808	950	CaOV3, mouse, DILI	boronate oxidation	[993]	2019
BTPB	FR	296	372/462	HepG2, DILI	boronic acid oxidation	[994]	2019
ONP	F	665	692	SH-SY5Y, mouse, epilepsy	boronate oxidation	[995]	2019
KC-ONOO	F	460	530	HepG2, mouse, DILI	boronate oxidation	[996]	2019
AzuFLuor 483-Bpin	F2P	800	483	RAW264.7	boronate oxidation	[1830]	2019
RTP-PN	FR2P	415/800	450/543	RAW264.7	boronate oxidation	[1831]	2019
DCM-Bpin	F	560	667	HeLa	boronate oxidation	[1832]	2019
CPD-ratio	FR	450	565/500	RAW264.7	boronate oxidation	[1833]	2019
NIR-PN	F	510	660	RAW264.7, zebrafish	boronate oxidation	[1834]	2019
CyBA	PA	700	PA	RAW264.7	boronate oxidation	[1835]	2019

MBTBE	F	520	569	HeLa	boronate oxidation, mitochondrial	[984]	2020
VO	F	420	635	HeLa, zebrafish, mouse, DILI	boronic acid oxidation	[997]	2020
FAM	F	587	625	RAW264.7	boronate oxidation, mitochondrial	[1836]	2020
LG-3	F	395	520	RAW264.7, AND-logic gate	boronate oxidation	[1837]	2020
BHBT	F	380	494	HepG2	boronate oxidation, endoplasmic reticulum	[1838]	2020
ACDM-BE	F	540	604	CHO-K1, zebrafish	boronate oxidation	[1839]	2020
CM, CL, CE	FR	340	400/ 450	RAW264.7	boronate oxidation oxidation, mitochondrial, lysosomal, endoplasmic reticulum	[1840]	2020
BTCBE	F	450	522	HeLa	boronate oxidation	[1841]	2020
QPP1	F	560	625	RAW264.7	boronate oxidation	[1842]	2020
QM-ONOO	F	430	620	EC1	boronate oxidation	[1843]	2020
Eu.1	L	321	550- 720	HeLa	boronic acid oxidation	[1844]	2020
^{mito}Probe-PN	F	520	660	RAW264.7, HeLa, MCF-7, HepG2	boronate oxidation, mitochondrial	[1845]	2020
BN-PN	F2P	750	508	HeLa, RAW264.7, mouse, DILI	boronate oxidation	[998]	2021
DPP-DH-P	FR	465	645/ 538	HepG2, mouse, DILI	boronate oxidation	[999]	2021
DPP-DEG-P	FR	465	645/ 538	buffer	boronate oxidation	[999]	2021
DDM-R	F	580	770	HepG2, mouse, DILI	boronate oxidation	[1000]	2021
ADB	F	362	440/ 520	RAW264.7	boronate oxidation	[1846]	2021
ANB	F	362	440/ 520	buffer	boronate oxidation	[1846]	2021
L	F	421	500	HepG2, HL772	boronate oxidation	[1847]	2021
DDAO-PN	F	600	657	RAW264.7, mouse	boronate oxidation	[1848]	2021
NAB-BE	F2P	340/ 745	512	RAW264.7	boronate oxidation	[1849]	2021
PN-1	F	440	540	A549, HeLa, HepG2, RAW264.7, HEK293	boronate oxidation	[1850]	2021
TPE-BOH	FR	400	625/ 510	HeLa, RAW264.7	boronic acid oxidation, mitochondrial	[1851]	2021
NIR-dCl	F	470	680	RAW264.7	boronate oxidation	[1852]	2021
BHID-Bpin	F2P	750	515	HeLa, rat	boronate oxidation	[1853]	2021
BC-BE	F	442	488	HT29	boronate oxidation	[1854]	2021
PE-XY	F	478	580	HeLa, *C. elegans*	boronate oxidation	[1855]	2021
TPE-DMAB	F	365	530	RAW264.7, mouse	boronic acid oxidation	[1856]	2021
DPTS-ONOO	F	436	505	RAW264.7	boronate oxidation	[1857]	2021
CBRV	F	460	710	HeLa	boronate oxidation, dual with viscosity	[1858]	2021
TCF-BA	F	587	607	Buffer	boronate oxidation	[1859]	2017
TCF-BA-2	F	629	650	Buffer	boronate oxidation	[1859]	2017
CI-Bz-BE	F2P	355/ 735	520	RAW264.7	boronate oxidation	[460]	2022
DPPO-PN	F	490	632	HeLa, mouse, arthritis	boronate oxidation	[1001]	2022
K-ONOO	FR	302	570/ 678	HeLa, zebrafish	boronate oxidation	[1002]	2022
BS2	F	405	430	buffer	boronate oxidation	[1003]	2022
JQ-2	FR	461	569/ 657	HeLa, HepG2, zebrafish, DILI	boronate oxidation	[1004]	2022
JQ-2	FR	461	569/ 657	HeLa, RAW264.7, HepG2, zebrafish	boronate oxidation	[1004]	2022
PTZ-H	FR	400	640/ 450	RAW264.7, zebrafish	boronate oxidation	[1350]	2022
Gol-ONOO$^-$	F	420	600	HeLa, GT	boronate oxidation	[1860]	2022
***p*-Borate**	F	470- 572	590	HepG2, RAW264.7, mouse	boronate oxidation	[1861]	2022
HND-ONOO	F	450	590	HeLa, RAW264.7	boronate oxidation	[1862]	2022
HDBT-ONOO	F2P	450/ 880	558	HeLa, HepG2, RAW264.7, zebrafish	boronate oxidation, mitochondrial	[1863]	2022
BTMO-PN	F	365	477	HeLa, mouse	boronate oxidation	[1864]	2022
NAB	FR2P	450/ 820	458/ 558	HeLa, HepG2, mouse	boronate oxidation endoplasmic reticulum	[1865]	2022
DCI-OV	F	580	690	Beas-2B, A549, HepG2,	boronate oxidation, dual with viscosity	[1866]	2022
YXP	F	397	535	BEAS, mouse	boronate oxidation	[1867]	2022
YV	F	460	533	HeLa, zebrafish	boronate oxidation	[1868]	2022

Rhod-CN-B	F	500	573	HL-7702, mouse	boronate oxidation	[1869]	2022
PV	F	447	507	HeLa, RAW264.7	boronic acid oxidation, mitochondrial	[1870]	2022
ATP-LW	F	488	568	HL-7702	boronate oxidation, dual with ATP	[1871]	2022
BDP-Py+	F	465	613	HepG2, mouse	boronate oxidation	[1885]	2022
MC-V-P	F	633	670-800	HepG2	boronate oxidation	[1872]	2022
Coumn-pHP-ONOO-	F	506	650	HeLa	boronate oxidation	[1873]	2022
RhNp-ClO-ONOO	F	483	518	RAW264.7, mouse	boronic acid oxidation, dual with HOCl	[1874]	2022
ATV-PPB	F	488	600-700	HepG2	boronate oxidation	[1875]	2022
BICBzBF	F	549	576	HeLa, RAW264.7, zebrafish	boronate oxidation, mitochondrial	[1876]	2022
RHOD-DCM-B	FR	480	670/570	HepG2, mouse, DILI, design strategy	boronate oxidation oxidation, spirolactam	[1005]	2022
CNN2-B	F	440	517	RAW264.7, A549, mouse	boronate oxidation, aminocoumarin, mitochondrial	[989]	2023
MBDP-Py$^+$	F	540-580	590-670	HepG2, mouse, DILI	boronate oxidation	[1006]	2023
TL	F	550-630	667	HeLa, HUVEC	boronate oxidation	[1877]	2023
Lyso-ONOO	F	450	555	L02, LX-2, mouse	boronate oxidation, lysosomal	[1878]	2023
Cy-OH-ONOO	F	640	710	RAW264.7, zebrafish, mouse	boronate oxidation	[1879]	2023
HDM-Cl-PN	FR	455	590/676	HeLa, RAW264.7, mouse	boronate oxidation	[1880]	2023
3a, 3b	F	365	510	HepG2	boronate oxidation	[1881]	2023
TCM-1-2	F	560	625	HeLa, RAW264.7	boronate oxidation	[1882]	2023
BTNB	FR	442	530/605	RAW264.7, zebrafish	boronate oxidation, mitochondrial	[1883]	2023
NAF-BN	F	600	695	HL-7702, Drosophila	boronate oxidation	[1884]	2023
BDP-ENE-S-Py$^+$	F	630	694	HepG2, mouse	boronate oxidation	[1885]	2023
NOSTracker	F	645	696	U251, U87-MG, HT22	boronate oxidation	[1886]	2023
GYP	FR	345	655/538	PC12, mouse	boronate oxidation	[1887]	2023
NN1	F	475	658	RAW264.7, mouse	boronic acid oxidation	[1888]	2023
W-2a	FR	426/564	563/684	EMT6, mouse	boronate oxidation, dual with Hg	[1889]	2023
DPB	F	570	658	HeLa, MPC5, RAW264.7	boronate oxidation, mitochondrial, dual with polarity and viscosity	[1890]	2023
P-1	F	670	570	HeLa, SMMC-7721, zebrafish	boronate oxidation, dual with viscosity	[1891]	2023
TPPB	F	365	655	HeLa	boronate oxidation	[1892]	2023
B-PD	CL	-	500-570	RAW264.7, mouse	boronate oxidation	[1893]	2023
Section 7 - Diphenylphosphinate							
DCPO-DP	F	556	690	HeLa	diphenylphosphinate	[1008]	2016
NOF2	F	670	742	RAW264.7, mouse	diphenylphosphinate	[1017]	2018
DCIPP	F	527	665	HeLa, zebrafish	diphenylphosphinate	[1011]	2019
HPP	F	403	520	HeLa	diphenylphosphinate	[1894]	2019
AN-DP	F	514	670	HepG2, colorimetric	diphenylphosphinate	[1012]	2020
CPC	FR	503	643/538	HepG2	diphenylphosphinate, mitochondrial	[1013]	2020
NR-ONOO	F	560	678	HeLa	diphenylphosphinate	[1014]	2020
NIR-HO	F	550	680	MCF-7, mouse	diphenylphosphinate, dual with Hg	[1018]	2020
RFP	F	525	590	RAW264.7, mouse	diphenylphosphinate	[1009]	2021
BTCV-PN	FR	440	632/525	HeLa, mouse	diphenylphosphinate, aminocoumarin	[1010]	2021
ANI-DP	FR	426	535/628	HeLa, zebrafish	diphenylphosphinate, mitochondrial	[1015]	2021
DCM-ONOO	F2P	520/820	685	HT22, RAW264.7, mouse	diphenylphosphinate	[1895]	2021
BDPP	F	465	613	HepG2, mouse	diphenylphosphinate	[1761]	2022
BS1	F	405	430	HepG2, DILI	diphenylphosphinate	[1003]	2022
JQ-3	F	488	557	HeLa, HepG2, zebrafish, DILI	diphenylphosphinate	[1016]	2022

GXY-ADP-2	FR	560	739/ 484/ 583	HepG2	diphenylphosphinate oxidation	[1896]	2022
MQA-P	F	405	645	HeLa, mouse	diphenylphosphinate, mitochondrial	[1019]	2023
XND-1	F	370	589	HeLa, zebrafish	diphenylphosphinate, dual with viscosity, mitochondrial	[1020]	2023
QCy7-DP	F	580	710	HepG2, mouse, DILI	diphenylphosphinate	[1021]	2023
NOP	F	560	656	HepG2, mouse, DILI	diphenylphosphinate	[1022]	2023
XPC	F	550	750	HeLa	diphenylphosphinate	[1897]	2023
Section 8 - Aryl chalcogenides							
Cy-PSe	F	758	775	RAW 264.7	selenide oxidation, reversible with GSH	[1024]	2011
BzSe-Cy	F	770	800	RAW 264.7	selenide oxidation, redox cycles	[1029]	2011
BOD-Se	FR	594	567/ 680	RAW264.7	diarylselenide oxidation	[1030]	2013
Cy-NTe	F	793	820	RAW264.7, mice	organotellurium oxidation	[1898]	2013
BDP-NGM	F	502	512	HeLa, RAW264.7	selenide oxidation	[1026]	2017
TP-Se	F2P	430/ 865	565	HeLa	selenide oxidation, mitochondrial	[1031]	2017
NMOF	FR	365	595	HeLa	sulfide oxidation	[1899]	2018
3a	FR	370	630/ 480	MCF-7, EC1	sulfide oxidation	[1027]	2020
CDMS	FR	500	662/ 548	RAW264.7, mouse	sulfide oxidation	[1028]	2021
NA-ONOO	F	365	500-570	HeLa, zebrafish	thiocarbonate oxidation	[1900]	2021
Section 9 - p-Phenols and p-aminophenols							
APF	F	490	515	neutrophils	*O*-dearylation	[607]	2003
HPF	F	490	515	neutrophils	*O*-dearylation	[607]	2003
Ds-DAB	F	350	505	RAW264.7	aminophenol oxidation	[1901]	2013
HKGreen-4	F2P	517/ 730	535	RAW264.7	*N*-dearylation, *p*-phenol	[1035]	2014
NP3	FP	375/ 760-820	470	EA.hy926	*N*-dearylation, *p*-phenol	[1036]	2015
1	F	440	545	RAW264.7	*N*-dearylation, *p*-aminophenol, mitochondrial	[1040]	2015
HKYellow	F	545	570	SH-SY5Y, mouse liver	*N*-dearylation, *p*-phenol	[1902]	2016
BHAni	F	519	530	RAW264.7	*N*-dearylation, *p*-phenol	[1903]	2016
probe	F2P	405/ 750	501	RAW264.7	*N*-dearylation, *p*-phenol	[1904]	2017
NP	F	445	545	RAW264.7	*N*-dearylation, *p*-phenol, mitochondrial	[1905]	2017
ASiR-P	F2P	460/ 750	610	HepG2. mouse	*N*-dearylation, *p*-phenol, lysosomal	[1042]	2018
3	F	526	538	RAW264.7	*N*-dearylation, *p*-phenol, endoplasmic reticulum	[1043]	2018
TPHQ	F2P	450/ 800	550	RAW 264.7	*O*-dearylation, *p*-phenol,	[1906]	2018
PX-1	F2P	405/ 800	553	SMMC-7721, mouse, DILI	*O*-dearylation, *p*-phenol	[1039]	2019
Gal-NHP	F	473	555	HepG2, hepatoma-specific	*O*-dearylation, *p*-phenol	[1044]	2019
DCM-OH	F	498	650	HepG2, mouse	*N*-dearylation, *p*-phenol	[1907]	2019
SiNH	F	470	595	HeLa	*N*-dearylation, *p*-phenol	[1908]	2019
FNO2	F	500	660	MCF-7, mouse	*N*-dearylation, time-resolved photoluminescence	[1909]	2019
Mito-PN	F	456	530	MCF-7	*N*-dearylation, dual with mitophagy, mitochondrial	[1052]	2021
NIR-PN2	F	510	670	PC12, drosophila, mouse, PD	*N*-dearylation	[1038]	2020
HCA-OH	F	460	548	HepG2, C. elegans, DFT	*N*-dearylation	[1910]	2020
HCA-OH	F	460	548	HepG2, C. elegans	*N*-dearylation, *p*-phenol	[1910]	2020
Ir-NIR	F	405	702	RAW264.7, HepG2, L02, mouse	*N*-dearylation, lysosomal	[1911]	2020
PS3	F	480	525	THP-1, J774A.1	*N*-dearylation, *p*-phenol	[1912]	2020
B545a,b	F	475	545	EA.hy926, mouse	*N*-dearylation, *p*-phenol	[1913]	2020
NNP	F	405	560	MX-2, mouse, DILI	*N*-dearylation	[1037]	2021

ER-PN	F2P	450	540	PC12, C. elegans	*N*-dearylation, endoplasmic reticulum	1914	2021
PDBE-PN	F	434	550	RAW264.7, zebrafish	*O*-dearylation	1915	2021
KNP-1	F	625	679	HK-2, RAW264.7, mouse	*N*-dearylation	1916	2021
NC-NP	FR	405	460/ 530	HepG2, HeLa	*N*-dearylation	1917	2022
Rd-DPA3	F	564	698	PC12, mouse, AD	*N*-dearylation	1918	2022
PMFP	F	435	553	HepG2, zebrafish	*O*-dearylation, mitochondrial	1919	2022
ER-ONOO	F2P	488	557	H1299, HUVEC	*N*-dearylation, endoplasmic reticulum	1920	2023
Section 10 - Hydrazide spirocycles							
RBPH	F	560	580	MCF-7	hydrazide spirolactam	1046	2013
RPTPP	F	530	578	RAW264.7	hydrazide spirolactam, mitochondrial	1048	2017
Probe 1	F	600	638	HeLa, RAW264.7	hydrazide spirolactam	1921	2017
Mito-PN	F	520	630	HeLa	hydrazide spirolactam, mitochondrial	1049	2018
CC-ONOO	F	640	698	RAW264.7	hydrazide spirolactam	1922	2018
CS-ONOO	FR	400/ 640	515/ 700	HeLa, RAW264.7, mouse	hydrazide spirolactam	1923	2019
RDMH-PN	F	520	585	RAW264.7, zebrafish	hydrazide spirolactam	1924	2019
RHHP-PN	F	570	585	RAW264.7, zebrafish	hydrazide spirolactam	1925	2019
Lyso-ONOO	F	590	650	HeLa, RAW264.7, mouse	hydrazide spirolactam	1926	2019
Red-PN	F	563	585	RAW 264.7, zebrafish	hydrazide spirolactam	1053	2019
NpRh-ONOO	FR2P	400/ 780	505/ 578	HeLa, zebrafish, rat	hydrazide spirolactam, lysosomal	1927	2020
KzRhONOO	FR2P	500/ 760	535/ 585	HeLa, zebrafish	hydrazide spirolactam	1928	2020
RHPN	F	540	581	HepG2, RAW264.7	hydrazide spirolactam	1929	2020
RH-PN	FR	360	454/ 581	RAW264.7, zebrafish	hydrazide spirolactam	1930	2020
P2	F2PR	405/ 800	474/ 574	RAW264.7, mouse	hydrazide spirolactam	1047	2021
NIR-ONOO	F2P	820	650	HeLa, RAW264.7, mouse, DILI	hydrazide spirolactam	1050	2021
ONOO-LysopH	F	595	678	HeLa	hydrazide spirolactam, lysosomal	1051	2021
Probe-OH	F	480	525	LM-3, mouse	hydrazide spirolactam, dual with HOCl	1432	2021
RB-PN	F	550	575	HESC-2, Cal-27, MC-3, HUVEC	hydrazide spirolactam	1931	2021
SZ	F	540	570	HUEVC	hydrazide spirolactam	1932	2021
Ru-FL-ONOO	FR	490	635/ 512	HeLa, RAW264.7	hydrazide spirolactam, lysosomal	1054	2022
CB2-H	F	631	669	HeLa, zebrafish, DFT	hydrazide spirolactam, dual with HOCl	1713	2022
F3ONOO	F	660	785	HeLa, mouse	hydrazide spirolactam	1933	2023
PN	F	680	732	buffer	hydrazide spirolactam	1934	2023
SPN	F	680	732	HepG2, zebrafish, mouse	hydrazide spirolactam	1934	2023
Section 11 - N-oxidation							
PN600	FR	355/ 475/ 576	525/ 585/ 595	SIN-1	*N*-oxidation, aromatization, dual with HOCl	1935	2012
Mito-A2	F	485	517	HeLa, RAW264.7, EA.hy926	*N*-oxidation/*N*-nitrosation, mitochondrial	1041	2016
Lyso-A2	F	485	517	HeLa, RAW264.7, EA.hy926	*N*-oxidation/*N*-nitrosation, lysosomal	1041	2016
2H	F	356	496	RAW264.7	dihydrorhodamine oxidation	1061	2017
SiRTA	F	650	680	EA.hy926, mouse	*N*-oxidation	1055	2018
HBTP	F	590	600	RAW264.7, mouse	*N*-oxidation, aromatization, dual with viscosity, lysosomal	1062	2019
ML-NAP-DPPEA	F	445	532	HeLa	*N*-oxidation, lysosomal	1056	2019
HSiO1-3	F	700	760	RAW264.7, mouse	*N*-oxidation, aromatization	1063	2020
L	F	477	599	SMMC-7721	*N*-oxidation	1057	2020
PR1/2-ONOO	F	708	730	RAW264.7, 293T, COS-7, A549, HeLa	*N*-oxidation, aromatization, lysosomal	1059	2022
HSiBM3	F	680	702	HeLa, RAW264.7, mouse	*N*-oxidation, aromatization, lysosomal	1064	2023

Probe	FR	380	545/ 435	RAW264.7, zebrafish	*N*-oxidation	[1058]	2023
1	FR	360	545/ 485	HeLa, zebrafish	*N*-oxidation	[1936]	2023
Section 12 - C=N bond cleavage							
BTP	F	433	524	HeLa	C=N bond cleavage	[1066]	2018
1	F	440	480	RAW264.7	C=N bond cleavage	[1937]	2019
Probe 1	F	405	504	HeLa, zebrafish	C=N bond cleavage	[1938]	2021
L-1	F	360	525	HeLa	C=N bond cleavage, mitochondrial	[1069]	2021
RN	F	488	571	HeLa	C=N bond cleavage	[1939]	2022
DMX	F	405	510	HeLa, zebrafish	C=N bond cleavage	[1940]	2022
BQ	F	450	550	HeLa	C=N bond cleavage	[1068]	2022
Section 13 - Other triggers							
Folic acid	F	380	460	HeLa	not reported	[1941]	2007
ROS/RNS Sensor	F	620	655	mouse neutrophils	arylamide cleavage	[1071]	2009
ARS-NBA	F	460	550	buffer	de-dimerization	[1942]	2015
[Eu(HDPH)$_3$(DPBT)]	L	335/ 400	610	HepG2	β-diketonate oxidation, Eu^{3+} release	[1943]	2017
Eu(hdph)$_3$(tpy)	L	337	607	HepG2	β-diketonate oxidation, Eu^{3+} release	[1944]	2018
FPP-Blue	F	375	447	HepG2	arylformamide	[1070]	2019
FPP-Green	F	385	506	HepG2	arylformamide	[1070]	2019
FPP-Yellow	F	435	560	HepG2, A549, mouse ex vivo	arylformamide	[1070]	2019
FPP-Red	F	530	620	HepG2	arylformamide	[1070]	2019
HOPy-PhOSi	FR	381	415/ 594	RAW264.7	silyl-ether bond cleavage	[1945]	2019
SiONNOH	FR	365	520/ 595/ 540	MCF-7	deprotonation, silyl deprotection, multicolor	[1081]	2020
Ac-BODIPY	F	499	504	HeLa	arylester cleavage	[1072]	2020
GCR1	FCL	535	700	HK2, mouse	aryltriflate and arylformate cleavage, dual with superoxide	[312]	2020
GCR2	FCL	535	700	HK2, mouse	aryltriflate and arylformate cleavage, dual with superoxide	[312]	2020
Probe 1	F	405	490	RAW264.7, design strategy	diketone	[1075]	2021
BTNPO	F2P	340	427	PC12, AD	oxindole oxidation	[1077]	2021
LAP	F	561	628	SMMC-7721, RAW264.7, DFT	nitration	[1946]	2021
Si-B1	FR	360-460	450/ 525	HeLa, RAW264.7, zebrafish	siloxane	[1947]	2021
Cy717	FR	550	815/ 650	RAW264.7, mouse	arylester cleavage	[1073]	2021
Ir-diol	F	405	704	HepG2, RAW264.7, mouse	hydroquinone oxidation, Iridium, dual with GSH	[1948]	2021
NATP	F2P	445	565	PC12, mouse, AD	oxindole oxidation	[1078]	2022
ON-RB	F	405	672	RAW264.7, atherosclerosis	1,4-oxazepine	[1083]	2022
BCN	F	405	490	HepG2, RAW264.7, zebrafish, mouse	diketone	[1076]	2022
PCPA	F	445	645	HeLa	phosphorothionate, mitochondrial	[1949]	2023
TPA-F-NO2	F	454	640	RAW264.7	arylester	[1074]	2023
HOPyNa-2-OH	F	372	652	buffer	deprotonation	[1079]	2023
HOPyNa-6-OH	F	372	652	MCF-7, RAW264.7	deprotonation	[1079]	2023

[a] F = fluorescence, R = ratiometric, 2P = two-photon, L= luminescence, CL = chemiluminescence, BL = bioluminescence, PA = photoacoustic. [b] Wavelengths given in nanometers.

Notes

A.R.L. declares a financial stake in BioLum Science, LLC. The other authors declare no financial stake.

Biographies

Maidileyvis Castro Cabello is currently working as a postdoctoral researcher in Prof. Alexander Lippert's group at Southern Methodist University, Dallas, Texas. Her research focuses on the field

of mechanistic and applied organic chemiluminescence. She obtained her undergraduate degree in Radiochemistry from the Higher Institute of Technologies and Applied Sciences (INTEC), Havana, Cuba. She received her M.Sc. and Ph.D. in Chemistry at the University of São Paulo under the supervision of Prof. Josef Wilhelm Baader, acting mainly on studies on the mechanism of peroxyoxalate chemiluminescence in aqueous media. This was followed by postdoctoral research in the laboratory of Prof. Roberto Kopke Salinas at the same university, where she gained a general experimental background in cell culture techniques, gene cloning, and purification of membrane proteins.

Gen Chen is currently a PhD student in Prof. Alexander Lippert's group at Southern Methodist University, Dallas, Texas. His research focuses on the synthesis of near-IR chemiluminescent probes. He obtained his bachelor's degree in applied chemistry from Anhui University of Science and Technology (AUST), Huainan, China and a master's degree of Chemistry from University of Science and Technology of China (USTC) under the supervision of Prof. Chen Gao, for the designing and building optical imaging equipment for the multiple chemiluminescent samples and its application in the rapid diagnosis of acute myocardial infarction.

Michael J. Mellvile earned two associate degrees from Sacramento City College in California before transferring to the Colorado School of Mines in 2019. As an undergraduate, Michael performed research under Mike McGuirk, where he gained experience performing air-free chemistry and setting up a new research lab. In 2021, he graduated *cum laude* with his B.S. in Biochemistry. Following graduation, Michael entered the Applied Chemistry Ph.D. program at Mines. He briefly continued his work in the McGuirk group, developing methods for performing organic isothermal titration experiments on supramolecular systems. Ultimately, Michael moved to the Domaille research group in the fall of 2022, where his fascination with chemical biology was ignited. His current work involves the development of small-molecule fluorescent probes to detect biologically relevant species such as hydrogen peroxide and peroxynitrite.

Rokia Osman is currently a PhD student in Prof. Alexander Lippert's group at Southern Methodist University, Dallas, Texas. Her research focuses on chemiluminescence and its application for detecting analytes such as nitric oxide. She obtained her master's degree in organic chemistry at Helwan University in Egypt under supervision of Prof. Galal Elgemeie where she worked on new synthetic approaches for 2-aryl, 2-pyridyl and 2-pyrimidylbenzothiazoles and their use in medicinal chemistry. After completing her master work, she joined the laboratory of Prof. Junha Jeon, at the University of Texas at Arlington as a visiting researcher, where she worked on chemical synthesis and catalysis. She completed her bachelor's degree at Al-Azhar University.

Dinesh Kumar earned an M.S. degree in Organic Chemistry from the University of Bangalore, India. He completed his Ph.D. in organic chemistry under the guidance of Daniel Gryko at the Institute of Organic Chemistry of the Polish Academy of Sciences, Warsaw, Poland working on the development of diketopyrrolopyrrole-based fluorescent probes for cations and applying them to bio-imaging. He joined the Domaille lab at the Colorado School of Mines in 2023 as a postdoctoral fellow where he is developing small-molecule fluorescent probes for tracking ROS/RNS in living cells as well as organic functional materials for optoelectronic applications.

Dylan W. Domaille earned B.S. degrees in chemistry and molecular and cell biology from the University of Oregon, where he worked on the synthesis of f-block ligands for nuclear waste separations. He completed his Ph.D. under the guidance of Chris Chang at UC Berkeley, developing small-molecule fluorophores for studying Cu in living cells. He transitioned to a postdoctoral position with Jen Cha at CU Boulder in Chemical Engineering, which ignited his interest in dynamic covalent chemistry, biomaterials, and biocompatible chemical synthesis. He

began his tenure track career at the Colorado School of Mines in 2017, where his research program develops sustainable chemical synthetic strategies, small-molecule fluorescent probes, and stimuli-responsive materials.

Alexander R. Lippert is a student of Nature and currently a Professor of Chemistry at Southern Methodist University. He earned his B.S. degree in Chemistry at the California Institute of Technology in 2003 and began his PhD at the University of California, Santa Barbara that same year. In 2007, he moved with his advisor to the University of Pennsylvania, where he was awarded his PhD in chemistry in 2008 for working on the synthesis and applications of fluxional bullvalene molecules and peptide ligation chemistry. Dr. Lippert then worked as a postdoctoral researcher at the University of California, Berkeley, where he developed luminescence and magnetic resonance imaging probes for hydrogen peroxide and hydrogen sulfide. He began at Southern Methodist University in 2012, where he built research programs around luminescent probes for reactive sulfur, oxygen, and nitrogen species and chemiluminescence imaging agents. Dr. Lippert also has interests in molecular devices, volumetric 3D displays, microscopic 3D printing, and rides the winds of science wherever they make take him.

Acknowledgements
This work is based upon work supported by start-up funds from the Colorado School of Mines (D.W.D), a Colorado Office of Economic Development and International Trade (COEDIT) Proof-of-Concept grant (D.W.D), the Arnold and Mabel Beckman Foundation, and an NSF CAREER award (2238563). This work is also based on work supported by the National Science Foundation (CHE 2155170) and the Welch Research Foundation (N-2038-20200401).

References
(1) Dickinson, B. C.; Chang, C. J. Chemistry and Biology of Reactive Oxygen Species in Signaling or Stress Responses. *Nat. Chem. Biol.* **2011**, *7* (8), 504–511. https://doi.org/10.1038/nchembio.607.
(2) Cortese-Krott, M. M.; Koning, A.; Kuhnle, G. G. C.; Nagy, P.; Bianco, C. L.; Pasch, A.; Wink, D. A.; Fukuto, J. M.; Jackson, A. A.; Van Goor, H.; Olson, K. R.; Feelisch, M. The Reactive Species Interactome: Evolutionary Emergence, Biological Significance, and Opportunities for Redox Metabolomics and Personalized Medicine. *Antioxid. Redox Signal.* **2017**, *27* (10), 684–712. https://doi.org/10.1089/ars.2017.7083.
(3) Sies, H.; Jones, D. P. Reactive Oxygen Species (ROS) as Pleiotropic Physiological Signalling Agents. *Nat. Rev. Mol. Cell Biol.* **2020**, *21* (7), 363–383. https://doi.org/10.1038/s41580-020-0230-3.
(4) Juan, C. A.; Pérez De La Lastra, J. M.; Plou, F. J.; Pérez-Lebeña, E. The Chemistry of Reactive Oxygen Species (ROS) Revisited: Outlining Their Role in Biological Macromolecules (DNA, Lipids and Proteins) and Induced Pathologies. *Int. J. Mol. Sci.* **2021**, *22* (9), 4642. https://doi.org/10.3390/ijms22094642.
(5) Heinrich, T. A.; Da Silva, R. S.; Miranda, K. M.; Switzer, C. H.; Wink, D. A.; Fukuto, J. M. Biological Nitric Oxide Signalling: Chemistry and Terminology: NO Chemical Biology and Terminology. *Br. J. Pharmacol.* **2013**, *169* (7), 1417–1429. https://doi.org/10.1111/bph.12217.
(6) Fukuto, J. M.; Carrington, S. J.; Tantillo, D. J.; Harrison, J. G.; Ignarro, L. J.; Freeman, B. A.; Chen, A.; Wink, D. A. Small Molecule Signaling Agents: The Integrated Chemistry and Biochemistry of Nitrogen Oxides, Oxides of Carbon, Dioxygen, Hydrogen Sulfide, and Their Derived Species. *Chem. Res. Toxicol.* **2012**, *25* (4), 769–793. https://doi.org/10.1021/tx2005234.

(7) Lau, N.; Pluth, M. D. Reactive Sulfur Species (RSS): Persulfides, Polysulfides, Potential, and Problems. *Curr. Opin. Chem. Biol.* **2019**, *49*, 1–8. https://doi.org/10.1016/j.cbpa.2018.08.012.
(8) Olson, K. R. Reactive Oxygen Species or Reactive Sulfur Species: Why We Should Consider the Latter. *J. Exp. Biol.* **2020**, *223* (4), jeb196352. https://doi.org/10.1242/jeb.196352.
(9) Ohata, J.; Bruemmer, K. J.; Chang, C. J. Activity-Based Sensing Methods for Monitoring the Reactive Carbon Species Carbon Monoxide and Formaldehyde in Living Systems. *Acc. Chem. Res.* **2019**, *52* (10), 2841–2848. https://doi.org/10.1021/acs.accounts.9b00386.
(10) Hammarlund, E. U.; Flashman, E.; Mohlin, S.; Licausi, F. Oxygen-Sensing Mechanisms across Eukaryotic Kingdoms and Their Roles in Complex Multicellularity. *Science* **2020**, *370* (6515), eaba3512. https://doi.org/10.1126/science.aba3512.
(11) Auten, R. L.; Davis, J. M. Oxygen Toxicity and Reactive Oxygen Species: The Devil Is in the Details. *Pediatr. Res.* **2009**, *66* (2), 121–127. https://doi.org/10.1203/PDR.0b013e3181a9eafb.
(12) Bezner, B. J.; Ryan, L. S.; Lippert, A. R. Reaction-Based Luminescent Probes for Reactive Sulfur, Oxygen, and Nitrogen Species: Analytical Techniques and Recent Progress. *Anal. Chem.* **2020**, *92* (1), 309–326. https://doi.org/10.1021/acs.analchem.9b04990.
(13) Sies, H.; Belousov, V. V.; Chandel, N. S.; Davies, M. J.; Jones, D. P.; Mann, G. E.; Murphy, M. P.; Yamamoto, M.; Winterbourn, C. Defining Roles of Specific Reactive Oxygen Species (ROS) in Cell Biology and Physiology. *Nat. Rev. Mol. Cell Biol.* **2022**, *23* (7), 499–515. https://doi.org/10.1038/s41580-022-00456-z.
(14) Murphy, M. P.; Bayir, H.; Belousov, V.; Chang, C. J.; Davies, K. J. A.; Davies, M. J.; Dick, T. P.; Finkel, T.; Forman, H. J.; Janssen-Heininger, Y.; Gems, D.; Kagan, V. E.; Kalyanaraman, B.; Larsson, N. G.; Milne, G. L.; Nyström, T.; Poulson, H. E.; Radi, R.; Remmen, H. V.; Schumacker, P. T.; Thornalley, P. J.; Toyokuni, S.; Winterbourn, C. C.; Yin, H.; Halliwell, B. Guidelines for Measuring Reactive Oxygen Species and Oxidative Damage in Cells and in Vivo. *Nat. Metab.* **2022**, *4* (6), 651–662. https://doi.org/10.1038/s42255-022-00591-z.
(15) Bruemmer, K.; Crossley, S.; Chang, C. Activity-Based Sensing: A Synthetic Methods Approach for Selective Molecular Imaging and Beyond. *Angew. Chem.-Int. Ed.* **2020**, *59* (33), 13734–13762. https://doi.org/10.1002/anie.201909690.
(16) Tsien, R. Y. New Calcium Indicators and Buffers with High Selectivity against Magnesium and Protons: Design, Synthesis, and Properties of Prototype Structures. *Biochemistry* **1980**, *19* (11), 2396–2404. https://doi.org/10.1021/bi00552a018.
(17) Palmer, A. E.; Tsien, R. Y. Measuring Calcium Signaling Using Genetically Targetable Fluorescent Indicators. *Nat. Protoc.* **2006**, *1* (3), 1057–1065. https://doi.org/10.1038/nprot.2006.172.
(18) Lippert, A. R.; Van de Bittner, G. C.; Chang, C. J. Boronate Oxidation as a Bioorthogonal Reaction Approach for Studying the Chemistry of Hydrogen Peroxide in Living Systems. *Acc. Chem. Res.* **2011**, *44* (9), 793–804. https://doi.org/10.1021/ar200126t.
(19) Wu, L.; Sedgwick, A. C.; Sun, X.; Bull, S. D.; He, X.-P.; James, T. D. Reaction-Based Fluorescent Probes for the Detection and Imaging of Reactive Oxygen, Nitrogen, and Sulfur Species. *Acc. Chem. Res.* **2019**, *52* (9), 2582–2597. https://doi.org/10.1021/acs.accounts.9b00302.
(20) Que, E. L.; Domaille, D. W.; Chang, C. J. Metals in Neurobiology: Probing Their Chemistry and Biology with Molecular Imaging. *Chem. Rev.* **2008**, *108* (5), 1517–1549. https://doi.org/10.1021/cr078203u.
(21) Domaille, D. W.; Que, E. L.; Chang, C. J. Synthetic Fluorescent Sensors for Studying the Cell Biology of Metals. *Nat. Chem. Biol.* **2008**, *4* (3), 168–175. https://doi.org/10.1038/nchembio.69.

(22) Jiao, X.; Li, Y.; Niu, J.; Xie, X.; Wang, X.; Tang, B. Small-Molecule Fluorescent Probes for Imaging and Detection of Reactive Oxygen, Nitrogen, and Sulfur Species in Biological Systems. *Anal. Chem.* **2018**, *90* (1), 533–555. https://doi.org/10.1021/acs.analchem.7b04234.
(23) Keston, A. S.; Brandt, R. The Fluorometric Analysis of Ultramicro Quantities of Hydrogen Peroxide. *Anal. Biochem.* **1965**, *11* (1), 1–5. https://doi.org/10.1016/0003-2697(65)90034-5.
(24) Hempel, S. L.; Buettner, G. R.; O'Malley, Y. Q.; Wessels, D. A.; Flaherty, D. M. Dihydrofluorescein Diacetate Is Superior for Detecting Intracellular Oxidants: Comparison with 2′,7′-Dichlorodihydrofluorescein Diacetate, 5(and 6)-Carboxy-2′,7′-Dichlorodihydrofluorescein Diacetate, and Dihydrorhodamine 123. *Free Radic. Biol. Med.* **1999**, *27* (1–2), 146–159. https://doi.org/10.1016/S0891-5849(99)00061-1.
(25) Zhou, M.; Diwu, Z.; Panchuk-Voloshina, N.; Haugland, R. P. A Stable Nonfluorescent Derivative of Resorufin for the Fluorometric Determination of Trace Hydrogen Peroxide: Applications in Detecting the Activity of Phagocyte NADPH Oxidase and Other Oxidases. *Anal. Biochem.* **1997**, *253* (2), 162–168. https://doi.org/10.1006/abio.1997.2391.
(26) Bezner, B. J.; Ryan, L. S.; Lippert, A. R. Reaction-Based Luminescent Probes for Reactive Sulfur, Oxygen, and Nitrogen Species: Analytical Techniques and Recent Progress. *Anal. Chem.* **2020**, *92* (1), 309–326. https://doi.org/10.1021/acs.analchem.9b04990.
(27) Hardy, M.; Zielonka, J.; Karoui, H.; Sikora, A.; Michalski, R.; Podsiadly, R.; Lopez, M.; Vasquez-Vivar, J.; Kalyanaraman, B.; Ouari, O. Detection and Characterization of Reactive Oxygen and Nitrogen Species in Biological Systems by Monitoring Species-Specific Products. *Antioxid. Redox Signal.* **2018**, *28* (15), 1416–1432. https://doi.org/10.1089/ars.2017.7398.
(28) Kwon, N.; Kim, D.; Swamy, K. M. K.; Yoon, J. Metal-Coordinated Fluorescent and Luminescent Probes for Reactive Oxygen Species (ROS) and Reactive Nitrogen Species (RNS). *Coord. Chem. Rev.* **2021**, *427*, 213581. https://doi.org/10.1016/j.ccr.2020.213581.
(29) Nguyen, V.-N.; Ha, J.; Cho, M.; Li, H.; Swamy, K. M. K.; Yoon, J. Recent Developments of BODIPY-Based Colorimetric and Fluorescent Probes for the Detection of Reactive Oxygen/Nitrogen Species and Cancer Diagnosis. *Coord. Chem. Rev.* **2021**, *439*, 213936. https://doi.org/10.1016/j.ccr.2021.213936.
(30) Zielonka, J.; Kalyanaraman, B. Small-Molecule Luminescent Probes for the Detection of Cellular Oxidizing and Nitrating Species. *Free Radic. Biol. Med.* **2018**, *128*, 3–22. https://doi.org/10.1016/j.freeradbiomed.2018.03.032.
(31) Bai, X.; Ng, K. K.-H.; Hu, J. J.; Ye, S.; Yang, D. Small-Molecule-Based Fluorescent Sensors for Selective Detection of Reactive Oxygen Species in Biological Systems. *Annu. Rev. Biochem.* **2019**, *88*, 605–633. https://doi.org/10.1146/annurev-biochem-013118-111754.
(32) Huang, J.; Pu, K. Activatable Molecular Probes for Second Near-Infrared Fluorescence, Chemiluminescence, and Photoacoustic Imaging. *Angew. Chem. Int. Ed.* **2020**, *59* (29), 11717–11731. https://doi.org/10.1002/anie.202001783.
(33) Liu, Y.; Teng, L.; Yin, B.; Meng, H.; Yin, X.; Huan, S.; Song, G.; Zhang, X. Chemical Design of Activatable Photoacoustic Probes for Precise Biomedical Applications. *Chem. Rev.* **2022**, *122* (6), 6850–6918. https://doi.org/10.1021/acs.chemrev.1c00875.
(34) Merkes, J. M.; Hasenbach, A.; Kiessling, F.; Hermann, S.; Banala, S. Sensing Reactive Oxygen Species with Photoacoustic Imaging Using Conjugation-Extended BODIPYs. *ACS Sens.* **2021**, *6* (12), 4379–4388. https://doi.org/10.1021/acssensors.1c01674.
(35) Lee, M. C.; Landers, K.; Chan, J. Activity-Based Photoacoustic Probes for Detection of Disease Biomarkers beyond Oncology. *ACS Bio Med Chem Au* **2023**, *3* (3), 223–232. https://doi.org/10.1021/acsbiomedchemau.3c00009.

(36) Rosenthal, J.; Lippard, S. J. Direct Detection of Nitroxyl in Aqueous Solution Using a Tripodal Copper(II) BODIPY Complex. *J. Am. Chem. Soc.* **2010**, *132* (16), 5536–5537. https://doi.org/10.1021/ja909148v.
(37) Reisz, J.; King, S. Progress toward the Development of Fluorescent Phosphine Probes for the Specific Detection and Quantification of Nitroxyl (HNO) in Biological Systems. *Nitric Oxide* **2011**, *24*, S27–S27. https://doi.org/10.1016/j.niox.2011.03.261.
(38) Liu, C.; Wang, Y.; Tang, C.; Liu, F.; Ma, Z.; Zhao, Q.; Wang, Z.; Zhu, B.; Zhang, X. A Reductant-Resistant Ratiometric, Colorimetric and Far-Red Fluorescent Probe for Rapid and Ultrasensitive Detection of Nitroxyl. *J. Mater. Chem. B* **2017**, *5* (19), 3557–3564. https://doi.org/10.1039/c6tb03359h.
(39) Miao, Z.; Reisz, J. A.; Mitroka, S. M.; Pan, J.; Xian, M.; King, S. B. A Selective Phosphine-Based Fluorescent Probe for Nitroxyl in Living Cells. *Bioorg. Med. Chem. Lett.* **2015**, *25*, 16–19. https://doi.org/10.1016/j.bmcl.2014.11.041.
(40) Pino, N.; Davis, J.; Yu, Z.; Chan, J. NitroxylFluor: A Thiol-Based Fluorescent Probe for Live-Cell Imaging of Nitroxyl. *J. Am. Chem. Soc.* **2017**, *139* (51), 18476–18479. https://doi.org/10.1021/jacs.7b11471.
(41) Rivera-Fuentes, P.; Lippard, S. Metal-Based Optical Probes for Live Cell Imaging of Nitroxyl (HNO). *Acc. Chem. Res.* **2015**, *48* (11), 2927–2934. https://doi.org/10.1021/acs.accounts.5b00388.
(42) An, W.; Ryan, L. S.; Reeves, A. G.; Bruemmer, K. J.; Mouhaffel, L.; Gerberich, J. L.; Winters, A.; Mason, R. P.; Lippert, A. R. A Chemiluminescent Probe for HNO Quantification and Real-Time Monitoring in Living Cells. *Angew. Chem. Int. Ed.* **2019**, *58* (5), 1361–1365. https://doi.org/10.1002/anie.201811257.
(43) Smulik-Izydorczyk, R.; Dębowska, K.; Pięta, J.; Michalski, R.; Marcinek, A.; Sikora, A. Fluorescent Probes for the Detection of Nitroxyl (HNO). *Free Radic. Biol. Med.* **2018**, *128*, 69–83. https://doi.org/10.1016/j.freeradbiomed.2018.04.564.
(44) Tanaka, K.; Miura, T.; Umezawa, N.; Urano, Y.; Kikuchi, K.; Higuchi, T.; Nagano, T. Rational Design of Fluorescein-Based Fluorescence Probes. Mechanism-Based Design of a Maximum Fluorescence Probe for Singlet Oxygen. *J. Am. Chem. Soc.* **2001**, *123*, 2530–2536. https://doi.org/10.1021/ja0035708.
(45) Pedersen, S. K.; Holmehave, J.; Blaikie, F. H.; Gollmer, A.; Breitenbach, T.; Jensen, H. H.; Ogilby, P. R. Aarhus Sensor Green: A Fluorescent Probe for Singlet Oxygen. *J. Org. Chem.* **2014**, *79*, 3079–3087. https://doi.org/10.1021/jo500219y.
(46) Xu, K.; Wang, L.; Qiang, M.; Wang, L.; Li, P.; Tang, B. A Selective Near-Infrared Fluorescent Probe for Singlet Oxygen in Living Cells. *Chem. Commun.* **2011**, *47*, 7386–7388. https://doi.org/10.1039/c1cc12473k.
(47) Gunduz, H.; Kolemen, S.; Akkaya, E. U. Singlet Oxygen Probes: Diversity in Signal Generation Mechanisms Yields a Larger Color Palette. *Coord. Chem. Rev.* **2021**, *429*, 213641. https://doi.org/10.1016/j.ccr.2020.213641.
(48) Cao, J.; Campbell, J.; Liu, L.; Mason, R. P.; Lippert, A. R. In Vivo Chemiluminescent Imaging Agents for Nitroreductase and Tissue Oxygenation. *Anal. Chem.* **2016**, *88* (9), 4995–5002. https://doi.org/10.1021/acs.analchem.6b01096.
(49) Ryan, L. S.; Gerberich, J.; Cao, J.; An, W.; Jenkins, B. A.; Mason, R. P.; Lippert, A. R. Kinetics-Based Measurement of Hypoxia in Living Cells and Animals Using an Acetoxymethyl Ester Chemiluminescent Probe. *ACS Sens.* **2019**, *4* (5), 1391–1398. https://doi.org/10.1021/acssensors.9b00360.
(50) Kagalwala, H. N.; Gerberich, J.; Smith, C. J.; Mason, R. P.; Lippert, A. R. Chemiluminescent 1,2-Dioxetane Iridium Complexes for Near-Infrared Oxygen Sensing. *Angew. Chem. Int. Ed.* **2022**, *61* (12), e202115704. https://doi.org/10.1002/anie.202115704.
(51) Kagalwala, H. N.; Bueno, L.; Wanniarachchi, H.; Unruh, D. K.; Hamal, K. B.; Pavlich, C. I.; Carlson, G. J.; Pinney, K. G.; Mason, R. P.; Lippert, A. R. Oxygen-Sensing

Chemiluminescent Iridium(III) 1,2-Dioxetanes: Unusual Coordination and Activity. *Anal. Sens.* **2023**, *3* (1), e202200085. https://doi.org/10.1002/anse.202200085.
(52) Qiao, J.; Wang, M.; Cui, M.; Fang, Y.; Li, H.; Zheng, C.; Li, Z.; Xu, Y.; Hua, H.; Li, D. Small-Molecule Probes for Fluorescent Detection of Cellular Hypoxia-Related Nitroreductase. *J. Pharm. Biomed. Anal.* **2021**, *203*, 114199. https://doi.org/10.1016/j.jpba.2021.114199.
(53) Qu, X.; Kirschenbaum, L. J.; Borish, E. T. Hydroxyterephthalate as a Fluorescent Probe for Hydroxyl Radicals: Application to Hair Melanin. *Photochem. Photobiol.* **2000**, *71* (3), 307–313. https://doi.org/10.1562/0031-8655(2000)0710307HAAFPF2.0.CO2.
(54) Deng, T.; Wang, X.; Wu, S.; Hu, S.; Liu, W.; Chen, T.; Yu, Z.; Xu, Q.; Liu, F. A New FRET Probe for Ratiometric Fluorescence Detecting Mitochondria-Localized Drug Activation and Imaging Endogenous Hydroxyl Radicals in Zebrafish. *Chem. Commun.* **2020**, *56* (32), 4432–4435. https://doi.org/10.1039/d0cc00382d.
(55) Zhang, B.; Xu, L.; Zhou, Y.; Zhang, W.; Wang, Y.; Zhu, Y. Synthesis and Activity of a Coumarin-Based Fluorescent Probe for Hydroxyl Radical Detection. *Luminescence* **2020**, *35* (2), 305–311. https://doi.org/10.1002/bio.3728.
(56) Ueno, T.; Urano, Y.; Kojima, H.; Nagano, T. Mechanism-Based Molecular Design of Highly Selective Fluorescence Probes for Nitrative Stress. *J. Am. Chem. Soc.* **2006**, *128* (33), 10640–10641. https://doi.org/10.1021/ja061972v.
(57) Yan, Y.; Krishnakumar, S.; Yu, H.; Ramishetti, S.; Deng, L.-W.; Wang, S.; Huang, L.; Huang, D. Nickel(II) Dithiocarbamate Complexes Containing Sulforhodamine B as Fluorescent Probes for Selective Detection of Nitrogen Dioxide. *J. Am. Chem. Soc.* **2013**, *135* (14), 5312–5315. https://doi.org/10.1021/ja401555y.
(58) Lippert, A. R.; New, E. J.; Chang, C. J. Reaction-Based Fluorescent Probes for Selective Imaging of Hydrogen Sulfide in Living Cells. *J. Am. Chem. Soc.* **2011**, *133* (26), 10078–10080. https://doi.org/10.1021/ja203661j.
(59) Liu, C.; Pan, J.; Li, S.; Zhao, Y.; Wu, L. Y.; Berkman, C. E.; Whorton, A. R.; Xian, M. Capture and Visualization of Hydrogen Sulfide by a Fluorescent Probe. *Angew. Chem.* **2011**, *123* (44), 10511–10513. https://doi.org/10.1002/ange.201104305.
(60) Peng, H.; Cheng, Y.; Dai, C.; King, A. L.; Predmore, B. L.; Lefer, D. J.; Wang, B. A Fluorescent Probe for Fast and Quantitative Detection of Hydrogen Sulfide in Blood. *Angew. Chem.* **2011**, *123* (41), 9846–9849. https://doi.org/10.1002/ange.201104236.
(61) Sasakura, K.; Hanaoka, K.; Shibuya, N.; Mikami, Y.; Kimura, Y.; Komatsu, T.; Ueno, T.; Terai, T.; Kimura, H.; Nagano, T. Development of a Highly Selective Fluorescence Probe for Hydrogen Sulfide. *J. Am. Chem. Soc.* **2011**, *133* (45), 18003–18005. https://doi.org/10.1021/ja207851s.
(62) Qian, Y.; Karpus, J.; Kabil, O.; Zhang, S.-Y.; Zhu, H.-L.; Banerjee, R.; Zhao, J.; He, C. Selective Fluorescent Probes for Live-Cell Monitoring of Sulphide. *Nat. Commun.* **2011**, *2* (1), 495. https://doi.org/10.1038/ncomms1506.
(63) Lin, V. S.; Lippert, A. R.; Chang, C. J. Cell-Trappable Fluorescent Probes for Endogenous Hydrogen Sulfide Signaling and Imaging H_2O_2 -Dependent H_2S Production. *Proc. Natl. Acad. Sci.* **2013**, *110* (18), 7131–7135. https://doi.org/10.1073/pnas.1302193110.
(64) Cao, J.; Lopez, R.; Thacker, J. M.; Moon, J. Y.; Jiang, C.; Morris, S. N. S.; Bauer, J. H.; Tao, P.; Mason, R. P.; Lippert, A. R. Chemiluminescent Probes for Imaging H_2S in Living Animals. *Chem. Sci.* **2015**, *6* (3), 1979–1985. https://doi.org/10.1039/C4SC03516J.
(65) Michel, B. W.; Lippert, A. R.; Chang, C. J. A Reaction-Based Fluorescent Probe for Selective Imaging of Carbon Monoxide in Living Cells Using a Palladium-Mediated Carbonylation. *J. Am. Chem. Soc.* **2012**, *134* (38), 15668–15671. https://doi.org/10.1021/ja307017b.
(66) Reeves, A. G.; Subbarao, M.; Lippert, A. R. Imaging Acetaldehyde Formation during Ethanol Metabolism in Living Cells Using a Hydrazinyl Naphthalimide Fluorescent Probe. *Anal. Methods* **2017**, *9* (23), 3418–3421. https://doi.org/10.1039/C7AY01238A.

(67) Lippert, A. R. Designing Reaction-Based Fluorescent Probes for Selective Hydrogen Sulfide Detection. *J. Inorg. Biochem.* **2014**, *133*, 136–142. https://doi.org/10.1016/j.jinorgbio.2013.10.010.
(68) Li, B.; Kim, Y. L.; Lippert, A. R. Chemiluminescence Measurement of Reactive Sulfur and Nitrogen Species. *Antioxid. Redox Signal.* **2022**, *36* (4–6), 337–353. https://doi.org/10.1089/ars.2021.0195.
(69) Jiang, Y.; Pu, K. Molecular Probes for Autofluorescence-Free Optical Imaging. *Chem. Rev.* **2021**, *121* (21), 13086–13131. https://doi.org/10.1021/acs.chemrev.1c00506.
(70) Li, X.; Yin, C.; Liew, S. S.; Lee, C.; Pu, K. Organic Semiconducting Luminophores for Near-Infrared Afterglow, Chemiluminescence, and Bioluminescence Imaging. *Adv. Funct. Mater.* **2021**, *31* (46), 2106154. https://doi.org/10.1002/adfm.202106154.
(71) Li, J.; Pu, K. Development of Organic Semiconducting Materials for Deep-Tissue Optical Imaging, Phototherapy and Photoactivation. *Chem. Soc. Rev.* **2019**, *48* (1), 38–71. https://doi.org/10.1039/C8CS00001H.
(72) Jablonski, A. Efficiency of Anti-Stokes Fluorescence in Dyes. *Nature* **1933**, *131* (3319), 839–840. https://doi.org/10.1038/131839b0.
(73) Lakowicz, J. R. *Principles of Fluorescence Spectroscopy*, 3rd ed.; Springer: New York, 2006.
(74) Anslyn, E. V.; Dougherty, D. A. *Modern Physical Organic Chemistry*; University Science: Sausalito, CA, 2006.
(75) O'Riordan, T. C.; Fitzgerald, K.; Ponomarev, G. V.; Mackrill, J.; Hynes, J.; Taylor, C.; Papkovsky, D. B. Sensing Intracellular Oxygen Using Near-Infrared Phosphorescent Probes and Live-Cell Fluorescence Imaging. *Am. J. Physiol.* **2007**, *292*, R1613. https://doi.org/10.1152/ajpregu.00707.2006.
(76) Sun, W.; Li, M.; Fan, J.; Peng, X. Activity-Based Sensing and Theranostic Probes Based on Photoinduced Electron Transfer. *Acc. Chem. Res.* **2019**, *52* (10), 2818–2831. https://doi.org/10.1021/acs.accounts.9b00340.
(77) Daly, B.; Ling, J.; De Silva, A. P. Current Developments in Fluorescent PET (Photoinduced Electron Transfer) Sensors and Switches. *Chem. Soc. Rev.* **2015**, *44* (13), 4203–4211. https://doi.org/10.1039/C4CS00334A.
(78) Escudero, D. Revising Intramolecular Photoinduced Electron Transfer (PET) from First-Principles. *Acc. Chem. Res.* **2016**, *49* (9), 1816–1824. https://doi.org/10.1021/acs.accounts.6b00299.
(79) De Silva, A. P.; Moody, T. S.; Wright, G. D. Fluorescent PET (Photoinduced Electron Transfer) Sensors as Potent Analytical Tools. *The Analyst* **2009**, *134* (12), 2385. https://doi.org/10.1039/b912527m.
(80) Algar, W. R.; Hildebrandt, N.; Vogel, S. S.; Medintz, I. L. FRET as a Biomolecular Research Tool — Understanding Its Potential While Avoiding Pitfalls. *Nat. Methods* **2019**, *16* (9), 815–829. https://doi.org/10.1038/s41592-019-0530-8.
(81) Wu, L.; Huang, C.; Emery, B. P.; Sedgwick, A. C.; Bull, S. D.; He, X.-P.; Tian, H.; Yoon, J.; Sessler, J. L.; James, T. D. Förster Resonance Energy Transfer (FRET)-Based Small-Molecule Sensors and Imaging Agents. *Chem. Soc. Rev.* **2020**, *49* (15), 5110–5139. https://doi.org/10.1039/C9CS00318E.
(82) Fan, J.; Hu, M.; Zhan, P.; Peng, X. Energy Transfer Cassettes Based on Organic Fluorophores: Construction and Applications in Ratiometric Sensing. *Chem. Soc. Rev.* **2013**, *42* (1), 29–43. https://doi.org/10.1039/C2CS35273G.
(83) Förster, Th. Zwischenmolekulare Energiewanderung Und Fluoreszenz. *Ann. Phys.* **1948**, *437* (1–2), 55–75. https://doi.org/10.1002/andp.19484370105.
(84) Ryan, L. S.; Gerberich, J.; Haris, U.; Nguyen, D.; Mason, R. P.; Lippert, A. R. Ratiometric pH Imaging Using a 1,2-Dioxetane Chemiluminescence Resonance Energy Transfer

Sensor in Live Animals. *ACS Sens.* **2020**, *5* (9), 2925–2932. https://doi.org/10.1021/acssensors.0c01393.
(85) Digby, E. M.; Tung, M. T.; Kagalwala, H. N.; Ryan, L. S.; Lippert, A. R.; Beharry, A. A. Dark Dynamic Therapy: Photosensitization without Light Excitation Using Chemiluminescence Resonance Energy Transfer in a Dioxetane–Erythrosin B Conjugate. *ACS Chem. Biol.* **2022**, *17* (5), 1082–1091. https://doi.org/10.1021/acschembio.1c00925.
(86) Han, J.; Jose, J.; Mei, E.; Burgess, K. Chemiluminescent Energy-Transfer Cassettes Based on Fluorescein and Nile Red. *Angew. Chem. Int. Ed.* **2007**, *46* (10), 1684–1687. https://doi.org/10.1002/anie.200603307.
(87) Slama-Schwok, A.; Blanchard-Desce, M.; Lehn, J. M. Intramolecular Charge Transfer in Donor-Acceptor Molecules. *J. Phys. Chem.* **1990**, *94* (10), 3894–3902. https://doi.org/10.1021/j100373a007.
(88) De Silva, A. P.; Gunaratne, H. Q. N.; Gunnlaugsson, T.; Huxley, A. J. M.; McCoy, C. P.; Rademacher, J. T.; Rice, T. E. Signaling Recognition Events with Fluorescent Sensors and Switches. *Chem. Rev.* **1997**, *97* (5), 1515–1566. https://doi.org/10.1021/cr960386p.
(89) Grabowski, Z. R.; Rotkiewicz, K.; Rettig, W. Structural Changes Accompanying Intramolecular Electron Transfer: Focus on Twisted Intramolecular Charge-Transfer States and Structures. *Chem. Rev.* **2003**, *103* (10), 3899–4032. https://doi.org/10.1021/cr940745l.
(90) Wang, C.; Chi, W.; Qiao, Q.; Tan, D.; Xu, Z.; Liu, X. Twisted Intramolecular Charge Transfer (TICT) and Twists beyond TICT: From Mechanisms to Rational Designs of Bright and Sensitive Fluorophores. *Chem. Soc. Rev.* **2021**, *50* (22), 12656–12678. https://doi.org/10.1039/D1CS00239B.
(91) Sedgwick, A. C.; Wu, L.; Han, H.-H.; Bull, S. D.; He, X.-P.; James, T. D.; Sessler, J. L.; Tang, B. Z.; Tian, H.; Yoon, J. Excited-State Intramolecular Proton-Transfer (ESIPT) Based Fluorescence Sensors and Imaging Agents. *Chem. Soc. Rev.* **2018**, *47* (23), 8842–8880. https://doi.org/10.1039/C8CS00185E.
(92) Zhao, Z.; Zhang, H.; Lam, J. W. Y.; Tang, B. Z. Aggregation-Induced Emission: New Vistas at the Aggregate Level. *Angew. Chem. Int. Ed.* **2020**, *59* (25), 9888–9907. https://doi.org/10.1002/anie.201916729.
(93) Hong, Y.; Lam, J. W. Y.; Tang, B. Z. Aggregation-Induced Emission. *Chem. Soc. Rev.* **2011**, *40* (11), 5361. https://doi.org/10.1039/c1cs15113d.
(94) Cai, X.; Liu, B. Aggregation-Induced Emission: Recent Advances in Materials and Biomedical Applications. *Angew. Chem. Int. Ed.* **2020**, *59* (25), 9868–9886. https://doi.org/10.1002/anie.202000845.
(95) Kwok, R. T. K.; Leung, C. W. T.; Lam, J. W. Y.; Tang, B. Z. Biosensing by Luminogens with Aggregation-Induced Emission Characteristics. *Chem. Soc. Rev.* **2015**, *44* (13), 4228–4238. https://doi.org/10.1039/C4CS00325J.
(96) Liu, H.; Song, P.; Wei, R.; Li, K.; Tong, A. A Facile, Sensitive and Selective Fluorescent Probe for Heparin Based on Aggregation-Induced Emission. *Talanta* **2014**, *118*, 348–352. https://doi.org/10.1016/j.talanta.2013.09.055.
(97) Vacher, M.; Fdez. Galván, I.; Ding, B.-W.; Schramm, S.; Berraud-Pache, R.; Naumov, P.; Ferré, N.; Liu, Y.-J.; Navizet, I.; Roca-Sanjuán, D.; Baader, W. J.; Lindh, R. Chemi- and Bioluminescence of Cyclic Peroxides. *Chem. Rev.* **2018**, *118* (15), 6927–6974. https://doi.org/10.1021/acs.chemrev.7b00649.
(98) Haris, U.; Kagalwala, H.; Kim, Y.; Lippert, A. Seeking Illumination: The Path to Chemiluminescent 1,2-Dioxetanes for Quantitative Measurements and In Vivo Imaging. *Acc. Chem. Res.* **2021**, *54* (13), 2844–2857. https://doi.org/10.1021/acs.accounts.1c00185.
(99) Kagalwala, H. N.; Reeves, R. T.; Lippert, A. R. Chemiluminescent Spiroadamantane-1,2-Dioxetanes: Recent Advances in Molecular Imaging and Biomarker Detection. *Curr. Opin. Chem. Biol.* **2022**, *68*, 102134. https://doi.org/10.1016/j.cbpa.2022.102134.

(100) Haris, U.; Lippert, A. R. Exploring the Structural Space of Chemiluminescent 1,2-Dioxetanes. *ACS Sens.* **2023**, *8* (1), 3–11. https://doi.org/10.1021/acssensors.2c02371.
(101) Allen, R. C.; Loose, L. D. Phagocytic Activation of a Luminol-Dependent Chemiluminescence in Rabbit Alveolar and Peritoneal Macrophages. *Biochem. Biophys. Res. Commun.* **1976**, *69* (1), 245–252. https://doi.org/10.1016/S0006-291X(76)80299-9.
(102) Daiber, A.; Oelze, M.; August, M.; Wendt, M.; Sydow, K.; Wieboldt, H.; Kleschyov, A. L.; Munzel, T. Detection of Superoxide and Peroxynitrite in Model Systems and Mitochondria by the Luminol Analogue L-012. *Free Radic. Res.* **2004**, *38* (3), 259–269. https://doi.org/10.1080/10715760410001659773.
(103) Zielonka, J.; Lambeth, J. D.; Kalyanaraman, B. On the Use of L-012, a Luminol-Based Chemiluminescent Probe, for Detecting Superoxide and Identifying Inhibitors of NADPH Oxidase: A Reevaluation. *Free Radic. Biol. Med.* **2013**, *65*, 1310–1314. https://doi.org/10.1016/j.freeradbiomed.2013.09.017.
(104) Delafresnaye, L.; Bloesser, F. R.; Kockler, K. B.; Schmitt, C. W.; Irshadeen, I. M.; Barner-Kowollik, C. All Eyes on Visible-Light Peroxyoxalate Chemiluminescence Read-Out Systems. *Chem. – Eur. J.* **2020**, *26* (1), 114–127. https://doi.org/10.1002/chem.201904054.
(105) Quimbar, M. E.; Davis, S. Q.; Al-Farra, S. T.; Hayes, A.; Jovic, V.; Masuda, M.; Lippert, A. R. Chemiluminescent Measurement of Hydrogen Peroxide in the Exhaled Breath Condensate of Healthy and Asthmatic Adults. *Anal. Chem.* **2020**, *92* (21), 14594–14600. https://doi.org/10.1021/acs.analchem.0c02929.
(106) Goto, T.; Takagi, T. Chemiluminescence of a *Cypridina* Luciferin Analogue, 2-Methyl-6-Phenyl-3,7-Dihydroimidazo[1,2- *a*]Pyrazin-3-One, in the Presence of the Xanthine–Xanthine Oxidase System. *Bull. Chem. Soc. Jpn.* **1980**, *53* (3), 833–834. https://doi.org/10.1246/bcsj.53.833.
(107) Teranishi, K.; Shimomura, O. Coelenterazine Analogs as Chemiluminescent Probe for Superoxide Anion. *Anal. Biochem.* **1997**, *249* (1), 37–43. https://doi.org/10.1006/abio.1997.2150.
(108) Li, B.; Kim, Y. L.; Lippert, A. R. Chemiluminescence Measurement of Reactive Sulfur and Nitrogen Species. *Antioxid. Redox Signal.* **2022**, *36* (4–6), 337–353. https://doi.org/10.1089/ars.2021.0195.
(109) Haris, U.; Kagalwala, H. N.; Kim, Y. L.; Lippert, A. R. Seeking Illumination: The Path to Chemiluminescent 1,2-Dioxetanes for Quantitative Measurements and *In Vivo* Imaging. *Acc. Chem. Res.* **2021**, *54* (13), 2844–2857. https://doi.org/10.1021/acs.accounts.1c00185.
(110) Zhan, Z.; Dai, Y.; Li, Q.; Lv, Y. Small Molecule-Based Bioluminescence and Chemiluminescence Probes for Sensing and Imaging of Reactive Species. *TrAC Trends Anal. Chem.* **2021**, *134*, 116129. https://doi.org/10.1016/j.trac.2020.116129.
(111) Choi, N.-E.; Lee, J.-Y.; Park, E.-C.; Lee, J.-H.; Lee, J. Recent Advances in Organelle-Targeted Fluorescent Probes. *Molecules* **2021**, *26* (1), 217. https://doi.org/10.3390/molecules26010217.
(112) Dickinson, B. C.; Srikun, D.; Chang, C. J. Mitochondrial-Targeted Fluorescent Probes for Reactive Oxygen Species. *Curr. Opin. Chem. Biol.* **2010**, *14* (1), 50–56. https://doi.org/10.1016/j.cbpa.2009.10.014.
(113) Yousif, L. F.; Stewart, K. M.; Kelley, S. O. Targeting Mitochondria with Organelle-Specific Compounds: Strategies and Applications. *ChemBioChem* **2009**, *10* (12), 1939–1950. https://doi.org/10.1002/cbic.200900185.
(114) Smith, R. A. J.; Hartley, R. C.; Murphy, M. P. Mitochondria-Targeted Small Molecule Therapeutics and Probes. *Antioxid. Redox Signal.* **2011**, *15* (12), 3021–3038. https://doi.org/10.1089/ars.2011.3969.
(115) Ballabio, A. The Awesome Lysosome. *EMBO Mol. Med.* **2016**, *8* (2), 73–76. https://doi.org/10.15252/emmm.201505966.

(116) Duan, X.; Tong, Q.; Fu, C.; Chen, L. Lysosome-Targeted Fluorescent Probes: Design Mechanism and Biological Applications. *Bioorganic Chem.* **2023**, *140*, 106832. https://doi.org/10.1016/j.bioorg.2023.106832.
(117) Voeltz, G. K.; Rolls, M. M.; Rapoport, T. A. Structural Organization of the Endoplasmic Reticulum. *EMBO Rep.* **2002**, *3* (10), 944–950. https://doi.org/10.1093/embo-reports/kvf202.
(118) Schwarz, D. S.; Blower, M. D. The Endoplasmic Reticulum: Structure, Function and Response to Cellular Signaling. *Cell. Mol. Life Sci.* **2016**, *73* (1), 79–94. https://doi.org/10.1007/s00018-015-2052-6.
(119) Liu, C.; Zhu, H.; Zhang, Y.; Su, M.; Liu, M.; Zhang, X.; Wang, X.; Rong, X.; Wang, K.; Li, X.; Zhu, B. Recent Advances in Golgi-Targeted Small-Molecule Fluorescent Probes. *Coord. Chem. Rev.* **2022**, *462*, 214504. https://doi.org/10.1016/j.ccr.2022.214504.
(120) Wang, H.; Liu, C.; Zhang, X.; Xiu, T.; Li, P.; Zhang, W.; Zhang, W.; Wang, X.; Liu, Z.; Tang, B. Simultaneous Fluorescence Imaging of Golgi $O2^{\bullet-}$ and Golgi H_2O_2 in Mice with Hypertension. *Biosens. Bioelectron.* **2022**, *213*, 114480. https://doi.org/10.1016/j.bios.2022.114480.
(121) Li, A.; Liu, Y.; Labapuchi; Chen, Z.; Li, S.; Zhong, R.; Cheng, D.; Chen, L.; He, L. Development of a Golgi-Targeted Superoxide Anion Fluorescent Probe for Elucidating Protein GOLPH3 Function in Myocardial Ischemia-Reperfusion Injury. *Anal. Chim. Acta* **2023**, *1255*, 341100. https://doi.org/10.1016/j.aca.2023.341100.
(122) Liu, F.; Zhang, X.; Jing, J.; Zhang, X. A Golgi-Targeted Fluorescent Probe for Imaging H_2O_2 and Releasing H_2S during Golgi Stress. *Dyes Pigments* **2023**, *219*, 111521. https://doi.org/10.1016/j.dyepig.2023.111521.
(123) Qiao, L.; Shao, X.; Gao, S.; Ming, Z.; Fu, X.; Wei, Q. Research on Endoplasmic Reticulum–Targeting Fluorescent Probes and Endoplasmic Reticulum Stress–Mediated Nanoanticancer Strategies: A Review. *Colloids Surf. B Biointerfaces* **2021**, *208*, 112046. https://doi.org/10.1016/j.colsurfb.2021.112046.
(124) Jani, M. S.; Zou, J.; Veetil, A. T.; Krishnan, Y. A DNA-Based Fluorescent Probe Maps NOS3 Activity with Subcellular Spatial Resolution. *Nat. Chem. Biol.* **2020**, *16* (6), 660–666. https://doi.org/10.1038/s41589-020-0491-3.
(125) Xue, L.; Karpenko, I. A.; Hiblot, J.; Johnsson, K. Imaging and Manipulating Proteins in Live Cells through Covalent Labeling. *Nat. Chem. Biol.* **2015**, *11* (12), 917–923. https://doi.org/10.1038/nchembio.1959.
(126) Keppler, A.; Gendreizig, S.; Gronemeyer, T.; Pick, H.; Vogel, H.; Johnsson, K. A General Method for the Covalent Labeling of Fusion Proteins with Small Molecules in Vivo. *Nat. Biotechnol.* **2003**, *21* (1), 86–89. https://doi.org/10.1038/nbt765.
(127) Gautier, A.; Juillerat, A.; Heinis, C.; Corrêa, I. R.; Kindermann, M.; Beaufils, F.; Johnsson, K. An Engineered Protein Tag for Multiprotein Labeling in Living Cells. *Chem. Biol.* **2008**, *15* (2), 128–136. https://doi.org/10.1016/j.chembiol.2008.01.007.
(128) Los, G. V.; Encell, L. P.; McDougall, M. G.; Hartzell, D. D.; Karassina, N.; Zimprich, C.; Wood, M. G.; Learish, R.; Ohana, R. F.; Urh, M.; Simpson, D.; Mendez, J.; Zimmerman, K.; Otto, P.; Vidugiris, G.; Zhu, J.; Darzins, A.; Klaubert, D. H.; Bulleit, R. F.; Wood, K. V. HaloTag: A Novel Protein Labeling Technology for Cell Imaging and Protein Analysis. *ACS Chem. Biol.* **2008**, *3* (6), 373–382. https://doi.org/10.1021/cb800025k.
(129) Srikun, D.; Albers, A. E.; Nam, C. I.; Iavarone, A. T.; Chang, C. J. Organelle-Targetable Fluorescent Probes for Imaging Hydrogen Peroxide in Living Cells via SNAP-Tag Protein Labeling. *J. Am. Chem. Soc.* **2010**, *132*, 4455–4465. https://doi.org/10.1021/ja100117u.
(130) Abo, M.; Minakami, R.; Miyano, K.; Kamiya, M.; Nagano, T.; Urano, Y.; Sumimoto, H. Visualization of Phagosomal Hydrogen Peroxide Production by a Novel Fluorescent Probe That Is Localized via SNAP-Tag Labeling. *Anal. Chem.* **2014**, *86*, 5983–5990. https://doi.org/10.1021/ac501041w.

(131) Wang, J.; Zhao, Y.; Wang, C.; Zhu, Q.; Du, Z.; Hu, A.; Yang, Y. Organelle-Specific Nitric Oxide Detection in Living Cells via HaloTag Protein Labeling. *PLOS ONE* **2015**, *10* (4), e0123986. https://doi.org/10.1371/journal.pone.0123986.
(132) Yao, H.-W.; Chen, J.-B.; Guo, X.-F.; Wang, H. Simultaneous Monitoring of Intra- and Extracellular Nitric Oxide in Living Cells by Means of Dual-Color Fluorescence Imaging. *Nitric Oxide* **2017**, *67*, 30–38. https://doi.org/10.1016/j.niox.2017.04.008.
(133) Zhang, X.; Wang, B.; Xiao, Y.; Wang, C.; He, L. Targetable, Two-Photon Fluorescent Probes for Local Nitric Oxide Capture in the Plasma Membranes of Live Cells and Brain Tissues. *The Analyst* **2018**, *143* (17), 4180–4188. https://doi.org/10.1039/C8AN00905H.
(134) Fan, X.-P.; Yang, W.; Ren, T.-B.; Xu, S.; Gong, X.-Y.; Zhang, X.-B.; Yuan, L. Engineering a Ratiometric Photoacoustic Probe with a Hepatocyte-Specific Targeting Ability for Liver Injury Imaging. *Anal. Chem.* **2022**, *94* (2), 1474–1481. https://doi.org/10.1021/acs.analchem.1c05026.
(135) An, P.; Lewandowski, T. M.; Lin, Q. Design and Synthesis of a BODIPY-Tetrazole Based "Off-On" in-Cell Fluorescence Reporter of Hydrogen Peroxide. *ChemBioChem* **2018**, *19* (12), 1326–1333. https://doi.org/10.1002/cbic.201700656.
(136) Jia, S.; Chang, C. J. A Microtubule-Localizing Activity-Based Sensing Fluorescent Probe for Imaging Hydrogen Peroxide in Living Cells. *Bioorg. Med. Chem. Lett.* **2021**, *48*, 128252. https://doi.org/10.1016/j.bmcl.2021.128252.
(137) Jiang, G.; Li, C.; Liu, X.; Chen, Q.; Li, X.; Gu, X.; Zhang, P.; Lai, Q.; Wang, J. Lipid Droplet-Targetable Fluorescence Guided Photodynamic Therapy of Cancer Cells with an Activatable AIE-Active Fluorescent Probe for Hydrogen Peroxide. *Adv. Opt. Mater.* **2020**, *8* (20), 2001119. https://doi.org/10.1002/adom.202001119.
(138) Li, M.; Wang, B.; Liu, J.; Zhang, Z.; Chen, L.; Li, Y.; Yan, X. Lipid Droplet-Specific Dual-Response Fluorescent Probe for the Detection of Polarity and H_2O_2 and Its Application in Living Cells. *Anal. Chem.* **2022**, *94* (27), 9732–9739. https://doi.org/10.1021/acs.analchem.2c01243.
(139) Li, X.; Xu, W.; Yang, Z.; Li, S.; Gu, X.; Yuan, T.; Li, C.; Wang, Y.; Hua, J. A Lipid Droplet-Targeted Multifunctional AIE-Active Fluorescent Probe for Hydrogen Peroxide Detection and Imaging-Guided Photodynamic Therapy. *Sens. Actuators B Chem.* **2023**, *375*, 132892. https://doi.org/10.1016/j.snb.2022.132892.
(140) Zhao, P.; Wang, K.; Zhu, X.; Zhou, Y.; Wu, J. A Fluorescent Probe for Imaging Hydrogen Peroxide in Ovarian Cancer Cells. *Dyes Pigments* **2018**, *155*, 143–149. https://doi.org/10.1016/j.dyepig.2018.03.038.
(141) He, P.; Deng, X.; Xu, B.; Xie, B.; Zou, W.; Zhou, H.; Dong, C. Development of Highly Efficient Estrogen Receptor β-Targeted Near-Infrared Fluorescence Probes Triggered by Endogenous Hydrogen Peroxide for Diagnostic Imaging of Prostate Cancer. *Molecules* **2023**, *28* (5), 2309. https://doi.org/10.3390/molecules28052309.
(142) Yang, J.; Yang, J.; Liang, S. H.; Xu, Y.; Moore, A.; Ran, C. Imaging Hydrogen Peroxide in Alzheimer's Disease via Cascade Signal Amplification. *Sci. Rep.* **2016**, *6*, 35613. https://doi.org/10.1038/srep35613.
(143) Ma, J.; Wang, X.; Li, N.; Cheng, Y. A Bifunctional Probe That Allows Dual-Channel Fluorescence Turn-on Detection of Protein Aggregates and Hydrogen Peroxide in Neurodegenerative Diseases. *Sens. Actuators B Chem.* **2021**, *346*, 130536. https://doi.org/10.1016/j.snb.2021.130536.
(144) Wang, X.; Iyaswamy, A.; Xu, D.; Krishnamoorthi, S.; Sreenivasmurthy, S. G.; Yang, Y.; Li, Y.; Chen, C.; Li, M.; Li, H.-W.; Wong, M. S. Real-Time Detection and Visualization of Amyloid-β Aggregates Induced by Hydrogen Peroxide in Cell and Mouse Models of Alzheimer's Disease. *ACS Appl. Mater. Interfaces* **2023**, *15* (1), 39–47. https://doi.org/10.1021/acsami.2c07859.

(145) Guo, Y.; Leng, H.; Wang, Y.; Shi, W.-J.; Zhang, L.; Yan, J. A Novel H_2O_2 -Activated NIR Fluorescent Probe for Imaging β-Amyloid Fibrils and Mitochondrial Viscosity. *Dyes Pigments* **2022**, *206*, 110665. https://doi.org/10.1016/j.dyepig.2022.110665.
(146) Gharai, P. K.; Khan, J.; Mallesh, R.; Garg, S.; Saha, A.; Ghosh, S.; Ghosh, S. Vanillin Benzothiazole Derivative Reduces Cellular Reactive Oxygen Species and Detects Amyloid Fibrillar Aggregates in Alzheimer's Brain. *ACS Chem. Neurosci.* **2023**, *14* (4), 773–786. https://doi.org/10.1021/acschemneuro.2c00771.
(147) Dickinson, B. C.; Huynh, C.; Chang, C. J. A Palette of Fluorescent Probes with Varying Emission Colors for Imaging Hydrogen Peroxide Signaling in Living Cells. *J. Am. Chem. Soc.* **2010**, *132*, (16), 5906–5915. https://doi.org/10.1021/ja1014103.
(148) Kolanowski, J. L.; Liu, F.; New, E. J. Fluorescent Probes for the Simultaneous Detection of Multiple Analytes in Biology. *Chem. Soc. Rev.* **2018**, *47* (1), 195–208. https://doi.org/10.1039/C7CS00528H.
(149) Wu, L.; Sedgwick, A. C.; Sun, X.; Bull, S. D.; He, X.-P.; James, T. D. Reaction-Based Fluorescent Probes for the Detection and Imaging of Reactive Oxygen, Nitrogen, and Sulfur Species. *Acc. Chem. Res.* **2019**, *52* (9), 2582–2597. https://doi.org/10.1021/acs.accounts.9b00302.
(150) Grienberger, C.; Konnerth, A. Imaging Calcium in Neurons. *Neuron* **2012**, *73* (5), 862–885. https://doi.org/10.1016/j.neuron.2012.02.011.
(151) Jiang, X.; Chen, J.; Bajić, A.; Zhang, C.; Song, X.; Carroll, S. L.; Cai, Z.-L.; Tang, M.; Xue, M.; Cheng, N.; Schaaf, C. P.; Li, F.; MacKenzie, K. R.; Ferreon, A. C. M.; Xia, F.; Wang, M. C.; Maletić-Savatić, M.; Wang, J. Quantitative Real-Time Imaging of Glutathione. *Nat. Commun.* **2017**, *8* (1), 16087. https://doi.org/10.1038/ncomms16087.
(152) Chen, J.; Jiang, X.; Zhang, C.; MacKenzie, K. R.; Stossi, F.; Palzkill, T.; Wang, M. C.; Wang, J. Reversible Reaction-Based Fluorescent Probe for Real-Time Imaging of Glutathione Dynamics in Mitochondria. *ACS Sens.* **2017**, *2* (9), 1257–1261. https://doi.org/10.1021/acssensors.7b00425.
(153) Jiang, X.; Zhang, C.; Chen, J.; Choi, S.; Zhou, Y.; Zhao, M.; Song, X.; Chen, X.; Maletić-Savatić, M.; Palzkill, T.; Moore, D.; Wang, M. C.; Wang, J. Quantitative Real-Time Imaging of Glutathione with Subcellular Resolution. *Antioxid. Redox Signal.* **2019**, *30* (16), 1900–1910. https://doi.org/10.1089/ars.2018.7605.
(154) Zhang, Y.; Guan, L.; Yu, H.; Yan, Y.; Du, L.; Liu, Y.; Sun, M.; Huang, D.; Wang, S. Reversible Fluorescent Probe for Selective Detection and Cell Imaging of Oxidative Stress Indicator Bisulfite. *Anal. Chem.* **2016**, *88* (8), 4426–4431. https://doi.org/10.1021/acs.analchem.6b00061.
(155) Zhang, W.; Liu, T.; Huo, F.; Ning, P.; Meng, X.; Yin, C. Reversible Ratiometric Fluorescent Probe for Sensing Bisulfate/ H_2O_2 and Its Application in Zebrafish. *Anal. Chem.* **2017**, *89* (15), 8079–8083. https://doi.org/10.1021/acs.analchem.7b01580.
(156) Zhang, W.; Huo, F.; Zhang, Y.; Chao, J.; Yin, C. Mitochondria-Targeted NIR Fluorescent Probe for Reversible Imaging H_2O_2 /SO_2 Redox Dynamics in Vivo. *Sens. Actuators B Chem.* **2019**, *297* (15), 126747. https://doi.org/10.1016/j.snb.2019.126747.
(157) Kim, Y. L.; Plank, J. T.; Li, B.; Lippert, A. R. Kinetics-Based Quantification of Peroxynitrite Using the Oxidative Decarbonylation of Isatin. *Anal. Chem.* **2022**, *94* (51), 17803–17809. https://doi.org/10.1021/acs.analchem.2c03474.
(158) Steiger, A. K.; Pardue, S.; Kevil, C. G.; Pluth, M. D. Self-Immolative Thiocarbamates Provide Access to Triggered H_2S Donors and Analyte Replacement Fluorescent Probes. *J. Am. Chem. Soc.* **2016**, *138* (23), 7256–7259. https://doi.org/10.1021/jacs.6b03780.
(159) Popova, M.; Lazarus, L. S.; Benninghoff, A. D.; Berreau, L. M. CO Sense and Release Flavonols: Progress toward the Development of an Analyte Replacement PhotoCORM for Use in Living Cells. *ACS Omega* **2020**, *5* (17), 10021–10033. https://doi.org/10.1021/acsomega.0c00409.

(160) Lichtman, J. W.; Conchello, J.-A. Fluorescence Microscopy. *Nat. Methods* **2005**, *2* (12), 910–919. https://doi.org/10.1038/nmeth817.
(161) Wolf, D. E. Fundamentals of Fluorescence and Fluorescence Microscopy. In *Methods in Cell Biology*; Elsevier, 2013; Vol. 114, pp 69–97. https://doi.org/10.1016/B978-0-12-407761-4.00004-X.
(162) Jonkman, J.; Brown, C. M.; Wright, G. D.; Anderson, K. I.; North, A. J. Guidance for Quantitative Confocal Microscopy. *Nat. Protoc.* **2020**, s41596-020-0307–7. https://doi.org/10.1038/s41596-020-0307-7.
(163) Power, R. M.; Huisken, J. A Guide to Light-Sheet Fluorescence Microscopy for Multiscale Imaging. *Nat. Methods* **2017**, *14* (4), 360–373. https://doi.org/10.1038/nmeth.4224.
(164) Blom, H.; Widengren, J. Stimulated Emission Depletion Microscopy. *Chem. Rev.* **2017**, *117* (11), 7377–7427. https://doi.org/10.1021/acs.chemrev.6b00653.
(165) Samanta, K.; Joseph, J. An Overview of Structured Illumination Microscopy: Recent Advances and Perspectives. *J. Opt.* **2021**, *23* (12), 123002. https://doi.org/10.1088/2040-8986/ac3675.
(166) Sauer, M.; Heilemann, M. Single-Molecule Localization Microscopy in Eukaryotes. *Chem. Rev.* **2017**, *117* (11), 7478–7509. https://doi.org/10.1021/acs.chemrev.6b00667.
(167) Von Diezmann, L.; Shechtman, Y.; Moerner, W. E. Three-Dimensional Localization of Single Molecules for Super-Resolution Imaging and Single-Particle Tracking. *Chem. Rev.* **2017**, *117* (11), 7244–7275. https://doi.org/10.1021/acs.chemrev.6b00629.
(168) Stennett, E. M. S.; Ciuba, M. A.; Levitus, M. Photophysical Processes in Single Molecule Organic Fluorescent Probes. *Chem. Soc. Rev.* **2014**, *43* (4), 1057–1075. https://doi.org/10.1039/C3CS60211G.
(169) Li, H.; Vaughan, J. C. Switchable Fluorophores for Single-Molecule Localization Microscopy. *Chem. Rev.* **2018**, *118* (18), 9412–9454. https://doi.org/10.1021/acs.chemrev.7b00767.
(170) Helmchen, F.; Denk, W. Deep Tissue Two-Photon Microscopy. *Nat. Methods* **2005**, *2* (12), 932–940. https://doi.org/10.1038/nmeth818.
(171) Kim, H. M.; Cho, B. R. Small-Molecule Two-Photon Probes for Bioimaging Applications. *Chem. Rev.* **2015**, *115* (11), 5014–5055. https://doi.org/10.1021/cr5004425.
(172) Jin, D.; Piper, J. A. Time-Gated Luminescence Microscopy Allowing Direct Visual Inspection of Lanthanide-Stained Microorganisms in Background-Free Condition. *Anal. Chem.* **2011**, *83* (6), 2294–2300. https://doi.org/10.1021/ac103207r.
(173) Krohn, K. A.; Link, J. M.; Mason, R. P. Molecular Imaging of Hypoxia. *J. Nucl. Med.* **2008**, *49* (Suppl 2), 129S-148S. https://doi.org/10.2967/jnumed.107.045914.
(174) Gallagher, F. A. An Introduction to Functional and Molecular Imaging with MRI. *Clin. Radiol.* **2010**, *65* (7), 557–566. https://doi.org/10.1016/j.crad.2010.04.006.
(175) Gessner, R.; Dayton, P. A. Advances in Molecular Imaging with Ultrasound. *Mol. Imaging* **2010**, *9* (3), 7290.2010.00022. https://doi.org/10.2310/7290.2010.00022.
(176) Dobrucki, L. W.; Sinusas, A. J. PET and SPECT in Cardiovascular Molecular Imaging. *Nat. Rev. Cardiol.* **2010**, *7* (1), 38–47. https://doi.org/10.1038/nrcardio.2009.201.
(177) Weber, W. A.; Grosu, A. L.; Czernin, J. Technology Insight: Advances in Molecular Imaging and an Appraisal of PET/CT Scanning. *Nat. Clin. Pract. Oncol.* **2008**, *5* (3), 160–170. https://doi.org/10.1038/ncponc1041.
(178) Frangioni, J. In Vivo Near-Infrared Fluorescence Imaging. *Curr. Opin. Chem. Biol.* **2003**, *7* (5), 626–634. https://doi.org/10.1016/j.cbpa.2003.08.007.
(179) Hong, G.; Antaris, A. L.; Dai, H. Near-Infrared Fluorophores for Biomedical Imaging. *Nat. Biomed. Eng.* **2017**, *1* (1), 0010. https://doi.org/10.1038/s41551-016-0010.
(180) Alander, J. T.; Kaartinen, I.; Laakso, A.; Pätilä, T.; Spillmann, T.; Tuchin, V. V.; Venermo, M.; Välisuo, P. A Review of Indocyanine Green Fluorescent Imaging in Surgery. *Int. J. Biomed. Imaging* **2012**, *2012*, 1–26. https://doi.org/10.1155/2012/940585.

(181) Hong, G.; Antaris, A. L.; Dai, H. Near-Infrared Fluorophores for Biomedical Imaging. *Nat. Biomed. Eng.* **2017**, *1* (1), 0010. https://doi.org/10.1038/s41551-016-0010.
(182) Grimm, J. B.; Lavis, L. D. Caveat Fluorophore: An Insiders' Guide to Small-Molecule Fluorescent Labels. *Nat. Methods* **2022**, *19* (2), 149–158. https://doi.org/10.1038/s41592-021-01338-6.
(183) Schnermann, M. J.; Lavis, L. D. Rejuvenating Old Fluorophores with New Chemistry. *Curr. Opin. Chem. Biol.* **2023**, *75*, 102335. https://doi.org/10.1016/j.cbpa.2023.102335.
(184) Dai, M.; Yang, Y. J.; Sarkar, S.; Ahn, K. H. Strategies to Convert Organic Fluorophores into Red/near-Infrared Emitting Analogues and Their Utilization in Bioimaging Probes. *Chem. Soc. Rev.* **2023**, *52* (18), 6344–6358. https://doi.org/10.1039/D3CS00475A.
(185) Wong, K. C. Y.; Sletten, E. M. Extending Optical Chemical Tools and Technologies to Mice by Shifting to the Shortwave Infrared Region. *Curr. Opin. Chem. Biol.* **2022**, *68*, 102131. https://doi.org/10.1016/j.cbpa.2022.102131.
(186) Thimsen, E.; Sadtler, B.; Berezin, M. Y. Shortwave-Infrared (SWIR) Emitters for Biological Imaging: A Review of Challenges and Opportunities. *Nanophotonics* **2017**, *6* (5), 1043–1054. https://doi.org/10.1515/nanoph-2017-0039.
(187) Chen, Z.; Su, L.; Wu, Y.; Liu, J.; Wu, R.; Li, Q.; Wang, C.; Liu, L.; Song, J. Design and Synthesis of a Small Molecular NIR-II Chemiluminescence Probe for in Vivo - Activated H_2S Imaging. *Proc. Natl. Acad. Sci.* **2023**, *120* (8), e2205186120. https://doi.org/10.1073/pnas.2205186120.
(188) Yao, Z.; Zhang, B. S.; Prescher, J. A. Advances in Bioluminescence Imaging: New Probes from Old Recipes. *Curr. Opin. Chem. Biol.* **2018**, *45*, 148–156. https://doi.org/10.1016/j.cbpa.2018.05.009.
(189) Bronsart, L. L.; Stokes, C.; Contag, C. H. Chemiluminescence Imaging of Superoxide Anion Detects Beta-Cell Function and Mass. *PLOS ONE* **2016**, *11* (1), e0146601. https://doi.org/10.1371/journal.pone.0146601.
(190) Ntziachristos, V.; Razansky, D. Molecular Imaging by Means of Multispectral Optoacoustic Tomography (MSOT). *Chem. Rev.* **2010**, *110* (5), 2783–2794. https://doi.org/10.1021/cr9002566.
(191) Wang, L. V.; Yao, J. A Practical Guide to Photoacoustic Tomography in the Life Sciences. *Nat. Methods* **2016**, *13* (8), 627–638. https://doi.org/10.1038/nmeth.3925.
(192) Knox, H. J.; Chan, J. Acoustogenic Probes: A New Frontier in Photoacoustic Imaging. *Acc. Chem. Res.* **2018**, *51* (11), 2897–2905. https://doi.org/10.1021/acs.accounts.8b00351.
(193) Murphy, M. P. How Mitochondria Produce Reactive Oxygen Species. *Biochem. J.* **2009**, *417* (1), 1–13. https://doi.org/10.1042/BJ20081386.
(194) Whittaker, J. W. Oxygen Reactions of the Copper Oxidases. *Essays Biochem.* **1999**, *34*, 155–172. https://doi.org/10.1042/bse0340155.
(195) Romero, E.; Gómez Castellanos, J. R.; Gadda, G.; Fraaije, M. W.; Mattevi, A. Same Substrate, Many Reactions: Oxygen Activation in Flavoenzymes. *Chem. Rev.* **2018**, *118* (4), 1742–1769. https://doi.org/10.1021/acs.chemrev.7b00650.
(196) Semenza, G. L. Oxygen Sensing, Hypoxia-Inducible Factors, and Disease Pathophysiology. *Annu. Rev. Pathol. Mech. Dis.* **2014**, *9* (1), 47–71. https://doi.org/10.1146/annurev-pathol-012513-104720.
(197) Walsh, J. C.; Lebedev, A.; Aten, E.; Madsen, K.; Marciano, L.; Kolb, H. C. The Clinical Importance of Assessing Tumor Hypoxia: Relationship of Tumor Hypoxia to Prognosis and Therapeutic Opportunities. *Antioxid. Redox Signal.* **2014**, *21* (10), 1516–1554. https://doi.org/10.1089/ars.2013.5378.
(198) Winterbourn, C. C. Biological Chemistry of Superoxide Radicals. *ChemTexts* **2020**, *6* (1), 7. https://doi.org/10.1007/s40828-019-0101-8.

(199) Hayyan, M.; Hashim, M. A.; AlNashef, I. M. Superoxide Ion: Generation and Chemical Implications. *Chem. Rev.* **2016**, *116* (5), 3029–3085. https://doi.org/10.1021/acs.chemrev.5b00407.
(200) Bedard, K.; Krause, K.-H. The NOX Family of ROS-Generating NADPH Oxidases: Physiology and Pathophysiology. *Physiol. Rev.* **2007**, *87* (1), 245–313. https://doi.org/10.1152/physrev.00044.2005.
(201) Babior, B. M.; Kipnes, R. S.; Curnutte, J. T. Biological Defense Mechanisms. The Production by Leukocytes of Superoxide, A Potential Bactericidal Agent. *J. Clin. Invest.* **1973**, *52* (3), 741–744. https://doi.org/10.1172/JCI107236.
(202) Burdon, R. H. Superoxide and Hydrogen Peroxide in Relation to Mammalian Cell Proliferation. *Free Radic. Biol. Med.* **1995**, *18* (4), 775–794. https://doi.org/10.1016/0891-5849(94)00198-S.
(203) Winterbourn, C. C. Are Free Radicals Involved in Thiol-Based Redox Signaling? *Free Radic. Biol. Med.* **2015**, *80*, 164–170. https://doi.org/10.1016/j.freeradbiomed.2014.08.017.
(204) Boveris, A. [57] Determination of the Production of Superoxide Radicals and Hydrogen Peroxide in Mitochondria. In *Methods in Enzymology*; Elsevier, 1984; Vol. 105, pp 429–435. https://doi.org/10.1016/S0076-6879(84)05060-6.
(205) Daiber, A.; Oelze, M.; August, M.; Wendt, M.; Sydow, K.; Wieboldt, H.; Kleschyov, A. L.; Munzel, T. Detection of Superoxide and Peroxynitrite in Model Systems and Mitochondria by the Luminol Analogue L-012. *Free Radic. Res.* **2004**, *38* (3), 259–269. https://doi.org/10.1080/10715760410001659773.
(206) Johnson, F.; Giulivi, C. Superoxide Dismutases and Their Impact upon Human Health. *Mol. Aspects Med.* **2005**, *26* (4–5), 340–352. https://doi.org/10.1016/j.mam.2005.07.006.
(207) Flint, D. H.; Tuminello, J. F.; Emptage, M. H. The Inactivation of Fe-S Cluster Containing Hydro-Lyases by Superoxide. *J. Biol. Chem.* **1993**, *268* (30), 22369–22376. https://doi.org/10.1016/S0021-9258(18)41538-4.
(208) Gardner, P. R.; Fridovich, I. Superoxide Sensitivity of the Escherichia Coli Aconitase. *J. Biol. Chem.* **1991**, *266* (29), 19328–19333. https://doi.org/10.1016/S0021-9258(18)55001-8.
(209) Winterbourn, C. C.; Kettle, A. J. Radical–Radical Reactions of Superoxide: A Potential Route to Toxicity. *Biochem. Biophys. Res. Commun.* **2003**, *305* (3), 729–736. https://doi.org/10.1016/S0006-291X(03)00810-6.
(210) Toledo, J. C.; Augusto, O. Connecting the Chemical and Biological Properties of Nitric Oxide. *Chem. Res. Toxicol.* **2012**, *25* (5), 975–989. https://doi.org/10.1021/tx300042g.
(211) Ferrer-Sueta, G.; Radi, R. Chemical Biology of Peroxynitrite: Kinetics, Diffusion, and Radicals. *ACS Chem. Biol.* **2009**, *4* (3), 161–177. https://doi.org/10.1021/cb800279q.
(212) Ferrer-Sueta, G.; Radi, R. Chemical Biology of Peroxynitrite: Kinetics, Diffusion, and Radicals. *ACS Chem. Biol.* **2009**, *4* (3), 161–177. https://doi.org/10.1021/cb800279q.
(213) Cabelli, D. E.; Bielski, B. H. J. Kinetics and Mechanism for the Oxidation of Ascorbic Acid/Ascorbate by HO_2/O_2^- (Hydroperoxyl/Superoxide) Radicals. A Pulse Radiolysis and Stopped-Flow Photolysis Study. *J. Phys. Chem.* **1983**, *87* (10), 1809–1812. https://doi.org/10.1021/j100233a031.
(214) Winterbourn, C. C.; Metodiewa, D. The Reaction of Superoxide with Reduced Glutathione. *Arch. Biochem. Biophys.* **1994**, *314* (2), 284–290. https://doi.org/10.1006/abbi.1994.1444.
(215) Nauseef, W. M. Detection of Superoxide Anion and Hydrogen Peroxide Production by Cellular NADPH Oxidases. *Biochim. Biophys. Acta BBA - Gen. Subj.* **2014**, *1840* (2), 757–767. https://doi.org/10.1016/j.bbagen.2013.04.040.
(216) McCord, J. M.; Fridovich, I. The Reduction of Cytochrome *c* by Milk Xanthine Oxidase. *J. Biol. Chem.* **1968**, *243* (21), 5753–5760. https://doi.org/10.1016/S0021-9258(18)91929-0.

(217) Peskin, A. V.; Winterbourn, C. C. Assay of Superoxide Dismutase Activity in a Plate Assay Using WST-1. *Free Radic. Biol. Med.* **2017**, *103*, 188–191. https://doi.org/10.1016/j.freeradbiomed.2016.12.033.
(218) Jie, Z.; Liu, J.; Shu, M.; Ying, Y.; Yang, H. Detection Strategies for Superoxide Anion: A Review. *Talanta* **2022**, *236*, 122892. https://doi.org/10.1016/j.talanta.2021.122892.
(219) Gopalakrishnan, B.; Nash, K. M.; Velayutham, M.; Villamena, F. A. Detection of Nitric Oxide and Superoxide Radical Anion by Electron Paramagnetic Resonance Spectroscopy from Cells Using Spin Traps. *J. Vis. Exp.* **2012**, No. 66, 2810. https://doi.org/10.3791/2810.
(220) Dharmaraja, A. T.; Alvala, M.; Sriram, D.; Yogeeswari, P.; Chakrapani, H. Design, Synthesis and Evaluation of Small Molecule Reactive Oxygen Species Generators as Selective Mycobacterium Tuberculosis Inhibitors. *Chem. Commun.* **2012**, *48* (83), 10325. https://doi.org/10.1039/c2cc35343a.
(221) Nishinaka, Y.; Aramaki, Y.; Yoshida, H.; Masuya, H.; Sugawara, T.; Ichimori, Y. A New Sensitive Chemiluminescence Probe, L-012, for Measuring the Production of Superoxide Anion by Cells. *Biochem. Biophys. Res. Commun.* **1993**, *193* (2), 554–559. https://doi.org/10.1006/bbrc.1993.1659.
(222) Allen, R. C. [36] Phagocytic Leukocyte Oxygenation Activities and Chemiluminescence: A Kinetic Approach to Analysis. In *Methods in Enzymology*; Elsevier, 1986; Vol. 133, pp 449–493. https://doi.org/10.1016/0076-6879(86)33085-4.
(223) Rembish, S. J.; Trush, M. A. Further Evidence That Lucigenin-Derived Chemiluminescence Monitors Mitochondrial Superoxide Generation in Rat Alveolar Macrophages. *Free Radic. Biol. Med.* **1994**, *17* (2), 117–126. https://doi.org/10.1016/0891-5849(94)90109-0.
(224) Sasaki, S.; Yamada, S.; Iwamura, M.; Kobayashi, Y. Specific Detection of Intramitochondrial Superoxide Produced by Either Cell Activation or Apoptosis by Employing a Newly Developed Cell-Permeative Lucigenin Derivative, 10,10'-Dimethyl-9,9'-Biacridinium Bis(Monomethyl Terephthalate). *Free Radic. Biol. Med.* **2013**, *65*, 1005–1011. https://doi.org/10.1016/j.freeradbiomed.2013.08.175.
(225) Kotani, H.; Ohkubo, K.; Crossley, M. J.; Fukuzumi, S. An Efficient Fluorescence Sensor for Superoxide with an Acridinium Ion-Linked Porphyrin Triad. *J. Am. Chem. Soc.* **2011**, *133* (29), 11092–11095. https://doi.org/10.1021/ja204161j.
(226) Spasojevic, I.; Liochev, S. I.; Fridovich, I. Lucigenin: Redox Potential in Aqueous Media and Redox Cycling with O2 β Production. *Free Radic. Biol. Med.* **1999**, *27*, S15. https://doi.org/10.1016/S0891-5849(99)90543-9.
(227) Li, Y.; Zhu, H.; Kuppusamy, P.; Roubaud, V.; Zweier, J. L.; Trush, M. A. Validation of Lucigenin (Bis-N-Methylacridinium) as a Chemilumigenic Probe for Detecting Superoxide Anion Radical Production by Enzymatic and Cellular Systems. *J. Biol. Chem.* **1998**, *273* (4), 2015–2023. https://doi.org/10.1074/jbc.273.4.2015.
(228) Minakami, H.; Arai, H.; Nakano, M.; Sugioka, K.; Suzuki, S.; Sotomatsu, A. A New and Suitable Reconstructed System for NADPH-Dependent Microsomal Lipid Peroxidation. *Biochem. Biophys. Res. Commun.* **1988**, *153* (3), 973–978. https://doi.org/10.1016/S0006-291X(88)81323-8.
(229) Takahashi, A.; Totsune-Nakano, H.; Nakano, M.; Mashiko, S.; Suzuki, N.; Ohma, C.; Inaba, H. Generation of O_2^- and Tyrosine Cation-Mediated Chemiluminescence during the Fertilization of Sea Urchin Eggs. *FEBS Lett.* **1989**, *246* (1–2), 117–119. https://doi.org/10.1016/0014-5793(89)80265-0.
(230) Toya, Y.; Kayano, T.; Sato, K.; Goto, T. Synthesis and Chemiluminescence Properties of 6-(4-Methoxyphenyl)-2-Methylimidazo[1,2- *a*]Pyrazin-3(7 *H*)-One and 2-Methyl-6-(2-Naphthyl)Imidazo[1,2- *a*]Pyrazin-3(7 *H*)-One. *Bull. Chem. Soc. Jpn.* **1992**, *65* (9), 2475–2479. https://doi.org/10.1246/bcsj.65.2475.

(231) Lucas, M.; Solano, F. Coelenterazine Is a Superoxide Anion-Sensitive Chemiluminescent Probe: Its Usefulness in the Assay of Respiratory Burst in Neutrophils. *Anal. Biochem.* **1992**, *206* (2), 273–277. https://doi.org/10.1016/0003-2697(92)90366-F.
(232) Teranishi, K.; Shimomura, O. Coelenterazine Analogs as Chemiluminescent Probe for Superoxide Anion. *Anal. Biochem.* **1997**, *249* (1), 37–43. https://doi.org/10.1006/abio.1997.2150.
(233) Pinto Da Silva, L.; Núnez-Montenegro, A.; Magalhães, C. M.; Ferreira, P. J. O.; Duarte, D.; González-Berdullas, P.; Rodríguez-Borges, J. E.; Vale, N.; Esteves Da Silva, J. C. G. Single-Molecule Chemiluminescent Photosensitizer for a Self-Activating and Tumor-Selective Photodynamic Therapy of Cancer. *Eur. J. Med. Chem.* **2019**, *183*, 111683. https://doi.org/10.1016/j.ejmech.2019.111683.
(234) Silva, J. P.; González-Berdullas, P.; Esteves Da Silva, J. C. G.; Pinto Da Silva, L. Development of a Coelenterazine Derivative with Enhanced Superoxide Anion-Triggered Chemiluminescence in Aqueous Solution. *Chemosensors* **2022**, *10* (5), 174. https://doi.org/10.3390/chemosensors10050174.
(235) Sousa, J.; Magalhães, C. M.; González-Berdullas, P.; Esteves Da Silva, J. C. G.; Pinto Da Silva, L. Comparative Investigation of the Chemiluminescent Properties of a Dibrominated Coelenterazine Analog. *Int. J. Mol. Sci.* **2022**, *23* (15), 8490. https://doi.org/10.3390/ijms23158490.
(236) Pedro Silva, J.; González-Berdullas, P.; Pereira, M.; Duarte, D.; Rodríguez-Borges, J. E.; Vale, N.; Esteves Da Silva, J. C. G.; Pinto Da Silva, L. Evaluation of the Anticancer Activity and Chemiluminescence of a Halogenated Coelenterazine Analog. *J. Photochem. Photobiol. Chem.* **2023**, *434*, 114228. https://doi.org/10.1016/j.jphotochem.2022.114228.
(237) Suzuki, N.; Suetsuna, K.; Mashiko, S.; Yoda, B.; Nomoto, T.; Toya, Y.; Inaba, H.; Goto, T. Reaction Rates for the Chemiluminescence of *Cypridina* Luciferin Analogues with Superoxide: A Quenching Experiment with Superoxide Dismutase. *Agric. Biol. Chem.* **1991**, *55* (1), 157–160. https://doi.org/10.1080/00021369.1991.10870523.
(238) Teranishi, K.; Nishiguchi, T. Cyclodextrin-Bound 6-(4-Methoxyphenyl)Imidazo[1,2-α]Pyrazin-3(7H)-Ones with Fluorescein as Green Chemiluminescent Probes for Superoxide Anions. *Anal. Biochem.* **2004**, *325* (2), 185–195. https://doi.org/10.1016/j.ab.2003.10.042.
(239) Teranishi, K. Development of Imidazopyrazinone Red-Chemiluminescent Probes for Detecting Superoxide Anions via a Chemiluminescence Resonance Energy Transfer Method. *Luminescence* **2007**, *22* (2), 147–156. https://doi.org/10.1002/bio.939.
(240) Saito, R.; Ohno, A.; Ito, E. Synthesis of Boradiazaindacene-Imidazopyrazinone Conjugate as Lipophilic and Yellow-Chemiluminescent Chemosensor for Superoxide Radical Anion. *Tetrahedron* **2010**, *66* (3), 583–590. https://doi.org/10.1016/j.tet.2009.11.086.
(241) Teranishi, K. Non-Invasive and Accurate Readout of Superoxide Anion in Biological Systems by near-Infrared Light. *Anal. Chim. Acta* **2021**, *1179*, 338827. https://doi.org/10.1016/j.aca.2021.338827.
(242) Teranishi, K. Near-Infrared Chemiluminescence Imaging of Superoxide Anion Production in Kidneys with $Iron^{3+}$-Nitrilotriacetate-Induced Acute Renal Oxidative Stress in Rats. *J. Photochem. Photobiol. B* **2022**, *228*, 112391. https://doi.org/10.1016/j.jphotobiol.2022.112391.
(243) Bindokas, V.; Jordan, J.; Lee, C.; Miller, R. Superoxide Production in Rat Hippocampal Neurons: Selective Imaging with Hydroethidine. *J. Neurosci.* **1996**, *16* (4), 1324–1336. https://doi.org/10.1523/JNEUROSCI.16-04-01324.1996.
(244) Robinson, K. M.; Janes, M. S.; Pehar, M.; Monette, J. S.; Ross, M. F.; Hagen, T. M.; Murphy, M. P.; Beckman, J. S. Selective Fluorescent Imaging of Superoxide *in Vivo* Using Ethidium-Based Probes. *Proc. Natl. Acad. Sci.* **2006**, *103* (41), 15038–15043. https://doi.org/10.1073/pnas.0601945103.

(245) Zhao, H.; Kalivendi, S.; Zhang, H.; Joseph, J.; Nithipatikom, K.; Vásquez-Vivar, J.; Kalyanaraman, B. Superoxide Reacts with Hydroethidine but Forms a Fluorescent Product That Is Distinctly Different from Ethidium: Potential Implications in Intracellular Fluorescence Detection of Superoxide. *Free Radic. Biol. Med.* **2003**, *34* (11), 1359–1368. https://doi.org/10.1016/S0891-5849(03)00142-4.
(246) Zhao, H.; Joseph, J.; Fales, H. M.; Sokoloski, E. A.; Levine, R. L.; Vasquez-Vivar, J.; Kalyanaraman, B. Detection and Characterization of the Product of Hydroethidine and Intracellular Superoxide by HPLC and Limitations of Fluorescence. *Proc. Natl. Acad. Sci.* **2005**, *102* (16), 5727–5732. https://doi.org/10.1073/pnas.0501719102.
(247) Zielonka, J.; Hardy, M.; Kalyanaraman, B. HPLC Study of Oxidation Products of Hydroethidine in Chemical and Biological Systems: Ramifications in Superoxide Measurements. *Free Radic. Biol. Med.* **2009**, *46* (3), 329–338. https://doi.org/10.1016/j.freeradbiomed.2008.10.031.
(248) Zielonka, J.; Kalyanaraman, B. Hydroethidine- and MitoSOX-Derived Red Fluorescence Is Not a Reliable Indicator of Intracellular Superoxide Formation: Another Inconvenient Truth. *Free Radic. Biol. Med.* **2010**, *48* (8), 983–1001. https://doi.org/10.1016/j.freeradbiomed.2010.01.028.
(249) Michalski, R.; Zielonka, J.; Hardy, M.; Joseph, J.; Kalyanaraman, B. Hydropropidine: A Novel, Cell-Impermeant Fluorogenic Probe for Detecting Extracellular Superoxide. *Free Radic. Biol. Med.* **2013**, *54*, 135–147. https://doi.org/10.1016/j.freeradbiomed.2012.09.018.
(250) Chu, W.; Chepetan, A.; Zhou, D.; Shoghi, K. I.; Xu, J.; Dugan, L. L.; Gropler, R. J.; Mintun, M. A.; Mach, R. H. Development of a PET Radiotracer for Non-Invasive Imaging of the Reactive Oxygen Species, Superoxide, in Vivo. *Org. Biomol. Chem.* **2014**, *12* (25), 4421–4431. https://doi.org/10.1039/C3OB42379D.
(251) Shchepinova, M. M.; Cairns, A. G.; Prime, T. A.; Logan, A.; James, A. M.; Hall, A. R.; Vidoni, S.; Arndt, S.; Caldwell, S. T.; Prag, H. A.; Pell, V. R.; Krieg, T.; Mulvey, J. F.; Yadav, P.; Cobley, J. N.; Bright, T. P.; Senn, H. M.; Anderson, R. F.; Murphy, M. P.; Hartley, R. C. MitoNeoD: A Mitochondria-Targeted Superoxide Probe. *Cell Chem. Biol.* **2017**, *24* (10), 1285-1298.e12. https://doi.org/10.1016/j.chembiol.2017.08.003.
(252) Kundu, K.; Knight, S. F.; Willett, N.; Lee, S.; Taylor, W. R.; Murthy, N. Hydrocyanines: A Class of Fluorescent Sensors That Can Image Reactive Oxygen Species in Cell Culture, Tissue, and In Vivo. *Angew. Chem. Int. Ed.* **2009**, *48* (2), 299–303. https://doi.org/10.1002/anie.200804851.
(253) Prunty, M. C.; Aung, M. H.; Hanif, A. M.; Allen, R. S.; Chrenek, M. A.; Boatright, J. H.; Thule, P. M.; Kundu, K.; Murthy, N.; Pardue, M. T. In Vivo Imaging of Retinal Oxidative Stress Using a Reactive Oxygen Species–Activated Fluorescent Probe. *Investig. Opthalmology Vis. Sci.* **2015**, *56* (10), 5862. https://doi.org/10.1167/iovs.15-16810.
(254) Yu, F.; Gao, M.; Li, M.; Chen, L. A Dual Response Near-Infrared Fluorescent Probe for Hydrogen Polysulfides and Superoxide Anion Detection in Cells and in Vivo. *Biomaterials* **2015**, *63*, 93–101. https://doi.org/10.1016/j.biomaterials.2015.06.007.
(255) Huang, Y.; Yu, F.; Wang, J.; Chen, L. Near-Infrared Fluorescence Probe for in Situ Detection of Superoxide Anion and Hydrogen Polysulfides in Mitochondrial Oxidative Stress. *Anal. Chem.* **2016**, *88*, (7) 4122–4129. https://doi.org/10.1021/acs.analchem.6b00458.
(256) Gao, M.; Zhang, X.; Wang, Y.; Liu, Q.; Yu, F.; Huang, Y.; Ding, C.; Chen, L. Sequential Detection of Superoxide Anion and Hydrogen Polysulfides under Hypoxic Stress via a Spectral-Response-Separated Fluorescent Probe Functioned with a Nitrobenzene Derivative. *Anal. Chem.* **2019**, *91* (12), 7774–7781. https://doi.org/10.1021/acs.analchem.9b01189.
(257) Wang, Y.; Gao, M.; Chen, Q.; Yu, F.; Jiang, G.; Chen, L. Associated Detection of Superoxide Anion and Mercury(II) under Chronic Mercury Exposure in Cells and Mice Models via a

Three-Channel Fluorescent Probe. *Anal. Chem.* **2018**, *90* (16), 9769–9778. https://doi.org/10.1021/acs.analchem.8b01442.
(258) Wang, Z.; Do Cong, T.; Zhong, W.; Lau, J. W.; Kwek, G.; Chan-Park, M. B.; Xing, B. Cyanine-Dyad Molecular Probe for the Simultaneous Profiling of the Evolution of Multiple Radical Species During Bacterial Infections. *Angew. Chem. Int. Ed.* **2021**, *60* (31), 16900–16905. https://doi.org/10.1002/anie.202104100.
(259) Wang, Y.; Han, J.; Xu, Y.; Gao, Y.; Wen, H.; Cui, H. Taking Advantage of the Aromatization of 7-Diethylamino-4-Methyl-3,4-Dihydrocoumarin in the Fluorescence Sensing of Superoxide Anion. *Chem. Commun.* **2020**, *56* (68), 9827–9829. https://doi.org/10.1039/d0cc02282a.
(260) Wang, Y.; Jia, S.; Yu, Z.; Wen, H.; Cui, H. Insights Into the Detection Selectivity of Redox and Non-Redox Based Probes for the Superoxide Anion Using Coumarin and Chromone as the Fluorophores. *Front. Chem.* **2021**, *9*, 753621. https://doi.org/10.3389/fchem.2021.753621.
(261) Tang, B.; Zhang, L.; Zhang, L. Study and Application of Flow Injection Spectrofluorimetry with a Fluorescent Probe of 2-(2-Pyridyl)-Benzothiazoline for Superoxide Anion Radicals. *Anal. Biochem.* **2004**, *326* (2), 176–182. https://doi.org/10.1016/j.ab.2003.11.023.
(262) Gao, J. J.; Xu, K. H.; Tang, B.; Yin, L. L.; Yang, G. W.; An, L. G. Selective Detection of Superoxide Anion Radicals Generated from Macrophages by Using a Novel Fluorescent Probe. *FEBS J.* **2007**, *274* (7), 1725–1733. https://doi.org/10.1111/j.1742-4658.2007.05720.x.
(263) Li, P.; Zhang, W.; Li, K.; Liu, X.; Xiao, H.; Zhang, W.; Tang, B. Mitochondria-Targeted Reaction-Based Two-Photon Fluorescent Probe for Imaging of Superoxide Anion in Live Cells and in Vivo. *Anal. Chem.* **2013**, *85* (20), 9877–9881. https://doi.org/10.1021/ac402409m.
(264) Xiao, H.; Liu, X.; Wu, C.; Wu, Y.; Li, P.; Guo, X.; Tang, B. A New Endoplasmic Reticulum-Targeted Two-Photon Fluorescent Probe for Imaging of Superoxide Anion in Diabetic Mice. *Biosens. Bioelectron.* **2017**, *91*, 449–455. https://doi.org/10.1016/j.bios.2016.12.068.
(265) Xuan, Y.; Qu, J. A Fast-Responsive Two-Photon Fluorescent Probe for in Vivo Imaging Superoxide Radical Anion with a Large Stokes Shift. *RSC Adv.* **2018**, *8* (8), 4125–4129. https://doi.org/10.1039/c7ra11695k.
(266) Zhang, W.; Li, P.; Yang, F.; Hu, X.; Sun, C.; Zhang, W.; Chen, D.; Tang, B. Dynamic and Reversible Fluorescence Imaging of Superoxide Anion Fluctuations in Live Cells and in Vivo. *J. Am. Chem. Soc.* **2013**, *135* (40), 14956–14959. https://doi.org/10.1021/ja408524j.
(267) Sun, C.; Du, W.; Zhang, W.; Wu, Y.; Yao, Z.; Wang, B.; Wu, T.; Yang, H.; Wang, Y.; Ren, L. A Novel Near-Infrared Probe for the Imaging of Superoxide Anion Fluctuations and Hydrogen Ion Enhancement in Vivo. *Anal. Methods* **2018**, *10* (30), 3727–3736. https://doi.org/10.1039/c8ay01190g.
(268) Zhang, W.; Su, D.; Li, P.; Zhang, J.; Liu, J.; Wang, H.; Zhang, W.; Tang, B. Two-Photon Fluorescence Imaging of Mitochondrial Superoxide Anion Transport Mediating Liver Ischemia-Reperfusion Injury in Mice. *Chem. Commun.* **2019**, *55* (72), 10740–10743. https://doi.org/10.1039/c9cc04585f.
(269) Liu, H.-W.; Zhu, X.; Zhang, J.; Zhang, X.-B.; Tan, W. A Red Emitting Two-Photon Fluorescent Probe for Dynamic Imaging of Redox Balance Meditated by a Superoxide Anion and GSH in Living Cells and Tissues. *The Analyst* **2016**, *141* (20), 5893–5899. https://doi.org/10.1039/C6AN01178K.
(270) Zhang, W.; Wang, X.; Li, P.; Xiao, H.; Zhang, W.; Wang, H.; Tang, B. Illuminating Superoxide Anion and pH Enhancements in Apoptosis of Breast Cancer Cells Induced by Mitochondrial Hyperfusion Using a New Two-Photon Fluorescence Probe. *Anal. Chem.* **2017**, *89* (12), 6840–6845. https://doi.org/10.1021/acs.analchem.7b01290.

(271) Zhang, W.; Liu, J.; Li, P.; Wang, X.; Bi, S.; Zhang, J.; Zhang, W.; Wang, H.; Tang, B. In Situ and Real-Time Imaging of Superoxide Anion and Peroxynitrite Elucidating Arginase 1 Nitration Aggravating Hepatic Ischemia-Reperfusion Injury. *Biomaterials* **2019**, *225*, 119499. https://doi.org/10.1016/j.biomaterials.2019.119499.
(272) Zhang, W.; Zhang, J.; Li, P.; Liu, J.; Su, D.; Tang, B. Two-Photon Fluorescence Imaging Reveals a Golgi Apparatus Superoxide Anion-Mediated Hepatic Ischaemia-Reperfusion Signalling Pathway. *Chem. Sci.* **2019**, *10* (3), 879–883. https://doi.org/10.1039/c8sc03917h.
(273) Lin, W.; Huang, J.; Guo, S.; Zhao, M.; Chen, X.; Shang, Q.; Zhang, R.; Liao, G.; Zheng, J.; Liao, Y. A Tunable Fluorescent Probe for Superoxide Anion Detection during Inflammation Caused by *Treponema Pallidum*. *J. Mater. Chem. B* **2023**, *11* (20), 4523–4528. https://doi.org/10.1039/D3TB00747B.
(274) Xiao, H.; Wu, C.; Li, P.; Tang, B. Simultaneous Fluorescence Visualization of Endoplasmic Reticulum Superoxide Anion and Polarity in Myocardial Cells and Tissue. *Anal. Chem.* **2018**, *90* (10), 6081–6088. https://doi.org/10.1021/acs.analchem.7b05440.
(275) Singh, A. P.; Murale, D. P.; Ha, Y.; Liew, H.; Lee, K. M.; Segev, A.; Suh, Y.-H.; Churchill, D. G. A Novel, Selective, and Extremely Responsive Thienyl-Based Dual Fluorogenic Probe for Tandem Superoxide and Hg^{2+} Chemosensing. *Dalton Trans* **2013**, *42* (10), 3285–3290. https://doi.org/10.1039/C2DT32135A.
(276) Manjare, S. T.; Kim, S.; Heo, W. D.; Churchill, D. G. Selective and Sensitive Superoxide Detection with a New *Diselenide* -Based Molecular Probe in Living Breast Cancer Cells. *Org. Lett.* **2014**, *16* (2), 410–412. https://doi.org/10.1021/ol4033013.
(277) Deshmukh, P. P.; Navalkar, A.; Maji, S. K.; Manjare, S. T. Phenylselenyl Containing Turn-on Dibodipy Probe for Selective Detection of Superoxide in Mammalian Breast Cancer Cell Line. *Sens. Actuators B Chem.* **2019**, *281* (15), 8–13. https://doi.org/10.1016/j.snb.2018.10.072.
(278) Madibone, K. S.; Deshmukh, P. P.; Navalkar, A.; Maji, S. K.; Badani, P. M.; Manjare, S. T. Cyclic Organoselenide BODIPY-Based Probe: Targeting Superoxide in MCF-7 Cancer Cells. *ACS Omega* **2020**, *5* (23), 14186–14193. https://doi.org/10.1021/acsomega.0c02074.
(279) Salunke, S. T.; Shelar, D. S.; Manjare, S. T. Synthesis and Photophysical Study of Tetraphenyl Substituted BODIPY Based Phenyl-Monoselenide Probe for Selective Detection of Superoxide. *J. Fluoresc.* **2023**, *33* (2), 437–444. https://doi.org/10.1007/s10895-022-03096-w.
(280) Malankar, G. S.; Shelar, D. S.; Butcher, R. J.; Manjare, S. T. Synthesis and Single Crystal X-Ray Study of Phenylselenyl Embedded Coumarin-Based Sensors for Selective Detection of Superoxide. *Dalton Trans.* **2022**, *51* (27), 10518–10526. https://doi.org/10.1039/d2dt01079h.
(281) Ohyashiki, T.; Nunomura, M.; Katoh, T. Detection of Superoxide Anion Radical in Phospholipid Liposomal Membrane by Fluorescence Quenching Method Using 1,3-Diphenylisobenzofuran. *Biochim. Biophys. Acta BBA - Biomembr.* **1999**, *1421* (1), 131–139. https://doi.org/10.1016/S0005-2736(99)00119-4.
(282) Ma, S.; Mu, W.; Gao, J.; Zhou, J. Spectroscopic Study of 2-(2-Pyridyliminomethyl)Phenol as a Novel Fluorescent Probe for Superoxide Anion Radicals and Superoxide Dismutase Activity. *J. Fluoresc.* **2009**, *19* (3), 487–493. https://doi.org/10.1007/s10895-008-0437-8.
(283) Vinatier, V.; Guieu, V.; Madaule, Y.; Maturano, M.; Payrastre, C.; Hoffmann, P. Superoxide-Induced Bleaching of Streptocyanine Dyes: Application to Assay the Enzymatic Activity of Superoxide Dismutases. *Anal. Biochem.* **2010**, *405* (2), 255–259. https://doi.org/10.1016/j.ab.2010.06.006.
(284) Liu, H.; Zhang, L.; Chen, J.; Zhai, Y.; Zeng, Y.; Li, L. A Novel Functional Imidazole Fluorescent Ionic Liquid: Simple and Efficient Fluorescent Probes for Superoxide Anion

Radicals. *Anal. Bioanal. Chem.* **2013**, *405* (29), 9563–9570. https://doi.org/10.1007/s00216-013-7357-4.
(285) Ma, H.; Yang, M.; Zhang, S.; Yin, P.; Wang, T.; Yang, Y.; Lei, Z.; Ma, Y.; Qin, Y.; Yang, Z. Two Aggregation-Induced Emission (AIE)-Active Reaction-Type Probes: For Real-Time Detecting and Imaging of Superoxide Anions. *Analyst* **2019**, *144* (2), 536–542. https://doi.org/10.1039/c8an01811a.
(286) Ye, Y.-X.; Pan, J.-C.; Chen, X.-Y.; Jiang, L.; Jiao, Q.-C.; Zhu, H.-L.; Liu, J.-Z.; Wang, Z.-C. A New Mitochondria-Targeted Fluorescent Probe for Exogenous and Endogenous Superoxide Anion Imaging in Living Cells and Pneumonia Tissue. *Analyst* **2022**, *147* (15), 3534–3541. https://doi.org/10.1039/d2an00690a.
(287) Olojo, R. O.; Xia, R. H.; Abramson, J. J. Spectrophotometric and Fluorometric Assay of Superoxide Ion Using 4-Chloro-7-Nitrobenzo-2-Oxa-1,3-Diazole. *Anal. Biochem.* **2005**, *339* (2), 338–344. https://doi.org/10.1016/j.ab.2005.01.032.
(288) Maeda, H.; Yamamoto, K.; Kohno, I.; Hafsi, L.; Itoh, N.; Nakagawa, S.; Kanagawa, N.; Suzuki, K.; Uno, T. Design of a Practical Fluorescent Probe for Superoxide Based on Protection-Deprotection Chemistry of Fluoresceins with Benzenesulfonyl Protecting Groups. *Chem. - Eur. J.* **2007**, *13* (7), 1946–1954. https://doi.org/10.1002/chem.200600522.
(289) Hu, J. J.; Wong, N.-K.; Ye, S.; Chen, X.; Lu, M.-Y.; Zhao, A. Q.; Guo, Y.; Ma, A. C.-H.; Leung, A. Y.-H.; Shen, J.; Yang, D. Fluorescent Probe HKSOX-1 for Imaging and Detection of Endogenous Superoxide in Live Cells and In Vivo. *J. Am. Chem. Soc.* **2015**, *137* (21), 6837–6843. https://doi.org/10.1021/jacs.5b01881.
(290) Lu, D.; Zhou, L.; Wang, R.; Zhang, X.-B.; He, L.; Zhang, J.; Hu, X.; Tan, W. A Two-Photon Fluorescent Probe for Endogenous Superoxide Anion Radical Detection and Imaging in Living Cells and Tissues. *Sens. Actuators B Chem.* **2017**, *250*, 259–266. https://doi.org/10.1016/j.snb.2017.04.041.
(291) Lv, Y.; Dan Cheng; Dongdong Su; Chen, M.; Yin, B.-C.; Yuan, L.; Zhang, X.-B. Visualization of Oxidative Injury in the Mouse Kidney Using Selective Superoxide Anion Fluorescent Probes. *Chem. Sci.* **2018**, *9* (39), 7606–7613. https://doi.org/10.1039/c8sc03308k.
(292) Yao, S.; Ma, C.; Lu, Y.; Wei, X.; Feng, X.; Miao, P.; Yang, G.; Zhang, J.; Yan, M.; Yu, J. A FRET-Based Ratiometric Two-Photon Fluorescent Probe for Superoxide Anion Detection and Imaging in Living Cells and Tissues. *Analyst* **2019**, *144* (5), 1704–1710. https://doi.org/10.1039/c8an02196a.
(293) Wang, Y.; Wang, X.; Zhang, L.; Huang, Y.; Bi, L.; Lv, C.; Chen, L. A Ratiometric Fluorescent Probe for Detecting the Endogenous Biological Signaling Molecule Superoxide Anion and Bioimaging during Tumor Treatment. *J. Mater. Chem. B* **2020**, *8* (5), 1017–1025. https://doi.org/10.1039/c9tb02453k.
(294) Zuo, Q.; Wu, Q.; Lv, Y.; Gong, X.; Cheng, D. Imaging of Endoplasmic Reticulum Superoxide Anion Fluctuation in a Liver Injury Model by a Selective Two-Photon Fluorescent Probe. *New J. Chem.* **2020**, *44* (14), 5457–5462. https://doi.org/10.1039/d0nj00487a.
(295) Ma, S.; Ma, Y.; Liu, Q.; Lin, W. A Two-Photon Fluorescent Probe with Lysosome Targetability for Imaging Endogenous Superoxide Anion in Living Cells, Zebrafish and Pneumonia Tissue. *Sens. Actuators B Chem.* **2021**, *332*, 129523. https://doi.org/10.1016/j.snb.2021.129523.
(296) Lu, Y.; Wang, R.; Sun, Y.; Tian, M.; Dong, B. Endoplasmic Reticulum-Specific Fluorescent Probe for the Two-Photon Imaging of Endogenous Superoxide Anion ($O2^{\bullet-}$) in Live Cells and Zebrafishes. *Talanta* **2021**, *225*, 122020. https://doi.org/10.1016/j.talanta.2020.122020.
(297) Zhang, C.; Qiu, Z.; Zhang, L.; Wang, S.; Zhao, S.; Pang, Q.; Liang, H. Mitochondria-Targeted Fluorescence/Photoacoustic Dual-Modality Imaging Probe Tailored for Visual

Precise Diagnosis of Drug-Induced Liver Injury. *Anal. Chem.* **2022**, *94* (16), 6251–6260. https://doi.org/10.1021/acs.analchem.2c00041.
(298) Wu, L.; Liu, L.; Han, H.-H.; Tian, X.; Odyniec, M. L.; Feng, L.; Sedgwick, A. C.; He, X.-P.; Bull, S. D.; James, T. D. ESIPT-Based Fluorescence Probe for the Ratiometric Detection of Superoxide. *New J. Chem.* **2019**, *43* (7), 2875–2877. https://doi.org/10.1039/C8NJ05656K.
(299) Jiao, S.; Zhai, J.; Yang, S.; Meng, X. A Highly Responsive, Sensitive NIR Fluorescent Probe for Imaging of Superoxide Anion in Mitochondria of Oral Cancer Cells. *Talanta* **2021**, *222*, 121566. https://doi.org/10.1016/j.talanta.2020.121566.
(300) Ji, K.; Shan, J.; Wang, X.; Tan, X.; Hou, J.; Liu, Y.; Song, Y. Rational Design of Near-Infrared Fluorescent Probes for Superoxide Anion Radical: Enhancement of Self-Stability and Sensitivity by Self-Immolative Linker. *Free Radic. Biol. Med.* **2021**, *167*, 36–44. https://doi.org/10.1016/j.freeradbiomed.2021.02.029.
(301) Wu, L.; Liu, J.; Tian, X.; Groleau, R. R.; Bull, S. D.; Li, P.; Tang, B.; James, T. D. Fluorescent Probe for the Imaging of Superoxide and Peroxynitrite during Drug-Induced Liver Injury. *Chem. Sci.* **2021**, *12* (11), 3921–3928. https://doi.org/10.1039/d0sc05937d.
(302) Yang, W.; Liu, R.; Yin, X.; Wu, K.; Yan, Z.; Wang, X.; Fan, G.; Tang, Z.; Li, Y.; Jiang, H. Novel Near-Infrared Fluorescence Probe for Bioimaging and Evaluating Superoxide Anion Fluctuations in Ferroptosis-Mediated Epilepsy. *Anal. Chem.* **2023**, *95* (33), 12240–12246. https://doi.org/10.1021/acs.analchem.3c00852.
(303) Geng, Y.; Zhang, H.; Zhang, G.; Zhou, J.; Zhu, M.; Ma, L.; Wang, X.; James, T. D.; Wang, Z. Near-Infrared Fluorescent Probe for the In Situ Visualization of Oxidative Stress in the Brains of Neuroinflammatory and Schizophrenic Mice. *Anal. Chem.* **2023**, *95* (32), 11943–11952. https://doi.org/10.1021/acs.analchem.3c01447.
(304) Tang, Z.; Song, B.; Zhang, W.; Guo, L.; Yuan, J. Precise Monitoring of Drug-Induced Kidney Injury Using an Endoplasmic Reticulum-Targetable Ratiometric Time-Gated Luminescence Probe for Superoxide Anions. *Anal. Chem.* **2019**, *91* (21), 14019–14028. https://doi.org/10.1021/acs.analchem.9b03602.
(305) Wei, H.; Wang, Y.; Chen, Q.; Sun, Y.; Yue, T.; Dong, B. Development of an Endoplasmic Reticulum-Targeting Fluorescent Probe for the Imaging of Superoxide Anion in Living Cells. *J. Fluoresc.* **2023**, *33* (2), 509–515. https://doi.org/10.1007/s10895-022-03079-x.
(306) Zhang, Y.; Li, W.; Chen, X.; Xiong, S.; Bian, Y.; Yuan, L.; Gao, X.; Su, D. Liver-Targeted Near-Infrared Fluorescence/Photoacoustic Dual-Modal Probe for Real-Time Imaging of In Situ Hepatic Inflammation. *Anal. Chem.* **2023**, *95* (4), 2579–2587. https://doi.org/10.1021/acs.analchem.2c05476.
(307) Yan, K.-C.; Patenall, B. L.; Gardiner, J. E.; Heylen, R. A.; Thet, N.; He, X.-P.; Sedgwick, A. C.; James, T. D.; Jenkins, A. T. A. TCF-Based Fluorescent Probe for Monitoring Superoxide Anion Produced in Bacteria under Chloramphenicol- and Heat-Induced Stress. *Chem. Commun.* **2022**, *58* (94), 13103–13106. https://doi.org/10.1039/d2cc04662h.
(308) Han, X.; Wang, R.; Song, X.; Yu, F.; Lv, C.; Chen, L. A Mitochondrial-Targeting near-Infrared Fluorescent Probe for Bioimaging and Evaluating Endogenous Superoxide Anion Changes during Ischemia/Reperfusion Injury. *Biomaterials* **2018**, *156*, 134–146. https://doi.org/10.1016/j.biomaterials.2017.11.039.
(309) Huang, L.; Li, Z.; Zhang, D.; Li, H.; Shi, C.; Zhang, P.; Su, X.; Zhang, X. Highly Specific and Sensitive Radioiodinated Agent for In Vivo Imaging of Superoxide through Superoxide-Initiated Retention. *Anal. Chem.* **2018**, *90* (21), 12971–12978. https://doi.org/10.1021/acs.analchem.8b03642.
(310) Huang, J.; Li, J.; Lyu, Y.; Miao, Q.; Pu, K. Molecular Optical Imaging Probes for Early Diagnosis of Drug-Induced Acute Kidney Injury. *Nat. Mater.* **2019**, *18* (10), 1133–1143. https://doi.org/10.1038/s41563-019-0378-4.

(311) Cheng, P.; Miao, Q.; Li, J.; Huang, J.; Xie, C.; Pu, K. Unimolecular Chemo-Fluoro-Luminescent Reporter for Crosstalk-Free Duplex Imaging of Hepatotoxicity. *J. Am. Chem. Soc.* **2019**, *141* (27), 10581–10584. https://doi.org/10.1021/jacs.9b02580.
(312) Huang, J.; Huang, J.; Cheng, P.; Jiang, Y.; Pu, K. Near-Infrared Chemiluminescent Reporters for In Vivo Imaging of Reactive Oxygen and Nitrogen Species in Kidneys. *Adv. Funct. Mater.* **2020**, *30* (39), 2003628. https://doi.org/10.1002/adfm.202003628.
(313) Gong, Y.; Yang, M.; Lv, J.; Li, H.; Gao, J.; Yuan, Z. A 1,2-Dioxetane-Based Chemiluminescent Probe for Highly Selective and Sensitive Detection of Superoxide Anions in Vitro and in Vivo. *ChemPlusChem* **2022**, *87* (4), e202200054. https://doi.org/10.1002/cplu.202200054.
(314) Ruan, B.; Yu, M.; Zhou, Y.; Xu, W.; Liu, Y.; Liu, B.; Zhu, L.; Yi, S.; Jiang, Y.; Huang, J. Size-Transformable Superoxide-Triggered Nanoreporters for Crosstalk-Free Dual Fluorescence/Chemiluminescence Imaging and Urinalysis in Living Mice. *Angew. Chem.* **2023**, *135* (31), e202305812. https://doi.org/10.1002/ange.202305812.
(315) Sun, T.; Chen, Q.; Zhou, Z.; Li, C.; Yu, T.; Jiang, C. A Chemiluminescent Reporter Assisted by In-Situ Neutrophils for Imaging O2− at Inflammatory Sites. *J. Controlled Release* **2023**, *358*, 382–397. https://doi.org/10.1016/j.jconrel.2023.04.035.
(316) Hong, S. C.; Murale, D. P.; Jang, S.-Y.; Haque, M. Md.; Seo, M.; Lee, S.; Woo, D. H.; Kwon, J.; Song, C.-S.; Kim, Y. K.; Lee, J.-S. Discrimination of Avian Influenza Virus Subtypes Using Host-Cell Infection Fingerprinting by a Sulfinate-Based Fluorescence Superoxide Probe. *Angew. Chem. Int. Ed.* **2018**, *57* (31), 9716–9721. https://doi.org/10.1002/anie.201804412.
(317) Xu, K.; Liu, X.; Tang, B.; Yang, G.; Yang, Y.; An, L. Design of a Phosphinate-Based Fluorescent Probe for Superoxide Detection in Mouse Peritoneal Macrophages. *Chem. - Eur. J.* **2007**, *13* (5), 1411–1416. https://doi.org/10.1002/chem.200600497.
(318) Xu, K.; Liu, X.; Tang, B. A Phosphinate-Based Red Fluorescent Probe for Imaging the Superoxide Radical Anion Generated by RAW264.7 Macrophages. *ChemBioChem* **2007**, *8* (4), 453–458. https://doi.org/10.1002/cbic.200600392.
(319) Song, W.; Dong, B.; Lu, Y.; Li, Z.; Zhang, W.; Lin, W. Two-Photon Fluorescent Sensors for Visual Detection of Abnormal Superoxide Anion in Diabetes Mice. *Sens. Actuators B Chem.* **2021**, *332*, 129537. https://doi.org/10.1016/j.snb.2021.129537.
(320) Wang, S.-Y.; Liu, J.-R.; Ju, Z.-H.; Tian, D.-H.; Chai, Z.-H.; Zhang, Y.; Dai, F.; Zhang, S.; Zhou, B. Simultaneous Two-Photon Intravital Imaging of Viscosity and Superoxide Radical Anion by a Styrylpyridinium-Based Fluorescent Probe. *Sens. Actuators B Chem.* **2023**, *381*, 133470. https://doi.org/10.1016/j.snb.2023.133470.
(321) Yang, J.; Liu, X.; Wang, H.; Tan, H.; Xie, X.; Zhang, X.; Liu, C.; Qu, X.; Hua, J. A Turn-on near-Infrared Fluorescence Probe with Aggregation-Induced Emission Based on Dibenzo[a,c]Phenazine for Detection of Superoxide Anions and Its Application in Cell Imaging. *Analyst* **2018**, *143* (5), 1242–1249. https://doi.org/10.1039/c7an01860f.
(322) Lv, J.-Y.; Nawaz, M. A. H.; Liu, N.; Zhou, H.-P.; Hussain, E.; Wen, X.; Gou, X.-Y.; Jin, X.; Yu, C. A Nile Red-Based near-Infrared Fluorescent Probe for the Detection of Superoxide Radical Anion in Living Cells. *Chin. J. Anal. Chem.* **2022**, *50* (9), 100140. https://doi.org/10.1016/j.cjac.2022.100140.
(323) Ying, W.; Dong, F.; Shi, Y.; Zhan, Z.; Wang, S.; Lv, L.; Liu, H.; Liu, L.; Zheng, Y.; Zhang, L. Superoxide Anion Monitoring in Epileptic Brains with a Near-Infrared Fluorescent Probe. *Dyes Pigments* **2023**, *213*, 111155. https://doi.org/10.1016/j.dyepig.2023.111155.
(324) Gao, X.; Feng, G.; Manghnani, P. N.; Hu, F.; Jiang, N.; Liu, J.; Liu, B.; Sun, J. Z.; Tang, B. Z. A Two-Channel Responsive Fluorescent Probe with AIE Characteristics and Its Application for Selective Imaging of Superoxide Anions in Living Cells. *Chem. Commun.* **2017**, *53*, 1653–1656. https://doi.org/10.1039/c6cc09307h.

(325) Zhang, Z.; Fan, J.; Zhao, Y.; Kang, Y.; Du, J.; Peng, X. Mitochondria-Accessing Ratiometric Fluorescent Probe for Imaging Endogenous Superoxide Anion in Live Cells and Daphnia Magna. *ACS Sens.* **2018**, *3* (3), 735–741. https://doi.org/10.1021/acssensors.8b00082.
(326) Zhang, N.; He, Y.; Tang, Q.; Wang, Y.; Zheng, Q.; Hu, P. A Mitochondrial Targeting Two-Channel Responsive Fluorescence Probe for Imaging the Superoxide Radical Anion in Vitro and in Vivo. *Talanta* **2019**, *194*, 79–85. https://doi.org/10.1016/j.talanta.2018.09.109.
(327) Wang, J.; Liu, L.; Xu, W.; Yang, Z.; Yan, Y.; Xie, X.; Wang, Y.; Yi, T.; Wang, C.; Hua, J. Mitochondria-Targeted Ratiometric Fluorescent Probe Based on Diketopyrrolopyrrole for Detecting and Imaging of Endogenous Superoxide Anion in Vitro and in Vivo. *Anal. Chem.* **2019**, *91* (9), 5786–5793. https://doi.org/10.1021/acs.analchem.9b00014.
(328) Huang, S.; Zhang, X.; Liu, Y.; Gui, J.; Wang, R.; Han, L.; Jia, H.; Du, L. Phosphinate-Based Mitochondria-Targeted Fluorescent Probe for Imaging and Detection of Endogenous Superoxide in Live Cells and in Vivo. *Talanta* **2019**, *197*, 239–248. https://doi.org/10.1016/j.talanta.2018.12.080.
(329) Xu, C.; Xu, W.; Yang, Z.; Li, S.; Wang, Y.; Hua, J. A Turn-on Mitochondria-Targeted near-Infrared Fluorescent Probe with a Large Stokes Shift for Detecting and Imaging Endogenous Superoxide Anion in Cells. *J. Photochem. Photobiol. Chem.* **2021**, *415*, 113304. https://doi.org/10.1016/j.jphotochem.2021.113304.
(330) Liu, W.; Wang, Y.; Wang, T.; Wang, L.; Hu, S.; Tian, D. A Versatile AIE Probe with Mitochondria Targeting for Dual-Channel Detection of Superoxide Anion and Viscosity. *Anal. Chim. Acta* **2023**, *1253*, 341099. https://doi.org/10.1016/j.aca.2023.341099.
(331) Liu, X.; Tian, X.; Xu, X.; Lu, J. Design of a Phosphinate-Based Bioluminescent Probe for Superoxide Radical Anion Imaging in Living Cells. *Luminescence* **2018**, *33* (6), 1101–1106. https://doi.org/10.1002/bio.3515.
(332) Jang, Y. J.; Murale, D. P.; Churchill, D. G. Novel Reversible and Selective Nerve Agent Simulant Detection in Conjunction with Superoxide “Turn-on” Probing. *The Analyst* **2014**, *139* (7), 1614. https://doi.org/10.1039/c3an02267f.
(333) Chen, L.; Cho, M. K.; Wu, D.; Kim, H. M.; Yoon, J. Two-Photon Fluorescence Probe for Selective Monitoring of Superoxide in Live Cells and Tissues. *Anal. Chem.* **2019**, *91* (22), 14691–14696. https://doi.org/10.1021/acs.analchem.9b03937.
(334) Murale, D. P.; Kim, H.; Choi, W. S.; Churchill, D. G. Highly Fluorescent and Specific Molecular Probing of (Homo)Cysteine or Superoxide: Biothiol Detection Confirmed in Living Neuronal Cells. *Org. Lett.* **2013**, *15* (14), 3630–3633. https://doi.org/10.1021/ol401480w.
(335) Murale, D. P.; Kim, H.; Choi, W. S.; Churchill, D. G. Highly Selective Excited State Intramolecular Proton Transfer (ESIPT)-Based Superoxide Probing. *Org. Lett.* **2013**, *15* (15), 3946–3949. https://doi.org/10.1021/ol4017222.
(336) Wang, T.; Shah, I.; Yang, Z.; Yin, W.; Zhang, S.; Yang, Y.; Yin, P.; Ma, H. Incorporating Thiourea into Fluorescent Probes: A Reliable Strategy for Mitochondrion-Targeted Imaging and Superoxide Anion Tracking in Living Cells. *Anal. Chem.* **2020**, *92* (3), 2824–2829. https://doi.org/10.1021/acs.analchem.9b05320.
(337) Merkes, J. M.; Rueping, M.; Kiessling, F.; Banala, S. Photoacoustic Detection of Superoxide Using Oxoporphyrinogen and Porphyrin. *ACS Sens.* **2019**, *4* (8), 2001–2008. https://doi.org/10.1021/acssensors.9b00224.
(338) Yu, Z. H.; Chung, C. Y.-S.; Tang, F. K.; Brewer, T. F.; Au-Yeung, H. Y. A Modular Trigger for the Development of Selective Superoxide Probes. *Chem. Commun.* **2017**, *53* (72), 10042–10045. https://doi.org/10.1039/C7CC05405J.
(339) Prigge, S. T.; Eipper, B. A.; Mains, R. E.; Amzel, L. M. Dioxygen Binds End-On to Mononuclear Copper in a Precatalytic Enzyme Complex. *Science* **2004**, *304* (5672), 864–867. https://doi.org/10.1126/science.1094583.

(340) Tang, F. K.; Yu, Z. H.; Wong, T. H.-F.; Chung, C. Y.-S.; Hirao, H.; Au-Yeung, H. Y. Fluorescein-Containing Superoxide Probes with a Modular Copper-Based Trigger. *ChemPlusChem* **2020**, *85* (4), 653–658. https://doi.org/10.1002/cplu.202000059.
(341) Halle, M. B.; Lee, K. J.; Yudhistira, T.; Choi, J. H.; Park, H.-S.; Churchill, D. G. A Hemicyanine-Embedded Diphenylselenide-Containing Probe "HemiSe" in Which SePh2 Stays Reduced for Selective Detection of Superoxide in Living Cells. *Chem. - Asian J.* **2018**, *13* (24), 3895–3902. https://doi.org/10.1002/asia.201801339.
(342) Wang, J.; Dang, V.; Zhao, W.; Lu, D.; Rivera, B. K.; Villamena, F. A.; Wang, P. G.; Kuppusamy, P. Perchlorotrityl Radical-Fluorophore Conjugates as Dual Fluorescence and EPR Probes for Superoxide Radical Anion. *Bioorg. Med. Chem.* **2010**, *18* (2), 922–929. https://doi.org/10.1016/j.bmc.2009.11.034.
(343) Hideg, É.; Barta, C.; Kálai, T.; Vass, I.; Hideg, K.; Asada, K. Detection of Singlet Oxygen and Superoxide with Fluorescent Sensors in Leaves Under Stress by Photoinhibition or UV Radiation. *Plant Cell Physiol.* **2002**, *43* (10), 1154–1164. https://doi.org/10.1093/pcp/pcf145.
(344) Jiang, X.; Li, M.; Wang, Y.; Wang, C.; Wang, Y.; Shen, T.; Shen, L.; Liu, X.; Wang, Y.; Li, X. 1,2,4,5-Tetrazine-Tethered Probes for Fluorogenically Imaging Superoxide in Live Cells with Ultrahigh Specificity. *Nat. Commun.* **2023**, *14* (1), 1401. https://doi.org/10.1038/s41467-023-37121-8.
(345) Yu, F.; Li, P.; Song, P.; Wang, B.; Zhao, J.; Han, K. Facilitative Functionalization of Cyanine Dye by an On-off-on Fluorescent Switch for Imaging of H_2O_2 Oxidative Stress and Thiols Reducing Repair in Cells and Tissues. *Chem. Commun.* **2012**, *48*, 4980–4982. https://doi.org/10.1039/c2cc30985h.
(346) Reja, S. I.; Gupta, M.; Gupta, N.; Bhalla, V.; Ohri, P.; Kaur, G.; Kumar, M. A Lysosome Targetable Fluorescent Probe for Endogenous Imaging of Hydrogen Peroxide in Living Cells. *Chem. Commun.* **2017**, *53*, 3701–3704. https://doi.org/10.1039/c6cc09127j.
(347) Veal, E. A.; Day, A. M.; Morgan, B. A. Hydrogen Peroxide Sensing and Signaling. *Mol. Cell* **2007**, *26* (1), 1–14. https://doi.org/10.1016/j.molcel.2007.03.016.
(348) Lennicke, C.; Cochemé, H. M. Redox Metabolism: ROS as Specific Molecular Regulators of Cell Signaling and Function. *Mol. Cell* **2021**, *81* (18), 3691–3707. https://doi.org/10.1016/j.molcel.2021.08.018.
(349) Winterbourn, C. C. The Biological Chemistry of Hydrogen Peroxide. In *Methods in Enzymology*; Elsevier, 2013; Vol. 528, pp 3–25. https://doi.org/10.1016/B978-0-12-405881-1.00001-X.
(350) Lippert, A. R.; Keshari, K. R.; Kurhanewicz, J.; Chang, C. J. A Hydrogen Peroxide-Responsive Hyperpolarized ^{13}C MRI Contrast Agent. *J. Am. Chem. Soc.* **2011**, *133* (11), 3776–3779. https://doi.org/10.1021/ja111589a.
(351) Tang, Z.; Zhao, P.; Wang, H.; Liu, Y.; Bu, W. Biomedicine Meets Fenton Chemistry. *Chem. Rev.* **2021**, *121* (4), 1981–2019. https://doi.org/10.1021/acs.chemrev.0c00977.
(352) Lim, J. B.; Huang, B. K.; Deen, W. M.; Sikes, H. D. Analysis of the Lifetime and Spatial Localization of Hydrogen Peroxide Generated in the Cytosol Using a Reduced Kinetic Model. *Free Radic. Biol. Med.* **2015**, *89*, 47–53. https://doi.org/10.1016/j.freeradbiomed.2015.07.009.
(353) Giorgio, M.; Trinei, M.; Migliaccio, E.; Pelicci, P. G. Hydrogen Peroxide: A Metabolic by-Product or a Common Mediator of Ageing Signals? *Nat. Rev. Mol. Cell Biol.* **2007**, *8* (9), 722–728. https://doi.org/10.1038/nrm2240.
(354) Reth, M. Hydrogen Peroxide as Second Messenger in Lymphocyte Activation. *Nat. Immunol.* **2002**, *3* (12), 1129–1134. https://doi.org/10.1038/ni1202-1129.
(355) Rojkind, M.; Domínguez-Rosales, J.-A.; Nieto, N.; Greenwel, P. Role of Hydrogen Peroxide and Oxidative Stress in Healing Responses. *Cell. Mol. Life Sci.* **2002**, *59* (11), 1872–1891. https://doi.org/10.1007/PL00012511.

(356) Marinho, H. S.; Real, C.; Cyrne, L.; Soares, H.; Antunes, F. Hydrogen Peroxide Sensing, Signaling and Regulation of Transcription Factors. *Redox Biol.* **2014**, *2*, 535–562. https://doi.org/10.1016/j.redox.2014.02.006.
(357) Afanas'ev, I. Mechanisms of Superoxide Signaling in Epigenetic Processes: Relation to Aging and Cancer. *Aging Dis.* **2015**, *6* (3), 216. https://doi.org/10.14336/AD.2014.0924.
(358) Hardeland, R.; Coto-Montes, A.; Poeggeler, B. Circadian Rhythms, Oxidative Stress, and Antioxidative Defense Mechanisms. *Chronobiol. Int.* **2003**, *20* (6), 921–962. https://doi.org/10.1081/CBI-120025245.
(359) Rhee, S. G.; Chang, T.-S.; Jeong, W.; Kang, D. Methods for Detection and Measurement of Hydrogen Peroxide inside and Outside of Cells. *Mol. Cells* **2010**, *29* (6), 539–549. https://doi.org/10.1007/s10059-010-0082-3.
(360) Rota, C.; Chignell, C. F.; Mason, R. P. Evidence for Free Radical Formation during the Oxidation of 2′-7′-Dichlorofluorescin to the Fluorescent Dye 2′-7′-Dichlorofluorescein by Horseradish Peroxidase:Possible Implications for Oxidative Stress Measurements. *Free Radic. Biol. Med.* **1999**, *27* (7–8), 873–881. https://doi.org/10.1016/S0891-5849(99)00137-9.
(361) Possel, H.; Noack, H.; Augustin, W.; Keilhoff, G.; Wolf, G. 2,7-Dihydrodichlorofluorescein Diacetate as a Fluorescent Marker for Peroxynitrite Formation. *FEBS Lett.* **1997**, *416* (2), 175–178. https://doi.org/10.1016/S0014-5793(97)01197-6.
(362) Hool, Kevin.; Nieman, T. A. Immobilized Luminol Chemiluminescence Reagent System for Hydrogen Peroxide Determinations in Flowing Streams. *Anal. Chem.* **1988**, *60* (9), 834–837. https://doi.org/10.1021/ac00160a002.
(363) Zhang, W.-Z.; Du, Z.-B.; Song, B.; Ye, Z.-Q.; Yuan, J.-L. Development of a Triple Channel Detection Probe for Hydrogen Peroxide. *Chin. Chem. Lett.* **2015**, *26* (12), 1465–1469. https://doi.org/10.1016/j.cclet.2015.10.022.
(364) Wang, H.; Zhang, R.; Bridle, K. R.; Jayachandran, A.; Thomas, J. A.; Zhang, W.; Yuan, J.; Xu, Z. P.; Crawford, D. H. G.; Liang, X.; Liu, X.; Roberts, M. S. Two-Photon Dual Imaging Platform for in Vivo Monitoring Cellular Oxidative Stress in Liver Injury. *Sci. Rep.* **2017**, *7*, 45374. https://doi.org/10.1038/srep45374.
(365) Deepa, S.; Rajendrakumar, K. Luminol-Pendant Chemiluminescent Polymethacrylamide-Based Polymers for Peroxide Sensing in Live Cell Imaging. *ChemistrySelect* **2019**, *4* (4), 1158–1165. https://doi.org/10.1002/slct.201803354.
(366) McCapra, F.; Richardson, D. G.; Chang, Y. C. Chemiluminescence Involving Peroxide Decompositions. *Photochem. Photobiol.* **1965**, *4* (6), 1111–1121. https://doi.org/10.1111/j.1751-1097.1965.tb09300.x.
(367) Sato, N. Synthesis and Properties of New Luminescent 10-Carboxymethylacridinium Derivatives. *Tetrahedron Lett.* **1996**, *37* (47), 8519–8522. https://doi.org/10.1016/0040-4039(96)01980-6.
(368) Renotte, R.; Sarlet, G.; Thunus, L.; Lejeune, R. High Stability and High Efficiency Chemiluminescent Acridinium Compounds Obtained from 9-Acridine Carboxylic Esters of Hydroxamic and Sulphohydroxamic Acids. *Luminescence* **2000**, *15* (5), 311–320. https://doi.org/10.1002/1522-7243(200009/10)15:5<311::AID-BIO600>3.0.CO;2-3.
(369) Nakazono, M.; Nanbu, S.; Akita, T.; Hamase, K. Synthesis, Chemiluminescence, and Application of 2,4-Disubstituted Phenyl 10-Methyl-10λ4-Acridine-9-Carboxylates. *Dyes Pigments* **2019**, *170*, 107628. https://doi.org/10.1016/j.dyepig.2019.107628.
(370) Nakazono, M.; Hamase, K. Strong Chemiluminescence Intensities of Bis-Acridinium Esters under Neutral and Alkaline Conditions. *Dyes Pigments* **2023**, *213*, 111175. https://doi.org/10.1016/j.dyepig.2023.111175.
(371) Nelson, N. C.; Cheikh, A. B.; Matsuda, E.; Becker, M. M. Simultaneous Detection of Multiple Nucleic Acid Targets in a Homogeneous Format. *Biochemistry* **1996**, *35* (25), 8429–8438. https://doi.org/10.1021/bi960085+.

(372) Scott, G.; Seitz, W. R.; Ambrose, J. Improved Determination of Hydrogen Peroxide by Measurement of Peroxyoxalate Chemiluminescence. *Anal. Chim. Acta* **1980**, *115*, 221–228. https://doi.org/10.1016/S0003-2670(01)93160-5.
(373) Quimbar, M. E.; Krenek, K. M.; Lippert, A. R. A Chemiluminescent Platform for Smartphone Monitoring of H_2O_2 in Human Exhaled Breath Condensates. *Methods* **2016**, *109*, 123–130. https://doi.org/10.1016/j.ymeth.2016.05.017.
(374) Lee, D.; Khaja, S.; Velasquez-Castano, J. C.; Dasari, M.; Sun, C.; Petros, J.; Taylor, W. R.; Murthy, N. In Vivo Imaging of Hydrogen Peroxide with Chemiluminescent Nanoparticles. *Nat. Mater.* **2007**, *6* (10), 765–769. https://doi.org/10.1038/nmat1983.
(375) Yue, Y.; Zhao, T.; Xu, Z.; Chi, W.; Chai, X.; Ai, J.; Zhang, J.; Huo, F.; Strongin, R.; Yin, C. Enlarging the Stokes Shift by Weakening the Pi-Conjugation of Cyanines for High Signal-to-Noise Ratiometric Imaging. *Adv. Sci.* https://doi.org/10.1002/advs.202205080.
(376) Yang, Y.; Wang, S.; Lu, L.; Zhang, Q.; Yu, P.; Fan, Y.; Zhang, F. NIR-II Chemiluminescence Molecular Sensor for In Vivo High-Contrast Inflammation Imaging. *Angew. Chem. Int. Ed.* **2020**, *59* (42), 18380–18385. https://doi.org/10.1002/anie.202007649.
(377) Belousov, V. V.; Fradkov, A. F.; Lukyanov, K. A.; Staroverov, D. B.; Shakhbazov, K. S.; Terskikh, A. V.; Lukyanov, S. Genetically Encoded Fluorescent Indicator for Intracellular Hydrogen Peroxide. *Nat. Methods* **2006**, *3* (4), 281–286. https://doi.org/10.1038/nmeth866.
(378) Bilan, D. S.; Belousov, V. V. *In Vivo* Imaging of Hydrogen Peroxide with HyPer Probes. *Antioxid. Redox Signal.* **2018**, *29* (6), 569–584. https://doi.org/10.1089/ars.2018.7540.
(379) Akasaka, K.; Suzuki, T.; Ohrui, H.; Meguro, H. Study on Aromatic Phosphines for Novel Fluorometry of Hydroperoxides (II) -The Determination of Lipid Hydroperoxides with Diphenyl-1-Pyrenylphosphine -. *Anal. Lett.* **1987**, *20* (5), 797–807. https://doi.org/10.1080/00032718708062929.
(380) Okimoto, Y.; Watanabe, A.; Niki, E.; Yamashita, T.; Noguchi, N. A Novel Fluorescent Probe Diphenyl-1-Pyrenylphosphine to Follow Lipid Peroxidation in Cell Membranes. *FEBS Lett.* **2000**, *474* (2–3), 137–140. https://doi.org/10.1016/S0014-5793(00)01587-8.
(381) Onoda, M.; Tokuyama, H.; Uchiyama, S.; Mawatari, K.; Santa, T.; Kaneko, K.; Imai, K.; Nakagomi, K. Fluorescence Enhancement by Hydroperoxides Based on a Change in the Intramolecular Charge Transfer Character of Benzofurazan. *Chem. Commun.* **2005**, 1848–1850. https://doi.org/10.1039/b500419e.
(382) Soh, N.; Sakawaki, O.; Makihara, K.; Odo, Y.; Fukaminato, T.; Kawai, T.; Irie, M.; Imato, T. Design and Development of a Fluorescent Probe for Monitoring Hydrogen Peroxide Using Photoinduced Electron Transfer. *Bioorg. Med. Chem.* **2005**, *13* (4), 1131–1139. https://doi.org/10.1016/j.bmc.2004.11.023.
(383) Soh, N.; Ariyoshi, T.; Fukaminato, T.; Nakano, K.; Irie, M.; Imato, T. Novel Fluorescent Probe for Detecting Hydroperoxides with Strong Emission in the Visible Range. *Bioorg. Med. Chem. Lett.* **2006**, *16* (4), 2943–2946. https://doi.org/10.1016/j.bmcl.2006.02.078.
(384) Shioji, K.; Oyama, Y.; Okuma, K.; Nakagawa, H. Synthesis and Properties of Fluorescence Probe for Detection of Peroxides in Mitochondria. *Bioorg. Med. Chem. Lett.* **2010**, *20* (13), 3911–3915. https://doi.org/10.1016/j.bmcl.2010.05.017.
(385) Huang, Y.; Yu, L.; Lu, P.; Wei, Y.; Fu, L.; Hou, J.; Wang, Y.; Wang, X.; Chen, L. Evaluate the Bisphenol A-Induced Redox State in Cells, Zebrafish and in Vivo with a Hydrogen Peroxide Turn-on Fluorescent Probe. *J. Hazard. Mater.* **2022**, *424* (Part_B), 127425. https://doi.org/10.1016/j.jhazmat.2021.127425.
(386) Lo, L.-C.; Chu, C.-Y. Development of Highly Selective and Sensitive Probes for Hydrogen Peroxide. *Chem. Commun.* **2003**, No. 21, 2728. https://doi.org/10.1039/b309393j.
(387) Chang, M. C. Y.; Pralle, A.; Isacoff, E. Y.; Chang, C. J. A Selective, Cell-Permeable Optical Probe for Hydrogen Peroxide in Living Cells. *J. Am. Chem. Soc.* **2004**, *126* (47), 15392–15393. https://doi.org/10.1021/ja0441716.

(388) Miller, E. W.; Albers, A. E.; Pralle, A.; Isacoff, E. Y.; Chang, C. J. Boronate-Based Fluorescent Probes for Imaging Cellular Hydrogen Peroxide. *J. Am. Chem. Soc.* **2005**, *127* (47), 16652–16659. https://doi.org/10.1021/ja054474f.
(389) Albers, A. E.; Okreglak, V. S.; Chang, C. J. A FRET-Based Approach to Ratiometric Fluorescence Detection of Hydrogen Peroxide. *J. Am. Chem. Soc.* **2006**, *128* (30), 9640–9641. https://doi.org/10.1021/ja063308k.
(390) Srikun, D.; Miller, E. W.; Domaille, D. W.; Chang, C. J. An ICT-Based Approach to Ratiometric Fluorescence Imaging of Hydrogen Peroxide Produced in Living Cells. *J. Am. Chem. Soc.* **2008**, *130* (14), 4596–4597. https://doi.org/10.1021/ja711480f.
(391) Chung, C.; Srikun, D.; Lim, C. S.; Chang, C. J.; Cho, B. R. A Two-Photon Fluorescent Probe for Ratiometric Imaging of Hydrogen Peroxide in Live Tissue. *Chem. Commun.* **2011**, *47*, 9618–9620. https://doi.org/10.1039/c1cc13583j.
(392) Masanta, G.; Heo, C. H.; Lim, C. S.; Bae, S. K.; Cho, B. R.; Kim, H. M. A Mitochondria-Localized Two-Photon Fluorescent Probe for Ratiometric Imaging of Hydrogen Peroxide in Live Tissue. *Chem. Commun.* **2012**, *48*, 3518–3520. https://doi.org/10.1039/c2cc00034b.
(393) Kumar, M.; Kumar, N.; Bhalla, V.; Sharma, P. R.; Qurishi, Y. A Charge Transfer Assisted Fluorescent Probe for Selective Detection of Hydrogen Peroxide among Different Reactive Oxygen Species. *Chem. Commun.* **2012**, *48*, 4719–4721. https://doi.org/10.1039/c2cc30932g.
(394) Qian, Y.-Y.; Xue, L.; Hu, D.-X.; Li, G.-P.; Jiang, H. Quinoline-Based Fluorescent Probe for Ratiometric Detection of Hydrogen Peroxide in Aqueous Solution. *Dyes Pigments* **2012**, *95* (2), 373–376. https://doi.org/10.1016/j.dyepig.2012.05.013.
(395) Zhu, B.; Jiang, H.; Guo, B.; Shao, C.; Wu, H.; Du, B.; Wei, Q. A Highly Selective Ratiometric Fluorescent Probe for Hydrogen Peroxide Displaying a Large Emission Shift. *Sens. Actuators B Chem.* **2013**, *186*, 681–686. https://doi.org/10.1016/j.snb.2013.06.058.
(396) Lee, S. W.; Rhee, H.-W.; Chang, Y.-T.; Hong, J.-I. Ratiometric Fluorescent Probes for Hydrogen Peroxide from a Focused Library. *Chem. - Eur. J.* **2013**, *19* (44), 14791–14794. https://doi.org/10.1002/chem.201302523.
(397) Bortolozzi, R.; von Gradowski, S.; Ihmels, H.; Schafer, K.; Viola, G. Selective Ratiometric Detection of H_2O_2 in Water and in Living Cells with Boronobenzo[b]Quinolizinium Derivatives. *Chem. Commun.* **2014**, *50*, 8242–8245. https://doi.org/10.1039/c4cc02283a.
(398) Liu, C.; Shao, C.; Wu, H.; Guo, B.; Zhu, B.; Zhang, X. A Fast-Response, Highly Sensitive and Selective Fluorescent Probe for the Ratiometric Imaging of Hydrogen Peroxide with a 100 nm Red-Shifted Emission. *RSC Adv.* **2014**, *4* (31), 16055. https://doi.org/10.1039/C4RA01039F.
(399) Wen, Y.; Liu, K.; Yang, H.; Li, Y.; Lan, H.; Liu, Y.; Zhang, X.; Yi, T. A Highly Sensitive Ratiometric Fluorescent Probe for the Detection of Cytoplasmic and Nuclear Hydrogen Peroxide. *Anal. Chem.* **2014**, *86* (19), 9970–9976. https://doi.org/10.1021/ac502909c.
(400) Wen, Y.; Liu, K.; Yang, H.; Liu, Y.; Chen, L.; Liu, Z.; Huang, C.; Yi, T. Mitochondria-Directed Fluorescent Probe for the Detection of Hydrogen Peroxide near Mitochondrial DNA. *Anal. Chem.* **2015**, *87* (20), 10579–10584. https://doi.org/10.1021/acs.analchem.5b03326.
(401) Rong, L.; Zhang, C.; Lei, Q.; Hu, M.-M.; Feng, J.; Shu, H.-B.; Liu, Y.; Zhang, X.-Z. Hydrogen Peroxide Detection with High Specificity in Living Cells and Inflamed Tissues. *Regen. Biomater.* **2016**, *3* (4), 217–222. https://doi.org/10.1093/rb/rbw022.
(402) Xu, J.; Zhai, J.; Xu, Y.; Zhu, J.; Qin, Y.; Jiang, D. A Near-Infrared Fluorescent Aza-Bodipy Probe for Dual-Wavelength Detection of Hydrogen Peroxide in Living Cells. *Analyst* **2016**, *141* (8), 2380–2383. https://doi.org/10.1039/c6an00262e.
(403) Liu, K.; Shang, H.; Kong, X.; Ren, M.; Wang, J.-Y.; Liu, Y.; Lin, W. A Novel Near-Infrared Fluorescent Probe for H_2O_2 in Alkaline Environment and the Application for H_2O_2 Imaging in Vitro and in Vivo. *Biomaterials* **2016**, *100*, 162–171. https://doi.org/10.1016/j.biomaterials.2016.05.029.

(404) Lei, Y.; Xue, C.; Zhang, S.; Sha, Y. A Ratiometric Fluorescent Probe for Sensing Hydrogen Peroxide Based on a Hemicyanine-Naphthol Fluorophore. *Luminescence* **2016**, *31* (3), 660–664. https://doi.org/10.1002/bio.3008.
(405) Xu, F.; Li, H.; Yao, Q.; Fan, J.; Wang, J.; Peng, X. A NIR Fluorescent Probe: Imaging Endogenous Hydrogen Peroxide during an Autophagy Process Induced by Rapamycin. *J. Mater. Chem. B* **2016**, *4* (46), 7363–7367. https://doi.org/10.1039/C6TB02463G.
(406) Liu, Y.; Nie, J.; Niu, J.; Meng, F.; Lin, W. Ratiometric Fluorescent Probe with AIE Property for Monitoring Endogenous Hydrogen Peroxide in Macrophages and Cancer Cells. *Sci. Rep.* **2017**, *7*, 1–10. https://doi.org/10.1038/s41598-017-07465-5.
(407) Liang, X.; Xu, X.; Qiao, D.; Yin, Z.; Shang, L. Dual Mechanism of an Intramolecular Charge Transfer (ICT)-FRET-Based Fluorescent Probe for the Selective Detection of Hydrogen Peroxide. *Chem. - Asian J.* **2017**, *12*, 3187–3194. https://doi.org/10.1002/asia.201701382.
(408) Dai, F.; Jin, F.; Long, Y.; Jin, X.; Zhou, B. A 1,8-Naphthalimide-Based Turn-on Fluorescent Probe for Imaging Mitochondrial Hydrogen Peroxide in Living Cells. *FREE Radic. Res.* **2018**, *52* (11–12), 1288–1295. https://doi.org/10.1080/10715762.2018.1446530.
(409) Shen, Y.; Zhang, X.; Zhang, Y.; Wu, Y.; Zhang, C.; Chen, Y.; Jin, J.; Li, H. A Mitochondria-Targeted Colorimetric and Ratiometric Fluorescent Probe for Hydrogen Peroxide with a Large Emission Shift and Bio-Imaging in Living Cells. *Sens. Actuators B Chem.* **2018**, *255*, 42–48. https://doi.org/10.1016/j.snb.2017.08.020.
(410) Hu, Y.; Gao, X.; Li, X.; Liang, H.; Zhang, D.; Liu, C. The Application of Flavonoid Derivatives as Redox-Responsive Fluorescent Probes in Hydrophobic Microenvironment. *Sens. Actuators B Chem.* **2018**, *262*, 144–152. https://doi.org/10.1016/j.snb.2018.01.184.
(411) Hou, J.; Qian, M.; Zhao, H.; Li, Y.; Liao, Y.; Han, G.; Xu, Z.; Wang, F.; Song, Y.; Liu, Y. A Near-Infrared Ratiometric/Turn-on Fluorescent Probe for in Vivo Imaging of Hydrogen Peroxide in a Murine Model of Acute Inflammation. *Anal. Chim. ACTA* **2018**, *1024*, 169–176. https://doi.org/10.1016/j.aca.2018.03.028.
(412) Li, Y.; Shu, Y.; Liang, M.; Xie, X.; Jiao, X.; Wang, X.; Tang, B. A Two-Photon H_2O_2-Activated CO Photoreleaser. *Angew. Chem.-Int. Ed.* **2018**, *57* (38), 12415–12419. https://doi.org/10.1002/anie.201805806.
(413) Xu, K.; He, L.; Yang, X.; Yang, Y.; Lin, W. A Ratiometric Fluorescent Hydrogen Peroxide Chemosensor Manipulated by an ICT- Activated FRET Mechanism and Its Bioimaging Application in Living Cells and Zebrafish. *Analyst* **2018**, *143* (15), 3555–3559. https://doi.org/10.1039/c8an00842f.
(414) Wang, J.; Zhu, W.; Niu, G.; Jiang, G.; Chen, Q.; Gao, P.; Li, Y.; Zhang, G.; Fan, X.; Tang, B. Z. Selectively Light-up Hydrogen Peroxide in Hypoxic Cancer Cells with a Novel Fluorescent Probe. *Chem. Commun.* **2018**, *54* (99), 13957–13960. https://doi.org/10.1039/c8cc07771a.
(415) Lim, C. S.; Cho, M. K.; Park, M. Y.; Kim, H. M. A Two-Photon Ratiometric Fluorescent Probe for Imaging of Hydrogen Peroxide Levels in Rat Organ Tissues. *ChemistryOpen* **2018**, *7* (1), 53–56. https://doi.org/10.1002/open.201700155.
(416) Tang, L.; Tian, M.; Chen, H.; Yan, X.; Zhong, K.; Bian, Y. An ESIPT-Based Mitochondria-Targeted Ratiometric and NIR-Emitting Fluorescent Probe for Hydrogen Peroxide and Its Bioimaging in Living Cells. *Dyes Pigments* **2018**, *158*, 482–489. https://doi.org/10.1016/j.dyepig.2017.12.028.
(417) He, L.; Liu, X.; Zhang, Y.; Yang, L.; Fang, Q.; Geng, Y.; Chen, W.; Song, X. A Mitochondria-Targeting Ratiometric Fluorescent Probe for Imaging Hydrogen Peroxide with Long-Wavelength Emission and Large Stokes Shift. *Sens. Actuators B Chem.* **2018**, *276*, 247–253. https://doi.org/10.1016/j.snb.2018.08.119.
(418) Liu, Y.; Bai, L.; Li, Y.; Ni, Y.; Xin, C.; Zhang, C.; Liu, J.; Liu, Z.; Li, L.; Huang, W. Visualizing Hydrogen Peroxide in Parkinson's Disease Models via a Ratiometric NIR Fluorogenic

Probe. *Sens. Actuators B Chem.* **2019**, *279*, 38–43. https://doi.org/10.1016/j.snb.2018.09.107.
(419) Xu, R.; Wang, Y.; You, H.; Zhang, L.; Wang, Y.; Chen, L. A Near-Infrared Fluorescent Probe for Evaluating Endogenous Hydrogen Peroxide during Ischemia/Reperfusion Injury. *Analyst* **2019**, *144* (8), 2556–2564. https://doi.org/10.1039/c9an00243j.
(420) Zhai, B.; Hu, W.; Hao, R.; Ni, W.; Liu, Z. Development of a Ratiometric Two-Photon Fluorescent Probe for Imaging of Hydrogen Peroxide in Ischemic Brain Injury. *Analyst* **2019**, *144* (20), 5965–5970. https://doi.org/10.1039/c9an01326a.
(421) Lee, J.; Yoon, S.; Chun, J.; Kang, C.; Lee, M. A Red-Emitting Styrylnaphthalimide-Based Fluorescent Probe Providing a Ratiometric Signal Change for the Precise and Quantitative Detection of H_2O_2. *Anal. Chim. Acta.* **2019**, *1080*, 153–161. https://doi.org/10.1016/j.aca.2019.07.008.
(422) Wen, Y.; Huo, F.; Wang, J.; Yin, C. Multicolor Fluorescence Based on FRET Regulated by Functional Peptides To Screen High Metastatic Potential Cancer Cells. *Anal. Chem.* **2019**, *91* (23), 15057–15063. https://doi.org/10.1021/acs.analchem.9b03731.
(423) Makau, J. N.; Kitagawa, A.; Kitamura, K.; Yamaguchi, T.; Mizuta, S. Design and Development of an HBT-Based Ratiometric Fluorescent Probe to Monitor Stress-Induced Premature Senescence. *ACS Omega* **2020**, *5* (20), 11299–11307. https://doi.org/10.1021/acsomega.9b04208.
(424) Xie, Y.; Chen, Z.; Hu, L.; Zhang, H.; Xu, P.; Pan, K. A Novel Ratiometric Fluorescent Probe for the Detection of Hydrogen Peroxide in Human Gastric Carcinoma HGC-27 Cells. *Anal. Methods* **2020**, *12* (12), 1567–1569. https://doi.org/10.1039/C9AY02263E.
(425) Wang, C.; Wang, Y.; Wang, G.; Huang, C.; Jia, N. A New Mitochondria-Targeting Fluorescent Probe for Ratiometric Detection of H_2O_2 in Live Cells. *Anal. Chim. Acta.* **2020**, *1097*, 230–237. https://doi.org/10.1016/j.aca.2019.11.024.
(426) Chen, Q.; Cheng, K.; Wang, W.; Yang, L.; Xie, Y.; Feng, L.; Zhang, J.; Zhang, H.; Sun, H. A Pyrene-Based Ratiometric Fluorescent Probe with a Large Stokes Shift for Selective Detection of Hydrogen Peroxide in Living Cells. *J. Pharm. Anal.* **2020**, *10* (5), 490–497. https://doi.org/10.1016/j.jpha.2020.07.003.
(427) Wu, X.; Lin, Q. A Novel Ratiometric Cationic Iridium(III) Complex Phosphorescent Probe for Hydrogen Peroxide. *Anal. Sci.* **2020**, *36* (4), 435–440. https://doi.org/10.2116/analsci.19P383.
(428) Yang, M.; Xia, L.; Zhou, X.; Jia, C.; Ji, M.; Wang, P. A Ratiometric Fluorescent Probe for Imaging Hydrogen Peroxide in Living Cells. *Chin. J. Org. Chem.* **2020**, *40* (9), 2888. https://doi.org/10.6023/cjoc202002030.
(429) Han, J.; Liu, X.; Xiong, H.; Wang, J.; Wang, B.; Song, X.; Wang, W. Investigation of the Relationship Between H_2O_2 and HClO in Living Cells by a Bifunctional, Dual-Ratiometric Responsive Fluorescent Probe. *Anal. Chem.* **2020**, *92* (7), 5134–5142. https://doi.org/10.1021/acs.analchem.9b05604.
(430) Yang, L.; Zhang, Y.; Ren, X.; Wang, B.; Yang, Z.; Song, X.; Wang, W. Fluorescent Detection of Dynamic H_2O_2/H_2S Redox Event in Living Cells and Organisms. *Anal. Chem.* **2020**, *92* (6), 4387–4394. https://doi.org/10.1021/acs.analchem.9b05270.
(431) Cho, S. W.; Jun, Y. W.; Reo, Y. J.; Sarkar, S.; Ahn, K. H. Environment-Insensitive Two-Photon Ratiometric Probe for in Cellulo Quantitative Measurement of Hydrogen Peroxide. *Results Chem.* **2021**, *3*, 100117. https://doi.org/10.1016/j.rechem.2021.100117.
(432) Xu, H.; Zhong, J.; Zhuang, W.; Jiang, J.; Ma, B.; He, H.; Li, G.; Liao, Y.; Wang, Y. A Bifunctional Mitochondrial Targeting AIE-Active Fluorescent Probe with High Sensitivity to Hydrogen Peroxide and Viscosity for Fatty Liver Diagnosis. *New J. Chem.* **2021**, *45* (27), 12138–12144. https://doi.org/10.1039/D1NJ01712H.
(433) Rim Kim, H.; Sarkar, S.; Han Ahn, K. A Two-Photon Ratiometric Sensing Platform Based on Solid-State Luminescent Benzocoumarin: Application to Prolonged Bioimaging of

Hydrogen Peroxide. *Chem. - Asian J.* **2022**, *17* (4), e202101317. https://doi.org/10.1002/asia.202101317.
(434) Grzelakowska, A.; Zielonka, M.; Debowska, K.; Modrzejewska, J.; Szala, M.; Sikora, A.; Zielonka, J.; Podsiadly, R. Two-Photon Fluorescent Probe for Cellular Peroxynitrite: Fluorescence Detection, Imaging, and Identification of Peroxynitrite-Specific Products. *Free Radic. Biol. Med.* **2021**, *169*, 24–35. https://doi.org/10.1016/j.freeradbiomed.2021.04.011.
(435) Yang, G.; Zhu, T.; Wang, D.; Liu, Z.; Zhang, R.; Han, G.; Tian, X.; Liu, B.; Han, M.; Zhang, Z. Revealing the Signaling Regulation of Hydrogen Peroxide to Cell Pyroptosis Using a Ratiometric Fluorescent Probe in Living Cells. *Chem. Commun.* **2021**, *57* (54), 6628–6631. https://doi.org/10.1039/d1cc02008k.
(436) Li, Z.; Ren, T.-B.; Zhang, X.-X.; Xu, S.; Gong, X.-Y.; Yang, Y.; Ke, G.; Yuan, L.; Zhang, X.-B. Precipitated Fluorophore-Based Probe for Accurate Detection of Mitochondrial Analytes. *Anal. Chem.* **2021**, *93* (4), 2235–2243. https://doi.org/10.1021/acs.analchem.0c04094.
(437) Lee, J.; Kim, H. S.; Jangili, P.; Kang, H.-G.; Sharma, A.; Kim, J. S. Fluorescent Probe for Monitoring Hydrogen Peroxide in COX-2-Positive Cancer Cells. *ACS Appl. Bio Mater.* **2021**, *4* (3), 2073–2079. https://doi.org/10.1021/acsabm.0c01135.
(438) Liu, D.; Chen, G.; Fang, G. A Near-Infrared, Colorimetric and Ratiometric Fluorescent Sensor with High Sensitivity to Hydrogen Peroxide and Viscosity for Solutions Detection and Imaging Living Cells. *Bioorganic Chem.* **2022**, *119*, 105513. https://doi.org/10.1016/j.bioorg.2021.105513.
(439) Chen, M.; Liang, Z.; Zeng, G.; Wang, Y.; Mai, Z.; Chen, X.; Wu, G.; Chen, T. An ESIPT-Based NIR-Emitting Ratiometric Fluorescent Probe for Monitoring Hydrogen Peroxide in Living Cells and Zebrafish. *Dyes Pigments* **2022**, *198*, 109995. https://doi.org/10.1016/j.dyepig.2021.109995.
(440) Tian, D.-H.; Liu, J.-R.; Wang, S.-Y.; Yan, S.; Chai, Z.-H.; Dai, F.; Zhang, S.; Zhou, B. Selective Imaging of Hydrogen Peroxide over Peroxynitrite by a Boronate-Based Fluorescent Probe Engineered via a Doubly Activated Electrophilicity-Increasing Strategy. *Sens. Actuators B Chem.* **2022**, *368*, 132149. https://doi.org/10.1016/j.snb.2022.132149.
(441) Chen, M.; Liang, Z.; Fan, X.; Qu, R.; Wang, H.; Chen, T. A Ratiometric ESIPT Fluorescent Probe for Detection of Anticancer-Associated H_2O_2 Level in Vitro and in Vivo. *Spectrochim. Acta. A. Mol. Biomol. Spectrosc.* **2022**, *276*. https://doi.org/10.1016/j.saa.2022.121163.
(442) Wang, Y.; Gao, H.; Gong, C.; Rizvi, S. F. A.; Liu, X.; Shi, X.; Zhang, H.; Wu, L. N-Quaternization of Heterocyclic Compound Extended the Emission to NIR with Large Stokes Shift and Its Application in Constructing Fluorescent Probe. *Spectrochim. Acta. A. Mol. Biomol. Spectrosc.* **2022**, *267*, 120566. https://doi.org/10.1016/j.saa.2021.120566.
(443) Niu, P.; Liu, J.; Xu, F.; Yang, L.; Li, Y.; Sun, A.; Wei, L.; Liu, X.; Song, X. Dual-Ratiometric Fluorescent Probe for H_2O_2 and HClO in Living Cells and Zebrafish and Application in Alcoholic Liver Injury Monitoring. *ACS Appl. Bio Mater.* **2022**, *5* (4), 1683–1691. https://doi.org/10.1021/acsabm.2c00058.
(444) Li, Z.; Xiao, L.; Sun, X.; Luo, C.; Li, R.; Zhang, W.; Wang, Z.; Xiao, H.; Shu, W. An ESIPT-Based Ratiometric Fluorescent Probe for Detecting H_2O_2 in Water Environment and Biosystems. *Sci. Total Environ.* **2023**, *867*, 161609. https://doi.org/10.1016/j.scitotenv.2023.161609.
(445) Feng, Z.; Wu, J.; Liu, W.; Ren, H.; Zheng, X.; Zhang, W.; Lee, C.-S.; Wang, P. A Ratiometric Fluorescent Probe for Single and Two-Photon Bioimaging of Hydrogen Peroxide in Vitro and in Vivo. *Sens. Actuators B Chem.* **2023**, *384*, 133668. https://doi.org/10.1016/j.snb.2023.133668.
(446) Zhu, M.; Wang, T.; Zhang, Y.; Nong, J.; Guo, Z. A Mitochondrial-Targeted Curcumin-Based Fluorescent Probe for Real-Time Tracking Endogenous Hydrogen Peroxide in Living Cells. *Sens. Actuators B Chem.* **2023**, *391*, 134039. https://doi.org/10.1016/j.snb.2023.134039.

(447) Kim, H. M.; Cho, B. R. Mitochondrial-Targeted Two-Photon Fluorescent Probes for Zinc Ions, H_2O_2, and Thiols in Living Tissues. *Oxid. Med. Cell. Longev.* **2013**, https://doi.org/10.1155/2013/323619.
(448) Ren, M.; Deng, B.; Wang, J.-Y.; Kong, X.; Liu, Z.-R.; Zhou, K.; He, L.; Lin, W. A Fast Responsive Two-Photon Fluorescent Probe for Imaging H_2O_2 in Lysosomes with a Large Turn-on Fluorescence Signal. *Biosens. Bioelectron.* **2016**, *79*, 237–243. https://doi.org/10.1016/j.bios.2015.12.046.
(449) Lindberg, E.; Winssinger, N. High Spatial Resolution Imaging of Endogenous Hydrogen Peroxide in Living Cells by Solid-State Fluorescence. *ChemBioChem* **2016**, *17* (17), 1612–1615. https://doi.org/10.1002/cbic.201600211.
(450) Zhang, K.; Wu, W.; Li, Y.; Sun, M.; Yu, H.; Wong, M. S. Carbazole-Based Two-Photon Fluorescent Probe for Selective Imaging of Mitochondrial Hydrogen Peroxide in Living Cells and Tissues. *RSC Adv.* **2016**, *6* (116), 115298–115302. https://doi.org/10.1039/C6RA21260C.
(451) Li, H.; Yao, Q.; Fan, J.; Du, J.; Wang, J.; Peng, X. A Two-Photon NIR-to-NIR Fluorescent Probe for Imaging Hydrogen Peroxide in Living Cells. *Biosens. Bioelectron.* **2017**, *94*, 536–543. https://doi.org/10.1016/j.bios.2017.03.039.
(452) Ma, Q.; Li, X.; Zhang, J.; Zhu, X.; Zhou, L.; Liu, H. A Novel Two-Photon Fluorescent Probe for the Selective Detection of Hydrogen Peroxide Based on a Naphthalene Derivative. *Anal. Methods* **2017**, *9* (31), 4558–4565. https://doi.org/10.1039/C7AY01249G.
(453) Zhou, L.; Peng, Y.; Wang, Q.; Lin, Q. An ESIPT-Based Two-Photon Fluorescent Probe Detection of Hydrogen Peroxide in Live Cells and Tissues. *J. Photochem. Photobiol. B* **2017**, *167*, 264–268. https://doi.org/10.1016/j.jphotobiol.2017.01.011.
(454) Lu, Y.; Shi, X.; Fan, W.; Black, C. A.; Lu, Z.; Fan, C. A Fast-Response Two-Photon Fluorescent Probe for Imaging Endogenous H_2O_2 in Living Cells and Tissues. *Spectrochim. Acta. A. Mol. Biomol. Spectrosc.* **2018**, *190*, 353–359. https://doi.org/10.1016/j.saa.2017.09.034.
(455) Zhou, L.; Ding, H.; Zhao, W.; Hu, S. A Mitochondria Targetable Two-Photon Excited near-Infrared Fluorescent Probe for Imaging of H_2O_2 in Live Cells and Tissues. *Spectrochim. Acta A. Mol. Biomol. Spectrosc.* **2019**, *206*, 529–534. https://doi.org/10.1016/j.saa.2018.08.042.
(456) Murfin, L. C.; Weber, M.; Park, S. J.; Kim, W. T.; Lopez-Alled, C. M.; McMullin, C. L.; Pradaux-Caggiano, F.; Lyall, C. L.; Kociok-Kohn, G.; Wenk, J.; Bull, S. D.; Yoon, J.; Kim, H. M.; James, T. D.; Lewis, S. E. Azulene-Derived Fluorescent Probe for Bioimaging: Detection of Reactive Oxygen and Nitrogen Species by Two-Photon Microscopy. *J. Am. Chem. Soc.* **2019**, *141* (49), 19389–19396. https://doi.org/10.1021/jacs.9b09813.
(457) Wu, Z.; Liu, M.; Liu, Z.; Tian, Y. Real-Time Imaging and Simultaneous Quantification of Mitochondrial H_2O_2 and ATP in Neurons with a Single Two-Photon Fluorescence-Lifetime-Based Probe. *J. Am. Chem. Soc.* **2020**, *142* (16), 7532–7541. https://doi.org/10.1021/jacs.0c00771.
(458) Wang, K.; Ma, W.; Xu, Y.; Liu, X.; Chen, G.; Yu, M.; Pan, Q.; Huang, C.; Li, X.; Mu, Q.; Sun, Y.; Yu, Z. Design of a Novel Mitochondria Targetable Turn-on Fluorescence Probe for Hydrogen Peroxide and Its Two-Photon Bioimaging Applications. *Chin. Chem. Lett.* **2020**, *31* (12), 3149–3152. https://doi.org/10.1016/j.cclet.2020.08.039.
(459) Ren, M.; Dong, D.; Xu, Q.; Yin, J.; Kong, F. A Biotin-Guided Two-Photon Fluorescent Probe for Detection of Hydrogen Peroxide in Cancer Cells Ferroptosis Process. *Talanta* **2021**, *234*. https://doi.org/10.1016/j.talanta.2021.122684.
(460) Grzelakowska, A.; Modrzejewska, J.; Kolinska, J.; Szala, M.; Zielonka, M.; Debowska, K.; Zaklos-Szyda, M.; Sikora, A.; Zielonka, J.; Podsiadly, R. Water-Soluble Cationic Boronate Probe Based on Coumarin Imidazolium Scaffold: Synthesis, Characterization, and

Application to Cellular Peroxynitrite Detection. *Free Radic. Biol. Med.* **2022**, *179*, 34–46. https://doi.org/10.1016/j.freeradbiomed.2021.12.260.
(461) Wang, X.; Ding, Q.; Tian, Y.; Wu, W.; Che, F.; Li, P.; Zhang, W.; Zhang, W.; Tang, B. In Situ Fluorescence Imaging Reveals That Mitochondrial H_2O_2 Mediates Lysosomal Dysfunction in Depression. *Chem. Commun.* **2022**, *58* (43), 6320–6323. https://doi.org/10.1039/d2cc00431c.
(462) Miller, E. W.; Tulyanthan, O.; Isacoff, E. Y.; Chang, C. J. Molecular Imaging of Hydrogen Peroxide Produced for Cell Signaling. *Nat. Chem. Biol.* **2007**, *3*, 263–267. https://doi.org/10.1038/nchembio871.
(463) Dickinson, B. C.; Chang, C. J. A Targetable Fluorescent Probe for Imaging Hydrogen Peroxide in the Mitochondria of Living Cells. *J. Am. Chem. Soc.* **2008**, *130* (30), 9638–9639. https://doi.org/10.1021/ja802355u.
(464) Xiao, H.; Li, P.; Zhang, S.; Zhang, W.; Zhang, W.; Tang, B. Simultaneous Fluorescence Visualization of Mitochondrial Hydrogen Peroxide and Zinc Ions in Live Cells and in Vivo. *Chem. Commun.* **2016**, *52*, 12741–12744. https://doi.org/10.1039/c6cc07182a.
(465) Xiao, H.; Li, P.; Hu, X.; Shi, X.; Zhang, W.; Tang, B. Simultaneous Fluorescence Imaging of Hydrogen Peroxide in Mitochondria and Endoplasmic Reticulum during Apoptosis. *Chem. Sci.* **2016**, *7* (9), 6153–6159. https://doi.org/10.1039/C6SC01793B.
(466) Xu, J.; Zhang, Y.; Yu, H.; Gao, X.; Shao, S. Mitochondria-Targeted Fluorescent Probe for Imaging Hydrogen Peroxide in Living Cells. *Anal. Chem.* **2016**, *88*, 1455–1461. https://doi.org/10.1021/acs.analchem.5b04424.
(467) Liu, Y.; Niu, J.; Nie, J.; Meng, F.; Lin, W. A Mitochondria-Targetable Fluorescent Probe with a Large Stokes Shift for Detecting Hydrogen Peroxide in Aqueous Solution and Living Cells. *New J. Chem.* **2017**, *41* (9), 3320–3325. https://doi.org/10.1039/C7NJ00107J.
(468) Yang, L.; Niu, J.-Y.; Sun, R.; Xu, Y.-J.; Ge, J.-F. Rosamine with Pyronine-Pyridinium Skeleton: Unique Mitochondrial Targetable Structure for Fluorescent Probes. *The Analyst* **2018**, *143* (8), 1813–1819. https://doi.org/10.1039/C7AN02041D.
(469) Liang, X.; Zhang, L.; Xu, X.; Qiao, D.; Shen, T.; Yin, Z.; Shang, L. An ICT-Based Mitochondria-Targeted Fluorescent Probe for Hydrogen Peroxide with a Large Turn-On Fluorescence Signal. *ChemistrySelect* **2019**, *4* (4), 1330–1336. https://doi.org/10.1002/slct.201803185.
(470) Yang, G.; Liu, Z.; Zhang, R.; Tian, X.; Chen, J.; Han, G.; Liu, B.; Han, X.; Fu, Y.; Hu, Z.; Zhang, Z. A Multi-Responsive Fluorescent Probe Reveals Mitochondrial Nucleoprotein Dynamics with Reactive Oxygen Species Regulation through Super-Resolution Imaging. *Angew. Chem. Int. Ed.* **2020**, *59* (37), 16154–16160. https://doi.org/10.1002/anie.202005959.
(471) Li, S.; Wang, P.; Feng, W.; Xiang, Y.; Dou, K.; Liu, Z. Simultaneous Imaging of Mitochondrial Viscosity and Hydrogen Peroxide in Alzheimer's Disease by a Single near-Infrared Fluorescent Probe with a Large Stokes Shift. *Chem. Commun.* **2020**, *56* (7), 1050–1053. https://doi.org/10.1039/c9cc08267k.
(472) Chen, X.; Ren, X.; Zhang, L.; Liu, Z.; Hai, Z. Mitochondria-Targeted Fluorescent and Photoacoustic Imaging of Hydrogen Peroxide in Inflammation. *Anal. Chem.* **2020**, *92* (20), 14244–14250. https://doi.org/10.1021/acs.analchem.0c03506.
(473) Song, X.; Bai, S.; He, N.; Wang, R.; Xing, Y.; Lv, C.; Yu, F. Real-Time Evaluation of Hydrogen Peroxide Injuries in Pulmonary Fibrosis Mice Models with a Mitochondria-Targeted Near-Infrared Fluorescent Probe. *ACS Sens.* **2021**, *6* (3), 1228–1239. https://doi.org/10.1021/acssensors.0c02519.
(474) Xu, J.-Q.; Guo, J.-S.; Xie, K.-F.; Gao, M.-J.; Wei, R.; Xin, Z.-H.; Kang, Y.-F. A Turn-on Mitochondria-Targeted Fluorescent Probe for Detecting and Imaging Hydrogen Peroxide in Vitro and in Vivo. *Dyes Pigments* **2022**, *204*, 110437. https://doi.org/10.1016/j.dyepig.2022.110437.

(475) Zhong, S.; Huang, S.; Feng, B.; Luo, T.; Chu, F.; Zheng, F.; Zhu, Y.; Chen, F.; Zeng, W. An ESIPT-Based AIE Fluorescent Probe to Visualize Mitochondrial Hydrogen Peroxide and Its Application in Living Cells and Rheumatoid Arthritis. *Org. Biomol. Chem.* **2023**, *21* (24), 5063–5071. https://doi.org/10.1039/D3OB00546A.
(476) Ciou, J.-J.; Wu, T.-C.; Chen, Z.-J.; Cheng, B.; Lai, C.-H. A Selective Fluorescent Turn-on Probe for Imaging and Sensing of Hydrogen Peroxide in Living Cells. *Anal. Bioanal. Chem.* **2023**, *415* (20), 4949–4959. https://doi.org/10.1007/s00216-023-04800-w.
(477) Feng, G.; Zhai, P.; Li, Z.; Fan, M.; Jiang, Y.; Qiao, N.; Chen, R.; Tang, S.; Xu, Z.; Wang, X.; Lin, G.; Yang, C.; Ying, M.; Dong, B.; Shao, Y.; Xu, G. In-Situ Construction of Fluorescent Probes for Hydrogen Peroxide Detection in Mitochondria and Lysosomes with on-Demand Modular Assembling and Double Turn-on Features. *Bioorganic Chem.* **2023**, *130*. https://doi.org/10.1016/j.bioorg.2022.106199.
(478) Dickinson, B. C.; Tang, Y.; Chang, Z.; Chang, C. J. A Nuclear-Localized Fluorescent Hydrogen Peroxide Probe for Monitoring Sirtuin-Mediated Oxidative Stress Responses In Vivo. *Chem. Biol.* **2011**, *18* (8), 943–948. https://doi.org/10.1016/j.chembiol.2011.07.005.
(479) Kim, D.; Kim, G.; Nam, S.-J.; Yin, J.; Yoon, J. Visualization of Endogenous and Exogenous Hydrogen Peroxide Using A Lysosome-Targetable Fluorescent Probe. *Sci. Rep.* **2015**, *5*, 8488. https://doi.org/10.1038/srep08488.
(480) Liu, J.; Ren, J.; Bao, X.; Gao, W.; Wu, C.; Zhao, Y. pH-Switchable Fluorescent Probe for Spatially-Confined Visualization of Intracellular Hydrogen Peroxide. *Anal. Chem.* **2016**, *88* (11), 5865–5870. https://doi.org/10.1021/acs.analchem.6b00654.
(481) Liu, J.; Zhou, S.; Ren, J.; Wu, C.; Zhao, Y. A Lysosome-Locating and Acidic pH-Activatable Fluorescent Probe for Visualizing Endogenous H_2O_2 in Lysosomes. *Analyst* **2017**, *142* (23), 4522–4528. https://doi.org/10.1039/c7an01280b.
(482) Zhu, Y.; Zhou, T.; Yang, L.; Yuan, L.; Liang, L.; Xu, P. Revelation of the Dynamic Progression of Hypoxia-Reoxygenation Injury by Visualization of the Lysosomal Hydrogen Peroxide. *Biochem. Biophys. Res. Commun.* **2017**, *486* (4), 904–908. https://doi.org/10.1016/j.bbrc.2017.03.121.
(483) Qiao, D.; Li, L.; Shen, T.; Yang, J.; Chang, H.; Liang, X.; Zhang, L.; Wang, Q.; Liu, N.; Zhao, W.; Shang, L. Establishment of a Customizable Fluorescent Probe Platform for the Organelle-Targeted Bioactive Species Detection. *ACS Sens.* **2020**, *5* (7), 2247–2254. https://doi.org/10.1021/acssensors.0c00992.
(484) Zhou, Z.; Yuan, X.; Long, D.; Liu, M.; Li, K.; Xie, Y. A Pyridine-Si-Rhodamine-Based near-Infrared Fluorescent Probe for Visualizing Reactive Oxygen Species in Living Cells. *Spectrochim. Acta. A. Mol. Biomol. Spectrosc.* **2021**, *246*, 118927. https://doi.org/10.1016/j.saa.2020.118927.
(485) Zhou, R.; Peng, Q.; Wan, D.; Yu, C.; Zhang, Y.; Hou, Y.; Luo, Q.; Li, X.; Zhang, S.; Xie, L.; Ou, P.; Peng, Y. Construction of a Lysosome-Targetable Ratiometric Fluorescent Probe for H_2O_2 Tracing and Imaging in Living Cells and an Inflamed Model. *RSC Adv.* **2021**, *11* (39), 24032–24037. https://doi.org/10.1039/d1ra04026j.
(486) Zhu, N.; Xu, J.; Ma, Q.; Mao, G.; Zhang, J.; Li, L.; Liu, S. A New Lysosome-Targeted Fluorescent Probe for Hydrogen Peroxide Based on a Benzothiazole Derivative. *Methods* **2023**, *215*, 38–45. https://doi.org/10.1016/j.ymeth.2023.05.005.
(487) Mao, W.; Zhu, M.; Yan, C.; Ma, Y.; Guo, Z.; Zhu, W. Rational Design of Ratiometric Near-Infrared Aza-BODIPY-Based Fluorescent Probe for *in Vivo* Imaging of Endogenous Hydrogen Peroxide. *ACS Appl. Bio Mater.* **2020**, *3* (1), 45–52. https://doi.org/10.1021/acsabm.9b00842.
(488) Albers, A. E.; Dickinson, B. C.; Miller, E. W.; Chang, C. J. A Red-Emitting Naphthofluorescein-Based Fluorescent Probe for Selective Detection of Hydrogen Peroxide in Living Cells. *Bioorg. Med. Chem. Lett.* **2008**, *18* (22), 5948–5950. https://doi.org/10.1016/j.bmcl.2008.08.035.

(489) Karton-Lifshin, N.; Segal, E.; Omer, L.; Portnoy, M.; Satchi-Fainaro, R.; Shabat, D. A Unique Paradigm for a Turn-ON Near-Infrared Cyanine-Based Probe: Noninvasive Intravital Optical Imaging of Hydrogen Peroxide. *J. Am. Chem. Soc.* **2011**, *133* (28), 10960–10965. https://doi.org/10.1021/ja203145v.
(490) Redy-Keisar, O.; Kisin-Finfer, E.; Ferber, S.; Satchi-Fainaro, R.; Shabat, D. Synthesis and Use of QCy7-Derived Modular Probes for the Detection and Imaging of Biologically Relevant Analytes. *Nat. Protoc.* **2014**, *9*, 27–36. https://doi.org/10.1038/nprot.2013.166.
(491) Zhang, X.; Zhang, L.; Liu, Y.; Bao, B.; Zang, Y.; Li, J.; Lu, W. A Near-Infrared Fluorescent Probe for Rapid Detection of Hydrogen Peroxide in Living Cells. *Tetrahedron* **2015**, *71* (29), 4842–4845. https://doi.org/10.1016/j.tet.2015.05.025.
(492) Wang, P.; Wang, K.; Chen, D.; Mao, Y.; Gu, Y. A Novel Colorimetric and Near-Infrared Fluorescent Probe for Hydrogen Peroxide Imaging in Vitro and in Vivo. *RSC Adv.* **2015**, *5* (104), 85957–85963. https://doi.org/10.1039/C5RA16827A.
(493) Narayanaswamy, N.; Narra, S.; Nair, R. R.; Saini, D. K.; Kondaiah, P.; Govindaraju, T. Stimuli-Responsive Colorimetric and NIR Fluorescence Combination Probe for Selective Reporting of Cellular Hydrogen Peroxide. *Chem. Sci.* **2016**, *7* (4), 2832–2841. https://doi.org/10.1039/C5SC03488D.
(494) Wang, P.; Wang, K.; Gu, Y. A Highly Selective Fluorescent Turn-on NIR Probe for the Bioimaging of Hydrogen Peroxide in Vitro and in Vivo. *Sens. Actuators B Chem.* **2016**, *228*, 174–179. https://doi.org/10.1016/j.snb.2016.01.025.
(495) Wen, Y.; Xue, F.; Lan, H.; Li, Z.; Xiao, S.; Yi, T. Multicolor Imaging of Hydrogen Peroxide Level in Living and Apoptotic Cells by a Single Fluorescent Probe. *Biosens. Bioelectron.* **2017**, *91*, 115–121. https://doi.org/10.1016/j.bios.2016.12.027.
(496) Green, O.; Gnaim, S.; Blau, R.; Eldar-Boock, A.; Satchi-Fainaro, R.; Shabat, D. Near-Infrared Dioxetane Luminophores with Direct Chemiluminescence Emission Mode. *J. Am. Chem. Soc.* **2017**, *139* (37), 13243–13248. https://doi.org/10.1021/jacs.7b08446.
(497) Chai, X.; Xiao, J.; Li, M.; Wang, C.; An, H.; Li, C.; Li, Y.; Zhang, D.; Cui, X.; Wang, T. Bridge-Caging Strategy in Phosphorus-Substituted Rhodamine for Modular Development of Near-Infrared Fluorescent Probes. *Chem. - Eur. J.* **2018**, *24* (54), 14506–14512. https://doi.org/10.1002/chem.201802875.
(498) Zhang, L.; Qian, M.; Xia, J.; Chen, L.; Cui, H.; Xia, Y.; Xu, L.; Wang, J.; Peng, X. A NIR Fluorescent Sensor with Large Stokes Shift for the Real-Time Visualization of Endogenous Hydrogen Peroxide in Living Cells. *J. Photochem. Photobiol. Chem.* **2019**, *370*, 12–17. https://doi.org/10.1016/j.jphotochem.2018.10.030.
(499) Weber, J.; Bollepalli, L.; Belenguer, A.; Di Antonio, M.; De Mitri, N.; Joseph, J.; Balasubramanian, S.; Hunter, C.; Bohndiek, S. An Activatable Cancer-Targeted Hydrogen Peroxide Probe for Photoacoustic and Fluorescence Imaging. *Cancer Res.* **2019**, *79* (20), 5407–5417. https://doi.org/10.1158/0008-5472.CAN-19-0691.
(500) Diao, Q.; Guo, H.; Yang, Z.; Luo, W.; Li, T.; Hou, D. Design of a Nile Red-Based NIR Fluorescent Probe for the Detection of Hydrogen Peroxide in Living Cells. *Spectrochim. Acta. A. Mol. Biomol. Spectrosc.* **2019**, *223*, 117284. https://doi.org/10.1016/j.saa.2019.117284.
(501) Zhang, J.; Shi, L.; Li, Z.; Li, D.; Tian, X.; Zhang, C. Near-Infrared Fluorescence Probe for Hydrogen Peroxide Detection: Design, Synthesis, and Application in Living Systems. *Analyst* **2019**, *144* (11), 3643–3648. https://doi.org/10.1039/c9an00385a.
(502) Wang, T.; Yang, X.; Men, J.; Zhou, J.; Zhang, H. A Near-Infrared Fluorescent Probe Based on Boric Acid Hydrolysis for Hydrogen Peroxide Detection and Imaging in HeLa Cells. *Luminescence* **2020**, *35* (2), 208–214. https://doi.org/10.1002/bio.3715.
(503) Yan, Y.; Liu, L.; Li, C.; Yang, Z.; Yi, T.; Hua, J. A NIR Fluorescent Probe Based on Phenazine with a Large Stokes Shift for the Detection and Imaging of Endogenous H_2O_2 in RAW 264.7 Cells. *Analyst* **2020**, *145* (12), 4196–4203. https://doi.org/10.1039/d0an00153h.

(504) Bi, X.; Wang, Y.; Wang, D.; Liu, L.; Zhu, W.; Zhang, J.; Zha, X. A Mitochondrial-Targetable Dual Functional near-Infrared Fluorescent Probe to Monitor pH and H_2O_2 in Living Cells and Mice. *RSC Adv.* **2020**, *10* (45), 26874–26879. https://doi.org/10.1039/D0RA03905E.
(505) Liang, T.; Zhang, D.; Hu, W.; Tian, C.; Zeng, L.; Wu, T.; Lei, D.; Qiang, T.; Yang, X.; Sun, X. A Dual Lock-and-Key Two Photon Fluorescence Probe in Response to Hydrogen Peroxide and Viscosity: Application in Cellular Imaging and Inflammation Therapy. *Talanta* **2021**, *235*. https://doi.org/10.1016/j.talanta.2021.122719.
(506) Gong, Y.; Feng, D.; Liu, W.; Fang, J.; Feng, S. A Self-Immolative near-Infrared Probe Based on Hemi-Benzothiazolecyanine for Visualizing Hydrogen Peroxide in Living Cells and Mice. *Dyes Pigments* **2021**, *186*, 108954. https://doi.org/10.1016/j.dyepig.2020.108954.
(507) Gardner, S. H.; Brady, C. J.; Keeton, C.; Yadav, A. K.; Mallojjala, S. C.; Lucero, M. Y.; Su, S.; Yu, Z.; Hirschi, J. S.; Mirica, L. M.; Chan, J. A General Approach to Convert Hemicyanine Dyes into Highly Optimized Photoacoustic Scaffolds for Analyte Sensing. *Angew. Chem. Int. Ed.* **2021**, *60* (34), 18860–18866. https://doi.org/10.1002/anie.202105905.
(508) Wang, W.; Jiang, W.; Mao, G.; Tan, Z.; Tan, M.; Li, C. A Novel Near-Infrared Theranostic Probe for Accurate Cancer Chemotherapy in Vivo by a Dual Activation Strategy. *Chem. Commun.* **2021**, *57* (100), 13768–13771. https://doi.org/10.1039/d1cc05864a.
(509) Li, X.; Zhao, Y.; Zheng, J.; Zhang, T. Boron Dipyrromethene-Based near-Infrared Fluorescent Probe for the Selective Imaging and Analyzing Hydrogen Peroxide in Living Cells. *J. Lumin.* **2021**, *229*, 117642. https://doi.org/10.1016/j.jlumin.2020.117642.
(510) Wang, W.; Jiang, W.; Mao, G.; Tan, M.; Fei, J.; Li, Y.; Li, C. Monitoring the Fluctuation of Hydrogen Peroxide in Diabetes and Its Complications with a Novel Near-Infrared Fluorescent Probe. *Anal. Chem.* **2021**, *93* (6), 3301–3307. https://doi.org/10.1021/acs.analchem.0c05364.
(511) Lv, X.; Han, T.; Wu, Y.; Zhang, B.; Guo, W. Improving the Fluorescence Brightness of Distyryl Bodipys by Inhibiting the Twisted Intramolecular Charge Transfer Excited State. *Chem. Commun.* **2021**, *57* (76), 9744–9747. https://doi.org/10.1039/d1cc03360c.
(512) Yu, W.; Huang, J.; Lin, M.; Wei, G.; Yang, F.; Tang, Z.; Zeng, F.; Wu, S. Fluorophore-Dapagliflozin Dyad for Detecting Diabetic Liver/Kidney Damages via Fluorescent Imaging and Treating Diabetes via Inhibiting SGLT2. *Anal. Chem.* **2021**, *93* (10), 4647–4656. https://doi.org/10.1021/acs.analchem.1c00223.
(513) Chunpo, G.; Yan, Y.; Pengfei, T.; Hu, S.; Yibo, J.; Yuyang, S.; Yun, Y.; Feng, R. A NIR Fluorescent Probe for the in Vitro and in Vivo Selective Detection of Hydrogen Peroxide. *Sens. Actuators B Chem.* **2022**, *350*, 130831. https://doi.org/10.1016/j.snb.2021.130831.
(514) Gao, M.-J.; Hua, Y.; Xu, J.-Q.; Zhang, L.-X.; Wang, S.; Kang, Y.-F. Near-Infrared Fluorescence Probe with a Large Stokes Shift for Selectively Imaging of Hydrogen Peroxide in Living Cells and in Vivo. *Dyes Pigments* **2022**, *197*, 109930. https://doi.org/10.1016/j.dyepig.2021.109930.
(515) Bolland, H. R.; Hammond, E. M.; Sedgwick, A. C. A Fluorescent Probe Strategy for the Detection and Discrimination of Hydrogen Peroxide and Peroxynitrite in Cells. *Chem. Commun.* **2022**, *58* (76), 10699–10702. https://doi.org/10.1039/d2cc03406a.
(516) Hao, Y.; Li, Z.; Ding, N.; Tang, X.; Zhang, C. A New Near-Infrared Fluorescence Probe Synthesized from IR-783 for Detection and Bioimaging of Hydrogen Peroxide in Vitro and in Vivo. *Spectrochim. Acta. A. Mol. Biomol. Spectrosc.* **2022**, *268*. https://doi.org/10.1016/j.saa.2021.120642.
(517) Peng, H.; Wang, T.; Li, G.; Huang, J.; Yuan, Q. Dual-Locked Near-Infrared Fluorescent Probes for Precise Detection of Melanoma via Hydrogen Peroxide-Tyrosinase Cascade Activation. *Anal. Chem.* **2022**, *94* (2), 1070–1075. https://doi.org/10.1021/acs.analchem.1c04058.

(518) An, B.; Pang, S.; Zhang, Y.; Wei, N. A Novel Near-Infrared Fluorescent Probe for Visualization of Intracellular Hydrogen Peroxide. *Front. Chem.* **2022**, *10*, 1025723. https://doi.org/10.3389/fchem.2022.1025723.
(519) Liu, X.; Yan, M.; Chen, Z.; Zhang, B.; Yao, N.; Zhao, S.; Zhao, X.; Zhang, T.; Hai, G. A Dual-Site Multifunctional Fluorescent Probe for Selective Detection of Endogenous H_2O_2 and SO2 Derivatives Based on ICT Process and Its Bioimaging Application. *Spectrochim. Acta. A. Mol. Biomol. Spectrosc.* **2023**, *286*. https://doi.org/10.1016/j.saa.2022.121955.
(520) Gao, J.; Wang, R.; Yin, K.; Zhu, T.; Sun, J.; Dong, C.; Dong, X.; Zhao, M.; Gu, X.; Zhao, C. Visualizing Hydrogen Peroxide and Hydrogen Sulfide Fluctuations in Living Cells via Dynamic-Reversible Fluorescent Probes. *Chem. Eng. J.* **2023**, *466*, 143102. https://doi.org/10.1016/j.cej.2023.143102.
(521) Wu, Y.; Jing, F.; Huang, H.; Wang, H.; Chen, S.; Fan, W.; Li, Y.; Wang, L.; Wang, Y.; Hou, S. A Near-Infrared Fluorescent Probe for Tracking Endogenous and Exogenous H_2O_2 in Cells and Zebrafish. *Spectrochim. Acta. A. Mol. Biomol. Spectrosc.* **2023**, *302*, 123158. https://doi.org/10.1016/j.saa.2023.123158.
(522) Zhou, Y.; Liu, T.; Lin, P.; Yuan, X.; Luo, K.; Xie, C.; Zhou, L. Fluorescence Probes Evaluated the Hydrogen Peroxide Level in Rice Roots under Cadmium Ion Stress. *Spectrochim. Acta. A. Mol. Biomol. Spectrosc.* **2023**, *303*, 123178. https://doi.org/10.1016/j.saa.2023.123178.
(523) Van de Bittner, G. C.; Dubikovskaya, E. a; Bertozzi, C. R.; Chang, C. J. In Vivo Imaging of Hydrogen Peroxide Production in a Murine Tumor Model with a Chemoselective Bioluminescent Reporter. *Proc. Natl. Acad. Sci. U.S.A.* **2010**, *107* (50), 21316. https://doi.org/10.1073/pnas.1012864107.
(524) O'Sullivan, J. J.; Heffern, M. C. Development of an ATP-Independent Bioluminescent Probe for Detection of Extracellular Hydrogen Peroxide. *Org. Biomol. Chem.* **2022**, *20* (31), 6231–6238. https://doi.org/10.1039/d2ob00436d.
(525) Seven, O.; Sozmen, F.; Simsek Turan, I. Self Immolative Dioxetane Based Chemiluminescent Probe for H_2O_2 Detection. *Sens. Actuators B Chem.* **2017**, *239*, 1318–1324. https://doi.org/10.1016/j.snb.2016.09.120.
(526) Green, O.; Eilon, T.; Hananya, N.; Gutkin, S.; Bauer, C. R.; Shabat, D. Opening a Gateway for Chemiluminescence Cell Imaging: Distinctive Methodology for Design of Bright Chemiluminescent Dioxetane Probes. *ACS Cent. Sci.* **2017**, *3* (4), 349–358. https://doi.org/10.1021/acscentsci.7b00058.
(527) Calabria, D.; Guardigli, M.; Mirasoli, M.; Punzo, A.; Porru, E.; Zangheri, M.; Simoni, P.; Pagnotta, E.; Ugolini, L.; Lazzeri, L.; Caliceti, C.; Roda, A. Selective Chemiluminescent TURN-ON Quantitative Bioassay and Imaging of Intracellular Hydrogen Peroxide in Human Living Cells. *Anal. Biochem.* **2020**, *600*, 113760. https://doi.org/10.1016/j.ab.2020.113760.
(528) Gnaim, S.; Shabat, D. Chemiluminescence Molecular Probe with a Linear Chain Reaction Amplification Mechanism. *Org. Biomol. Chem.* **2019**, *17* (6), 1389–1394. https://doi.org/10.1039/c8ob03042a.
(529) Zhang, X.; Chen, Y.; He, H.; Wang, S.; Lei, Z.; Zhang, F. ROS/RNS and Base Dual Activatable Merocyanine-Based NIR-II Fluorescent Molecular Probe for in Vivo Biosensing. *Angew. Chem. Int. Ed.* **2021**, *60* (50), 26337–26341. https://doi.org/10.1002/anie.202109728.
(530) Tian, Y.; Liu, S.; Cao, W.; Wu, P.; Chen, Z.; Xiong, H. H_2O_2 -Activated NIR-II Fluorescent Probe with a Large Stokes Shift for High-Contrast Imaging in Drug-Induced Liver Injury Mice. *Anal. Chem.* **2022**, *94* (32), 11321–11328. https://doi.org/10.1021/acs.analchem.2c02052.
(531) Zeng, C.; Ouyang, J.; Sun, L.; Zeng, Z.; Tan, Y.; Zeng, F.; Wu, S. An Activatable Probe for Detection and Therapy of Food-Additive-Related Hepatic Injury via NIR-II Fluorescence/Optoacoustic Imaging and Biomarker-Triggered Drug Release. *Anal. Chim. Acta.* **2022**, *1208*. https://doi.org/10.1016/j.aca.2022.339831.

(532) Maeda, H.; Fukuyasu, Y.; Yoshida, S.; Fukuda, M.; Saeki, K.; Matsuno, H.; Yamauchi, Y.; Yoshida, K.; Hirata, K.; Miyamoto, K. Fluorescent Probes for Hydrogen Peroxide Based on a Non-Oxidative Mechanism. *Angew. Chem. Int. Ed.* **2004**, *43* (18), 2389–2391. https://doi.org/10.1002/anie.200452381.
(533) Xu, K.; Tang, B.; Huang, H.; Yang, G.; Chen, Z.; Li, P.; An, L. Strong Red Fluorescent Probes Suitable for Detecting Hydrogen Peroxide Generated by Mice Peritoneal Macrophages. *Chem. Commun.* **2005**, 5974–5976. https://doi.org/10.1039/b512440a.
(534) Xu, K.; Liu, F.; Wang, H.; Wang, S.; Wang, L.; Tang, B. Sulfonate-Based Fluorescent Probes for Imaging Hydrogen Peroxide in Living Cells. *Sci. China Ser. B Chem.* **2009**, *52* (6), 734–740. https://doi.org/10.1007/s11426-009-0109-9.
(535) Hu, L.; Liu, J.; Zhang, J.; Zhang, H.; Xu, P.; Chen, Z.; Xiao, E. A Novel Ratiometric Fluorescent Probe for Rapid Detection of Hydrogen Peroxide in Living Cells. *RSC Adv.* **2019**, *9* (67), 39532–39535. https://doi.org/10.1039/C9RA07517H.
(536) Guo, H.; Chen, G.; Gao, M.; Wang, R.; Liu, Y.; Yu, F. Imaging of Endogenous Hydrogen Peroxide during the Process of Cell Mitosis and Mouse Brain Development with a Near-Infrared Ratiometric Fluorescent Probe. *Anal. Chem.* **2019**, *91* (1), 1203–1210. https://doi.org/10.1021/acs.analchem.8b05326.
(537) Su, J.; Zhang, S.; Wang, C.; Li, M.; Wang, J.; Su, F.; Wang, Z. A Fast and Efficient Method for Detecting H $_2$ O $_2$ by a Dual-Locked Model Chemosensor. *ACS Omega* **2021**, *6* (23), 14819–14823. https://doi.org/10.1021/acsomega.1c00384.
(538) Abo, M.; Urano, Y.; Hanaoka, K.; Terai, T.; Komatsu, T.; Nagano, T. Development of a Highly Sensitive Fluorescence Probe for Hydrogen Peroxide. *J. Am. Chem. Soc.* **2011**, *133* (27), 10629–10637. https://doi.org/10.1021/ja203521e.
(539) Zhang, K.-M.; Dou, W.; Li, P.-X.; Shen, R.; Ru, J.-X.; Liu, W.; Cui, Y.-M.; Chen, C.-Y.; Liu, W.-S.; Bai, D.-C. A Coumarin-Based Two-Photon Probe for Hydrogen Peroxide. *Biosens. Bioelectron.* **2015**, *64*, 542–546. https://doi.org/10.1016/j.bios.2014.09.073.
(540) Li, B.; Chen, J.-B.; Xiong, Y.; Yang, X.; Zhao, C.; Sun, J. Development of Turn-on Fluorescent Probes for the Detection of H_2O_2 Vapor with High Selectivity and Sensitivity. *Sens. Actuators B Chem.* **2018**, *268*, 475–484. https://doi.org/10.1016/j.snb.2018.04.140.
(541) Purdey, M. S.; McLennan, H. J.; Sutton-McDowall, M. L.; Drumm, D. W.; Zhang, X.; Capon, P. K.; Heng, S.; Thompson, J. G.; Abell, A. D. Biological Hydrogen Peroxide Detection with Aryl Boronate and Benzil BODIPY-Based Fluorescent Probes. *Sens. Actuators B Chem.* **2018**, *262*, 750–757. https://doi.org/10.1016/j.snb.2018.01.198.
(542) Xie, X.; Yang, X.; Wu, T.; Li, Y.; Li, M.; Tan, Q.; Wang, X.; Tang, B. Rational Design of an α-Ketoamide-Based Near-Infrared Fluorescent Probe Specific for Hydrogen Peroxide in Living Systems. *Anal. Chem.* **2016**, *88* (16), 8019–8025. https://doi.org/10.1021/acs.analchem.6b01256.
(543) Cheng, D.; Xu, W.; Yuan, L.; Zhang, X. Investigation of Drug-Induced Hepatotoxicity and Its Remediation Pathway with Reaction-Based Fluorescent Probes. *Anal. Chem.* **2017**, *89* (14), 7693–7700. https://doi.org/10.1021/acs.analchem.7b01671.
(544) Peng, J.; Hou, X.; Zeng, F.; Wu, S. Fluorescent Nanoprobe for In-Vivo Ratiometric Imaging of Endogenous Hydrogen Peroxide Resulted from Drug-Induced Organ Damages. *Biosens. Bioelectron.* **2017**, *94*, 278–285. https://doi.org/10.1016/j.bios.2017.03.003.
(545) Gao, C.; Tian, Y.; Zhang, R.; Jing, J.; Zhang, X. Endoplasmic Reticulum-Directed Ratiometric Fluorescent Probe for Quantitive Detection of Basal H_2O_2. *Anal. Chem.* **2017**, *89* (23), 12945–12950. https://doi.org/10.1021/acs.analchem.7b03809.
(546) Huang, X.; Li, Z.; Liu, Z.; Zeng, C.; Hu, L. A Near-Infrared Fluorescent Probe for Endogenous Hydrogen Peroxide Real-Time Imaging in Living Cells and Zebrafish. *Dyes Pigments* **2019**, *165*, 518–523. https://doi.org/10.1016/j.dyepig.2019.02.042.
(547) Gu, T.; Mo, S.; Mu, Y.; Huang, X.; Hu, L. Detection of Endogenous Hydrogen Peroxide in Living Cells with Para-Nitrophenyl Oxoacetyl Rhodamine as Turn-on Mitochondria-

Targeted Fluorescent Probe. *Sens. Actuators B Chem.* **2020**, *309*, 127731. https://doi.org/10.1016/j.snb.2020.127731.
(548) Chen, J.; Chen, L.; Wu, Y.; Fang, Y.; Zeng, F.; Wu, S.; Zhao, Y. A(2)O(2)-Activatable Nanoprobe for Diagnosing Interstitial Cystitis and Liver Ischemia-Reperfusion Injury via Multispectral Optoacoustic Tomography and NIR-II Fluorescent Imaging. *Nat. Commun.* **2021**, *12* (1). https://doi.org/10.1038/s41467-021-27233-4.
(549) Wang, S.; Zhang, Y.; Wang, T.; Liu, Y.; Shen, S.; Cao, X. A Near-Infrared Fluorescent Probe Based on the Hemicyanine Skeleton for the Detection of Hydrogen Peroxide in Vivo. *Spectrochim. Acta. A. Mol. Biomol. Spectrosc.* **2022**, *266*. https://doi.org/10.1016/j.saa.2021.120435.
(550) Hitomi, Y.; Takeyasu, T.; Funabiki, T.; Kodera, M. Detection of Enzymatically Generated Hydrogen Peroxide by Metal-Based Fluorescent Probe. *Anal. Chem.* **2011**, *83* (24), 9213–9216. https://doi.org/10.1021/ac202534g.
(551) Hitomi, Y.; Takeyasu, T.; Kodera, M. Iron Complex-Based Fluorescent Probes for Intracellular Hydrogen Peroxide Detection. *Chem. Commun.* **2013**, *49*, 9929–9931. https://doi.org/10.1039/c3cc44471f.
(552) Albers, A. E.; Rawls, K. A.; Chang, C. J. Activity-Based Fluorescent Reporters for Monoamine Oxidases in Living Cells. *Chem. Commun.* **2007**, No. 44, 4647. https://doi.org/10.1039/b713190a.
(553) Hitomi, Y.; Takeyasu, T.; Kodera, M. Development of Green-Emitting Iron Complex-Based Fluorescent Probes for Intracellular Hydrogen Peroxide Imaging. *Bull. Chem. Soc. Jpn.* **2014**, *87* (7), 819–824. https://doi.org/10.1246/bcsj.20140055.
(554) Song, D.; Lim, J. M.; Cho, S.; Park, S.-J.; Cho, J.; Kang, D.; Rhee, S. G.; You, Y.; Nam, W. A Fluorescence Turn-on H_2O_2 Probe Exhibits Lysosome-Localized Fluorescence Signals. *Chem. Commun.* **2012**, *48*, 5449–5451. https://doi.org/10.1039/c2cc31632c.
(555) Yang, X.; Zhao, P.; Qu, J.; Liu, R. Fluorescent Sensors Based on Quinoline-Containing Styrylcyanine: Determination of Ferric Ions, Hydrogen Peroxide, and Glucose, pH-Sensitive Properties and Bioimaging. *Luminescence* **2015**, *30*, 592–599. https://doi.org/10.1002/bio.2791.
(556) Miller, E. W.; Bian, S. X.; Chang, C. J. A Fluorescent Sensor for Imaging Reversible Redox Cycles in Living Cells. *J. Am. Chem. Soc.* **2007**, *129* (12), 3458–3459. https://doi.org/10.1021/ja0668973.
(557) Xu, K.; Qiang, M.; Gao, W.; Su, R.; Li, N.; Gao, Y.; Xie, Y.; Kong, F.; Tang, B. A Near-Infrared Reversible Fluorescent Probe for Real-Time Imaging of Redox Status Changes in Vivo. *Chem. Sci.* **2013**, *4* (3), 1079. https://doi.org/10.1039/c2sc22076h.
(558) Liao, Y.-X.; Li, K.; Wu, M.-Y.; Wu, T.; Yu, X.-Q. A Selenium-Contained Aggregation-Induced "Turn-on" Fluorescent Probe for Hydrogen Peroxide. *Org. Biomol. Chem.* **2014**, *12*, 3004–3008. https://doi.org/10.1039/c4ob00206g.
(559) Zhang, C.; Nie, S.; Ding, Y.; Liu, C.; Zhang, Y.; Zhang, Y.; Guo, J. A 3-Position Modified Naphthalimide Fluorescent Probe for Reversible Response to H_2O_2 and GSH and Cell Imaging. *J. Iran. Chem. Soc.* **2023**. https://doi.org/10.1007/s13738-023-02867-x.
(560) Pham, D.; Basu, U.; Pohorilets, I.; St Croix, C. M.; Watkins, S. C.; Koide, K. Fluorogenic Probe Using a Mislow-Evans Rearrangement for Real-Time Imaging of Hydrogen Peroxide. *Angew. Chem. Int. Ed.* **2020**, *59* (40), 17435–17441. https://doi.org/10.1002/anie.202007104.
(561) Shanmugapriya, J.; Rajaguru, K.; Sivaraman, G.; Muthusubramanian, S.; Bhuvanesh, N. Boranil Dye Based "Turn-on" Fluorescent Probes for Detection of Hydrogen Peroxide and Their Cell Imaging Application. *RSC Adv.* **2016**, *6* (89), 85838–85843. https://doi.org/10.1039/C6RA17863D.
(562) Griesbeck, A. G.; Öngel, B.; Atar, M. New Phthalimide-Methionine Dyad-Based Fluorescence Probes for Reactive Oxygen Species: Singlet Oxygen, Hydrogen Peroxide,

and Hypochlorite. *J. Phys. Org. Chem.* **2017**, *30* (9), e3741. https://doi.org/10.1002/poc.3741.
(563) Chen, Y.; Zhu, W.-J.; Wei, X.-R.; Xu, Y.-J.; Sun, R.; Ge, J.-F. Near-Infrared and Lysosome-Targetable Fluorescent Probe Based on Phenoxazinium for Hydrogen Peroxide Detection. *Anal. Methods* **2018**, *10* (30), 3754–3758. https://doi.org/10.1039/C8AY01403E.
(564) Kaur, M.; Yang, D. S.; Choi, K.; Cho, M. J.; Choi, D. H. A Fluorescence Turn-on and Colorimetric Probe Based on a Diketopyrrolopyrrole–Tellurophene Conjugate for Efficient Detection of Hydrogen Peroxide and Glutathione. *Dyes Pigments* **2014**, *100*, 118–126. https://doi.org/10.1016/j.dyepig.2013.09.001.
(565) Wang, Y.; Chen, R.-X.; Tian, R.; Li, Y.; Guo, Z.; Fang, Y.; Zhang, Q.; Chen, S.; Wang, K.-P.; Hu, Z.-Q. A Mitochondria-Targeted Fluorescent Probe for Real-Time Imaging SO_2/ H_2O_2. *Spectrochim. Acta. A. Mol. Biomol. Spectrosc.* **2021**, *262*, 120134. https://doi.org/10.1016/j.saa.2021.120134.
(566) Qi, H.; Zhao, X.; Tang, Y.; Qian, M.; Gao, H.; Qi, H. Cyclometalated Iridium Complex as Off-On-Off Reversible Photoluminescence Probe for Redox Cycle HSO_3^-/ H_2O_2 in Living Cells. *Appl. Spectrosc.* **2019**, *73* (11), 1292–1298. https://doi.org/10.1177/0003702819861573.
(567) Wang, Y.; Zhou, F.; Meng, Q.; Zhang, S.; Jia, H.; Wang, C.; Zhang, R.; Zhang, Z. A Novel Fluorescence Probe for the Reversible Detection of Bisulfite and Hydrogen Peroxide Pair in Vitro and in Vivo. *Chem.- Asian J.* **2021**, *16* (21), 3419–3426. https://doi.org/10.1002/asia.202100926.
(568) Fang, Y.; Wang, J.; Yu, H.; Zhang, Q.; Chen, S.; Wang, K.-P.; Hu, Z.-Q. A Sequential Dual-Key-Dual-Lock Fluorescent Probe for Detection of SO_2 and H_2O_2 in Cells and Mice. *Sens. Actuators B Chem.* **2022**, *371*, 132514. https://doi.org/10.1016/j.snb.2022.132514.
(569) Li, Y.; Huang, Y.; Sun, X.; Zhong, K.; Tang, L. An AIE Mechanism-Based Fluorescent Probe for Relay Recognition of HSO3−/ H_2O_2 and Its Application in Food Detection and Bioimaging. *Talanta* **2023**, *258*, 124412. https://doi.org/10.1016/j.talanta.2023.124412.
(570) Tian, L.; Sun, X.; Zhou, L.; Zhong, K.; Li, S.; Yan, X.; Tang, L. Reversible Colorimetric and NIR Fluorescent Probe for Sensing SO_2/H_2O_2 in Living Cells and Food Samples. *Food Chem.* **2023**, *407*, 135031. https://doi.org/10.1016/j.foodchem.2022.135031.
(571) Ye, S.; Hu, J. J.; Yang, D. Tandem Payne/Dakin Reaction: A New Strategy for Hydrogen Peroxide Detection and Molecular Imaging. *Angew. Chem.* **2018**, *130* (32), 10330–10334. https://doi.org/10.1002/ange.201805162.
(572) Ye, S.; Hananya, N.; Green, O.; Chen, H.; Zhao, A.; Shen, J.; Shabat, D.; Yang, D. A Highly Selective and Sensitive Chemiluminescent Probe for Real-Time Monitoring of Hydrogen Peroxide in Cells and Animals. *Angew. Chem.-Int. Ed.* **2020**, *59* (34), 14326–14330. https://doi.org/10.1002/anie.202005429.
(573) Ye, S.; Hu, J. J.; Zhao, Q. A.; Yang, D. Fluorescent Probes for *in Vitro* and *in Vivo* Quantification of Hydrogen Peroxide. *Chem. Sci.* **2020**, *11* (44), 11989–11997. https://doi.org/10.1039/D0SC04888G.
(574) Wu, F.; Yu, H.; Wang, Q.; Zhang, J.; Li, Z.; Yang, X.-F. Development of a Coumarin-Based Fluorescent Probe for Hydrogen Peroxide Based on the Payne/Dakin Tandem Reaction. *Dyes Pigments* **2021**, *190*, 109335. https://doi.org/10.1016/j.dyepig.2021.109335.
(575) Maeda, H.; Matsu-ura, S.; Nishida, M.; Yamauchi, Y.; Ohmori, H. Assessment of Acyl Groups and Reaction Conditions in the Competition between Perhydrolysis and Hydrolysis of Acyl Resorufins for Developing an Indicator Reaction for Fluorometric Analysis of Hydrogen Peroxide. *Chem. Pharm. Bull.* **2002**, *50* (2), 169–174. https://doi.org/10.1248/cpb.50.169.
(576) Murale, D. P.; Liew, H.; Suh, Y.-H.; Churchill, D. G. Mercuric-Triggered Hydrogen Peroxide “Turn-on” Fluorescence Detection in Neuronal Cells with Novel Fluorescein-Based Probe Obtained in One Pot. *Anal. Methods* **2013**, *5* (11), 2650. https://doi.org/10.1039/c3ay40296g.

(577) Zhan, F.; Yang, Q.; Wang, Q.; Zhang, Q.; Zhuang, Z.; Feng, X.; Zhang, G.; Zheng, G. An Extremely Rapid-Response Fluorescent Probe for Hydrogen Peroxide and Its Application in Living Cells. *RSC Adv.* **2016**, *6* (92), 89940–89943. https://doi.org/10.1039/C6RA12984F.
(578) Zeng, X.; Jiang, C.; Zhang, Q.; Chai, D.; Ma, M.; Chen, J.; Liu, Z. A Novel Simple Fluorescent Probe for the Detection of Hydrogen Peroxide in Vivo with High Selectivity. *J. Lumin.* **2021**, *240*, 118422. https://doi.org/10.1016/j.jlumin.2021.118422.
(579) Mao, C.; Tian, Y.; Wang, S.; Wang, B.; Liu, X. New Strategy for Detection of Hydrogen Peroxide Based on Bi-Nucleophilic Reaction. *Spectrochim. Acta. A. Mol. Biomol. Spectrosc.* **2021**, *262*, 120131. https://doi.org/10.1016/j.saa.2021.120131.
(580) Li, Y.; Zhou, Y.; Lei, J.; Lu, Q.; Qin, X.; Xu, Q.; Wang, Y.; Wu, C.; Yang, Z.; He, B. A NIR Fluorescent Probe for the Selective Detection of Hydrogen Peroxide by Acetyl-Hydrolyzing in Cells. *J. Mol. Struct.* **2023**, *1271*, 134042. https://doi.org/10.1016/j.molstruc.2022.134042.
(581) Lippert, A. R.; Gschneidtner, T.; Chang, C. J. Lanthanide-Based Luminescent Probes for Selective Time-Gated Detection of Hydrogen Peroxide in Water and in Living Cells. *Chem. Commun.* **2010**, *46* (40), 7510. https://doi.org/10.1039/c0cc01560a.
(582) Ye, Z.; Chen, J.; Wang, G.; Yuan, J. Development of Terbium Complex-Based Luminescent Probe for Imaging Endogenous Hydrogen Peroxide Generation in Plant Tissues. *Anal. Chem.* **2011**, *83* (11), 4163–4169. https://doi.org/10.1021/ac200438g.
(583) Wolfbeis, O. S.; Dürkop, A.; Wu, M.; Lin, Z. A Europium-Ion-Based Luminescent Sensing Probe for Hydrogen Peroxide. *Angew. Chem. Int. Ed.* **2002**, *41* (23), 4495–4498. https://doi.org/10.1002/1521-3773(20021202)41:23<4495::AID-ANIE4495>3.0.CO;2-I.
(584) Dürkop, A.; Wolfbeis, O. S. Nonenzymatic Direct Assay of Hydrogen Peroxide at Neutral pH Using the Eu3Tc Fluorescent Probe. *J. Fluoresc.* **2005**, *15* (5), 755–761. https://doi.org/10.1007/s10895-005-2984-6.
(585) Zscharnack, K.; Kreisig, T.; Prasse, A. A.; Zuchner, T. A Luminescence-Based Probe for Sensitive Detection of Hydrogen Peroxide in Seconds. *Anal. Chim. Acta* **2014**, *834*, 51–57. https://doi.org/10.1016/j.aca.2014.05.019.
(586) Dong, B.; Song, X.; Kong, X.; Wang, C.; Tang, Y.; Liu, Y.; Lin, W. Simultaneous Near-Infrared and Two-Photon In Vivo Imaging of H_2O_2 Using a Ratiometric Fluorescent Probe Based on the Unique Oxidative Rearrangement of Oxonium. *Adv. Mater.* **2016**, *28* (39), 8755–8759. https://doi.org/10.1002/adma.201602939.
(587) Jiang, W.-L.; Wang, W.-X.; Liu, J.; Li, Y.; Li, C.-Y. A Novel Hepatocyte-Targeting Ratiometric Fluorescent Probe for Imaging Hydrogen Peroxide in Zebrafish. *Sens. Actuators B Chem.* **2020**, *313*, 128054. https://doi.org/10.1016/j.snb.2020.128054.
(588) Groegel, D. B. M.; Link, M.; Duerkop, A.; Wolfbeis, O. S. A New Fluorescent PET Probe for Hydrogen Peroxide and Its Use in Enzymatic Assays for L-Lactate and D-Glucose. *ChemBioChem* **2011**, *12* (18), 2779–2785. https://doi.org/10.1002/cbic.201100561.
(589) Li, X.; Yu, W.; Zhao, H.; Fan, Z.; Xiao, M.; Xi, R.; Xu, Y.; Meng, M. Fluorogenic Biosensors Constructed via Aggregation-Induced Emission Based on Enzyme-Catalyzed Coupling Reactions for Detection of Hydrogen Peroxide. *Anal. Sci.* **2021**, *37* (9), 1275–1279. https://doi.org/10.2116/analsci.20P463.
(590) Yin, Y.; Wang, G.; Liu, Y.; Wang, X.; Gao, W.; Zhang, S.; You, C. Simple Phenotypic Sensor for Visibly Tracking H_2O_2 Fluctuation to Detect Plant Health Status. *J. Agric. Food Chem.* **2022**, *70* (32), 10058–10064. https://doi.org/10.1021/acs.jafc.2c02170.
(591) Nakahara, R.; Fujimoto, T.; Doi, M.; Morita, K.; Yamaguchi, T.; Fujita, Y. Fluorophotometric Determination of Hydrogen Peroxide and Other Reactive Oxygen Species with Fluorescein Hydrazide (FH) and Its Crystal Structure. *Chem. Pharm. Bull.* **2008**, *56* (7), 977–981. https://doi.org/10.1248/cpb.56.977.

(592) Kumar, M.; Kumar, N.; Bhalla, V. A Naphthalimide Based Chemosensor for Zn^{2+}, Pyrophosphate and H_2O_2: Sequential Logic Operations at the Molecular Level. *Chem. Commun.* **2013**, *49*, 877–879. https://doi.org/10.1039/c2cc37728d.
(593) Zhou, X.; Lesiak, L.; Lai, R.; Beck, J. R.; Zhao, J.; Elowsky, C. G.; Li, H.; Stains, C. I. Chemoselective Alteration of Fluorophore Scaffolds as a Strategy for the Development of Ratiometric Chemodosimeters. *Angew. Chem. Int. Ed.* **2017**, *56* (15), 4197–4200. https://doi.org/10.1002/anie.201612628.
(594) Cheng, Y.; Dai, J.; Sun, C.; Liu, R.; Zhai, T.; Lou, X.; Xia, F. An Intracellular H_2O_2-Responsive AIEgen for the Peroxidase-Mediated Selective Imaging and Inhibition of Inflammatory Cells. *Angew. Chem. Int. Ed.* **2018**, *57* (12), 3123–3127. https://doi.org/10.1002/anie.201712803.
(595) Quan, Z.; Mao, L.; Tang, Y.; Lei, M.; Zhu, B.; Liu, Y. Mechanistic Investigation of H_2O_2 - Dependent Chemiluminescence from Tetrabromo-1,4-Benzoquinone. *ChemPhysChem* **2022**, *23* (5). https://doi.org/10.1002/cphc.202100885.
(596) Johnson, R.; van der Zalm, J.; Chen, A.; Bell, I.; Van Raay, T.; Al-Abdul-Wahid, M.; Manderville, R. Unraveling the Chemosensing Mechanism by the 7-(Diethylamino)Coumarin-Hemicyanine Hybrid: A Ratiometric Fluorescent Probe for Hydrogen Peroxide. *Anal. Chem.* **2022**, *94* (31), 11047–11054. https://doi.org/10.1021/acs.analchem.2c01852.
(597) Fang, J.; Liao, S.; Gao, C.; Gao, S.; Li, W.; Pi, D.; Zhou, H. *Oxidative Cleavage of Alkene: A New Strategy to Construct a Mitochondria-Targeted Fluorescent Probe for Hydrogen Peroxide Imaging in Vitro And In Vivo*; preprint; SSRN, **2023**. https://doi.org/10.2139/ssrn.4377212.
(598) Fukuzaki, S. Mechanisms of Actions of Sodium Hypochlorite in Cleaning and Disinfection Processes. *Biocontrol Sci.* **2006**, *11* (4), 147–157. https://doi.org/10.4265/bio.11.147.
(599) Pullar, J. M.; Vissers, M. C. M.; Winterbourn, C. C. Living with a Killer: The Effects of Hypochlorous Acid on Mammalian Cells. *IUBMB Life* **2000**, *50* (4–5), 259–266. https://doi.org/10.1080/713803731.
(600) Klebanoff, S. J. Myeloperoxidase: Friend and Foe. *J. Leukoc. Biol.* **2005**, *77* (5), 598–625. https://doi.org/10.1189/jlb.1204697.
(601) Winterbourn, C. C. Biological Reactivity and Biomarkers of the Neutrophil Oxidant, Hypochlorous Acid. *Toxicology* **2002**, *181–182*, 223–227. https://doi.org/10.1016/S0300-483X(02)00286-X.
(602) Winterbourn, C. C.; Kettle, A. J. Biomarkers of Myeloperoxidase-Derived Hypochlorous Acid. *Free Radic. Biol. Med.* **2000**, *29* (5), 403–409. https://doi.org/10.1016/S0891-5849(00)00204-5.
(603) Woods, A. A.; Linton, S. M.; Davies, M. J. Detection of HOCl-Mediated Protein Oxidation Products in the Extracellular Matrix of Human Atherosclerotic Plaques. *Biochem. J.* **2003**, *370* (2), 729–735. https://doi.org/10.1042/bj20021710.
(604) Winterbourn, C. C.; van den Berg, J. J. M.; Roitman, E.; Kuypers, F. A. Chlorohydrin Formation from Unsaturated Fatty Acids Reacted with Hypochlorous Acid. *Arch. Biochem. Biophys.* **1992**, *296* (2), 547–555. https://doi.org/10.1016/0003-9861(92)90609-Z.
(605) Kettle, A. J. Neutrophils Convert Tyrosyl Residues in Albumin to Chlorotyrosine. *FEBS Lett.* **1996**, *379* (1), 103–106. https://doi.org/10.1016/0014-5793(95)01494-2.
(606) van der Vliet, A.; Jenner, A.; Eiserich, J. P.; Cross, C. E.; Halliwell, B. [48] Analysis of Aromatic Nitration, Chlorination, and Hydroxylation by Gas Chromatography-Mass Spectrometry. In *Methods in Enzymology*; Nitric Oxide Part C: Biological and Antioxidant Activities; Academic Press, 1999; Vol. 301, pp 471–483. https://doi.org/10.1016/S0076-6879(99)01110-6.
(607) Setsukinai, K.; Urano, Y.; Kakinuma, K.; Majima, H. J.; Nagano, T. Development of Novel Fluorescence Probes That Can Reliably Detect Reactive Oxygen Species and Distinguish

Specific Species. *J. Biol. Chem.* **2003**, *278* (5), 3170–3175. https://doi.org/10.1074/jbc.M209264200.
(608) Setsukinai, K.; Urano, Y.; Kikuchi, K.; Higuchi, T.; Nagano, T. Fluorescence Switching by O-Dearylation of 7-Aryloxycoumarins. Development of Novel Fluorescence Probes to Detect Reactive Oxygen Species with High Selectivity. *J. Chem. Soc. Perkin Trans. 2* **2000**, No. 12, 2453–2457. https://doi.org/10.1039/B006449L.
(609) Shepherd, J.; Hilderbrand, S. A.; Waterman, P.; Heinecke, J. W.; Weissleder, R.; Libby, P. A Fluorescent Probe for the Detection of Myeloperoxidase Activity in Atherosclerosis-Associated Macrophages. *Chem. Biol.* **2007**, *14* (11), 1221–1231. https://doi.org/10.1016/j.chembiol.2007.10.005.
(610) Xiao, Y.; Zhang, R.; Ye, Z.; Dai, Z.; An, H.; Yuan, J. Lanthanide Complex-Based Luminescent Probes for Highly Sensitive Time-Gated Luminescence Detection of Hypochlorous Acid. *Anal. Chem.* **2012**, *84* (24), 10785–10792. https://doi.org/10.1021/ac3028189.
(611) Ye, Z.; Zhang, R.; Song, B.; Dai, Z.; Jin, D.; Goldys, E. M.; Yuan, J. Development of a Functional Ruthenium(II) Complex for Probing Hypochlorous Acid in Living Cells. *Dalton Trans.* **2014**, *43* (22), 8414–8420. https://doi.org/10.1039/C4DT00179F.
(612) Lu, F.; Nabeshima, T. A Highly Selective and Sensitive Turn-on Chemodosimeter for Hypochlorous Acid Based on an Iridium(III) Complex and Its Application to Bioimaging. *Dalton Trans.* **2014**, *43* (25), 9529–9536. https://doi.org/10.1039/C4DT00616J.
(613) Huang, Y.; He, N.; Wang, Y.; Zhang, L.; Kang, Q.; Wang, Y.; Shen, D.; Choo, J.; Chen, L. Detection of Hypochlorous Acid Fluctuation via a Selective Near-Infrared Fluorescent Probe in Living Cells and in Vivo under Hypoxic Stress. *J. Mater. Chem. B* **2019**, *7* (15), 2557–2564. https://doi.org/10.1039/C9TB00079H.
(614) Zhao, C.; An, J.; Zhou, L.; Fei, Q.; Wang, F.; Tan, J.; Shi, B.; Wang, R.; Guo, Z.; Zhu, W.-H. Transforming the Recognition Site of 4-Hydroxyaniline into 4-Methoxyaniline Grafted onto a BODIPY Core Switches the Selective Detection of Peroxynitrite to Hypochlorous Acid. *Chem. Commun.* **2016**, *52* (10), 2075–2078. https://doi.org/10.1039/C5CC08936K.
(615) Zhou, X.-H.; Jiang, Y.-R.; Zhao, X.-J.; Guo, D. A Naphthalene-Based Two-Photon Fluorescent Probe for Selective and Sensitive Detection of Endogenous Hypochlorous Acid. *Talanta* **2016**, *160*, 470–474. https://doi.org/10.1016/j.talanta.2016.07.047.
(616) Lin, X.; Chen, Y.; Bao, L.; Wang, S.; Liu, K.; Qin, W.; Kong, F. A Two-Photon near-Infrared Fluorescent Probe for Imaging Endogenous Hypochlorite in Cells, Tissue and Living Mouse. *Dyes Pigments* **2020**, *174*, 108113. https://doi.org/10.1016/j.dyepig.2019.108113.
(617) Wu, G.-S.; Thirumalaivasan, N.; Lin, T.-C.; Wu, S.-P. Ultrasensitive and Specific Two-Photon Fluorescence Detection of Hypochlorous Acid by a Lysosome-Targeting Fluorescent Probe for Cell Imaging. *J. Pharm. Biomed. Anal.* **2020**, *190*, 113545. https://doi.org/10.1016/j.jpba.2020.113545.
(618) Duan, Q.; Jia, P.; Zhuang, Z.; Liu, C.; Zhang, X.; Wang, Z.; Sheng, W.; Li, Z.; Zhu, H.; Zhu, B.; Zhang, X. Rational Design of a Hepatoma-Specific Fluorescent Probe for HOCl and Its Bioimaging Applications in Living HepG2 Cells. *Anal. Chem.* **2019**, *91* (3), 2163–2168. https://doi.org/10.1021/acs.analchem.8b04726.
(619) Liu, X.; Tang, Z.; Song, B.; Ma, H.; Yuan, J. A Mitochondria-Targeting Time-Gated Luminescence Probe for Hypochlorous Acid Based on a Europium Complex. *J. Mater. Chem. B* **2017**, *5* (15), 2849–2855. https://doi.org/10.1039/C6TB02991D.
(620) Bai, X.; Yang, B.; Chen, H.; Shen, J.; Yang, D. HKOCl-4: A Rhodol-Based Yellow Fluorescent Probe for the Detection of Hypochlorous Acid in Living Cells and Tissues. *Org. Chem. Front.* **2020**, *7* (8), 993–996. https://doi.org/10.1039/D0QO00081G.
(621) Yang, T.; Sun, J.; Yao, W.; Gao, F. A Two-Photon Fluorescent Probe for Turn-on Monitoring HOCl Level in Endoplasmic Reticulum. *Dyes Pigments* **2020**, *180*, 108435. https://doi.org/10.1016/j.dyepig.2020.108435.

(622) Kenmoku, S.; Urano, Y.; Kojima, H.; Nagano, T. Development of a Highly Specific Rhodamine-Based Fluorescence Probe for Hypochlorous Acid and Its Application to Real-Time Imaging of Phagocytosis. *J. Am. Chem. Soc.* **2007**, *129* (23), 7313–7318. https://doi.org/10.1021/ja068740g.
(623) Zhou, J.; Li, L.; Shi, W.; Gao, X.; Li, X.; Ma, H. HOCl Can Appear in the Mitochondria of Macrophages during Bacterial Infection as Revealed by a Sensitive Mitochondrial-Targeting Fluorescent Probe. *Chem. Sci.* **2015**, *6* (8), 4884–4888. https://doi.org/10.1039/C5SC01562F.
(624) Koide, Y.; Urano, Y.; Hanaoka, K.; Terai, T.; Nagano, T. Development of an Si-Rhodamine-Based Far-Red to Near-Infrared Fluorescence Probe Selective for Hypochlorous Acid and Its Applications for Biological Imaging. *J. Am. Chem. Soc.* **2011**, *133* (15), 5680–5682. https://doi.org/10.1021/ja111470n.
(625) Ikeno, T.; Hanaoka, K.; Iwaki, S.; Myochin, T.; Murayama, Y.; Ohde, H.; Komatsu, T.; Ueno, T.; Nagano, T.; Urano, Y. Design and Synthesis of an Activatable Photoacoustic Probe for Hypochlorous Acid. *Anal. Chem.* **2019**, *91* (14), 9086–9092. https://doi.org/10.1021/acs.analchem.9b01529.
(626) Best, Q. A.; Sattenapally, N.; Dyer, D. J.; Scott, C. N.; McCarroll, M. E. pH-Dependent Si-Fluorescein Hypochlorous Acid Fluorescent Probe: Spirocycle Ring-Opening and Excess Hypochlorous Acid-Induced Chlorination. *J. Am. Chem. Soc.* **2013**, *135* (36), 13365–13370. https://doi.org/10.1021/ja401426s.
(627) Wu, X.; Li, Z.; Yang, L.; Han, J.; Han, S. A Self-Referenced Nanodosimeter for Reaction Based Ratiometric Imaging of Hypochlorous Acid in Living Cells. *Chem. Sci.* **2013**, *4* (1), 460–467. https://doi.org/10.1039/C2SC21485G.
(628) Zhu, B.; Li, P.; Shu, W.; Wang, X.; Liu, C.; Wang, Y.; Wang, Z.; Wang, Y.; Tang, B. Highly Specific and Ultrasensitive Two-Photon Fluorescence Imaging of Native HOCl in Lysosomes and Tissues Based on Thiocarbamate Derivatives. *Anal. Chem.* **2016**, *88* (24), 12532–12538. https://doi.org/10.1021/acs.analchem.6b04392.
(629) Wang, X.; Zhou, Y.; Xu, C.; Song, H.; Li, L.; Zhang, J.; Guo, M. A Highly Selective Fluorescent Probe for the Detection of Hypochlorous Acid in Tap Water and Living Cells. *Spectrochim. Acta. A. Mol. Biomol. Spectrosc.* **2018**, *203*, 415–420. https://doi.org/10.1016/j.saa.2018.06.012.
(630) Zhu, B.; Wu, L.; Zhu, H.; Wang, Z.; Duan, Q.; Fang, Z.; Jia, P.; Li, Z.; Liu, C. A Highly Specific and Ultrasensitive Two-Photon Fluorescent Probe for Imaging Native Hypochlorous Acid in Living Cells. *Sens. Actuators B Chem.* **2018**, *269*, 1–7. https://doi.org/10.1016/j.snb.2018.04.115.
(631) Li, X.; Wu, L.; Zhao, Z.; Liu, C.; Zhu, B. A Novel Highly Specific and Ultrasensitive Fluorescent Probe for Monitoring Hypochlorous Acid and Its Application in Live Cells. *RSC Adv.* **2019**, *9* (8), 4659–4664. https://doi.org/10.1039/C8RA09551E.
(632) Fan, G.; Wang, N.; Zhang, J.; Ji, X.; Qin, S.; Tao, Y.; Zhao, W. BODIPY-Based near-Infrared Fluorescent Probe for Diagnosis Drug-Induced Liver Injury via Imaging of HClO in Cells and in Vivo. *Dyes Pigments* **2022**, *199*, 110073. https://doi.org/10.1016/j.dyepig.2021.110073.
(633) Mu, S.; Jiang, L.; Gao, H.; Zhang, J.; Sun, H.; Shi, X.; Liu, X.; Zhang, H. A Novel Fluorescent Probe with Large Stokes Shift for Accurate Detection of HOCl in Mitochondria and Its Imaging Application. *Anal. Chim. Acta* **2022**, *1191*, 339287. https://doi.org/10.1016/j.aca.2021.339287.
(634) Lu, Y.; Dong, B.; Song, W.; Kong, X.; Mehmood, A. H.; Lin, W. An Endoplasmic Reticulum-Targeting Fluorescent Probe for the Imaging of Hypochlorous Acid in Living Cells and Zebrafishes. *J. Photochem. Photobiol. Chem.* **2019**, *384*, 111980. https://doi.org/10.1016/j.jphotochem.2019.111980.

(635) Liu, J.; Zhai, Z.; Niu, H.; Zhang, Y.; Song, X.; Zhang, P.; Ye, Y. Endoplasmic Reticulum-Targetable Fluorescent Probe for Visualizing HClO in EC1 Cells. *Tetrahedron Lett.* **2020**, *61* (37), 152301. https://doi.org/10.1016/j.tetlet.2020.152301.
(636) Liu, S.-Z.; Xu, J.-H.; Ma, Q.-J.; Wang, B.-Y.; Li, L.-K.; Zhu, N.-N.; Liu, S.-Y.; Wang, G.-G. A Naphthalimide-Based and Golgi-Targetable Fluorescence Probe for Quantifying Hypochlorous Acid. *Spectrochim. Acta. A. Mol. Biomol. Spectrosc.* **2023**, *286*, 121986. https://doi.org/10.1016/j.saa.2022.121986.
(637) Shi, D.; Chen, S.; Dong, B.; Zhang, Y.; Sheng, C.; James, T. D.; Guo, Y. Evaluation of HOCl-Generating Anticancer Agents by an Ultrasensitive Dual-Mode Fluorescent Probe. *Chem. Sci.* **2019**, *10* (13), 3715–3722. https://doi.org/10.1039/C9SC00180H.
(638) Ji, D.; Li, G.; Zhang, S.; Zhu, M.; Li, C.; Qiao, R. Mitochondria-Targeted Fluorescence Probe for Endogenous Hypochlorite Imaging in Living Cells and Zebrafishs. *Sens. Actuators B Chem.* **2018**, *259*, 816–824. https://doi.org/10.1016/j.snb.2017.12.089.
(639) Liu, C.; Jia, P.; Wu, L.; Li, Z.; Zhu, H.; Wang, Z.; Deng, S.; Shu, W.; Zhang, X.; Yu, Y.; Zhu, B. Rational Design of a Highly Efficient Two-Photon Fluorescent Probe for Tracking Intracellular Basal Hypochlorous Acid and Its Applications in Identifying Tumor Cells and Tissues. *Sens. Actuators B Chem.* **2019**, *297*, 126731. https://doi.org/10.1016/j.snb.2019.126731.
(640) Zhou, K.; Ren, M.; Wang, L.; Li, Z.; Lin, W. Preparation of a Two-Photon Fluorescent Probe with a Large Turn-on Signal for Imaging Hypochlorous Acid in Living Tissues. *Anal. Methods* **2018**, *10* (22), 2546–2550. https://doi.org/10.1039/C8AY00607E.
(641) Liu, J.; Yin, Z. A Novel NIR-Emissive Probe with Large Stokes Shift for Hypochlorite Detection and Imaging in Living Cells. *Talanta* **2019**, *196*, 352–356. https://doi.org/10.1016/j.talanta.2018.12.086.
(642) Fang, X.; Jin, X.; Ma, X.; Guan, L.; Chen, W.; She, M. Rational Construction of Deep-Red Fluorescent Probe for Rapid Detection of HClO and Its Application in Bioimaging and Paper-Based Sensing. *Anal. Bioanal. Chem.* **2022**, *414* (19), 5887–5897. https://doi.org/10.1007/s00216-022-04154-9.
(643) Zhang, H.; Yin, X.; Hong, J.; Deng, Y.; Feng, G. A NIR Fluorescence Probe Having Significant Fluorescence Turn-on Signal at 700 nm and Large Stokes Shift for Rapid Detection of HOCl in Vivo. *Talanta* **2021**, *223*, 121768. https://doi.org/10.1016/j.talanta.2020.121768.
(644) Tang, C.; Gao, Y.; Liu, T.; Lin, Y.; Zhang, X.; Zhang, C.; Li, X.; Zhang, T.; Du, L.; Li, M. Bioluminescent Probe for Detecting Endogenous Hypochlorite in Living Mice. *Org. Biomol. Chem.* **2018**, *16* (4), 645–651. https://doi.org/10.1039/C7OB02842C.
(645) Choi, S. H.; Kim, K.; Jeon, J.; Meka, B.; Bucella, D.; Pang, K.; Khatua, S.; Lee, J.; Churchill, D. G. Optical Effects of S-Oxidation and M^{n+} Binding in Meso-Thienyl Dipyrrin Systems and of Stepwise Bromination of 4,4-Difluoro-8-(2,5-Dibromo-3-Thienyl)-4-Bora-3a,4a-Diaza-s-Indacene. *Inorg. Chem.* **2008**, *47* (23), 11071–11083. https://doi.org/10.1021/ic801354y.
(646) Kim, T.-I.; Park, S.; Choi, Y.; Kim, Y. A BODIPY-Based Probe for the Selective Detection of Hypochlorous Acid in Living Cells. *Chem. – Asian J.* **2011**, *6* (6), 1358–1361. https://doi.org/10.1002/asia.201100025.
(647) Liang, L.; Liu, C.; Jiao, X.; Zhao, L.; Zeng, X. A Highly Selective and Sensitive Photoinduced Electron Transfer (PET) Based HOCl Fluorescent Probe in Water and Its Endogenous Imaging in Living Cells. *Chem. Commun.* **2016**, *52* (51), 7982–7985. https://doi.org/10.1039/C6CC02603F.
(648) Zhang, B.; Yang, X.; Zhang, R.; Liu, Y.; Ren, X.; Xian, M.; Ye, Y.; Zhao, Y. Lysosomal-Targeted Two-Photon Fluorescent Probe to Sense Hypochlorous Acid in Live Cells. *Anal. Chem.* **2017**, *89* (19), 10384–10390. https://doi.org/10.1021/acs.analchem.7b02361.

(649) Liu, C.; Jiao, X.; He, S.; Zhao, L.; Zeng, X. A Highly Selective and Sensitive Fluorescent Probe for Hypochlorous Acid and Its Lysosome-Targetable Biological Applications. *Talanta* **2017**, *174*, 234–242. https://doi.org/10.1016/j.talanta.2017.06.012.
(650) Feng, H.; Meng, Q.; Wang, Y.; Duan, C.; Wang, C.; Jia, H.; Zhang, Z.; Zhang, R. Responsive Fluorescence Probe for Selective and Sensitive Detection of Hypochlorous Acid in Live Cells and Animals. *Chem. – Asian J.* **2018**, *13* (18), 2611–2618. https://doi.org/10.1002/asia.201800957.
(651) Baruah, M.; Jana, A.; Ali, M.; Mapa, K.; Samanta, A. An Efficient PeT Based Fluorescent Probe for Mapping Mitochondrial Oxidative Stress Produced via the Nox2 Pathway. *J. Mater. Chem. B* **2022**, *10* (13), 2230–2237. https://doi.org/10.1039/D2TB00356B.
(652) Bao, X.; Cao, X.; Yuan, Y.; Zhou, B.; Huo, C. A Water-Soluble, Highly Sensitive and Ultrafast Fluorescence Probe for Imaging of Mitochondrial Hypochlorous Acid. *Sens. Actuators B Chem.* **2021**, *344*, 130210. https://doi.org/10.1016/j.snb.2021.130210.
(653) Wang, B.; Yuan, F.; Wang, S.; Duan, R.; Ren, W. X.; Hou, J.-T. Detection of Atherosclerosis-Associated HOCl Using a Mitochondria-Targeted Fluorescent Probe. *Sens. Actuators B Chem.* **2021**, *348*, 130695. https://doi.org/10.1016/j.snb.2021.130695.
(654) Liu, X.; Zheng, A.; Luan, D.; Wang, X.; Kong, F.; Tong, L.; Xu, K.; Tang, B. High-Quantum-Yield Mitochondria-Targeting Near-Infrared Fluorescent Probe for Imaging Native Hypobromous Acid in Living Cells and in Vivo. *Anal. Chem.* **2017**, *89* (3), 1787–1792. https://doi.org/10.1021/acs.analchem.6b04094.
(655) Gong, J.; Liu, C.; Cai, S.; He, S.; Zhao, L.; Zeng, X. Novel Near-Infrared Fluorescent Probe with a Large Stokes Shift for Sensing Hypochlorous Acid in Mitochondria. *Org. Biomol. Chem.* **2020**, *18* (38), 7656–7662. https://doi.org/10.1039/D0OB01563F.
(656) Liu, J.; Niu, P.; Rong, Y.; Chen, W.; Liu, X.; Wei, L.; Song, X. A Phenothiazine Coumarin Based Ratiometric Fluorescent Probe for Real-Time Detection of Lysosomal Hypochlorite in Living Cell and Zebra Fish. *Spectrochim. Acta. A. Mol. Biomol. Spectrosc.* **2021**, *261*, 120024. https://doi.org/10.1016/j.saa.2021.120024.
(657) Hou, P.; Chen, S.; Liang, G.; Li, H.; Zhang, H. A Lysosome-Targeted Ratiometric Fluorescent Probe with a Large Blue Shift for Monitoring Hypochlorous Acid in Living Cells and Zebrafish. *Spectrochim. Acta. A. Mol. Biomol. Spectrosc.* **2020**, *229*, 117866. https://doi.org/10.1016/j.saa.2019.117866.
(658) Xie, X.; Wang, J.; Yan, Y.; Zhang, X.; Liu, C.; Yang, J.; Hua, J. A New Mitochondria-Targeted Ratiometric Fluorescent Probe Based on Diketopyrrolopyrrole for Imaging Endogenous HOCl in Living Cells. *Analyst* **2018**, *143* (23), 5736–5743. https://doi.org/10.1039/C8AN01469H.
(659) Song, W.; Dong, B.; Lu, Y.; Kong, X.; Mehmood, A. H.; Lin, W. Development of an Endoplasmic Reticulum-Targeting Fluorescent Probe for the Two-Photon Imaging of Hypochlorous Acid (HClO) in Living Cells. *Anal. Methods* **2019**, *11* (35), 4450–4455. https://doi.org/10.1039/C9AY01390C.
(660) Xia, Q.; Wang, X.; Liu, Y.; Shen, Z.; Ge, Z.; Huang, H.; Li, X.; Wang, Y. An Endoplasmic Reticulum-Targeted Two-Photon Fluorescent Probe for Bioimaging of HClO Generated during Sleep Deprivation. *Spectrochim. Acta. A. Mol. Biomol. Spectrosc.* **2020**, *229*, 117992. https://doi.org/10.1016/j.saa.2019.117992.
(661) Chen, W.-C.; Venkatesan, P.; Wu, S.-P. A Highly Selective Turn-on Fluorescent Probe for Hypochlorous Acid Based on Hypochlorous Acid-Induced Oxidative Intramolecular Cyclization of Boron Dipyrromethene-Hydrazone. *Anal. Chim. Acta* **2015**, *882*, 68–75. https://doi.org/10.1016/j.aca.2015.04.012.
(662) Liu, S.-R.; Vedamalai, M.; Wu, S.-P. Hypochlorous Acid Turn-on Boron Dipyrromethene Probe Based on Oxidation of Methyl Phenyl Sulfide. *Anal. Chim. Acta* **2013**, *800*, 71–76. https://doi.org/10.1016/j.aca.2013.09.018.

(663) Qu, Z.; Ding, J.; Zhao, M.; Li, P. Development of a Selenide-Based Fluorescent Probe for Imaging Hypochlorous Acid in Lysosomes. *J. Photochem. Photobiol. Chem.* **2015**, *299*, 1–8. https://doi.org/10.1016/j.jphotochem.2014.10.015.
(664) Lv, X.; Yuan, X.; Wang, Y.; Guo, W. A Naphthalimide Based Fast and Selective Fluorescent Probe for Hypochlorous Acid/Hypochlorite and Its Application for Bioimaging. *New J. Chem.* **2018**, *42* (18), 15105–15110. https://doi.org/10.1039/C8NJ03208D.
(665) Venkatesan, P.; Wu, S.-P. A Turn-on Fluorescent Probe for Hypochlorous Acid Based on the Oxidation of Diphenyl Telluride. *Analyst* **2015**, *140* (4), 1349–1355. https://doi.org/10.1039/C4AN02116A.
(666) Li, G.; Zhu, D.; Liu, Q.; Xue, L.; Jiang, H. A Strategy for Highly Selective Detection and Imaging of Hypochlorite Using Selenoxide Elimination. *Org. Lett.* **2013**, *15* (8), 2002–2005. https://doi.org/10.1021/ol4006823.
(667) Xie, X.; Wu, T.; Wang, X.; Li, Y.; Wang, K.; Zhao, Z.; Jiao, X.; Tang, B. A Two-Photon Fluorescent Probe for Ratiometric Visualization of Hypochlorous Acid in Live Cells and Animals Based on a Selenide Oxidation/Elimination Tandem Reaction. *Chem. Commun.* **2018**, *54* (84), 11965–11968. https://doi.org/10.1039/C8CC07312K.
(668) Hwang, J.; Choi, M. G.; Bae, J.; Chang, S.-K. Signaling of Hypochlorous Acid by Selective Deprotection of Dithiolane. *Org. Biomol. Chem.* **2011**, *9* (20), 7011–7015. https://doi.org/10.1039/C1OB06012K.
(669) Yuan, L.; Wang, L.; Agrawalla, B. K.; Park, S.-J.; Zhu, H.; Sivaraman, B.; Peng, J.; Xu, Q.-H.; Chang, Y.-T. Development of Targetable Two-Photon Fluorescent Probes to Image Hypochlorous Acid in Mitochondria and Lysosome in Live Cell and Inflamed Mouse Model. *J. Am. Chem. Soc.* **2015**, *137* (18), 5930–5938. https://doi.org/10.1021/jacs.5b00042.
(670) Jun, Y. W.; Sarkar, S.; Singha, S.; Reo, Y. J.; Kim, H. R.; Kim, J.-J.; Chang, Y.-T.; Ahn, K. H. A Two-Photon Fluorescent Probe for Ratiometric Imaging of Endogenous Hypochlorous Acid in Live Cells and Tissues. *Chem. Commun.* **2017**, *53* (78), 10800–10803. https://doi.org/10.1039/C7CC05834A.
(671) Liu, Z.; Li, G.; Wang, Y.; Li, J.; Mi, Y.; Guo, L.; Xu, W.; Zou, D.; Li, T.; Wu, Y. A Novel Fluorescent Probe for Imaging the Process of HOCl Oxidation and Cys/Hcy Reduction in Living Cells. *RSC Adv.* **2018**, *8* (17), 9519–9523. https://doi.org/10.1039/C7RA13419C.
(672) Liu, F.; Tang, Y.; Kuang, Y.; Pan, D.; Liu, X.; Yu, R.-Q.; Jiang, J.-H. An Activatable Fluorescent Probe with an Ultrafast Response and Large Stokes Shift for Live Cell Bioimaging of Hypochlorous Acid. *RSC Adv.* **2016**, *6* (109), 107910–107915. https://doi.org/10.1039/C6RA22686H.
(673) Mao, Z.; Ye, M.; Hu, W.; Ye, X.; Wang, Y.; Zhang, H.; Li, C.; Liu, Z. Design of a Ratiometric Two-Photon Probe for Imaging of Hypochlorous Acid (HClO) in Wounded Tissues. *Chem. Sci.* **2018**, *9* (28), 6035–6040. https://doi.org/10.1039/C8SC01697F.
(674) Chen, X.; Wang, X.; Wang, S.; Shi, W.; Wang, K.; Ma, H. A Highly Selective and Sensitive Fluorescence Probe for the Hypochlorite Anion. *Chem. – Eur. J.* **2008**, *14* (15), 4719–4724. https://doi.org/10.1002/chem.200701677.
(675) Ren, M.; Li, Z.; Nie, J.; Wang, L.; Lin, W. A Photocaged Fluorescent Probe for Imaging Hypochlorous Acid in Lysosomes. *Chem. Commun.* **2018**, *54* (66), 9238–9241. https://doi.org/10.1039/C8CC04926B.
(676) Ren, M.; Li, Z.; Deng, B.; Wang, L.; Lin, W. Single Fluorescent Probe Separately and Continuously Visualize H2S and HClO in Lysosomes with Different Fluorescence Signals. *Anal. Chem.* **2019**, *91* (4), 2932–2938. https://doi.org/10.1021/acs.analchem.8b05116.
(677) Ren, M.; Nie, J.; Deng, B.; Zhou, K.; Wang, J.-Y.; Lin, W. A Fluorescent Probe for Ratiometric Imaging of Exogenous and Intracellular Formed Hypochlorous Acid in Lysosomes. *New J. Chem.* **2017**, *41* (13), 5259–5262. https://doi.org/10.1039/C7NJ00949F.

(678) Jiang, C.; Xu, X.; Yao, C. A Ratiometric Fluorescence Probe for Imaging Endoplasmic Reticulum (ER) Hypochlorous Acid in Living Cells Undergoing Excited State Intramolecular Proton Transfer. *Spectrochim. Acta. A. Mol. Biomol. Spectrosc.* **2022**, *273*, 121075. https://doi.org/10.1016/j.saa.2022.121075.
(679) Zhu, N.; Guo, X.; Chang, Y.; Shi, Z.; Jin, L. Y.; Feng, S. A Mitochondria-Tracing Fluorescent Probe for Real-Time Detection of Mitochondrial Dynamics and Hypochlorous Acid in Live Cells. *Dyes Pigments* **2022**, *201*, 110227. https://doi.org/10.1016/j.dyepig.2022.110227.
(680) Yang, Y.-K.; Cho, H. J.; Lee, J.; Shin, I.; Tae, J. A Rhodamine−Hydroxamic Acid-Based Fluorescent Probe for Hypochlorous Acid and Its Applications to Biological Imagings. *Org. Lett.* **2009**, *11* (4), 859–861. https://doi.org/10.1021/ol802822t.
(681) Jia, J.; Ma, H. A Water-Soluble Fluorescence Resonance Energy Transfer Probe for Hypochlorous Acid and Its Application to Cell Imaging. *Chin. Sci. Bull.* **2011**, *56* (31), 3266–3272. https://doi.org/10.1007/s11434-011-4645-2.
(682) Zhang, Y.-R.; Chen, X.-P.; Jing-Shao; Zhang, J.-Y.; Yuan, Q.; Miao, J.-Y.; Zhao, B.-X. A Ratiometric Fluorescent Probe for Sensing HOCl Based on a Coumarin–Rhodamine Dyad. *Chem. Commun.* **2014**, *50* (91), 14241–14244. https://doi.org/10.1039/C4CC05976J.
(683) Kathiravan, A.; Manjunathan, T.; Velusamy, M.; Guru, A.; Arockiaraj, J.; Jhonsi, M. A.; Gopinath, P. Nano-Sized Aggregation Induced Emissive Probe for Highly Sensitive Hypochlorous Acid Detection. *Dyes Pigments* **2023**, *210*, 111016. https://doi.org/10.1016/j.dyepig.2022.111016.
(684) Cheng, X.; Jia, H.; Long, T.; Feng, J.; Qin, J.; Li, Z. A “Turn-on” Fluorescent Probe for Hypochlorous Acid: Convenient Synthesis, Good Sensing Performance, and a New Design Strategy by the Removal of CN Isomerization. *Chem. Commun.* **2011**, *47* (43), 11978–11980. https://doi.org/10.1039/C1CC15214A.
(685) Han, J.; Li, Y.; Wang, Y.; Bao, X.; Wang, L.; Ren, L.; Ni, L.; Li, C. A Water-Soluble Fluorescent Probe for Monitoring Hypochlorite in Water and in Living Cells. *Sens. Actuators B Chem.* **2018**, *273*, 778–783. https://doi.org/10.1016/j.snb.2018.06.065.
(686) Hu, C.; Li, J.; Yan, L. A Fluorescent Probe for Hypochlorite with Colorimetric and Fluorometric Characteristics and Imaging in Living Cells. *Anal. Biochem.* **2019**, *566*, 32–36. https://doi.org/10.1016/j.ab.2018.11.011.
(687) Ding, Y.; Xu, C.; Li, Z.; Qin, W.; Han, X.; Han, X.; Zhang, C.; Yu, C.; Wang, X.; Li, L.; Huang, W. Fast-Response Fluorogenic Probe for Visualizing Hypochlorite in Living Cells and in Zebrafish. *ChemBioChem* **2019**, *20* (6), 831–837. https://doi.org/10.1002/cbic.201800659.
(688) Xu, H.; Wu, S.-L.; Lin, N.-J.; Lu, Y.; Xiao, J.; Wang, Y.-W.; Peng, Y. A NIR Fluorescent Probe for Rapid Turn-on Detection and Bioimaging of Hypochlorite Anion. *Sens. Actuators B Chem.* **2021**, *346*, 130484. https://doi.org/10.1016/j.snb.2021.130484.
(689) Emrullahoğlu, M.; Üçüncü, M.; Karakuş, E. A BODIPY Aldoxime-Based Chemodosimeter for Highly Selective and Rapid Detection of Hypochlorous Acid. *Chem. Commun.* **2013**, *49* (71), 7836–7838. https://doi.org/10.1039/C3CC44463E.
(690) Wu, G.; Zeng, F.; Wu, S. A Water-Soluble and Specific BODIPY-Based Fluorescent Probe for Hypochlorite Detection and Cell Imaging. *Anal. Methods* **2013**, *5* (20), 5589–5596. https://doi.org/10.1039/C3AY41268G.
(691) Huang, C.; Qian, Y. A Fast-Responsed Lysosomal-Targeted Fluorescent Probe Based on BODIPY with Low Limit Detection for Hypochlorous Acid and Its Application of Intracellular Hypochlorous Acid Bioimaging. *Opt. Mater.* **2019**, *92*, 53–59. https://doi.org/10.1016/j.optmat.2019.04.012.
(692) Li, D.; Feng, Y.; Lin, J.; Chen, M.; Wang, S.; Wang, X.; Sheng, H.; Shao, Z.; Zhu, M.; Meng, X. A Mitochondria-Targeted Two-Photon Fluorescent Probe for Highly Selective and Rapid Detection of Hypochlorite and Its Bio-Imaging in Living Cells. *Sens. Actuators B Chem.* **2016**, *222*, 483–491. https://doi.org/10.1016/j.snb.2015.08.098.

(693) Wan, Z.; Yu, S.; Wang, Q.; Tobia, J.; Chen, H.; Li, Z.; Liu, X.; Zhang, Y. A BODIPY-Based Far-Red-Absorbing Fluorescent Probe for Hypochlorous Acid Imaging. *ChemPhotoChem* **2022**, *6* (4), e202100250. https://doi.org/10.1002/cptc.202100250.
(694) Nguyen, K. H.; Hao, Y.; Zeng, K.; Fan, S.; Li, F.; Yuan, S.; Ding, X.; Xu, M.; Liu, Y.-N. A Benzothiazole-Based Fluorescent Probe for Hypochlorous Acid Detection and Imaging in Living Cells. *Spectrochim. Acta. A. Mol. Biomol. Spectrosc.* **2018**, *199*, 189–193. https://doi.org/10.1016/j.saa.2018.03.055.
(695) Wang, L.; Liu, J.; Zhang, H.; Guo, W. Discrimination between Cancerous and Normal Cells/Tissues Enabled by a near-Infrared Fluorescent HClO Probe. *Sens. Actuators B Chem.* **2021**, *334*, 129602. https://doi.org/10.1016/j.snb.2021.129602.
(696) Xu, C.; Qian, Y.; Qi, Z.; Lu, C.; Cui, Y. A Conjugated BODIPY–Triphenylamine Multi-Aldoxime: Sonogashira Coupling, Ratiometric Chemodosimeter and Rapid Detection of Hypochlorite with Two-Photon Excited Fluorescence. *New J. Chem.* **2018**, *42* (9), 6910–6917. https://doi.org/10.1039/C8NJ00368H.
(697) Yuan, L.; Lin, W.; Song, J.; Yang, Y. Development of an ICT-Based Ratiometric Fluorescent Hypochlorite Probe Suitable for Living Cell Imaging. *Chem. Commun.* **2011**, *47* (47), 12691–12693. https://doi.org/10.1039/C1CC15762K.
(698) Goswami, S.; Paul, S.; Manna, A. Highly Reactive (<1 Min) Ratiometric “Naked Eye” Detection of Hypochlorite with Real Application in Tap Water. *Dalton Trans.* **2013**, *42* (28), 10097–10101. https://doi.org/10.1039/C3DT51238J.
(699) Yan, L.; Hu, C.; Li, J. A Fluorescence Turn-on Probe for Rapid Monitoring of Hypochlorite Based on Coumarin Schiff Base. *Anal. Bioanal. Chem.* **2018**, *410* (28), 7457–7464. https://doi.org/10.1007/s00216-018-1352-8.
(700) Tang, X.; Zhu, Z.; Liu, R.; Tang, Y. A Novel Ratiometric and Colorimetric Fluorescent Probe for Hypochlorite Based on Cyanobiphenyl and Its Applications. *Spectrochim. Acta. A. Mol. Biomol. Spectrosc.* **2019**, *219*, 576–581. https://doi.org/10.1016/j.saa.2019.04.042.
(701) Wang, Z.; Zhang, Y.; Song, J.; Li, M.; Yang, Y.; Gu, W.; Xu, X.; Xu, H.; Wang, S. A Highly Specific and Sensitive Turn-on Fluorescence Probe for Hypochlorite Detection Based on Anthracene Fluorophore and Its Bioimaging Applications. *Dyes Pigments* **2019**, *161*, 172–181. https://doi.org/10.1016/j.dyepig.2018.09.046.
(702) Sun, Z.-N.; Liu, F.-Q.; Chen, Y.; Tam, P. K. H.; Yang, D. A Highly Specific BODIPY-Based Fluorescent Probe for the Detection of Hypochlorous Acid. *Org. Lett.* **2008**, *10* (11), 2171–2174. https://doi.org/10.1021/ol800507m.
(703) Yuan, L.; Lin, W.; Xie, Y.; Chen, B.; Song, J. Fluorescent Detection of Hypochlorous Acid from Turn-On to FRET-Based Ratiometry by a HOCl-Mediated Cyclization Reaction. *Chem. – Eur. J.* **2012**, *18* (9), 2700–2706. https://doi.org/10.1002/chem.201101918.
(704) Zuo, Q.-P.; Li, Z.-J.; Hu, Y.-H.; Li, B.; Huang, L.-H.; Wang, C.-J.; Liu, S.-K.; Liao, H.-Q. A Highly Sensitive Fluorescent Probe for HClO and Its Application in Live Cell Imaging. *J. Fluoresc.* **2012**, *22* (5), 1201–1207. https://doi.org/10.1007/s10895-012-1067-8.
(705) Zhang, Y.-R.; Meng, N.; Miao, J.-Y.; Zhao, B.-X. A Ratiometric Fluorescent Probe Based on a Through-Bond Energy Transfer (TBET) System for Imaging HOCl in Living Cells. *Chem. – Eur. J.* **2015**, *21* (52), 19058–19063. https://doi.org/10.1002/chem.201503500.
(706) Chen, W.-C.; Venkatesan, P.; Wu, S.-P. A Turn-on Fluorescent Probe for Hypochlorous Acid Based on HOCl-Promoted Removal of the CN Bond in BODIPY-Hydrazone. *New J. Chem.* **2015**, *39* (9), 6892–6898. https://doi.org/10.1039/C5NJ01083G.
(707) Ding, F.; Wen, H.; Zhuo, R.; Li, J.; Zheng, H.; Deng, Y.; Shen, J.; He, X. A Novel Ratiometric and Colorimetric Chemosensor for Highly Sensitive, Selective and Ultrafast Tracing of HClO in Live Cells, Bacteria and Zebrafish. *Anal. Chim. Acta* **2021**, *1161*, 338472. https://doi.org/10.1016/j.aca.2021.338472.
(708) Wang, Y.; Ding, F.; Sun, X.; Chen, S.; Huang, H.; Chen, H. A Reaction-Based Colorimetric and Ratiometric Chemosensor for Imaging Identification of HClO in Live Cells, Mung Bean

Sprouts, and Paper Strips. *Talanta* **2021**, *234*, 122655. https://doi.org/10.1016/j.talanta.2021.122655.
(709) Tang, Y.; Li, Y.; Liu, L.; Ni, H.; Han, J.; Wang, L.; Mao, Y.; Ni, L.; Wang, Y. A Water-Soluble Colorimetric and Fluorescent Probe for Rapidly Sensing of ClO^- in Organisms. *J. Photochem. Photobiol. Chem.* **2020**, *387*, 112166. https://doi.org/10.1016/j.jphotochem.2019.112166.
(710) Zhang, Y.; Teng, H.; Gao, Y.; Afzal, M. W.; Tian, J.; Chen, X.; Tang, H.; James, T. D.; Guo, Y. A General Strategy for Selective Detection of Hypochlorous Acid Based on Triazolopyridine Formation. *Chin. Chem. Lett.* **2020**, *31* (11), 2917–2920. https://doi.org/10.1016/j.cclet.2020.03.020.
(711) Teng, H.; Tian, J.; Sun, D.; Xiu, M.; Zhang, Y.; Qiang, X.; Tang, H.; Guo, Y. A Mitochondria-Specific Fluorescent Probe Based on Triazolopyridine Formation for Visualizing Endogenous Hypochlorous Acid in Living Cells and Zebrafish. *Sens. Actuators B Chem.* **2020**, *319*, 128288. https://doi.org/10.1016/j.snb.2020.128288.
(712) Chen, S.; Lu, J.; Sun, C.; Ma, H. A Highly Specific Ferrocene-Based Fluorescent Probe for Hypochlorous Acid and Its Application to Cell Imaging. *Analyst* **2010**, *135* (3), 577–582. https://doi.org/10.1039/B921187J.
(713) Sun, M.; Yu, H.; Zhu, H.; Ma, F.; Zhang, S.; Huang, D.; Wang, S. Oxidative Cleavage-Based Near-Infrared Fluorescent Probe for Hypochlorous Acid Detection and Myeloperoxidase Activity Evaluation. *Anal. Chem.* **2014**, *86* (1), 671–677. https://doi.org/10.1021/ac403603r.
(714) Shi, Y.; Huo, F.; Yin, C. Malononitrile as the 'Double-Edged Sword' of Passivation-Activation Regulating Two ICT to Highly Sensitive and Accurate Ratiometric Fluorescent Detection for Hypochlorous Acid in Biological System. *Sens. Actuators B Chem.* **2020**, *325*, 128793. https://doi.org/10.1016/j.snb.2020.128793.
(715) Lou, Z.; Li, P.; Song, P.; Han, K. Ratiometric Fluorescence Imaging of Cellular Hypochlorous Acid Based on Heptamethine Cyanine Dyes. *Analyst* **2013**, *138* (21), 6291–6295. https://doi.org/10.1039/C3AN00198A.
(716) Zhang, X.; Zhao, W.; Li, B.; Li, W.; Zhang, C.; Hou, X.; Jiang, J.; Dong, Y. Ratiometric Fluorescent Probes for Capturing Endogenous Hypochlorous Acid in the Lungs of Mice. *Chem. Sci.* **2018**, *9* (43), 8207–8212. https://doi.org/10.1039/C8SC03226B.
(717) Xiao, H.; Li, J.; Zhao, J.; Yin, G.; Quan, Y.; Wang, J.; Wang, R. A Colorimetric and Ratiometric Fluorescent Probe for ClO− Targeting in Mitochondria and Its Application in Vivo. *J. Mater. Chem. B* **2015**, *3* (8), 1633–1638. https://doi.org/10.1039/C4TB02003K.
(718) Yuan, Y.; Wang, D.; Long, W.; Deng, F.; Yu, S.; Tian, J.; Ouyang, H.; Lin, S.; Zhang, X.; Wei, Y. Ratiometric Fluorescent Detection of Hypochlorite in Aqueous Solution and Living Cells Using an Ionic Probe with Aggregation-Induced Emission Feature. *Sens. Actuators B Chem.* **2021**, *330*, 129324. https://doi.org/10.1016/j.snb.2020.129324.
(719) Kang, J.; Huo, F.; Zhang, Y.; Chao, J.; Strongin, R. M.; Yin, C. Detecting Intracellular ClO- with Ratiometric Fluorescent Signal and Its Application in Vivo. *Sens. Actuators B Chem.* **2018**, *273*, 1532–1538. https://doi.org/10.1016/j.snb.2018.07.072.
(720) Park, J.; Kim, H.; Choi, Y.; Kim, Y. A Ratiometric Fluorescent Probe Based on a BODIPY–DCDHF Conjugate for the Detection of Hypochlorous Acid in Living Cells. *Analyst* **2013**, *138* (12), 3368–3371. https://doi.org/10.1039/C3AN36820C.
(721) Hu, Q.; Qin, C.; Huang, L.; Wang, H.; Liu, Q.; Zeng, L. Selective Visualization of Hypochlorite and Its Fluctuation in Cancer Cells by a Mitochondria-Targeting Ratiometric Fluorescent Probe. *Dyes Pigments* **2018**, *149*, 253–260. https://doi.org/10.1016/j.dyepig.2017.10.002.
(722) Zhou, L.; Lu, D.-Q.; Wang, Q.; Hu, S.; Wang, H.; Sun, H.; Zhang, X. A High-Resolution Mitochondria-Targeting Ratiometric Fluorescent Probe for Detection of the Endogenous Hypochlorous Acid. *Spectrochim. Acta. A. Mol. Biomol. Spectrosc.* **2016**, *166*, 129–134. https://doi.org/10.1016/j.saa.2016.05.019.

(723) Xu, J.; Yuan, H.; Qin, C.; Zeng, L.; Bao, G.-M. A Mitochondria-Targeted near-Infrared Probe for Colorimetric and Ratiometric Fluorescence Detection of Hypochlorite in Living Cells. *RSC Adv.* **2016**, *6* (109), 107525–107532. https://doi.org/10.1039/C6RA22868B.
(724) Chen, Y.; Wei, T.; Zhang, Z.; Zhang, W.; Lv, J.; Chen, T.; Chi, B.; Wang, F.; Chen, X. A Mitochondria-Targeted Fluorescent Probe for Ratiometric Detection of Hypochlorite in Living Cells. *Chin. Chem. Lett.* **2017**, *28* (10), 1957–1960. https://doi.org/10.1016/j.cclet.2017.05.010.
(725) Chen, Y.; Zhu, Z.; Liu, X.; Jiang, Y.; Shen, J. Lysosome-Targeting Benzothiazole-Based Fluorescent Probe for Imaging Viscosity and Hypochlorite Levels in Living Cells and Zebrafish. *Spectrochim. Acta. A. Mol. Biomol. Spectrosc.* **2022**, *275*, 121141. https://doi.org/10.1016/j.saa.2022.121141.
(726) Xu, Q.; Lee, K.-A.; Lee, S.; Lee, K. M.; Lee, W.-J.; Yoon, J. A Highly Specific Fluorescent Probe for Hypochlorous Acid and Its Application in Imaging Microbe-Induced HOCl Production. *J. Am. Chem. Soc.* **2013**, *135* (26), 9944–9949. https://doi.org/10.1021/ja404649m.
(727) Lin, W.; Long, L.; Chen, B.; Tan, W. A Ratiometric Fluorescent Probe for Hypochlorite Based on a Deoximation Reaction. *Chem. – Eur. J.* **2009**, *15* (10), 2305–2309. https://doi.org/10.1002/chem.200802054.
(728) Peterson, W. H.; Burris, R. H.; Sant, R.; Little, H. N. Toxic Gases in Silage, Production of Toxic Gas (Nitrogen Oxides) in Silage Making. *J. Agric. Food Chem.* **1958**, *6* (2), 121–126. https://doi.org/10.1021/jf60084a006.
(729) Ignarro, L. J. Nitric Oxide Is Not Just Blowing in the Wind. *Br. J. Pharmacol.* **2019**, *176* (2), 131–134. https://doi.org/10.1111/bph.14540.
(730) Tejero, J.; Shiva, S.; Gladwin, M. T. Sources of Vascular Nitric Oxide and Reactive Oxygen Species and Their Regulation. *Physiol. Rev.* **2019**, *99* (1), 311–379. https://doi.org/10.1152/physrev.00036.2017.
(731) Francis, S. H.; Busch, J. L.; Corbin, J. D. cGMP-Dependent Protein Kinases and cGMP Phosphodiesterases in Nitric Oxide and cGMP Action. *Pharmacol. Rev.* **2010**, *62* (3), 525–563. https://doi.org/10.1124/pr.110.002907.
(732) Evangelista, A. M.; Kohr, M. J.; Murphy, E. *S* -Nitrosylation: Specificity, Occupancy, and Interaction with Other Post-Translational Modifications. *Antioxid. Redox Signal.* **2013**, *19* (11), 1209–1219. https://doi.org/10.1089/ars.2012.5056.
(733) DeMartino, A. W.; Kim-Shapiro, D. B.; Patel, R. P.; Gladwin, M. T. Nitrite and Nitrate Chemical Biology and Signalling. *Br. J. Pharmacol.* **2019**, *176* (2), 228–245. https://doi.org/10.1111/bph.14484.
(734) Ferrer-Sueta, G.; Campolo, N.; Trujillo, M.; Bartesaghi, S.; Carballal, S.; Romero, N.; Alvarez, B.; Radi, R. Biochemistry of Peroxynitrite and Protein Tyrosine Nitration. *Chem. Rev.* **2018**, *118* (3), 1338–1408. https://doi.org/10.1021/acs.chemrev.7b00568.
(735) Farah, C.; Michel, L. Y. M.; Balligand, J.-L. Nitric Oxide Signalling in Cardiovascular Health and Disease. *Nat. Rev. Cardiol.* **2018**, *15* (5), 292–316. https://doi.org/10.1038/nrcardio.2017.224.
(736) Bogdan, C. Nitric Oxide and the Immune Response. *Nat. Immunol.* **2001**, *2* (10), 907–916. https://doi.org/10.1038/ni1001-907.
(737) Garthwaite, J. NO as a Multimodal Transmitter in the Brain: Discovery and Current Status. *Br. J. Pharmacol.* **2019**, *176* (2), 197–211. https://doi.org/10.1111/bph.14532.
(738) Basudhar, D.; Bharadwaj, G.; Somasundaram, V.; Cheng, R. Y. S.; Ridnour, L. A.; Fujita, M.; Lockett, S. J.; Anderson, S. K.; McVicar, D. W.; Wink, D. A. Understanding the Tumour Micro-environment Communication Network from an NOS2/COX2 Perspective. *Br. J. Pharmacol.* **2019**, *176* (2), 155–176. https://doi.org/10.1111/bph.14488.

(739) Wallace, J. L. Nitric Oxide in the Gastrointestinal Tract: Opportunities for Drug Development. *Br. J. Pharmacol.* **2019**, *176* (2), 147–154. https://doi.org/10.1111/bph.14527.
(740) Ritz, T.; Salsman, M. L.; Young, D. A.; Lippert, A. R.; Khan, D. A.; Ginty, A. T. Boosting Nitric Oxide in Stress and Respiratory Infection: Potential Relevance for Asthma and COVID-19. *Brain Behav. Immun. - Health* **2021**, *14*, 100255. https://doi.org/10.1016/j.bbih.2021.100255.
(741) Sun, J.; Zhang, X.; Broderick, M.; Fein, H. Measurement of Nitric Oxide Production in Biological Systems by Using Griess Reaction Assay. *Sensors* **2003**, *3* (8), 276–284. https://doi.org/10.3390/s30800276.
(742) Hogg, N. Detection of Nitric Oxide by Electron Paramagnetic Resonance Spectroscopy. *Free Radic. Biol. Med.* **2010**, *49* (2), 122–129. https://doi.org/10.1016/j.freeradbiomed.2010.03.009.
(743) Bedioui, F.; Ismail, A.; Griveau, S. Electrochemical Detection of Nitric Oxide and S-Nitrosothiols in Biological Systems: Past, Present & Future. *Curr. Opin. Electrochem.* **2018**, *12*, 42–50. https://doi.org/10.1016/j.coelec.2018.04.014.
(744) Wiersma, J. H. 2,3-Diaminonaphthalene as a Spectrophotometric and Fluorometric Reagent for the Determination of Nitrite Ion. *Anal. Lett.* **1970**, *3* (3), 123–132. https://doi.org/10.1080/00032717008067789.
(745) Sawicki, C. R. Fluorimetric Determination of Nitrate. *Anal. Lett.* **1971**, *4* (11), 761–775. https://doi.org/10.1080/00032717108058676.
(746) Miles, A. M.; Wink, D. A.; Cook, J. C.; Grisham, M. B. Determination of Nitric Oxide Using Fluorescence Spectroscopy. In *Methods in Enzymology*; Elsevier, 1996; Vol. 268, pp 105–120. https://doi.org/10.1016/S0076-6879(96)68013-6.
(747) Kojima, H.; Sakurai, K.; Kikuchi, K.; Kawahara, S.; Kirino, Y.; Nagoshi, H.; Hirata, Y.; Akaike, T.; Maeda, H.; Nagano, T. Development of a Fluorescent Indicator for the Bioimaging of Nitric Oxide. *Biol. Pharm. Bull.* **1997**, *20* (12), 1229–1232. https://doi.org/10.1248/bpb.20.1229.
(748) Kojima, H.; Sakurai, K.; Kikuchi, K.; Kawahara, S.; Kirino, Y.; Nagoshi, H.; Hirata, Y.; Nagano, T. Development of a Fluorescent Indicator for Nitric Oxide Based on the Fluorescein Chromophore. *Chem. Pharm. Bull. (Tokyo)* **1998**, *46* (2), 373–375. https://doi.org/10.1248/cpb.46.373.
(749) Kojima, H.; Nakatsubo, N.; Kikuchi, K.; Kawahara, S.; Kirino, Y.; Nagoshi, H.; Hirata, Y.; Nagano, T. Detection and Imaging of Nitric Oxide with Novel Fluorescent Indicators: Diaminofluoresceins. *Anal. Chem.* **1998**, *70* (13), 2446–2453. https://doi.org/10.1021/ac9801723.
(750) Itoh, Y.; Ma, F. H.; Hoshi, H.; Oka, M.; Noda, K.; Ukai, Y.; Kojima, H.; Nagano, T.; Toda, N. Determination and Bioimaging Method for Nitric Oxide in Biological Specimens by Diaminofluorescein Fluorometry. *Anal. Biochem.* **2000**, *287* (2), 203–209. https://doi.org/10.1006/abio.2000.4859.
(751) Schwendemann, J.; Sehringer, B.; Noethling, C.; Zahradnik, H. P.; Schaefer, W. R. Nitric Oxide Detection by DAF (Diaminofluorescein) Fluorescence in Human Myometrial Tissue. *Gynecol. Endocrinol.* **2008**, *24* (6), 306–311. https://doi.org/10.1080/09513590801994063.
(752) Giliano, N. Y.; Konevega, L. V.; Noskin, L. A. Dynamics of Intracellular Superoxide and NO Content in Human Endotheliocytes and Carcinoma Cells after Treatment with NO Synthase Inhibitors. *Bull. Exp. Biol. Med.* **2010**, *149*, 78–81. https://doi.org/10.1007/s10517-010-0880-9.
(753) Namin, S. M.; Nofallah, S.; Joshi, M. S.; Kavallieratos, K.; Tsoukias, N. M. Kinetic Analysis of DAF-FM Activation by NO: Toward Calibration of a NO-Sensitive Fluorescent Dye. *Nitric Oxide* **2013**, *28*, 39–46. https://doi.org/10.1016/j.niox.2012.10.001.

(754) Kojima, H.; Hirotani, M.; Nakatsubo, N.; Kikuchi, K.; Urano, Y.; Higuchi, T.; Hirata, Y.; Nagano, T. Bioimaging of Nitric Oxide with Fluorescent Indicators Based on the Rhodamine Chromophore. *Anal. Chem.* **2001**, *73* (9), 1967–1973. https://doi.org/10.1021/ac001136i.
(755) Zhang, X.; Wang, H.; Li, J.-S.; Zhang, H.-S. Development of a Fluorescent Probe for Nitric Oxide Detection Based on Difluoroboradiaza-s-Indacene Fluorophore. *Anal. Chim. Acta* **2003**, *481* (1), 101–108. https://doi.org/10.1016/S0003-2670(03)00064-3.
(756) Gabe, Y.; Urano, Y.; Kikuchi, K.; Kojima, H.; Nagano, T. Highly Sensitive Fluorescence Probes for Nitric Oxide Based on Boron Dipyrromethene Chromophore-Rational Design of Potentially Useful Bioimaging Fluorescence Probe. *J. Am. Chem. Soc.* **2004**, *126* (10), 3357–3367. https://doi.org/10.1021/ja037944j.
(757) Tu, F.-Q.; Zhang, L.-Y.; Guo, X.-F.; Zhang, Z.-X.; Wang, H.; Zhang, H.-S. Dual Labeling for Simultaneous Determination of Nitric Oxide, Glutathione and Cysteine in Macrophage RAW264.7 Cells by Microchip Electrophoresis with Fluorescence Detection. *J. Chromatogr. A* **2014**, *1359*, 309–316. https://doi.org/10.1016/j.chroma.2014.07.026.
(758) Zhang, X.; Chi, R.; Zou, J.; Zhang, H.-S. Development of a Novel Fluorescent Probe for Nitric Oxide Detection: 8-(3′,4′-Diaminophenyl)-Difluoroboradiaza-S-Indacence. *Spectrochim. Acta. A. Mol. Biomol. Spectrosc.* **2004**, *60* (13), 3129–3134. https://doi.org/10.1016/j.saa.2004.02.028.
(759) Zhang, X.; Zhang, H. Design, Synthesis and Characterization of a Novel Fluorescent Probe for Nitric Oxide Based on Difluoroboradiaza-s-Indacene Fluorophore. *Spectrochim. Acta. A. Mol. Biomol. Spectrosc.* **2005**, *61* (6), 1045–1049. https://doi.org/10.1016/j.saa.2004.05.041.
(760) Huang, K.-J.; Wang, H.; Zhang, Q.-Y.; Ma, M.; Hu, J.-F.; Zhang, H.-S. Direct Detection of Nitric Oxide in Human Blood Serum by Use of 1,3,5,7-Tetramethyl-8-(3′,4′-Diaminophenyl)Difluoroboradiaza-s-Indacene with HPLC. *Anal. Bioanal. Chem.* **2006**, *384* (6), 1284–1290. https://doi.org/10.1007/s00216-006-0312-x.
(761) Huang, K.-J.; Zhang, M.; Xie, W.-Z.; Zhang, H.-S.; Feng, Y.-Q.; Wang, H. Sensitive Determination of Nitric Oxide in Some Rat Tissues Using Polymer Monolith Microextraction Coupled to High-Performance Liquid Chromatography with Fluorescence Detection. *Anal. Bioanal. Chem.* **2007**, *388*, 939–946. https://doi.org/10.1007/s00216-007-1283-2.
(762) Gabe, Y.; Ueno, T.; Urano, Y.; Kojima, H.; Nagano, T. Tunable Design Strategy for Fluorescence Probes Based on 4-Substituted BODIPY Chromophore: Improvement of Highly Sensitive Fluorescence Probe for Nitric Oxide. *Anal. Bioanal. Chem.* **2006**, *386* (3), 621–626. https://doi.org/10.1007/s00216-006-0587-y.
(763) Huang, K.-J.; Zhang, M.; Xie, W.-Z.; Zhang, H.-S.; Feng, Y.-Q.; Wang, H. Determination of Nitric Oxide in Hydrophytes Using Poly(Methacrylic Acid-Ethylene Glycol Dimethacrylate) Monolith Microextraction Coupled to High-Performance Liquid Chromatography with Fluorescence Detection. *J. Chromatogr. B Analyt. Technol. Biomed. Life. Sci.* **2007**, *854* (1), 135–142. https://doi.org/10.1016/j.jchromb.2007.04.012.
(764) Huang, K.-J.; Wang, H.; Ma, M.; Sha, M.-L.; Zhang, H.-S. Ultrasound-Assisted Liquid-Phase Microextraction and High-Performance Liquid Chromatographic Determination of Nitric Oxide Produced in PC12 Cells Using 1,3,5,7-Tetramethyl-2,6-Dicarbethoxy-8-(3’,4’-Diaminophenyl)-Difluoroboradiaza-s-Indacene. *J. Chromatogr. A* **2006**, *1103* (2), 193–201. https://doi.org/10.1016/j.chroma.2005.11.015.
(765) Zhang, H.-X.; Chen, J.-B.; Guo, X.-F.; Wang, H.; Zhang, H.-S. Highly Sensitive Determination of Nitric Oxide in Biologic Samples by a Near-Infrared BODIPY-Based Fluorescent Probe Coupled with High-Performance Liquid Chromatography. *Talanta* **2013**, *116*, 335–342. https://doi.org/10.1016/j.talanta.2013.05.043.
(766) K. Vegesna, G.; Sripathi, S. R.; Zhang, J.; Zhu, S.; He, W.; Luo, F.-T.; Jahng, W. J.; Frost, M.; Liu, H. Highly Water-Soluble BODIPY-Based Fluorescent Probe for Sensitive and

Selective Detection of Nitric Oxide in Living Cells. *ACS Appl. Mater. Interfaces* **2013**, *5* (10), 4107–4112. https://doi.org/10.1021/am303247s.
(767) Chen, J.-B.; Zhang, H.-X.; Guo, X.-F.; Wang, H.; Zhang, H.-S. Novel B,O-Chelated Fluorescent Probe for Nitric Oxide Imaging in Raw 264.7 Macrophages and Onion Tissues. *Anal. Chim. Acta* **2013**, *800*, 77–86. https://doi.org/10.1016/j.aca.2013.09.019.
(768) Zhang, W.; Zhang, J.; Zhang, H.; Cao, L.; Zhang, R.; Ye, Z.; Yuan, J. Development and Application of a Ruthenium(II) Complex-Based Photoluminescent and Electrochemiluminescent Dual-Signaling Probe for Nitric Oxide. *Talanta* **2013**, *116*, 354–360. https://doi.org/10.1016/j.talanta.2013.05.064.
(769) Zhang, H.-X.; Chen, J.-B.; Guo, X.-F.; Wang, H.; Zhang, H.-S. Highly Sensitive Low-Background Fluorescent Probes for Imaging of Nitric Oxide in Cells and Tissues. *Anal. Chem.* **2014**, *86* (6), 3115–3123. https://doi.org/10.1021/ac4041718.
(770) Zhang, Z.-X.; Guo, X.-F.; Wang, H.; Zhang, H.-S. Capillary Electrophoresis Strategy to Monitor the Released and Remaining Nitric Oxide from the Same Single Cell Using a Specially Designed Water-Soluble Fluorescent Probe. *Anal. Chem.* **2015**, *87* (7), 3989–3995. https://doi.org/10.1021/acs.analchem.5b00191.
(771) Yao, H.-W.; Zhu, X.-Y.; Guo, X.-F.; Wang, H. An Amphiphilic Fluorescent Probe Designed for Extracellular Visualization of Nitric Oxide Released from Living Cells. *Anal. Chem.* **2016**, *88* (18), 9014–9021. https://doi.org/10.1021/acs.analchem.6b01532.
(772) Bobba, K.; Saranya, G.; Alex, S.; Velusamy, N.; Maiti, K.; Bhuniya, S. SERS-Active Multi-Channel Fluorescent Probe for NO: Guide to Discriminate Intracellular Biothiols. *Sens. ACTUATORS B-Chem.* **2018**, *260*, 165–173. https://doi.org/10.1016/j.snb.2017.12.174.
(773) Zhang, J.; Pan, F.; Jin, Y.; Wang, N.; He, J.; Zhang, W.; Zhao, W. A BODIPY-Based Dual-Responsive Turn-on Fluorescent Probe for NO and Nitrite. *Dyes Pigments* **2018**, *155*, 276–283. https://doi.org/10.1016/j.dyepig.2018.03.035.
(774) Chen, X.-X.; Niu, L.-Y.; Shao, N.; Yang, Q.-Z. BODIPY-Based Fluorescent Probe for Dual-Channel Detection of Nitric Oxide and Glutathione: Visualization of Cross-Talk in Living Cells. *Anal. Chem.* **2019**, *91* (7), 4301–4306. https://doi.org/10.1021/acs.analchem.9b00169.
(775) Xue, Q.; Wang, S.; Bi, X.; Chen, Z.; Zhu, H.; Chen, W.; Lu, H.; Guo, Z. An Electronic-Tuning Strategy to Improve the Responsiveness of Nitric Oxide Probe. *Dyes Pigments* **2023**, *218*, 111486. https://doi.org/10.1016/j.dyepig.2023.111486.
(776) Jiang, Z.; Liang, Z.; Cui, Y.; Zhang, C.; Wang, J.; Wang, H.; Wang, T.; Chen, Y.; He, W.; Liu, Z.; Guo, Z. Blood–Brain Barrier Permeable Photoacoustic Probe for High-Resolution Imaging of Nitric Oxide in the Living Mouse Brain. *J. Am. Chem. Soc.* **2023**, *145* (14), 7952–7961. https://doi.org/10.1021/jacs.2c13315.
(777) Sasaki, E.; Kojima, H.; Nishimatsu, H.; Urano, Y.; Kikuchi, K.; Hirata, Y.; Nagano, T. Highly Sensitive Near-Infrared Fluorescent Probes for Nitric Oxide and Their Application to Isolated Organs. *J. Am. Chem. Soc.* **2005**, *127* (11), 3684–3685. https://doi.org/10.1021/ja042967z.
(778) Zhegalova, N. G.; Gonzales, G.; Berezin, M. Y. Synthesis of Nitric Oxide Probes with Fluorescence Lifetime Sensitivity. *Org. Biomol. Chem.* **2013**, *11* (47), 8228. https://doi.org/10.1039/c3ob41498a.
(779) Mao, Z.; Feng, W.; Li, Z.; Zeng, L.; Lv, W.; Liu, Z. NIR in, Far-Red out: Developing a Two-Photon Fluorescent Probe for Tracking Nitric Oxide in Deep Tissue. *Chem. Sci.* **2016**, *7* (8), 5230–5235. https://doi.org/10.1039/C6SC01313A.
(780) Wang, B.; Yu, S.; Chai, X.; Li, T.; Wu, Q.; Wang, T. A Lysosome-Compatible Near-Infrared Fluorescent Probe for Targeted Monitoring of Nitric Oxide. *Chem. - Eur. J.* **2016**, *22*, 5649–5656. https://doi.org/10.1002/chem.201505054.

(781) Tang, J.; Guo, Z.; Zhang, Y.; Bai, B.; Zhu, W.-H. Rational Design of a Fast and Selective Near-Infrared Fluorescent Probe for Targeted Monitoring of Endogenous Nitric Oxide. *Chem. Commun.* **2017**, *53*, 10520–10523. https://doi.org/10.1039/c7cc05971j.
(782) Huo, Y.; Miao, J.; Han, L.; Li, Y.; Li, Z.; Shi, Y.; Guo, W. Selective and Sensitive Visualization of Endogenous Nitric Oxide in Living Cells and Animals by a Si-Rhodamine Deoxylactam-Based near-Infrared Fluorescent Probe. *Chem. Sci.* **2017**, *8* (10), 6857–6864. https://doi.org/10.1039/C7SC02608K.
(783) Liu, S.; Zhu, Y.; Wu, P.; Xiong, H. Highly Sensitive D-A-D-Type Near-Infrared Fluorescent Probe for Nitric Oxide Real-Time Imaging in Inflammatory Bowel Disease. *Anal. Chem.* **2021**, *93* (11), 4975–4983. https://doi.org/10.1021/acs.analchem.1c00281.
(784) Zheng, H.; Shang, G.-Q.; Yang, S.-Y.; Gao, X.; Xu, J.-G. Fluorogenic and Chromogenic Rhodamine Spirolactam Based Probe for Nitric Oxide by Spiro Ring Opening Reaction. *Org. Lett.* **2008**, *10* (12), 2357–2360. https://doi.org/10.1021/ol800206x.
(785) Yuan, L.; Lin, W.; Xie, Y.; Chen, B.; Song, J. Development of a Ratiometric Fluorescent Sensor for Ratiometric Imaging of Endogenously Produced Nitric Oxide in Macrophage Cells. *Chem. Commun.* **2011**, *47*, 9372–9374. https://doi.org/10.1039/c1cc13047a.
(786) Yu, H.; Jin, L.; Dai, Y.; Li, H.; Xiao, Y. From a BODIPY-Rhodamine Scaffold to a Ratiometric Fluorescent Probe for Nitric Oxide. *New J. Chem.* **2013**, *37*, 1688–1691. https://doi.org/10.1039/c3nj41127c.
(787) Ong, J.; Pang, V.; Tng, L.; Ang, W. Pre-Assembled Coumarin-Rhodamine Scaffold for Ratiometric Sensing of Nitric Oxide and Hypochlorite. *Chem.- Eur. J.* **2018**, *24* (8), 1870–1876. https://doi.org/10.1002/chem.201703554.
(788) Zhu, X.; Chen, J.-Q.; Ma, C.; Liu, X.; Cao, X.-P.; Zhang, H. A Ratiometric Mitochondria-Targeting Two-Photon Fluorescent Probe for Imaging of Nitric Oxide in Vivo. *Analyst* **2017**, *142*, 4623–4628. https://doi.org/10.1039/c7an01461a.
(789) Chen, L.; Wu, D.; Yoon, J. An ESIPT Based Fluorescence Probe for Ratiometric Monitoring of Nitric Oxide. *Sens. Actuators B Chem.* **2018**, *259*, 347–353. https://doi.org/10.1016/j.snb.2017.12.073.
(790) Reinhardt, C.; Zhou, E.; Jorgensen, M.; Partipilo, G.; Chan, J. A Ratiometric Acoustogenic Probe for in Vivo Imaging of Endogenous Nitric Oxide. *J. Am. Chem. Soc.* **2018**, *140* (3), 1011–1018. https://doi.org/10.1021/jacs.7b10783.
(791) Zhao, L.; Huang, Z.; Ma, D.; Yan, Y.; Zhang, X.; Xiao, Y. A Nucleus Targetable Fluorescent Probe for Ratiometric Imaging of Endogenous NO in Living Cells and Zebrafishes. *ANALYST* **2021**, *146* (13), 4130–4134. https://doi.org/10.1039/d1an00426c.
(792) Wang, L.; Wang, Z.; Chen, Y.; Huang, Z.; Huang, X.; Xue, M.; Cheng, H.; Li, B.; Liu, P. A Novel Dual-Channel Fluorescent Probe for Selectively and Sensitively Imaging Endogenous Nitric Oxide in Living Cells and Zebrafish. *Spectrochim. Acta. A. Mol. Biomol. Spectrosc.* **2022**, *277*, 121280. https://doi.org/10.1016/j.saa.2022.121280.
(793) Han, S.; Yang, L.; Liu, M.; Li, H.; Song, X. Accurate Diagnosis of Hepatic Fibrosis with Dual Detection of Nitric Oxide and Viscosity by a Ratiometric Fluorescent Probe. *Chem. Eng. J.* **2023**, *463*, 142383. https://doi.org/10.1016/j.cej.2023.142383.
(794) Seo, E. W.; Han, J. H.; Heo, C. H.; Shin, J. H.; Kim, H. M.; Cho, B. R. A Small-Molecule Two-Photon Probe for Nitric Oxide in Living Tissues. *Chem. - Eur. J.* **2012**, *18*, 12388. https://doi.org/10.1002/chem.201201197.
(795) Yu, H.; Xiao, Y.; Jin, L. A Lysosome-Targetable and Two-Photon Fluorescent Probe for Monitoring Endogenous and Exogenous Nitric Oxide in Living Cells. *J. Am. Chem. Soc.* **2012**, *134* (42), 17486–17489. https://doi.org/10.1021/ja308967u.
(796) Liu, Q.; Xue, L.; Zhu, D.-J.; Li, G.-P.; Jiang, H. Highly Selective Two-Photon Fluorescent Probe for Imaging of Nitric Oxide in Living Cells. *Chin. Chem. Lett.* **2014**, *25*, 19–23. https://doi.org/10.1016/j.cclet.2013.11.024.

(797) Dong, X.; Heo, C. H.; Chen, S.; Kim, H. M.; Liu, Z. Quinoline-Based Two-Photon Fluorescent Probe for Nitric Oxide in Live Cells and Tissues. *Anal. Chem.* **2014**, *86* (1), 308–311. https://doi.org/10.1021/ac403226h.
(798) Chen, X.; Sun, L.; Chen, Y.; Cheng, X.; Wu, W.; Ji, L.; Chao, H. A Fast and Selective Two-Photon Phosphorescent Probe for the Imaging of Nitric Oxide in Mitochondria. *Biomaterials* **2015**, *58*, 72–81. https://doi.org/10.1016/j.biomaterials.2015.04.012.
(799) Li, S.; Zhou, D.; Li, Y.; Liu, H.; Wu, P.; Ou-Yang, J.; Jiang, W.; Li, C. Efficient Two-Photon Fluorescent Probe for Imaging of Nitric Oxide during Endoplasmic Reticulum Stress. *ACS Sens.* **2018**, *3* (11), 2311–2319. https://doi.org/10.1021/acssensors.8b00567.
(800) Xu, C.; Xin, C.; Yu, C.; Wu, M.; Xu, J.; Qin, W.; Ding, Y.; Wang, X.; Li, L.; Huang, W. Fast Response Two-Photon Fluorogenic Probe Based on Schiff Base Derivatives for Monitoring Nitric Oxide Levels in Living Cells and Zebrafish. *Chem. Commun.* **2018**, *54* (96). https://doi.org/10.1039/c8cc06698a.
(801) Wu, W.; Guan, R.; Liao, X.; Yan, X.; Rees, T. W.; Ji, L.; Chao, H. Bimodal Visualization of Endogenous Nitric Oxide in Lysosomes with a Two-Photon Iridium(III) Phosphorescent Probe. *Anal. Chem.* **2019**, *91* (15), 10266–10272. https://doi.org/10.1021/acs.analchem.9b02415.
(802) Tang, C.; Wang, M.; Shang, X.; Chen, X.; Huang, D.; Zheng, Q. Real-Time Monitoring of Intracellular Nitric Oxide Using a Long-Wavelength-Emitting Probe via One-Photon or Two-Photon Excitation. *J. Mater. Chem. C* **2019**, *7* (11), 3246–3252. https://doi.org/10.1039/c8tc06238b.
(803) Yu, H.; Zhang, X.; Xiao, Y.; Zou, W.; Wang, L.; Jin, L. Targetable Fluorescent Probe for Monitoring Exogenous and Endogenous NO in Mitochondria of Living Cells. *Anal. Chem.* **2013**, *85* (15), 7076–7084. https://doi.org/10.1021/ac401916z.
(804) Wang, C.; Song, X.; Han, Z.; Li, X.; Xu, Y.; Xiao, Y. Monitoring Nitric Oxide in Subcellular Compartments by Hybrid Probe Based on Rhodamine Spirolactam and SNAP-Tag. *ACS Chem. Biol.* **2016**, *11* (7), 2033–2040. https://doi.org/10.1021/acschembio.5b01032.
(805) Veetil, A. T.; Zou, J.; Henderson, K. W.; Jani, M. S.; Shaik, S. M.; Sisodia, S. S.; Hale, M. E.; Krishnan, Y. DNA-Based Fluorescent Probes of NOS2 Activity in Live Brains. *Proc. Natl. Acad. Sci.* **2020**, *117* (26), 14694–14702. https://doi.org/10.1073/pnas.2003034117.
(806) Zhou, L.; Liu, C.; Zheng, Y.; Huang, Z.; Zhang, X.; Xiao, Y. Bio-Orthogonal Toolbox for Monitoring Nitric Oxide in Targeted Organelles of Live Cells and Zebrafishes. *Anal. Chem.* **2022**, *94* (45), 15678–15685. https://doi.org/10.1021/acs.analchem.2c02768.
(807) Sun, Y.-Q.; Liu, J.; Zhang, H.; Huo, Y.; Lv, X.; Shi, Y.; Guo, W. A Mitochondria-Targetable Fluorescent Probe for Dual-Channel NO Imaging Assisted by Intracellular Cysteine and Glutathione. *J. Am. Chem. Soc.* **2014**, *136* (36), 12520–12523. https://doi.org/10.1021/ja504156a.
(808) Feng, W.; Qiao, Q.-L.; Leng, S.; Miao, L.; Yin, W.-T.; Wang, L.-Q.; Xu, Z.-C. A 1,8-Naphthalimide-Derived Turn-on Fluorescent Probe for Imaging Lysosomal Nitric Oxide in Living Cells. *Chin. Chem. Lett.* **2016**, *27* (9), 1554–1558. https://doi.org/10.1016/j.cclet.2016.06.016.
(809) Dai, Z.; Tian, L.; Song, B.; Liu, X.; Yuan, J. Development of a Novel Lysosome-Targetable Time-Gated Luminescence Probe for Ratiometric and Luminescence Lifetime Detection of Nitric Oxide in Vivo. *Chem. Sci.* **2017**, *8* (3), 1969–1976. https://doi.org/10.1039/C6SC03667H.
(810) Wang, F.; Yu, S.; Xu, Z.; Li, L.; Dang, Y.; Xu, X.; Luo, Y.; Cheng, Z.; Yu, H.; Zhang, W.; Zhang, A.; Ding, C. Acid-Promoted D-A-D Type Far-Red Fluorescent Probe with High Photostability for Lysosomal Nitric Oxide Imaging. *Anal. Chem.* **2018**, *90* (13), 7953–7962. https://doi.org/10.1021/acs.analchem.8b00612.

(811) Zhang, P.; Tian, Y.; Liu, H.; Ren, J.; Wang, H.; Zeng, R.; Long, Y.; Chen, J. In Vivo Imaging of Hepatocellular Nitric Oxide Using a Hepatocyte-Targeting Fluorescent Sensor. *Chem. Commun.* **2018**, *54* (52), 7231–7234. https://doi.org/10.1039/c8cc03240h.
(812) He, Z.; Liu, D.; Liu, Y.; Li, X.; Shi, W.; Ma, H. Golgi-Targeted Fluorescent Probe for Imaging NO in Alzheimer's Disease. *Anal. Chem.* **2022**, *94* (28), 10256–10262. https://doi.org/10.1021/acs.analchem.2c01885.
(813) Takakura, H.; Kojima, R.; Kamiya, M.; Kobayashi, E.; Komatsu, T.; Ueno, T.; Terai, T.; Hanaoka, K.; Nagano, T.; Urano, Y. New Class of Bioluminogenic Probe Based on Bioluminescent Enzyme-Induced Electron Transfer: BioLeT. *J. Am. Chem. Soc.* **2015**, *137* (12), 4010–4013. https://doi.org/10.1021/ja511014w.
(814) Yadav, A. K.; Lee, M. C.; Lucero, M. Y.; Su, S.; Reinhardt, C. J.; Chan, J. Activity-Based NIR Bioluminescence Probe Enables Discovery of Diet-Induced Modulation of the Tumor Microenvironment via Nitric Oxide. *ACS Cent. Sci.* **2022**, *8* (4), 461–472. https://doi.org/10.1021/acscentsci.1c00317.
(815) Wang, S.; Li, Z.; Liu, Y.; Feng, G.; Zheng, J.; Yuan, Z.; Zhang, X. Activatable Photoacoustic and Fluorescent Probe of Nitric Oxide for Cellular and in Vivo Imaging. *Sens. Actuators B-Chem.* **2018**, *267*, 403–411. https://doi.org/10.1016/j.snb.2018.04.052.
(816) Rathnamalala, C. S. L.; Hernandez, S.; Lucero, M. Y.; Swartchick, C. B.; Kalam Shaik, A.; Hammer, N. I.; East, A. K.; Gwaltney, S. R.; Chan, J.; Scott, C. N. Xanthene-Based Nitric Oxide-Responsive Nanosensor for Photoacoustic Imaging in the SWIR Window. *Angew. Chem. Int. Ed.* **2023**, *62* (13). https://doi.org/10.1002/anie.202214855.
(817) Hu, J.; Yin, L.; Xu, K.; Gao, J.; Tong, L.; Tang, B. Vicinal Diaminobenzoacridine Used as the Fluorescent Probe for Trace Nitric Oxide Determination by Flow Injection Spectrofluorimetry and Macrophage Cells Imaging. *Anal. Chim. Acta* **2008**, *606* (1), 57–62. https://doi.org/10.1016/j.aca.2007.10.055.
(818) Ding, L.; Yuan, F.; Huang, L.; Huang, J.; Liu, X.; Liang, B. A Novel Fluorescence Probe 9-(4-(1,2-Diamine)Benzene-N1-Phenyl)Acridine for Nitric Oxide Determination. *J. Wuhan Univ. Technol. Mater. Sci. Ed.* **2014**, *29*, 848–853. https://doi.org/10.1007/s11595-014-1007-3.
(819) Wang, M.; Xu, Z.; Wang, X.; Cui, J. A Fluorescent and Colorimetric Chemosensor for Nitric Oxide Based on 1,8-Naphthalimide. *Dyes Pigments* **2013**, *96* (2), 333–337. https://doi.org/10.1016/j.dyepig.2012.08.024.
(820) Huang, C.-B.; Huang, J.; Xu, L. A Highly Selective Fluorescent Probe for Fast Detection of Nitric Oxide in Aqueous Solution. *RSC Adv.* **2015**, *5* (18), 13307–13310. https://doi.org/10.1039/C4RA08337G.
(821) Gupta, N.; Imam Reja, S.; Bhalla, V.; Gupta, M.; Kaur, G.; Kumar, M. An Approach for the Selective Detection of Nitric Oxide in Biological Systems: An in Vitro and in Vivo Perspective. *Chem. - Asian J.* **2016**, *11*, 1020–1027. https://doi.org/10.1002/asia.201501333.
(822) Zhang, R.; Ye, Z.; Wang, G.; Zhang, W.; Yuan, J. Development of a Ruthenium(II) Complex Based Luminescent Probe for Imaging Nitric Oxide Production in Living Cells. *Chem. - Eur. J.* **2010**, *16* (23), 6884–6891. https://doi.org/10.1002/chem.200903267.
(823) Vidanapathirana, A.; Pullen, B.; Zhang, R.; Duong, M.; Goyne, J.; Zhang, X.; Bonder, C.; Abell, A.; Bursill, C.; Nicholls, S.; Psaltis, P. A Novel Ruthenium-Based Molecular Sensor to Detect Endothelial Nitric Oxide. *Sci. Rep.* **2019**, *9*. https://doi.org/10.1038/s41598-019-39123-3.
(824) Yu, X.; Zhang, R.; Ye, Z.; Song, B.; Yuan, J. Design and Synthesis of a Ruthenium(II) Complex-Based Luminescent Probe for Highly Selective and Sensitive Luminescence Detection of Nitric Oxide. *J. Fluoresc.* **2013**, *23* (6), 1113–1120. https://doi.org/10.1007/s10895-013-1240-8.

(825) Wu, C.; Wu, K.; Kang, T.; Wang, H.; Leung, C.; Liu, J.; Ma, D. Iridium-Based Probe for Luminescent Nitric Oxide Monitoring in Live Cells. *Sci. Rep.* **2018**, *8*. https://doi.org/10.1038/s41598-018-30991-9.
(826) Chen, Y.; Guo, W.; Ye, Z.; Wang, G.; Yuan, J. A Europium(Iii) Chelate as an Efficient Time-Gated Luminescent Probe for Nitric Oxide. *Chem. Commun.* **2011**, *47* (22), 6266. https://doi.org/10.1039/c0cc05658h.
(827) Liu, M.; Ye, Z.; Wang, G.; Yuan, J. Development of a Novel Europium(III) Complex-Based Luminescence Probe for Time-Resolved Luminescence Imaging of the Nitric Oxide Production in Neuron Cells. *Talanta* **2012**, *99*, 951–958. https://doi.org/10.1016/j.talanta.2012.07.064.
(828) Lin, L.-Y.; Lin, X.-Y.; Lin, F.; Wong, K.-T. A New Spirobifluorene-Bridged Bipolar System for a Nitric Oxide Turn-On Fluorescent Probe. *Org. Lett.* **2011**, *13* (9), 2216–2219. https://doi.org/10.1021/ol200463m.
(829) Liu, W.; Fan, C.; Sun, R.; Xu, Y.-J.; Ge, J.-F. Near-Infrared Emission of Dibenzoxanthenium and Its Application in the Design of Nitric Oxide Probes. *Org. Biomol. Chem.* **2015**, *13* (15), 4532–4538. https://doi.org/10.1039/C5OB00042D.
(830) Weng, M.; Yang, X.; Ni, Y.; Xu, C.; Zhang, H.; Shao, J.; Shi, N.; Zhang, C.; Wu, Q.; Li, L.; Huang, W. Deep-Red Fluorogenic Probe for Rapid Detection of Nitric Oxide in Parkinson's Disease Models. *Sens. Actuators B Chem.* **2019**, *283*, 769–775. https://doi.org/10.1016/j.snb.2018.12.071.
(831) Yuan, L.; Lin, W.; Xie, Y.; Chen, B.; Zhu, S. Single Fluorescent Probe Responds to H_2O_2, NO, and H_2O_2/NO with Three Different Sets of Fluorescence Signals. *J. Am. Chem. Soc.* **2012**, *134* (2), 1305–1315. https://doi.org/10.1021/ja2100577.
(832) Zhang, P.; Li, J.; Li, B.; Xu, J.; Zeng, F.; Lv, J.; Wu, S. A Logic Gate-Based Fluorescent Sensor for Detecting H2S and NO in Aqueous Media and inside Live Cells. *Chem. Commun.* **2015**, *51*, 4414–4416. https://doi.org/10.1039/c4cc09737h.
(833) Chen, X.; Niu, L.; Yang, Q. Visualizing the Underlying Signaling Pathway Related to Nitric Oxide and Glutathione in Cardiovascular Disease Therapy by a Sequentially Activated Fluorescent Probe. *Anal. Chem.* **2021**, *93* (8), 3922–3928. https://doi.org/10.1021/acs.analchem.0c04754.
(834) Chen, X.; Wu, Y.; Ge, X.; Lei, L.; Niu, L.; Yang, Q.; Zheng, L. In Vivo Imaging of Heart Failure with Preserved Ejection Fraction by Simultaneous Monitoring of Cardiac Nitric Oxide and Glutathione Using a Three-Channel Fluorescent Probe. *Biosens. Bioelectron.* **2022**, *214*. https://doi.org/10.1016/j.bios.2022.114510.
(835) Zhang, X.; Kim, W.-S.; Hatcher, N.; Potgieter, K.; Moroz, L. L.; Gillette, R.; Sweedler, J. V. Interfering with Nitric Oxide Measurements. *J. Biol. Chem.* **2002**, *277* (50), 48472–48478. https://doi.org/10.1074/jbc.M209130200.
(836) Ye, X.; Rubakhin, S. S.; Sweedler, J. V. Simultaneous Nitric Oxide and Dehydroascorbic Acid Imaging by Combining Diaminofluoresceins and Diaminorhodamines. *J. Neurosci. Methods* **2008**, *168* (2), 373–382. https://doi.org/10.1016/j.jneumeth.2007.10.026.
(837) Yang, Y.; Seidlits, S. K.; Adams, M. M.; Lynch, V. M.; Schmidt, C. E.; Anslyn, E. V.; Shear, J. B. A Highly Selective Low-Background Fluorescent Imaging Agent for Nitric Oxide. *J. Am. Chem. Soc.* **2010**, *132* (38), 13114–13116. https://doi.org/10.1021/ja1040013.
(838) Lv, X.; Wang, Y.; Zhang, S.; Liu, Y.; Zhang, J.; Guo, W. A Specific Fluorescent Probe for NO Based on a New NO-Binding Group. *Chem. Commun.* **2014**, *50*, 7499–7502. https://doi.org/10.1039/c4cc03540b.
(839) Dai, C.-G.; Wang, J.-L.; Fu, Y.-L.; Zhou, H.-P.; Song, Q.-H. Selective and Real-Time Detection of Nitric Oxide by a Two-Photon Fluorescent Probe in Live Cells and Tissue Slices. *Anal. Chem.* **2017**, *89* (19), 10511–10519. https://doi.org/10.1021/acs.analchem.7b02680.

(840) Li, C.; Tang, W.; Feng, W.; Liu, C.; Song, Q. A Rapid-Response and Ratiometric Fluorescent Probe for Nitric Oxide: From the Mitochondria to the Nucleus in Live Cells. *Anal. Chim. ACTA* **2020**, *1096*, 148–158. https://doi.org/10.1016/j.aca.2019.10.047.
(841) Escamilla, P.; Shen, Y.; Zhang, Q.; Hernandez, D.; Howard, C.; Qian, X.; Filonov, D.; Kinev, A.; Shear, J.; Anslyn, E.; Yang, Y. 2-Amino-3 '-Dialkylaminobiphenyl-Based Fluorescent Intracellular Probes for Nitric Oxide Surrogate N_2O_3. *Chem. Sci.* **2020**, *11* (5), 1394–1403. https://doi.org/10.1039/c9sc04304g.
(842) Yu, Y.; Zhang, X.; Dong, Y.; Luo, X.; Qian, X.; Yang, Y. Fusing the Nagano's and the Anslyn's Chemistry for Lyso-Specific NO Detection. *Sens. Actuators B-Chem.* **2021**, *346*. https://doi.org/10.1016/j.snb.2021.130562.
(843) Tang, C.; Wang, M.; Wu, C.; Zheng, Q. Selective Visualization of Nitric Oxide in Living Cells and Tissue Slices Using a Mitochondria-Targetable Fluorescent Probe. *Dyes Pigments* **2023**, *217*, 111443. https://doi.org/10.1016/j.dyepig.2023.111443.
(844) Ghebremariam, Y. T.; Huang, N. F.; Kambhampati, S.; Volz, K. S.; Joshi, G. G.; Anslyn, E. V.; Cooke, J. P. Characterization of a Fluorescent Probe for Imaging Nitric Oxide. *J. Vasc. Res.* **2014**, *51*, 68–79. https://doi.org/10.1159/000356445.
(845) Shen, Y.-M.; Song, L.-L.; Qian, X.-H.; Yang, Y.-J. A Scalable Synthesis of 1-Amino-5-Cyanonaphthalene, a Precursor for a Nitric Oxide Probe (NO550) Designed via the Dye Assembly Principle. *Chin. Chem. Lett.* **2013**, *24*, 7–8. https://doi.org/10.1016/j.cclet.2013.01.019.
(846) Shiue, T.-W.; Chen, Y.-H.; Wu, C.-M.; Singh, G.; Chen, H.-Y.; Hung, C.-H.; Liaw, W.-F.; Wang, Y.-M. Nitric Oxide Turn-on Fluorescent Probe Based on Deamination of Aromatic Primary Monoamines. *Inorg. Chem.* **2012**, *51* (9), 5400–5408. https://doi.org/10.1021/ic300379u.
(847) Adarsh, N.; Krishnan, M. S.; Ramaiah, D. Sensitive Naked Eye Detection of Hydrogen Sulfide and Nitric Oxide by Aza-BODIPY Dyes in Aqueous Medium. *Anal. Chem.* **2014**, *86* (18), 9335–9342. https://doi.org/10.1021/ac502849d.
(848) Zhao, B.; Yang, Y.; Wu, Y.; Yang, B.; Chai, J.; Hu, X.; Liu, B. To Re-Evaluate the Emission Mechanism, AIE Activity of 5-Azidofluorescein and Its Reaction with H2S and NO. *Sens. Actuators B-Chem.* **2018**, *256*, 79–88. https://doi.org/10.1016/j.snb.2017.10.020.
(849) Beltran, A.; Isabel Burguete, M.; Abanades, D. R.; Perez-Sala, D.; Luis, S. V.; Galindo, F. Turn-on Fluorescent Probes for Nitric Oxide Sensing Based on the Ortho-Hydroxyamino Structure Showing No Interference with Dehydroascorbic Acid. *Chem. Commun.* **2014**, *50*, 3579–3581. https://doi.org/10.1039/c3cc49555h.
(850) Resta, I.; Bedrina, B.; Martinez-Planes, E.; Minguela, A.; Galindo, F. Detection of Subcellular Nitric Oxide in Mitochondria Using a Pyrylium Probe: Assays in Cell Cultures and Peripheral Blood. *J. Mater. Chem. B* **2021**, *9* (48), 9885–9892. https://doi.org/10.1039/d1tb02326h.
(851) Li, X.; Chen, H.; Wang, Y.; Chen, H.; Gao, Y. BODIPY-Based NO Probe for Macrophage-Targeted Immunotherapy Response Monitoring. *Anal. Chem.* **2023**, *95* (18), 7320–7328. https://doi.org/10.1021/acs.analchem.3c00409.
(852) Miao, J.; Huo, Y.; Lv, X.; Li, Z.; Cao, H.; Shi, H.; Shi, Y.; Guo, W. Fast-Response and Highly Selective Fluorescent Probes for Biological Signaling Molecule NO Based on N-Nitrosation of Electron-Rich Aromatic Secondary Amines. *Biomaterials* **2016**, *78*, 11–19. https://doi.org/10.1016/j.biomaterials.2015.11.011.
(853) Mao, Z.; Jiang, H.; Song, X.; Hu, W.; Liu, Z. Development of a Silicon-Rhodamine Based Near-Infrared Emissive Two-Photon Fluorescent Probe for Nitric Oxide. *Anal. Chem.* **2017**, *89* (18), 9620–9624. https://doi.org/10.1021/acs.analchem.7b02697.
(854) Islam, A.; Sasmal, M.; Maiti, D.; Dutta, A.; Show, B.; Ali, M. Design of a Pyrene Scaffold Multifunctional Material: Real-Time Turn-On Chemosensor for Nitric Oxide, AIEE Behavior,

and Detection of TNP Explosive. *ACS Omega* **2018**, *3* (8), 10306–10316. https://doi.org/10.1021/acsomega.8b01294.
(855) Maiti, D.; Islam, A.; Sasmal, M.; Prodhan, C.; Ali, M. Selective Sensing of Nitric Oxide by a 9,10-Phenanthroquinone-Pyridoxal Based Fluorophore. *Photochem. Photobiol. Sci.* **2018**, *17* (9), 1213–1221. https://doi.org/10.1039/c8pp00115d.
(856) Dutta, A.; Islam, A.; Maiti, D.; Sasmal, M.; Pradhan, C.; Ali, M. A Smart Molecular Probe for Selective Recognition of Nitric Oxide in 100% Aqueous Solution with Cell Imaging Application and DFT Studies. *Org. Biomol. Chem.* **2019**, *17* (9), 2492–2501. https://doi.org/10.1039/c9ob00177h.
(857) Reinhardt, C. J.; Xu, R.; Chan, J. Nitric Oxide Imaging in Cancer Enabled by Steric Relaxation of a Photoacoustic Probe Platform. *Chem. Sci.* **2020**, *11* (6), 1587–1592. https://doi.org/10.1039/C9SC05600A.
(858) Huo, Y.; Miao, J.; Fang, J.; Shi, H.; Wang, J.; Guo, W. Aromatic Secondary Amine-Functionalized Fluorescent NO Probes: Improved Detection Sensitivity for NO and Potential Applications in Cancer Immunotherapy Studies. *Chem. Sci.* **2019**, *10* (1), 145–152. https://doi.org/10.1039/C8SC03694B.
(859) Sun, L.; Ouyang, J.; Ma, Y.; Zeng, Z.; Zeng, C.; Zeng, F.; Wu, S. An Activatable Probe with Aggregation-Induced Emission for Detecting and Imaging Herbal Medicine Induced Liver Injury with Optoacoustic Imaging and NIR-II Fluorescence Imaging. *Adv. Healthc. Mater.* **2021**, *10* (24). https://doi.org/10.1002/adhm.202100867.
(860) Lucero, M. Y.; East, A. K.; Reinhardt, C. J.; Sedgwick, A. C.; Su, S.; Lee, M. C.; Chan, J. Development of NIR-II Photoacoustic Probes Tailored for Deep-Tissue Sensing of Nitric Oxide. *J. Am. Chem. Soc.* **2021**, *143* (18), 7196–7202. https://doi.org/10.1021/jacs.1c03004.
(861) Liu, Y.; Fan, H.; Wen, Y.; Jia, T.; Su, Q.; Li, F. ICT-Based near Infrared Fluorescent Switch-on Probe for Nitric Oxide Bioimaging in Vivo. *Dyes Pigments* **2019**, *166*, 211–216. https://doi.org/10.1016/j.dyepig.2019.03.012.
(862) Ye, M.; Hu, W.; He, M.; Li, C.; Zhai, S.; Liu, Z.; Wang, Y.; Zhang, H.; Li, C. Deep Imaging for Visualizing Nitric Oxide in Lipid Droplets: Discovering the Relationship between Nitric Oxide and Resistance to Cancer Chemotherapy Drugs. *Chem. Commun.* **2020**, *56* (46), 6233–6236. https://doi.org/10.1039/D0CC01856B.
(863) Shu, L.; Shang, Z.; Li, J.; Gao, Y.; Bi, W. A Dual-Response Triphenylamine-Based Fluorescent Probe for Selective Sensing of Copper(II) and Nitric Oxide in Live Cells. *J. Mol. Struct.* **2023**, *1271*. https://doi.org/10.1016/j.molstruc.2022.134032.
(864) Liu, P.; Li, B.; Zheng, J.; Liang, Q.; Wu, C.; Huang, L.; Zhang, P.; Jia, Y.; Wang, S. A Novel N-Nitrosation-Based Ratiometric Fluorescent Probe for Highly Selective Imaging Endogenous Nitric Oxide in Living Cells and Zebrafish. *Sens. Actuators B-Chem.* **2021**, *329*. https://doi.org/10.1016/j.snb.2020.129147.
(865) Pan, Y.; Chen, X.; Dong, L.; Shao, N.; Niu, L.; Yang, Q. Visualizing Nitric Oxide-Dependent HIF-1 Activity under Hypoxia with a Lipid Droplet-Targeting Fluorescent Probe. *Chin. Chem. Lett.* **2021**, *32* (12), 3895–3898. https://doi.org/10.1016/j.cclet.2021.06.024.
(866) Li, C.; Hu, W.; Wang, J.; Song, X.; Xiong, X.; Liu, Z. A Highly Specific Probe for the Imaging of Inflammation-Induced Endogenous Nitric Oxide Produced during the Stroke Process. *The Analyst* **2020**, *145* (18), 6125–6129. https://doi.org/10.1039/D0AN00824A.
(867) Wang, X.-Y.; Lin, Y.-M.; Sun, X.-Y.; Wu, Y.-Q.; Miao, H.; Chu, J.; Bai, T.-W.; Fu, Y.-L. A Lysosomal Targeted Fluorescent Probe Based on BODIPY for Monitoring NO in Living Cells and Zebrafish Imaging. *Sens. Actuators B Chem.* **2023**, *383*, 133592. https://doi.org/10.1016/j.snb.2023.133592.
(868) Mou, J.; Qi, H.; Xiang, R.; Xu, S.; Liu, J.; Meng, S.; Chen, N.; Xue, Y.; Pei, D. A Novel Fluorescence Sensor for Relay Recognition of Zinc Ions and Nitric Oxide through

Fluorescence “off-on-off” Functionality. *New J. Chem.* **2021**, *45* (6), 2958–2966. https://doi.org/10.1039/d0nj05018k.
(869) Wang, L.-L.; Bai, J.-Y.; Li, X.-F.; Zheng, M.-H.; Miao, Y.; Jin, J.-Y. Simultaneous Imaging of Hypochlorous Acid and Nitric Oxide in Live Cells Based on a Dual-Channel Fluorescent Probe. *Anal. Chim. Acta* **2021**, *1183*, 338980. https://doi.org/10.1016/j.aca.2021.338980.
(870) Zhu, T.; Ren, N.; Liu, X.; Dong, Y.; Wang, R.; Gao, J.; Sun, J.; Zhu, Y.; Wang, L.; Fan, C.; Tian, H.; Li, J.; Zhao, C. Probing the Intracellular Dynamics of Nitric Oxide and Hydrogen Sulfide Using an Activatable NIR II Fluorescence Reporter. *Angew. Chem.-Int. Ed.* **2021**, *60* (15), 8450–8454. https://doi.org/10.1002/anie.202015650.
(871) Rieth, T.; Sasamoto, K. Detection of Nitric Oxide and Nitrite by Using a Rhodamine-Type Fluorescent Indicator. *Anal. Commun.* **1998**, *35* (6), 195–198. https://doi.org/10.1039/a802897d.
(872) Wu, C.-M.; Chen, Y.-H.; Dayananda, K.; Shiue, T.-W.; Hung, C.-H.; Liaw, W.-F.; Chen, P.-Y.; Wang, Y.-M. Sensitivity Evaluation of Rhodamine B Hydrazide towards Nitric Oxide and Its Application for Macrophage Cells Imaging. *Anal. Chim. Acta* **2011**, *708*, 141–148. https://doi.org/10.1016/j.aca.2011.10.005.
(873) Fu, Y.-L.; Li, H.; Wei, X.-Z.; Song, Q.-H. BODIPY-Based Hydrazine as a Fluorescent Probe for Sensitive and Selective Detection of Nitric Oxide: A New Strategy. *J. Mater. Chem. B* **2019**, *7* (24), 3792–3795. https://doi.org/10.1039/C9TB00626E.
(874) Guo, R.-Y.; Zhang, Y.-T.; Chanmungkalakul, S.; Guo, H.-R.; Hu, Y.; Li, J.; Liu, X.; Zang, Y.; Li, X. Bioinspired Design of Reversible Fluorescent Probes for Tracking Nitric Oxide Dynamics in Live Cells. *CCS Chem.* **2021**, *3* (10), 116–128. https://doi.org/10.31635/ccschem.021.202000501.
(875) Raveendran, A. V.; Gouthaman, S.; Ponnuvel, K.; Gandhi, S.; P., C. A. S. Rhodamine Spirolactam Based Photoswitchable Chemodosimeter for Nitric Oxide Detection and Their Live Cell Imaging Utility. *Dyes Pigments* **2023**, *215*, 111284. https://doi.org/10.1016/j.dyepig.2023.111284.
(876) Xu, Q.; Zhang, Y.; Zhu, M.; Yan, C.; Mao, W.; Zhu, W.-H.; Guo, Z. Bent-to-Planar Si-Rhodamines: A Distinct Rehybridization Lights up NIR-II Fluorescence for Tracking Nitric Oxide in the Alzheimer’s Disease Brain. *Chem. Sci.* **2023**, *14* (15), 4091–4101. https://doi.org/10.1039/D3SC00193H.
(877) Katayama, Y.; Takahashi, S.; Maeda, M. Design, Synthesis and Characterization of a Novel Fluorescent Probe for Nitric Oxide (Nitrogen Monoxide). *Anal. Chim. Acta* **1998**, *365*, 159–167. https://doi.org/10.1016/s0003-2670(98)00089-0.
(878) Soh, N.; Katayama, Y.; Maeda, M. A Fluorescent Probe for Monitoring Nitric Oxide Production Using a Novel Detection Concept. *The Analyst* **2001**, *126* (5), 564–566. https://doi.org/10.1039/b101600h.
(879) Soh, N.; Imato, T.; Kawamura, K.; Maeda, M.; Katayama, Y. Ratiometric Direct Detection of Nitric Oxide Based on a Novel Signal-Switching Mechanism. *Chem. Commun.* **2002**, 2650–2651. https://doi.org/10.1039/b207726d.
(880) Franz, K. J.; Singh, N.; Lippard, S. J. Metal-Based NO Sensing by Selective Ligand Dissociation. *Angew. Chem. Int. Ed.* **2000**, *39* (12), 2120–2122. https://doi.org/10.1002/1521-3773(20000616)39:12<2120::AID-ANIE2120>3.0.CO;2-M.
(881) Franz, K. J.; Singh, N.; Spingler, B.; Lippard, S. J. Aminotroponiminates as Ligands for Potential Metal-Based Nitric Oxide Sensors. *Inorg. Chem.* **2000**, *39* (18), 4081–4092. https://doi.org/10.1021/ic000344q.
(882) Hilderbrand, S. A.; Lim, M. H.; Lippard, S. J. Dirhodium Tetracarboxylate Scaffolds as Reversible Fluorescence-Based Nitric Oxide Sensors. *J. Am. Chem. Soc.* **2004**, *126* (15), 4972–4978. https://doi.org/10.1021/ja038471j.

(883) Hilderbrand, S. A.; Lippard, S. J. Nitric Oxide Reactivity of Fluorophore Coordinated Carboxylate-Bridged Diiron(II) and Dicobalt(II) Complexes. *Inorg. Chem.* **2004**, *43* (17), 5294–5301. https://doi.org/10.1021/ic049649l.
(884) Lim, M. H.; Lippard, S. J. Fluorescence-Based Nitric Oxide Detection by Ruthenium Porphyrin Fluorophore Complexes. *Inorg. Chem.* **2004**, *43* (20), 6366–6370. https://doi.org/10.1021/ic035418n.
(885) Lim, M. H.; Lippard, S. J. Copper Complexes for Fluorescence-Based NO Detection in Aqueous Solution. *J. Am. Chem. Soc.* **2005**, *127* (35), 12170–12171. https://doi.org/10.1021/ja053150o.
(886) Lim, M. H.; Lippard, S. J. Fluorescent Nitric Oxide Detection by Copper Complexes Bearing Anthracenyl and Dansyl Fluorophore Ligands. *Inorg. Chem.* **2006**, *45* (22), 8980–8989. https://doi.org/10.1021/ic0609913.
(887) Lim, M. H.; Wong, B. A.; Pitcock, W. H.; Mokshagundam, D.; Baik, M.-H.; Lippard, S. J. Direct Nitric Oxide Detection in Aqueous Solution by Copper(II) Fluorescein Complexes. *J. Am. Chem. Soc.* **2006**, *128* (44), 14364–14373. https://doi.org/10.1021/ja064955e.
(888) McQuade, L. E.; Pluth, M. D.; Lippard, S. J. Mechanism of Nitric Oxide Reactivity and Fluorescence Enhancement of the NO-Specific Probe CuFL1. *Inorg. Chem.* **2010**, *49* (17), 8025–8033. https://doi.org/10.1021/ic101054u.
(889) Lim, M. H.; Xu, D.; Lippard, S. J. Visualization of Nitric Oxide in Living Cells by a Copper-Based Fluorescent Probe. *Nat. Chem. Biol.* **2006**, *2*, 375–380. https://doi.org/10.1038/nchembio794.
(890) Pluth, M. D.; McQuade, L. E.; Lippard, S. J. Cell-Trappable Fluorescent Probes for Nitric Oxide Visualization in Living Cells. *Org. Lett.* **2010**, *12* (10), 2318–2321. https://doi.org/10.1021/ol1006289.
(891) McQuade, L. E.; Lippard, S. J. Fluorescence-Based Nitric Oxide Sensing by Cu(II) Complexes That Can Be Trapped in Living Cells. *Inorg. Chem.* **2010**, *49* (16), 7464–7471. https://doi.org/10.1021/ic100802q.
(892) McQuade, L. E.; Mab, J.; Lowe, G.; Ghatpande, A.; Gelperin, A.; Lippard, S. J. Visualization of Nitric Oxide Production in the Mouse Main Olfactory Bulb by a Cell-Trappable Copper(II) Fluorescent Probe. *Proc. Natl. Acad. Sci. U. S. A.* **2010**, *107*, 8525. https://doi.org/10.1073/pnas.0914794107.
(893) Ghosh, M.; van den Akker, N. M. S.; Wijnands, K. A. P.; Poeze, M.; Weber, C.; McQuade, L. E.; Pluth, M. D.; Lippard, S. J.; Post, M. J.; Molin, D. G. M.; van Zandvoort, M. A. M. J. Specific Visualization of Nitric Oxide in the Vasculature with Two-Photon Microscopy Using a Copper Based Fluorescent Probe. *PLoS One* **2013**, *8*, e75331. https://doi.org/10.1371/journal.pone.0075331.
(894) Ouyang, J.; Hong, H.; Shen, C.; Zhao, Y.; Ouyang, C.; Dong, L.; Zhu, J.; Guo, Z.; Zeng, K.; Chen, J.; Zhang, C.; Zhang, J. A Novel Fluorescent Probe for the Detection of Nitric Oxide in Vitro and in Vivo. *Free Radic. Biol. Med.* **2008**, *45*, 1426–1436. https://doi.org/10.1016/j.freeradbiomed.2008.08.016.
(895) Hu, X.; Wang, J.; Zhu, X.; Dong, D.; Zhang, X.; Wu, S.; Duan, C. A Copper(II) Rhodamine Complex with a Tripodal Ligand as a Highly Selective Fluorescence Imaging Agent for Nitric Oxide. *Chem. Commun.* **2011**, *47*, 11507–11509. https://doi.org/10.1039/c1cc14032a.
(896) Meng, Q.; Zhang, Y.; Hou, D.; Xin, G.; Li, T.; He, C.; Duan, C. Fluorimetric and Colorimetric Detection of Nitric Oxide in Living Cells by Rhodamine Derivatives Assisted by Cu^{2+}. *Tetrahedron* **2013**, *69* (2), 636–641. https://doi.org/10.1016/j.tet.2012.11.010.
(897) Srivastava, P.; Verma, M.; Sivakumar, S.; Patra, A. K. A Smart FRET Probe Exhibiting a Molecular Keypad Lock Device Based on Rapid Detection of Nitric Oxide Mediated by Cu^{2+} Ion. *Sens. Actuators B Chem.* **2019**, *291*, 478–484. https://doi.org/10.1016/j.snb.2019.04.093.

(898) Pluth, M. D.; Chan, M. R.; McQuade, L. E.; Lippard, S. J. Seminaphthofluorescein-Based Fluorescent Probes for Imaging Nitric Oxide in Live Cells. *Inorg. Chem.* **2011**, *50* (19), 9385–9392. https://doi.org/10.1021/ic200986v.
(899) Apfel, U.-P.; Buccella, D.; Wilson, J. J.; Lippard, S. J. Detection of Nitric Oxide and Nitroxyl with Benzoresorufin-Based Fluorescent Sensors. *Inorg. Chem.* **2013**, *52* (6), 3285–3294. https://doi.org/10.1021/ic302793w.
(900) Phenazine-Embedded Copper(II) Complex as a Fluorescent Probe for the Detection of NO and HNO with a Bioimaging Application.
(901) Loas, A.; Lippard, S. J. Direct Ratiometric Detection of Nitric Oxide with Cu(II)-Based Fluorescent Probes. *J. Mater. Chem. B* **2017**, *5*, 8929–8933. https://doi.org/10.1039/c7tb02666h.
(902) Hu, X.; Zhang, X.; Song, H.; He, C.; Bao, Y.; Tang, Q.; Duan, C. A Novel Copper(II) Complex-Based Fluorescence Probe for Nitric Oxide Detecting and Imaging. *Tetrahedron* **2012**, *68* (39), 8371–8375. https://doi.org/10.1016/j.tet.2012.04.002.
(903) Sun, X.; Xu, Y.; Zhu, W.; He, C.; Xu, L.; Yang, Y.; Qian, X. Copper-Promoted Probe for Nitric Oxide Based on o-Phenylenediamine: Large Blue-Shift in Absorption and Fluorescence Enhancement. *Anal. Methods* **2012**, *4* (4), 919. https://doi.org/10.1039/c2ay25039j.
(904) Mondal, B.; Kumar, P.; Ghosh, P.; Kalita, A. Fluorescence-Based Detection of Nitric Oxide in Aqueous and Methanol Media Using a Copper(Ii) Complex. *Chem. Commun.* **2011**, *47* (10), 2964. https://doi.org/10.1039/c0cc04054a.
(905) Kumar, P.; Kalita, A.; Mondal, B. Reduction of Copper(Ii) Complexes of Tridentate Ligands by Nitric Oxide and Fluorescent Detection of NO in Methanol and Water Media. *Dalton Trans.* **2011**, *40* (34), 8656. https://doi.org/10.1039/c1dt10773a.
(906) Kumar, P.; Kalita, A.; Mondal, B. Copper(II) Complexes as Turn on Fluorescent Sensors for Nitric Oxide. *Dalton Trans.* **2012**, *41*, 10543–10548. https://doi.org/10.1039/c2dt31068f.
(907) Kumar, P.; Kalita, A.; Mondal, B. Nitric Oxide Sensors Based on Copper(II) Complexes of N-Donor Ligands. *Inorganica Chim. Acta* **2013**, *404*, 88–96. https://doi.org/10.1016/j.ica.2013.04.015.
(908) Sivaraman, G.; Anand, T.; Chellappa, D. A Fluorescence Switch for the Detection of Nitric Oxide and Histidine and Its Application in Live Cell Imaging. *ChemPlusChem* **2014**, *79* (12), 1761–1766. https://doi.org/10.1002/cplu.201402217.
(909) Juárez, L. A.; Barba-Bon, A.; Costero, A. M.; Martínez-Máñez, R.; Sancenón, F.; Parra, M.; Gaviña, P.; Terencio, M. C.; Alcaraz, M. J. A Boron Dipyrromethene (BODIPY)-Based Cu ^{II} -Bipyridine Complex for Highly Selective NO Detection. *Chem. - Eur. J.* **2015**, *21* (44), 15486–15490. https://doi.org/10.1002/chem.201502191.
(910) Wilson, N.; Mak, L. H.; Cilibrizzi, A.; Gee, A. D.; Long, N. J.; Woscholski, R.; Vilar, R. A Lipophilic Copper(II) Complex as an Optical Probe for Intracellular Detection of NO. *Dalton Trans.* **2016**, *45*, 18177–18182. https://doi.org/10.1039/c6dt02880b.
(911) Barzegar Amiri Olia, M.; Zavras, A.; Schiesser, C. H.; Alexander, S.-A. Blue “turn-on” Fluorescent Probes for the Direct Detection of Free Radicals and Nitric Oxide in Pseudomonas Aeruginosa Biofilms. *Org. Biomol. Chem.* **2016**, *14*, 2272–2281. https://doi.org/10.1039/c5ob02441b.
(912) Sadek, M. M.; Barzegar Amiri Olia, M.; Nowell, C. J.; Barlow, N.; Schiesser, C. H.; Nicholson, S. E.; Norton, R. S. Characterisation of a Novel Coumarin-Based Fluorescent Probe for Monitoring Nitric Oxide Production in Macrophages. *Bioorg. Med. Chem.* **2017**, *25* (20), 5743–5748. https://doi.org/10.1016/j.bmc.2017.08.054.
(913) Jain, P.; David, A.; Bhatla, S. C. A Novel Protocol for Detection of Nitric Oxide in Plants. In *Plant Nitric Oxide*; Gupta, K. J., Ed.; Methods in Molecular Biology; Springer New York: New York, NY, 2016; Vol. 1424, pp 69–79. https://doi.org/10.1007/978-1-4939-3600-7_7.
(914) Rodriguez-Nuevalos, S.; Parra, M.; Ceballos, S.; Gil, S.; Costero, A. A Nitric Oxide Induced “Click” Reaction to Trigger the Aggregation Induced Emission (AIE) Phenomena of a

Tetraphenyl Ethylene Derivative: A New Fluorescent Probe for NO. *J. Photochem. Photobiol. -Chem.* **2020**, *388*. https://doi.org/10.1016/j.jphotochem.2019.112132.
(915) Bätz, M.; Korth, H.; Sustmann, R. A Novel Method for Detecting Nitric Oxide (NO) by Formation of Fluorescent Products Based on Cheletropic Spin Traps. *Angew. Chem. Int. Ed. Engl.* **1997**, *36* (13–14), 1501–1503. https://doi.org/10.1002/anie.199715011.
(916) Hornig, F. S.; Korth, H.; Rauen, U.; de Groot, H.; Sustmann, R. Synthesis and Properties of a pH-Insensitive Fluorescent Nitric Oxide Cheletropic Trap (FNOCT). *Helv. Chim. Acta* **2006**, *89* (10), 2281–2296. https://doi.org/10.1002/hlca.200690212.
(917) Meineke, P.; Rauen, U.; De Groot, H.; Korth, H.-G.; Sustmann, R. Cheletropic Traps for the Fluorescence Spectroscopic Detection of Nitric Oxide (Nitrogen Monoxide) in Biological Systems. *Chem. - Eur. J.* **1999**, *5* (6), 1738–1747. https://doi.org/10.1002/(SICI)1521-3765(19990604)5:6<1738::AID-CHEM1738>3.0.CO;2-T.
(918) Dueppe, P. M.; Talbierski, P. M.; Hornig, F. S.; Rauen, U.; Korth, H.-G.; Wille, T.; Boese, R.; Omlor, T.; de Groot, H.; Sustmann, R. Pyrene-Based Fluorescent Nitric Oxide Cheletropic Traps (FNOCTs) for the Detection of Nitric Oxide in Cell Cultures and Tissues. *Chem. - Eur. J.* **2010**, *16*, 11121. https://doi.org/10.1002/chem.201000029.
(919) Wang, J.; He, C.; Wu, P.; Wang, J.; Duan, C. An Amide-Containing Metal-Organic Tetrahedron Responding to a Spin-Trapping Reaction in a Fluorescent Enhancement Manner for Biological Imaging of NO in Living Cells. *J. Am. Chem. Soc.* **2011**, *133* (32), 12402–12405. https://doi.org/10.1021/ja2048489.
(920) Sun, C.-D.; Shi, W.; Song, Y.-C.; Chen, W.; Ma, H.-M. An Unprecedented Strategy for Selective and Sensitive Fluorescence Detection of Nitric Oxide Based on Its Reaction with a Selenide. *Chem. Commun.* **2011**, *47*, 8638–8640. https://doi.org/10.1039/c1cc12174j.
(921) Jiao, S.; Yang, S.; Wang, Y.; Ma, A. A High-Selectivity NIR Fluorescent Probe for Detection of Nitric Oxide in Saliva Samples and Living Cells Imaging. *Sens. Actuators B,* **2023**, *374*. https://doi.org/10.1016/j.snb.2022.132790.
(922) Ma, S.; Fang, D.-C.; Ning, B.; Li, M.; He, L.; Gong, B. The Rational Design of a Highly Sensitive and Selective Fluorogenic Probe for Detecting Nitric Oxide. *Chem. Commun.* **2014**, *50*, 6475–6478. https://doi.org/10.1039/c4cc01142b.
(923) Wang, H.-L.; Liu, F.-T.; Ding, A.-X.; Ma, S.-F.; He, L.; Lin, L.; Lu, Z.-L. Water-Soluble Hantzsch Ester as Switch-on Fluorescent Probe for Efficiently Detecting Nitric Oxide. *Spectrochim. Acta. A. Mol. Biomol. Spectrosc.* **2016**, *169*, 1–6. https://doi.org/10.1016/j.saa.2016.06.014.
(924) Ma, S.; Sun, X.; Yu, Q.; Liu, R.; Lu, Z.; He, L. Dihydropyridine-Coumarin-Based Fluorescent Probe for Imaging Nitric Oxide in Living Cells. *Photochem. Photobiol. Sci.* **2020**, *19* (9), 1230–1235. https://doi.org/10.1039/d0pp00201a.
(925) Mahapatra, A. K.; Ali, S. S.; Maiti, K.; Mondal, S.; Maji, R.; Manna, S.; Manna, S. K.; Uddin, Md. R.; Mandal, S. Highly Sensitive Ratiometric Fluorescence Probes for Nitric Oxide Based on Dihydropyridine and Potentially Useful in Bioimaging. *RSC Adv.* **2016**, *6* (114), 113219–113227. https://doi.org/10.1039/C6RA23139J.
(926) Li, H.; Zhang, D.; Gao, M.; Huang, L.; Tang, L.; Li, Z.; Chen, X.; Zhang, X. Highly Specific C–C Bond Cleavage Induced FRET Fluorescence for in Vivo Biological Nitric Oxide Imaging. *Chem. Sci.* **2017**, *8* (3), 2199–2203. https://doi.org/10.1039/C6SC04071C.
(927) Gao, C.; Lin, L.; Sun, W.; Tan, Z.; Huang, J.; He, L.; Lu, Z. Dihydropyridine-Derived BODIPY Probe for Detecting Exogenous and Endogenous Nitric Oxide in Mitochondria. *Talanta* **2018**, *176*, 382–388. https://doi.org/10.1016/j.talanta.2017.08.044.
(928) Islam, A. S. M.; Bhowmick, R.; Pal, K.; Katarkar, A.; Chaudhuri, K.; Ali, M. A Smart Molecule for Selective Sensing of Nitric Oxide: Conversion of NO to HSNO; Relevance of Biological HSNO Formation. *Inorg. Chem.* **2017**, *56* (8), 4324–4331. https://doi.org/10.1021/acs.inorgchem.6b02787.

(929) Han, Q.; Liu, J.; Meng, Q.; Wang, Y.; Peng, H.; Zhang, Z.; Xu, Z.; Zhang, R. Turn-On Fluorescence Probe for Nitric Oxide Detection and Bioimaging in Live Cells and Zebrafish. *ACS Sens.* **2019**, *4* (2), 309-+. https://doi.org/10.1021/acssensors.8b00776.
(930) Kim, S. J.; Park, S. Y.; Yoon, S. A.; Kim, C.; Kang, C.; Lee, M. H. Naphthalimide-4-(4-Nitrophenyl)Thiosemicarbazide: A Fluorescent Probe for Simultaneous Monitoring of Viscosity and Nitric Oxide in Living Cells. *Anal. Chem.* **2021**, *93* (10), 4391–4397. https://doi.org/10.1021/acs.analchem.0c04019.
(931) Islam, A.; Bhowmick, R.; Garain, B.; Katarkar, A.; Ali, M. Nitric Oxide Sensing through 1,2,3,4-Oxatriazole Formation from Acylhydrazide: A Kinetic Study. *J. Org. Chem.* **2018**, *83* (21), 13287–13295. https://doi.org/10.1021/acs.joc.8b02110.
(932) Maiti, D.; Islam, A.; Sasmal, M.; Dutta, A.; Katarkar, A.; Ali, M. A Coumarin Embedded Highly Sensitive Nitric Oxide Fluorescent Sensor: Kinetic Assay and Bio-Imaging Applications. *Org. Biomol. Chem.* **2020**, *18* (41), 8450–8458. https://doi.org/10.1039/d0ob00567c.
(933) Jenni, S.; Renault, K.; Dejouy, G.; Debieu, S.; Laly, M.; Romieu, A. In Situ Synthesis of Phenoxazine Dyes in Water: Application for “Turn-On” Fluorogenic and Chromogenic Detection of Nitric Oxide. *ChemPhotoChem* **2022**, *6* (5). https://doi.org/10.1002/cptc.202100268.
(934) Wang, W.; Yang, T.; Zhang, Q.; Lu, K.; Zheng, Z.; Tian, C.; Ping, J.; Qi, B.; Wu, S. Development of a Facile Lysosome-Targeting Nitric Oxide Fluorescent Probe Based on a Novel Reaction Mechanism. *Anal. Chem.* **2023**, *95* (15), 6279–6286. https://doi.org/10.1021/acs.analchem.2c04896.
(935) Pacher, P.; Beckman, J. S.; Liaudet, L. Nitric Oxide and Peroxynitrite in Health and Disease. *Physiol. Rev.* **2007**, *87* (1), 315–424. https://doi.org/10.1152/physrev.00029.2006.
(936) Ferrer-Sueta, G.; Radi, R. Chemical Biology of Peroxynitrite: Kinetics, Diffusion, and Radicals. *ACS Chem. Biol.* **2009**, *4* (3), 161–177. https://doi.org/10.1021/cb800279q.
(937) Koppenol, W. H.; Moreno, J. J.; Pryor, W. A.; Ischiropoulos, H.; Beckman, J. S. Peroxynitrite, a Cloaked Oxidant Formed by Nitric Oxide and Superoxide. *Chem. Res. Toxicol.* **1992**, *5* (6), 834–842. https://doi.org/10.1021/tx00030a017.
(938) Radi, R. Peroxynitrite, a Stealthy Biological Oxidant. *J. Biol. Chem.* **2013**, *288* (37), 26464–26472. https://doi.org/10.1074/jbc.R113.472936.
(939) Ferrer-Sueta, G.; Campolo, N.; Trujillo, M.; Bartesaghi, S.; Carballal, S.; Romero, N.; Alvarez, B.; Radi, R. Biochemistry of Peroxynitrite and Protein Tyrosine Nitration. *Chem. Rev.* **2018**, *118* (3), 1338–1408. https://doi.org/10.1021/acs.chemrev.7b00568.
(940) Cammack, R.; Shergill, J. K.; Ananda Inalsingh, V.; Hughes, M. N. Applications of Electron Paramagnetic Resonance Spectroscopy to Study Interactions of Iron Proteins in Cells with Nitric Oxide. *Spectrochim. Acta. A. Mol. Biomol. Spectrosc.* **1998**, *54* (14), 2393–2402. https://doi.org/10.1016/S1386-1425(98)00219-4.
(941) Bonini, M. G.; Radi, R.; Ferrer-Sueta, G.; Ferreira, A. M. D. C.; Augusto, O. Direct EPR Detection of the Carbonate Radical Anion Produced from Peroxynitrite and Carbon Dioxide. *J. Biol. Chem.* **1999**, *274* (16), 10802–10806. https://doi.org/10.1074/jbc.274.16.10802.
(942) Viera, L.; Ye, Y. Z.; Estévez, A. G.; Beckman, J. S. [39] Immunohistochemical Methods to Detect Nitrotyrosine. In *Methods in Enzymology*; Nitric Oxide Part C: Biological and Antioxidant Activities; Academic Press, 1999; Vol. 301, pp 373–381. https://doi.org/10.1016/S0076-6879(99)01101-5.
(943) Rabbani, N.; Thornalley, P. J. Assay of 3-Nitrotyrosine in Tissues and Body Fluids by Liquid Chromatography with Tandem Mass Spectrometric Detection. In *Methods in Enzymology*; Nitric Oxide, Part F; Academic Press, 2008; Vol. 440, pp 337–359. https://doi.org/10.1016/S0076-6879(07)00822-1.
(944) Kooy, N. W.; Royall, J. A.; Ischiropoulos, H.; Beckman, J. S. Peroxynitrite-Mediated Oxidation of Dihydrorhodamine 123. *Free Radic. Biol. Med.* **1994**, *16* (2), 149–156. https://doi.org/10.1016/0891-5849(94)90138-4.

(945) Roychowdhury, S.; Luthe, A.; Keilhoff, G.; Wolf, G.; Horn, T. F. W. Oxidative Stress in Glial Cultures: Detection by DAF-2 Fluorescence Used as a Tool to Measure Peroxynitrite Rather than Nitric Oxide. *Glia* **2002**, *38* (2), 103–114. https://doi.org/10.1002/glia.10024.
(946) Ueno, T.; Urano, Y.; Kojima, H.; Nagano, T. Mechanism-Based Molecular Design of Highly Selective Fluorescence Probes for Nitrative Stress. *J. Am. Chem. Soc.* **2006**, *128* (33), 10640–10641. https://doi.org/10.1021/ja061972v.
(947) Yang, D.; Wang, H.-L.; Sun, Z.-N.; Chung, N.-W.; Shen, J.-G. A Highly Selective Fluorescent Probe for the Detection and Imaging of Peroxynitrite in Living Cells. *J. Am. Chem. Soc.* **2006**, *128* (18), 6004–6005. https://doi.org/10.1021/ja0603756.
(948) Sun, Z.-N.; Wang, H.-L.; Liu, F.-Q.; Chen, Y.; Tam, P. K. H.; Yang, D. BODIPY-Based Fluorescent Probe for Peroxynitrite Detection and Imaging in Living Cells. *Org. Lett.* **2009**, *11* (9), 1887–1890. https://doi.org/10.1021/ol900279z.
(949) Peng, T.; Yang, D. HKGreen-3: A Rhodol-Based Fluorescent Probe for Peroxynitrite. *Org. Lett.* **2010**, *12* (21), 4932–4935. https://doi.org/10.1021/ol102182j.
(950) Zhang, J.; Zhen, X.; Zeng, J.; Pu, K. A Dual-Modal Molecular Probe for Near-Infrared Fluorescence and Photoacoustic Imaging of Peroxynitrite. *Anal. Chem.* **2018**, *90* (15), 9301–9307. https://doi.org/10.1021/acs.analchem.8b01879.
(951) Huang, Y.; Yu, L.; Fu, L.; Hou, J.; Wang, L.; Sun, M.; Wang, X.; Chen, L. Molecular Fluorescent Probes for Imaging and Evaluation of Peroxynitrite Fluctuations in Living Cells and in Vivo under Hypoxic Stress. *Sens. Actuators B Chem.* **2022**, *370*, 132410. https://doi.org/10.1016/j.snb.2022.132410.
(952) Bruemmer, K. J.; Merrikhihaghi, S.; Lollar, C. T.; Morris, S. N. S.; Bauer, J. H.; Lippert, A. R. ^{19}F Magnetic Resonance Probes for Live-Cell Detection of Peroxynitrite Using an Oxidative Decarbonylation Reaction. *Chem Commun* **2014**, *50* (82), 12311–12314. https://doi.org/10.1039/C4CC04292A.
(953) Cao, J.; An, W.; Reeves, A. G.; Lippert, A. R. A Chemiluminescent Probe for Cellular Peroxynitrite Using a Self-Immolative Oxidative Decarbonylation Reaction. *Chem. Sci.* **2018**, *9* (9), 2552–2558. https://doi.org/10.1039/C7SC05087A.
(954) Wortel, R. C.; Mizrachi, A.; Li, H.; Markovsky, E.; Enyedi, B.; Jacobi, J.; Brodsky, O.; Cao, J.; Lippert, A. R.; Incrocci, L.; Mulhall, J. P.; Haimovitz-Friedman, A. Sildenafil Protects Endothelial Cells From Radiation-Induced Oxidative Stress. *J. Sex. Med.* **2019**, *16* (11), 1721–1733. https://doi.org/10.1016/j.jsxm.2019.08.015.
(955) Wang, W.; Xiong, J.; Song, X.; Wang, Z.; Zhang, F.; Mao, Z. Activatable Two-Photon Near-Infrared Fluorescent Probe Tailored toward Peroxynitrite In Vivo Imaging in Tumors. *Anal. Chem.* **2020**, *92* (19), 13305–13312. https://doi.org/10.1021/acs.analchem.0c02587.
(956) Xiong, J.; Wang, W.; Wang, C.; Zhong, C.; Ruan, R.; Mao, Z.; Liu, Z. Visualizing Peroxynitrite in Microvessels of the Brain with Stroke Using an Engineered Highly Specific Fluorescent Probe. *ACS Sens.* **2020**, *5* (10), 3237–3245. https://doi.org/10.1021/acssensors.0c01555.
(957) Lu, X.; Su, H.; Zhang, J.; Wang, N.; Wang, H.; Liu, J.; Zhao, W. Resorufin-Based Fluorescent Probe with Elevated Water Solubility for Visualizing Fluctuant Peroxynitrite in Progression of Inflammation. *Spectrochim. Acta. A. Mol. Biomol. Spectrosc.* **2022**, *267*, 120620. https://doi.org/10.1016/j.saa.2021.120620.
(958) An, Q.; Su, S.; Chai, L.; Wang, Y.; Wang, X.; Li, X.; Liang, T.; Hu, W.; Song, X.; Li, C. Imaging of Peroxynitrite in Mitochondria by a Near-Infrared Fluorescent Probe with a Large Stokes Shift. *Talanta* **2023**, *253*, 124073. https://doi.org/10.1016/j.talanta.2022.124073.
(959) Gong, J.; Wang, X.; Fan, H.-E.; Wang, J.; Zhang, F.; Mao, Z. Engineering an Activatable Fluorescent Probe for Studying $ONOO^-$ in Pyroptotic Process. *Talanta* **2023**, *267*, 125216. https://doi.org/10.1016/j.talanta.2023.125216.

(960) Li, Y.; Xie, X.; Yang, X.; Li, M.; Jiao, X.; Sun, Y.; Wang, X.; Tang, B. Two-Photon Fluorescent Probe for Revealing Drug-Induced Hepatotoxicity via Mapping Fluctuation of Peroxynitrite. *Chem. Sci.* **2017**, *8* (5), 4006–4011. https://doi.org/10.1039/C7SC00303J.
(961) Cheng, D.; Peng, J.; Lv, Y.; Su, D.; Liu, D.; Chen, M.; Yuan, L.; Zhang, X. De Novo Design of Chemical Stability Near-Infrared Molecular Probes for High-Fidelity Hepatotoxicity Evaluation In Vivo. *J. Am. Chem. Soc.* **2019**, *141* (15), 6352–6361. https://doi.org/10.1021/jacs.9b01374.
(962) Qian, W. U.; Dan, C.; Yun, L.; Lin, Y.; Xiaobing, Z. Monitoring of Peroxynitrite Variation During Liver Injury Adopting a Far Red to Near-Infrared Fluorescent Probe with Large Stokes Shift. *Chem. J. Chin. Univ.* **2020**, *41* (11), 2426. https://doi.org/10.7503/cjcu20209236.
(963) Yan, Z.; Tang, Z.; Wang, X.; Zheng, Z.; Tian, Z.; Geng, X.; Li, Y.; Jiang, H. A Novel Golgi-Targetable Fluorescent Probe for Imaging Peroxynitrite in Golgi Stress and Sepsis-Induced Acute Lung Injury. *Sens. Actuators B Chem.* **2022**, *369*, 132352. https://doi.org/10.1016/j.snb.2022.132352.
(964) Shao, T.; Xu, X.; Wang, L.; Shen, Y.; Zhao, J.; Li, H.; Zhang, D.; Du, W.; Bai, H.; Peng, B.; Li, L. A Novel α-Ketoamide Reactivity-Based Two-Photon Fluorogenic Probe for Visualizing Peroxynitrite in Parkinson's Disease Models. *J. Innov. Opt. Health Sci.* **2023**, *16* (04), 2250039. https://doi.org/10.1142/S1793545822500390.
(965) Xiong, J.; Wang, W.; Wang, C.; Zhong, C.; Ruan, R.; Mao, Z.; Liu, Z. Visualizing Peroxynitrite in Microvessels of the Brain with Stroke Using an Engineered Highly Specific Fluorescent Probe. *ACS Sens.* **2020**, *5* (10), 3237–3245. https://doi.org/10.1021/acssensors.0c01555.
(966) Merényi, G.; Lind, J.; Goldstein, S. The Rate of Homolysis of Adducts of Peroxynitrite to the CO Double Bond. *J. Am. Chem. Soc.* **2002**, *124* (1), 40–48. https://doi.org/10.1021/ja011799x.
(967) Koppenol, W. H.; Serrano-Luginbuehl, S.; Nauser, T.; Kissner, R. Thinking Outside the Cage: A New Hypothesis That Accounts for Variable Yields of Radicals from the Reaction of CO_2 with $ONOO^-$. *Chem. Res. Toxicol.* **2020**, *33* (7), 1516–1527. https://doi.org/10.1021/acs.chemrestox.9b00309.
(968) Hou, J.-T.; Yang, J.; Li, K.; Liao, Y.-X.; Yu, K.-K.; Xie, Y.-M.; Yu, X.-Q. A Highly Selective Water-Soluble Optical Probe for Endogenous Peroxynitrite. *Chem. Commun.* **2014**, *50* (69), 9947–9950. https://doi.org/10.1039/C4CC04192E.
(969) Zhou, X.; Kwon, Y.; Kim, G.; Ryu, J.-H.; Yoon, J. A Ratiometric Fluorescent Probe Based on a Coumarin–Hemicyanine Scaffold for Sensitive and Selective Detection of Endogenous Peroxynitrite. *Biosens. Bioelectron.* **2015**, *64*, 285–291. https://doi.org/10.1016/j.bios.2014.08.089.
(970) Guo, B.; Jing, J.; Nie, L.; Xin, F.; Gao, C.; Yang, W.; Zhang, X. A Lysosome Targetable Versatile Fluorescent Probe for Imaging Viscosity and Peroxynitrite with Different Fluorescence Signals in Living Cells. *J. Mater. Chem. B* **2018**, *6* (4), 580–585. https://doi.org/10.1039/C7TB02615C.
(971) Zhan, Z.; Liu, R.; Chai, L.; Dai, Y.; Lv, Y. Visualization of Lung Inflammation to Pulmonary Fibrosis via Peroxynitrite Fluctuation. *Anal. Chem.* **2019**, *91* (17), 11461–11466. https://doi.org/10.1021/acs.analchem.9b02971.
(972) Wang, H.; Nie, J.; Li, P.; Zhang, X.; Wang, Y.; Zhang, W.; Zhang, W.; Tang, B. Exploring Idiopathic Pulmonary Fibrosis Biomarker by Simultaneous Two-Photon Fluorescence Imaging of Cysteine and Peroxynitrite. *Anal. Chem.* **2022**, *94* (32), 11272–11281. https://doi.org/10.1021/acs.analchem.2c01866.
(973) Feng, S.; Zheng, Z.; Gong, S.; Feng, G. A Unique Probe Enables Labeling Cell Membrane and Golgi Apparatus and Tracking Peroxynitrite in Golgi Oxidative Stress and Drug-Induced

Liver Injury. *Sens. Actuators B Chem.* **2022**, *361*, 131751. https://doi.org/10.1016/j.snb.2022.131751.
(974) Cheng, D.; Pan, Y.; Wang, L.; Zeng, Z.; Yuan, L.; Zhang, X.; Chang, Y.-T. Selective Visualization of the Endogenous Peroxynitrite in an Inflamed Mouse Model by a Mitochondria-Targetable Two-Photon Ratiometric Fluorescent Probe. *J. Am. Chem. Soc.* **2017**, *139* (1), 285–292. https://doi.org/10.1021/jacs.6b10508.
(975) Jiang, W.-L.; Li, Y.; Wang, W.-X.; Zhao, Y.-T.; Fei, J.; Li, C.-Y. A Hepatocyte-Targeting near-Infrared Ratiometric Fluorescent Probe for Monitoring Peroxynitrite during Drug-Induced Hepatotoxicity and Its Remediation. *Chem. Commun.* **2019**, *55* (95), 14307–14310. https://doi.org/10.1039/C9CC07017F.
(976) Gong, X.; Cheng, D.; Li, W.; Shen, Y.; Peng, R.; Shi, L.; He, L.; Yuan, L. A Highly Selective Ratiometric Molecular Probe for Imaging Peroxynitrite during Drug-Induced Acute Liver Injury. *J. Mater. Chem. B* **2021**, *9* (39), 8246–8252. https://doi.org/10.1039/D1TB01534F.
(977) Cheng, D.; Gong, X.; Wu, Q.; Yuan, J.; Lv, Y.; Yuan, L.; Zhang, X. High-Selectivity Fluorescent Reporter toward Peroxynitrite in a Coexisting Nonalcoholic Fatty Liver and Drug-Induced Liver Diseases Model. *Anal. Chem.* **2020**, *92* (16), 11396–11404. https://doi.org/10.1021/acs.analchem.0c02277.
(978) Wang, Y.; Liu, Y.; Song, X.; Feng, Y.; Jing, C.; Zhang, G.; Huang, Y.; Liu, W. Dual-Targetable Fluorescent Probe for Mapping the Fluctuation of Peroxynitrite in Drug-Induced Liver Injury Model. *Spectrochim. Acta. A. Mol. Biomol. Spectrosc.* **2023**, *286*, 121892. https://doi.org/10.1016/j.saa.2022.121892.
(979) Xu, W.; Yang, Q.; Zeng, J.; Tan, L.; Zhou, L.; Peng, L.; Zhou, Y.; Xie, C.; Luo, K.; Zhang, Z. A Biomarker ($ONOO^-$)-Activated Multicolor Fluorescent Probe for Early Detection and Assessment of Arthritis. *Sens. Actuators B Chem.* **2022**, *359*, 131565. https://doi.org/10.1016/j.snb.2022.131565.
(980) Xu, W.; Tan, L.; Zeng, J.; Yang, Q.; Zhou, Y.; Zhou, L. Molecular Engineering for Construction of a Novel $ONOO^-$- Activated Multicolor Fluorescent Nanoprobe for Early Diagnosis and Assessing Treatment of Arthritis in Vivo. *Biosens. Bioelectron.* **2022**, *209*, 114242. https://doi.org/10.1016/j.bios.2022.114242.
(981) Sikora, A.; Zielonka, J.; Lopez, M.; Joseph, J.; Kalyanaraman, B. Direct Oxidation of Boronates by Peroxynitrite: Mechanism and Implications in Fluorescence Imaging of Peroxynitrite. *Free Radic. Biol. Med.* **2009**, *47* (10), 1401–1407. https://doi.org/10.1016/j.freeradbiomed.2009.08.006.
(982) Sikora, A.; Zielonka, J.; Lopez, M.; Dybala-Defratyka, A.; Joseph, J.; Marcinek, A.; Kalyanaraman, B. Reaction between Peroxynitrite and Boronates: EPR Spin-Trapping, HPLC Analyses, and Quantum Mechanical Study of the Free Radical Pathway. *Chem. Res. Toxicol.* **2011**, *24* (5), 687–697. https://doi.org/10.1021/tx100439a.
(983) Zielonka, J.; Sikora, A.; Joseph, J.; Kalyanaraman, B. Peroxynitrite Is the Major Species Formed from Different Flux Ratios of Co-Generated Nitric Oxide and Superoxide: Direct Reaction with Boronate-Based Fluorescent Probe. *J. Biol. Chem.* **2010**, *285* (19), 14210–14216. https://doi.org/10.1074/jbc.M110.110080.
(984) Shu, W.; Wu, Y.; Zang, S.; Su, S.; Kang, H.; Jing, J.; Zhang, X. A Mitochondria-Targeting Highly Specific Fluorescent Probe for Fast Sensing of Endogenous Peroxynitrite in Living Cells. *Sens. Actuators B Chem.* **2020**, *303*, 127284. https://doi.org/10.1016/j.snb.2019.127284.
(985) Wang, Z.; Wang, W.; Wang, P.; Song, X.; Mao, Z.; Liu, Z. Highly Sensitive Near-Infrared Imaging of Peroxynitrite Fluxes in Inflammation Progress. *Anal. Chem.* **2021**, *93* (5), 3035–3041. https://doi.org/10.1021/acs.analchem.0c05118.
(986) Zhou, J.; Li, Y.; Shen, J.; Li, Q.; Wang, R.; Xu, Y.; Qian, X. A Ratiometric Fluorescent Probe for Fast and Sensitive Detection of Peroxynitrite: A Boronate Ester as the Receptor to

Initiate a Cascade Reaction. *RSC Adv* **2014**, *4* (93), 51589–51592. https://doi.org/10.1039/C4RA10048D.
(987) Zhang, J.; Li, Y.; Zhao, J.; Guo, W. An Arylboronate-Based Fluorescent Probe for Selective and Sensitive Detection of Peroxynitrite and Its Applications for Fluorescence Imaging in Living Cells. *Sens. Actuators B Chem.* **2016**, *237*, 67–74. https://doi.org/10.1016/j.snb.2016.06.054.
(988) Zhang, J.; Li, Y.; Guo, W. An Arylboronate-Based Fluorescent Probe for Peroxynitrite with Fast Response and High Selectivity. *Anal. Methods* **2015**, *7* (12), 4885–4888. https://doi.org/10.1039/C5AY01219H.
(989) Sang, M.; Huang, Y.; Liu, Z.; Li, G.; Wang, Y.; Yuan, Z.; Dai, C.; Zheng, J. Peroxynitrite/Lipid Droplet Sequence-Activated Dual-Lock Fluorescent Probes Enable Precise Intraoperative Imaging of Atherosclerotic Plaques. *ACS Sens.* **2023**, *8* (2), 893–903. https://doi.org/10.1021/acssensors.2c02590.
(990) Li, Z.; Huang, S.; He, Y.; Duan, Q.; Zheng, G.; Jiang, Y.; Cai, L.; Jia, Y.; Zhang, H.; Ho, D. AND Logic Gate Based Fluorescence Probe for Simultaneous Detection of Peroxynitrite and Hypochlorous Acid. *Spectrochim. Acta. A. Mol. Biomol. Spectrosc.* **2020**, *230*, 118073. https://doi.org/10.1016/j.saa.2020.118073.
(991) Sedgwick, A. C.; Han, H.-H.; Gardiner, J. E.; Bull, S. D.; He, X.-P.; James, T. D. The Development of a Novel AND Logic Based Fluorescence Probe for the Detection of Peroxynitrite and GSH. *Chem. Sci.* **2018**, *9* (15), 3672–3676. https://doi.org/10.1039/C8SC00733K.
(992) Odyniec, M. L.; Han, H.-H.; Gardiner, J. E.; Sedgwick, A. C.; He, X.-P.; Bull, S. D.; James, T. D. Peroxynitrite Activated Drug Conjugate Systems Based on a Coumarin Scaffold Toward the Application of Theranostics. *Front. Chem.* **2019**, *7*.
(993) Li, D.; Wang, S.; Lei, Z.; Sun, C.; El-Toni, A. M.; Alhoshan, M. S.; Fan, Y.; Zhang, F. Peroxynitrite Activatable NIR-II Fluorescent Molecular Probe for Drug-Induced Hepatotoxicity Monitoring. *Anal. Chem.* **2019**, *91* (7), 4771–4779. https://doi.org/10.1021/acs.analchem.9b00317.
(994) Ma, Y.; Tian, H.; Jin, Z.; Li, X.; Li, Y. Observation of the Generation of Peroxynitrite in Mouse Liver after Acetaminophen Overdose with a Boronate-Based Ratiometric Fluorescence Probe. *RSC Adv.* **2019**, *9* (12), 6510–6514. https://doi.org/10.1039/C8RA10053E.
(995) Hu, J.; Shao, C.; Wang, X.; Di, X.; Xue, X.; Su, Z.; Zhao, J.; Zhu, H.-L.; Liu, H.-K.; Qian, Y. Imaging Dynamic Peroxynitrite Fluxes in Epileptic Brains with a Near-Infrared Fluorescent Probe. *Adv. Sci.* **2019**, *6* (15), 1900341. https://doi.org/10.1002/advs.201900341.
(996) Xia, L.; Tong, Y.; Li, L.; Cui, M.; Gu, Y.; Wang, P. A Selective Fluorescent Turn-on Probe for Imaging Peroxynitrite in Living Cells and Drug-Damaged Liver Tissues. *Talanta* **2019**, *204*, 431–437. https://doi.org/10.1016/j.talanta.2019.06.032.
(997) Deng, Y.; Feng, G. Visualization of ONOO– and Viscosity in Drug-Induced Hepatotoxicity with Different Fluorescence Signals by a Sensitive Fluorescent Probe. *Anal. Chem.* **2020**, *92* (21), 14667–14675. https://doi.org/10.1021/acs.analchem.0c03199.
(998) Wang, Z.; Zhang, F.; Xiong, J.; Mao, Z.; Liu, Z. Investigations of Drug-Induced Liver Injury by a Peroxynitrite Activatable Two-Photon Fluorescence Probe. *Spectrochim. Acta. A. Mol. Biomol. Spectrosc.* **2021**, *246*, 118960. https://doi.org/10.1016/j.saa.2020.118960.
(999) Wang, N.; Wang, H.; Zhang, J.; Ji, X.; Su, H.; Liu, J.; Wang, J.; Zhao, W. Diketopyrrolopyrrole-Based Sensor for over-Expressed Peroxynitrite in Drug-Induced Hepatotoxicity via Ratiometric Fluorescence Imaging. *Sens. Actuators B Chem.* **2022**, *352*, 130992. https://doi.org/10.1016/j.snb.2021.130992.
(1000) Tian, Y.; Zhou, D.-Y.; Jiang, W.-L.; She, Z.-P.; Li, Y.; Li, C.-Y. Novel Near-Infrared Fluorescence Probe with Large Stokes Shift for Monitoring CCl4-Induced Toxic Hepatitis. *Talanta* **2021**, *223*, 121720. https://doi.org/10.1016/j.talanta.2020.121720.

(1001) Wang, Z.; Gong, J.; Wang, P.; Xiong, J.; Zhang, F.; Mao, Z. An Activatable Fluorescent Probe Enables in Vivo Evaluation of Peroxynitrite Levels in Rheumatoid Arthritis. *Talanta* **2023**, *252*, 123811. https://doi.org/10.1016/j.talanta.2022.123811.
(1002) Kang, H.; Shu, W.; Yu, J.; Gao, M.; Han, R.; Jing, J.; Zhang, R.; Zhang, X. A Near-Infrared Fluorescent Probe for Ratiometric Imaging Peroxynitrite in Parkinson's Disease Model. *Sens. Actuators B Chem.* **2022**, *359*, 131393. https://doi.org/10.1016/j.snb.2022.131393.
(1003) Kong, Y.; Wu, R.; Wang, X.; Qin, G.; Wu, F.; Wang, C.; Chen, M.; Wang, N.; Wang, Q.; Cao, D. Highly Sensitive Benzothiazole-Based Chemosensors for Detection and Bioimaging of Peroxynitrite in Living Cells. *RSC Adv.* **2022**, *12* (43), 27933–27939. https://doi.org/10.1039/D2RA04549D.
(1004) Xu, J.-Q.; Gao, M.-J.; Guo, J.-S.; Wang, Y.-H.; Wei, R.; Meng, Y.-L.; Kang, Y.-F. A Highly Selective Probe for Ratiometric Imaging Peroxynitrite in Living Cells and in Vivo. *Bioorganic Chem.* **2022**, *128*, 106055. https://doi.org/10.1016/j.bioorg.2022.106055.
(1005) Wen, L.; Ma, X.; Yang, J.; Jiang, M.; Peng, C.; Ma, Z.; Yu, H.; Li, Y. A New Ratiometric Design Strategy Based on Modulation of π-Conjugation Unit for Developing Fluorescent Probe and Imaging of Cellular Peroxynitrite. *Anal. Chem.* **2022**, *94* (11), 4763–4769. https://doi.org/10.1021/acs.analchem.1c05447.
(1006) Wang, N.; Lu, X.; Wang, J.; Wang, H.; Zhang, B.; Zhao, W.; Zhang, J. Quasi-LD-Targeted and ONOO−-Responsive Fluorescent Probe for Investigating the Interaction of Nonalcoholic Fatty Liver with Drug-Induced Liver Injury. *Anal. Chem.* **2023**, *95* (14), 5967–5975. https://doi.org/10.1021/acs.analchem.2c05674.
(1007) Haggett, J.; Domaille, D. *A Diazaborine-Based Fluorescent Probe Tracks Endogenously Produced Peroxynitrite in Live Cells*; preprint; Chemistry, 2022. https://doi.org/10.26434/chemrxiv-2022-3c4ht.
(1008) Mulay, S. V.; Kim, Y.; Lee, K. J.; Yudhistira, T.; Park, H.-S.; Churchill, D. G. Fluorogenic and Red-Shifted Diphenyl Phosphinate-Based Probe for Selective Peroxynitrite Detection as Demonstrated in Fixed Cells. *New J. Chem.* **2016**, *41* (20), 11934–11940. https://doi.org/10.1039/c7nj02530k.
(1009) Su, H.; Wang, N.; Wang, J.; Wang, H.; Zhang, J.; Zhao, W. A Resorufin-Based Red-Emitting Fluorescent Probe with High Selectivity for Tracking Endogenous Peroxynitrite in Living Cells and Inflammatory Mice. *Spectrochim. Acta. A. Mol. Biomol. Spectrosc.* **2021**, *252*, 119502. https://doi.org/10.1016/j.saa.2021.119502.
(1010) Jiang, G.; Li, C.; Lai, Q.; Liu, X.; Chen, Q.; Zhang, P.; Wang, J.; Tang, B. Z. An Easily Available Ratiometric AIE Probe for Peroxynitrite in Vitro and in Vivo Imaging. *Sens. Actuators B Chem.* **2021**, *329*, 129223. https://doi.org/10.1016/j.snb.2020.129223.
(1011)Yuan, R.; Ma, Y.; Du, J.; Meng, F.; Guo, J.; Hong, M.; Yue, Q.; Li, X.; Li, C. A Novel Highly Selective Near-Infrared and Naked-Eye Fluorescence Probe for Imaging Peroxynitrite. *Anal. Methods* **2019**, *11* (11), 1522–1529. https://doi.org/10.1039/C8AY02632G.
(1012) Gu, B.; Liu, C.; Wu, Y.; Zhang, C.; Shen, Y.; Liu, M. Application of a Colorimetric and Near-Infrared Fluorescent Probe in Peroxynitrite Detection and Imaging in Living Cells. *ACS Omega* **2020**, *5* (42), 27530–27535. https://doi.org/10.1021/acsomega.0c04073.
(1013) Shen, Y.; Dai, L.; Zhang, Y.; Li, H.; Chen, Y.; Zhang, C. A Novel Pyridinium-Based Fluorescent Probe for Ratiometric Detection of Peroxynitrite in Mitochondria. *Spectrochim. Acta. A. Mol. Biomol. Spectrosc.* **2020**, *228*, 117762. https://doi.org/10.1016/j.saa.2019.117762.
(1014) Zhang, Y.; Ma, D. Selective Detection of Peroxynitrite in Living Cells by a Near-Infrared Diphenyl Phosphinate-Based Dicyanoisophorone Probe. *Spectrochim. Acta. A. Mol. Biomol. Spectrosc.* **2021**, *244*, 118890. https://doi.org/10.1016/j.saa.2020.118890.
(1015) Gu, B.; Liu, M.; Dai, C.; Zhou, Z.; Tang, D.; Tang, S.; Shen, Y.; Li, H. Rational Construction of a Novel Ratiometric Far-Red Fluorescent Probe with Excellent Water Solubility for

Sensing Mitochondrial Peroxynitrite. *Sens. Actuators B Chem.* **2021**, *344*, 130246. https://doi.org/10.1016/j.snb.2021.130246.
(1016) Wang, B.-D.; Wei, R.; Gao, M.-J.; Wang, Y.-H.; Zhang, C.-F.; Guo, X.-H.; Liang, Z.; Zhou, J.-T.; Sun, J.-X.; Xu, J.-Q.; Kang, Y.-F. Development of Peroxynitrite-Responsive Fluorescence Probe for Recognition of Drug-Induced Liver Injury. *Spectrochim. Acta. A. Mol. Biomol. Spectrosc.* **2022**, *283*, 121755. https://doi.org/10.1016/j.saa.2022.121755.
(1017) Wu, Y.; Shi, A.; Li, Y.; Zeng, H.; Chen, X.; Wu, J.; Fan, X. A Near-Infrared Xanthene Fluorescence Probe for Monitoring Peroxynitrite in Living Cells and Mouse Inflammation Model. *Analyst* **2018**, *143* (22), 5512–5519. https://doi.org/10.1039/C8AN01107A.
(1018) Yang, X.; Han, X.; Zhang, Y.; Liu, J.; Tang, J.; Zhang, D.; Zhao, Y.; Ye, Y. Imaging Hg2+-Induced Oxidative Stress by NIR Molecular Probe with "Dual-Key-and-Lock" Strategy. *Anal. Chem.* **2020**, *92* (17), 12002–12009. https://doi.org/10.1021/acs.analchem.0c02509.
(1019) Fan, L.; Yang, Q.; Zan, Q.; Zhao, K.; Lu, W.; Wang, X.; Wang, Y.; Shuang, S.; Dong, C. Multifunctional Fluorescent Probe for Simultaneous Detection of ONOO–, Viscosity, and Polarity and Its Application in Ferroptosis and Cancer Models. *Anal. Chem.* **2023**, *95* (13), 5780–5787. https://doi.org/10.1021/acs.analchem.3c00142.
(1020) Liu, Y.; Ma, Y.; Lin, W. Construction of a Large Stokes Shift Fluorescent Probe for Dual Detection of Mitochondrial Viscosity and ONOO− and Its Application in Bioimaging. *Talanta* **2023**, *253*, 124023. https://doi.org/10.1016/j.talanta.2022.124023.
(1021) Chai, X.; Li, B.; Chen, C.; Zhang, W.; Sun, L.; Han, H.-H.; Zhang, Y.; Sun, S.; Yang, J.; Zhang, J.; He, X.-P. A Highly Sensitive and Selective Near-Infrared Fluorescent Probe for Imaging Peroxynitrite in Living Cells and Drug-Induced Liver Injury Mice. *Anal. Chem.* **2023**, *95* (13), 5747–5753. https://doi.org/10.1021/acs.analchem.3c00007.
(1022) Dong, J.; Yang, Y.; Fan, X.; Zhu, H.-L.; Li, Z. Accurate Imaging in the Processes of Formation and Inhibition of Drug-Induced Liver Injury by an Activable Fluorescent Probe for $ONOO^-$. *Mater. Today Bio* **2023**, *21*, 100689. https://doi.org/10.1016/j.mtbio.2023.100689.
(1023) Zhang, Q.; Zhang, N.; Long, Y.-T.; Qian, X.; Yang, Y. Understanding the Selectivity of a Multichannel Fluorescent Probe for Peroxynitrite Over Hypochlorite. *Bioconjug. Chem.* **2016**, *27* (2), 341–353. https://doi.org/10.1021/acs.bioconjchem.5b00396.
(1024) Yu, F.; Li, P.; Li, G.; Zhao, G.; Chu, T.; Han, K. A Near-IR Reversible Fluorescent Probe Modulated by Selenium for Monitoring Peroxynitrite and Imaging in Living Cells. *J. Am. Chem. Soc.* **2011**, *133* (29), 11030–11033. https://doi.org/10.1021/ja202582x.
(1025) Yu, F.; Li, P.; Wang, B.; Han, K. Reversible Near-Infrared Fluorescent Probe Introducing Tellurium to Mimetic Glutathione Peroxidase for Monitoring the Redox Cycles between Peroxynitrite and Glutathione in Vivo. *J. Am. Chem. Soc.* **2013**, *135* (20), 7674–7680. https://doi.org/10.1021/ja401360a.
(1026) Yudhistira, T.; Mulay, S. V.; Lee, K. J.; Kim, Y.; Park, H.-S.; Churchill, D. G. Thiomaleimide Functionalization for Selective Biological Fluorescence Detection of Peroxynitrite as Tested in HeLa and RAW 264.7 Cells. *Chem. – Asian J.* **2017**, *12* (15), 1927–1934. https://doi.org/10.1002/asia.201700527.
(1027) Hou, J.-T.; Wang, B.; Zhang, Y.; Cui, B.; Cao, X.; Zhang, M.; Ye, Y.; Wang, S. Observation of Peroxynitrite Overproduction in Cells during 5-Fluorouracil Treatment via a Ratiometric Fluorescent Probe. *Chem. Commun.* **2020**, *56* (18), 2759–2762. https://doi.org/10.1039/C9CC09652C.
(1028) Li, Z.; Lu, J.; Pang, Q.; You, J. Construction of a Near-Infrared Fluorescent Probe for Ratiometric Imaging of Peroxynitrite during Tumor Progression. *Analyst* **2021**, *146* (16), 5204–5211. https://doi.org/10.1039/D1AN00980J.
(1029) Xu, K.; Chen, H.; Tian, J.; Ding, B.; Xie, Y.; Qiang, M.; Tang, B. A Near-Infrared Reversible Fluorescent Probe for Peroxynitrite and Imaging of Redox Cycles in Living Cells. *Chem. Commun.* **2011**, *47* (33), 9468–9470. https://doi.org/10.1039/C1CC12994E.

(1030) Wang, B.; Yu, F.; Li, P.; Sun, X.; Han, K. A BODIPY Fluorescence Probe Modulated by Selenoxide Spirocyclization Reaction for Peroxynitrite Detection and Imaging in Living Cells. *Dyes Pigments* **2013**, *96* (2), 383–390. https://doi.org/10.1016/j.dyepig.2012.09.006.
(1031) Sun, C.; Du, W.; Wang, P.; Wu, Y.; Wang, B.; Wang, J.; Xie, W. A Novel Mitochondria-Targeted Two-Photon Fluorescent Probe for Dynamic and Reversible Detection of the Redox Cycles between Peroxynitrite and Glutathione. *Biochem. Biophys. Res. Commun.* **2017**, *494* (3), 518–525. https://doi.org/10.1016/j.bbrc.2017.10.123.
(1032) *APF (Hydroxyl Radical, Hypochlorite or Peroxynitrite Sensor)*. https://www.thermofisher.com/order/catalog/product/A36003?SID=srch-srp-A36003 (accessed 2023-07-22).
(1033) *HPF (Hydroxyl Radical and Peroxynitrite Sensor)*. https://www.thermofisher.com/order/catalog/product/H36004 (accessed 2023-07-22).
(1034) Setsukinai, K.; Urano, Y.; Kakinuma, K.; Majima, H. J.; Nagano, T. Development of Novel Fluorescence Probes That Can Reliably Detect Reactive Oxygen Species and Distinguish Specific Species. *J. Biol. Chem.* **2003**, *278* (5), 3170–3175. https://doi.org/10.1074/jbc.M209264200.
(1035) Peng, T.; Wong, N.-K.; Chen, X.; Chan, Y.-K.; Ho, D. H.-H.; Sun, Z.; Hu, J. J.; Shen, J.; El-Nezami, H.; Yang, D. Molecular Imaging of Peroxynitrite with HKGreen-4 in Live Cells and Tissues. *J. Am. Chem. Soc.* **2014**, *136* (33), 11728–11734. https://doi.org/10.1021/ja504624q.
(1036) Li, X.; Tao, R.-R.; Hong, L.-J.; Cheng, J.; Jiang, Q.; Lu, Y.-M.; Liao, M.-H.; Ye, W.-F.; Lu, N.-N.; Han, F.; Hu, Y.-Z.; Hu, Y.-H. Visualizing Peroxynitrite Fluxes in Endothelial Cells Reveals the Dynamic Progression of Brain Vascular Injury. *J. Am. Chem. Soc.* **2015**, *137* (38), 12296–12303. https://doi.org/10.1021/jacs.5b06865.
(1037) Jin, C.; Wu, P.; Yang, Y.; He, Z.; Zhu, H.; Li, Z. A Novel Fluorescent Probe for the Detection of Peroxynitrite and Its Application in Acute Liver Injury Model. *Redox Biol.* **2021**, *46*, 102068. https://doi.org/10.1016/j.redox.2021.102068.
(1038) Sun, Q.; Xu, J.; Ji, C.; Shaibani, M. S. S.; Li, Z.; Lim, K.; Zhang, C.; Li, L.; Liu, Z. Ultrafast Detection of Peroxynitrite in Parkinson's Disease Models Using a Near-Infrared Fluorescent Probe. *Anal. Chem.* **2020**, *92* (5), 4038–4045. https://doi.org/10.1021/acs.analchem.9b05599.
(1039) Zhou, Y.; Li, P.; Fan, N.; Wang, X.; Liu, X.; Wu, L.; Zhang, W.; Zhang, W.; Ma, C.; Tang, B. In Situ Visualization of Peroxisomal Peroxynitrite in the Livers of Mice with Acute Liver Injury Induced by Carbon Tetrachloride Using a New Two-Photon Fluorescent Probe. *Chem. Commun.* **2019**, *55* (47), 6767–6770. https://doi.org/10.1039/C9CC02483B.
(1040) Zhang, H.; Liu, J.; Sun, Y.-Q.; Huo, Y.; Li, Y.; Liu, W.; Wu, X.; Zhu, N.; Shi, Y.; Guo, W. A Mitochondria-Targetable Fluorescent Probe for Peroxynitrite: Fast Response and High Selectivity. *Chem. Commun.* **2015**, *51* (13), 2721–2724. https://doi.org/10.1039/C4CC09122A.
(1041) Miao, J.; Huo, Y.; Liu, Q.; Li, Z.; Shi, H.; Shi, Y.; Guo, W. A New Class of Fast-Response and Highly Selective Fluorescent Probes for Visualizing Peroxynitrite in Live Cells, Subcellular Organelles, and Kidney Tissue of Diabetic Rats. *Biomaterials* **2016**, *107*, 33–43. https://doi.org/10.1016/j.biomaterials.2016.08.032.
(1042) Zhang, H.; Liu, J.; Wang, L.; Sun, M.; Yan, X.; Wang, J.; Guo, J.-P.; Guo, W. Amino-Si-Rhodamines: A New Class of Two-Photon Fluorescent Dyes with Intrinsic Targeting Ability for Lysosomes. *Biomaterials* **2018**, *158*, 10–22. https://doi.org/10.1016/j.biomaterials.2017.12.013.
(1043) Knewtson, K. E.; Rane, D.; Peterson, B. R. Targeting Fluorescent Sensors to Endoplasmic Reticulum Membranes Enables Detection of Peroxynitrite During Cellular Phagocytosis. *ACS Chem. Biol.* **2018**, *13* (9), 2595–2602. https://doi.org/10.1021/acschembio.8b00535.

(1044) Liu, C.; Duan, Q.; Zhang, X.; Li, Z.; Jia, P.; Zhu, H.; Yu, Y.; Wang, Z.; Zhu, B.; Sheng, W. A Novel Hepatoma-Specific Fluorescent Probe for Imaging Endogenous Peroxynitrite in Live HepG2 Cells. *Sens. Actuators B Chem.* **2019**, *289*, 124–130. https://doi.org/10.1016/j.snb.2019.03.068.
(1045) Shu, W.; Wu, Y.; Shen, T.; Cui, J.; Kang, H.; Jing, J.; Zhang, X. A Mitochondria-Targeted Far Red Fluorescent Probe for Ratiometric Imaging of Endogenous Peroxynitrite. *Dyes Pigments* **2019**, *170*, 107609. https://doi.org/10.1016/j.dyepig.2019.107609.
(1046) Ambikapathi, G.; Kempahanumakkagari, S. K.; Ramappa Lamani, B.; Kuramkote Shivanna, D.; Bodagur Maregowda, H.; Gupta, A.; Malingappa, P. Bioimaging of Peroxynitrite in MCF-7 Cells by a New Fluorescent Probe Rhodamine B Phenyl Hydrazide. *J. Fluoresc.* **2013**, *23* (4), 705–712. https://doi.org/10.1007/s10895-013-1205-y.
(1047) Chen, S.; Vurusaner, B.; Pena, S.; Thu, C. T.; Mahal, L. K.; Fisher, Edward. A.; Canary, James. W. Two-Photon, Ratiometric, Quantitative Fluorescent Probe Reveals Fluctuation of Peroxynitrite Regulated by Arginase 1. *Anal. Chem.* **2021**, *93* (29), 10090–10098. https://doi.org/10.1021/acs.analchem.1c00911.
(1048) Li, H.; Li, X.; Wu, X.; Shi, W.; Ma, H. Observation of the Generation of $ONOO^-$ in Mitochondria under Various Stimuli with a Sensitive Fluorescence Probe. *Anal. Chem.* **2017**, *89* (10), 5519–5525. https://doi.org/10.1021/acs.analchem.7b00503.
(1049) Zhu, B.; Zhang, M.; Wu, L.; Zhao, Z.; Liu, C.; Wang, Z.; Duan, Q.; Wang, Y.; Jia, P. A Highly Specific Far-Red Fluorescent Probe for Imaging Endogenous Peroxynitrite in the Mitochondria of Living Cells. *Sens. Actuators B Chem.* **2018**, *257*, 436–441. https://doi.org/10.1016/j.snb.2017.10.170.
(1050) Mao, G.-J.; Gao, G.-Q.; Dong, W.-P.; Wang, Q.-Q.; Wang, Y.-Y.; Li, Y.; Su, L.; Zhang, G. A Two-Photon Excited near-Infrared Fluorescent Probe for Imaging Peroxynitrite during Drug-Induced Hepatotoxicity and Its Remediation. *Talanta* **2021**, *221*, 121607. https://doi.org/10.1016/j.talanta.2020.121607.
(1051) Xia, Q.; Feng, S.; Hong, J.; Feng, G. One Probe for Multiple Targets: A NIR Fluorescent Rhodamine-Based Probe for ONOO− and Lysosomal pH Detection in Live Cells. *Sens. Actuators B Chem.* **2021**, *337*, 129732. https://doi.org/10.1016/j.snb.2021.129732.
(1052) Liu, Z.; Sun, Q.; Yan, M.; Zhang, C.; Yuan, H.; He, W. Activity-Based Fluorescent Molecular Logic Gate Probe for Dynamic Tracking of Mitophagy Induced by Oxidative Stress. *Anal. Chem.* **2021**, *93* (7), 3502–3509. https://doi.org/10.1021/acs.analchem.0c04854.
(1053) Li, Z.; Liu, C.; Yu, C.; Chen, Y.; Jia, P.; Zhu, H.; Zhang, X.; Yu, Y.; Zhu, B.; Sheng, W. A Highly Selective and Sensitive Red-Emitting Fluorescent Probe for Visualization of Endogenous Peroxynitrite in Living Cells and Zebrafish. *Analyst* **2019**, *144* (10), 3442–3449. https://doi.org/10.1039/C9AN00347A.
(1054) Ren, J.; Du, Z.; Zhang, W.; Zhang, R.; Song, B.; Yuan, J. Development of a Fluorescein Modified Ruthenium(II) Complex Probe for Lysosome-Targeted Ratiometric Luminescence Detection and Imaging of Peroxynitrite in Living Cells. *Anal. Chim. Acta* **2022**, *1205*, 339784. https://doi.org/10.1016/j.aca.2022.339784.
(1055) Miao, J.; Huo, Y.; Shi, H.; Fang, J.; Wang, J.; Guo, W. A Si-Rhodamine-Based near-Infrared Fluorescent Probe for Visualizing Endogenous Peroxynitrite in Living Cells, Tissues, and Animals. *J. Mater. Chem. B* **2018**, *6* (27), 4466–4473. https://doi.org/10.1039/C8TB00987B.
(1056) Qian, J.; Gong, D.; Ru, J.; Guo, Y.; Cao, T.; Liu, W.; Iqbal, A.; Iqbal, K.; Qin, W.; Guo, H. A Naphthalimide-Based Lysosome-Targeting Fluorescent Probe for the Selective Detection and Imaging of Endogenous Peroxynitrite in Living Cells. *Anal. Bioanal. Chem.* **2019**, *411* (17), 3929–3939. https://doi.org/10.1007/s00216-019-01866-3.
(1057) Li, M.; Gong, X.; Li, H.-W.; Han, H.; Shuang, S.; Song, S.; Dong, C. A Fast Detection of Peroxynitrite in Living Cells. *Anal. Chim. Acta* **2020**, *1106*, 96–102. https://doi.org/10.1016/j.aca.2020.02.009.

(1058) Zeng, X.; Chen, X.; Chen, J.; Ma, M.; Jin, H.; Yu, S.; Liu, Z. A Simple Highly Selective Ratiometric Fluorescent Probe for Detection of Peroxynitrite and Its Bioimaging Applications. *Dyes Pigments* **2023**, *210*, 110993. https://doi.org/10.1016/j.dyepig.2022.110993.
(1059) Lin, X.; Fan, M.; Li, N.; Yang, J.; Zhu, H.; Chen, B.; Zhu, J.; Zhang, D.; Wang, T.; Cui, X. Phosphorus-Substituted Rhodamines for Bioimaging of the Lysosomal Peroxynitrite in Vivo. *Dyes Pigments* **2022**, *201*, 110201. https://doi.org/10.1016/j.dyepig.2022.110201.
(1060) Zhang, Q.; Zhu, Z.; Zheng, Y.; Cheng, J.; Zhang, N.; Long, Y.-T.; Zheng, J.; Qian, X.; Yang, Y. A Three-Channel Fluorescent Probe That Distinguishes Peroxynitrite from Hypochlorite. *J. Am. Chem. Soc.* **2012**, *134* (45), 18479–18482. https://doi.org/10.1021/ja305046u.
(1061) Li, Z.; Liu, R.; Tan, Z.; He, L.; Lu, Z.; Gong, B. Aromatization of 9,10-Dihydroacridine Derivatives: Discovering a Highly Selective and Rapid-Responding Fluorescent Probe for Peroxynitrite. *ACS Sens.* **2017**, *2* (4), 501–505. https://doi.org/10.1021/acssensors.7b00139.
(1062) Ren, M.; Wang, L.; Lv, X.; Liu, J.; Chen, H.; Wang, J.; Guo, W. Development of a Benzothiazole-Functionalized Red-Emission Pyronin Dye and Its Dihydro Derivative for Imaging Lysosomal Viscosity and Tracking Endogenous Peroxynitrite. *J. Mater. Chem. B* **2019**, *7* (40), 6181–6186. https://doi.org/10.1039/C9TB01525F.
(1063) Wang, L.; Liu, J.; Zhao, S.; Zhang, H.; Sun, Y.; Wei, A.; Guo, W. Fluorescence Imaging of Hypochlorous Acid and Peroxynitrite in Vitro and in Vivo with Emission Wavelength beyond 750 nm. *Chem. Commun.* **2020**, *56* (56), 7718–7721. https://doi.org/10.1039/D0CC02322A.
(1064) Ren, M.; Zhou, C.; Wang, L.; Lv, X.; Guo, W. Rationally Designed Meso-Benzimidazole-Pyronin with Emission Wavelength beyond 700 Nm Enabling in Vivo Visualization of Acute-Liver-Injury-Induced Peroxynitrite. *Chin. Chem. Lett.* **2023**, *34* (4), 107646. https://doi.org/10.1016/j.cclet.2022.06.069.
(1065) Sun, J.; Cao, X.; Lu, W.; Wei, Y.; Kong, L.; Chen, W.; Shao, X.; Wang, Y. Recent Advances in Fluorescent Probes of Peroxynitrite: Structural, Strategies and Biological Applications. *Theranostics* **2023**, *13* (5), 1716–1744. https://doi.org/10.7150/thno.80529.
(1066) Shen, Y.; Zhang, X.; Zhang, Y.; Li, H.; Dai, L.; Peng, X.; Peng, Z.; Xie, Y. A Fluorescent Sensor for Fast Detection of Peroxynitrite by Removing of C=N in a Benzothiazole Derivative. *Anal. Chim. Acta* **2018**, *1014*, 71–76. https://doi.org/10.1016/j.aca.2018.01.046.
(1067) Wang, C.; Shu, W.; Chen, Q.; Yang, C.; Su, S.; Gao, M.; Zhang, R.; Jing, J.; Zhang, X. A Simple Dual-Response Fluorescent Probe for Imaging of Viscosity and $ONOO^-$ through Different Fluorescence Signals in Living Cells and Zebrafish. *Spectrochim. Acta. A. Mol. Biomol. Spectrosc.* **2021**, *260*, 119990. https://doi.org/10.1016/j.saa.2021.119990.
(1068) Wang, F.; Guo, B.; Guo, X.; Gu, B.; Shen, Y.; Long, J. A Rapidly Responding and Highly Sensitive Biosensor for pH-Universal Detection of $ONOO^-$ and Its Cellular Imaging. *J. Photochem. Photobiol. Chem.* **2022**, *427*, 113796. https://doi.org/10.1016/j.jphotochem.2022.113796.
(1069) Liu, Y.; Zhang, C.; Wei, Y.; Chen, H.; Kong, L.; Chen, Q.; Wang, Y. De Novo-Designed Landmine Warfare Strategy Luminophore for Super-Resolution Imaging Reveal $ONOO^-$ Evolution in Living Cells. *Chem. Eng. J.* **2021**, *422*, 130151. https://doi.org/10.1016/j.cej.2021.130151.
(1070) Xie, X.; Liu, G.; Su, X.; Li, Y.; Liu, Y.; Jiao, X.; Wang, X.; Tang, B. A Facile, Versatile, and Highly Efficient Strategy for Peroxynitrite Bioimaging Enabled by Formamide Deformylation. *Anal. Chem.* **2019**, *91* (10), 6872–6879. https://doi.org/10.1021/acs.analchem.9b01175.
(1071) Panizzi, P.; Nahrendorf, M.; Wildgruber, M.; Waterman, P.; Figueiredo, J.-L.; Aikawa, E.; McCarthy, J.; Weissleder, R.; Hilderbrand, S. A. Oxazine Conjugated Nanoparticle Detects

in Vivo Hypochlorous Acid and Peroxynitrite Generation. *J. Am. Chem. Soc.* **2009**, *131* (43), 15739–15744. https://doi.org/10.1021/ja903922u.
(1072) Xiaolong, Z.; Na, L.; Fayu, L.; Chao, G.; Jiubiao, F.; Leping, L.; Xiaolin, G.; Na, Y. Synthesis and Application of Water-Soluble Reaction-Based Boron-Dipyrromethene (BODIPY) Probes for Fluorescent Detection of Peroxynitrite with High Selectivity. *Chin. J. Org. Chem.* **2020**, *40* (12), 4339. https://doi.org/10.6023/cjoc202007022.
(1073) Lu, J.; Li, Z.; Gao, Q.; Tan, J.; Sun, Z.; Chen, L.; You, J. Nonoxidative Strategy for Monitoring Peroxynitrite Fluctuations in Immune Responses of Tumorigenesis. *Anal. Chem.* **2021**, *93* (7), 3426–3435. https://doi.org/10.1021/acs.analchem.0c04512.
(1074) Zhang, J.; Liu, L.; Wang, Y.; Wang, C.; Guo, Y.; Yuan, Z.; Jia, Y.; Li, P.; Sun, S.; Zhao, G. A Highly Selective Red-Emitting Fluorescent Probe and Its Micro-Nano-Assembly for Imaging Endogenous Peroxynitrite (ONOO−) in Living Cells. *Anal. Chim. Acta* **2023**, *1241*, 340778. https://doi.org/10.1016/j.aca.2022.340778.
(1075) Yang, R.; Dou, Y.; Zhang, Y.; Qu, L.; Sun, Y.; Li, Z. A Facile and Highly Efficient Fluorescent Turn-on Switch Strategy Based on Diketone Isomerization and Its Application in Peroxynitrite Fluorescent Imaging. *Sens. Actuators B Chem.* **2021**, *337*, 129805. https://doi.org/10.1016/j.snb.2021.129805.
(1076) Sun, Y.; Tang, X.; Li, X.; Kong, X.; Tian, M.; Wang, Y.; Dong, B. PET-ESIPT-Based Fluorescent Probes for Revealing the Fluctuation of Peroxynitrite ($ONOO^-$) in Living Cells, Zebrafishes and Brain Tissues. *Sens. Actuators B Chem.* **2022**, *353*, 131121. https://doi.org/10.1016/j.snb.2021.131121.
(1077) Xie, X.; Liu, G.; Niu, Y.; Xu, C.; Li, Y.; Zhang, J.; Jiao, X.; Wang, X.; Tang, B. Dual-Channel Imaging of Amyloid-β Plaques and Peroxynitrite To Illuminate Their Correlations in Alzheimer's Disease Using a Unimolecular Two-Photon Fluorescent Probe. *Anal. Chem.* **2021**, *93* (45), 15088–15095. https://doi.org/10.1021/acs.analchem.1c03334.
(1078) Xie, X.; Liu, Y.; Liu, G.; Zhao, Y.; Liu, J.; Li, Y.; Zhang, J.; Jiao, X.; Wang, X.; Tang, B. Two-Photon Fluorescence Imaging of the Cerebral Peroxynitrite Stress in Alzheimer's Disease. *Chem. Commun.* **2022**, *58* (43), 6300–6303. https://doi.org/10.1039/D2CC01744J.
(1079) Zhuo, J.; Hui, J.; Chi, H.; Guo, Y.; Lu, G. Near-Infrared Fluorescent Probes with Long-Acting Cyclic Monitoring and Effectively Eliminating Peroxynitrite. *Chem. – Asian J.* **2023**, *n/a* (n/a), e202300717. https://doi.org/10.1002/asia.202300717.
(1080) Lu, G.; Guo, Y.; Zhuo, J.; Li, X.; Chi, H.; Zhang, Z. A General Strategy for Through-Bond Energy Transfer Fluorescence Probes Combining Intramolecular Charge Transfer: A Silyl Ether System for Endogenous Peroxynitrite Sensing. *Chem. – Eur. J.* **2019**, *25* (71), 16350–16357. https://doi.org/10.1002/chem.201903880.
(1081) Zhuo, J.; Gong, K.; Guo, Y.; Lu, G.; Chi, H.; Duan, Y.; Zhang, Z.; Li, X. A Silyl Ether Based Fluorescent Probe for Rapid Monitoring of Endogenous Peroxynitrite Concentration and Imaging in Living Cells through Multicolor Emission. *ChemPlusChem* **2020**, *85* (4), 684–688. https://doi.org/10.1002/cplu.202000100.
(1082) Wu, W.; Liao, X.; Chen, Y.; Ji, L.; Chao, H. Mitochondria-Targeting and Reversible Near-Infrared Emissive Iridium(III) Probe for in Vivo $ONOO^-$/GSH Redox Cycles Monitoring. *Anal. Chem.* **2021**, *93* (22), 8062–8070. https://doi.org/10.1021/acs.analchem.1c01409.
(1083) Zhang, H.; Xu, Y.; Li, H.; Shi, W.; Li, X.; Ma, H. New Rhodamines with Changeable π-Conjugation for Lengthening Fluorescence Wavelengths and Imaging Peroxynitrite. *Chem* **2022**, *8* (1), 287–295. https://doi.org/10.1016/j.chempr.2021.11.023.
(1084) Sikora, A.; Zielonka, J.; Dębowska, K.; Michalski, R.; Smulik-Izydorczyk, R.; Pięta, J.; Podsiadły, R.; Artelska, A.; Pierzchała, K.; Kalyanaraman, B. Boronate-Based Probes for Biological Oxidants: A Novel Class of Molecular Tools for Redox Biology. *Front. Chem.* **2020**, *8*.
(1085) Hu, Q.; Qin, C.; Huang, L.; Wang, H.; Liu, Q.; Zeng, L. Selective Visualization of Hypochlorite and Its Fluctuation in Cancer Cells by a Mitochondria-Targeting Ratiometric

Fluorescent Probe. *Dyes Pigments* **2018**, *149*, 253–260. https://doi.org/10.1016/j.dyepig.2017.10.002.
(1086) Lv, X.; Yuan, X.; Wang, Y.; Guo, W. A Naphthalimide Based Fast and Selective Fluorescent Probe for Hypochlorous Acid/Hypochlorite and Its Application for Bioimaging. *New J. Chem.* **2018**, *42* (18), 15105–15110. https://doi.org/10.1039/C8NJ03208D.
(1087) Mao, Z.; Ye, M.; Hu, W.; Ye, X.; Wang, Y.; Zhang, H.; Li, C.; Liu, Z. Design of a Ratiometric Two-Photon Probe for Imaging of Hypochlorous Acid (HClO) in Wounded Tissues. *Chem. Sci.* **2018**, *9* (28), 6035–6040. https://doi.org/10.1039/C8SC01697F.
(1088) Zhu, B.; Wu, L.; Zhang, M.; Wang, Y.; Zhao, Z.; Wang, Z.; Duan, Q.; Jia, P.; Liu, C. A Fast-Response, Highly Specific Fluorescent Probe for the Detection of Picomolar Hypochlorous Acid and Its Bioimaging Applications. *Sens. Actuators B Chem.* **2018**, *263*, 103–108. https://doi.org/10.1016/j.snb.2018.02.083.
(1089) Carballal, S.; Bartesaghi, S.; Radi, R. Kinetic and Mechanistic Considerations to Assess the Biological Fate of Peroxynitrite. *Biochim. Biophys. Acta BBA - Gen. Subj.* **2014**, *1840* (2), 768–780. https://doi.org/10.1016/j.bbagen.2013.07.005.
(1090) Lyublinskaya, O.; Antunes, F. Measuring Intracellular Concentration of Hydrogen Peroxide with the Use of Genetically Encoded H_2O_2 Biosensor HyPer. *Redox Biol.* **2019**, *24*, 101200. https://doi.org/10.1016/j.redox.2019.101200.
(1091) Haris, U.; Plank, J. T.; Li, B.; Page, Z. A.; Lippert, A. R. Visible Light Chemical Micropatterning Using a Digital Light Processing Fluorescence Microscope. *ACS Cent. Sci.* **2022**, *8* (1), 67–76. https://doi.org/10.1021/acscentsci.1c01234.
(1092) Chandrasiri, I.; Loku Yaddehige, M.; Li, B.; Sun, Y.; Meador, W. E.; Dorris, A.; Farid Zia, M.; Hammer, N. I.; Flynt, A.; Delcamp, J. H.; Davis, E.; Lippert, A.; Watkins, D. L. Cross-Linking Poly(Caprolactone)–Polyamidoamine Linear Dendritic Block Copolymers for Theranostic Nanomedicine. *ACS Appl. Polym. Mater.* **2022**, *4* (5), 2972–2986. https://doi.org/10.1021/acsapm.1c01131.
(1093) Ryan, L. S.; Nakatsuka, A.; Lippert, A. R. Photoactivatable 1,2-Dioxetane Chemiluminophores. *Results Chem.* **2021**, *3*, 100106. https://doi.org/10.1016/j.rechem.2021.100106.
(1094) Li, B.; Haris, U.; Aljowni, M.; Nakatsuka, A.; Patel, S. K.; Lippert, A. R. Tuning the Photophysical Properties of Spirolactam Rhodamine Photoswitches. *Isr. J. Chem.* **2021**, *61* (3–4), 244–252. https://doi.org/10.1002/ijch.202000083.
(1095) Patel, S. K.; Cao, J.; Lippert, A. R. A Volumetric Three-Dimensional Digital Light Photoactivatable Dye Display. *Nat. Commun.* **2017**, *8* (1), 15239. https://doi.org/10.1038/ncomms15239.
(1096) Bezner, B. J.; Ryan, L. S.; Lippert, A. R. Reaction-Based Luminescent Probes for Reactive Sulfur, Oxygen, and Nitrogen Species: Analytical Techniques and Recent Progress. *Anal. Chem.* **2020**, *92* (1), 309–326. https://doi.org/10.1021/acs.analchem.9b04990.
(1097) Lyublinskaya, O.; Antunes, F. Measuring Intracellular Concentration of Hydrogen Peroxide with the Use of Genetically Encoded H_2O_2 Biosensor HyPer. *Redox Biol.* **2019**, *24*, 101200. https://doi.org/10.1016/j.redox.2019.101200.
(1098) Wang, X.; Pu, K. Molecular Substrates for the Construction of Afterglow Imaging Probes in Disease Diagnosis and Treatment. *Chem. Soc. Rev.* **2023**, *52* (14), 4549–4566. https://doi.org/10.1039/D3CS00006K.
(1099) Zlitni, A.; Gambhir, S. S. Molecular Imaging Agents for Ultrasound. *Curr. Opin. Chem. Biol.* **2018**, *45*, 113–120. https://doi.org/10.1016/j.cbpa.2018.03.017.
(1100) Jiang, Y.; Pu, K. Multimodal Biophotonics of Semiconducting Polymer Nanoparticles. *Acc. Chem. Res.* **2018**, *51* (8), 1840–1849. https://doi.org/10.1021/acs.accounts.8b00242.
(1101) Sohn, H.-Y.; Gloe, T.; Keller, M.; Schoenafinger, K.; Pohl, U. Sensitive Superoxide Detection in Vascular Cells by the New Chemiluminescence Dye L-012. *J. Vasc. Res.* **1999**, *36* (6), 456–464. https://doi.org/10.1159/000025688.

(1102) Daiber, A.; August, M.; Baldus, S.; Wendt, M.; Oelze, M.; Sydow, K.; Kleschyov, A. L.; Munzel, T. Measurement of NAD(P)H Oxidase-Derived Superoxide with the Luminol Analogue L-012. *Free Radic. Biol. Med.* **2004**, *36* (1), 101–111. https://doi.org/10.1016/j.freeradbiomed.2003.10.012.
(1103) Niu, J.; Fan, J.; Wang, X.; Xiao, Y.; Xie, X.; Jiao, X.; Sun, C.; Tang, B. Simultaneous Fluorescence and Chemiluminescence Turned on by Aggregation-Induced Emission for Real-Time Monitoring of Endogenous Superoxide Anion in Live Cells. *Anal. Chem.* **2017**, *89* (13), 7210–7215. https://doi.org/10.1021/acs.analchem.7b01425.
(1104) Ying, A.; Ying, L. A New Hydrocyanine Probe for Imaging Reactive Oxygen Species in the Mitochondria of Live Cells. *Bioorg. Med. Chem. Lett.* **2023**, *87*, 129262. https://doi.org/10.1016/j.bmcl.2023.129262.
(1105) Li, R.-Q.; Mao, Z.-Q.; Rong, L.; Wu, N.; Lei, Q.; Zhu, J.-Y.; Zhuang, L.; Zhang, X.-Z.; Liu, Z.-H. A Two-Photon Fluorescent Probe for Exogenous and Endogenous Superoxide Anion Imaging in Vitro and in Vivo. *Biosens. Bioelectron.* **2017**, *87*, 73–80. https://doi.org/10.1016/j.bios.2016.08.008.
(1106) Zhang, W.; Wang, X.; Li, P.; Huang, F.; Wang, H.; Zhang, W.; Tang, B. Elucidating the Relationship between Superoxide Anion Levels and Lifespan Using an Enhanced Two-Photon Fluorescence Imaging Probe. *Chem. Commun.* **2015**, *51*, 9710–9713. https://doi.org/10.1039/c5cc01670c.
(1107) Long, R.; Tang, C.; Xu, J.; Li, T.; Tong, C.; Guo, Y.; Shi, S.; Wang, D. Novel Natural Myricetin with AIE and ESIPT Characteristics for Selective Detection and Imaging of Superoxide Anions in Vitro and in Vivo. *Chem. Commun.* **2019**, *55* (73), 10912–10915. https://doi.org/10.1039/c9cc05212g.
(1108) Zhang, W.; Fan, W.; Wang, X.; Li, P.; Zhang, W.; Wang, H.; Tang, B. Uncovering Endoplasmic Reticulum Superoxide Regulating Hepatic Ischemia-Reperfusion Injury by Dynamic Reversible Fluorescence Imaging. *Anal. Chem.* **2023**, *95* (21), 8367–8375. https://doi.org/10.1021/acs.analchem.3c01068.
(1109) Ma, S.; Gao, J.; Li, Z.; Zhou, J. Spectrofluorometric Determination of Superoxide Anion Radicals and Superoxide Dismutase Activity Using a 2-(2-Thienyl)Benzothiazoline Probe. *Anal. Lett.* **2010**, *43* (2), 280–288. https://doi.org/10.1080/00032710903325815.
(1110) Wang, Y.; Gao, M.; Liao, C.; Yu, F.; Chen, L. A Sulfydryl-Based near-Infrared Ratiometic Fluorescent Probe for Assessment of Acute/Chronic Mercury Exposure via Associated Determination of Superoxide Anion and Mercury Ion in Cells and in Vivo. *Sens. Actuators B Chem.* **2019**, *301* (12), 127038. https://doi.org/10.1016/j.snb.2019.127038.
(1111) Shelar, D. S.; Malankar, G. S.; Singh, P. R.; Vaidya, S. P.; Pinjari, R. V.; Manjare, S. T. Superoxide Targeted “Turn-on” Fluorescence Sensing Enabled by a Diselenide Based Quinoline Probe and Its *in Vitro* Anticancer Activity in Cancer Cells. *New J. Chem.* **2023**, *47* (14), 6653–6660. https://doi.org/10.1039/D2NJ06241K.
(1112) Maeda, H.; Yamamoto, K.; Nomura, Y.; Kohno, I.; Hafsi, L.; Ueda, N.; Yoshida, S.; Fukuda, M.; Fukuyasu, Y.; Yamauchi, Y.; Itoh, N. A Design of Fluorescent Probes for Superoxide Based on a Nonredox Mechanism. *J. Am. Chem. Soc.* **2005**, *127* (1), 68–69. https://doi.org/10.1021/ja047018k.
(1113) Si, F.; Liu, Y.; Yan, K.; Zhong, W. A Mitochondrion Targeting Fluorescent Probe for Imaging of Intracellular Superoxide Radicals. *Chem. Commun.* **2015**, *51*, 7931–7934. https://doi.org/10.1039/c5cc01075f.
(1114) Lu, X.; Chen, Z.; Dong, X.; Zhao, W. Water-Soluble Fluorescent Probe with Dual Mitochondria/Lysosome Targetability for Selective Superoxide Detection in Live Cells and in Zebrafish Embryos. *ACS Sens.* **2018**, *3* (1), 59–64. https://doi.org/10.1021/acssensors.7b00831.
(1115) Shin, J.; Kang, D. M.; Yoo, J.; Heo, J.; Jeong, K.; Chung, J. H.; Han, Y. S.; Kim, S. Superoxide-Responsive Fluorogenic Molecular Probes for Optical Bioimaging of

Neurodegenerative Events in Alzheimer′s Disease. *Analyst* **2021**, *146* (15), 4748–4755. https://doi.org/10.1039/d1an00692d.
(1116) Chen, L.; Lu, X.; Xiao, F.; Wu, D. A Sensitive and Selective Fluorescence Probe for the Detection of Superoxide Radical Anion in Vivo Based on a Protection-Deprotection Process. *Dyes Pigments* **2021**, *194*, 109614. https://doi.org/10.1016/j.dyepig.2021.109614.
(1117) Liu, M.; Xu, N.; Wang, Z.; Li, X.; Ma, Z.; Qu, X.; Wang, X.; Tian, Z. A Merocyanine Dye-Based Superoxide Anion Fluorescent Probe with Second-Level Response Agility Enables Evaluating Interstitial Cystitis via Two-Photon Excitation Imaging. *Dyes Pigments* **2023**, *219*, 111526. https://doi.org/10.1016/j.dyepig.2023.111526.
(1118) Chang, J.; Wang, Y.; Wei, H.; Kong, X.; Dong, B.; Yue, T. Development of a “Double Reaction” Type-Based Fluorescent Probe for the Imaging of Superoxide Anion in Living Cells. *Spectrochim. Acta. A. Mol. Biomol. Spectrosc.* **2023**, *302*, 123080. https://doi.org/10.1016/j.saa.2023.123080.
(1119) Huang, J.; Lyu, Y.; Li, J.; Cheng, P.; Jiang, Y.; Pu, K. A Renal-Clearable Duplex Optical Reporter for Real-Time Imaging of Contrast-Induced Acute Kidney Injury. *Angew. Chem. Int. Ed.* **2019**, *58* (49), 17796–17804. https://doi.org/10.1002/anie.201910137.
(1120) Li, Z.; Li, S.; Lv, H.; Shen, J.; He, X.; Peng, B. BODIPY-Based Rapid Response Fluorescence Probe for Sensing and Bioimaging Endogenous Superoxide Anion in Living Cells. *Spectrochim. Acta. A. Mol. Biomol. Spectrosc.* **2022**, *269*, 120766. https://doi.org/10.1016/j.saa.2021.120766.
(1121) Zhang, J.; Li, C.; Zhang, R.; Zhang, F.; Liu, W.; Liu, X.; Lee, S. M.-Y.; Zhang, H. A Phosphinate-Based near-Infrared Fluorescence Probe for Imaging the Superoxide Radical Anion in Vitro and in Vivo. *Chem. Commun.* **2016**, *52*, 2679–2682. https://doi.org/10.1039/c5cc09976e.
(1122) Zhao, Y. Q.; Lin, H.; Li, L. H.; Yang, X. Q.; Hao, S. X.; Cen, J. W.; Wei, Y.; Qi, B.; Huang, H. Study on Synthesis and Characterization of a Fluorescence Probe and Its Application for Determination of Superoxide Anion Radical. *Adv. Mater. Res.* **2011**, *393–395*, 1483–1487. https://doi.org/10.4028/www.scientific.net/AMR.393-395.1483.
(1123) Delafresnaye, L.; Schmitt, C. W.; Barner, L.; Barner-Kowollik, C. A Photochemical Ligation System Enabling Solid-Phase Chemiluminescence Read-Out. *Chem. - Eur. J.* **2019**, *25* (54), 12538–12544. https://doi.org/10.1002/chem.201901858.
(1124) Rink, S.; Duerkop, A.; Jacobi von Wangelin, A.; Seidel, M.; Baeumner, A. Next Generation Luminol Derivative as Powerful Benchmark Probe for Chemiluminescence Assays. *Anal. Chim. Acta.* **2021**, *1188*. https://doi.org/10.1016/j.aca.2021.339161.
(1125) Onoda, M.; Uchiyama, S.; Endo, A.; Tokuyama, H.; Santa, T.; Imai, K. First Fluorescent Photoinduced Electron Transfer (PET) Reagent for Hydroperoxides. *Org. Lett.* **2003**, *5* (9), 1459–1461. https://doi.org/10.1021/ol0342150.
(1126) Inoue, N.; Suzuki, Y.; Yokoyama, K.; Karube, I. Novel Fluorescent Probe for Analysis of Hydroperoxides Based on Boron Dipyrromethane Fluorophore. *Biosci. Biotechnol. Biochem.* **2009**, *73*, 1215–1217. https://doi.org/10.1271/bbb.80899.
(1127) Du, L.; Li, M.; Zheng, S.; Wang, B. Rational Design of a Fluorescent Hydrogen Peroxide Probe Based on the Umbelliferone Fluorophore. *Tetrahedron Lett.* **2008**, *49* (19), 3045–3048. https://doi.org/10.1016/j.tetlet.2008.03.063.
(1128) Wei, Y.; Zhang, Y.; Liu, Z.; Guo, M. A Novel Profluorescent Probe for Detecting Oxidative Stress Induced by Metal and H_2O_2 in Living Cells. *Chem. Commun.* **2010**, *46*, 4472–4474. https://doi.org/10.1039/c000254b.
(1129) Du Ý, L.; Ni Ý, N.; Li, M.; Wang, B. A Fluorescent Hydrogen Peroxide Probe Based on a ‘Click’ Modified Coumarin Fluorophore. *Tetrahedron Lett.* **2010**, *51* (8), 1152–1154. https://doi.org/10.1016/j.tetlet.2009.12.049.

(1130)Sella, E.; Lubelski, A.; Klafter, J.; Shabat, D. Two-Component Dendritic Chain Reactions: Experiment and Theory. *J. Am. Chem. Soc.* **2010**, *132* (11), 3945–3952. https://doi.org/10.1021/ja910839n.
(1131)Miller, E. W.; Dickinson, B. C.; Chang, C. J. Aquaporin-3 Mediates Hydrogen Peroxide Uptake to Regulate Downstream Intracellular Signaling. *Proc. Natl. Acad. Sci.* **2010**, *107* (36), 15681–15686. https://doi.org/10.1073/pnas.1005776107.
(1132)Lu, C.-P.; Lin, C.-T.; Chang, C.-M.; Wu, S.-H.; Lo, L.-C. Nitrophenylboronic Acids as Highly Chemoselective Probes To Detect Hydrogen Peroxide in Foods and Agricultural Products. *J. Agric. Food Chem.* **2011**, *59* (21), 11403–11406. https://doi.org/10.1021/jf202874r.
(1133)Hyman, L. M.; Franz, K. J. A Cell-Permeable Fluorescent Prochelator Responds to Hydrogen Peroxide and Metal Ions by Decreasing Fluorescence. *Inorganica Chim. Acta* **2012**, *380*, 125–134. https://doi.org/10.1016/j.ica.2011.11.056.
(1134)Li, G.; Zhu, D.; Liu, Q.; Xue, L.; Jiang, H. Rapid Detection of Hydrogen Peroxide Based on Aggregation Induced Ratiometric Fluorescence Change. *Org. Lett.* **2013**, *15* (4), 924–927. https://doi.org/10.1021/ol4000845.
(1135)Sun, W.; Ma, Z.; Li, J.; Li, W.; Du, L.; Li, M. Bifunctional Fluorescent Probes for Hydrogen Peroxide and Diols Based on a 1,8-Naphthalimide Fluorophore. *Sci. China Chem.* **2013**, *56* (10), 1440–1445. https://doi.org/10.1007/s11426-013-4870-4.
(1136)Sun, X.; Xu, S.-Y.; Flower, S. E.; Fossey, J. S.; Qian, X.; James, T. D. “Integrated” and “Insulated” Boronate-Based Fluorescent Probes for the Detection of Hydrogen Peroxide. *Chem. Commun.* **2013**, *49*, 8311–8313. https://doi.org/10.1039/c3cc43265c.
(1137)Xu, M.; Han, J.-M.; Zhang, Y.; Yang, X.; Zang, L. A Selective Fluorescence Turn-on Sensor for Trace Vapor Detection of Hydrogen Peroxide. *Chem. Commun.* **2013**, *49* (100), 11779. https://doi.org/10.1039/c3cc47631f.
(1138)Daniel, K. B.; Agrawal, A.; Manchester, M.; Cohen, S. M. Readily Accessible Fluorescent Probes for Sensitive Biological Imaging of Hydrogen Peroxide. *ChemBioChem* **2013**, *14* (5), 593–598. https://doi.org/10.1002/cbic.201200724.
(1139)Hu, F.; Huang, Y.; Zhang, G.; Zhao, R.; Zhang, D. A Highly Selective Fluorescence Turn-on Detection of Hydrogen Peroxide and d-Glucose Based on the Aggregation/Deaggregation of a Modified Tetraphenylethylene. *Tetrahedron Lett.* **2014**, *55* (8), 1471–1474. https://doi.org/10.1016/j.tetlet.2014.01.056.
(1140)Xu, J.; Li, Q.; Yue, Y.; Guo, Y.; Shao, S. A Water-Soluble BODIPY Derivative as a Highly Selective “Turn-On” Fluorescent Sensor for H_2O_2 Sensing in Vivo. *Biosens. Bioelectron.* **2014**, *56*, 58–63. https://doi.org/10.1016/j.bios.2013.12.065.
(1141)Wu, W.; Li, J.; Chen, L.; Ma, Z.; Zhang, W.; Liu, Z.; Cheng, Y.; Du, L.; Li, M. Bioluminescent Probe for Hydrogen Peroxide Imaging in Vitro and in Vivo. *Anal. Chem.* **2014**, *86* (19), 9800–9806. https://doi.org/10.1021/ac502396g.
(1142)Shen, Y. M.; Kong, B.; Peng, X. F.; Feng, S. D.; Zhang, X. Y.; Zhang, C. X.; Jin, J. L.; Zhen, Q. Y. A New Turn-Off Fluorescence Chemosensor for Hydrogen Peroxide Based on Carbazole Derivative in Aqueous Solution. *Adv. Mater. Res.* **2014**, *1006–1007*, 821–825. https://doi.org/10.4028/www.scientific.net/AMR.1006-1007.821.
(1143)Franks, A. T.; Franz, K. J. A Prochelator with a Modular Masking Group Featuring Hydrogen Peroxide Activation with Concurrent Fluorescent Reporting. *Chem. Commun.* **2014**, *50*, 11317–11320. https://doi.org/10.1039/c4cc05076b.
(1144)Shen, Y. M.; Yang, S. M.; Xi, L. C.; Cao, W. Y.; Zhou, L. L.; Yang, Y.; Feng, S. D.; Peng, X. F.; Zhang, X. Y.; Zhang, C. X.; Jin, J. L.; Zhen, Q. Y. A Water-Solution Fluorescence Probe for H_2O_2 Based on Naphthalimide Derivative. *Adv. Mater. Res.* **2014**, *1061–1062*, 978–982. https://doi.org/10.4028/www.scientific.net/AMR.1061-1062.978.
(1145)Yi, L.; Wei, L.; Wang, R.; Zhang, C.; Zhang, J.; Tan, T.; Xi, Z. A Dual-Response Fluorescent Probe Reveals the H_2O_2 -Induced H_2S Biogenesis through a Cystathionine β-Synthase

Pathway. *Chem. - Eur. J.* **2015**, *21*, 15167–15172. https://doi.org/10.1002/chem.201502832.
(1146)Purdey, M. S.; Connaughton, H. S.; Whiting, S.; Schartner, E. P.; Monro, T. M.; Thompson, J. G.; Aitken, R. J.; Abell, A. D. Boronate Probes for the Detection of Hydrogen Peroxide Release from Human Spermatozoa. *Free Radic. Biol. Med.* **2015**, *81*, 69–76. https://doi.org/10.1016/j.freeradbiomed.2015.01.015.
(1147)Cai, Z.-J.; Kuang, Y.-Q.; Pan, D.; Liu, W.; Jiang, J.-H. Synthesis and Characterization of a Novel ELF-97-Based Fluorescent Probe for Hydrogen Peroxide Detection. *Chin. J. Anal. Chem.* **2015**, *43* (11), 1671–1675. https://doi.org/10.1016/S1872-2040(15)60875-1.
(1148)Zhang, W.; Liu, W.; Li, P.; Huang, F.; Wang, H.; Tang, B. Rapid-Response Fluorescent Probe for Hydrogen Peroxide in Living Cells Based on Increased Polarity of C-B Bonds. *Anal. Chem.* **2015**, *87* (19), 9825–9828. https://doi.org/10.1021/acs.analchem.5b02194.
(1149)Fu, Y.; Yao, J.; Xu, W.; Fan, T.; Jiao, Z.; He, Q.; Zhu, D.; Cao, H.; Cheng, J. Schiff Base Substituent-Triggered Efficient Deboration Reaction and Its Application in Highly Sensitive Hydrogen Peroxide Vapor Detection. *Anal. Chem.* **2016**, *88* (10), 5507–5512. https://doi.org/10.1021/acs.analchem.6b01057.
(1150)Ang, C. Y.; Tan, S. Y.; Wu, S.; Qu, Q.; Wong, M. F. E.; Luo, Z.; Li, P.-Z.; Tamil Selvan, S.; Zhao, Y. A Dual Responsive “Turn-on” Fluorophore for Orthogonal Selective Sensing of Biological Thiols and Hydrogen Peroxide. *J. Mater. Chem. C* **2016**, *4* (14), 2761–2774. https://doi.org/10.1039/C5TC01465D.
(1151)Song, Z.; Kwok, R. T. K.; Ding, D.; Nie, H.; Lam, J. W. Y.; Liu, B.; Tang, B. Z. An AIE-Active Fluorescence Turn-on Bioprobe Mediated by Hydrogen-Bonding Interaction for Highly Sensitive Detection of Hydrogen Peroxide and Glucose. *Chem. Commun.* **2016**, *52* (65), 10076–10079. https://doi.org/10.1039/C6CC05049B.
(1152)Han, Z.; Liang, X.; Ren, X.; Shang, L.; Yin, Z. A 3,7-Dihydroxyphenoxazine-Based Fluorescent Probe for Selective Detection of Intracellular Hydrogen Peroxide. *Chem. - Asian J.* **2016**, *11*, 818–822. https://doi.org/10.1002/asia.201501304.
(1153)Chen, Y.; Shi, X.; Lu, Z.; Wang, X.; Wang, Z. A Fluorescent Probe for Hydrogen Peroxide in Vivo Based on the Modulation of Intramolecular Charge Transfer. *Anal. Chem.* **2017**, *89*, 5278–5284. https://doi.org/10.1021/acs.analchem.6b04810.
(1154)Wang, X.; Huang, Y.; Lv, W.; Li, C.; Zeng, W.; Zhang, Y.; Feng, X. A Novel Fluorescent Probe Based on ESIPT and AIE Processes for the Detection of Hydrogen Peroxide and Glucose and Its Application in Nasopharyngeal Carcinoma Imaging. *Anal. Methods* **2017**, *9* (12), 1872–1875. https://doi.org/10.1039/C7AY00167C.
(1155)Ren, M.; Deng, B.; Zhou, K.; Kong, X.; Wang, J.-Y.; Lin, W. Single Fluorescent Probe for Dual-Imaging Viscosity and H_2O_2 in Mitochondria with Different Fluorescence Signals in Living Cells. *Anal. Chem.* **2017**, *89* (1), 552–555. https://doi.org/10.1021/acs.analchem.6b04385.
(1156)Zhang, Y.; Jiao, Z.; Xu, W.; Fu, Y.; Zhu, D.; Xu, J.; He, Q.; Cao, H.; Cheng, J. Design, Synthesis and Properties of a Reactive Chromophoric/Fluorometric Probe for Hydrogen Peroxide Detection. *New J. Chem.* **2017**, *41* (10), 3790–3797. https://doi.org/10.1039/C7NJ00851A.
(1157)Li, X.; Li, J.; Tao, Y.; Peng, Z.; Lu, P.; Wang, Y. Oxazole-Based High Resolution Ratiometric Fluorescent Probes for Hydrogen Peroxide Detection. *Sens. Actuators B Chem.* **2017**, *247*, 609–616. https://doi.org/10.1016/j.snb.2017.03.060.
(1158)Huang, J.; Li, T.; Liu, R.; Zhang, R.; Wang, Q.; Li, N.; Gu, Y.; Wang, P. Rational Designed Benzochalcone-Based Fluorescent Probe for Molecular Imaging of Hydrogen Peroxide in Live Cells and Tissues. *Sens. Actuators B Chem.* **2017**, *248*, 257–264. https://doi.org/10.1016/j.snb.2017.04.001.
(1159)Nie, J.; Liu, Y.; Niu, J.; Ni, Z.; Lin, W. A New Pyrene-Based Fluorescent Probe with Large Stokes Shift for Detecting Hydrogen Peroxide in Aqueous Solution and Living Cells. *J.*

Photochem. Photobiol. Chem. **2017**, *348*, 1–7. https://doi.org/10.1016/j.jphotochem.2017.08.008.
(1160)Yin, R.; Fang, Y.; Zhou, X.; Stains, C. I. Synthesis and Application of a Ratiometric Probe for Hydrogen Peroxide. *Methods Enzymol.* **2020**, *639*, 23–36. https://doi.org/10.1016/bs.mie.2020.04.007.
(1161)Xu, F.; Tang, W.; Kang, S.; Song, J.; Duan, X. A Highly Sensitive and Photo-Stable Fluorescent Probe for Endogenous Intracellular H_2O_2 Imaging in Live Cancer Cells. *Dyes Pigments* **2018**, *153*, 61–66. https://doi.org/10.1016/j.dyepig.2018.02.015.
(1162)Liu, X.; Tian, H.; Yang, L.; Su, Y.; Guo, M.; Song, X. A Sensitive and Selective Fluorescent Probe for the Detection of Hydrogen Peroxide with a Red Emission and a Large Stokes Shift. *Sens. Actuators B Chem.* **2018**, *255*, 1160–1165. https://doi.org/10.1016/j.snb.2017.05.151.
(1163)Zhang, N.; Dong, B.; Kong, X.; Wang, C.; Song, W.; Lin, W. Development of a Xanthene-Based Red-Emissive Fluorescent Probe for Visualizing H_2O_2 in Living Cells, Tissues and Animals. *J. Fluoresc.* **2018**, *28* (2), 681–687. https://doi.org/10.1007/s10895-018-2231-6.
(1164)Ni, Y.; Liu, H.; Dai, D.; Mu, X.; Xu, J.; Shao, S. Chromogenic, Fluorescent, and Redox Sensors for Multichannel Imaging and Detection of Hydrogen Peroxide in Living Cell Systems. *Anal. Chem.* **2018**, *90* (17), 10152–10158. https://doi.org/10.1021/acs.analchem.7b04435.
(1165)Han, J.; Chu, C.; Cao, G.; Mao, W.; Wang, S.; Zhao, Z.; Gao, M.; Ye, H.; Xu, X. A Simple Boronic Acid-Based Fluorescent Probe for Selective Detection of Hydrogen Peroxide in Solutions and Living Cells. *Bioorganic Chem.* **2018**, *81*, 362–366. https://doi.org/10.1016/j.bioorg.2018.08.036.
(1166)Huang, Z.; Yao, Q.; Chen, J.; Gao, Y. Redox Supramolecular Self-Assemblies Nonlinearly Enhance Fluorescence to Identify Cancer Cells. *Chem. Commun.* **2018**, *54* (42), 5385–5388. https://doi.org/10.1039/c8cc02648c.
(1167)Liu, X.; He, L.; Yang, L.; Geng, Y.; Yang, L.; Song, X. Iminocoumarin-Based Fluorescence Probe for Intracellular H_2O_2 Detection with a Red Emission and a Large Stokes Shift. *Sens. Actuators B Chem.* **2018**, *259*, 803–808. https://doi.org/10.1016/j.snb.2017.12.140.
(1168)Yik-Sham Chung, C.; Timblin, G. A.; Saijo, K.; Chang, C. J. Versatile Histochemical Approach to Detection of Hydrogen Peroxide in Cells and Tissues Based on Puromycin Staining. *J. Am. Chem. Soc.* **2018**, *140* (19), 6109–6121. https://doi.org/10.1021/jacs.8b02279.
(1169)Hoshi, K.; Messina, M. S.; Ohata, J.; Chung, C. Y.-S.; Chang, C. J. A Puromycin-Dependent Activity-Based Sensing Probe for Histochemical Staining of Hydrogen Peroxide in Cells and Animal Tissues. *Nat. Protoc.* **2022**, *17* (7), 1691–1710. https://doi.org/10.1038/s41596-022-00694-7.
(1170)Liu, J.; Liang, J.; Wu, C.; Zhao, Y. A Doubly-Quenched Fluorescent Probe for Low-Background Detection of Mitochondrial H_2O_2. *Anal. Chem.* **2019**, *91* (10), 6902–6909. https://doi.org/10.1021/acs.analchem.9b01294.
(1171)Zhou, Z.; Li, Y.; Su, W.; Gu, B.; Xu, H.; Wu, C.; Yin, P.; Li, H.; Zhang, Y. A Dual-Signal Colorimetric and near-Infrared Fluorescence Probe for the Detection of Exogenous and Endogenous Hydrogen Peroxide in Living Cells. *Sens. Actuators B Chem.* **2019**, *280*, 120–128. https://doi.org/10.1016/j.snb.2018.09.126.
(1172)Qiu, X.; Xin, C.; Qin, W.; Li, Z.; Zhang, D.; Zhang, G.; Peng, B.; Han, X.; Yu, C.; Li, L.; Huang, W. A Novel Pyrimidine Based Deep-Red Fluorogenic Probe for Detecting Hydrogen Peroxide in Parkinson's Disease Models. *TALANTA* **2019**, *199*, 628–633. https://doi.org/10.1016/j.talanta.2019.03.017.
(1173)Li, W.; Wang, L.; Tang, H.; Cao, D. An Interface-Targeting and H_2O_2 -Activatable Probe Liberating AIEgen: Enabling on-Site Imaging and Dynamic Movement Tracking of Lipid Droplets. *Chem. Commun.* **2019**, *55* (31), 4491–4494. https://doi.org/10.1039/c9cc01404g.

(1174)Velusamy, N.; Thirumalaivasan, N.; Bobba, K.; Podder, A.; Wu, S.; Bhuniya, S. FRET-Based Dual Channel Fluorescent Probe for Detecting Endogenous/Exogenous H_2O_2/H_2S Formation through Multicolor Images. *J. Photochem. Photobiol. B-Biol.* **2019**, *191*, 99–106. https://doi.org/10.1016/j.jphotobiol.2018.12.016.
(1175)Wu, Y.; Li, Z.; Shen, Y. A Novel ESIPT Phthalimide-Based Fluorescent Probe for Quantitative Detection of H_2O_2. *ACS Omega* **2019**, *4* (14), 16242–16246. https://doi.org/10.1021/acsomega.9b02594.
(1176)Wang, W.-X.; Jiang, W.-L.; Liu, Y.; Li, Y.; Zhang, J.; Li, C.-Y. Near-Infrared Fluorescence Probe with a Large Stokes Shift for Visualizing Hydrogen Peroxide in Ulcerative Colitis Mice. *Sens. Actuators B Chem.* **2020**, *320*, 128296. https://doi.org/10.1016/j.snb.2020.128296.
(1177)Zhang, G.; Li, Z.; Chen, F.; Zhang, D.; Ji, W.; Yang, Z.; Wu, Q.; Zhang, C.; Li, L.; Huang, W. A Novel Fluorogenic Probe for Visualizing the Hydrogen Peroxide in Parkinson's Disease Models. *J. Innov. Opt. Health Sci.* **2020**, *13* (03), 2050013. https://doi.org/10.1142/S1793545820500133.
(1178)Williams, G. T.; Sedgwick, A. C.; Sen, S.; Gwynne, L.; Gardiner, J. E.; Brewster, J. T. I.; Hiscock, J. R.; James, T. D.; Jenkins, A. T. A.; Sessler, J. L. Boronate Ester Cross-Linked PVA Hydrogels for the Capture and H_2O_2 -Mediated Release of Active Fluorophores. *Chem. Commun.* **2020**, *56* (41), 5516–5519. https://doi.org/10.1039/d0cc01904f.
(1179)Hou, P.; Chen, S.; Liang, G.; Li, H.; Zhang, H. Design of a Facile Fluorescent Probe with a Large Stokes Shift for Hydrogen Peroxide Imaging in Vitro and in Vivo. *Spectrochim. Acta. A. Mol. Biomol. Spectrosc.* **2020**, *236*. https://doi.org/10.1016/j.saa.2020.118338.
(1180)Hankins, R. A.; Suarez, S. I.; Kalk, M. A.; Green, N. M.; Harty, M. N.; Lukesh, J. C. An Innovative Hydrogen Peroxide-Sensing Scaffold and Insight Towards Its Potential as an ROS-Activated Persulfide Donor. *Angew. Chem. Int. Ed.* **2020**, *59* (49), 22238–22245. https://doi.org/10.1002/anie.202010530.
(1181)Cheng, J.; Ren, Y.; Huang, Y.; Li, X.; Huang, M.; Han, F.; Liang, X.; Li, X. Sequentially Activated Probe Design Strategy for Analyzing Metabolite Crosstalk in a Biochemical Cascade. *Anal. Chem.* **2020**, *92* (1), 1409–1415. https://doi.org/10.1021/acs.analchem.9b04576.
(1182)Li, Z. Imaging of Hydrogen Peroxide (H_2O_2) during the Ferroptosis Process in Living Cancer Cells with a Practical Fluorescence Probe. *TALANTA* **2020**, *212*. https://doi.org/10.1016/j.talanta.2020.120804.
(1183)Du, Y.; Wang, B.; Jin, D.; Li, M.; Li, Y.; Yan, X.; Zhou, X.; Chen, L. Dual-Site Fluorescent Probe for Multi-Response Detection of ClO- and H_2O_2 and Bio-Imaging. *Anal. Chim. Acta.* **2020**, *1103*, 174–182. https://doi.org/10.1016/j.aca.2019.12.059.
(1184)Zhou, R.; Niu, L.; Hu, Y.; Qi, Q.; Huang, W.; Yang, L. A Novel Dual-Function Fluorescent Probe for the Rapid Detection of Bisulfite and Hydrogen Peroxide in Aqueous Solution and Living Cells. *Spectrochim. Acta. A. Mol. Biomol. Spectrosc.* **2021**, *248*, 119226. https://doi.org/10.1016/j.saa.2020.119226.
(1185)Sufian, A.; Bhattacherjee, D.; Mishra, T.; Bhabak, K. P. Peroxide-Responsive Boronate Ester-Coupled Turn-on Fluorogenic Probes: Direct Linkers Supersede Self-Immolative Linkers for Sensing Peroxides. *Dyes Pigments* **2021**, *191*, 109363. https://doi.org/10.1016/j.dyepig.2021.109363.
(1186)Xu, L.; Zhang, Y.; Zhao, L.; Han, H.; Zhang, S.; Huang, Y.; Wang, X.; Song, D.; Ma, P.; Ren, P.; Sun, Y. A Neoteric Dual-Signal Colorimetric Fluorescent Probe for Detecting Endogenous/Exogenous Hydrogen Peroxide in Cells and Monitoring Drug-Induced Hepatotoxicity. *Talanta* **2021**, *233*. https://doi.org/10.1016/j.talanta.2021.122578.
(1187)Wang, Y.-B.; Luo, H.-Z.; Wang, C.-Y.; Guo, Z.-Q.; Zhu, W.-H. A Turn-on Fluorescent Probe Based on π-Extended Coumarin for Imaging Endogenous Hydrogen Peroxide in RAW

264.7 Cells. *J. Photochem. Photobiol. Chem.* **2021**, *414*, 113270. https://doi.org/10.1016/j.jphotochem.2021.113270.
(1188)Iwashita, H.; Castillo, E.; Messina, M. S.; Swanson, R. A.; Chang, C. J. A Tandem Activity-Based Sensing and Labeling Strategy Enables Imaging of Transcellular Hydrogen Peroxide Signaling. *Proc. Natl. Acad. Sci. U. S. A.* **2021**, *118* (9), e2018513118. https://doi.org/10.1073/pnas.2018513118.
(1189)Ma, K.; Yue, Y.; Zhao, L.; Chao, J.; Yin, C. A Sequentially Activated Bioluminescent Probe for Observation of Cellular H_2O_2 Production Induced by Cysteine. *Chem. Commun.* **2021**, *57* (78), 10015–10018. https://doi.org/10.1039/d1cc04015d.
(1190)Zhang, H.; Tian, D.; Zheng, Y.; Dai, F.; Zhou, B. Designing an ESIPT-Based Fluorescent Probe for Imaging of Hydrogen Peroxide during the Ferroptosis Process. *Spectrochim. Acta. A. Mol. Biomol. Spectrosc.* **2021**, *248*. https://doi.org/10.1016/j.saa.2020.119264.
(1191)Zuo, Y.; Jiao, Y.; Ma, C.; Duan, C. A Novel Fluorescent Probe for Hydrogen Peroxide and Its Application in Bio-Imaging. *Molecules* **2021**, *26* (11). https://doi.org/10.3390/molecules26113352.
(1192)Yao, W.; Cao, Y.; She, M.; Yan, Y.; Li, J.; Leng, X.; Liu, P.; Zhang, S.; Li, J. Imaging and Monitoring the Hydrogen Peroxide Level in Heart Failure by a Fluorescent Probe with a Large Stokes Shift. *ACS Sens.* **2021**, *6* (1), 54–62. https://doi.org/10.1021/acssensors.0c01707.
(1193)Lu, J.; Ji, L.; Yu, Y. Rational Design of a Selective and Sensitive “Turn-on” Fluorescent Probe for Monitoring and Imaging Hydrogen Peroxide in Living Cells. *RSC Adv.* **2021**, *11* (56), 35093–35098. https://doi.org/10.1039/D1RA06620J.
(1194)Gatin-Fraudet, B.; Ottenwelter, R.; Le Saux, T.; Norsikian, S.; Pucher, M.; Lombès, T.; Baron, A.; Durand, P.; Doisneau, G.; Bourdreux, Y.; Iorga, B. I.; Erard, M.; Jullien, L.; Guianvarc’h, D.; Urban, D.; Vauzeilles, B. Evaluation of Borinic Acids as New, Fast Hydrogen Peroxide–Responsive Triggers. *Proc. Natl. Acad. Sci.* **2021**, *118* (50), e2107503118. https://doi.org/10.1073/pnas.2107503118.
(1195)Li, X.; Gao, N.; Liu, C.; Yu, M.; Rong, X.; Zhang, Y.; Su, M.; Wang, X.; Zhu, H.; Wang, K.; Liu, Y.; Sheng, W.; Zhu, B. A Melatonin-Based Targetable Fluorescent Probe Activated by Hydrogen Peroxide for Tumor Cells Screening. *Sens. Actuators B Chem.* **2022**, *353*, 131051. https://doi.org/10.1016/j.snb.2021.131051.
(1196)Hua, Y.; Shang, Y.; Gao, M.; Li, J.; Kang, Y. A “Turn-on” Fluorescent Probe with High Selectivity and Large Stokes Shift for the Detection of Hydrogen Peroxide and Its Bioimaging Applications. *Spectrochim. ACTA PART -Mol. Biomol. Spectrosc.* **2022**, *265*. https://doi.org/10.1016/j.saa.2021.120320.
(1197)Wang, Y.; Li, S.; Zhu, X.; Shi, X.; Liu, X.; Zhang, H. A Novel H_2O_2 Activated NIR Fluorescent Probe for Accurately Visualizing H_2S Fluctuation during Oxidative Stress. *Anal. Chim. ACTA* **2022**, *1202*. https://doi.org/10.1016/j.aca.2022.339670.
(1198)Chen, S.; Fan, W.; Sun, Z.; Zheng, E.; Wang, L.; Wu, Y.; Hou, S.; Ma, X. Acetyl Group Assisted Rapid Intramolecular Recognition of Hydrogen Peroxide: A Novel Promising Approach for Efficient Hydrogen Peroxide Probe. *Spectrochim. Acta. A. Mol. Biomol. Spectrosc.* **2022**, *276*, 121162. https://doi.org/10.1016/j.saa.2022.121162.
(1199)Tang, J.; Li, F.; Liu, C.; Shu, J.; Yue, J.; Xu, B.; Liu, X.; Zhang, K.; Jiang, W. Attractive Benzothiazole-Based Fluorescence Probe for the Highly Efficient Detection of Hydrogen Peroxide. *Anal. Chim. Acta.* **2022**, *1214*. https://doi.org/10.1016/j.aca.2022.339939.
(1200) Ma, T.; Zhang, Y.; Fu, K.; Li, Z.; Yuan, C.; Ma, W. Design, Synthesis and Properties of Hydrogen Peroxide Fluorescent Probe Based on Benzothiazole. *Bioorganic Chem.* **2022**, *123*. https://doi.org/10.1016/j.bioorg.2022.105798.
(1201) Zeng, G.; Liang, Z.; Jiang, X.; Quan, T.; Chen, T. An ESIPT-Dependent AIE Fluorophore Based on HBT Derivative: Substituent Positional Impact on Aggregated Luminescence and

Its Application for Hydrogen Peroxide Detection. *Chem. - Eur. J.* **2022**, *28* (5), e202103241. https://doi.org/10.1002/chem.202103241.
(1202) Ouyang, J.; Sun, L.; Zeng, F.; Wu, S. Rational Design of Stable Heptamethine Cyanines and Development of a Biomarker-Activatable Probe for Detecting Acute Lung/Kidney Injuries via NIR-II Fluorescence Imaging. *Analyst* **2022**, *147* (3), 410–416. https://doi.org/10.1039/d1an02183d.
(1203) Yang, Y.; Qiu, W.; Xu, Z.; Sun, Z.; Qing, M.; Li, N.; Luo, H. Rational Design of a Fluorescent Probe for Specific Sensing of Hydrogen Peroxide/Glucose and Intracellular Imaging Applications. *Spectrochim. Acta. A. Mol. Biomol. Spectrosc.* **2022**, *277*. https://doi.org/10.1016/j.saa.2022.121254.
(1204) Zang, L.; Huang, H.; Li, X.; Ju, Y.; Feng, B.; Lu, J. PEGylated Near-Infrared Fluorescence Probe for Mitochondria-Targetable Hydrogen Peroxide Detection. *Talanta* **2022**, *243*. https://doi.org/10.1016/j.talanta.2022.123370.
(1205) Zhang, Y.; Yang, M.; Wang, Y.; Huang, W.; Ji, M. Lighting up Hydrogen Peroxide in Living Cells by a Novel Quinoxalinamine Based Fluorescent Probe. *Spectrochim. Acta. A. Mol. Biomol. Spectrosc.* **2022**, *267* (Part_1), 120528. https://doi.org/10.1016/j.saa.2021.120528.
(1206) Li, L.; Zheng, M.; Yan, X.; Huang, H.; Cao, S.; Liu, K.; Liu, J.-B. Quantitative Detection of H_2O_2 with a Composite Fluorescent Probe of 8-Quinoline Boronic Acid-Al(III). *J. Photochem. Photobiol. Chem.* **2022**, *432*, 114069. https://doi.org/10.1016/j.jphotochem.2022.114069.
(1207) Li, Y.; Ren, L.; Gao, T.; Chen, T.; Han, J.; Wang, Y. A Coumarin-Based Fluorescent Probe for Sensitive Monitoring H_2O_2 in Water and Living Cells. *Tetrahedron Lett.* **2023**, *114*, 154291. https://doi.org/10.1016/j.tetlet.2022.154291.
(1208) Wang, K.; Yao, T.; Xue, J.; Guo, Y.; Xu, X. A Novel Fluorescent Probe for the Detection of Hydrogen Peroxide. *Biosensors* **2023**, *13* (6), 658. https://doi.org/10.3390/bios13060658.
(1209) Xia, H.-C.; Li, H.; Zhang, W.-L.; Kong, Y.-Y. Synthesis and Application of Dual-Channel Fluorescent Probes for Selective Recognition of SO_2/ H_2O_2. *Sens. Actuators B Chem.* **2023**, *378*, 133146. https://doi.org/10.1016/j.snb.2022.133146.
(1210) Tang, J.; Zhang, K.; Ni, T.; Xu, B.; Hou, B.; Liu, X.; Jiang, W. Multiple Fluorescence and Hydrogen Peroxide-Responsive Properties of Novel Triphenylamine–Benzothiazole Derivatives. *Anal. Methods* **2023**, *15* (32), 4021–4031. https://doi.org/10.1039/D3AY01038D.
(1211)Wang, Y. M.; Li, J.; Chen, J. H.; Liu, B.; Zeng, Y.; Lim, J.-Y.; Liu, Y. T.; Zhang, J. F.; Wu, X. H.; Ren, W. X. A Dual-Responsive Fluorescent Probe for Detection of H_2O_2 and HClO in Living Cells and Caenorhabditis Elegans. *Dyes Pigments* **2023**, *215*, 111218. https://doi.org/10.1016/j.dyepig.2023.111218.
(1212) Wang, M.; Zhang, F.; Wang, C.-Q.; Yin, N.; Wang, Y.; Qin, G.; Xu, Q.; Gong, J.; Liu, H.; Duan, X. Target-Binding Accelerated Response for Sensitive Detection of Basal H_2O_2 in Tumor Cells and Tissues via a Dual-Functional Fluorescence Probe. *Anal. Chem.* **2022**, *94* (15), 5962–5969. https://doi.org/10.1021/acs.analchem.2c00400.
(1213) He, Y.; Miao, L.; Yu, L.; Chen, Q.; Qiao, Y.; Zhang, J.-F.; Zhou, Y. A Near-Infrared Fluorescent Probe for Detection of Exogenous and Endogenous Hydrogen Peroxide in Vivo. *Dyes Pigments* **2019**, *168*, 160–165. https://doi.org/10.1016/j.dyepig.2019.04.055.
(1214) Singh, A. P.; Lee, K. M.; Murale, D. P.; Jun, T.; Liew, H.; Suh, Y.-H.; Churchill, D. G. Novel Sulphur-Rich BODIPY Systems That Enable Stepwise Fluorescent O-Atom Turn-on and H_2O_2 Neuronal System Probing. *Chem. Commun.* **2012**, *48*, 7298–7300. https://doi.org/10.1039/c2cc33076h.
(1215) Xu, C.; Qian, Y. A Selenamorpholine-Based Redox-Responsive Fluorescent Probe for Targeting Lysosome and Visualizing Exogenous/Endogenous Hydrogen Peroxide in Living

Cells and Zebrafish. *J. Mater. Chem. B* **2019**, *7* (16), 2714–2721. https://doi.org/10.1039/c8tb03010c.
(1216) Ma, T.; Li, Y.; Yuan, C.; Li, Z.; Ma, W.; Ma, L. Design, Synthesis and Performance Test of a Hydrogen Peroxide Fluorescent Probe Based on Selenomorpholine and Pyrimidine. *Int. J. Environ. Anal. Chem.* **2022**, 1–13. https://doi.org/10.1080/03067319.2022.2047183.
(1217) Ma, T.; Fu, K.; Li, Z.; Yuan, C.; Ma, W. A Novel Hydrogen Peroxide Fluorescent Probe for Bioimaging Detection and Enables Multiple Redox Cycles. *Spectrochim. Acta. A. Mol. Biomol. Spectrosc.* **2022**, *276*, 121218. https://doi.org/10.1016/j.saa.2022.121218.
(1218) Zhuang, Z.; Yang, Q.; Zhang, Z.; Zhang, Q.; Zheng, G.; Zhan, F. A Highly Selective Fluorescent Probe for Hydrogen Peroxide and Its Applications in Living Cells. *J. Photochem. Photobiol. Chem.* **2017**, *344*, 8–14. https://doi.org/10.1016/j.jphotochem.2017.04.009.
(1219) Xiong, J.; Xia, L.; Li, L.; Cui, M.; Gu, Y.; Wang, P. An Acetate-Based NIR Fluorescent Probe for Selectively Imaging of Hydrogen Peroxide in Living Cells and in Vivo. *Sens. Actuators B Chem.* **2019**, *288*, 127–132. https://doi.org/10.1016/j.snb.2019.02.100.
(1220) Han, H.; He, X.; Wu, M.; Huang, Y.; Zhao, L.; Xu, L.; Ma, P.; Sun, Y.; Song, D.; Wang, X. A Novel Colorimetric and Near-Infrared Fluorescence Probe for Detecting and Imaging Exogenous and Endogenous Hydrogen Peroxide in Living Cells. *Talanta* **2020**, *217*. https://doi.org/10.1016/j.talanta.2020.121000.
(1221) Li, Y.; Zhou, Y.; Lei, J.; Qin, X.; Xu, Q.; Lu, Q.; Wu, C.; Yang, Z.; He, B. An Acetyl-Hydrolyzing Nir Fluorescent Probe for Selective Detection of Hydrogen Peroxide in Cells. *SSRN Electron. J.* **2022**. https://doi.org/10.2139/ssrn.4093449.
(1222) Lv, L.; Luo, W.; Diao, Q. A Mitochondria-Targeted Rhodol Fluorescent Probe for Imaging of Hydrogen Peroxide in Living Cells. *Anal. Methods* **2022**, *14* (21), 2117–2122. https://doi.org/10.1039/D2AY00522K.
(1223) Peng, T.; Ye, S.; Liu, R.; Qu, J. Colorimetric and Fluorescent Dual-Signals Probes for Naked-Eye Detection of Hydrogen Peroxide and Applications in Milk Samples and in Vivo. *Spectrochim. Acta. A. Mol. Biomol. Spectrosc.* **2023**, *297*, 122757. https://doi.org/10.1016/j.saa.2023.122757.
(1224) Ma, Q.; Ma, H.; Wang, Z.; Su, M.; Xiao, H.; Liang, S. Synthesis of a Novel Chemiluminescent Reagent for the Determination of Hydrogen Peroxide in Snow Waters. *Talanta* **2001**, *53* (5), 983–990. https://doi.org/10.1016/s0039-9140(00)00598-1.
(1225) Sekiya, M.; Umezawa, K.; Sato, A.; Citterio, D.; Suzuki, K. A Novel Luciferin-Based Bright Chemiluminescent Probe for the Detection of Reactive Oxygen Species. *Chem. Commun.* **2009**, No. 21, 3047. https://doi.org/10.1039/b903751a.
(1226) Zamojc, K.; Zdrowowicz, M.; Rudnicki-Velasquez, P. B.; Krzyminski, K.; Zaborowski, B.; Niedzialkowski, P.; Jacewicz, D.; Chmurzynski, L. The Development of 1,3-Diphenylisobenzofuran as a Highly Selective Probe for the Detection and Quantitative Determination of Hydrogen Peroxide. *Free Radic. Res.* **2017**, *51* (1), 38–46. https://doi.org/10.1080/10715762.2016.1262541.
(1227) Li, N.; Huang, J.; Wang, Q.; Gu, Y.; Wang, P. A Reaction Based One- and Two-Photon Fluorescent Probe for Selective Imaging H_2O_2 in Living Cells and Tissues. *Sens. Actuators B Chem.* **2018**, *254*, 411–416. https://doi.org/10.1016/j.snb.2017.07.133.
(1228) Han, X.; Tian, C.; Yuan, M.-S.; Li, Z.; Wang, W.; Li, T.; Chen, S.-W.; Wang, J. Colorimetric Hydrazine Detection and Fluorescent Hydrogen Peroxide Imaging by Using a Multifunctional Chemical Probe. *Anal. Chim. Acta* **2019**, *1052*, 137–144. https://doi.org/10.1016/j.aca.2018.11.039.
(1229) Mao, L.; Gao, H.-Y.; Huang, C.-H.; Qin, L.; Huang, R.; Shao, B.; Shao, J.; Zhu, B.-Z. Unprecedented Strong Intrinsic Chemiluminescence Generation from Degradation of Halogenated Hydroxy-Quinoid Pollutants by Co(II)-Mediated Advanced Oxidation

Processes: The Critical Role of Site-Specific Production of Hydroxyl Radicals. *Chem. Eng. J.* **2020**, *394*, 125023. https://doi.org/10.1016/j.cej.2020.125023.
(1230) Wei, Y.; Wang, X.; Shi, W.; Chen, R.; Zheng, L.; Wang, Z.; Chen, K.; Gao, L. A Novel Methylenemalononitrile-BODIPY-Based Fluorescent Probe for Highly Selective Detection of Hydrogen Peroxide in Living Cells. *Eur. J. Med. Chem.* **2021**, *226*. https://doi.org/10.1016/j.ejmech.2021.113828.
(1231) Li, T.; Cao, K.; Yang, X.; Liu, Y.; Wang, X.; Wu, F.; Chen, G.; Wang, Q. An Oral Ratiometric NIR-II Fluorescent Probe for Reliable Monitoring of Gastrointestinal Diseases in Vivo. *Biomaterials* **2023**, *293*. https://doi.org/10.1016/j.biomaterials.2022.121956.
(1232) Liao, Y.-X.; Wang, M.-D.; Li, K.; Yang, Z.-X.; Hou, J.-T.; Wu, M.-Y.; Liu, Y.-H.; Yu, X.-Q. A Highly Sensitive and Selective "Turn-on" Fluorescent Probe for Hypochlorous Acid Monitoring. *RSC Adv.* **2015**, *5* (24), 18275–18278. https://doi.org/10.1039/C4RA14579H.
(1233) Hu, J. J.; Wong, N.-K.; Lu, M.-Y.; Chen, X.; Ye, S.; Zhao, A. Q.; Gao, P.; Kao, R. Y.-T.; Shen, J.; Yang, D. HKOCl-3: A Fluorescent Hypochlorous Acid Probe for Live-Cell and in Vivo Imaging and Quantitative Application in Flow Cytometry and a 96-Well Microplate Assay. *Chem. Sci.* **2016**, *7* (3), 2094–2099. https://doi.org/10.1039/C5SC03855C.
(1234) Zhang, C.; Nie, Q.; Ismail, I.; Xi, Z.; Yi, L. A Highly Sensitive and Selective Fluorescent Probe for Fast Sensing of Endogenous HClO in Living Cells. *Chem. Commun.* **2018**, *54* (31), 3835–3838. https://doi.org/10.1039/C8CC01917G.
(1235) Jia, P.; Zhuang, Z.; Liu, C.; Wang, Z.; Duan, Q.; Li, Z.; Zhu, H.; Du, B.; Zhu, B.; Sheng, W.; Kang, B. A Highly Specific and Ultrasensitive P-Aminophenylether-Based Fluorescent Probe for Imaging Native HOCl in Live Cells and Zebrafish. *Anal. Chim. Acta* **2019**, *1052*, 131–136. https://doi.org/10.1016/j.aca.2018.11.031.
(1236) Song, X.; Hu, W.; Wang, D.; Mao, Z.; Liu, Z. A Highly Specific and Ultrasensitive Probe for the Imaging of Inflammation-Induced Endogenous Hypochlorous Acid. *Analyst* **2019**, *144* (11), 3546–3551. https://doi.org/10.1039/C9AN00390H.
(1237) Shi, W.; Song, B.; Liu, Z.; Zhang, W.; Tan, M.; Song, F.; Yuan, J. Smart Bimodal Imaging of Hypochlorous Acid In Vivo Using a Heterobimetallic Ruthenium(II)–Gadolinium(III) Complex Probe. *Anal. Chem.* **2020**, *92* (16), 11145–11154. https://doi.org/10.1021/acs.analchem.0c01198.
(1238) Zhang, M.; Ma, Y.-H.; Li, P.; Jia, Y.; Han, K.-L. Detection of Atherosclerosis-Related Hypochlorous Acid Produced in Foam Cells with a Localized Endoplasmic Reticulum Probe. *Chem. Commun.* **2020**, *56* (17), 2610–2613. https://doi.org/10.1039/D0CC00090F.
(1239) Wang, K.; Jia, P.; Li, X.; Zhang, X.; Liu, C.; Yu, Y.; Zhu, H.; Li, Z.; Sheng, W.; Zhu, B. A Simple P-Methylaminophenylether-Based Fluorescent Probe for Detecting Native Hypochlorous Acid in Live Cells and Zebrafish. *Dyes Pigments* **2020**, *177*, 108310. https://doi.org/10.1016/j.dyepig.2020.108310.
(1240) Wang, K.; Liu, Y.; Liu, C.; Zhu, H.; Li, X.; Zhang, F.; Gao, N.; Pang, X.; Sheng, W.; Zhu, B. A Simple Pyridine-Based Highly Specific Fluorescent Probe for Tracing Hypochlorous Acid in Lysosomes of Living Cells. *New J. Chem.* **2021**, *45* (32), 14548–14553. https://doi.org/10.1039/D1NJ02256C.
(1241) Wang, K.; Liu, Y.; Liu, C.; Zhu, H.; Li, X.; Yu, M.; Liu, L.; Sang, G.; Sheng, W.; Zhu, B. A New-Type HOCl-Activatable Fluorescent Probe and Its Applications in Water Environment and Biosystems. *Sci. Total Environ.* **2022**, *839*, 156164. https://doi.org/10.1016/j.scitotenv.2022.156164.
(1242) Zhan, X.-Q.; Yan, J.-H.; Su, J.-H.; Wang, Y.-C.; He, J.; Wang, S.-Y.; Zheng, H.; Xu, J.-G. Thiospirolactone as a Recognition Site: Rhodamine B-Based Fluorescent Probe for Imaging Hypochlorous Acid Generated in Human Neutrophil Cells. *Sens. Actuators B Chem.* **2010**, *150* (2), 774–780. https://doi.org/10.1016/j.snb.2010.07.057.
(1243) Chen, X.; Lee, K.-A.; Ha, E.-M.; Lee, K. M.; Seo, Y. Y.; Choi, H. K.; Kim, H. N.; Kim, M. J.; Cho, C.-S.; Lee, S. Y.; Lee, W.-J.; Yoon, J. A Specific and Sensitive Method for Detection

of Hypochlorous Acid for the Imaging of Microbe-Induced HOCl Production. *Chem. Commun.* **2011**, *47* (15), 4373–4375. https://doi.org/10.1039/C1CC10589B.
(1244) Moon, J. O.; Lee, J. W.; Choi, M. G.; Ahn, S.; Chang, S.-K. Dual Signaling of Hypochlorous Acid by Desulfurization of Thiocoumarin. *Tetrahedron Lett.* **2012**, *53* (48), 6594–6597. https://doi.org/10.1016/j.tetlet.2012.09.110.
(1245) Yuan, L.; Lin, W.; Chen, H. Analogs of Changsha Near-Infrared Dyes with Large Stokes Shifts for Bioimaging. *Biomaterials* **2013**, *34* (37), 9566–9571. https://doi.org/10.1016/j.biomaterials.2013.08.081.
(1246) Zhang, Z.; Deng, C.; Meng, L.; Zheng, Y.; Yan, X. A Rhodamine Hydrazide-Based Fluorescent Probe for Sensitive and Selective Detection of Hypochlorous Acid and Its Application in Living Cells. *Anal. Methods* **2014**, *7* (1), 107–114. https://doi.org/10.1039/C4AY02281E.
(1247) Ding, S.; Zhang, Q.; Xue, S.; Feng, G. Real-Time Detection of Hypochlorite in Tap Water and Biological Samples by a Colorimetric, Ratiometric and near-Infrared Fluorescent Turn-on Probe. *Analyst* **2015**, *140* (13), 4687–4693. https://doi.org/10.1039/C5AN00465A.
(1248) Chen, X.; Lee, K.-A.; Ren, X.; Ryu, J.-C.; Kim, G.; Ryu, J.-H.; Lee, W.-J.; Yoon, J. Synthesis of a Highly HOCl-Selective Fluorescent Probe and Its Use for Imaging HOCl in Cells and Organisms. *Nat. Protoc.* **2016**, *11* (7), 1219–1228. https://doi.org/10.1038/nprot.2016.062.
(1249) Liu, Y.; Zhao, Z.-M.; Miao, J.-Y.; Zhao, B.-X. A Ratiometric Fluorescent Probe Based on Boron Dipyrromethene and Rhodamine Förster Resonance Energy Transfer Platform for Hypochlorous Acid and Its Application in Living Cells. *Anal. Chim. Acta* **2016**, *921*, 77–83. https://doi.org/10.1016/j.aca.2016.03.045.
(1250) Manna, A.; Sarkar, D.; Goswami, S.; Quah, C. K.; Fun, H.-K. Single Excited State Intramolecular Proton Transfer (ESIPT) Chemodosimeter Based on Rhodol for Both Hg^{2+} and OCl^{-}: Ratiometric Detection with Live-Cell Imaging. *RSC Adv.* **2016**, *6* (62), 57417–57423. https://doi.org/10.1039/C6RA11009F.
(1251) Guo, R.; Wang, Q.; Lin, W. A Carbazole-Fused-RhodamineProbe for Detection of HOCl in Living Cells. *J. Fluoresc.* **2017**, *27* (6), 1969–1974. https://doi.org/10.1007/s10895-017-2134-y.
(1252) Albrett, A. M.; Ashby, L. V.; Dickerhof, N.; Kettle, A. J.; Winterbourn, C. C. Heterogeneity of Hypochlorous Acid Production in Individual Neutrophil Phagosomes Revealed by a Rhodamine-Based Probe. *J. Biol. Chem.* **2018**, *293* (40), 15715–15724. https://doi.org/10.1074/jbc.RA118.004789.
(1253) Jiao, X.; Xiao, Y.; Li, Y.; Liang, M.; Xie, X.; Wang, X.; Tang, B. Evaluating Drug-Induced Liver Injury and Its Remission via Discrimination and Imaging of HClO and H_2S with a Two-Photon Fluorescent Probe. *Anal. Chem.* **2018**, *90* (12), 7510–7516. https://doi.org/10.1021/acs.analchem.8b01106.
(1254) Gong, Y.-J.; Lv, M.-K.; Zhang, M.-L.; Kong, Z.-Z.; Mao, G.-J. A Novel Two-Photon Fluorescent Probe with Long-Wavelength Emission for Monitoring HClO in Living Cells and Tissues. *Talanta* **2019**, *192*, 128–134. https://doi.org/10.1016/j.talanta.2018.08.089.
(1255) Wang, J.; Cheng, D.; Zhu, L.; Wang, P.; Liu, H.-W.; Chen, M.; Yuan, L.; Zhang, X.-B. Engineering Dithiobenzoic Acid Lactone-Decorated Si-Rhodamine as a Highly Selective near-Infrared HOCl Fluorescent Probe for Imaging Drug-Induced Acute Nephrotoxicity. *Chem. Commun.* **2019**, *55* (73), 10916–10919. https://doi.org/10.1039/C9CC04736K.
(1256) Wang, L.; Ren, M.; Li, Z.; Dai, L.; Lin, W. A Ratiometric Two-Photon Fluorescent Probe for the Rapid Detection of HClO in Living Systems. *Anal. Methods* **2019**, *11* (12), 1580–1584. https://doi.org/10.1039/C9AY00205G.
(1257) Lu, P.; Zhang, X.; Ren, T.; Yuan, L. Molecular Engineering of Ultra-Sensitive Fluorescent Probe with Large Stokes Shift for Imaging of Basal HOCl in Tumor Cells and Tissues. *Chin. Chem. Lett.* **2020**, *31* (11), 2980–2984. https://doi.org/10.1016/j.cclet.2020.08.016.

(1258) Zhang, D.; Ma, Z.; Wang, Y.; Yin, H.; Li, M.; Wang, Y.; Wang, H.; Jia, B.; Liu, J. Dual-Binding Benzene and Rhodamine B Conjugate Derivatives as Fluorescent Chemodosimeter for Hypochlorite in Living Cell Imaging. *Spectrochim. Acta. A. Mol. Biomol. Spectrosc.* **2020**, *229*, 117908. https://doi.org/10.1016/j.saa.2019.117908.
(1259) Zhang, M.; Wang, T.; Lin, X.; Fan, M.; Zho, Y.; Li, N.; Cui, X. Boron-Substituted Rhodamine for Ratiometric Monitoring Dynamic of H_2O_2 and HOCl in Vivo. *Sens. Actuators B Chem.* **2021**, *331*, 129411. https://doi.org/10.1016/j.snb.2020.129411.
(1260) Cho, M.; Nguyen, V.-N.; Yoon, J. Simultaneous Detection of Hypochlorite and Singlet Oxygen by a Thiocoumarin-Based Ratiometric Fluorescent Probe. *ACS Meas. Sci. Au* **2022**, *2* (3), 219–223. https://doi.org/10.1021/acsmeasuresciau.1c00055.
(1261) Wang, X.; Zhou, Y.; Xu, C.; Song, H.; Li, L.; Zhang, J.; Guo, M. A Highly Selective Fluorescent Probe for the Detection of Hypochlorous Acid in Tap Water and Living Cells. *Spectrochim. Acta. A. Mol. Biomol. Spectrosc.* **2018**, *203*, 415–420. https://doi.org/10.1016/j.saa.2018.06.012.
(1262) Xing, P.; Zhang, Z.; Niu, Y.; Qi, Y.; Dong, L.; Wang, C. Water Solubility Is Essential for Fluorescent Probes to Image Hypochlorous Acid in Live Cells. *Chem. Commun.* **2018**, *54* (71), 9889–9892. https://doi.org/10.1039/C8CC04631J.
(1263) Zhu, B.; Wu, L.; Zhang, M.; Wang, Y.; Zhao, Z.; Wang, Z.; Duan, Q.; Jia, P.; Liu, C. A Fast-Response, Highly Specific Fluorescent Probe for the Detection of Picomolar Hypochlorous Acid and Its Bioimaging Applications. *Sens. Actuators B Chem.* **2018**, *263*, 103–108. https://doi.org/10.1016/j.snb.2018.02.083.
(1264) Zhu, B.; Wu, L.; Zhang, M.; Zhao, Z.; Wang, Z.; Duan, Q.; Jia, P.; Li, Z.; Zhu, H.; Liu, C. A Highly Specific and Ultrasensitive Fluorescent Probe for Monitoring Hypochlorous Acid and Its Applications in Live Cells. *Sens. Actuators B-Chem.* **2018**, *267*, 589–596. https://doi.org/10.1016/j.snb.2018.04.011.
(1265) Wu, L.; Yang, Q.; Liu, L.; C. Sedgwick, A.; J. Cresswell, A.; D. Bull, S.; Huang, C.; D. James, T. ESIPT-Based Fluorescence Probe for the Rapid Detection of Hypochlorite (HOCl/ClO^-). *Chem. Commun.* **2018**, *54* (61), 8522–8525. https://doi.org/10.1039/C8CC03717E.
(1266) Liu, C.; Jia, P.; Zhuang, Z.; Wang, Z.; Duan, Q.; Li, Z.; Zhu, H.; Zhang, X.; Zhu, B.; Sheng, W. A Water-Soluble and Highly Specific Fluorescent Probe with Large Stokes Shift for Imaging Basal HOCl in Living Cells and Zebrafish. *Sens. Actuators B Chem.* **2019**, *291*, 243–249. https://doi.org/10.1016/j.snb.2019.04.068.
(1267) Shen, S.-L.; Huang, X.-Q.; Lin, X.-H.; Cao, X.-Q. A Ratiometric Fluorescent Probe for Lysosomal Hypochlorous Acid Based on Through-Bond Energy Transfer Strategy. *Anal. Chim. Acta* **2019**, *1052*, 124–130. https://doi.org/10.1016/j.aca.2018.11.030.
(1268) Tong, L.; Qian, Y. A Naphthalimide–Rhodamine Chemodosimeter for Hypochlorite Based on TBET: High Quantum Yield and Endogeous Imaging in Living Cells. *J. Photochem. Photobiol. Chem.* **2019**, *368*, 62–69. https://doi.org/10.1016/j.jphotochem.2018.09.027.
(1269) Wang, J.; Men, Y.; Niu, L.; Luo, Y.; Zhang, J.; Zhao, W.; Wang, J. A Reaction-Based Fluorescent Probe for Imaging of Native Hypochlorous Acid. *Chem. – Asian J.* **2019**, *14* (21), 3893–3897. https://doi.org/10.1002/asia.201901041.
(1270) Zhang, Y.-Y.; Chen, X.-Z.; Liu, X.-Y.; Zhang, X.-Y.; Gao, G.; Hou, S.-C.; Wang, H.-M. A Highly Selective and Ultrafast Near-Infrared Fluorescent Turn-on and Colorimetric Probe for Hypochlorite in Living Cells. *Anal. Chim. Acta* **2019**, *1078*, 135–141. https://doi.org/10.1016/j.aca.2019.06.014.
(1271) Deng, Y.; Feng, S.; Xia, Q.; Gong, S.; Feng, G. A Novel Reaction-Based Fluorescence Probe for Rapid Imaging of HClO in Live Cells, Animals, and Injured Liver Tissues. *Talanta* **2020**, *215*, 120901. https://doi.org/10.1016/j.talanta.2020.120901.

(1272) He, N.; Wang, Y.; Huang, Y.; Chen, L.; Wang, X.; Lv, C.; Yue, S. Detection of Hypochlorous Acid Fluctuation via a Selective Fluorescent Probe in Acute Lung Injury Cells and Mouse Models. *J. Mater. Chem. B* **2020**, *8* (43), 9899–9905. https://doi.org/10.1039/D0TB01969K.
(1273) Jiao, C.; Liu, Y.; Pang, J.; Lu, W.; Zhang, P.; Wang, Y. A Simple Lysosome-Targeted Probe for Detection of Hypochlorous Acid in Living Cells. *J. Photochem. Photobiol. Chem.* **2020**, *392*, 112399. https://doi.org/10.1016/j.jphotochem.2020.112399.
(1274) Wang, X.; Tao, Y.; Zhang, J.; Chen, M.; Wang, N.; Ji, X.; Zhao, W. Selective Detection and Visualization of Exogenous/Endogenous Hypochlorous Acid in Living Cells Using a BODIPY-Based Red-Emitting Fluorescent Probe. *Chem. – Asian J.* **2020**, *15* (6), 770–774. https://doi.org/10.1002/asia.201901709.
(1275) Shi, L.; Yang, S.; Hong, H.-J.; Li, Y.; Yu, H.-J.; Shao, G.; Zhang, K.; Gong, S.-Z. A Novel Target and pH Dual-Activatable Fluorescent Probe for Precisely Detecting Hypochlorite in Lysosomes. *Anal. Chim. Acta* **2020**, *1094*, 122–129. https://doi.org/10.1016/j.aca.2019.10.004.
(1276) Zhang, Y.; Ma, Y.; Wang, Z.; Zhang, X.; Chen, X.; Hou, S.; Wang, H. A Novel Colorimetric and Far-Red Emission Ratiometric Fluorescent Probe for the Highly Selective and Ultrafast Detection of Hypochlorite in Water and Its Application in Bioimaging. *Analyst* **2020**, *145* (3), 939–945. https://doi.org/10.1039/C9AN02034A.
(1277) Du, Y.; Wang, B.; Jin, D.; Li, M.; Li, Y.; Yan, X.; Zhou, X.; Chen, L. Dual-Site Fluorescent Probe for Multi-Response Detection of ClO− and H_2O_2 and Bio-Imaging. *Anal. Chim. Acta* **2020**, *1103*, 174–182. https://doi.org/10.1016/j.aca.2019.12.059.
(1278) Gao, W.; Ma, Y.; Liu, Y.; Ma, S.; Lin, W. Observation of Endogenous HClO in Living Mice with Inflammation, Tissue Injury and Bacterial Infection by a near-Infrared Fluorescent Probe. *Sens. Actuators B Chem.* **2021**, *327*, 128884. https://doi.org/10.1016/j.snb.2020.128884.
(1279) He, M.; Ye, M.; Wang, Z.; Liu, P.; Li, H.; Lu, C.; Wang, Y.; Liang, T.; Li, H.; Li, C. A Ratiometric Near-Infrared Fluorescent Probe with a Large Emission Peak Shift for Sensing and Imaging Hypochlorous Acid. *Sens. Actuators B Chem.* **2021**, *343*, 130063. https://doi.org/10.1016/j.snb.2021.130063.
(1280) Liang, X.; Huo, Y.; Yan, J.; Huang, L.; Lin, W. The Development of a Highly Selective Fluorescent Probe for the Rapid Detection of HClO in Living Cells and Zebrafish. *New J. Chem.* **2021**, *45* (28), 12569–12575. https://doi.org/10.1039/D1NJ00891A.
(1281) Luo, P.; Zhao, X. A Sensitive and Selective Fluorescent Probe for Real-Time Detection and Imaging of Hypochlorous Acid in Living Cells. *ACS Omega* **2021**, *6* (18), 12287–12292. https://doi.org/10.1021/acsomega.1c01102.
(1282) Qian, X.; Yu, H.; Zhu, W.; Yao, X.; Liu, W.; Yang, S.; Zhou, F.; Liu, Y. Near Infrared Fluorescent Probe for in Vivo Bioimaging of Endogenous Hypochlorous Acid. *Dyes Pigments* **2021**, *188*, 109218. https://doi.org/10.1016/j.dyepig.2021.109218.
(1283) Wang, X.-B.; Zhang, D.-L.; Li, H.-J.; Lu, X.; Liu, Q.; Wu, Y.-C. Rational Design of an HClO-Specific Triggered Self-Immolative Fluorescent Turn-on Sensor and Its Bioimaging Applications. *J. Mater. Chem. B* **2021**, *9* (42), 8793–8800. https://doi.org/10.1039/D1TB01721G.
(1284) Tang, H.; Qiang, X.; Gao, Y.; Teng, H.; Chen, X.; Zhang, Y.; Tian, J.; Qin, B.; Guo, Y. Real-Time Tracking and Dual-Mode Imaging of Hypochlorous Acid in Vivo by a Small-Sized Fluorescence Probe. *Dyes Pigments* **2021**, *188*, 109219. https://doi.org/10.1016/j.dyepig.2021.109219.
(1285) Wang, M.; Han, X.; Yang, X.; Liu, J.; Song, X.; Zhu, W.; Ye, Y. A Long-Wavelength Activable AIEgen Fluorescent Probe for HClO and Cell Apoptosis Imaging. *Analyst* **2021**, *146* (21), 6490–6495. https://doi.org/10.1039/D1AN01430G.
(1286) Pang, Q.; Li, T.; Yin, C.; Ma, K.; Huo, F. Comparing the Abundance of HClO in Cancer/Normal Cells and Visualizing in Vivo Using a Mitochondria-Targeted Ultra-Fast

Fluorescent Probe. *Analyst* **2021**, *146* (10), 3361–3367. https://doi.org/10.1039/D1AN00375E.
(1287) Luo, P.; Xu, J.; Shen, B.; Xu, P. A Mitochondria-Targeted Fluorescence Probe for Visualizing Detection of Hypochlorite in Living Cells. *ChemistrySelect* **2021**, *6* (34), 9144–9148. https://doi.org/10.1002/slct.202102377.
(1288) Mao, S.; Ding, G.; Wang, Q.; Liu, X.; Wang, K.; Gao, Y.; Wang, X.; Liang, X.; Meng, D. A Novel Mitochondria-Targeted Fluorescent Sensor for the HOCl /ClO− Detection and Imaging Application in Living Cells. *Tetrahedron* **2022**, *123*, 132983. https://doi.org/10.1016/j.tet.2022.132983.
(1289) Li, L.-K.; Hou, Y.-M.; Liu, X.-C.; Tian, M.-J.; Ma, Q.-J.; Zhu, N.-N.; Liu, S.-Z. An ICT-FRET-Based Fluorescent Probe for the Ratiometric Sensing of Hypochlorous Acid Based on a Coumarin–Naphthalimide Derivative. *New J. Chem.* **2022**, *46* (14), 6596–6602. https://doi.org/10.1039/D2NJ00491G.
(1290) Qu, W.; Guo, T.; Yang, B.; Tian, R.; Qiu, S.; Chen, X.; Geng, Z.; Wang, Z. Tracking HOCl by an Incredibly Simple Fluorescent Probe with AIE plus ESIPT in Vitro and in Vivo. *Spectrochim. Acta. A. Mol. Biomol. Spectrosc.* **2022**, *281*, 121649. https://doi.org/10.1016/j.saa.2022.121649.
(1291) Chen, M.; Chen, X.; Wang, Y.; Fan, X.; Chen, T.; Liang, Z. An ESIPT Fluorescent Probe for Ultrarapid HClO Detection during Reagent-Stimulated Oxidative Stress in Cells and Zebrafish. *Sens. Actuators B Chem.* **2022**, *371*, 132545. https://doi.org/10.1016/j.snb.2022.132545.
(1292) Huang, H.; Yue, L.; Chen, Z.; Li, H.; Lin, W. Elevated Hypochlorous Acid Levels in Asthmatic Mice Were Disclosed by a Near-Infrared Fluorescence Probe. *Anal. Chim. Acta* **2022**, *1232*, 340480. https://doi.org/10.1016/j.aca.2022.340480.
(1293) Kafuti, Y. S.; Zeng, S.; Qian, M.; Zhang, C.; Liu, X.; Wang, J.; Chen, Q. A Novel NIR Fluorescent Probe with Fast Response and Large Stokes Shift for the Detection and Imaging of Hypochlorous Acid in Living Cells. *Dyes Pigments* **2022**, *199*, 110067. https://doi.org/10.1016/j.dyepig.2021.110067.
(1294) Li, L.; Wang, X.; Huang, J.; Ma, K.; Tan, X. A Novel Near-Infrared Fluorescent Probe for Rapid Sensing of HClO in Living Cells and Zebrafish. *Front. Chem.* **2022**, *10*.
(1295) Zeng, C.; Chen, Z.; Yang, M.; Lv, J.; Li, H.; Link to external site, this link will open in a new window; Gao, J.; Link to external site, this link will open in a new window; Yuan, Z.; Link to external site, this link will open in a new window. A Hydroxytricyanopyrrole-Based Fluorescent Probe for Sensitive and Selective Detection of Hypochlorous Acid. *Molecules* **2022**, *27* (21), 7237. https://doi.org/10.3390/molecules27217237.
(1296) Hu, W.; Zhao, M.; Gu, K.; Xie, L.; Liu, M.; Lu, D. Fluorescent Probe for the Detection of Hypochlorous Acid in Water Samples and Cell Models. *RSC Adv.* **2022**, *12* (2), 777–784. https://doi.org/10.1039/D1RA08116K.
(1297) Zeng, C.; Chen, Z.; Yang, M.; Lv, J.; Li, H.; Gao, J.; Yuan, Z. A Hydroxytricyanopyrrole-Based Fluorescent Probe for Sensitive and Selective Detection of Hypochlorous Acid. *Molecules* **2022**, *27* (21), 7237. https://doi.org/10.3390/molecules27217237.
(1298) Zhang, H.; Feng, Q.; Hou, J.-T.; Li, Z.; Shen, J. Carboxy Bodipy-Based Fast Trigger Fluorescent Probe for Imaging Endogenous Hypochlorous Acid. *Chemosensors* **2023**, *11* (1), 26. https://doi.org/10.3390/chemosensors11010026.
(1299) Sun, J.; Xu, J.; Ma, Q.; Mao, G.; Zhu, N.; Tian, M.; Li, L.; Liu, S. A Highly Selective Fluorescent Probe for Hypochlorous Acid in Living Cells Based on a Naphthalene Derivative. *Int. J. Anal. Chem.* **2022**, *2022*, e7649230. https://doi.org/10.1155/2022/7649230.
(1300) Fang, H.; Chen, Y.; Geng, S.; Yao, S.; Guo, Z.; He, W. Super-Resolution Imaging of Mitochondrial HClO during Cell Ferroptosis Using a Near-Infrared Fluorescent Probe. *Anal. Chem.* **2022**, *94* (51), 17904–17912. https://doi.org/10.1021/acs.analchem.2c03887.

(1301) Liu, K.; Zhang, J.; Li, X.; Xie, Y.; Li, Y.; Wang, X.; Jiao, X.; Xie, X.; Tang, B. Hypochlorous Acid-Activated Two-Photon Fluorescent Probe for Evaluation of Anticancer Drug-Induced Cardiotoxicity and Screening of Antioxidant Drugs. *Org. Chem. Front.* **2022**, *9* (24), 6795–6801. https://doi.org/10.1039/D2QO01408D.
(1302) Gai, L.; Mack, J.; Liu, H.; Xu, Z.; Lu, H.; Li, Z. A BODIPY Fluorescent Probe with Selective Response for Hypochlorous Acid and Its Application in Cell Imaging. *Sens. Actuators B Chem.* **2013**, *182*, 1–6. https://doi.org/10.1016/j.snb.2013.02.106.
(1303) Singh, A. P.; Tsay, O. G.; Murale, D. P.; Jun, T.; Liew, H.; Suh, Y.-H.; Churchill, D. G. Extremely Selective "Turn-on" Fluorescence Detection of Hypochlorite Confirmed by Proof-of-Principle Neurological Studies via Esterase Action in Living Cells. *Analyst* **2013**, *138* (10), 2829–2832. https://doi.org/10.1039/C3AN00297G.
(1304) Liu, F.; Gao, Y.; Wang, J.; Sun, S. Reversible and Selective Luminescent Determination of ClO−/H2S Redox Cycle in Vitro and in Vivo Based on a Ruthenium Trisbipyridyl Probe. *Analyst* **2014**, *139* (13), 3324–3329. https://doi.org/10.1039/C4AN00331D.
(1305) Tian, F.; Jia, Y.; Zhang, Y.; Song, W.; Zhao, G.; Qu, Z.; Li, C.; Chen, Y.; Li, P. A HClO-Specific near-Infrared Fluorescent Probe for Determination of Myeloperoxidase Activity and Imaging Mitochondrial HClO in Living Cells. *Biosens. Bioelectron.* **2016**, *86*, 68–74. https://doi.org/10.1016/j.bios.2016.06.039.
(1306) Wang, X.; Zhou, L.; Qiang, F.; Wang, F.; Wang, R.; Zhao, C. Development of a BODIPY-Based Ratiometric Fluorescent Probe for Hypochlorous Acid and Its Application in Living Cells. *Anal. Chim. Acta* **2016**, *911*, 114–120. https://doi.org/10.1016/j.aca.2016.01.022.
(1307) Zhang, B.; Yang, X.; Zhang, R.; Liu, Y.; Ren, X.; Xian, M.; Ye, Y.; Zhao, Y. Lysosomal-Targeted Two-Photon Fluorescent Probe to Sense Hypochlorous Acid in Live Cells. *Anal. Chem.* **2017**, *89* (19), 10384–10390. https://doi.org/10.1021/acs.analchem.7b02361.
(1308) Liu, C.; Jiao, X.; He, S.; Zhao, L.; Zeng, X. A Highly Selective and Sensitive Fluorescent Probe for Hypochlorous Acid and Its Lysosome-Targetable Biological Applications. *Talanta* **2017**, *174*, 234–242. https://doi.org/10.1016/j.talanta.2017.06.012.
(1309) Deng, B.; Ren, M.; Kong, X.; Zhou, K.; Lin, W. Development of an Enhanced Turn-on Fluorescent HOCl Probe with a Large Stokes Shift and Its Use for Imaging HOCl in Cells and Zebrafish. *Sens. Actuators B Chem.* **2018**, *255*, 963–969. https://doi.org/10.1016/j.snb.2017.08.146.
(1310) Jiao, X.; Huang, K.; He, S.; Liu, C.; Zhao, L.; Zeng, X. A Mitochondria-Targeted near-Infrared Fluorescent Probe with a Large Stokes Shift for Real-Time Detection of Hypochlorous Acid. *Org. Biomol. Chem.* **2019**, *17* (1), 108–114. https://doi.org/10.1039/C8OB02583E.
(1311)Sun, J.; Zhang, L.; Hu, Y.; Fang, J. Highly Selective Fluorometric Probes for Detection of HClO in Living Cells. *Sens. Actuators B Chem.* **2018**, *266*, 447–454. https://doi.org/10.1016/j.snb.2018.03.124.
(1312) Wang, S.; Zhang, B.; Wang, W.; Feng, G.; Yuan, D.; Zhang, X. Elucidating the Structure–Reactivity Correlations of Phenothiazine-Based Fluorescent Probes toward ClO^-. *Chem. – Eur. J.* **2018**, *24* (32), 8157–8166. https://doi.org/10.1002/chem.201800356.
(1313) Zheng, D.; Qiu, X.; Liu, C.; Jiao, X.; He, S.; Zhao, L.; Zeng, X. Synthesis and Bioapplication of a Highly Selective and Sensitive Fluorescent Probe for HOCl Based on a Phenothiazine–Dicyanoisophorone Conjugate with Large Stokes Shift. *New J. Chem.* **2018**, *42* (7), 5135–5141. https://doi.org/10.1039/C8NJ00279G.
(1314) Vedamalai, M.; Kedaria, D.; Vasita, R.; Gupta, I. Oxidation of Phenothiazine Based Fluorescent Probe for Hypochlorite and Its Application to Live Cell Imaging. *Sens. Actuators B Chem.* **2018**, *263*, 137–142. https://doi.org/10.1016/j.snb.2018.02.071.
(1315) Wang, L.; Chen, X.; Xia, Q.; Liu, R.; Qu, J. Deep-Red AIE-Active Fluorophore for Hypochlorite Detection and Bioimaging in Live Cells. *Ind. Eng. Chem. Res.* **2018**, *57* (23), 7735–7741. https://doi.org/10.1021/acs.iecr.8b01071.

(1316) Duan, C.; Won, M.; Verwilst, P.; Xu, J.; Kim, H. S.; Zeng, L.; Kim, J. S. In Vivo Imaging of Endogenously Produced HClO in Zebrafish and Mice Using a Bright, Photostable Ratiometric Fluorescent Probe. *Anal. Chem.* **2019**, *91* (6), 4172–4178. https://doi.org/10.1021/acs.analchem.9b00224.
(1317) He, L.; Zhang, Y.; Xiong, H.; Wang, J.; Geng, Y.; Wang, B.; Wang, Y.; Yang, Z.; Song, X. A Ratiometric Flavone-Based Fluorescent Probe for Hypochlorous Acid Detection with Large Stokes Shift and Long-Wavelength Emission. *Dyes Pigments* **2019**, *166*, 390–394. https://doi.org/10.1016/j.dyepig.2019.03.029.
(1318) Jiao, C.; Liu, Y.; Lu, W.; Zhang, P.; Ma, X.; Wang, Y. A Simple Sensor Based on 1,8-Naphthalimide with Large Stokes Shift for Detection of Hypochlorous Acid in Living Cells. *RSC Adv.* **2019**, *9* (54), 31196–31201. https://doi.org/10.1039/C9RA06174F.
(1319) Jin, Y.; Lv, M.; Tao, Y.; Xu, S.; He, J.; Zhang, J.; Zhao, W. A Water-Soluble BODIPY-Based Fluorescent Probe for Rapid and Selective Detection of Hypochlorous Acid in Living Cells. *Spectrochim. Acta. A. Mol. Biomol. Spectrosc.* **2019**, *219*, 569–575. https://doi.org/10.1016/j.saa.2019.04.085.
(1320) Liu, C.; Wang, Q.; Jiao, X.; Yao, H.; He, S.; Zhao, L.; Zeng, X. A Ratiometric Fluorescent Probe for Hypochlorous Acid and Its Biological Applications. *Dyes Pigments* **2019**, *160*, 989–994. https://doi.org/10.1016/j.dyepig.2018.07.001.
(1321) Natarajan, V.; Thirumalaivasan, N.; Wu, S.-P.; Sivan, V. A Far-Red to NIR Emitting Ultra-Sensitive Probe for the Detection of Endogenous HOCl in Zebrafish and the RAW 264.7 Cell Line. *Org. Biomol. Chem.* **2019**, *17* (14), 3538–3544. https://doi.org/10.1039/C9OB00143C.
(1322) Wang, J.-Y.; Qu, J.; Zhang, H.; Wei, K.; Ni, S.-X. A Fast-Responsive Two-Photon Fluorescent Probe for Monitoring Endogenous HClO with a Large Turn-on Signal and Its Application in Zebrafish Imaging. *RSC Adv.* **2019**, *9* (29), 16467–16471. https://doi.org/10.1039/C9RA02160D.
(1323) Zhang, H.; Li, Z.; Wang, M.; Luo, T.; Yi, L.; Wang, J. Novel Hepatocyte-Targeting Fluorescent Probes for Detection of Hypochlorous Acid: Synergistic Effect of Phosphate and Galactose. *Sens. Actuators B Chem.* **2019**, *279*, 102–110. https://doi.org/10.1016/j.snb.2018.09.123.
(1324) Zhang, Y.; Zuo, Y.; Yang, T.; Gou, Z.; Wang, X.; Lin, W. Novel Fluorescent Probe with a Bridged Si–O–Si Bond for the Reversible Detection of Hypochlorous Acid and Biothiol Amino Acids in Live Cells and Zebrafish. *Analyst* **2019**, *144* (17), 5075–5080. https://doi.org/10.1039/C9AN00844F.
(1325) Lou, Y.; Wang, C.; Chi, S.; Li, S.; Mao, Z.; Liu, Z. Construction of a Two-Photon Fluorescent Probe for Ratiometric Imaging of Hypochlorous Acid in Alcohol-Induced Liver Injury. *Chem. Commun.* **2019**, *55* (86), 12912–12915. https://doi.org/10.1039/C9CC06888K.
(1326) Pan, Y.; Yan, Y.; Li, Y.; Gao, X.-W.; Chao, D. A Fast-Responsive Fluorescent Probe Based on a Terpyridine-Zn^{2+} Complex for Sensing Hypochlorous Acid in Aqueous Solution and Its Application in Real Water Samples and Bioimaging. *New J. Chem.* **2019**, *43* (38), 15120–15125. https://doi.org/10.1039/C9NJ03801A.
(1327) Song, H.; Zhou, Y.; Xu, C.; Wang, X.; Zhang, J.; Wang, Y.; Liu, X.; Guo, M.; Peng, X. A Dual-Function Fluorescent Probe: Sensitive Detection of Water Content in Commercial Products and Rapid Detection of Hypochlorite with a Large Stokes Shift. *Dyes Pigments* **2019**, *162*, 160–167. https://doi.org/10.1016/j.dyepig.2018.10.023.
(1328) Wang, C.; Qian, Y. A TICT-Active Orthogonal D-A Type Probe Phenothiazine-BODIPY for Ratiometric Response of Hypochlorite and Its Application in Living Cells. *J. Lumin.* **2019**, *210*, 261–268. https://doi.org/10.1016/j.jlumin.2019.02.044.
(1329) Chen, W.; Li, G.; Chen, C.; Sheng, J.; Yang, L. Aggregation-Enhanced Emission Enables Phenothiazine Coumarin as a Robust Ratiometric Fluorescent for Rapid and Selective

Detection of HClO. *Spectrochim. Acta. A. Mol. Biomol. Spectrosc.* **2020**, *228*, 117724. https://doi.org/10.1016/j.saa.2019.117724.
(1330) Chu, C.-J.; Wu, G.-S.; Ma, H.-I.; Venkatesan, P.; Thirumalaivasan, N.; Wu, S.-P. A Fluorescent Turn-on Probe for Detection of Hypochlorus Acid and Its Bioimaging in Living Cells. *Spectrochim. Acta. A. Mol. Biomol. Spectrosc.* **2020**, *233*, 118234. https://doi.org/10.1016/j.saa.2020.118234.
(1331) Han, J.; Liu, X.; Xiong, H.; Wang, J.; Wang, B.; Song, X.; Wang, W. Investigation of the Relationship Between H_2O_2 and HClO in Living Cells by a Bifunctional, Dual-Ratiometric Responsive Fluorescent Probe. *Anal. Chem.* **2020**, *92* (7), 5134–5142. https://doi.org/10.1021/acs.analchem.9b05604.
(1332) Hou, J.-T.; Wang, B.; Zou, Y.; Fan, P.; Chang, X.; Cao, X.; Wang, S.; Yu, F. Molecular Fluorescent Probes for Imaging and Evaluation of Hypochlorite Fluctuations during Diagnosis and Therapy of Osteoarthritis in Cells and in a Mouse Model. *ACS Sens.* **2020**, *5* (7), 1949–1958. https://doi.org/10.1021/acssensors.0c00270.
(1333) Shen, Y.; Liu, X.; Zhang, X.; Zhang, Y.; Gu, B. Employing an ICT-ESIPT Strategy for Ratiometric Tracking of HClO Based on Sulfide Oxidation Reaction. *Spectrochim. Acta. A. Mol. Biomol. Spectrosc.* **2020**, *239*, 118515. https://doi.org/10.1016/j.saa.2020.118515.
(1334) Yue, X.; Wang, J.; Han, J.; Wang, B.; Song, X. A Dual-Ratiometric Fluorescent Probe for Individual and Continuous Detection of H_2S and HClO in Living Cells. *Chem. Commun.* **2020**, *56* (19), 2849–2852. https://doi.org/10.1039/C9CC10028H.
(1335) Li, H.; Miao, Y.; Liu, Z.; Wu, X.; Piao, C.; Zhou, X. A Mitochondria-Targeted Fluorescent Probe for Fast Detecting Hypochlorite in Living Cells. *Dyes Pigments* **2020**, *176*, 108192. https://doi.org/10.1016/j.dyepig.2020.108192.
(1336) Long, L.; Han, Y.; Liu, W.; Chen, Q.; Yin, D.; Li, L.; Yuan, F.; Han, Z.; Gong, A.; Wang, K. Simultaneous Discrimination of Hypochlorite and Single Oxygen during Sepsis by a Dual-Functional Fluorescent Probe. *Anal. Chem.* **2020**, *92* (8), 6072–6080. https://doi.org/10.1021/acs.analchem.0c00492.
(1337) Li, Y.; Li, H.; Di, G. Ratiometric Fluorescent Probe with Aggregation-Induced Emission Features for Monitoring HClO in Living Cells and Zebra Fish. *New J. Chem.* **2020**, *44* (33), 14286–14290. https://doi.org/10.1039/C9NJ06458C.
(1338) Hou, J.-T.; Wang, B.; Fan, P.; Duan, R.; Cao, X.; Zhu, L.; Wang, S. A Novel Benzothiazine-Fused Coumarin Derivative for Sensing Hypochlorite with High Performance. *Dyes Pigments* **2020**, *182*, 108675. https://doi.org/10.1016/j.dyepig.2020.108675.
(1339) Chen, J.; Lu, Y.; Wu, Y.; Chen, Z.; Liu, X.; Zhang, C.; Sheng, J.; Li, L.; Chen, W.; Song, X. De Novo Design of a Robust Fluorescent Probe for Basal HClO Imaging in a Mouse Parkinson's Disease Model. *ACS Chem. Neurosci.* **2021**, *12* (21), 4058–4064. https://doi.org/10.1021/acschemneuro.1c00431.
(1340) Hao, Y.; Zhang, Y.; Sun, Q.; Chen, S.; Tang, Z.; Zeng, R.; Xu, M. Phenothiazine-Coumarin-Pyridine Hybrid as an Efficient Fluorescent Probe for Ratiometric Sensing Hypochlorous Acid. *Microchem. J.* **2021**, *171*, 106851. https://doi.org/10.1016/j.microc.2021.106851.
(1341) Zheng, A.; Liu, H.; Peng, C.; Gao, X.; Xu, K.; Tang, B. A Mitochondria-Targeting near-Infrared Fluorescent Probe for Imaging Hypochlorous Acid in Cells. *Talanta* **2021**, *226*, 122152. https://doi.org/10.1016/j.talanta.2021.122152.
(1342) Zhan, Z.; Chai, L.; Lei, Q.; Zhou, X.; Wang, Y.; Deng, H.; Lv, Y.; Li, W. Two-Photon Ratiometric Fluorescent Probe for Imaging of Hypochlorous Acid in Acute Lung Injury and Its Remediation Effect. *Anal. Chim. Acta* **2021**, *1187*, 339159. https://doi.org/10.1016/j.aca.2021.339159.
(1343) Liang, L.; Sun, Y.; Liu, C.; Jiao, X.; Shang, Y.; Zeng, X.; Zhao, L.; Zhao, J. Highly Selective Turn-on Fluorescent Probe for Hypochlorite and Viscosity Detection. *J. Mol. Struct.* **2021**, *1227*, 129523. https://doi.org/10.1016/j.molstruc.2020.129523.

(1344) Cui, H.; Hou, P.; Li, Y.; Sun, J.; Zhang, H.; Zheng, Y.; Liu, Q.; Chen, S. Ratiometric Fluorescence Imaging of Hypochlorous Acid in Living Cells and Zebrafish Using a Novel Phenothiazine-Fused HPQ Probe. *J. Photochem. Photobiol. Chem.* **2021**, *417*, 113343. https://doi.org/10.1016/j.jphotochem.2021.113343.
(1345) Zhu, B.; Wu, X.; Rodrigues, J.; Hu, X.; Sheng, R.; Bao, G.-M. A Dual-Analytes Responsive Fluorescent Probe for Discriminative Detection of ClO^- and N_2H_4 in Living Cells. *Spectrochim. Acta. A. Mol. Biomol. Spectrosc.* **2021**, *246*, 118953. https://doi.org/10.1016/j.saa.2020.118953.
(1346) Wang, Q.; Zheng, D.; Cao, Q.; Huang, K.; Qin, D. A Dual-Response Fluoran-Phenothiazine Hybrid Fluorescent Probe for Selective Sensing of Fe^{3+} and ClO^- and Cell Imaging Application. *Spectrochim. Acta. A. Mol. Biomol. Spectrosc.* **2021**, *261*, 120061. https://doi.org/10.1016/j.saa.2021.120061.
(1347) Liang, L.; Sun, Y.; Liu, C.; Zeng, X.; Zhao, J. A Phenothiazine-Based Turn-on Fluorescent Probe for Selective Quantification of HClO in Living Cells. *Dyes Pigments* **2021**, *190*, 109344. https://doi.org/10.1016/j.dyepig.2021.109344.
(1348) Han, J.; Yang, S.; Wang, B.; Song, X. Tackling the Selectivity Dilemma of Benzopyrylium–Coumarin Dyes in Fluorescence Sensing of HClO and SO2. *Anal. Chem.* **2021**, *93* (12), 5194–5200. https://doi.org/10.1021/acs.analchem.0c05266.
(1349) Wu, P.; Xiong, H. An Acid-Enhanced OFF-ON Fluorescent Probe for the Detection of Hypochlorous Acid in Rheumatoid Arthritis. *Talanta* **2022**, *247*, 123584. https://doi.org/10.1016/j.talanta.2022.123584.
(1350) Huang, T.; Yan, S.; Yu, Y.; Xue, Y.; Yu, Y.; Han, C. Dual-Responsive Ratiometric Fluorescent Probe for Hypochlorite and Peroxynitrite Detection and Imaging In Vitro and In Vivo. *Anal. Chem.* **2022**, *94* (2), 1415–1424. https://doi.org/10.1021/acs.analchem.1c04729.
(1351) Zhang, R.; Lian, L.; Wang, B.; Zhu, L.; Ren, Y.; Shen, J.; Yu, X.-Q.; Hou, J.-T. Observation of HOCl Generation Associated with Diabetic Cataract Using a Highly Sensitive Fluorescent Probe. *Spectrochim. Acta. A. Mol. Biomol. Spectrosc.* **2022**, *278*, 121385. https://doi.org/10.1016/j.saa.2022.121385.
(1352) Zhou, G.; Hou, S.; Zhao, N.; Finney, N.; Wang, Y. A Novel Colorimetric and Ratiometric Fluorescent Probe for Monitoring Lysosomal HOCl in Real Time. *Dyes Pigments* **2022**, *204*, 110394. https://doi.org/10.1016/j.dyepig.2022.110394.
(1353) Bao, X.; Ai, K.; Cao, X.; Chen, D.; Zhou, B.; Huo, C. A Dual-Site and Dual-Turn-on Fluorescence Probe for Imaging Mitochondrial HClO and SO_2. *Dyes Pigments* **2022**, *197*, 109928. https://doi.org/10.1016/j.dyepig.2021.109928.
(1354) Liu, J.; Yin, H.; Shang, Z.; Gu, P.; He, G.; Meng, Q.; Zhang, R.; Zhang, Z. Sequential Detection of Hypochlorous Acid and Sulfur Dioxide Derivatives by a Red-Emitting Fluorescent Probe and Bioimaging Applications in Vitro and in Vivo. *RSC Adv.* **2022**, *12* (25), 15861–15869. https://doi.org/10.1039/D2RA01048H.
(1355) Zhang, K.; Gai, F.; Ding, G.; Zhang, Y.; Wang, X.; Tian, M.; Gou, Z.; Zuo, Y. Main-Chain Modified Polysiloxane towards Ratiometric Fluorescent Probes for Dynamic Visualization of ClO^-/GSH Oxidation Reduction Fluctuations in Vivo. *Sens. Actuators B Chem.* **2022**, *370*, 132469. https://doi.org/10.1016/j.snb.2022.132469.
(1356) Gu, B.; Liu, M.; Long, J.; Ye, X.; Xu, Z.; Shen, Y. An AIE Based Fluorescent Chemosensor for Ratiometric Detection of Hypochlorous Acid and Its Application. *Spectrochim. Acta. A. Mol. Biomol. Spectrosc.* **2022**, *278*, 121290. https://doi.org/10.1016/j.saa.2022.121290.
(1357) Zhang, C.; Wang, Y.; Zhang, L.; Li, X.; Nie, S.; Liu, C. A Near-Infrared Fluorescent Probe Based on Phenothiazine for Rapid Detecting of CN^- and ClO^-. *Opt. Mater.* **2022**, *133*, 112959. https://doi.org/10.1016/j.optmat.2022.112959.
(1358) Ye, Z.; Ji, M.; Wu, K.; Yang, J.; Liu, A.-A.; Sun, W.; Ding, D.; Liu, D. In-Sequence High-Specificity Dual-Reporter Unlocking of Fluorescent Probe Enables the Precise

Identification of Atherosclerotic Plaques. *Angew. Chem. Int. Ed.* **2022**, *61* (29), e202204518. https://doi.org/10.1002/anie.202204518.
(1359) Ramamoorthy, J.; Sathya, V.; Lavanya, R.; Padmini, V. Highly Selective and Sensitive Response of Curcumin Thioether Derivative for the Detection of Hypochlorous Acid by Fluorimetric Method. *J. Iran. Chem. Soc.* **2022**, *19* (8), 3327–3335. https://doi.org/10.1007/s13738-022-02528-5.
(1360) Niu, P.; Liu, J.; Xu, F.; Yang, L.; Li, Y.; Sun, A.; Wei, L.; Liu, X.; Song, X. Dual-Ratiometric Fluorescent Probe for H_2O_2 and HClO in Living Cells and Zebrafish and Application in Alcoholic Liver Injury Monitoring. *ACS Appl. Bio Mater.* **2022**, *5* (4), 1683–1691. https://doi.org/10.1021/acsabm.2c00058.
(1361) Xu, Q.; Heo, C. H.; Kim, J. A.; Lee, H. S.; Hu, Y.; Kim, D.; Swamy, K. M. K.; Kim, G.; Nam, S.-J.; Kim, H. M.; Yoon, J. A Selective Imidazoline-2-Thione-Bearing Two-Photon Fluorescent Probe for Hypochlorous Acid in Mitochondria. *Anal. Chem.* **2016**, *88* (12), 6615–6620. https://doi.org/10.1021/acs.analchem.6b01738.
(1362) Qiao, L.; Nie, H.; Wu, Y.; Xin, F.; Gao, C.; Jing, J.; Zhang, X. An Ultrafast Responsive BODIPY-Based Fluorescent Probe for the Detection of Endogenous Hypochlorite in Live Cells. *J. Mater. Chem. B* **2017**, *5* (3), 525–530. https://doi.org/10.1039/C6TB02774A.
(1363) Ye, W.; Bian, Q.; Huang, Y.; Lin, Q.; Zhan, X.; Zheng, H. Sulfonyl-Semicarbazide Group as a Recognition Site: A Novel Ratiometric Fluorescent Probe for Hypochlorous Acid and Imaging in Living Cells. *Dyes Pigments* **2020**, *173*, 107987. https://doi.org/10.1016/j.dyepig.2019.107987.
(1364) Tang, X.; Zhu, Z.; Wang, Z.; Tang, Y.; Wang, L.; Liu, L. Developed a Novel Quinazolinone Based Turn-on Fluorescence Probe for Highly Selective Monitoring Hypochlorite and Its Bioimaging Applications. *Spectrochim. Acta. A. Mol. Biomol. Spectrosc.* **2020**, *228*, 117845. https://doi.org/10.1016/j.saa.2019.117845.
(1365) Liu, J.; Shangguan, M.; Zeng, X.; Guo, Y.; Wang, T.; Hou, L. Phosphorescent Iridium(III) Complex for Efficient Sensing of Hypochlorite and Imaging in Living Cells. *Anal. Biochem.* **2020**, *592*, 113573. https://doi.org/10.1016/j.ab.2019.113573.
(1366) Yue, X.; Yang, Y.; Lan, M.; Li, K.; Wang, B. Dual-Ratiometric Fluorescence Sensing and Real-Time Detection of HOCl and NQO1 Using a Single Fluorescent Probe under One-Wavelength Excitation. *Anal. Chim. Acta* **2022**, *1224*, 340242. https://doi.org/10.1016/j.aca.2022.340242.
(1367) Wang, B.; Guo, X.; Liu, Z.; Wu, Y.; Hou, J.-T. A Long-Wavelength Emissive Phenothiazine Derived Fluorescent Probe for Detecting HOCl Upregulation in 5-FU Stimulated Living Cells. *Chem. Res. Chin. Univ.* **2022**, *38* (2), 609–615. https://doi.org/10.1007/s40242-021-1173-8.
(1368) Shi, W.-J.; Huang, Y.; Liu, W.; Xu, D.; Chen, S.-T.; Liu, F.; Hu, J.; Zheng, L.; Chen, K. A BODIPY-Based “OFF-ON” Fluorescent Probe for Fast and Selective Detection of Hypochlorite in Living Cells. *Dyes Pigments* **2019**, *170*, 107566. https://doi.org/10.1016/j.dyepig.2019.107566.
(1369) Jun, Y. W.; Sarkar, S.; Singha, S.; Reo, Y. J.; Kim, H. R.; Kim, J.-J.; Chang, Y.-T.; Ahn, K. H. A Two-Photon Fluorescent Probe for Ratiometric Imaging of Endogenous Hypochlorous Acid in Live Cells and Tissues. *Chem. Commun.* **2017**, *53* (78), 10800–10803. https://doi.org/10.1039/C7CC05834A.
(1370) Cao, J.; Jiang, D.-M.; Ren, X.; Li, T.; Gong, X.-T.; Yang, Y.-R.; Xu, Z.-G.; Sun, C.-L.; Shi, Z.-F.; Zhang, S.; Zhang, H.-L. A Highly Selective Two-Photon Probe with Large Turn-on Signal for Imaging Endogenous HOCl in Living Cells. *Dyes Pigments* **2017**, *146*, 279–286. https://doi.org/10.1016/j.dyepig.2017.07.006.
(1371) Chang, C.; Wang, F.; Qiang, J.; Zhang, Z.; Chen, Y.; Zhang, W.; Wang, Y.; Chen, X. Benzothiazole-Based Fluorescent Sensor for Hypochlorite Detection and Its Application for

Biological Imaging. *Sens. Actuators B Chem.* **2017**, *243*, 22–28. https://doi.org/10.1016/j.snb.2016.11.123.
(1372) Lohar, S.; Patra, A.; Roy, P.; Babu, S. P. S.; Chattopadhyay, P. A Highly Selective Fluorescence Turn-On Probe for the Sensing and Bioimaging of Hypochlorite Anion in Aqueous Media. *ChemistrySelect* **2018**, *3* (23), 6707–6713. https://doi.org/10.1002/slct.201800114.
(1373) He, L.; Xiong, H.; Wang, B.; Zhang, Y.; Wang, J.; Zhang, H.; Li, H.; Yang, Z.; Song, X. Rational Design of a Two-Photon Ratiometric Fluorescent Probe for Hypochlorous Acid with a Large Stokes Shift. *Anal. Chem.* **2020**, *92* (16), 11029–11034. https://doi.org/10.1021/acs.analchem.0c00030.
(1374) Li, Z.; Huang, S.; He, Y.; Duan, Q.; Zheng, G.; Jiang, Y.; Cai, L.; Jia, Y.; Zhang, H.; Ho, D. AND Logic Gate Based Fluorescence Probe for Simultaneous Detection of Peroxynitrite and Hypochlorous Acid. *Spectrochim. Acta. A. Mol. Biomol. Spectrosc.* **2020**, *230*, 118073. https://doi.org/10.1016/j.saa.2020.118073.
(1375) Zheng, G.; Li, Z.; Duan, Q.; Cheng, K.; He, Y.; Huang, S.; Zhang, H.; Jiang, Y.; Jia, Y.; Sun, H. Two Quenching Groups Are Better than One: A Robust Strategy for Constructing HOCl Fluorescent Probe with Minimized Background Fluorescence and Ultra-High Sensitivity and Its Application of HOCl Imaging in Living Cells and Tissues. *Sens. Actuators B Chem.* **2020**, *310*, 127890. https://doi.org/10.1016/j.snb.2020.127890.
(1376) Li, L.; Wang, X.; Sun, C.; Xu, T.; Yang, Z.; Zhang, Z.; Feng, Y.; Fang, M.; Chen, M.; Wang, X.; Meng, X. Design of a Two-Photon Fluorescent Probe for Ratiometric Imaging of Endogenous Hypochlorite in Mitochondria. *Dyes Pigments* **2020**, *181*, 108548. https://doi.org/10.1016/j.dyepig.2020.108548.
(1377) Xu, Z.; Wang, X.; Duan, T.; He, R.; Wang, F.; Zhou, X. Development of an Ultrafast Fluorescent Probe for Specific Recognition of Hypochlorous Acid and Its Application in Live Cells. *RSC Adv.* **2021**, *11* (40), 24669–24672. https://doi.org/10.1039/D1RA04082K.
(1378) Fang, S.; Wang, L.; Mei, Y.; Zheng, K. A Ratiometric Fluorescent Probe for Sensing Hypochlorite in Physiological Saline, Bovine Serum Albumin and Fetal Bovine/Calf Serum. *Spectrochim. Acta. A. Mol. Biomol. Spectrosc.* **2022**, *269*, 120738. https://doi.org/10.1016/j.saa.2021.120738.
(1379) Kong, X.; Shuang, S.-M.; Zhang, Y.; Wang, Y.; Dong, C. Dicyanoisophorone-Based Fluorescent Probe with Large Stokes Shift for Ratiometric Detection and Imaging of Exogenous/Endogenous Hypochlorite in Cell and Zebrafish. *Talanta* **2022**, *242*, 123293. https://doi.org/10.1016/j.talanta.2022.123293.
(1380) Liu, S.-R.; Wu, S.-P. Hypochlorous Acid Turn-on Fluorescent Probe Based on Oxidation of Diphenyl Selenide. *Org. Lett.* **2013**, *15* (4), 878–881. https://doi.org/10.1021/ol400011u.
(1381) Wang, B.; Li, P.; Yu, F.; Song, P.; Sun, X.; Yang, S.; Lou, Z.; Han, K. A Reversible Fluorescence Probe Based on Se–BODIPY for the Redox Cycle between HClO Oxidative Stress and H 2 S Repair in Living Cells. *Chem. Commun.* **2013**, *49* (10), 1014–1016. https://doi.org/10.1039/C2CC37803E.
(1382) Cheng, G.; Fan, J.; Sun, W.; Cao, J.; Hu, C.; Peng, X. A Near-Infrared Fluorescent Probe for Selective Detection of HClO Based on Se-Sensitized Aggregation of Heptamethine Cyanine Dye. *Chem. Commun.* **2013**, *50* (8), 1018–1020. https://doi.org/10.1039/C3CC47864E.
(1383) Zhang, W.; Liu, W.; Li, P.; Kang, J.; Wang, J.; Wang, H.; Tang, B. Reversible Two-Photon Fluorescent Probe for Imaging of Hypochlorous Acid in Live Cells and in Vivo. *Chem. Commun.* **2015**, *51* (50), 10150–10153. https://doi.org/10.1039/C5CC02537K.
(1384) Mulay, S. V.; Choi, M.; Jang, Y. J.; Kim, Y.; Jon, S.; Churchill, D. G. Enhanced Fluorescence Turn-on Imaging of Hypochlorous Acid in Living Immune and Cancer Cells. *Chem. – Eur. J.* **2016**, *22* (28), 9642–9648. https://doi.org/10.1002/chem.201601270.

(1385) Xu, X.-H.; Liu, C.; Mei, Y.; Song, Q.-H. BODIPY-Based Selenides as Fluorescent Probes for Rapid, Sensitive and Mitochondria-Specific Detection of Hypochlorous Acid. *J. Mater. Chem. B* **2019**, *7* (43), 6861–6867. https://doi.org/10.1039/C9TB01641D.
(1386) Li, P.; Jia, Y.; Zhao, N.; Zhang, Y.; Zhou, P.; Lou, Z.; Qiao, Y.; Zhang, P.; Wen, S.; Han, K. Quantifying the Fast Dynamics of HClO in Living Cells by a Fluorescence Probe Capable of Responding to Oxidation and Reduction Events within the Time Scale of Milliseconds. *Anal. Chem.* **2020**, *92* (19), 12987–12995. https://doi.org/10.1021/acs.analchem.0c01703.
(1387) Malankar, G. S.; Sakunthala, A.; Navalkar, A.; Maji, S. K.; Raju, S.; Manjare, S. T. Organoselenium-Based BOPHY as a Sensor for Detection of Hypochlorous Acid in Mammalian Cells. *Anal. Chim. Acta* **2021**, *1150*, 338205. https://doi.org/10.1016/j.aca.2021.338205.
(1388) Liu, C.; Shang, Y.; Zhao, T.; Liang, L.; He, S.; Zhao, L.; Zeng, X.; Wang, T. Facile Functionalized Fluorescein Derivative as a Reversible Fluorescence Probe for Selective Monitor of the Redox Cycle between Hypochlorous Acid and Cysteine. *Sens. Actuators B Chem.* **2021**, *348*, 130632. https://doi.org/10.1016/j.snb.2021.130632.
(1389) Liu, C.; Jiao, X.; Cai, S.; He, S.; Zhao, L.; Zeng, X. Reversible Fluorescent Probe for Visually Monitoring the Concentration-Dependent Dynamic Correlations among HOCl, H_2S, and Ca^{2+} in Neurons. *Sens. Actuators B Chem.* **2021**, *329*, 129213. https://doi.org/10.1016/j.snb.2020.129213.
(1390) Shelar, D. S.; Malankar, G. S.; M, M.; Patra, M.; Butcher, R. J.; Manjare, S. T. Selective Detection of Hypochlorous Acid in Living Cervical Cancer Cells with an Organoselenium-Based BOPPY Probe. *New J. Chem.* **2022**, *46* (36), 17610–17618. https://doi.org/10.1039/D2NJ02956A.
(1391) Hu, Z.-Q.; Zhu, J.-H.; Gu, Y.-Y.; Hu, W.-Z.; Li, M.; Jiang, Y. A Sensitive and Selective Turn-on Fluorescent Probe for Hypochlorous Acid Based on a Thiorhodamine 6G Amide, and Its Application in Cellular Imaging. *Microchim. Acta* **2014**, *181* (11), 1401–1406. https://doi.org/10.1007/s00604-014-1280-z.
(1392) Samanta, S.; Govindaraju, T. Unambiguous Detection of Elevated Levels of Hypochlorous Acid in Double Transgenic AD Mouse Brain. *ACS Chem. Neurosci.* **2019**, *10* (12), 4847–4853. https://doi.org/10.1021/acschemneuro.9b00554.
(1393) Sun, J.; Feng, F. An S-Alkyl Thiocarbamate-Based Biosensor for Highly Sensitive and Selective Detection of Hypochlorous Acid. *Analyst* **2018**, *143* (18), 4251–4255. https://doi.org/10.1039/C8AN01027G.
(1394) Tang, X.; Zhu, Z.; Wang, Y.; Han, J.; Ni, L.; Zhang, H.; Li, J.; Yanli, M. A Cyanobiphenyl Based Fluorescent Probe for Rapid and Specific Detection of Hypochlorite and Its Bio-Imaging Applications. *Sens. Actuators B Chem.* **2018**, *262*, 57–63. https://doi.org/10.1016/j.snb.2018.01.204.
(1395) Zhang, Y.-R.; Zhao, Z.-M.; Miao, J.-Y.; Zhao, B.-X. A Ratiometric Fluorescence Probe Based on a Novel FRET Platform for Imaging Endogenous HOCl in the Living Cells. *Sens. Actuators B Chem.* **2016**, *229*, 408–413. https://doi.org/10.1016/j.snb.2016.01.146.
(1396) Ma, P.; Zhang, B.; Diao, Q.; Li, L.; Sun, Y.; Wang, X.; Song, D. A Water-Soluble Fluorescent Probe for ClO^- and Cd^{2+} under Physiological pH and Its Applications in Living Cells Imaging. *Sens. Actuators B Chem.* **2016**, *233*, 639–645. https://doi.org/10.1016/j.snb.2016.04.142.
(1397) Feng, A.; Liu, P.; Liang, Q.; Zhang, X.; Huang, L.; Jia, Y.; Xie, M.; Yan, Q.; Li, C.; Wang, S. A New Carbazole-Based Colormetric and Ratiometric Fluorescent Probe for Hypochlorite Sensing in Living Cells and Zebrafishes. *Dyes Pigments* **2020**, *180*, 108492. https://doi.org/10.1016/j.dyepig.2020.108492.
(1398) Wang, L.; Pan, Q.; Chen, Y.; Ou, Y.; Li, H.; Li, B. A Dual-Response Ratiometric Fluorescent Probe for Hypochlorite and Hydrazine Detection and Its Imaging in Living Cells.

Spectrochim. Acta. A. Mol. Biomol. Spectrosc. **2020**, *241*, 118672. https://doi.org/10.1016/j.saa.2020.118672.
(1399) Guo, H.; Lin, J.; Zheng, L.; Yang, F. An Effective Fluorescent Sensor for ClO^- in Aqueous Media Based on Thiophene-Cyanostilbene Schiff-Base. *Spectrochim. Acta. A. Mol. Biomol. Spectrosc.* **2021**, *256*, 119744. https://doi.org/10.1016/j.saa.2021.119744.
(1400) Nguyen, V.-N.; Heo, S.; Kim, S.; Swamy, K. M. K.; Ha, J.; Park, S.; Yoon, J. A Thiocoumarin-Based Turn-on Fluorescent Probe for Hypochlorite Detection and Its Application to Live-Cell Imaging. *Sens. Actuators B Chem.* **2020**, *317*, 128213. https://doi.org/10.1016/j.snb.2020.128213.
(1401) Zhang, L.; Zhang, Y.-F.; Han, Y.-F. A Perylene Diimide-Based Fluorescent Probe for the Selective Detection of Hypochlorite in Living Cells. *Mater. Chem. Front.* **2022**, *6* (16), 2266–2273. https://doi.org/10.1039/D2QM00283C.
(1402) Xiao, H.; Xin, K.; Dou, H.; Yin, G.; Quan, Y.; Wang, R. A Fast-Responsive Mitochondria-Targeted Fluorescent Probe Detecting Endogenous Hypochlorite in Living RAW 264.7 Cells and Nude Mouse. *Chem. Commun.* **2015**, *51* (8), 1442–1445. https://doi.org/10.1039/C4CC07411D.
(1403) Shi, W.-J.; Feng, L.-X.; Wang, X.; Huang, Y.; Wei, Y.-F.; Huang, Y.-Y.; Ma, H.-J.; Wang, W.; Xiang, M.; Gao, L. A Near-Infrared-Emission Aza-BODIPY-Based Fluorescent Probe for Fast, Selective, and "Turn-on" Detection of HClO/ClO^-. *Talanta* **2021**, *233*, 122581. https://doi.org/10.1016/j.talanta.2021.122581.
(1404) Shu, W.; Jia, P.; Chen, X.; Li, X.; Huo, Y.; Liu, F.; Wang, Z.; Liu, C.; Zhu, B.; Yan, L.; Du, B. A Highly Selective Ratiometric Fluorescent Probe for the Sensitive Detection of Hypochlorous Acid and Its Bioimaging Applications. *RSC Adv.* **2016**, *6* (69), 64315–64322. https://doi.org/10.1039/C6RA15266J.
(1405) Wei, P.; Liu, L.; Yuan, W.; Yang, J.; Li, R.; Yi, T. A Fluorescent Probe Operating under Weak Acidic Conditions for the Visualization of HOCl in Solid Tumors in Vivo. *Sci. China Chem.* **2020**, *63* (8), 1153–1158. https://doi.org/10.1007/s11426-020-9737-y.
(1406) Yang, J.; Zheng, W.; Shen, Y.; Xu, Y.; Lv, G.; Li, C. A Novel Near-Infrared Fluorescent Probe Based on Phenoxazine for the Specific Detection of HOCl. *J. Lumin.* **2020**, *226*, 117460. https://doi.org/10.1016/j.jlumin.2020.117460.
(1407) Xu, J.; Wang, C.; Ma, Q.; Zhang, H.; Tian, M.; Sun, J.; Wang, B.; Chen, Y. Novel Mitochondria-Targeting and Naphthalimide-Based Fluorescent Probe for Detecting HClO in Living Cells. *ACS Omega* **2021**, *6* (22), 14399–14409. https://doi.org/10.1021/acsomega.1c01271.
(1408) Kim, K. H.; Kim, S. J.; Singha, S.; Yang, Y. J.; Park, S. K.; Ahn, K. H. Ratiometric Detection of Hypochlorous Acid in Brain Tissues of Neuroinflammation and Maternal Immune Activation Models with a Deep-Red/Near-Infrared Emitting Probe. *ACS Sens.* **2021**, *6* (9), 3253–3261. https://doi.org/10.1021/acssensors.1c00930.
(1409) Qiujuan, M.; Wang, C.; Mao, G.; Tian, M.; Sun, J.; Feng, S. An Endoplasmic Reticulum-Targeting and Ratiometric Fluorescent Probe for Hypochlorous Acid in Living Cells Based on a 1,8-Naphthalimide Derivative. *New J. Chem.* **2020**, No. 42, 18105–18510. https://doi.org/10.1039/D0NJ04045B.
(1410) Ma, Q.; Wang, C.; Bai, Y.; Xu, J.; Zhang, J.; Li, Z.; Guo, X. A Lysosome-Targetable and Ratiometric Fluorescent Probe for Hypochlorous Acid in Living Cells Based on a 1,8-Naphthalimide Derivative. *Spectrochim. Acta. A. Mol. Biomol. Spectrosc.* **2019**, *223*, 117334. https://doi.org/10.1016/j.saa.2019.117334.
(1411)Ma, F.; Sun, M.; Zhang, K.; Zhang, Y.; Zhu, H.; Wu, L.; Huang, D.; Wang, S. An Oxidative Cleavage-Based Ratiometric Fluorescent Probe for Hypochlorous Acid Detection and Imaging. *RSC Adv.* **2014**, *4* (104), 59961–59964. https://doi.org/10.1039/C4RA09611H.
(1412) Zhang, P.; Wang, H.; Zhang, D.; Zeng, X.; Zeng, R.; Xiao, L.; Tao, H.; Long, Y.; Yi, P.; Chen, J. Two-Photon Fluorescent Probe for Lysosome-Targetable Hypochlorous Acid

Detection within Living Cells. *Sens. Actuators B Chem.* **2018**, *255*, 2223–2231. https://doi.org/10.1016/j.snb.2017.09.025.
(1413) Li, S.; Huang, D.; Wan, J.; Yan, S.; Jiang, J.; Xiao, H. A Two-Photon Fluorescent Probe Derived from Spirobifluorene for Fast Sensing of Hypochlorite and Mercury Ions. *Sens. Actuators B Chem.* **2018**, *275*, 101–109. https://doi.org/10.1016/j.snb.2018.08.035.
(1414) Pan, D.; Don, Y.; Lu, Y.; Xiao, G.; Chi, H.; Hu, Z. AIE Fluorescent Probe Based on Tetraphenylethylene and Morpholine-Thiourea Structures for Detection of HClO. *Anal. Chim. Acta* **2022**, *1235*, 340559. https://doi.org/10.1016/j.aca.2022.340559.
(1415) Zhang, Z.; Zheng, Y.; Hang, W.; Yan, X.; Zhao, Y. Sensitive and Selective off–on Rhodamine Hydrazide Fluorescent Chemosensor for Hypochlorous Acid Detection and Bioimaging. *Talanta* **2011**, *85* (1), 779–786. https://doi.org/10.1016/j.talanta.2011.04.078.
(1416) Zhang, Z.; Zou, Y.; Deng, C.; Meng, L. A Simple Rhodamine Hydrazide-Based Turn-on Fluorescent Probe for HOCl Detection. *Luminescence* **2016**, *31* (4), 997–1004. https://doi.org/10.1002/bio.3064.
(1417) Huang, X.-Q.; Wang, Z.-Y.; Lv, Y.-J.; Shen, S.-L.; Zhu, Y.; Wang, J.; Zhang, Y.-R.; Wang, J.-M.; Ge, Y.-Q.; Cao, X.-Q. A Fluorescent Probe for the Detection of HOCl in Lysosomes. *New J. Chem.* **2018**, *42* (14), 11480–11484. https://doi.org/10.1039/C8NJ00831K.
(1418) Shen, S.-L.; Zhang, X.-F.; Ge, Y.-Q.; Zhu, Y.; Cao, X.-Q. A Novel Ratiometric Fluorescent Probe for the Detection of HOCl Based on FRET Strategy. *Sens. Actuators B Chem.* **2018**, *254*, 736–741. https://doi.org/10.1016/j.snb.2017.07.158.
(1419) Huo, F.-J.; Zhang, J.-J.; Yang, Y.-T.; Chao, J.-B.; Yin, C.-X.; Zhang, Y.-B.; Chen, T.-G. A Fluorescein-Based Highly Specific Colorimetric and Fluorescent Probe for Hypochlorites in Aqueous Solution and Its Application in Tap Water. *Sens. Actuators B Chem.* **2012**, *166–167*, 44–49. https://doi.org/10.1016/j.snb.2011.11.081.
(1420) Wei, F.; Lu, Y.; He, S.; Zhao, L.; Zeng, X. Selective and Sensitive Fluorescence Chemosensor for the Hypochlorite Anion in Water. *J. Fluoresc.* **2012**, *22* (5), 1257–1262. https://doi.org/10.1007/s10895-012-1066-9.
(1421) Xiong, K.; Huo, F.; Yin, C.; Chao, J.; Zhang, Y.; Xu, M. A Highly Selective Fluorescent Bioimaging Probe for Hypochlorite Based on 1,8-Naphthalimide Derivative. *Sens. Actuators B Chem.* **2015**, *221*, 1508–1514. https://doi.org/10.1016/j.snb.2015.07.116.
(1422) Tang, Z.; Ding, X.-L.; Liu, Y.; Zhao, Z.-M.; Zhao, B.-X. A New Probe Based on Rhodamine B and Benzothiazole Hydrazine for Sensing Hypochlorite in Living Cells and Real Water Samples. *RSC Adv.* **2015**, *5* (121), 99664–99668. https://doi.org/10.1039/C5RA20188H.
(1423) Zhang, R.; Zhao, J.; Han, G.; Liu, Z.; Liu, C.; Zhang, C.; Liu, B.; Jiang, C.; Liu, R.; Zhao, T.; Han, M.-Y.; Zhang, Z. Real-Time Discrimination and Versatile Profiling of Spontaneous Reactive Oxygen Species in Living Organisms with a Single Fluorescent Probe. *J. Am. Chem. Soc.* **2016**, *138* (11), 3769–3778. https://doi.org/10.1021/jacs.5b12848.
(1424) Guo, J.; Zhang, Z.; Kuai, Z.; Wang, R.; Yang, Q.; Shan, Y.; Li, Y. A New Turn-on Fluorescent Probe towards Hypochlorite in Living Cells. *Anal. Methods* **2017**, *9* (5), 864–870. https://doi.org/10.1039/C6AY02819E.
(1425) Jiang, Y.; Zhang, S.; Wang, B.; Qian, T.; Jin, C.; Wu, S.; Shen, J. Novel Triphenylamine-Based Fluorescent Probe for Specific Detection and Bioimaging of OCl^-. *Tetrahedron* **2018**, *74* (39), 5733–5738. https://doi.org/10.1016/j.tet.2018.08.010.
(1426) He, X.; Chen, H.; Xu, C.; Fan, J.; Xu, W.; Li, Y.; Deng, H.; Shen, J. Ratiometric and Colorimetric Fluorescent Probe for Hypochlorite Monitor and Application for Bioimaging in Living Cells, Bacteria and Zebrafish. *J. Hazard. Mater.* **2020**, *388*, 122029. https://doi.org/10.1016/j.jhazmat.2020.122029.
(1427) Zhu, Y.; Wang, K.; Wu, X.; Sun, Y.; Gong, X.; Cao, D.; Guan, R.; Liu, Z. A Highly Sensitive Turn-on Fluorescent Probe for Real-Time Detecting Hypochlorite and Its Application in Living Cells. *Talanta* **2020**, *209*, 120548. https://doi.org/10.1016/j.talanta.2019.120548.

(1428) Han, Z.; Dong, L.; Sun, F.; Long, L.; Jiang, S.; Dai, X.; Zhang, M. A Novel Fluorescent Probe with Extremely Low Background Fluorescence for Sensing Hypochlorite in Zebrafish. *Anal. Biochem.* **2020**, *602*, 113795. https://doi.org/10.1016/j.ab.2020.113795.
(1429) Wang, N.; Xu, W.; Song, D.; Ma, P. A Fluorescein-Carbazole-Based Fluorescent Probe for Imaging of Endogenous Hypochlorite in Living Cells and Zebrafish. *Spectrochim. Acta. A. Mol. Biomol. Spectrosc.* **2020**, *227*, 117692. https://doi.org/10.1016/j.saa.2019.117692.
(1430) Zhu, Y.; Ma, Y.; Liu, Y.; Liu, Z.; Ma, S.; Xing, M.; Cao, D.; Lin, W. Fluorescence Response of a Fluorescein Derivative for Hypochlorite Ion and Its Application for Biological Imaging in Wounded Zebrafish and Living Mice. *Sens. Actuators B Chem.* **2021**, *327*, 128848. https://doi.org/10.1016/j.snb.2020.128848.
(1431) Zhang, S.; Mu, X.; Yan, L. A Fluorescent Probe for the Fast Detection of Hypochlorite and Its Applications in Water, Test Strip and Living Cells. *J. Fluoresc.* **2021**, *31* (2), 569–576. https://doi.org/10.1007/s10895-020-02675-z.
(1432) Zhang, K.; Dai, Y.; Li, Q.; Su, Y.; Lv, Y. Unimolecular Chemo-Fluoro-Luminescent Probe for Simultaneous Detection and Imaging of Peroxynitrite and Hypochlorite in Vitro and in Vivo. *Sens. Actuators B Chem.* **2021**, *347*, 130609. https://doi.org/10.1016/j.snb.2021.130609.
(1433) Afzal, M. W.; Wang, S.; Gao, Y.; Qin, B.; Tian, X.; Zhang, Y.; Tang, H.; Guo, Y. A Highly Water-Soluble Rhodol-Based Fluorescent Probe for the Organic-Solvent Independent Sensing of Biological Hypochlorous Acid. *Dyes Pigments* **2022**, *204*, 110435. https://doi.org/10.1016/j.dyepig.2022.110435.
(1434) Zhang, Z.-H.; Li, C.-C.; Qu, J.; Zhang, H.; Liu, K.; Wang, J.-Y. A Novel and Fast-Responsive Two-Photon Fluorescent Probe with Modified Group for Monitoring Endogenous HClO Accompanied by a Large Turn-on Signal and Its Application in Zebrafish Imaging. *Spectrochim. Acta. A. Mol. Biomol. Spectrosc.* **2022**, *278*, 121361. https://doi.org/10.1016/j.saa.2022.121361.
(1435) Shi, J.; Li, Q.; Zhang, X.; Peng, M.; Qin, J.; Li, Z. Simple Triphenylamine-Based Luminophore as a Hypochlorite Chemosensor. *Sens. Actuators B Chem.* **2010**, *145* (1), 583–587. https://doi.org/10.1016/j.snb.2009.11.003.
(1436) Cheng, G.; Fan, J.; Sun, W.; Sui, K.; Jin, X.; Wang, J.; Peng, X. A Highly Specific BODIPY-Based Probe Localized in Mitochondria for HClO Imaging. *Analyst* **2013**, *138* (20), 6091–6096. https://doi.org/10.1039/C3AN01152F.
(1437) Guo, B.; Nie, H.; Yang, W.; Tian, Y.; Jing, J.; Zhang, X. A Highly Sensitive and Rapidly Responding Fluorescent Probe with a Large Stokes Shift for Imaging Intracellular Hypochlorite. *Sens. Actuators B Chem.* **2016**, *236*, 459–465. https://doi.org/10.1016/j.snb.2016.06.004.
(1438) Gao, Y.; Pan, Y.; Chi, Y.; He, Y.; Chen, H.; Nemykin, V. N. A “Reactive” Turn-on Fluorescence Probe for Hypochlorous Acid and Its Bioimaging Application. *Spectrochim. Acta. A. Mol. Biomol. Spectrosc.* **2019**, *206*, 190–196. https://doi.org/10.1016/j.saa.2018.07.090.
(1439) Zhan, Z.; Su, Z.; Chai, L.; Li, C.; Liu, R.; Lv, Y. Multimodal Imaging Iridium(III) Complex for Hypochlorous Acid in Living Systems. *Anal. Chem.* **2020**, *92* (12), 8285–8291. https://doi.org/10.1021/acs.analchem.0c00536.
(1440) Zhan, Z.; Zhang, K.; Zhang, L.; Li, Q.; Lv, Y. Development of Iridium(III) Phosphorescent Probe for Hypochlorous Acid Detection in Macrophages Cells and Cancer Cells Co-Culture System and Application in Inflamed Mouse Model. *Sens. Actuators B Chem.* **2020**, *303*, 127016. https://doi.org/10.1016/j.snb.2019.127016.
(1441) Jiang, Q.; Wang, Z.; Li, M.; Song, J.; Yang, Y.; Xu, X.; Xu, H.; Wang, S. A Novel Nopinone-Based Fluorescent Probe for Colorimetric and Ratiometric Detection of Hypochlorite and Its Applications in Water Samples and Living Cells. *Analyst* **2020**, *145* (3), 1033–1040. https://doi.org/10.1039/C9AN01981B.

(1442) Haldar, U.; Sharma, R.; Ruidas, B.; Lee, H. Toward Rapid and Selective Detection of Hypochlorous Acid in Pure Aqueous Media and Its Application to Cell Imaging: BODIPY-Derived Water-Soluble Macromolecular Chemosensor with High Sensitivity. *Dyes Pigments* **2020**, *172*, 107858. https://doi.org/10.1016/j.dyepig.2019.107858.
(1443) Wang, Z.; Zhang, Y.; Liang, Y.; Li, M.; Meng, Z.; Gong, S.; Yang, Y.; Xu, X.; Wang, S. Rational Design of a Facile Camphor-Based Fluorescence Turn-on Probe for Real-Time Tracking of Hypochlorous Acid in Vivo and in Vitro. *Analyst* **2022**, *147* (10), 2080–2088. https://doi.org/10.1039/D2AN00321J.
(1444) Li, J.; Huo, F.; Yin, C. A Selective Colorimetric and Fluorescent Probe for the Detection of ClO− and Its Application in Bioimaging. *RSC Adv.* **2014**, *4* (84), 44610–44613. https://doi.org/10.1039/C4RA06435F.
(1445) Yang, Y.; Yin, C.; Huo, F.; Chao, J.; Zhang, Y.; Jin, S. Simple 1,8-Diaminonaphthalene-Based Fluorescence Chemosensor for Hypochlorites and Its Practical Application. *Sens. Actuators B Chem.* **2014**, *199*, 226–231. https://doi.org/10.1016/j.snb.2014.03.105.
(1446) Fan, J.; Mu, H.; Zhu, H.; Du, J.; Jiang, N.; Wang, J.; Peng, X. Recognition of HClO in Live Cells with Separate Signals Using a Ratiometric Fluorescent Sensor with Fast Response. *Ind. Eng. Chem. Res.* **2015**, *54* (36), 8842–8846. https://doi.org/10.1021/acs.iecr.5b01904.
(1447) Li, G.; Lin, Q.; Sun, L.; Feng, C.; Zhang, P.; Yu, B.; Chen, Y.; Wen, Y.; Wang, H.; Ji, L.; Chao, H. A Mitochondrial Targeted Two-Photon Iridium(III) Phosphorescent Probe for Selective Detection of Hypochlorite in Live Cells and in Vivo. *Biomaterials* **2015**, *53*, 285–295. https://doi.org/10.1016/j.biomaterials.2015.02.106.
(1448) Xiong, K.; Huo, F.; Yin, C.; Chu, Y.; Yang, Y.; Chao, J.; Zheng, A. A Novel Recognition Mechanism Supported by Experiment and Theoretical Calculation for Hypochlorites Recognition and Its Practical Application. *Sens. Actuators B Chem.* **2016**, *224*, 307–314. https://doi.org/10.1016/j.snb.2015.10.047.
(1449) Jiang, Y.; Wu, S.; Jin, C.; Wang, B.; Shen, J. Novel Diaminomaleonitrile-Based Fluorescent Probe for Ratiometric Detection and Bioimaging of Hypochlorite. *Sens. Actuators B Chem.* **2018**, *265*, 365–370. https://doi.org/10.1016/j.snb.2018.01.202.
(1450) Wang, L.-L.; Bai, J.-Y.; Li, X.-F.; Zheng, M.-H.; Miao, Y.; Jin, J.-Y. Simultaneous Imaging of Hypochlorous Acid and Nitric Oxide in Live Cells Based on a Dual-Channel Fluorescent Probe. *Anal. Chim. Acta* **2021**, *1183*, 338980. https://doi.org/10.1016/j.aca.2021.338980.
(1451) Lv, J.; Wang, F.; Wei, T.; Chen, X. Highly Sensitive and Selective Fluorescent Probes for the Detection of HOCl/OCl^- Based on Fluorescein Derivatives. *Ind. Eng. Chem. Res.* **2017**, *56* (13), 3757–3764. https://doi.org/10.1021/acs.iecr.7b00381.
(1452) Ponnuvel, K.; Ramamoorthy, J.; Sivaraman, G.; Padmini, V. Merocyanine Dye-Based Fluorescent Chemosensor for Highly Selective and Sensitive Detection of Hypochlorous Acid and Imaging in Live Cells. *ChemistrySelect* **2018**, *3* (1), 91–95. https://doi.org/10.1002/slct.201701833.
(1453) Santra, M.; Sarkar, S.; Jun, Y. W.; Reo, Y. J.; Ahn, K. H. Dual Probing of Redox Species, NAD(P)H and HOCl, with a Benzo[a]Phenoxazine Based Far Red-Emitting Dye. *Tetrahedron Lett.* **2018**, *59* (33), 3210–3213. https://doi.org/10.1016/j.tetlet.2018.07.031.
(1454) Yang, Y.; Zhang, D.; Xu, M.; Wang, J.; Chen, J.; Wang, L. An NBD–NH_2 Fluorescent Probe for Bioimaging: Existence of a Specific Detection of ClO^-. *Monatshefte Für Chem. - Chem. Mon.* **2018**, *149* (6), 1003–1008. https://doi.org/10.1007/s00706-018-2143-9.
(1455) Jin, L.; Xu, M.; Jiang, H.; Wang, W.; Wang, Q. A Simple Fluorescein Derived Colorimetric and Fluorescent 'off–on' Sensor for the Detection of Hypochlorite. *Anal. Methods* **2018**, *10* (37), 4562–4569. https://doi.org/10.1039/C8AY01489B.
(1456) Zhu, B.; Wu, L.; Zhang, M.; Wang, Y.; Liu, C.; Wang, Z.; Duan, Q.; Jia, P. A Highly Specific and Ultrasensitive Near-Infrared Fluorescent Probe for Imaging Basal Hypochlorite in the Mitochondria of Living Cells. *Biosens. Bioelectron.* **2018**, *107*, 218–223. https://doi.org/10.1016/j.bios.2018.02.023.

(1457) Wang, X.; Xu, C.; Song, H.; Liu, X.; Xie, X.; Pang, X.; Zhou, Y. Red-Emitting Fluorescent Probe for Selective and Sensitive Determination Hypochlorite in Living Cells. *J. Lumin.* **2019**, *210*, 472–478. https://doi.org/10.1016/j.jlumin.2019.03.006.
(1458) Mao, G.-J.; Gao, G.-Q.; Liang, Z.-Z.; Wang, Y.-Y.; Su, L.; Wang, Z.-X.; Zhang, H.; Ma, Q.-J.; Zhang, G. A Mitochondria-Targetable Two-Photon Fluorescent Probe with a Far-Red to near-Infrared Emission for Sensing Hypochlorite in Biosystems. *Anal. Chim. Acta* **2019**, *1081*, 184–192. https://doi.org/10.1016/j.aca.2019.07.040.
(1459) Lee, S. C.; Park, S.; So, H.; Lee, G.; Kim, K.-T.; Kim, C. An Acridine-Based Fluorescent Sensor for Monitoring ClO^- in Water Samples and Zebrafish. *Sensors* **2020**, *20* (17), 4764. https://doi.org/10.3390/s20174764.
(1460) Xu, L.; Wu, M.; Zhao, L.; Han, H.; Zhang, S.; Ma, P.; Sun, Y.; Wang, X.; Song, D. A Novel Highly Sensitive and Near-Infrared Fluorescent Probe for Detecting Hypochlorite and Its Application in Actual Water Sample and Bioimaging. *Talanta* **2020**, *215*, 120892. https://doi.org/10.1016/j.talanta.2020.120892.
(1461) Gao, G.; Zhao, P.; Zhou, J.; Guo, B.; Gong, H.; Fu, B. A Commercially Available NIR Fluorescence Probe for the Detection of Hypochlorite and Its Application in Cell Imaging. *Microchem. J.* **2020**, *159*, 105311. https://doi.org/10.1016/j.microc.2020.105311.
(1462) Zhang, A.-B.; Jin, L.; Wang, Q.-M.; Wang, W.-L.; Chen, Y.-L. Two Smart Coumarin-Based Fluorescent Probes with AIE Effect for Sensing ClO- and Imaging in Living Cells. *Spectrochim. Acta. A. Mol. Biomol. Spectrosc.* **2022**, *283*, 121690. https://doi.org/10.1016/j.saa.2022.121690.
(1463) Zeng, X.; Chen, J.; Yu, S.; Liu, Z.; Ma, M. The Development of a 4-Aminonaphthalimide-Based Highly Selective Fluorescent Probe for Rapid Detection of HOCl. *J. Fluoresc.* **2022**, *32* (5), 1843–1849. https://doi.org/10.1007/s10895-022-02996-1.
(1464) Mishra, A.; Dayal, N.; Beck-Speier, I. Effect of Sulphite on the Oxidative Metabolism of Human Neutrophils: Studies with Lucigenin- and Luminol-Dependent Chemiluminescence. *J. Biolumin. Chemilumin.* **1995**, *10* (1), 9–19. https://doi.org/10.1002/bio.1170100103.
(1465) Austin, K. A.; Paynter, K. T. Characterization of the Chemiluminescence Measured in Hemocytes of the Eastern Oyster, Crassostrea Virginica. *J. Exp. Zool.* **1995**, *273* (6), 461–471. https://doi.org/10.1002/jez.1402730603.
(1466) Daniels, I.; Bhatia, K. S.; Porter, C. J.; Lindsay, M. A.; Morgan, A. G.; Burden, R. P.; Fletcher, J. Hydrogen Peroxide Generation by Polymorphonuclear Leukocytes Exposed to Peritoneal Dialysis Effluent. *Clin. Diagn. Lab. Immunol.* **1996**, *3* (6), 682–688. https://doi.org/10.1128/cdli.3.6.682-688.1996.
(1467) Liu, Y.; Sun, Y.; Du, J.; Lv, X.; Zhao, Y.; Chen, M.; Wang, P.; Guo, W. Highly Sensitive and Selective Turn-on Fluorescent and Chromogenic Probe for Cu^{2+} and ClO^- Based on a N-Picolinyl Rhodamine B-Hydrazide Derivative. *Org. Biomol. Chem.* **2010**, *9* (2), 432–437. https://doi.org/10.1039/C0OB00411A.
(1468) Goswami, S.; Das, S.; Aich, K.; Nandi, P. K.; Ghoshal, K.; Quah, C. K.; Bhattacharyya, M.; Fun, H.-K.; Abdel-Aziz, H. A. A Rhodamine–Quinoline Based Chemodosimeter Capable of Recognising Endogenous OCl− in Human Blood Cells. *RSC Adv.* **2014**, *4* (47), 24881–24886. https://doi.org/10.1039/C4RA03200D.
(1469) Hou, J.-T.; Wu, M.-Y.; Li, K.; Yang, J.; Yu, K.-K.; Xie, Y.-M.; Yu, X.-Q. Mitochondria-Targeted Colorimetric and Fluorescent Probes for Hypochlorite and Their Applications for in Vivo Imaging. *Chem. Commun.* **2014**, *50* (63), 8640–8643. https://doi.org/10.1039/C4CC02673J.
(1470) Goswami, S.; Das, A. K.; Manna, A.; Maity, A. K.; Saha, P.; Quah, C. K.; Fun, H.-K.; Abdel-Aziz, H. A. Nanomolar Detection of Hypochlorite by a Rhodamine-Based Chiral Hydrazide in Absolute Aqueous Media: Application in Tap Water Analysis with Live-Cell Imaging. *Anal. Chem.* **2014**, *86* (13), 6315–6322. https://doi.org/10.1021/ac500418k.

(1471) Ren, M.; Deng, B.; Zhou, K.; Kong, X.; Wang, J.-Y.; Xu, G.; Lin, W. A Lysosome-Targeted and Ratiometric Fluorescent Probe for Imaging Exogenous and Endogenous Hypochlorous Acid in Living Cells. *J. Mater. Chem. B* **2016**, *4* (27), 4739–4745. https://doi.org/10.1039/C6TB01085G.
(1472) Ghoshal, K.; Das, S.; Aich, K.; Goswami, S.; Chowdhury, S.; Bhattacharyya, M. A Novel Sensor to Estimate the Prevalence of Hypochlorous (HOCl) Toxicity in Individuals with Type 2 Diabetes and Dyslipidemia. *Clin. Chim. Acta* **2016**, *458*, 144–153. https://doi.org/10.1016/j.cca.2016.05.006.
(1473) Wang, H.; Gravot, G.; Liang, X.; Thorling, C.; Zhang, R.; Liu, X.; Roberts, M. In Vivo Visualizing the Generation of Hypochlorous Acid Using a Novel Selective Fluorescent Probe. In *European Microscopy Congress 2016: Proceedings*; John Wiley & Sons, Ltd, 2016; pp 1022–1023. https://doi.org/10.1002/9783527808465.EMC2016.5886.
(1474) Long, Y.; Zhou, J.; Yang, M.; Liu, X.; Zhang, M.; Yang, B. Highly Selective, Sensitive and Naked-Eye Fluorescence Probes for the Direct Detection of Hypochlorite Anion and Their Application in Biological Environments. *Sens. Actuators B Chem.* **2016**, *232*, 327–335. https://doi.org/10.1016/j.snb.2016.03.157.
(1475) Ren, M.; Nie, J.; Deng, B.; Zhou, K.; Wang, J.-Y.; Lin, W. A Fluorescent Probe for Ratiometric Imaging of Exogenous and Intracellular Formed Hypochlorous Acid in Lysosomes. *New J. Chem.* **2017**, *41* (13), 5259–5262. https://doi.org/10.1039/C7NJ00949F.
(1476) Zhang, F.; Liang, X.; Zhang, W.; Wang, Y.-L.; Wang, H.; Mohammed, Y. H.; Song, B.; Zhang, R.; Yuan, J. A Unique Iridium(III) Complex-Based Chemosensor for Multi-Signal Detection and Multi-Channel Imaging of Hypochlorous Acid in Liver Injury. *Biosens. Bioelectron.* **2017**, *87*, 1005–1011. https://doi.org/10.1016/j.bios.2016.09.067.
(1477) Zhan, Z.; Liu, R.; Chai, L.; Li, Q.; Zhang, K.; Lv, Y. Turn-on Fluorescent Probe for Exogenous and Endogenous Imaging of Hypochlorous Acid in Living Cells and Quantitative Application in Flow Cytometry. *Anal. Chem.* **2017**, *89* (17), 9544–9551. https://doi.org/10.1021/acs.analchem.7b02613.
(1478) Li, K.; Hou, J.-T.; Yang, J.; Yu, X.-Q. A Tumor-Specific and Mitochondria-Targeted Fluorescent Probe for Real-Time Sensing of Hypochlorite in Living Cells. *Chem. Commun.* **2017**, *53* (40), 5539–5541. https://doi.org/10.1039/C7CC01679D.
(1479) Shen, S.-L.; Zhang, X.-F.; Ge, Y.-Q.; Zhu, Y.; Cao, X.-Q. A Mitochondria-Targeting Ratiometric Fluorescent Probe for the Detection of Hypochlorite Based on the FRET Strategy. *RSC Adv.* **2017**, *7* (87), 55296–55300. https://doi.org/10.1039/C7RA11086C.
(1480) Shen, S.-L.; Huang, X.-Q.; Zhang, Y.-Y.; Zhu, Y.; Hou, C.; Ge, Y.-Q.; Cao, X.-Q. Ratiometric Fluorescent Probe for the Detection of HOCl in Lysosomes Based on FRET Strategy. *Sens. Actuators B Chem.* **2018**, *263*, 252–257. https://doi.org/10.1016/j.snb.2018.02.121.
(1481) Song, G.-J.; Ma, H.-L.; Luo, J.; Cao, X.-Q.; Zhao, B.-X. A New Ratiometric Fluorescent Probe for Sensing HOCl Based on TBET in Real Time. *Dyes Pigments* **2018**, *148*, 206–211. https://doi.org/10.1016/j.dyepig.2017.09.022.
(1482) Yang, C.; Zuo, M.; Hu, X.; Chen, X.; Zhang, D.; Qi, Z.; Zhao, X.; Zuo, H. A Novel Rhodamine-Based Fluorescent Probe for Selective Detection of ClO– and Its Application in Living Cell Imaging. *Can. J. Chem.* **2018**, *96* (12), 1129–1133. https://doi.org/10.1139/cjc-2018-0123.
(1483) Li, T.; Wang, L.; Lin, S.; Xu, X.; Liu, M.; Shen, S.; Yan, Z.; Mo, R. Rational Design and Bioimaging Applications of Highly Specific “Turn-On” Fluorescent Probe for Hypochlorite. *Bioconjug. Chem.* **2018**, *29* (8), 2838–2845. https://doi.org/10.1021/acs.bioconjchem.8b00430.
(1484) Xue, L.; Feng, Y.; Song, Y.; Wang, R.; Liu, D.; Du, J.; Yang, Q.; Li, Y. A Highly Selective and Sensitive Ratiometric Fluorescent Probe for Hypochlorite and Its Application. *Chem. Res. Chin. Univ.* **2018**, *34* (4), 536–540. https://doi.org/10.1007/s40242-018-8028-y.

(1485) Xia, Y.; Liu, X.; Wang, D.; Wang, Z.; Liu, Q.; Yu, H.; Zhang, M.; Song, Y. A Fluorometric and Mitochondrion-Targetable Probe for Rapid, Naked-Eye Test of Hypochlorite in Real Samples. *Chin. Chem. Lett.* **2018**, *29* (10), 1517–1520. https://doi.org/10.1016/j.cclet.2018.01.054.
(1486) Duan, Q.; Zheng, G.; Li, Z.; Cheng, K.; Zhang, J.; Yang, L.; Jiang, Y.; Zhang, H.; He, J.; Sun, H. An Ultra-Sensitive Ratiometric Fluorescent Probe for Hypochlorous Acid Detection by the Synergistic Effect of AIE and TBET and Its Application of Detecting Exogenous/Endogenous HOCl in Living Cells. *J. Mater. Chem. B* **2019**, *7* (33), 5125–5131. https://doi.org/10.1039/C9TB01279F.
(1487) Hu, J.; Zhang, X.; Liu, T.; Gao, H.-W.; Lu, S.; Uvdal, K.; Hu, Z. Ratiometric Fluorogenic Determination of Endogenous Hypochlorous Acid in Living Cells. *Spectrochim. Acta. A. Mol. Biomol. Spectrosc.* **2019**, *219*, 232–239. https://doi.org/10.1016/j.saa.2019.04.024.
(1488) Shen, S.-L.; Huang, X.-Q.; Jiang, H.-L.; Lin, X.-H.; Cao, X.-Q. A Rhodamine B-Based Probe for the Detection of HOCl in Lysosomes. *Anal. Chim. Acta* **2019**, *1046*, 185–191. https://doi.org/10.1016/j.aca.2018.09.054.
(1489) Liu, L.; Wei, P.; Yuan, W.; Liu, Z.; Xue, F.; Zhang, X.; Yi, T. Detecting Basal Myeloperoxidase Activity in Living Systems with a Near-Infrared Emissive “Turn-On” Probe. *Anal. Chem.* **2020**, *92* (16), 10971–10978. https://doi.org/10.1021/acs.analchem.9b04601.
(1490) Zhu, N.; Guo, X.; Pang, S.; Chang, Y.; Liu, X.; Shi, Z.; Feng, S. Mitochondria-Immobilized Unimolecular Fluorescent Probe for Multiplexing Imaging of Living Cancer Cells. *Anal. Chem.* **2020**, *92* (16), 11103–11110. https://doi.org/10.1021/acs.analchem.0c01046.
(1491) Li, M.-Y.; Li, K.; Liu, Y.-H.; Zhang, H.; Yu, K.-K.; Liu, X.; Yu, X.-Q. Mitochondria-Immobilized Fluorescent Probe for the Detection of Hypochlorite in Living Cells, Tissues, and Zebrafishes. *Anal. Chem.* **2020**, *92* (4), 3262–3269. https://doi.org/10.1021/acs.analchem.9b05102.
(1492) Wang, T.-R.; Zhang, X.-F.; Huang, X.-Q.; Cao, X.-Q.; Shen, S.-L. Rapid and Selective Visualization of Mitochondrial Hypochlorite by a Red Region Water-Soluble Fluorescence Probe. *Spectrochim. Acta. A. Mol. Biomol. Spectrosc.* **2021**, *247*, 119115. https://doi.org/10.1016/j.saa.2020.119115.
(1493) Hu, W.; Qiang, T.; Li, C.; Ren, L.; Cheng, F.; Wang, B.; Li, M.; Song, X.; D. James, T. Imaging of Hypochlorous Acid in Mitochondria Using an Asymmetric Near-Infrared Fluorescent Probe with Large Stokes Shift. *Chem. Sci.* **2022**, *13* (37), 11140–11149. https://doi.org/10.1039/D2SC03833A.
(1494) He, M.; Ye, M.; Li, B.; Wu, T.; Lu, C.; Liu, P.; Li, H.; Zhou, X.; Wang, Y.; Liang, T.; Li, H.; Li, C. Bioimaging of Hypochlorous Acid Using a Near-Infrared Fluorescent Probe Derived from Rhodamine Dye with a Large Stokes Shift. *Sens. Actuators B Chem.* **2022**, *364*, 131868. https://doi.org/10.1016/j.snb.2022.131868.
(1495) Zhang, H.; Li, L.-L.; Shi, L.; Chen, S.-Y.; Li, K.; Yu, X.-Q. An ‘AND’-Based Ratiometric Fluorescence Probe for the Sequential Detection of Biothiols and Hypochlorous Acid. *Chem. Commun.* **2022**, *58* (99), 13720–13723. https://doi.org/10.1039/D2CC05782D.
(1496) Zhou, Y.; Zeng, J.; Yang, Q.; Zhou, L. Rational Construction of a Fluorescent Sensor for Simultaneous Detection and Imaging of Hypochlorous Acid and Peroxynitrite in Living Cells, Tissues and Inflammatory Rat Models. *Spectrochim. Acta. A. Mol. Biomol. Spectrosc.* **2022**, *282*, 121691. https://doi.org/10.1016/j.saa.2022.121691.
(1497) Hou, J.-T.; Li, K.; Yang, J.; Yu, K.-K.; Liao, Y.-X.; Ran, Y.-Z.; Liu, Y.-H.; Zhou, X.-D.; Yu, X.-Q. A Ratiometric Fluorescent Probe for in Situ Quantification of Basal Mitochondrial Hypochlorite in Cancer Cells. *Chem. Commun.* **2015**, *51* (31), 6781–6784. https://doi.org/10.1039/C5CC01217A.
(1498) Peng, P.; Li, H.; Bai, L.; Wang, L.; Chen, B.; Yu, C.; Zhang, C.; Ge, J.; Li, L.; Huang, W. Photocontrollable Fluorogenic Probe for Visualizing Near-Membrane Hypochlorite in Live Cells. *ChemistrySelect* **2018**, *3* (21), 5981–5986. https://doi.org/10.1002/slct.201800777.

(1499) Liu, Z.; Gao, K.; Wang, B.; Yan, H.; Xing, P.; Zhong, C.; Xu, Y.; Li, H.; Chen, J.; Wang, W.; Sun, S. A Dinuclear Ruthenium(II) Complex as Turn-on Luminescent Probe for Hypochlorous Acid and Its Application for in Vivo Imaging. *Sci. Rep.* **2016**, *6* (1), 29065. https://doi.org/10.1038/srep29065.
(1500) Wang, J.; Ni, Y.; Shao, S. A Reversible Fluorescence Probe for Detection of ClO−/AA Redox Cycle in Aqueous Solution and in Living Cells. *Talanta* **2016**, *147*, 468–472. https://doi.org/10.1016/j.talanta.2015.10.026.
(1501) He, M.; Sun, H.; Wei, J.; Zhang, R.; Han, X.; Ni, Z. A Highly Sensitive, Fast Responsive and Reversible Naphthalimide-Based Fluorescent Probe for Hypochlorous Acid and Ascorbic Acid in Aqueous Solution and Living Cells. *Spectrochim. Acta. A. Mol. Biomol. Spectrosc.* **2021**, *247*, 119138. https://doi.org/10.1016/j.saa.2020.119138.
(1502) Liu, Q.; Liu, C.; He, S.; Zhao, L.; Zeng, X.; Zhou, J.; Link to external site, this link will open in a new tab; Gong, J. A New Phenylazo-Based Fluorescent Probe for Sensitive Detection of Hypochlorous Acid in Aqueous Solution. *Molecules* **2022**, *27* (9), 2978. https://doi.org/10.3390/molecules27092978.
(1503) An, Z.; Zhao, Z.; Zhao, L.; Yue, Q.; Li, K.; Zhao, B.; Miao, J.; Su, L. The Novel HOCl Fluorescent Probe CAN Induced A549 Apoptosis by Inhibiting Chlorination Activity of MPO. *Bioorg. Med. Chem. Lett.* **2020**, *30* (18), 127394. https://doi.org/10.1016/j.bmcl.2020.127394.
(1504) Wang, L.; Liu, J.; Zhao, S.; Zhang, H.; Sun, Y.; Wei, A.; Guo, W. Fluorescence Imaging of Hypochlorous Acid and Peroxynitrite in Vitro and in Vivo with Emission Wavelength beyond 750 nm. *Chem. Commun.* **2020**, *56* (56), 7718–7721. https://doi.org/10.1039/D0CC02322A.
(1505) Samanta, S. K.; Maiti, K.; Manna, S. K.; Ali, S. S.; Guria, U. N.; Ghosh, A.; Datta, P.; Mahapatra, A. K. An Aggregation-Induced Emission (AIE)-Active Fluorescent Chemodosimeter for Selective Sensing of Hypochlorite in Water and Solid State: Endogenous Detection of Hypochlorite in Live Cells. *Dyes Pigments* **2021**, *196*, 109758. https://doi.org/10.1016/j.dyepig.2021.109758.
(1506) Shen, S.-L.; Ning, J.-Y.; Zhang, X.-F.; Miao, J.-Y.; Zhao, B.-X. Through-Bond Energy Transfer-Based Ratiometric Fluorescent Probe for the Imaging of HOCl in Living Cells. *Sens. Actuators B Chem.* **2017**, *244*, 907–913. https://doi.org/10.1016/j.snb.2017.01.073.
(1507) Shen, B.; Qian, Y.; Qi, Z.; Lu, C.; Sun, Q.; Xia, X.; Cui, Y. Near-Infrared BODIPY-Based Two-Photon ClO− Probe Based on Thiosemicarbazide Desulfurization Reaction: Naked-Eye Detection and Mitochondrial Imaging. *J. Mater. Chem. B* **2017**, *5* (29), 5854–5861. https://doi.org/10.1039/C7TB01344B.
(1508) Yuan, Q.; Zhao, Z.-M.; Zhang, Y.-R.; Su, L.; Miao, J.-Y.; Zhao, B.-X. A Lysosome-Targeted Ratiometric Fluorescent Probe for Detection of Hypochlorous Acid in Living Cells. *Sens. Actuators B Chem.* **2017**, *247*, 736–741. https://doi.org/10.1016/j.snb.2017.03.049.
(1509) Yao, S.; Qian, Y. A Naphthalimide–Rhodamine Two-Photon Fluorescent Turn-on Probe for Hypochlorous Acid by Desulfurization-Cyclization and Fluorescence Resonance Energy Transfer. *Sens. Actuators B Chem.* **2017**, *252*, 877–885. https://doi.org/10.1016/j.snb.2017.06.091.
(1510) Han, X.; Tian, C.; Jiang, J.; Yuan, M.-S.; Chen, S.-W.; Xu, J.; Li, T.; Wang, J. Two Ratiometric Fluorescent Probes for Hypochlorous Acid Detection and Imaging in Living Cells. *Talanta* **2018**, *186*, 65–72. https://doi.org/10.1016/j.talanta.2018.04.015.
(1511)Li, L.; Wang, S.; Lan, H.; Gong, G.; Zhu, Y.; Tse, Y. C.; Wong, K. M.-C. Rhodol Derivatives as Selective Fluorescent Probes for the Detection of HgII Ions and the Bioimaging of Hypochlorous Acid. *ChemistryOpen* **2018**, *7* (2), 136–143. https://doi.org/10.1002/open.201700154.
(1512) Wang, L.; Li, W.; Zhi, W.; Ye, D.; Zhang, W.; Ni, L. Rapid Detection of Hypochlorite by a Coumarin-Based Hydrazide in Aqueous Solution and Its Application in Live-Cell Imaging.

Sens. Actuators B Chem. **2018**, *255*, 1112–1118. https://doi.org/10.1016/j.snb.2017.08.039.
(1513) Mao, G.-J.; Liang, Z.-Z.; Bi, J.; Zhang, H.; Meng, H.-M.; Su, L.; Gong, Y.-J.; Feng, S.; Zhang, G. A Near-Infrared Fluorescent Probe Based on Photostable Si-Rhodamine for Imaging Hypochlorous Acid during Lysosome-Involved Inflammatory Response. *Anal. Chim. Acta* **2019**, *1048*, 143–153. https://doi.org/10.1016/j.aca.2018.10.014.
(1514) Meng, H.; Huang, X.-Q.; Lin, Y.; Yang, D.-Y.; Lv, Y.-J.; Cao, X.-Q.; Zhang, G.-X.; Dong, J.; Shen, S.-L. A New Ratiometric Fluorescent Probe for Sensing Lysosomal HOCl Based on Fluorescence Resonance Energy Transfer Strategy. *Spectrochim. Acta. A. Mol. Biomol. Spectrosc.* **2019**, *223*, 117355. https://doi.org/10.1016/j.saa.2019.117355.
(1515) Wang, Q.; Jin, L.; Wang, W.; Dai, L.; Tan, X.; Zhao, C. Two Coumarin-Based Turn-on Fluorescent Probes Based on for Hypochlorous Acid Detection and Imaging in Living Cells. *Spectrochim. Acta. A. Mol. Biomol. Spectrosc.* **2019**, *211*, 239–245. https://doi.org/10.1016/j.saa.2018.12.019.
(1516) Yang, J.; Fan, M.; Sun, Y.; Zhang, M.; Xue, Y.; Zhang, D.; Wang, T.; Cui, X. A Near-Infrared Fluorescent Probe Based on Phosphorus-Substituted Rhodamine for Deep Imaging of Endogenous Hypochlorous Acid in Vivo. *Sens. Actuators B Chem.* **2020**, *307*, 127652. https://doi.org/10.1016/j.snb.2019.127652.
(1517) Zhang, W.; Wang, H.; Li, F.; Chen, Y.; Kwok, R. T. K.; Huang, Y.; Zhang, J.; Hou, J.; Tang, B. Z. A Ratiometric Fluorescent Probe Based on AIEgen for Detecting HClO in Living Cells. *Chem. Commun.* **2020**, *56* (93), 14613–14616. https://doi.org/10.1039/D0CC06582J.
(1518) Ma, Z.; Chen, X.; Wang, C.; Lv, Q. A Novel Ratiometric Fluorescence Probe for Hypochlorite Detection and Its Application in Cell Imaging. *J. Mol. Struct.* **2020**, *1221*, 128812. https://doi.org/10.1016/j.molstruc.2020.128812.
(1519) Mao, G.-J.; Wang, Y.-Y.; Dong, W.-P.; Meng, H.-M.; Wang, Q.-Q.; Luo, X.-F.; Li, Y.; Zhang, G. A Lysosome-Targetable Two-Photon Excited near-Infrared Fluorescent Probe for Visualizing Hypochlorous Acid-Involved Arthritis and Its Treatment. *Spectrochim. Acta. A. Mol. Biomol. Spectrosc.* **2021**, *249*, 119326. https://doi.org/10.1016/j.saa.2020.119326.
(1520) Ruan, S.; Wu, S.; Yang, L.; Li, M.; Zhang, Y.; Wang, Z.; Wang, S. A Novel Turn-on Fluorescent Probe Based on Berberine for Detecting Hg2+ and ClO− with the Different Fluorescence Signals. *Microchem. J.* **2021**, *166*, 106199. https://doi.org/10.1016/j.microc.2021.106199.
(1521) Wang, Q.-Q.; Wang, Y.-Y.; Li, Y.; Zhang, S.-Y.; Guo, X.-Y.; Zha, W.-K.; Li, W.-J.; Mao, G.-J. A Lysosome-Targetable Fluorescent Probe Based on HClO-Mediated Cyclization Reaction for Imaging of Hypochlorous Acid. *Anal. Sci.* **2022**, *38* (1), 175–182. https://doi.org/10.2116/analsci.21P264.
(1522) Ai, Y.; Zhu, Z.; Ding, H.; Fan, C.; Liu, G.; Pu, S. Development of Dual-Fluorophore and Dual-Site Multifunctional Fluorescent Probe for Detecting HClO and H_2S Based on Rhodamine-Coumarin Units. *J. Photochem. Photobiol. Chem.* **2022**, *433*, 114144. https://doi.org/10.1016/j.jphotochem.2022.114144.
(1523) Jin, X.; Hao, L.; Hu, Y.; She, M.; Shi, Y.; Obst, M.; Li, J.; Shi, Z. Two Novel Fluorescein-Based Fluorescent Probes for Hypochlorite and Its Real Applications in Tap Water and Biological Imaging. *Sens. Actuators B Chem.* **2013**, *186*, 56–60. https://doi.org/10.1016/j.snb.2013.05.079.
(1524) Yang, Z.; Wang, M.; She, M.; Yin, B.; Huang, Y.; Liu, P.; Li, J.; Zhang, S. New Aliphatic and Aromatic Dialdehyde Bridged Turn-on Probes for Hypochlorite Detection in Biological Samples Based on Bis(Fluorescein). *Sens. Actuators B Chem.* **2014**, *202*, 656–662. https://doi.org/10.1016/j.snb.2014.05.130.
(1525) Wang, B.; Chen, D.; Kambam, S.; Wang, F.; Wang, Y.; Zhang, W.; Yin, J.; Chen, H.; Chen, X. A Highly Specific Fluorescent Probe for Hypochlorite Based on Fluorescein Derivative

and Its Endogenous Imaging in Living Cells. *Dyes Pigments* **2015**, *120*, 22–29. https://doi.org/10.1016/j.dyepig.2015.03.022.
(1526) Zang, L.; Liang, C.; Wang, Y.; Bu, W.; Sun, H.; Jiang, S. A Highly Specific Pyrene-Based Fluorescent Probe for Hypochlorite and Its Application in Cell Imaging. *Sens. Actuators B Chem.* **2015**, *211*, 164–169. https://doi.org/10.1016/j.snb.2015.01.046.
(1527) Wu, W.-L.; Zhao, Z.-M.; Dai, X.; Su, L.; Zhao, B.-X. A Fast-Response Colorimetric and Fluorescent Probe for Hypochlorite and Its Real Applications in Biological Imaging. *Sens. Actuators B Chem.* **2016**, *232*, 390–395. https://doi.org/10.1016/j.snb.2016.03.155.
(1528) Xing, P.; Gao, K.; Wang, B.; Gao, J.; Yan, H.; Wen, J.; Li, W.; Xu, Y.; Li, H.; Chen, J.; Wang, W.; Sun, S. HEPES Is Not Suitable for Fluorescence Detection of HClO: A Novel Probe for HClO in Absolute PBS. *Chem. Commun.* **2016**, *52* (28), 5064–5066. https://doi.org/10.1039/C6CC00880A.
(1529) High Efficient Approach for Hypochlorous Acid Sensing in Water Samples and Living Cells Based on Acylhydrazone Schiff Base Functionalized Fluorescent Probes. *New J. Chem.* **2017**. https://doi.org/10.1039/C7NJ01383C.
(1530) Jiao, X.; Liu, C.; Wang, Q.; Huang, K.; He, S.; Zhao, L.; Zeng, X. Fluorescence Probe for Hypochlorous Acid in Water and Its Applications for Highly Lysosome-Targetable Live Cell Imaging. *Anal. Chim. Acta* **2017**, *969*, 49–56. https://doi.org/10.1016/j.aca.2017.03.020.
(1531) Liu, X.; Guo, L.; Song, B.; Tang, Z.; Yuan, J. Development of a Novel Europium Complex-Based Luminescent Probe for Time-Gated Luminescence Imaging of Hypochlorous Acid in Living Samples. *Methods Appl. Fluoresc.* **2017**, *5* (1), 014009. https://doi.org/10.1088/2050-6120/aa61af.
(1532) He, Y.; Xu, Y.; Shang, Y.; Zheng, S.; Chen, W.; Pang, Y. An ESIPT-Based Fluorescent Probe for the Determination of Hypochlorous Acid (HClO): Mechanism Study and Its Application in Cell Imaging. *Anal. Bioanal. Chem.* **2018**, *410* (27), 7007–7017. https://doi.org/10.1007/s00216-018-1332-z.
(1533) Li, J.; Yang, X.; Zhang, D.; Liu, Y.; Tang, J.; Li, Y.; Zhao, Y.; Ye, Y. A Fluorescein-Based "Turn-on" Fluorescence Probe for Hypochlorous Acid Detection and Its Application in Cell Imaging. *Sens. Actuators B Chem.* **2018**, *265*, 84–90. https://doi.org/10.1016/j.snb.2018.03.027.
(1534) Xing, P.; Feng, Y.; Niu, Y.; Li, Q.; Zhang, Z.; Dong, L.; Wang, C. A Water-Soluble, Two-Photon Probe for Imaging Endogenous Hypochlorous Acid in Live Tissue. *Chem. – Eur. J.* **2018**, *24* (22), 5748–5753. https://doi.org/10.1002/chem.201800249.
(1535) Jia, H.; Xia, S.; Feng, H.; Meng, Q.; Duan, C.; Zhang, Z.; Zhang, R. A Fast Response Fluorescence Probe Specific for Hypochlorous Acid Detection and Its Applications in Bioimaging. *Org. Biomol. Chem.* **2018**, *16* (12), 2074–2082. https://doi.org/10.1039/C8OB00036K.
(1536) Li, Y.; Tang, Y.; Gao, M.; Wang, Y.; Han, J.; Xia, J.; Wang, L.; Tang, X.; Ni, L. A Sensitive BODIPY-Based Fluorescent Probe Suitable for Hypochlorite Detection in Living Cells. *J. Photochem. Photobiol. Chem.* **2018**, *352*, 65–72. https://doi.org/10.1016/j.jphotochem.2017.10.037.
(1537) Wang, Z.; Zhang, Q.; Liu, J.; Sui, R.; Li, Y.; Li, Y.; Zhang, X.; Yu, H.; Jing, K.; Zhang, M.; Xiao, Y. A Twist Six-Membered Rhodamine-Based Fluorescent Probe for Hypochlorite Detection in Water and Lysosomes of Living Cells. *Anal. Chim. Acta* **2019**, *1082*, 116–125. https://doi.org/10.1016/j.aca.2019.07.046.
(1538) Jin, L.; Tan, X.; Zhao, C.; Wang, Q. Two Highly Sensitive and Selective Coumarin-Based Fluorometric Probes for the Detection of ClO^- and Cell Imaging. *Anal. Methods* **2019**, *11* (14), 1916–1922. https://doi.org/10.1039/C9AY00105K.
(1539) Wang, K.; Xi, D.; Liu, C.; Chen, Y.; Gu, H.; Jiang, L.; Chen, X.; Wang, F. A Ratiometric Benzothiazole-Based Fluorescence Probe for Selectively Recognizing HClO and Its

Practical Applications. *Chin. Chem. Lett.* **2020**, *31* (11), 2955–2959. https://doi.org/10.1016/j.cclet.2020.03.064.
(1540) Naha, S.; Velmathi, S. "ESIPT-AIE" Based Sequential Fluorescence 'on-off' Marker for Endogenous Detection of Hypochlorite and Cobalt (II). *Microchem. J.* **2020**, *153*, 104499. https://doi.org/10.1016/j.microc.2019.104499.
(1541) Zhang, W.; Song, W.; Lin, W. A Novel ER-Targeted Two-Photon Fluorescent Probe for Monitoring Abnormal Concentrations of HClO in Diabetic Mice. *J. Mater. Chem. B* **2021**, *9* (36), 7381–7385. https://doi.org/10.1039/D1TB01327K.
(1542) Zhang, X.; Zhang, F.; Yang, B.; Liu, B. A Simple Strategy for Constructing PET Fluorescent Probe and Its Application in Hypochlorite Detection. *Spectrochim. Acta. A. Mol. Biomol. Spectrosc.* **2021**, *258*, 119827. https://doi.org/10.1016/j.saa.2021.119827.
(1543) Yan, L.; Yang, H.; Li, J.; Zhou, C.; Li, L.; Wu, X.; Lei, C. A near Infrared Fluorescent Probe for Detection and Bioimaging of Zinc Ions and Hypochlorous Acid. *Anal. Chim. Acta* **2022**, *1206*, 339750. https://doi.org/10.1016/j.aca.2022.339750.
(1544) Kim, P. A.; Choe, D.; So, H.; Park, S.; Suh, B.; Jeong, S.; Kim, K.-T.; Kim, C.; Harrison, R. G. A Selective Fluorescence Sensor for Hypochlorite Used for the Detection of Hypochlorite in Zebrafish. *Spectrochim. Acta. A. Mol. Biomol. Spectrosc.* **2021**, *261*, 120059. https://doi.org/10.1016/j.saa.2021.120059.
(1545) Liu, L.; Guo, C.; Zhang, Q.; Xu, P.; Cui, Y.; Zhu, W.; Fang, M.; Li, C. A Hydrazone Dual-Functional Fluorescent Probe Based on Carbazole and Coumarin Groups for the Detection of Cu^{2+} and ClO^{-}: Application in Live Cell Imaging and Actual Water Samples. *J. Photochem. Photobiol. Chem.* **2022**, *423*, 113593. https://doi.org/10.1016/j.jphotochem.2021.113593.
(1546) Zhang, C.; Li, X.; Jiang, Y.; Zhang, Y.; Xie, Y.; Sun, Y.; Liu, C. A Super Large Stokes Shift Ratiometric Fluorescent Probe for Highly Selective Sensing of ClO^{-} in Bio-Imaging and Real Water Samples. *Spectrochim. Acta. A. Mol. Biomol. Spectrosc.* **2022**, *283*, 121736. https://doi.org/10.1016/j.saa.2022.121736.
(1547) Chang, X.-C.; Han, X.-F.; Liu, B.-J.; Jiang, Z.-Y.; Li, S.-Z.; Lv, Y.-M.; Li, A.-L.; Wang, Y.; Wu, W.-N. A Tosylhydrazone-Based Probe for the Ratiometric Fluorescent Detection of Hypochlorite in Endoplasmic Reticulum of Living Cells. *J. Mol. Struct.* **2022**, *1255*, 132382. https://doi.org/10.1016/j.molstruc.2022.132382.
(1548) Zha, J.; Fu, B.; Qin, C.; Zeng, L.; Hu, X. A Ratiometric Fluorescent Probe for Rapid and Sensitive Visualization of Hypochlorite in Living Cells. *RSC Adv.* **2014**, *4* (81), 43110–43113. https://doi.org/10.1039/C4RA07009G.
(1549) Yue, Y.; Huo, F.; Yin, C.; Chao, J.; Yongbin Zhang, Y. Z.; Wei, X. An ICT Based Ultraselective and Sensitive Fluorescent Probe for Detection of HClO in Living Cells. *RSC Adv.* **2015**, *5* (95), 77670–77672. https://doi.org/10.1039/C5RA16097A.
(1550) Li, H.; Guan, L.; Zhang, X.; Yu, H.; Huang, D.; Sun, M.; Wang, S. A Cyanine-Based near-Infrared Fluorescent Probe for Highly Sensitive and Selective Detection of Hypochlorous Acid and Bioimaging. *Talanta* **2016**, *161*, 592–598. https://doi.org/10.1016/j.talanta.2016.09.008.
(1551) Li, J.; Li, P.; Huo, F.; Yin, C.; Liu, T.; Chao, J.; Zhang, Y. Ratiometric Fluorescent Probes for ClO− and in Vivo Applications. *Dyes Pigments* **2016**, *130*, 209–215. https://doi.org/10.1016/j.dyepig.2016.02.024.
(1552) Wang, B.; Wen, J.; Gao, K.; Yan, H.; Xu, Y.; Li, H.; Chen, J.; Wang, W.; Sun, S. Double-Mode Detection of HClO by Naked Eye and Concurrent Fluorescence Increasing in Absolute PBS. *RSC Adv.* **2016**, *6* (42), 35315–35317. https://doi.org/10.1039/C6RA03959F.
(1553) Wang, X.; Song, F.; Peng, X. A Versatile Fluorescent Probe for Imaging Viscosity and Hypochlorite in Living Cells. *Dyes Pigments* **2016**, *125*, 89–94. https://doi.org/10.1016/j.dyepig.2015.10.012.

(1554) Zhang, Z.; Fan, J.; Cheng, G.; Ghazali, S.; Du, J.; Peng, X. Fluorescence Completely Separated Ratiometric Probe for HClO in Lysosomes. *Sens. Actuators B Chem.* **2017**, *246*, 293–299. https://doi.org/10.1016/j.snb.2017.02.081.
(1555) Yu, H.; Wu, Y.; Hu, Y.; Gao, X.; Liang, Q.; Xu, J.; Shao, S. Dual-Functional Fluorescent Probe Responds to Hypochlorous Acid and SO2 Derivatives with Different Fluorescence Signals. *Talanta* **2017**, *165*, 625–631. https://doi.org/10.1016/j.talanta.2017.01.015.
(1556) Chen, Y.; Wei, T.; Zhang, Z.; Zhang, W.; Lv, J.; Chen, T.; Chi, B.; Wang, F.; Chen, X. A Mitochondria-Targeted Fluorescent Probe for Ratiometric Detection of Hypochlorite in Living Cells. *Chin. Chem. Lett.* **2017**, *28* (10), 1957–1960. https://doi.org/10.1016/j.cclet.2017.05.010.
(1557) Wu, W.-L.; Zhao, X.; Xi, L.-L.; Huang, M.-F.; Zeng, W.-H.; Miao, J.-Y.; Zhao, B.-X. A Mitochondria-Targeted Fluorescence Probe for Ratiometric Detection of Endogenous Hypochlorite in the Living Cells. *Anal. Chim. Acta* **2017**, *950*, 178–183. https://doi.org/10.1016/j.aca.2016.11.019.
(1558) Dou, K.; Fu, Q.; Chen, G.; Yu, F.; Liu, Y.; Cao, Z.; Li, G.; Zhao, X.; Xia, L.; Chen, L.; Wang, H.; You, J. A Novel Dual-Ratiometric-Response Fluorescent Probe for SO_2/ClO^- Detection in Cells and in Vivo and Its Application in Exploring the Dichotomous Role of SO_2 under the ClO^- Induced Oxidative Stress. *Biomaterials* **2017**, *133*, 82–93. https://doi.org/10.1016/j.biomaterials.2017.04.024.
(1559) Dou, K.; Chen, G.; Yu, F.; Sun, Z.; Li, G.; Zhao, X.; Chen, L.; You, J. A Two-Photon Ratiometric Fluorescent Probe for the Synergistic Detection of the Mitochondrial SO_2/HClO Crosstalk in Cells and in Vivo. *J. Mater. Chem. B* **2017**, *5* (42), 8389–8398. https://doi.org/10.1039/C7TB01900A.
(1560) Chen, H.; Sun, T.; Qiao, X.-G.; Tang, Q.-O.; Zhao, S.-C.; Zhou, Z. Red-Emitting Fluorescent Probe for Detecting Hypochlorite Acid in Vitro and in Vivo. *Spectrochim. Acta. A. Mol. Biomol. Spectrosc.* **2018**, *204*, 196–202. https://doi.org/10.1016/j.saa.2018.06.037.
(1561) Xi, L.-L.; Guo, X.-F.; Wang, C.-L.; Wu, W.-L.; Huang, M.-F.; Miao, J.-Y.; Zhao, B.-X. A Near-Infrared Ratiometric Fluorescent Probe for Rapid and Selective Detection of Hypochlorous Acid in Aqueous Solution and Living Cells. *Sens. Actuators B Chem.* **2018**, *255*, 666–671. https://doi.org/10.1016/j.snb.2017.08.073.
(1562) Zhang, L.-J.; Zhao, X.; Yang, D.; Jia, Z.-Z.; Han, X.; Sun, L.-Q.; Yu, L.-L.; Liu, J.-T.; He, X.-D.; Miao, J.-Y.; Zhao, B.-X. A New Water-Soluble and Mitochondria-Targeted Fluorescence Probe for Ratiometric Detection of Hypochlorous Acid in Living Cells. *Sens. Actuators B Chem.* **2018**, *276*, 8–12. https://doi.org/10.1016/j.snb.2018.08.071.
(1563) Lv, J.; Chen, Y.; Wang, F.; Wei, T.; Zhang, Z.; Qiang, J.; Chen, X. A Mitochondria-Targeted Fluorescent Probe Based on Fluorescein Derivative for Detection of Hypochlorite in Living Cells. *Dyes Pigments* **2018**, *148*, 353–358. https://doi.org/10.1016/j.dyepig.2017.09.037.
(1564) Zhang, L.-J.; Ning, J.-Y.; Miao, J.-Y.; Liu, J.-T.; Zhao, B.-X. A New Ratiometric Fluorescent Probe for Detecting Endogenous HClO in Living Cells. *New J. Chem.* **2018**, *42* (4), 2989–2993. https://doi.org/10.1039/C7NJ03907G.
(1565) Li, J.-P.; Xia, S.; Zhang, H.; Qu, G.-R.; Guo, H.-M. Three-Input “AND-Type” Fluorescent Logic Gate as Ratio Probe for Specific Imaging of Hypochlorite in Rough Endoplasmic Reticulum. *Sens. Actuators B Chem.* **2018**, *255*, 622–629. https://doi.org/10.1016/j.snb.2017.08.076.
(1566) Wang, X.; Min, J.; Wang, W.; Wang, Y.; Yin, G.; Wang, R. A Novel Porphyrin-Based near-Infrared Fluorescent Probe for Hypochlorite Detection and Its Application in Vitro and in Vivo. *Analyst* **2018**, *143* (11), 2641–2647. https://doi.org/10.1039/C8AN00586A.
(1567) Song, X.; Dong, B.; Kong, X.; Wang, C.; Zhang, N.; Lin, W. Construction of a Ratiometric Fluorescent Probe with an Extremely Large Emission Shift for Imaging Hypochlorite in Living Cells. *Spectrochim. Acta. A. Mol. Biomol. Spectrosc.* **2018**, *188*, 394–399. https://doi.org/10.1016/j.saa.2017.07.011.

(1568) Liu, Z.; Song, F.; Song, B.; Jiao, L.; An, J.; Yuan, J.; Peng, X. A FRET Chemosensor for Hypochlorite with Large Stokes Shifts and Long-Lifetime Emissions. *Sens. Actuators B Chem.* **2018**, *262*, 958–965. https://doi.org/10.1016/j.snb.2018.01.240.
(1569) Feng, H.; Wang, Y.; Liu, J.; Zhang, Z.; Yang, X.; Chen, R.; Meng, Q.; Zhang, R. A Highly Specific Fluorescent Probe for Rapid Detection of Hypochlorous Acid in Vivo and in Water Samples. *J. Mater. Chem. B* **2019**, *7* (24), 3909–3916. https://doi.org/10.1039/C9TB00551J.
(1570) Huang, Y.; Zhang, Y.; Huo, F.; Chao, J.; Yin, C. A Near-Infrared Ratiometric Fluorescent Probe with Large Stokes Based on Isophorone for Rapid Detection of ClO^- and Its Bioimaging in Cell and Mice. *Sens. Actuators B Chem.* **2019**, *287*, 453–458. https://doi.org/10.1016/j.snb.2019.02.075.
(1571) Liu, S.; Yang, D.; Liu, Y.; Pan, H.; Chen, H.; Qu, X.; Li, H. A Dual-Channel and Fast-Response Fluorescent Probe for Selective Detection of HClO and Its Applications in Live Cells. *Sens. Actuators B Chem.* **2019**, *299*, 126937. https://doi.org/10.1016/j.snb.2019.126937.
(1572) Ning, J.; Lin, Z.; Zhao, X.; Zhao, B.; Miao, J. Inhibiting Lysine 353 Oxidation of GRP78 by a Hypochlorous Probe Targeting Endoplasmic Reticulum Promotes Autophagy in Cancer Cells. *Cell Death Dis.* **2019**, *10* (11), 1–16. https://doi.org/10.1038/s41419-019-2095-y.
(1573) Xiong, H.; He, L.; Zhang, Y.; Wang, J.; Song, X.; Yang, Z. A Ratiometric Fluorescent Probe for the Detection of Hypochlorous Acid in Living Cells and Zebra Fish with a Long Wavelength Emission. *Chin. Chem. Lett.* **2019**, *30* (5), 1075–1077. https://doi.org/10.1016/j.cclet.2019.02.008.
(1574) Zhang, Q.; Zhang, P.; Gong, Y.; Ding, C. Two-Photon AIE Based Fluorescent Probe with Large Stokes Shift for Selective and Sensitive Detection and Visualization of Hypochlorite. *Sens. Actuators B Chem.* **2019**, *278*, 73–81. https://doi.org/10.1016/j.snb.2018.09.057.
(1575) Zhong, X.; Zhou, L.; Jin, C.; Wang, B.; Jiang, Y.; Shen, J. A Mitochondria-Target Probe for OCl^- "Naked Eye" Detection and Its Imaging in Living Cell. *Talanta* **2019**, *202*, 369–374. https://doi.org/10.1016/j.talanta.2019.04.062.
(1576) Wu, W.-L.; Ma, H.-L.; Xi, L.-L.; Huang, M.-F.; Wang, K.-M.; Miao, J.-Y.; Zhao, B.-X. A Novel Lipid Droplets-Targeting Ratiometric Fluorescence Probe for Hypochlorous Acid in Living Cells. *Talanta* **2019**, *194*, 308–313. https://doi.org/10.1016/j.talanta.2018.10.006.
(1577) Shangguan, M.; Jiang, X.; Lu, Z.; Zou, W.; Chen, Y.; Xu, P.; Pan, Y.; Hou, L. A Coumarin-Based Fluorescent Probe for Hypochlorite Ion Detection in Environmental Water Samples and Living Cells. *Talanta* **2019**, *202*, 303–307. https://doi.org/10.1016/j.talanta.2019.04.074.
(1578) Jantra, S.; Butta, P.; Jithavech, P.; Rojsitthisak, P.; Palaga, T.; Rashatasakhon, P.; Sukwattanasinitt, M.; Wacharasindhu, S. "Turn on" Orange Fluorescent Probe Based on Styryl-BODIPY for Detection of Hypochlorite and Its Application in Live Cell Imaging. *Dyes Pigments* **2019**, *162*, 189–195. https://doi.org/10.1016/j.dyepig.2018.10.007.
(1579) Ma, Z.; Wang, X.; Wang, C.; Chen, X.; Lv, Q. A Sensitive and Selective Fluorescence Probe for Detection of Hypochlorite (OCl^-) and Its Bioimaging in Live Cells. *Spectrochim. Acta. A. Mol. Biomol. Spectrosc.* **2019**, *213*, 370–374. https://doi.org/10.1016/j.saa.2019.01.083.
(1580) Lu, Z.; Shangguan, M.; Jiang, X.; Xu, P.; Hou, L.; Wang, T. A Water-Soluble Cyclometalated Iridium(III) Complex with Fluorescent Sensing Capability for Hypochlorite. *Dyes Pigments* **2019**, *171*, 107715. https://doi.org/10.1016/j.dyepig.2019.107715.
(1581) Gu, J.; Li, X.; Zhou, Z.; Liao, R.; Gao, J.; Tang, Y.; Wang, Q. Synergistic Regulation of Effective Detection for Hypochlorite Based on a Dual-Mode Probe by Employing Aggregation Induced Emission (AIE) and Intramolecular Charge Transfer (ICT) Effects. *Chem. Eng. J.* **2019**, *368*, 157–164. https://doi.org/10.1016/j.cej.2019.02.175.

(1582) Xiong, K.; Huo, F.; Zhang, Y.; Wen, Y.; Yin, C. A NIR Ratiometric Fluorescent Probe for the 'Naked-Eye' Detection of Endogenous Hypochlorous Acid in Practical Samples. *Anal. Methods* **2019**, *11* (13), 1751–1756. https://doi.org/10.1039/C9AY00011A.
(1583) Han, X.; Ma, Y.; Chen, Y.; Wang, X.; Wang, Z. Enhancement of the Aggregation-Induced Emission by Hydrogen Bond for Visualizing Hypochlorous Acid in an Inflammation Model and a Hepatocellular Carcinoma Model. *Anal. Chem.* **2020**, *92* (3), 2830–2838. https://doi.org/10.1021/acs.analchem.9b05347.
(1584) Huang, Y.; Zhang, Y.; Huo, F.; Liu, Y.; Yin, C. Mitochondrial-Targeted near-Infrared "Dual Mode" Fluorescent Dyes with Large Stokes Shift for Detection of Hypochlorous Acid and Its Bioimaging in Cell and Mice. *Dyes Pigments* **2020**, *179*, 108387. https://doi.org/10.1016/j.dyepig.2020.108387.
(1585) Shi, Y.; Huo, F.; Zhang, Y.; Yin, C. The Reduction Performance of Double Bonds Regulated by the Competition of Push–Pull Electron Groups to Realize the Colorimetric and Fluorescence Recognition of Hypochlorous Acid. *Analyst* **2020**, *145* (22), 7297–7302. https://doi.org/10.1039/D0AN01551B.
(1586) Li, M.; Chao, J.; Liu, Y.; Xu, M.; Zhang, Y.; Huo, F.; Wang, J.; Yin, C. Fast Detecting Hypochlorous Acid Based on Electron-Withdrawing Group Promoted Oxidation and Its Biological Applications in Cells and Root Tips of Plants. *Spectrochim. Acta. A. Mol. Biomol. Spectrosc.* **2020**, *229*, 118001. https://doi.org/10.1016/j.saa.2019.118001.
(1587) Nie, J.; Sun, H.; Miao, B.; Ni, Z. A Novel Coumarin-Based Ratiometric near-Infrared Fluorescence Probe for Hypochlorous Acid in Living Cells. *Dyes Pigments* **2020**, *181*, 108590. https://doi.org/10.1016/j.dyepig.2020.108590.
(1588) Wang, B.; Zhang, F.; Wang, S.; Yang, R.; Chen, C.; Zhao, W. Imaging Endogenous HClO in Atherosclerosis Using a Novel Fast-Response Fluorescence Probe. *Chem. Commun.* **2020**, *56* (17), 2598–2601. https://doi.org/10.1039/C9CC07256J.
(1589) Gao, L.-L.; Wang, W.-W.; Wu, W.-N.; Wang, Y.; Zhao, X.-L.; Fan, Y.-C.; Li, H.-J.; Xu, Z.-H. Sensitive and Selective Fluorescent Probe for Hypochlorite in 100% Aqueous Solution and Its Application for Lysosome-Targetable Cell Imaging. *Spectrochim. Acta. A. Mol. Biomol. Spectrosc.* **2020**, *231*, 118110. https://doi.org/10.1016/j.saa.2020.118110.
(1590) Lin, X.; Qin, W.; Chen, Y.; Bao, L.; Li, N.; Wang, S.; Liu, K.; Kong, F.; Yi, T. Construction of a Multi-Signal near-Infrared Fluorescent Probe for Sensing of Hypochlorite Concentration Fluctuation in Living Animals. *Sens. Actuators B Chem.* **2020**, *324*, 128732. https://doi.org/10.1016/j.snb.2020.128732.
(1591) Chao, J.; Duan, Y.; Liu, Y.; Xu, M.; Zhang, Y.; Huo, F.; Zhang, T.; Wang, J.; Yin, C. Carbazole-Conjugated-Coumarin by Enone Realizing Ratiometric and Colorimetric Detection of Hypochlorite Ions and Its Application in Plants and Animals. *Spectrochim. Acta. A. Mol. Biomol. Spectrosc.* **2020**, *243*, 118813. https://doi.org/10.1016/j.saa.2020.118813.
(1592) Chen, H.; He, X.; Yu, Y.; Qian, Y.; Shen, J.; Zhao, S. Execution of Aggregation-Induced Emission as Nano-Sensors for Hypochlorite Detection and Application for Bioimaging in Living Cells and Zebrafish. *Talanta* **2020**, *214*, 120842. https://doi.org/10.1016/j.talanta.2020.120842.
(1593) Gan, Y.; Yin, G.; Zhang, X.; Zhou, L.; Zhang, Y.; Li, H.; Yin, P. Turn-on Fluorescent Probe for Sensing Exogenous and Endogenous Hypochlorous Acid in Living Cells, Zebrafishes and Mice. *Talanta* **2021**, *225*, 122030. https://doi.org/10.1016/j.talanta.2020.122030.
(1594) Ren, H.; Huo, F.; Yin, C. An ESIPT-Based Colorimetric and Fluorescent Probe with Large Stokes Shift for the Sensitive Detection of Hypochlorous Acid and Its Bioimaging in Cells. *New J. Chem.* **2021**, *45* (10), 4724–4728. https://doi.org/10.1039/D0NJ05807F.
(1595) Wang, L.; Zhang, R.; Bu, Y.-C.; Huang, Z.; Kong, L.; Yang, J.-X. Two Novel "Turn on" Fluorescent Probes for Monitoring Hypochlorite in Living HeLa Cells. *Dyes Pigments* **2021**, *196*, 109749. https://doi.org/10.1016/j.dyepig.2021.109749.

(1596) Yang, X.; Liu, J.; Xie, P.; Han, X.; Zhang, D.; Ye, Y.; Zhao, Y. Visualization of Biothiols and HClO in Cancer Therapy via a Multi-Responsive Fluorescent Probe. *Sens. Actuators B Chem.* **2021**, *347*, 130620. https://doi.org/10.1016/j.snb.2021.130620.
(1597) Wu, H.; Chen, Y.; Ling, X.; Yuan, W.; Li, B.; Zhou, Z. A Novel D-π-A Molecule as ICT Type Fluorescent Probe for Endogenous Hypochlorite Imaging in Living Cells and Zebrafishes. *J. Mol. Liq.* **2021**, *329*, 115465. https://doi.org/10.1016/j.molliq.2021.115465.
(1598) Xu, C.; Zhou, Y.; Li, Z.; Zhou, Y.; Liu, X.; Peng, X. Rational Design of AIE-Based Fluorescent Probes for Hypochlorite Detection in Real Water Samples and Live Cell Imaging. *J. Hazard. Mater.* **2021**, *418*, 126243. https://doi.org/10.1016/j.jhazmat.2021.126243.
(1599) Huang, Y.; Zhang, Y.; Huo, F.; Yin, C. An Innovative Hypochlorite-Sensing Scaffold and Its Imaging Application in Vivo. *Dyes Pigments* **2021**, *191*, 109378. https://doi.org/10.1016/j.dyepig.2021.109378.
(1600) Cheng, S.; Li, A.; Pan, X.; Wang, H.; Zhang, C.; Li, J.; Qi, X. A Near-Infrared Fluorescent Probe for Highly Specific and Ultrasensitive Detection of Hypochlorite Ions in Living Cells. *Anal. Bioanal. Chem.* **2021**, *413* (17), 4441–4450. https://doi.org/10.1007/s00216-021-03398-1.
(1601) Luo, Q.; Luo, Z.; Zeng, H.; Xiao, Y.; Peng, Y.; Liu, G. A New HClO-Activated "Turn-off" Mitochondria-Targetable NIR Fluorescent Probe for Imaging of Osteoarthritis in Vivo. *Spectrochim. Acta. A. Mol. Biomol. Spectrosc.* **2022**, *273*, 121017. https://doi.org/10.1016/j.saa.2022.121017.
(1602) Liu, K.; Huang, S.; Li, T.; Sun, J.; Fan, L.; Wang, X.; Li, H.; Li, Y.; Zhang, W.; Yang, Z. A Benzocoumarin-Based Fluorescent Probe for Highly Specific Ultra-Sensitive Fast Detecting Endogenous/Exogenous Hypochlorous Acid and Its Applications. *J. Photochem. Photobiol. Chem.* **2022**, *427*, 113843. https://doi.org/10.1016/j.jphotochem.2022.113843.
(1603) Guo, F.-F.; Wu, W.-N.; Zhao, X.-L.; Wang, Y.; Fan, Y.-C.; Zhang, C.-X.; Xu, Z.-H. A Deep-Red Lysosome-Targetable Fluorescent Probe for Detection of Hypochlorous Acid in Pure Water and Its Imaging Application in Living Cells and Zebrafish. *Spectrochim. Acta. A. Mol. Biomol. Spectrosc.* **2022**, *264*, 120270. https://doi.org/10.1016/j.saa.2021.120270.
(1604) Shi, W.-J.; Wan, Q.-H.; Yang, F.; Wang, X.; Wei, Y.-F.; Lin, X.-R.; Zhang, J.-Y.; Deng, R.-H.; Chen, J.-Y.; Zheng, L.; Liu, F.; Gao, L. A Novel TCF-Aza-BODIPY-Based near-Infrared Fluorescent Probe for Highly Selective Detection of Hypochlorous Acid in Living Cells. *Spectrochim. Acta. A. Mol. Biomol. Spectrosc.* **2022**, *279*, 121490. https://doi.org/10.1016/j.saa.2022.121490.
(1605) Zhang, Y.; Yang, H.; Li, M.; Gong, S.; Song, J.; Wang, Z.; Wang, S. A Red-Emitting Ratiometric Fluorescent Probe with Large Stokes Shift and Emission Peak Shift for Imaging Hypochlorous Acid in Living Cells and Zebrafish. *Dyes Pigments* **2022**, *197*, 109861. https://doi.org/10.1016/j.dyepig.2021.109861.
(1606) Li, S.; Zeng, Y.; Tang, C.; Wang, F.; Gu, B.; Tang, S. A Red-Emissive Benzothiazole-Based Luminophore with ESIPT and AIE Natures and Its Application for Detecting and Imaging Hypochlorous Acid. *Spectrochim. Acta. A. Mol. Biomol. Spectrosc.* **2022**, *281*, 121601. https://doi.org/10.1016/j.saa.2022.121601.
(1607) Ma, M.; Chen, J.; Yu, S.; Liu, Z.; Zeng, X. Development of a Novel Highly Specific Fluorescent Probe for Detecting HOCl in Living Cells and Zebrafish, as Well as Real Water Samples. *J. Mol. Struct.* **2022**, *1268*, 133744. https://doi.org/10.1016/j.molstruc.2022.133744.
(1608) Xu, X.; Ding, H.; Zhang, Q.; Liu, G.; Pu, S. A Ratiometric Fluorescent Probe with an Extremely Large Emission Shift for Detecting ClO^- and Its Application in Test Strips and Cell Imaging. *Dyes Pigments* **2022**, *207*, 110776. https://doi.org/10.1016/j.dyepig.2022.110776.

(1609) Du, L.; Xie, Y.; Qian, H.; Zhou, W.; Yang, Q.; Sun, X.; Wang, L. A New Coumarin-Based "Turn-on" Fluorescence Probe with High Sensitivity and Specificity for Detecting Hypochlorite Ion. *Dyes Pigments* **2022**, *200*, 110137. https://doi.org/10.1016/j.dyepig.2022.110137.
(1610) Liu, L.; Yang, Y.; Cui, Y.; Zhu, W.; Fang, M.; Li, C. A Novel Dicyanisophorone-Based Colorimetric and Ratiometric Fluorescent Probe for the Detection of Hypochlorite in the Environment and Living Cells. *Dyes Pigments* **2023**, *208*, 110879. https://doi.org/10.1016/j.dyepig.2022.110879.
(1611)Jiang, C.; Li, Y.; Yan, L.; Ye, A.; He, Q.; Yao, C. A Ratiometric Fluorescence Mitochondrial-Targeted Probe for Imaging HOCl in Vitro and in Vivo. *Dyes Pigments* **2022**, *198*, 109975. https://doi.org/10.1016/j.dyepig.2021.109975.
(1612) Shi, S.; Guan, P.; Zhang, F.; Chai, J.; Yang, B.; Liu, B. A Near-Infrared Ratiometric Fluorescent Probe with Large Stokes Shift for Rapid Detection of ClO^- in Living Cells. *J. Mol. Struct.* **2022**, *1267*, 133570. https://doi.org/10.1016/j.molstruc.2022.133570.
(1613) Liu, S.-S.; Yan, J.-L.; Wu, W.-N.; Zhao, X.-L.; Fan, Y.-C.; Wang, Y.; Xu, Z.-H. Highly Selective Fluorescent Probe for Rapid Turn-on Detection and Cell Imaging of Hypochlorite Anion. *J. Photochem. Photobiol. Chem.* **2022**, *432*, 114082. https://doi.org/10.1016/j.jphotochem.2022.114082.
(1614) Shangguan, L.; Wang, J.; Qian, X.; Wu, Y.; Liu, Y. Mitochondria-Targeted Ratiometric Chemdosimeter to Detect Hypochlorite Acid for Monitoring the Drug-Damaged Liver and Kidney. *Anal. Chem.* **2022**, *94* (34), 11881–11888. https://doi.org/10.1021/acs.analchem.2c02431.
(1615) Yu, S.-Y.; Hsu, C.-Y.; Chen, W.-C.; Wei, L.-F.; Wu, S.-P. A Hypochlorous Acid Turn-on Fluorescent Probe Based on HOCl-Promoted Oxime Oxidation and Its Application in Cell Imaging. *Sens. Actuators B Chem.* **2014**, *196*, 203–207. https://doi.org/10.1016/j.snb.2014.01.121.
(1616) Goswami, S.; Aich, K.; Das, S.; Pakhira, B.; Ghoshal, K.; Quah, C. K.; Bhattacharyya, M.; Fun, H.-K.; Sarkar, S. A Triphenyl Amine-Based Solvatofluorochromic Dye for the Selective and Ratiometric Sensing of OCl^- in Human Blood Cells. *Chem. - Asian J.* **2015**, *10* (3), 694–700. https://doi.org/10.1002/asia.201403234.
(1617) Wang, E.; Qiao, H.; Zhou, Y.; Pang, L.; Yu, F.; Zhang, J.; Ma, T. A Novel "Turn-on" Fluorogenic Probe for Sensing Hypochlorous Acid Based on BODIPY. *RSC Adv.* **2015**, *5* (89), 73040–73045. https://doi.org/10.1039/C5RA14118D.
(1618) Kang, J.; Huo, F.; Yue, Y.; Wen, Y.; Chao, J.; Zhang, Y.; Yin, C. A Solvent Depend on Ratiometric Fluorescent Probe for Hypochlorous Acid and Its Application in Living Cells. *Dyes Pigments* **2017**, *136*, 852–858. https://doi.org/10.1016/j.dyepig.2016.09.048.
(1619) Zhao, Y.; Li, H.; Xue, Y.; Ren, Y.; Han, T. A Phenanthroimidazole-Based Fluorescent Probe for Hypochlorous Acid with High Selectivity and Its Bio-Imaging in Living Cells. *Sens. Actuators B Chem.* **2017**, *241*, 335–341. https://doi.org/10.1016/j.snb.2016.10.092.
(1620) Das, S.; Aich, K.; Patra, L.; Ghoshal, K.; Gharami, S.; Bhattacharyya, M.; Mondal, T. K. Development of a New Fluorescence Ratiometric Switch for Endogenous Hypochlorite Detection in Monocytes of Diabetic Subjects by Dye Release Method. *Tetrahedron Lett.* **2018**, *59* (12), 1130–1135. https://doi.org/10.1016/j.tetlet.2018.02.023.
(1621) Gao, Y.; Pan, Y.; He, Y.; Chen, H.; Nemykin, V. N. A Fast-Response, Red Emission Aza-BODIPY-Hydrazone-Based Chemodosimeter for Selective Detection of HClO. *Sens. Actuators B Chem.* **2018**, *269*, 151–157. https://doi.org/10.1016/j.snb.2018.04.135.
(1622) Yang, Q.; Zhong, X.; Chen, Y.; Yang, J.; Jin, C.; Jiang, Y. A Mitochondria-Targeted Fluorescent Probe for Hypochlorite Sensing and Its Application in Bioimaging. *Analyst* **2020**, *145* (8), 3100–3105. https://doi.org/10.1039/D0AN00245C.
(1623) Tian, T.; Xu, S.; Ru, Y.; Zhang, D.; Pu, S. A Red-Emission Iridium (Ⅲ) Complex-Based Fluorescent Probe with Schiff Base Structure for Selection Detection HOCl and Its

Application in Water Sample. *J. Organomet. Chem.* **2022**, *976*, 122351. https://doi.org/10.1016/j.jorganchem.2022.122351.
(1624) Wang, Q.; Liu, C.; Chang, J.; Lu, Y.; He, S.; Zhao, L.; Zeng, X. Novel Water Soluble Styrylquinolinium Boronic Acid as a Ratiometric Reagent for the Rapid Detection of Hypochlorite Ion. *Dyes Pigments* **2013**, *99* (3), 733–739. https://doi.org/10.1016/j.dyepig.2013.06.019.
(1625) Shu, W.; Yan, L.; Wang, Z.; Liu, J.; Zhang, S.; Liu, C.; Zhu, B. A Novel Visual and Far-Red Fluorescent Dual-Channel Probe for the Rapid and Sensitive Detection of Hypochlorite in Aqueous Solution and Living Cells. *Sens. Actuators B Chem.* **2015**, *221*, 1130–1136. https://doi.org/10.1016/j.snb.2015.07.066.
(1626) Wang, Y.; Shu, W.; Han, B.; Zhao, X.; Wu, L.; Liu, C.; Ma, Z.; Zhu, B.; Du, B. A Simple, Cyanovinylene-Based, Ratiometric, Colorimetric and Fluorescent Chemodosimeter for the Specific and Sensitive Detection of HClO in Living Cells. *New J. Chem.* **2017**, *41* (17), 9262–9267. https://doi.org/10.1039/C7NJ01654A.
(1627) Li, G.; Ji, D.; Zhang, S.; Li, J.; Li, C.; Qiao, R. A Mitochondria-Targeting Fluorescence Turn-on Probe for Hypochlorite and Its Applications for in Vivo Imaging. *Sens. Actuators B Chem.* **2017**, *252*, 127–133. https://doi.org/10.1016/j.snb.2017.05.138.
(1628) Tong, H.; Zhang, Y.; Ma, S.; Zhang, M.; Wang, N.; Wang, R.; Lou, K.; Wang, W. A Pinacol Boronate Caged NIAD-4 Derivative as a near-Infrared Fluorescent Probe for Fast and Selective Detection of Hypochlorous Acid. *Chin. Chem. Lett.* **2018**, *29* (1), 139–142. https://doi.org/10.1016/j.cclet.2017.07.007.
(1629) Zhang, P.; Zhang, Q.; Li, S.; Chen, W.; Guo, X.; Ding, C. Enhanced Fluorescence Sensing of Hypochlorous Acid Using Serum Albumin as a Signal Amplifier. *J. Mater. Chem. B* **2019**, *7* (8), 1238–1245. https://doi.org/10.1039/C8TB03023E.
(1630) Duan, Y.-M.; Wang, S.; Cao, F.; Zhang, Q.; Chen, S.; Zhang, Y.-B.; Wang, K.-P.; Hu, Z.-Q. Facile and Highly Selective Ratiometric Fluorescence Probe Based on Benzo[5]Helicene for the Detection of Hypochlorous Acid. *Ind. Eng. Chem. Res.* **2020**, *59* (2), 992–999. https://doi.org/10.1021/acs.iecr.9b05073.
(1631) Lan, J.; Guo, J.; Jiang, X.; Chen, Y.; Hu, Z.; Que, Y.; Li, H.; Gu, J.; Ho, R. J. Y.; Zeng, R.; Ding, Y.; Zhang, T. A New Dicyanoisophorone-Based Ratiometric and Colorimetric near-Infrared Fluorescent Probe for Specifically Detecting Hypochlorite and Its Bioimaging on a Model of Acute Inflammation. *Anal. Chim. Acta* **2020**, *1094*, 70–79. https://doi.org/10.1016/j.aca.2019.09.076.
(1632) Lan, J.; Wang, Y.; Qin, Y.; Li, Z.; Zeng, R.; Liu, L.; Chen, L.; Yang, K.; Ding, Y.; Zhang, T. Dual-Site Mitochondria-Targeted Fluorescent Probe for Simultaneous Distinguishing Detection of Hypochlorite and SO_2 Derivatives in Real Water Samples and Bioimaging. *Dyes Pigments* **2022**, *207*, 110706. https://doi.org/10.1016/j.dyepig.2022.110706.
(1633) Zhen, L.; Lan, J.; Zhang, S.; Liu, L.; Zeng, R.; Chen, Y.; Ding, Y. A NIR Fluorescent Probe for the Specific Detection of Hypochlorite and Its Application in Vitro and in Vivo. *Anal. Methods* **2022**, *14* (22), 2147–2152. https://doi.org/10.1039/D2AY00561A.
(1634) Chen, L.; Park, S. J.; Wu, D.; Kim, H. M.; Yoon, J. A Two-Photon ESIPT Based Fluorescence Probe for Specific Detection of Hypochlorite. *Dyes Pigments* **2018**, *158*, 526–532. https://doi.org/10.1016/j.dyepig.2018.01.027.
(1635) Ning, Y.; Cui, J.; Lu, Y.; Wang, X.; Xiao, C.; Wu, S.; Li, J.; Zhang, Y. De Novo Design and Synthesis of a Novel Colorimetric Fluorescent Probe Based on Naphthalenone Scaffold for Selective Detection of Hypochlorite and Its Application in Living Cells. *Sens. Actuators B Chem.* **2018**, *269*, 322–330. https://doi.org/10.1016/j.snb.2018.04.156.
(1636) zhang, H.; Huo, F.; Zhang, Y.; Yin, C. Mono- or Di- Naphthalimides as Fluorophore to Detect Hypochlorous Acid (HOCl) by Ratiometric Fluorescent Signal and Their Biological Application. *Sens. Actuators B Chem.* **2018**, *269*, 180–188. https://doi.org/10.1016/j.snb.2018.04.155.

(1637) Zhang, Y.; Ma, L.; Tang, C.; Pan, S.; Shi, D.; Wang, S.; Li, M.; Guo, Y. A Highly Sensitive and Rapidly Responding Fluorescent Probe Based on a Rhodol Fluorophore for Imaging Endogenous Hypochlorite in Living Mice. *J. Mater. Chem. B* **2018**, *6* (5), 725–731. https://doi.org/10.1039/C7TB02862H.
(1638) Feng, Y.; Li, S.; Li, D.; Wang, Q.; Ning, P.; Chen, M.; Tian, X.; Wang, X. Rational Design of a Diaminomaleonitrile-Based Mitochondria – Targeted Two-Photon Fluorescent Probe for Hypochlorite in Vivo: Solvent-Independent and High Selectivity over Cu^{2+}. *Sens. Actuators B Chem.* **2018**, *254*, 282–290. https://doi.org/10.1016/j.snb.2017.07.019.
(1639) Shi, R.; Chen, H.; Qi, Y.; Huang, W.; Yin, G.; Wang, R. From Aggregation-Induced to Solution Emission: A New Strategy for Designing Ratiometric Fluorescent Probes and Its Application for in Vivo HClO Detection. *Analyst* **2019**, *144* (5), 1696–1703. https://doi.org/10.1039/C8AN01950A.
(1640) Tang, Y.; Li, Y.; Han, J.; Mao, Y.; Ni, L.; Wang, Y. A Coumarin Based Fluorescent Probe for Rapidly Distinguishing of Hypochlorite and Copper (II) Ion in Organisms. *Spectrochim. Acta. A. Mol. Biomol. Spectrosc.* **2019**, *208*, 299–308. https://doi.org/10.1016/j.saa.2018.10.019.
(1641) Xu, C.; Zhou, Y.; Cui, Y.; Liu, X.; Peng, X. A Facile AIEgen-Based Fluorescent Probe Design Strategy and Its Application in Hypochlorite Probe Construction. *Sens. Actuators B Chem.* **2020**, *314*, 128083. https://doi.org/10.1016/j.snb.2020.128083.
(1642) Li, Q.; Zhan, Z.; Zhang, K.; Song, H.; Lv, Y. Ratiometric Two-Photon Fluorescent Probe for Detection of Hypochlorite in Living Cells. *Talanta* **2020**, *217*, 121099. https://doi.org/10.1016/j.talanta.2020.121099.
(1643) Li, M.; Du, F.; Xue, P.; Tan, X.; Liu, S.; Zhou, Y.; Chen, J.; Bai, L. An AIE Fluorescent Probe with a Naphthalimide Derivative and Its Application for Detection of Hypochlorite and Imaging inside Living Cells. *Spectrochim. Acta. A. Mol. Biomol. Spectrosc.* **2020**, *227*, 117760. https://doi.org/10.1016/j.saa.2019.117760.
(1644) Malkondu, S.; Erdemir, S.; Karakurt, S. Red and Blue Emitting Fluorescent Probe for Cyanide and Hypochlorite Ions: Biological Sensing and Environmental Analysis. *Dyes Pigments* **2020**, *174*, 108019. https://doi.org/10.1016/j.dyepig.2019.108019.
(1645) Zhong, X.; Yang, Q.; Chen, Y.; Jiang, Y.; Dai, Z. Aggregation-Induced Fluorescence Probe for Hypochlorite Imaging in Mitochondria of Living Cells and Zebrafish. *J. Mater. Chem. B* **2020**, *8* (33), 7375–7381. https://doi.org/10.1039/D0TB01496F.
(1646) Li, C.; Yin, P.; Li, T.; Wei, T.; Hu, T.; Chen, J.; Qin, X.; Niu, Q. Rapid and Sensitive Detection of Hypochlorite in ~100% Aqueous Solution Using a Bithiophene-Based Fluorescent Sensor: Application to Water Analysis and Live-Cell Imaging. *J. Mol. Liq.* **2020**, *320*, 114396. https://doi.org/10.1016/j.molliq.2020.114396.
(1647) Dai, Y.; Zhan, Z.; Chai, L.; Zhang, L.; Guo, Q.; Zhang, K.; Lv, Y. A Two-Photon Excited Near-Infrared Iridium(III) Complex for Multi-Signal Detection and Multimodal Imaging of Hypochlorite. *Anal. Chem.* **2021**, *93* (10), 4628–4634. https://doi.org/10.1021/acs.analchem.0c05460.
(1648) Zhang, X.; Zhang, F.; Chai, J.; Yang, B.; Liu, B. A TICT + AIE Based Fluorescent Probe for Ultrafast Response of Hypochlorite in Living Cells and Mouse. *Spectrochim. Acta. A. Mol. Biomol. Spectrosc.* **2021**, *256*, 119735. https://doi.org/10.1016/j.saa.2021.119735.
(1649) Zhan, Z.; Lei, Q.; Dai, Y.; Wang, D.; Yu, Q.; Lv, Y.; Li, W. Simultaneous Monitoring of HOCl and Viscosity with Drug-Induced Pyroptosis in Live Cells and Acute Lung Injury. *Anal. Chem.* **2022**, *94* (35), 12144–12151. https://doi.org/10.1021/acs.analchem.2c02235.
(1650) Leng, J.; Nie, W.; Yuan, L.; Liu, S.; Liu, T.; Cheng, J.; Liu, Z. A BODIPY-Diaminomaleonitrile Based Water-Soluble Fluorescent Probe for Selective “Off-On” Detection of Hypochlorite**. *ChemistrySelect* **2022**, *7* (12), e202200378. https://doi.org/10.1002/slct.202200378.
(1651) Zhang, W.; Guo, C.; Liu, L.; Qin, J.; Yang, C. Naked-Eye Visible and Fluorometric Dual-Signaling Chemodosimeter for Hypochlorous Acid Based on Water-Soluble p-

Methoxyphenol Derivative. *Org. Biomol. Chem.* **2011**, *9* (15), 5560–5563. https://doi.org/10.1039/C1OB05550J.
(1652) Zhou, Y.; Li, J.-Y.; Chu, K.-H.; Liu, K.; Yao, C.; Li, J.-Y. Fluorescence Turn-on Detection of Hypochlorous Acid via HOCl-Promoted Dihydrofluorescein- Ether Oxidation and Its Application in Vivo. *Chem. Commun.* **2012**, *48* (39), 4677–4679. https://doi.org/10.1039/C2CC30265A.
(1653) Yin, W.; Zhu, H.; Wang, R. A Sensitive and Selective Fluorescence Probe Based Fluorescein for Detection of Hypochlorous Acid and Its Application for Biological Imaging. *Dyes Pigments* **2014**, *107*, 127–132. https://doi.org/10.1016/j.dyepig.2014.03.012.
(1654) Hu, J. J.; Wong, N.-K.; Gu, Q.; Bai, X.; Ye, S.; Yang, D. HKOCl-2 Series of Green BODIPY-Based Fluorescent Probes for Hypochlorous Acid Detection and Imaging in Live Cells. *Org. Lett.* **2014**, *16* (13), 3544–3547. https://doi.org/10.1021/ol501496n.
(1655) Yue, Y.; Yin, C.; Huo, F.; Chao, J.; Zhang, Y. The Application of Natural Drug-Curcumin in the Detection Hypochlorous Acid of Real Sample and Its Bioimaging. *Sens. Actuators B Chem.* **2014**, *202*, 551–556. https://doi.org/10.1016/j.snb.2014.05.119.
(1656) Jiang, Y.; Zheng, G.; Cai, N.; Zhang, H.; Tan, Y.; Huang, M.; He, Y.; He, J.; Sun, H. A Fast-Response Fluorescent Probe for Hypochlorous Acid Detection and Its Application in Exogenous and Endogenous HOCl Imaging of Living Cells. *Chem. Commun.* **2017**, *53* (91), 12349–12352. https://doi.org/10.1039/C7CC07373A.
(1657) Ali, F.; Aute, S.; Sreedharan, S.; Anila, H. A.; Saeed, H. K.; Smythe, C. G.; Thomas, J. A.; Das, A. Tracking HOCl Concentrations across Cellular Organelles in Real Time Using a Super Resolution Microscopy Probe. *Chem. Commun.* **2018**, *54* (15), 1849–1852. https://doi.org/10.1039/C7CC09433G.
(1658) Tang, X.; Sun, H.; Nie, J.; Han, X.; Zhao, Y.; Zhang, R.; Ni, Z. An O-Hydroxyl Aldehyde Structure Based Naphthalimide Derivative: Reversible Photochromic Properties and Its Application in ClO^- Detection in Living Cells. *Spectrochim. Acta. A. Mol. Biomol. Spectrosc.* **2019**, *219*, 154–163. https://doi.org/10.1016/j.saa.2019.04.049.
(1659) Wang, Z.; Zhang, Y.; Song, J.; Li, M.; Yang, Y.; Xu, X.; Xu, H.; Wang, S. Three Novel Camphor-Based Fluorescence Probes for Ratiometric Detection of Hypochlorite and Bio-Imaging in Living Cells. *Sens. Actuators B Chem.* **2019**, *284*, 148–158. https://doi.org/10.1016/j.snb.2018.12.104.
(1660) Yadav, R.; Odera, K.; Rai, A.; Noguchi, A.; Takahashi, R.; Mishra, L. A Stable and Highly Sensitive Fluorescent Probe for Detection of Hypochlorite Ion In Vitro and in Living Cells. *Chem. Lett.* **2019**, *48* (2), 110–113. https://doi.org/10.1246/cl.180875.
(1661) Zhang, K.; Lv, Y.; Meng, J.; Wang, J.; Peng, A.; Wang, X.; Tian, Z. A Single-Chromophore-Based Agent Enables Rapid Sensing of Intracellular Hypochlorous Acid and in-Situ Photodynamic Therapy to Cancer Cells. *Anal. Chim. Acta* **2019**, *1061*, 142–151. https://doi.org/10.1016/j.aca.2019.02.005.
(1662) Chao, J.; Duan, Y.; Zhang, Y.; Huo, F.; Yin, C.; Xu, M.; Li, M. A Carbazole-Based Fluorescent Probe for Ultra-Fast Detection of ClO^- and Its Application to Live Cell Imaging. *Chem. Pap.* **2020**, *74* (4), 1171–1176. https://doi.org/10.1007/s11696-019-00958-9.
(1663) Yan, F.; Sun, X.; Jiang, Y.; Wang, R.; Zhang, Y.; Cui, Y. Dual-Function Fluorescent Probe with Red Emission for Sensing Viscosity and OCl− and Its Applications in Bioimaging. *Dyes Pigments* **2020**, *182*, 108531. https://doi.org/10.1016/j.dyepig.2020.108531.
(1664) Yang, X.; Wang, Y.; Shang, Z.; Zhang, Z.; Chi, H.; Zhang, Z.; Zhang, R.; Meng, Q. Quinoline-Based Fluorescent Probe for the Detection and Monitoring of Hypochlorous Acid in a Rheumatoid Arthritis Model. *RSC Adv.* **2021**, *11* (50), 31656–31662. https://doi.org/10.1039/D1RA06224G.
(1665) Zhi, X.; Qian, Y. A Novel Red-Emission Phenothiazine Fluorescent Protein Chromophore Based on Oxygen–chlorine Bond (O–Cl) Formation for Real-Time Detection of

Hypochlorous Acid in Cells. *Talanta* **2021**, *222*, 121503. https://doi.org/10.1016/j.talanta.2020.121503.
(1666) Ye, S.; Yang, B.; Wu, M.; Chen, Z.; Shen, J.; Shabat, D.; Yang, D. Recurring Real-Time Monitoring of Inflammations in Living Mice with a Chemiluminescent Probe for Hypochlorous Acid. *CCS Chem.* **2021**, *4* (6), 1871–1878. https://doi.org/10.31635/ccschem.021.202101108.
(1667) Bizyukin, A. V.; Soodaeva, S. K. Study of Oxidative Phagocyte Metabolism Using the Fluorescent Indicator Hydroethidine. *Pharm. Chem. J.* **1995**, *29* (4), 236–240. https://doi.org/10.1007/BF02219542.
(1668) Pyne, D. B.; Baker, M. S.; Smith, J. A.; Weidemann, M. J.; Telford, R. D. Exercise and the Neutrophil Oxidative Burst: Biological and Experimental Variability. *Eur. J. Appl. Physiol.* **1996**, *74* (6), 564–571. https://doi.org/10.1007/BF02376774.
(1669) Bizyukin, A. V.; Korkina, L. G.; Velichkovskii, B. T. Comparative Use of 2,7-Dichlorofluorescin Diacetate, Dihydrorhodamine 123, and Hydroethidine to Study Oxidative Metabolism in Phagocytic Cells. *Bull. Exp. Biol. Med.* **1995**, *119* (4), 347–351. https://doi.org/10.1007/BF02445889.
(1670) Wu, Z.; Wu, X.; Li, Z.; Yang, Y.; Han, J.; Han, S. Benzothiazoline Based Chemodosimeters for Fluorogenic Detection of Hypochlorous Acid. *Bioorg. Med. Chem. Lett.* **2013**, *23* (15), 4354–4357. https://doi.org/10.1016/j.bmcl.2013.05.083.
(1671) Goswami, S.; Manna, A.; Paul, S.; Quah, C. K.; Fun, H.-K. Rapid and Ratiometric Detection of Hypochlorite with Real Application in Tap Water: Molecules to Low Cost Devices (TLC Sticks). *Chem. Commun.* **2013**, *49* (99), 11656–11658. https://doi.org/10.1039/C3CC47121G.
(1672) Fan, J.; Mu, H.; Zhu, H.; Wang, J.; Peng, X. Light up ClO^- in Live Cells Using an Aza-Coumarin Based Fluorescent Probe with Fast Response and High Sensitivity. *Analyst* **2015**, *140* (13), 4594–4598. https://doi.org/10.1039/C5AN00777A.
(1673) Sen, B.; Sheet, S. K.; Patra, S. K.; Koner, D.; Saha, N.; Khatua, S. Highly Selective Detection of Hypochlorous Acid by a Bis-Heteroleptic Ru(II) Complex of Pyridyl-1,2,3-Triazole Ligand via C(sp^2)–H Hydroxylation. *Inorg. Chem.* **2019**, *58* (15), 9982–9991. https://doi.org/10.1021/acs.inorgchem.9b01125.
(1674) Yan, Y.-H.; He, X.-Y.; Su, L.; Miao, J.-Y.; Zhao, B.-X. A New FRET-Based Ratiometric Fluorescence Probe for Hypochlorous Acid and Its Imaging in Living Cells. *Talanta* **2019**, *201*, 330–334. https://doi.org/10.1016/j.talanta.2019.04.024.
(1675) Huang, X.; Luo, T.; Zhang, C.; Li, J.; Jia, Z.; Chen, X.; Hu, Y.; Huang, H. Dual-Ratiometric Fluorescence Probe for Viscosity and Hypochlorite Based on AIEgen with Mitochondria-Targeting Ability. *Talanta* **2022**, *241*, 123235. https://doi.org/10.1016/j.talanta.2022.123235.
(1676) Dunstan, S. L.; Sala-Newby, G. B.; Fajardo, A. B.; Taylor, K. M.; Campbell, A. K. Cloning and Expression of the Bioluminescent Photoprotein Pholasin from the Bivalve Mollusc Pholas Dactylus. *J. Biol. Chem.* **2000**, *275* (13), 9403–9409. https://doi.org/10.1074/jbc.275.13.9403.
(1677) Li, J.; Yin, C.; Liu, T.; Wen, Y.; Huo, F. A New Mechanism-Based Fluorescent Probe for the Detection of ClO^- by UV–Vis and Fluorescent Spectra and Its Applications. *Sens. Actuators B Chem.* **2017**, *252*, 1112–1117. https://doi.org/10.1016/j.snb.2017.07.171.
(1678) Reut, V. E.; Kozlov, S. O.; Kudryavtsev, I. V.; Grudinina, N. A.; Kostevich, V. A.; Gorbunov, N. P.; Grigorieva, D. V.; Kalvinkovskaya, J. A.; Bushuk, S. B.; Varfolomeeva, E. Y.; Fedorova, N. D.; Gorudko, I. V.; Panasenko, O. M.; Vasilyev, V. B.; Sokolov, A. V. New Application of the Commercially Available Dye Celestine Blue B as a Sensitive and Selective Fluorescent “Turn-On” Probe for Endogenous Detection of HOCl and Reactive Halogenated Species. *Antioxidants* **2022**, *11* (9), 1719. https://doi.org/10.3390/antiox11091719.

(1679) Zhang, R.; Song, B.; Dai, Z.; Ye, Z.; Xiao, Y.; Liu, Y.; Yuan, J. Highly Sensitive and Selective Phosphorescent Chemosensors for Hypochlorous Acid Based on Ruthenium(II) Complexes. *Biosens. Bioelectron.* **2013**, *50*, 1–7. https://doi.org/10.1016/j.bios.2013.06.005.
(1680) Zhang, R.; Ye, Z.; Song, B.; Dai, Z.; An, X.; Yuan, J. Development of a Ruthenium(II) Complex-Based Luminescent Probe for Hypochlorous Acid in Living Cells. *Inorg. Chem.* **2013**, *52* (18), 10325–10331. https://doi.org/10.1021/ic400767u.
(1681) Liu, X.; Tang, Z.; Song, B.; Ma, H.; Yuan, J. A Mitochondria-Targeting Time-Gated Luminescence Probe for Hypochlorous Acid Based on a Europium Complex. *J. Mater. Chem. B* **2017**, *5* (15), 2849–2855. https://doi.org/10.1039/C6TB02991D.
(1682) Wang, X.; Wang, R.; Ding, Q.; Wu, W.; Che, F.; Li, P.; Zhang, W.; Zhang, W.; Liu, Z.; Tang, B. Hypochlorous Acid-Activated Multifunctional Fluorescence Platform for Depression Therapy and Antidepressant Efficacy Evaluation. *Anal. Chem.* **2022**, *94* (27), 9811–9818. https://doi.org/10.1021/acs.analchem.2c01639.
(1683) Wang, X.-B.; Li, H.-J.; Li, Q.; Ding, Y.; Hu, C.; Wu, Y.-C. A Specifically Triggered Turn-on Fluorescent Probe Platform and Its Visual Imaging of HClO in Cells, Arthritis and Tumors. *J. Hazard. Mater.* **2022**, *427*, 127874. https://doi.org/10.1016/j.jhazmat.2021.127874.
(1684) Xiong, K.; Yin, C.; Chao, J.; Zhang, Y.; Huo, F. The Detection for Hypochlorite by UV–Vis and Fluorescent Spectra Based on Oxidized Ring Opening and Successive Hydrolysis Reaction. *Spectrochim. Acta. A. Mol. Biomol. Spectrosc.* **2016**, *166*, 79–83. https://doi.org/10.1016/j.saa.2016.05.016.
(1685) Jin, L.; Tan, X.; Dai, L.; Zhao, C.; Wang, W.; Wang, Q. A Novel Coumarin-Based Fluorescent Probe with Fine Selectivity and Sensitivity for Hypochlorite and Its Application in Cell Imaging. *Talanta* **2019**, *202*, 190–197. https://doi.org/10.1016/j.talanta.2019.04.070.
(1686) Wang, W.; Jin, L.; Shen, Z.; Li, Z.; Zhang, X.; Wang, Q. A Fluorescent Probe with a Significant Selective Turn-On Response for HClO Detection and Bioimaging in Living Cells. *ChemistrySelect* **2019**, *4* (25), 7425–7430. https://doi.org/10.1002/slct.201901587.
(1687) Jin, L.; Tan, X.; Dai, L.; Sheng, L.; Wang, Q. A Highly Specific and Sensitive Turn-on Fluorescence Probe for Hypochlorite Detection and Its Bioimaging Applications. *RSC Adv.* **2019**, *9* (28), 15926–15932. https://doi.org/10.1039/C9RA01457H.
(1688) Wang, Q.-M.; Jin, L.; Shen, Z.-Y.; Xu, J.-H.; Sheng, L.-Q.; Bai, H. Mitochondria-Targeting Turn-on Fluorescent Probe for HClO Detection and Imaging in Living Cells. *Spectrochim. Acta. A. Mol. Biomol. Spectrosc.* **2020**, *228*, 117825. https://doi.org/10.1016/j.saa.2019.117825.
(1689) Ma, H.; Song, B.; Wang, Y.; Liu, C.; Wang, X.; Yuan, J. Development of Organelle-Targetable Europium Complex Probes for Time-Gated Luminescence Imaging of Hypochlorous Acid in Live Cells and Animals. *Dyes Pigments* **2017**, *140*, 407–416. https://doi.org/10.1016/j.dyepig.2017.01.062.
(1690) Wu, J.; Che, W.; Liu, H.; Min, P.; Zheng, D. Development of a Lysosome-Targetable Visible-Light-Excited Europium(III) Complex-Based Luminescent Probe to Image Hypochlorous Acid in Living Cells. *Opt. Mater.* **2020**, *109*, 110273. https://doi.org/10.1016/j.optmat.2020.110273.
(1691) Ma, H.; Chen, K.; Song, B.; Tang, Z.; Huang, Y.; Zhang, T.; Wang, H.; Sun, W.; Yuan, J. A Visible-Light-Excitable Mitochondria-Targeted Europium Complex Probe for Hypochlorous Acid and Its Application to Time-Gated Luminescence Bioimaging. *Biosens. Bioelectron.* **2020**, *168*, 112560. https://doi.org/10.1016/j.bios.2020.112560.
(1692) Pak, Y. L.; Park, S. J.; Song, G.; Yim, Y.; Kang, H.; Kim, H. M.; Bouffard, J.; Yoon, J. Endoplasmic Reticulum-Targeted Ratiometric N-Heterocyclic Carbene Borane Probe for Two-Photon Microscopic Imaging of Hypochlorous Acid. *Anal. Chem.* **2018**, *90* (21), 12937–12943. https://doi.org/10.1021/acs.analchem.8b03565.

(1693) Pak, Y. L.; Park, S. J.; Wu, D.; Cheon, B.; Kim, H. M.; Bouffard, J.; Yoon, J. N-Heterocyclic Carbene Boranes as Reactive Oxygen Species-Responsive Materials: Application to the Two-Photon Imaging of Hypochlorous Acid in Living Cells and Tissues. *Angew. Chem. Int. Ed.* **2018**, *57* (6), 1567–1571. https://doi.org/10.1002/anie.201711188.
(1694) Wei, P.; Yuan, W.; Xue, F.; Zhou, W.; Li, R.; Zhang, D.; Yi, T. Deformylation Reaction-Based Probe for in Vivo Imaging of HOCl. *Chem. Sci.* **2018**, *9* (2), 495–501. https://doi.org/10.1039/C7SC03784H.
(1695) Liu, C.; Li, Z.; Yu, C.; Chen, Y.; Liu, D.; Zhuang, Z.; Jia, P.; Zhu, H.; Zhang, X.; Yu, Y.; Zhu, B.; Sheng, W. Development of a Concise Rhodamine-Formylhydrazine Type Fluorescent Probe for Highly Specific and Ultrasensitive Tracing of Basal HOCl in Live Cells and Zebrafish. *ACS Sens.* **2019**, *4* (8), 2156–2163. https://doi.org/10.1021/acssensors.9b01001.
(1696) Wei, P.; Liu, L.; Wen, Y.; Zhao, G.; Xue, F.; Yuan, W.; Li, R.; Zhong, Y.; Zhang, M.; Yi, T. Release of Amino- or Carboxy-Containing Compounds Triggered by HOCl: Application for Imaging and Drug Design. *Angew. Chem. Int. Ed.* **2019**, *58* (14), 4547–4551. https://doi.org/10.1002/anie.201813648.
(1697) Wei, P.; Guo, Y.; Liu, L.; Zhou, X.; Yi, T. Hypochlorous Acid Triggered Fluorescent Probes for in Situ Imaging of a Psoriasis Model. *J. Mater. Chem. B* **2022**, *10* (27), 5211–5217. https://doi.org/10.1039/D2TB00765G.
(1698) Xiong, K.; Huo, F.; Zhang, Y.; Wen, Y.; Chao, J.; Yin, C. A Novel Recognition Mechanism Based on Aldehyde Group Oxidized into Carboxyl Group by Hypochlorite for the Materials of Fluorescent Probes. *Sens. Actuators B Chem.* **2018**, *255*, 2378–2383. https://doi.org/10.1016/j.snb.2017.09.042.
(1699) Ding, H.-L.; Pu, Y.-Q.; Ye, D.-Y.; Dong, Z.-Y.; Yang, M.; Lü, C.-W.; An, Y. The Design and Synthesis of Two Imidazole Fluorescent Probes for the Special Recognition of HClO/$NaHSO_3$ and Their Applications. *Anal. Methods* **2020**, *12* (19), 2476–2483. https://doi.org/10.1039/D0AY00334D.
(1700) Zhu, H.; Zhang, Z.; Long, S.; Du, J.; Fan, J.; Peng, X. Synthesis of an Ultrasensitive BODIPY-Derived Fluorescent Probe for Detecting HOCl in Live Cells. *Nat. Protoc.* **2018**, *13* (10), 2348–2361. https://doi.org/10.1038/s41596-018-0041-6.
(1701) Choi, M. G.; Lee, Y. J.; Lee, K. M.; Park, K. Y.; Park, T. J.; Chang, S.-K. A Simple Hypochlorous Acid Signaling Probe Based on Resorufin Carbonodithioate and Its Biological Application. *Analyst* **2019**, *144* (24), 7263–7269. https://doi.org/10.1039/C9AN01884K.
(1702) Ma, J.; Yan, C.; Li, Y.; Duo, H.; Li, Q.; Lu, X.; Guo, Y. Unusual Hypochlorous Acid (HClO) Recognition Mechanism Based on Chlorine–Oxygen Bond (Cl−O) Formation. *Chem. – Eur. J.* **2019**, *25* (29), 7168–7176. https://doi.org/10.1002/chem.201806264.
(1703) Xie, Y.; Yan, L.; Tang, Y.; Tang, M.; Wang, S.; Bi, L.; Sun, W.; Li, J. A Smart Fluorescent Probe Based on Salicylaldehyde Schiff's Base with AIE and ESIPT Characteristics for the Detections of N2H4 and ClO−. *J. Fluoresc.* **2019**, *29* (2), 399–406. https://doi.org/10.1007/s10895-019-02348-6.
(1704) Wu, P.; Zhu, Y.; Chen, L.; Tian, Y.; Xiong, H. A Fast-Responsive OFF–ON Near-Infrared-II Fluorescent Probe for In Vivo Detection of Hypochlorous Acid in Rheumatoid Arthritis. *Anal. Chem.* **2021**, *93* (38), 13014–13021. https://doi.org/10.1021/acs.analchem.1c02831.
(1705) Ma, C.; Hou, S.; Zhou, X.; Wang, Z.; Yoon, J. Rational Design of Meso-Phosphino-Substituted BODIPY Probes for Imaging Hypochlorite in Living Cells and Mice. *Anal. Chem.* **2021**, *93* (27), 9640–9646. https://doi.org/10.1021/acs.analchem.1c02025.
(1706) Yang, J.; Yao, Y.; Shen, Y.; Xu, Y.; Lv, G.; Li, C. A Novel Phenoxazine-Based Fluorescent Probe for the Detection of HOCl in Living Cells. *Z. Für Anorg. Allg. Chem.* **2020**, *646* (9), 431–436. https://doi.org/10.1002/zaac.202000127.

(1707) Cheng, W.; Xue, X.; Gan, L.; Jin, P.; Zhang, B.; Guo, M.; Si, J.; Du, H.; Chen, H.; Fang, J. Individual and Successive Detection of H_2S and HClO in Living Cells and Zebrafish by a Dual-Channel Fluorescent Probe with Longer Emission Wavelength. *Anal. Chim. Acta* **2021**, *1156*, 338362. https://doi.org/10.1016/j.aca.2021.338362.
(1708) Jia, X.; Wei, C.; Li, Z.; Liu, L.; Wang, M.; Zhang, P.; Li, X. Selective Imaging of HClO in the Liver Tissue In Vivo Using a Near-Infrared Hepatocyte-Specific Fluorescent Probe. *Chem. – Asian J.* **2021**, *16* (14), 1967–1972. https://doi.org/10.1002/asia.202100476.
(1709) Chen, Y.; Lim, J.-Y.; Wu, X. H.; Heo, J. S.; FengyingYuan; Zhang, J. F.; Yoon, D. W.; Ren, W. X. Development of H_2S and HClO Dual-Responsive Fluorescent Probe for Cancer Recognition. *Dyes Pigments* **2021**, *195*, 109666. https://doi.org/10.1016/j.dyepig.2021.109666.
(1710) Hou, P.; Li, G.; Li, Z.; Yue, L.; Liu, L.; Sun, J.; Wang, H.; Chen, W.; Song, X.; Chen, S. A Robust Dual-Channel Fluorescence-Enhanced Probe for Duplex Imaging of Endogenous HClO/ClO^- in Living Cells and in Zebrafish. *Sens. Actuators B Chem.* **2022**, *359*, 131562. https://doi.org/10.1016/j.snb.2022.131562.
(1711)Zeng, Z.-X.; Gu, J.; Liu, Y.-N.; Li, D.-D.; Yang, Y.-S.; Wang, B.-Z.; Zhu, H.-L. A Fluorescent Sensor for Selective Detection of Hypochlorite and Its Application in Arabidopsis Thaliana. *Spectrochim. Acta. A. Mol. Biomol. Spectrosc.* **2021**, *244*, 118830. https://doi.org/10.1016/j.saa.2020.118830.
(1712) Hiranmartsuwan, P.; Wangngae, S.; Nootem, J.; Kamkaew, A.; Daengngern, R.; Wattanathana, W.; Chansaenpak, K. BODIPY-Based Fluorescent Probes for Selective Visualization of Endogenous Hypochlorous Acid in Living Cells via Triazolopyridine Formation. *Biosensors* **2022**, *12* (11), 923. https://doi.org/10.3390/bios12110923.
(1713) Huang, W.; Du, X.; Zhang, C.; Zhang, S.; Zhang, J.; Yang, X.-F. Rational Design of a Dual-Channel Fluorescent Probe for the Simultaneous Imaging of Hypochlorous Acid and Peroxynitrite in Living Organisms. *Anal. Chem.* **2022**, *94* (50), 17485–17493. https://doi.org/10.1021/acs.analchem.2c03661.
(1714) Heiduschka, P.; Thanos, S. NO Production during Neuronal Cell Death Can Be Directly Assessed by a Chemical Reaction in Vivo. *Neuroreport* **1998**, *9* (18), 4051–4057.
(1715) Chen, X. Direct Nitric Oxide Imaging in Cultured Hippocampal Neurons with Diaminoanthraquinone and Confocal Microscopy. *Cell Biol. Int.* **2001**, *25* (7), 593–598. https://doi.org/10.1006/cbir.2001.0734.
(1716) Schuchmann, S.; Albrecht, D.; Heinemann, U.; Von Bohlen Und Halbach, O. Nitric Oxide Modulates Low-Mg^{2+}-Induced Epileptiform Activity in Rat Hippocampal–Entorhinal Cortex Slices. *Neurobiol. Dis.* **2002**, *11* (1), 96–105. https://doi.org/10.1006/nbdi.2002.0533.
(1717) Marin, M. J.; Thomas, P.; Fabregat, V.; Luis, S. V.; Russell, D. A.; Galindo, F. Fluorescence of 1,2-Diaminoanthraquinone and Its Nitric Oxide Reaction Product within Macrophage Cells. *ChemBioChem* **2011**, *12* (16), 2471–2477. https://doi.org/10.1002/cbic.201100371.
(1718) Galindo, F.; Kabir, N.; Gavrilovic, J.; Russell, D. A. Spectroscopic Studies of 1,2-Diaminoanthraquinone (DAQ) as a Fluorescent Probe for the Imaging of Nitric Oxide in Living Cells. *Photochem. Photobiol. Sci.* **2008**, *7*(1), 126–130. https://doi.org/10.1039/b707528f.
(1719) Plater, M. J.; Greig, I.; Helfrich, M. H.; Ralston, S. H. The Synthesis and Evaluation of O-Phenylenediamine Derivatives as Fluorescent Probes for Nitric Oxide Detection. *J. Chem. Soc. Perkin 1* **2001**, No. 20, 2553–2559. https://doi.org/10.1039/b105953j.
(1720) Chen, J.-B.; Zhang, H.-X.; Guo, X.-F.; Wang, H.; Zhang, H.-S. “Off-on” Red-Emitting Fluorescent Probes with Large Stokes Shifts for Nitric Oxide Imaging in Living Cells. *Anal. Bioanal. Chem.* **2013**, *405* (23), 7447–7456. https://doi.org/10.1007/s00216-013-7177-6.
(1721) Liu, W.; Fan, C.; Sun, R.; Xu, Y.-J.; Ge, J.-F. Near-Infrared Emission of Dibenzoxanthenium and Its Application in the Design of Nitric Oxide Probes. *Org. Biomol. Chem.* **2015**, *13*, 4532–4538. https://doi.org/10.1039/c5ob00042d.

(1722) Liu, X.; Liu, S.; Liang, G. Fluorescence Turn-on for the Highly Selective Detection of Nitric Oxide in Vitro and in Living Cells. *Analyst* **2016**, *141*, 2600–2605. https://doi.org/10.1039/c6an00110f.
(1723) Wang, Q.; Jiao, X.; Liu, C.; He, S.; Zhao, L.; Zeng, X. A Rhodamine-Based Fast and Selective Fluorescent Probe for Monitoring Exogenous and Endogenous Nitric Oxide in Live Cells. *J. Mater. Chem. B* **2018**, *6* (24), 4096–4103. https://doi.org/10.1039/c8tb00646f.
(1724) Liu, Z.; Sun, C.; Wang, H.; Wu, T.; Qiu, B.; Xiong, X.; Liu, L. A Far-Red-Emitting Fluorescence Probe for Selective and Sensitive Detection of No in Live Cells and in C. Elegans. *Spectrochim. Acta. A. Mol. Biomol. Spectrosc.* **2021**, *261*. https://doi.org/10.1016/j.saa.2021.120030.
(1725) Panfilov, M.; Chernova, D.; Khalfina, I.; Moskalensky, A.; Vorob'ev, A. Design and Synthesis of New Acridone-Based Nitric Oxide Fluorescent Probe. *Molecules* **2021**, *26* (14). https://doi.org/10.3390/molecules26144340.
(1726) Kaushik, D.; Kaur, M.; Mutreja, V.; Pathania, K.; Salunke, D. B.; Sahoo, S. C.; Saini, V.; Pawar, S. V.; Kansal, S. K.; Mehta, S. K. Synthesis of Quinoline Based Molecular Probes for Detection of Nitric Oxide. *Dyes Pigments* **2022**, *201*, 110226. https://doi.org/10.1016/j.dyepig.2022.110226.
(1727) Zhou, T.; Wang, J.; Xu, J.; Zheng, C.; Niu, Y.; Wang, C.; Xu, F.; Yuan, L.; Zhao, X.; Liang, L.; Xu, P. A Smart Fluorescent Probe for NO Detection and Application in Myocardial Fibrosis Imaging. *Anal. Chem.* **2020**, *92* (7), 5064–5072. https://doi.org/10.1021/acs.analchem.9b05435.
(1728) Biswas, S.; Rajesh, Y.; Barman, S.; Bera, M.; Paul, A.; Mandal, M.; Singh, N. A Dual-Analyte Probe: Hypoxia Activated Nitric Oxide Detection with Phototriggered Drug Release Ability. *Chem. Commun.* **2018**, *54* (57), 7940–7943. https://doi.org/10.1039/c8cc01854e.
(1729) Duarte, A.; Esteves Da Silva, J. C. G. Reduced Fluoresceinamine as a Fluorescent Sensor for Nitric Oxide. *Sensors* **2010**, *10* (3), 1661–1669. https://doi.org/10.3390/s100301661.
(1730) Huo, Y.; Miao, J.; Li, Y.; Shi, Y.; Shi, H.; Guo, W. Aromatic Primary Monoamine-Based Fast-Response and Highly Specific Fluorescent Probes for Imaging the Biological Signaling Molecule Nitric Oxide in Living Cells and Organisms. *J. Mater. Chem. B* **2017**, *5* (13), 2483–2490. https://doi.org/10.1039/C6TB03382B.
(1731) Alam, R.; Islam, A.; Sasmal, M.; Katarkar, A.; Ali, M. A Rhodamine-Based Turn-on Nitric Oxide Sensor in Aqueous Medium with Endogenous Cell Imaging: An Unusual Formation of Nitrosohydroxylamine. *Org. Biomol. Chem.* **2018**, *16* (21), 3910–3920. https://doi.org/10.1039/c8ob00822a.
(1732) Li, H.; Hao, Y.-H.; Feng, W.; Song, Q.-H. Rapid and Sensitive Detection of Nitric Oxide by a BODIPY-Based Fluorescent Probe in Live Cells: Glutathione Effects. *J. Mater. Chem. B* **2020**, *8* (42), 9785–9793. https://doi.org/10.1039/D0TB01784A.
(1733) Liu, Y.; Jiao, C.; Wei, Y.; Lu, W.; Zhang, P.; Wang, Y. A Highly Specific Rhodamine B Based Turn-on Fluorescent Probe for Nitric Oxide and Application in Living Cells. *Tetrahedron* **2020**, *76* (46), 131622. https://doi.org/10.1016/j.tet.2020.131622.
(1734) Meghdadi, S.; Amirnasr, M.; Amiri, A.; Musavizadeh Mobarakeh, Z.; Azarkamanzad, Z. Benign Synthesis of N-(8-Quinolyl)Pyridine-2-Carboxamide) Ligand (Hbpq), and Its Ni(II) and Cu(II) Complexes. A Fluorescent Probe for Direct Detection of Nitric Oxide in Acetonitrile Solution Based on Hbpq Copper(II) Acetate Interaction. *Comptes Rendus Chim.* **2014**, *17* (5), 477–483. https://doi.org/10.1016/j.crci.2013.10.003.
(1735) Muthuraj, B.; Deshmukh, R.; Trivedi, V.; Iyer, P. K. Highly Selective Probe Detects Cu^{2+} and Endogenous NO Gas in Living Cell. *ACS Appl. Mater. Interfaces* **2014**, *6* (9), 6562–6569. https://doi.org/10.1021/am501476w.
(1736) Anand, T.; Sivaraman, G.; Chellappa, D. Quinazoline Copper(II) Ensemble as Turn-on Fluorescence Sensor for Cysteine and Chemodosimeter for NO. *J. Photochem. Photobiol. Chem.* **2014**, *281*, 47–52. https://doi.org/10.1016/j.jphotochem.2014.02.015.

(1737) Alam, R.; Mistri, T.; Mondal, P.; Das, D.; Mandal, S. K.; Khuda-Bukhsh, A. R.; Ali, M. A Novel Copper(II) Complex as a Nitric Oxide Turn-on Fluorosensor: Intracellular Applications and DFT Calculation. *Dalton Trans* **2014**, *43* (6), 2566–2576. https://doi.org/10.1039/C3DT52521J.
(1738) Vidanapathirana, A. K.; Goyne, J. M.; Williamson, A. E.; Pullen, B. J.; Chhay, P.; Sandeman, L.; Bensalem, J.; Sargeant, T. J.; Grose, R.; Crabtree, M. J.; Zhang, R.; Nicholls, S. J.; Psaltis, P. J.; Bursill, C. A. Biological Sensing of Nitric Oxide in Macrophages and Atherosclerosis Using a Ruthenium-Based Sensor. *Biomedicines* **2022**, *10* (8), 1807. https://doi.org/10.3390/biomedicines10081807.
(1739) Ma, S.-F.; Wang, Q.-H.; Liu, F.-T.; Wang, H.-L.; Fang, D.-C.; Gong, B.; He, L.; Lu, Z.-L. Dihydropyridine-Based Fluorescence Probe for Nitric Oxide. *RSC Adv.* **2016**, *6* (89), 85698–85703. https://doi.org/10.1039/C6RA16713F.
(1740) Su, W.; Huang, L.; Liang, X.; Zhu, L.; Lin, W. Dual Channel Mitochondria-Targeted Fluorescent Probe for Detection of Nitric Oxide in Living Cells and Zebrafish. *J. Photochem. Photobiol. -Chem.* **2021**, *412*. https://doi.org/10.1016/j.jphotochem.2021.113256.
(1741) Lu, K.; Wang, Y.; Zhang, H.; Tian, C.; Wang, W.; Yang, T.; Qi, B.; Wu, S. Rational Design of a Theranostic Agent Triggered by Endogenous Nitric Oxide in a Cellular Model of Alzheimer's Disease. *J. Med. Chem.* **2022**, *65* (13), 9193–9205. https://doi.org/10.1021/acs.jmedchem.2c00399.
(1742) Radi, R.; Cosgrove, T. P.; Beckman, J. S.; Freeman, B. A. Peroxynitrite-Induced Luminol Chemiluminescence. *Biochem. J.* **1993**, *290* (1), 51–57. https://doi.org/10.1042/bj2900051.
(1743) Daiber, A.; Oelze, M.; August, M.; Wendt, M.; Sydow, K.; Wieboldt, H.; Kleschyov, A. L.; Munzel, T. Detection of Superoxide and Peroxynitrite in Model Systems and Mitochondria by the Luminol Analogue L-012. *Free Radic. Res.* **2004**, *38* (3), 259–269. https://doi.org/10.1080/10715760410001659773.
(1744) Myhre, O.; Andersen, J. M.; Aarnes, H.; Fonnum, F. Evaluation of the Probes 2′,7′-Dichlorofluorescin Diacetate, Luminol, and Lucigenin as Indicators of Reactive Species Formation. *Biochem. Pharmacol.* **2003**, *65* (10), 1575–1582. https://doi.org/10.1016/S0006-2952(03)00083-2.
(1745) Yang, X.-F.; Guo, X.-Q.; Zhao, Y.-B. Development of a Novel Rhodamine-Type Fluorescent Probe to Determine Peroxynitrite. *Talanta* **2002**, *57* (5), 883–890. https://doi.org/10.1016/S0039-9140(02)00120-0.
(1746) Crow, J. P. Dichlorodihydrofluorescein and Dihydrorhodamine 123 Are Sensitive Indicators of Peroxynitritein Vitro:Implications for Intracellular Measurement of Reactive Nitrogen and Oxygen Species. *Nitric Oxide* **1997**, *1* (2), 145–157. https://doi.org/10.1006/niox.1996.0113.
(1747) Glebska, J.; Koppenol, W. H. Peroxynitrite-Mediated Oxidation of Dichlorodihydrofluorescein and Dihydrorhodamine. *Free Radic. Biol. Med.* **2003**, *35* (6), 676–682. https://doi.org/10.1016/S0891-5849(03)00389-7.
(1748) Possel, H.; Noack, H.; Augustin, W.; Keilhoff, G.; Wolf, G. 2,7-Dihydrodichlorofluorescein Diacetate as a Fluorescent Marker for Peroxynitrite Formation. *FEBS Lett.* **1997**, *416* (2), 175–178. https://doi.org/10.1016/S0014-5793(97)01197-6.
(1749) Cui, J.; Zang, S.; Nie, H.; Shen, T.; Su, S.; Jing, J.; Zhang, X. An ICT-Based Fluorescent Probe for Ratiometric Monitoring the Fluctuations of Peroxynitrite in Mitochondria. *Sens. Actuators B Chem.* **2021**, *328*, 129069. https://doi.org/10.1016/j.snb.2020.129069.
(1750) Xie, X.; Tang, F.; Liu, G.; Li, Y.; Su, X.; Jiao, X.; Wang, X.; Tang, B. Mitochondrial Peroxynitrite Mediation of Anthracycline-Induced Cardiotoxicity as Visualized by a Two-Photon Near-Infrared Fluorescent Probe. *Anal. Chem.* **2018**, *90* (19), 11629–11635. https://doi.org/10.1021/acs.analchem.8b03207.

(1751) Li, J.-B.; Chen, L.; Wang, Q.; Liu, H.-W.; Hu, X.-X.; Yuan, L.; Zhang, X.-B. A Bioluminescent Probe for Imaging Endogenous Peroxynitrite in Living Cells and Mice. *Anal. Chem.* **2018**, *90* (6), 4167–4173. https://doi.org/10.1021/acs.analchem.8b00198.
(1752) Cheng, D.; Peng, J.; Lv, Y.; Su, D.; Liu, D.; Chen, M.; Yuan, L.; Zhang, X. De Novo Design of Chemical Stability Near-Infrared Molecular Probes for High-Fidelity Hepatotoxicity Evaluation In Vivo. *J. Am. Chem. Soc.* **2019**, *141* (15), 6352–6361. https://doi.org/10.1021/jacs.9b01374.
(1753) Qu, W.; Niu, C.; Zhang, X.; Chen, W.; Yu, F.; Liu, H.; Zhang, X.; Wang, S. Construction of a Novel Far-Red Fluorescence Light-up Probe for Visualizing Intracellular Peroxynitrite. *Talanta* **2019**, *197*, 431–435. https://doi.org/10.1016/j.talanta.2019.01.065.
(1754) Wang, W.; Xiong, J.; Song, X.; Wang, Z.; Zhang, F.; Mao, Z. Activatable Two-Photon Near-Infrared Fluorescent Probe Tailored toward Peroxynitrite In Vivo Imaging in Tumors. *Anal. Chem.* **2020**, *92* (19), 13305–13312. https://doi.org/10.1021/acs.analchem.0c02587.
(1755) Yin, X.; Feng, W.; Gong, S.; Feng, G. Near-Infrared Fluorescent Probe with Rapid Response and Large Stokes Shift for Imaging Peroxynitrite in Living Cells, Zebrafish and Mice. *Dyes Pigments* **2020**, *172*, 107820. https://doi.org/10.1016/j.dyepig.2019.107820.
(1756) Zhang, K.; Wang, Z.; Hu, X.; Meng, J.; Bao, W.; Wang, X.; Ding, W.; Tian, Z. A Long-Wavelength Turn-on Fluorescent Probe for Intracellular Nanomolar Level Peroxynitrite Sensing with Second-Level Response. *Talanta* **2020**, *219*, 121354. https://doi.org/10.1016/j.talanta.2020.121354.
(1757) Ling, C.; Cui, M.; Chen, J.; Xia, L.; Deng, D.; Gu, Y.; Wang, P. A Novel Highly Selective Fluorescent Probe with New Chalcone Fluorophore for Monitoring and Imaging Endogenous Peroxynitrite in Living Cells and Drug-Damaged Liver Tissue. *Talanta* **2020**, *215*, 120934. https://doi.org/10.1016/j.talanta.2020.120934.
(1758) Xiao-Ping, W.; Rong, L.; Min, Z.; Lulu, Z.; Hongyan, R.; Meiling, P.; Gao-Hui, Z. Coumarin-Based Fluorescence Turn-on Probes for High Selectivity Peroxynitrite Detection and Imaging in Living Cells and γ-Carrageenan-Induced Inflammatory Tissue and Mice. *Microchem. J.* **2022**, *183*, 108003. https://doi.org/10.1016/j.microc.2022.108003.
(1759) Su, H.; Ji, X.; Zhang, J.; Wang, N.; Wang, H.; Liu, J.; Jiao, J.; Zhao, W. Red-Emitting Fluorescent Probe for Visualizing Endogenous Peroxynitrite in Live Cells and Inflamed Mouse Model. *J. Mol. Struct.* **2022**, *1265*, 133443. https://doi.org/10.1016/j.molstruc.2022.133443.
(1760) Wang, N.; Wang, H.; Zhang, J.; Ji, X.; Su, H.; Liu, J.; Wang, J.; Zhao, W. Endogenous Peroxynitrite Activated Fluorescent Probe for Revealing Anti-tuberculosis Drug Induced Hepatotoxicity. *Chin. Chem. Lett.* **2022**, *33* (3), 1584–1588. https://doi.org/10.1016/j.cclet.2021.09.046.
(1761) Su, H.; Wang, N.; Zhang, J.; Lu, X.; Qin, S.; Wang, J.; Zhao, W.; Wang, J. An Activatable Fluorescent Probe for Monitoring the Up-Regulation of Peroxynitrite in Drug-Induced Hepatotoxicity Model. *Dyes Pigments* **2022**, *203*, 110341. https://doi.org/10.1016/j.dyepig.2022.110341.
(1762) Qin, S.; Lu, H.; Zhang, J.; Ji, X.; Wang, N.; Liu, J.; Zhao, W.; Wang, J. An Activatable Reporter for Fluorescence Imaging Drug-Induced Liver Injury in Diverse Cell Lines and in Vivo. *Dyes Pigments* **2022**, *203*, 110345. https://doi.org/10.1016/j.dyepig.2022.110345.
(1763) Drummen, G. P. C.; van Liebergen, L. C. M.; Op den Kamp, J. A. F.; Post, J. A. C11-BODIPY581/591, an Oxidation-Sensitive Fluorescent Lipid Peroxidation Probe: (Micro)Spectroscopic Characterization and Validation of Methodology. *Free Radic. Biol. Med.* **2002**, *33* (4), 473–490. https://doi.org/10.1016/S0891-5849(02)00848-1.
(1764) Jia, X.; Chen, Q.; Yang, Y.; Tang, Y.; Wang, R.; Xu, Y.; Zhu, W.; Qian, X. FRET-Based Mito-Specific Fluorescent Probe for Ratiometric Detection and Imaging of Endogenous Peroxynitrite: Dyad of Cy3 and Cy5. *J. Am. Chem. Soc.* **2016**, *138* (34), 10778–10781. https://doi.org/10.1021/jacs.6b06398.

(1765) Liao, Y.-X.; Yang, Z.-X.; Li, K.; Yu, X.-Q. A Highly Selective Ratiometric Fluorescent Probe for Peroxynitrite Detection in Aqueous Media. *Chem. Lett.* **2016**, *45* (6), 691–693. https://doi.org/10.1246/cl.160213.
(1766) Li, Z.; Yan, S.-H.; Chen, C.; Geng, Z.-R.; Chang, J.-Y.; Chen, C.-X.; Huang, B.-H.; Wang, Z.-Lin. Molecular Visualizing and Quantifying Immune-Associated Peroxynitrite Fluxes in Phagocytes and Mouse Inflammation Model. *Biosens. Bioelectron.* **2017**, *90*, 75–82. https://doi.org/10.1016/j.bios.2016.11.036.
(1767) Peng, J.; Samanta, A.; Zeng, X.; Han, S.; Wang, L.; Su, D.; Loong, D. T. B.; Kang, N.-Y.; Park, S.-J.; All, A. H.; Jiang, W.; Yuan, L.; Liu, X.; Chang, Y.-T. Real-Time In Vivo Hepatotoxicity Monitoring through Chromophore-Conjugated Photon-Upconverting Nanoprobes. *Angew. Chem. Int. Ed.* **2017**, *56* (15), 4165–4169. https://doi.org/10.1002/anie.201612020.
(1768) Fu, Y.; Nie, H.; Zhang, R.; Xin, F.; Tian, Y.; Jing, J.; Zhang, X. An ESIPT Based Naphthalimide Chemosensor for Visualizing Endogenous $ONOO^-$ in Living Cells. *RSC Adv.* **2018**, *8* (4), 1826–1832. https://doi.org/10.1039/C7RA11774D.
(1769) Zhou, D.-Y.; Li, Y.; Jiang, W.-L.; Tian, Y.; Fei, J.; Li, C.-Y. A Ratiometric Fluorescent Probe for Peroxynitrite Prepared by de Novo Synthesis and Its Application in Assessing the Mitochondrial Oxidative Stress Status in Cells and in Vivo. *Chem. Commun.* **2018**, *54* (82), 11590–11593. https://doi.org/10.1039/C8CC07389A.
(1770) Sun, W.; Shi, Y.-D.; Ding, A.-X.; Tan, Z.-L.; Chen, H.; Liu, R.; Wang, R.; Lu, Z.-L. Imaging Viscosity and Peroxynitrite by a Mitochondria-Targeting Two-Photon Ratiometric Fluorescent Probe. *Sens. Actuators B Chem.* **2018**, *276*, 238–246. https://doi.org/10.1016/j.snb.2018.08.045.
(1771) Li, D.; Cheng, J.; Wang, C.-K.; Ying, H.; Hu, Y.; Han, F.; Li, X. Bis-Reaction-Trigger as a Strategy to Improve the Selectivity of Fluorescent Probes. *Chem. Commun.* **2018**, *54* (59), 8170–8173. https://doi.org/10.1039/C8CC02830C.
(1772) Hou, T.; Zhang, K.; Kang, X.; Guo, X.; Du, L.; Chen, X.; Yu, L.; Yue, J.; Ge, H.; Liu, Y.; Asiri, A. M.; Alamry, K. A.; Yu, H.; Wang, S. Sensitive Detection and Imaging of Endogenous Peroxynitrite Using a Benzo[d]Thiazole Derived Cyanine Probe. *Talanta* **2019**, *196*, 345–351. https://doi.org/10.1016/j.talanta.2018.12.083.
(1773) Zhou, D.-Y.; Ou-Yang, J.; Li, Y.; Jiang, W.-L.; Tian, Y.; Yi, Z.-M.; Li, C.-Y. A Ratiometric Fluorescent Probe for the Detection of Peroxynitrite with Simple Synthesis and Large Emission Shift and Its Application in Cells Image. *Dyes Pigments* **2019**, *161*, 288–295. https://doi.org/10.1016/j.dyepig.2018.09.059.
(1774) Zhang, J.; Liang, M.; Wang, X.; Li, Y.; Jiao, X.; Xie, X.; Tang, B. Visualizing Peroxynitrite Fluxes in Myocardial Cells Using a New Fluorescent Probe Reveals the Protective Effect of Estrogen. *Chem. Commun.* **2019**, *55* (47), 6719–6722. https://doi.org/10.1039/C9CC02591J.
(1775) Guria, U. N.; Gangopadhyay, A.; Ali, S. S.; Maiti, K.; Samanta, S. K.; Manna, S.; Ghosh, A. K.; Uddin, M. R.; Mandal, S.; Mahapatra, A. K. A Benzothiazole-Conjugated Hemicyanine Dye as a Ratiometric NIR Fluorescent Probe for the Detection and Imaging of Peroxynitrite in Living Cells. *Anal. Methods* **2019**, *11* (42), 5447–5454. https://doi.org/10.1039/C9AY01622H.
(1776) Zhang, W.; Liu, J.; Li, P.; Wang, X.; Bi, S.; Zhang, J.; Zhang, W.; Wang, H.; Tang, B. In Situ and Real-Time Imaging of Superoxide Anion and Peroxynitrite Elucidating Arginase 1 Nitration Aggravating Hepatic Ischemia-Reperfusion Injury. *Biomaterials* **2019**, *225*, 119499. https://doi.org/10.1016/j.biomaterials.2019.119499.
(1777) Liu, H.-W.; Zhang, H.; Lou, X.; Teng, L.; Yuan, J.; Yuan, L.; Zhang, X.-B.; Tan, W. Imaging of Peroxynitrite in Drug-Induced Acute Kidney Injury with a near-Infrared Fluorescence and Photoacoustic Dual-Modal Molecular Probe. *Chem. Commun.* **2020**, *56* (58), 8103–8106. https://doi.org/10.1039/D0CC01621G.

(1778) Lu, J.; Li, Z.; Zheng, X.; Tan, J.; Ji, Z.; Sun, Z.; You, J. A Rapid Response Near-Infrared Ratiometric Fluorescent Probe for the Real-Time Tracking of Peroxynitrite for Pathological Diagnosis and Therapeutic Assessment in a Rheumatoid Arthritis Model. *J. Mater. Chem. B* **2020**, *8* (40), 9343–9350. https://doi.org/10.1039/D0TB01970D.
(1779) Yu, C.; Keying, B.; Ruiting, H.; Ping, X.; Lina, H.; Yumin, W.; Junfeng, Z.; Rui, X.; Xianghua, W. Near-Infrared Ratiometric Fluorescent Probe for Detection of Peroxynitrite in HeLa Cells Based on Dicyanomethylene-4H-Pyran Coumarin System. *Chin. J. Org. Chem.* **2020**, *40* (2), 511. https://doi.org/10.6023/cjoc201907048.
(1780) Gu, B.; Wu, C.; Zhang, C.; He, S.; Tang, S.; Li, H.; Shen, Y. A Morpholino Hydrazone-Based Lysosome-Targeting Fluorescent Probe with Fast Response and High Sensitivity for Imaging Peroxynitrite in Living Cells. *Spectrochim. Acta. A. Mol. Biomol. Spectrosc.* **2021**, *262*, 120100. https://doi.org/10.1016/j.saa.2021.120100.
(1781) Fang, Y.; Chen, R.-X.; Qin, H.-F.; Wang, J.-J.; Zhang, Q.; Chen, S.; Wen, Y.-H.; Wang, K.-P.; Hu, Z.-Q. A Chromene Based Fluorescence Probe: Accurate Detection of Peroxynitrite in Mitochondria, Not Elsewhere. *Sens. Actuators B Chem.* **2021**, *334*, 129603. https://doi.org/10.1016/j.snb.2021.129603.
(1782) Yu, H.; Fang, Y.; Wang, J.; Zhang, Q.; Chen, S.; Wang, K.-P.; Hu, Z.-Q. Enhancing Probe's Sensitivity for Peroxynitrite through Alkoxy Modification of Dicyanovinylchromene. *Anal. Bioanal. Chem.* **2022**, *414* (23), 6779–6789. https://doi.org/10.1007/s00216-022-04239-5.
(1783) Bao, L.; Liu, K.; Chen, Y.; Yang, G. Construction of a Rational-Designed Multifunctional Platform Based on a Fluorescence Resonance Energy Transfer Process for Simultaneous Detection of pH and Endogenous Peroxynitrite. *Anal. Chem.* **2021**, *93* (26), 9064–9073. https://doi.org/10.1021/acs.analchem.1c00264.
(1784) Zhang, J.; Kan, J.; Sun, Y.; Won, M.; Kim, J. H.; Zhang, W.; Zhou, J.; Qian, Z.; Kim, J. S. Nanoliposomal Ratiometric Fluorescent Probe toward $ONOO^-$ Flux. *ACS Appl. Bio Mater.* **2021**, *4* (3), 2080–2088. https://doi.org/10.1021/acsabm.0c01178.
(1785) Du, Y.; Wang, H.; Zhang, T.; Wei, W.; Guo, M. ICT-Based Fluorescent Ratiometric Probe for Monitoring Mitochondrial Peroxynitrite in Living Cells. *New J. Chem.* **2021**, *45* (29), 12915–12921. https://doi.org/10.1039/D1NJ01713F.
(1786) Li, K.-Y.; Lu, P.-H.; Wu, B.-H.; Wu, S.-P. A Mitochondria-Targeting near-Infrared Fluorescent Probe for the in Vivo Detection of Peroxynitrite. *Dyes Pigments* **2022**, *205*, 110521. https://doi.org/10.1016/j.dyepig.2022.110521.
(1787) Liu, Y.; Feng, S.; Gong, S.; Feng, G. Dual-Channel Fluorescent Probe for Detecting Viscosity and $ONOO^-$ without Signal Crosstalk in Nonalcoholic Fatty Liver. *Anal. Chem.* **2022**, *94* (50), 17439–17447. https://doi.org/10.1021/acs.analchem.2c03419.
(1788) Liu, Y.; Ma, Y.; Lin, W. Construction of a Bi-Functional Ratiometric Fluorescent Probe for Detection of Endoplasmic Reticulum Viscosity and $ONOO^-$ in Cells and Zebrafish. *Sens. Actuators B Chem.* **2022**, *373*, 132742. https://doi.org/10.1016/j.snb.2022.132742.
(1789) Luo, X.; Zhang, C.; Yuan, F.; Cheng, S.; Zhu, Y.; Xiang, M.; Hu, X.; Xian, Y. Dual-Channel Fluorescent Probe for the Detection of Peroxynitrite and Glutathione in Mitochondria: Accurate Discrimination of Inflammatory and Progressing Tumor Cells. *Anal. Chem.* **2022**, *94* (45), 15790–15800. https://doi.org/10.1021/acs.analchem.2c03577.
(1790) He, L.; Liu, H.; Wu, J.; Cheng, Z.; Yu, F. Construction of a Mitochondria-Endoplasmic Reticulum Dual-Targeted Red-Emitting Fluorescent Probe for Imaging Peroxynitrite in Living Cells and Zebrafish. *Chem. – Asian J.* **2022**, *17* (14), e202200388. https://doi.org/10.1002/asia.202200388.
(1791) Han, R.; Shu, W.; Kang, H.; Duan, Q.; Zhang, X.; Liang, C.; Gao, M.; Xu, L.; Jing, J.; Zhang, X. A Deep Red Ratiometric Fluorescent Probe for Accurate Detection of Peroxynitrite in Mitochondria. *Anal. Chim. Acta* **2022**, *1203*, 339652. https://doi.org/10.1016/j.aca.2022.339652.

(1792) Li, J.; Peng, S.; Li, Z.; Zhao, F.; Han, X.; Liu, J.; Cao, W.; Ye, Y. Visualization of Peroxynitrite in Cyclophosphamide-Induced Oxidative Stress by an Activatable Probe. *Talanta* **2022**, *238*, 123007. https://doi.org/10.1016/j.talanta.2021.123007.
(1793) Zheng, Y.-L.; Li, X.-C.; Tang, W.; Xie, L.; Dai, F.; Zhou, B. A Coumarin-Based Fluorescent Probe: Small but Multi-Signal. *Sens. Actuators B Chem.* **2022**, *368*, 132169. https://doi.org/10.1016/j.snb.2022.132169.
(1794) Hu, W.; Qiang, T.; Chai, L.; Liang, T.; Ren, L.; Cheng, F.; Li, C.; D. James, T. Simultaneous Tracking of Autophagy and Oxidative Stress during Stroke with an ICT-TBET Integrated Ratiometric Two-Photon Platform. *Chem. Sci.* **2022**, *13* (18), 5363–5373. https://doi.org/10.1039/D1SC06805A.
(1795) Chen, W.; Liu, H.; Song, F.; Xin, L.; Zhang, Q.; Zhang, P.; Ding, C. pH-Switched Near-Infrared Fluorescent Strategy for Ratiometric Detection of $ONOO^-$ in Lysosomes and Precise Imaging of Oxidative Stress in Rheumatoid Arthritis. *Anal. Chem.* **2023**, *95* (2), 1301–1308. https://doi.org/10.1021/acs.analchem.2c04175.
(1796) Han, Y.; Luo, C.; Quan, Z.; Li, H.; Sun, S.; Xu, Y. New “Destruction Seek to Survive” Strategy Based on a Serum Albumin Assembly with a Squaraine Molecule for the Detection of Peroxynitrite. *Anal. Chem.* **2023**, *95* (18), 7278–7285. https://doi.org/10.1021/acs.analchem.3c00282.
(1797) Liu, Q.; Dong, C.; Zhang, J.; Zhao, B.; Zhou, Y.; Fan, C.; Lu, Z. A Mitochondria-Targeted Ratiometric NIR Fluorescent Probe for Simultaneously Monitoring Viscosity and $ONOO^-$ Based on Two Different Channels in Living HepG2 Cells. *Dyes Pigments* **2023**, *210*, 111045. https://doi.org/10.1016/j.dyepig.2022.111045.
(1798) Niu, L.; Cao, Q.; Zhang, T.; Zhang, Y.; Liang, T.; Wang, J. Simultaneous Detection of Mitochondrial Viscosity and Peroxynitrite in Livers from Subjects with Drug-Induced Fatty Liver Disease Using a Novel Fluorescent Probe. *Talanta* **2023**, *260*, 124591. https://doi.org/10.1016/j.talanta.2023.124591.
(1799) Wang, J.; Liu, S.-Y.; Yu, G.-H.; Hu, H.-R.; Fang, Y.; Chen, S.-J.; Wang, K.-P.; Hu, Z.-Q. Highly Selective and Sensitive Benzopyran-Based Fluorescent Probes for Imaging Exogenous and Endogenous Peroxynitrite. *Spectrochim. Acta. A. Mol. Biomol. Spectrosc.* **2023**, *297*, 122747. https://doi.org/10.1016/j.saa.2023.122747.
(1800) Xue, X.-L.; Zhang, H.; Chen, G.-H.; Yu, G.-H.; Hu, H.-R.; Niu, S.-Y.; Wang, K.-P.; Hu, Z.-Q. Coumarin-Cyanine Hybrid: A Ratiometric Fluorescent Probe for Accurate Detection of Peroxynitrite in Mitochondria. *Spectrochim. Acta. A. Mol. Biomol. Spectrosc.* **2023**, *292*, 122443. https://doi.org/10.1016/j.saa.2023.122443.
(1801) Yan, H.; Xu, X.; Li, J.; Xie, P.; Cao, W.; Yang, X.; Ye, Y. A Novel Fluorescence-on Fluorescent Probe for ONOO– Detection in HeLa Cells. *J. Photochem. Photobiol. Chem.* **2023**, *440*, 114638. https://doi.org/10.1016/j.jphotochem.2023.114638.
(1802) Shao, M.; Li, L.; Yu, F.; Zhu, L.; Jiang, M.; Yu, H. Peroxynitrite Activatable Double Spiral Ring Derived Fluorescent Probe for Imaging of Inflammation and Drug-Induced Liver Injury. *Dyes Pigments* **2023**, *215*, 111240. https://doi.org/10.1016/j.dyepig.2023.111240.
(1803) Ji, Y.; Liu, S.; Zhang, J.; Qu, L.; Wu, J.; Liu, H.; Cheng, Z. Construction of HPQ-Based Activatable Fluorescent Probe for Peroxynitrite and Its Application in Ferroptosis and Mice Model of LPS-Induced Inflammation. *Bioorganic Chem.* **2023**, *138*, 106650. https://doi.org/10.1016/j.bioorg.2023.106650.
(1804) Zhang, Q.; Zeng, S.-M.-Z.; Yuan, L.-C.; Wu, C.-J.; Wu, S.-Y.; Ren, S.-Z.; Zhao, M.-D.; Wang, X.-M.; Zhu, H.-L.; Wang, Z.-C. Real-Time Diagnosis of Glioblastoma by Sensing Peroxynitrite with a Highly Selective and Rapid-Responding Fluorescent Probe. *Sens. Actuators B Chem.* **2023**, *395*, 134502. https://doi.org/10.1016/j.snb.2023.134502.
(1805) Yang, W.; Liu, R.; Yin, X.; Jin, Y.; Wang, L.; Dong, M.; Wu, K.; Yan, Z.; Fan, G.; Tang, Z.; Li, Y.; Jiang, H. Peroxynitrite Activated Near-Infrared Fluorescent Probe for Evaluating

Ferroptosis-Mediated Acute Kidney Injury. *Sens. Actuators B Chem.* **2023**, *393*, 134180. https://doi.org/10.1016/j.snb.2023.134180.
(1806) Chen, S.; Huang, W.; Tan, H.; Yin, G.; Chen, S.; Zhao, K.; Huang, Y.; Zhang, Y.; Li, H.; Wu, C. A Large Stokes Shift NIR Fluorescent Probe for Visual Monitoring of Mitochondrial Peroxynitrite during Inflammation and Ferroptosis and in an Alzheimer's Disease Model. *Analyst* **2023**, *148* (18), 4331–4338. https://doi.org/10.1039/D3AN00956D.
(1807) Li, Y.; Lei, J.; Qin, X.; Li, G.; Zhou, Q.; Yang, Z. A Mitochondria-Targeted Dual-Response Sensor for Monitoring Viscosity and Peroxynitrite in Living Cells with Distinct Fluorescence Signals. *Bioorganic Chem.* **2023**, *138*, 106603. https://doi.org/10.1016/j.bioorg.2023.106603.
(1808) Kou, M.; Wang, K.; Zhang, X.; Cui, X.; Zhang, W.; Wang, B.; Tang, X.; Liu, W. Mitochondria-Targeted Ruthenium(II)-Based Phosphorescent Chemodosimeter for Peroxynitrite Detection in Drug-Induced Liver Injury. *Sens. Actuators B Chem.* **2023**, *396*, 134555. https://doi.org/10.1016/j.snb.2023.134555.
(1809) Li, Y.; Zhao, Z.; Xiao, Y.; Wang, X.; Jiao, X.; Xie, X.; Zhang, J.; Tang, B. Reactivity Modulation of Benzopyran-Coumarin Platform by Introducing Electron-Withdrawing Groups: Specific Detection of Biothiols and Peroxynitrite. *Anal. Chem.* **2019**, *91* (9), 6097–6102. https://doi.org/10.1021/acs.analchem.9b00636.
(1810) Jing, C.; Wang, Y.; Song, X.; Li, X.; Feng, Y.; Kou, M.; Zhang, G.; Dou, W.; Liu, W. A Dual-Fluorophore and Dual-Site Multifunctional Fluorescent Sensor for Real-Time Visualization of Mitochondrial $ONOO^-$/GSH Cross-Talk in Living Cells. *Sens. Actuators B Chem.* **2022**, *365*, 131847. https://doi.org/10.1016/j.snb.2022.131847.
(1811)Song, X.; Guo, Y.; Jing, C.; Feng, Y.; Cao, C.; Kou, M.; Liu, W.; Wang, D. Dual-Site Fluorescent Sensor as a Multiple Logic System for Studying the Dichotomous Function of Sulfur Dioxide under Oxidative Stress Induced by Peroxynitrite. *Anal. Chem.* **2022**, *94* (15), 5744–5751. https://doi.org/10.1021/acs.analchem.1c03792.
(1812) Li, J.; He, R.; Duan, S.; Li, J.; Han, X.; Ye, Y. Construction and Cell Imaging Study of a Novel Fluorescent Probe for ONOO– Detection. *Chin. J. Org. Chem.* **2022**, *42* (8), 2428. https://doi.org/10.6023/cjoc202203023.
(1813) Kim, J.; Park, J.; Lee, H.; Choi, Y.; Kim, Y. A Boronate-Based Fluorescent Probe for the Selective Detection of Cellular Peroxynitrite. *Chem. Commun.* **2014**, *50* (66), 9353–9356. https://doi.org/10.1039/C4CC02943G.
(1814) Rios, N.; Piacenza, L.; Trujillo, M.; Martínez, A.; Demicheli, V.; Prolo, C.; Álvarez, M. N.; López, G. V.; Radi, R. Sensitive Detection and Estimation of Cell-Derived Peroxynitrite Fluxes Using Fluorescein-Boronate. *Free Radic. Biol. Med.* **2016**, *101*, 284–295. https://doi.org/10.1016/j.freeradbiomed.2016.08.033.
(1815) Sedgwick, A. C.; Sun, X.; Kim, G.; Yoon, J.; Bull, S. D.; James, T. D. Boronate Based Fluorescence (ESIPT) Probe for Peroxynitrite. *Chem. Commun.* **2016**, *52* (83), 12350–12352. https://doi.org/10.1039/C6CC06829D.
(1816) Dębowska, K.; Dębski, D.; Michałowski, B.; Dybala-Defratyka, A.; Wójcik, T.; Michalski, R.; Jakubowska, M.; Selmi, A.; Smulik, R.; Piotrowski, Ł.; Adamus, J.; Marcinek, A.; Chlopicki, S.; Sikora, A. Characterization of Fluorescein-Based Monoboronate Probe and Its Application to the Detection of Peroxynitrite in Endothelial Cells Treated with Doxorubicin. *Chem. Res. Toxicol.* **2016**, *29* (5), 735–746. https://doi.org/10.1021/acs.chemrestox.5b00431.
(1817) Palanisamy, S.; Wu, P.-Y.; Wu, S.-C.; Chen, Y.-J.; Tzou, S.-C.; Wang, C.-H.; Chen, C.-Y.; Wang, Y.-M. In Vitro and in Vivo Imaging of Peroxynitrite by a Ratiometric Boronate-Based Fluorescent Probe. *Biosens. Bioelectron.* **2017**, *91*, 849–856. https://doi.org/10.1016/j.bios.2017.01.027.
(1818) Sedgwick, A. C.; Han, H.-H.; Gardiner, J. E.; Bull, S. D.; He, X.-P.; James, T. D. Long-Wavelength Fluorescent Boronate Probes for the Detection and Intracellular Imaging of

Peroxynitrite. *Chem. Commun.* **2017**, *53* (95), 12822–12825. https://doi.org/10.1039/C7CC07845E.
(1819) Li, K.-B.; Dong, L.; Zhang, S.; Shi, W.; Jia, W.-P.; Han, D.-M. Fluorogenic Boronate-Based Probe-Lactulose Complex for Full-Aqueous Analysis of Peroxynitrite. *Talanta* **2017**, *165*, 593–597. https://doi.org/10.1016/j.talanta.2017.01.028.
(1820) Li, Q.; Yang, Z. A Boronate-Based Ratiometric Fluorescent Probe for Fast Selective Detection of Peroxynitrite. *Tetrahedron Lett.* **2018**, *59* (2), 125–129. https://doi.org/10.1016/j.tetlet.2017.12.004.
(1821) Sedgwick, A. C.; Dou, W.-T.; Jiao, J.-B.; Wu, L.; Williams, G. T.; Jenkins, A. T. A.; Bull, S. D.; Sessler, J. L.; He, X.-P.; James, T. D. An ESIPT Probe for the Ratiometric Imaging of Peroxynitrite Facilitated by Binding to Aβ-Aggregates. *J. Am. Chem. Soc.* **2018**, *140* (43), 14267–14271. https://doi.org/10.1021/jacs.8b08457.
(1822) Guo, Y.; Lu, G.; Zhuo, J.; Wang, J.; Li, X.; Zhang, Z. A Visible-near-Infrared Fluorescent Probe for Peroxynitrite with Large Pseudo-Stokes and Emission Shift via through-Bond Energy and Charge Transfers Controlled by Energy Matching. *J. Mater. Chem. B* **2018**, *6* (16), 2489–2496. https://doi.org/10.1039/C8TB00452H.
(1823) Lee, D.; Lim, C. S.; Ko, G.; Kim, D.; Cho, M. K.; Nam, S.-J.; Kim, H. M.; Yoon, J. A Two-Photon Fluorescent Probe for Imaging Endogenous $ONOO^-$ near NMDA Receptors in Neuronal Cells and Hippocampal Tissues. *Anal. Chem.* **2018**, *90* (15), 9347–9352. https://doi.org/10.1021/acs.analchem.8b01960.
(1824) Weber, M.; Mackenzie, A. B.; Bull, S. D.; James, T. D. Fluorescence-Based Tool To Detect Endogenous Peroxynitrite in M1-Polarized Murine J774.2 Macrophages. *Anal. Chem.* **2018**, *90* (17), 10621–10627. https://doi.org/10.1021/acs.analchem.8b03035.
(1825) Li, W.; Wang, X.; Zhang, Y.; Zhang, S. Single Probe Giving Different Signals towards Reactive Oxygen Species and Nitroxyl. *Dyes Pigments* **2018**, *148*, 348–352. https://doi.org/10.1016/j.dyepig.2017.09.033.
(1826) Wu, L.; Wang, Y.; Weber, M.; Liu, L.; Sedgwick, A. C.; Bull, S. D.; Huang, C.; James, T. D. ESIPT-Based Ratiometric Fluorescence Probe for the Intracellular Imaging of Peroxynitrite. *Chem. Commun.* **2018**, *54* (71), 9953–9956. https://doi.org/10.1039/C8CC04919J.
(1827) L. Odyniec, M.; Park, S.-J.; E. Gardiner, J.; C. Webb, E.; C. Sedgwick, A.; Yoon, J.; D. Bull, S.; Myung Kim, H.; D. James, T. A Fluorescent ESIPT-Based Benzimidazole Platform for the Ratiometric Two-Photon Imaging of $ONOO^-$ in Vitro and Ex Vivo. *Chem. Sci.* **2020**, *11* (28), 7329–7334. https://doi.org/10.1039/D0SC02347G.
(1828) Wu, L.; Han, H.-H.; Liu, L.; E. Gardiner, J.; C. Sedgwick, A.; Huang, C.; D. Bull, S.; He, X.-P.; D. James, T. ESIPT-Based Fluorescence Probe for the Rapid Detection of Peroxynitrite 'AND' Biological Thiols. *Chem. Commun.* **2018**, *54* (80), 11336–11339. https://doi.org/10.1039/C8CC06917D.
(1829) Zhu, B.; Wu, L.; Wang, Y.; Zhang, M.; Zhao, Z.; Liu, C.; Wang, Z.; Duan, Q.; Jia, P. A Highly Selective and Ultrasensitive Ratiometric Far-Red Fluorescent Probe for Imaging Endogenous Peroxynitrite in Living Cells. *Sens. Actuators B Chem.* **2018**, *259*, 797–802. https://doi.org/10.1016/j.snb.2017.12.135.
(1830) Murfin, L. C.; Weber, M.; Park, S. J.; Kim, W. T.; Lopez-Alled, C. M.; McMullin, C. L.; Pradaux-Caggiano, F.; Lyall, C. L.; Kociok-Köhn, G.; Wenk, J.; Bull, S. D.; Yoon, J.; Kim, H. M.; James, T. D.; Lewis, S. E. Azulene-Derived Fluorescent Probe for Bioimaging: Detection of Reactive Oxygen and Nitrogen Species by Two-Photon Microscopy. *J. Am. Chem. Soc.* **2019**, *141* (49), 19389–19396. https://doi.org/10.1021/jacs.9b09813.
(1831) Wang, Z.; Wu, L.; Wang, Y.; Zhang, M.; Zhao, Z.; Liu, C.; Duan, Q.; Jia, P.; Zhu, B. A Highly Selective and Ultrasensitive Ratiometric Fluorescent Probe for Peroxynitrite and Its Two-Photon Bioimaging Applications. *Anal. Chim. Acta* **2019**, *1049*, 219–225. https://doi.org/10.1016/j.aca.2018.05.064.

(1832) Wu, L.; Tian, X.; Han, H.-H.; Wang, J.; Groleau, R. R.; Tosuwan, P.; Wannalerse, B.; Sedgwick, A. C.; Bull, S. D.; He, X.-P.; James, T. D. A Simple Near-Infrared Fluorescent Probe for the Detection of Peroxynitrite. *ChemistryOpen* **2019**, *8* (12), 1407–1409. https://doi.org/10.1002/open.201900301.
(1833) Li, Z.; Yu, C.; Chen, Y.; Liu, C.; Jia, P.; Zhu, H.; Zhang, X.; Sheng, W.; Zhu, B. A Novel Ratiometric Fluorescent Probe for Highly Sensitive and Selective Detection of Peroxynitrite and Its Application for Tracing Endogenous Peroxynitrite in Live Cells. *Anal. Methods* **2019**, *11* (44), 5699–5703. https://doi.org/10.1039/C9AY02069A.
(1834) Jia, P.; Liu, D.; Zhuang, Z.; Liu, C.; Li, Z.; Yu, C.; Chen, Y.; Zhu, H.; Zhang, X.; Yu, Y.; Zhu, B.; Sheng, W. Dicyanoisophorone-Derived Near-Infrared Fluorescent Probe for Ultrasensitive Detection of Peroxynitrite in Living Cells and Zebrafish. *Ind. Eng. Chem. Res.* **2019**, *58* (43), 19778–19784. https://doi.org/10.1021/acs.iecr.9b03854.
(1835) Hariri, A.; Zhao, E.; Jeevarathinam, A. S.; Lemaster, J.; Zhang, J.; Jokerst, J. V. Molecular Imaging of Oxidative Stress Using an LED-Based Photoacoustic Imaging System. *Sci. Rep.* **2019**, *9* (1), 11378. https://doi.org/10.1038/s41598-019-47599-2.
(1836) Li, M.; Han, H.; Zhang, H.; Song, S.; Shuang, S.; Dong, C. Boronate Based Sensitive Fluorescent Probe for the Detection of Endogenous Peroxynitrite in Living Cells. *Spectrochim. Acta. A. Mol. Biomol. Spectrosc.* **2020**, *243*, 118683. https://doi.org/10.1016/j.saa.2020.118683.
(1837) Li, Z.; Huang, S.; He, Y.; Duan, Q.; Zheng, G.; Jiang, Y.; Cai, L.; Jia, Y.; Zhang, H.; Ho, D. AND Logic Gate Based Fluorescence Probe for Simultaneous Detection of Peroxynitrite and Hypochlorous Acid. *Spectrochim. Acta. A. Mol. Biomol. Spectrosc.* **2020**, *230*, 118073. https://doi.org/10.1016/j.saa.2020.118073.
(1838) Wang, D.; Huyan, Y.; Nan, X.; Li, H.; Sun, S.; Xu, Y. Product-Boosted Fluorescence Signal: A New Approach for Designing Small-Molecule Probes for Detection of Peroxynitrite. *Chem. Commun.* **2020**, *56* (57), 7925–7928. https://doi.org/10.1039/D0CC02963G.
(1839) Wang, G.; Wang, Y.; Wang, C.; Huang, C.; Jia, N. A New Long-Wavelength Fluorescent Probe for Tracking Peroxynitrite in Live Cells and Inflammatory Sites of Zebrafish. *Analyst* **2020**, *145* (3), 828–835. https://doi.org/10.1039/C9AN01934K.
(1840) Weber, M.; Yamada, N.; Tian, X.; Bull, S. D.; Minoshima, M.; Kikuchi, K.; Mackenzie, A. B.; James, T. D. Sensing Peroxynitrite in Different Organelles of Murine RAW264.7 Macrophages With Coumarin-Based Fluorescent Probes. *Front. Chem.* **2020**, *8*.
(1841) Shu, W.; Wu, Y.; Duan, Q.; Zang, S.; Su, S.; Jing, J.; Zhang, X. A Highly Selective Fluorescent Probe for Monitoring Exogenous and Endogenous $ONOO^-$ Fluctuations in HeLa Cells. *Dyes Pigments* **2020**, *175*, 108069. https://doi.org/10.1016/j.dyepig.2019.108069.
(1842) Kang, S. H.; Chung, B. Y.; Park, J. E.; Jeon, J.; Park, Y. D. Activatable Red Emitting Fluorescent Probe for Rapid and Sensitive Detection of Intracellular Peroxynitrite. *Talanta* **2020**, *217*, 121053. https://doi.org/10.1016/j.talanta.2020.121053.
(1843) Han, X.; Yang, X.; Zhang, Y.; Li, Z.; Cao, W.; Zhang, D.; Ye, Y. A Novel Activatable AIEgen Fluorescent Probe for Peroxynitrite Detection and Its Application in EC1 Cells. *Sens. Actuators B Chem.* **2020**, *321*, 128510. https://doi.org/10.1016/j.snb.2020.128510.
(1844) Breen, C.; Pal, R.; J. Elsegood, M. R.; J. Teat, S.; Iza, F.; Wende, K.; R. Buckley, B.; J. Butler, S. Time-Resolved Luminescence Detection of Peroxynitrite Using a Reactivity-Based Lanthanide Probe. *Chem. Sci.* **2020**, *11* (12), 3164–3170. https://doi.org/10.1039/C9SC06053G.
(1845) Liu, M.; Zhai, W.; Chen, H.; Zhang, H.; Li, C. Halogen Effects-Induced Bright D−π–A Fluorophore as Scaffold for NIR Fluorogenic Probes with High Contrast. *Anal. Chem.* **2020**, *92* (15), 10792–10799. https://doi.org/10.1021/acs.analchem.0c02247.

(1846) Li, M.; Han, H.; Song, S.; Shuang, S.; Dong, C. AIE-Based Fluorescent Boronate Probe and Its Application in Peroxynitrite Imaging. *Spectrochim. Acta. A. Mol. Biomol. Spectrosc.* **2021**, *261*, 120044. https://doi.org/10.1016/j.saa.2021.120044.
(1847) Wang, M.; Wang, C.; Song, W.; Zhong, W.; Sun, T.; Zhu, J.; Wang, J. A Novel Borate Fluorescent Probe for Rapid Selective Intracellular Peroxynitrite Imaging. *Spectrochim. Acta. A. Mol. Biomol. Spectrosc.* **2021**, *251*, 119398. https://doi.org/10.1016/j.saa.2020.119398.
(1848) Wang, Z.; Wang, W.; Wang, P.; Song, X.; Mao, Z.; Liu, Z. Highly Sensitive Near-Infrared Imaging of Peroxynitrite Fluxes in Inflammation Progress. *Anal. Chem.* **2021**, *93* (5), 3035–3041. https://doi.org/10.1021/acs.analchem.0c05118.
(1849) Grzelakowska, A.; Zielonka, M.; Dębowska, K.; Modrzejewska, J.; Szala, M.; Sikora, A.; Zielonka, J.; Podsiadły, R. Two-Photon Fluorescent Probe for Cellular Peroxynitrite: Fluorescence Detection, Imaging, and Identification of Peroxynitrite-Specific Products. *Free Radic. Biol. Med.* **2021**, *169*, 24–35. https://doi.org/10.1016/j.freeradbiomed.2021.04.011.
(1850) Zeng, X.; Li, Z.; Fu, J.; Jiang, C.; Ma, M.; Zhu, L.; Jin, X. A Novel Ultrasensitive Peroxynitrite-Specific Fluorescent Probe and Its Bioimaging Applications in Living Systems. *Dyes Pigments* **2021**, *186*, 108982. https://doi.org/10.1016/j.dyepig.2020.108982.
(1851) Guo, B.; Shu, W.; Liu, W.; Wang, H.; Xing, S.; Chen, J.; Zhang, X. Mitochondria-Specific Ultrasensitive Ratiometric AIE Probe for Imaging Endogenous Peroxynitrite. *Sens. Actuators B Chem.* **2021**, *344*, 130206. https://doi.org/10.1016/j.snb.2021.130206.
(1852) Chung, J.; Kim, H.; Li, H.; Yoon, J. Reasonably Constructed NIR Fluorescent Probes Based on Dicyanoisophorone Skeleton for Imaging ONOO− in Living Cells. *Dyes Pigments* **2021**, *195*, 109665. https://doi.org/10.1016/j.dyepig.2021.109665.
(1853) Wu, L.; Tian, X.; Lee, D. J.; Yoon, J.; Lim, C. S.; Kim, H. M.; James, T. D. Two-Photon ESIPT-Based Fluorescent Probe Using 4-Hydroxyisoindoline-1,3-Dione for the Detection of Peroxynitrite. *Chem. Commun.* **2021**, *57* (84), 11084–11087. https://doi.org/10.1039/D1CC03160K.
(1854) Modrzejewska, J.; Szala, M.; Link to external site, this link will open in a new window; Grzelakowska, A.; Zakłos-Szyda, M.; Link to external site, this link will open in a new window; Zielonka, J.; Podsiadły, R.; Link to external site, this link will open in a new window. Novel Boronate Probe Based on 3-Benzothiazol-2-Yl-7-Hydroxy-Chromen-2-One for the Detection of Peroxynitrite and Hypochlorite. *Molecules* **2021**, *26* (19), 5940. https://doi.org/10.3390/molecules26195940.
(1855) Ye, Y.-X.; Chen, X.-Y.; Yu, Y.-W.; Zhang, Q.; Wei, X.-W.; Wang, Z.-C.; Wang, B.-Z.; Jiao, Q.-C.; Zhu, H.-L. A Novel Fast-Response and Highly Selective AIEgen Fluorescent Probe for Visualizing Peroxynitrite in Living Cells, C. Elegans and Inflammatory Mice. *Analyst* **2021**, *146* (21), 6556–6565. https://doi.org/10.1039/D1AN01374B.
(1856) Xie, H.; Zhang, J.; Chen, C.; Sun, F.; Liu, H.; He, X.; Lam, K. W. K.; Li, Z.; Lam, J. W. Y.; Zhang, G. Q.; Ding, D.; Kwok, R. T. K.; Tang, B. Z. Sensitive and Specific Detection of Peroxynitrite and in Vivo Imaging of Inflammation by a “Simple” AIE Bioprobe. *Mater. Chem. Front.* **2021**, *5* (4), 1830–1835. https://doi.org/10.1039/D0QM01004A.
(1857) Li, M.; Lei, P.; Song, S.; Shuang, S.; Wang, R.; Dong, C. A Butterfly-Shaped ESIPT Molecule with Solid-State Fluorescence for the Detection of Latent Fingerprints and Exogenous and Endogenous ONOO− by Caging of the Phenol Donor. *Talanta* **2021**, *233*, 122593. https://doi.org/10.1016/j.talanta.2021.122593.
(1858) Li, H.; Liu, Y.; Li, X.; Li, X.; Ma, H. Design, Synthesis and Application of a Dual-Functional Fluorescent Probe for Reactive Oxygen Species and Viscosity. *Spectrochim. Acta. A. Mol. Biomol. Spectrosc.* **2021**, *246*, 119059. https://doi.org/10.1016/j.saa.2020.119059.
(1859) Siarkiewicz, P.; Michalski, R.; Sikora, A.; Smulik-Izydorczyk, R.; Szala, M.; Grzelakowska, A.; Modrzejewska, J.; Bailey, A.; Nycz, J. E.; Kalyanaraman, B.; Malecki, J. G.; Zielonka,

J.; Podsiadły, R. On the Chemical Reactivity of Tricyanofuran(TCF)-Based near-Infrared Fluorescent Redox Probes – Effects of Glutathione on the Probe Response and Product Fluorescence. *Dyes Pigments* **2021**, *192*, 109405. https://doi.org/10.1016/j.dyepig.2021.109405.

(1860) Li, J.; Tang, J.; Yang, X.; Xie, P.; Liu, J.; Zhang, D.; Ye, Y. A Novel Aggregation-Induced Emission Fluorescent Probe to Visualize Peroxynitrite Levels during Golgi Stress. *Sens. Actuators B Chem.* **2022**, *358*, 131513. https://doi.org/10.1016/j.snb.2022.131513.

(1861) Ji, X.; Zhou, J.; Liu, C.; Zhang, J.; Dong, X.; Zhang, F.; Zhao, W. Regulating the Activity of Boronate Moiety to Construct Fluorescent Probes for the Detection of $ONOO^-$in Vitro and in Vivo. *Anal. Methods* **2022**, *14* (48), 5027–5033. https://doi.org/10.1039/D2AY01727J.

(1862) Wang, X.; Xiao, S.; Zhou, X.; Duan, T. An Ultrafast Fluorescent Probe for the Detection of Peroxynitrite in Living Cells. *J. Chem.* **2022**, *2022*, e8995440. https://doi.org/10.1155/2022/8995440.

(1863) Xu, Z.; Qian, J.; Ge, Y.; Wang, Y.; Chen, H. A Two-Photon Fluorescent Probe for the Visual Detection of Peroxynitrite in Living Cells and Zebrafish. *Molecules* **2022**, *27* (15), 4858. https://doi.org/10.3390/molecules27154858.

(1864) Ma, L.; Yang, Q.; Zan, Q.; Tian, H.; Zhang, X.; Dong, C.; Fan, L. A Benzothiazole-Based Fluorescence Probe for Imaging of Peroxynitrite during Ferroptosis and Diagnosis of Tumor Tissues. *Anal. Bioanal. Chem.* **2022**, *414* (27), 7753–7762. https://doi.org/10.1007/s00216-022-04307-w.

(1865) Sun, Y.; Wang, R.; Wang, J.; Wei, H.; Chen, Q.; Wang, Y.; Dong, B. Construction of a Ratiometric Two-Photon ER-Targeting Fluorescent Probe for the Imaging of Peroxynitrite in Living Systems. *Sens. Actuators B Chem.* **2022**, *370*, 132439. https://doi.org/10.1016/j.snb.2022.132439.

(1866) Shi, B.; Wang, H.; Wan, X.; Guo, Y.; Liu, S.-Y.; Gong, Q. A Novel "Dual-Locked" Fluorescent Probe for $ONOO^-$ and Viscosity Enables Serum-Based Rapid Disease Screening. *Spectrochim. Acta. A. Mol. Biomol. Spectrosc.* **2022**, *278*, 121375. https://doi.org/10.1016/j.saa.2022.121375.

(1867) Chen, C.; Yang, Y.; Chen, H.; Fan, X.; Zhu, H.-L.; Li, Z. Imaging Pulmonary Fibrosis with a Practical Probe for the Detection of Peroxynitrite in Living Cells and Mice. *Dyes Pigments* **2022**, *204*, 110443. https://doi.org/10.1016/j.dyepig.2022.110443.

(1868) Yu, J.; Shu, W.; Kang, H.; Han, R.; Zhang, X.; Zhang, R.; Jing, J.; Zhang, X. An ESIPT-Based Fluorescent Probe with Large Stokes Shift for Peroxynitrite Detection in HeLa Cells and Zebrafish. *Dyes Pigments* **2022**, *204*, 110334. https://doi.org/10.1016/j.dyepig.2022.110334.

(1869) Peng, C.; Yang, J.; Li, W.; Lin, D.; Fei, Y.; Chen, X.; Yuan, L.; Li, Y. Development of Probes with High Signal-to-Noise Ratios Based on the Facile Modification of Xanthene Dyes for Imaging Peroxynitrite during the Liver Ischemia/Reperfusion Process. *Anal. Chem.* **2022**, *94* (30), 10773–10780. https://doi.org/10.1021/acs.analchem.2c01496.

(1870) Li, M.; Huang, Y.; Song, S.; Shuang, S.; Dong, C. A Bifunctional Fluorescence Probe for Dual-Channel Detecting of Mitochondrial Viscosity and Endogenous/Exogenous Peroxynitrite. *Bioorganic Chem.* **2022**, *119*, 105484. https://doi.org/10.1016/j.bioorg.2021.105484.

(1871) Wu, L.; Liu, J.; Tian, X.; Groleau, R. R.; Feng, B.; Yang, Y.; Sedgwick, A. C.; Han, H.-H.; Wang, Y.; Wang, H.-M.; Huang, F.; Bull, S. D.; Zhang, H.; Huang, C.; Zang, Y.; Li, J.; He, X.-P.; Li, P.; Tang, B.; James, T. D.; Sessler, J. L. Dual-Channel Fluorescent Probe for the Simultaneous Monitoring of Peroxynitrite and Adenosine-5′-Triphosphate in Cellular Applications. *J. Am. Chem. Soc.* **2022**, *144* (1), 174–183. https://doi.org/10.1021/jacs.1c07954.

(1872) Xu, C.; Li, Y.; Wu, X.; Li, X.; Li, L.; Kong, F.; Tang, B. A Dual-Responsive Probe for the Simultaneous Monitoring of Viscosity and Peroxynitrite with Different Fluorescence Signals

in Living Cells. *Chem. Commun.* **2022**, *58* (40), 5976–5979. https://doi.org/10.1039/D2CC01607A.
(1873) Parthiban, C.; Manivannan, R.; Son, Y.-A. A Novel Near-Infrared Fluorescent Probe for Rapid Detection of Peroxynitrite with Large Stokes Shift and Imaging in Living Cells. *J. Photochem. Photobiol. Chem.* **2022**, *423*, 113579. https://doi.org/10.1016/j.jphotochem.2021.113579.
(1874) Zhou, Y.; Zeng, J.; Yang, Q.; Zhou, L. Rational Construction of a Fluorescent Sensor for Simultaneous Detection and Imaging of Hypochlorous Acid and Peroxynitrite in Living Cells, Tissues and Inflammatory Rat Models. *Spectrochim. Acta. A. Mol. Biomol. Spectrosc.* **2022**, *282*, 121691. https://doi.org/10.1016/j.saa.2022.121691.
(1875) Chau, J. H. C.; Zhang, R.; Lee, M. M. S.; Lam, K. W. K.; Yu, E. Y.; Lam, J. W. Y.; Kwok, R. T. K.; Tang, B. Z. A Ratiometric Theranostic System for Visualization of $ONOO^-$ Species and Reduction of Drug-Induced Hepatotoxicity. *Biomater. Sci.* **2022**, *10* (4), 1083–1089. https://doi.org/10.1039/D1BM01675J.
(1876) Sonawane, P. M.; Lee, W.; Kim, Y.; Roychaudhury, A.; Bhosale, V. K.; Kim, D.; Park, H.-S.; Kim, C.-H.; Churchill, D. G. Phosphinate–Benzoindocyanin Fluorescent Probe for Endogenous Mitochondrial Peroxynitrite Detection in Living Cells and Gallbladder Access in Inflammatory Zebrafish Animal Models. *Spectrochim. Acta. A. Mol. Biomol. Spectrosc.* **2022**, *267*, 120568. https://doi.org/10.1016/j.saa.2021.120568.
(1877) Tang, J.; Li, Z.; Qiang, C.; Han, Y.; Yang, L.; Zhu, L.; Dang, T.; Chen, G.; Ye, Y. A Long-Wavelength Mitochondria-Targeted Fluorescent Probe for Imaging of Peroxynitrite during Dexamethasone Treatment. *Spectrochim. Acta. A. Mol. Biomol. Spectrosc.* **2023**, *292*, 122429. https://doi.org/10.1016/j.saa.2023.122429.
(1878) Wang, K.; Guo, R.; Chen, X.-Y.; Yang, Y.-S.; Qiao, L.-Q.; Wang, M.-L. Multifunctional Lysosome-Targetable Fluorescent Probe for Imaging Peroxynitrite in Acute Liver Injury Model. *Chem. Eng. J.* **2023**, *455*, 140491. https://doi.org/10.1016/j.cej.2022.140491.
(1879) Xu, Z.; Xu, Z.; Zhang, D. A near Infrared Fluorescent Probe for Rapid Sensing of Peroxynitrite in Living Cells and Breast Cancer Mice. *RSC Adv.* **2023**, *13* (12), 8262–8269. https://doi.org/10.1039/D3RA01024D.
(1880) Zhou, Z.; Wang, X.; Wang, Z.; Wu, J.; Zhang, F.; Mao, Z. Evaluation of Peroxynitrite Fluxes in Inflammatory Mice with a Ratiometric Fluorescence Probe. *Spectrochim. Acta. A. Mol. Biomol. Spectrosc.* **2023**, *294*, 122503. https://doi.org/10.1016/j.saa.2023.122503.
(1881) Xie, F.; Zhou, R.; Jian, C.; Zhang, L.; He, Y. A Borate-Based Peroxynitrite Fluorescent Probe and Its Application in Fluorescence Imaging of Living Cells. *Anal. Methods* **2023**, *15* (26), 3268–3274. https://doi.org/10.1039/D3AY00517H.
(1882) Jr, H. T.; Guo, C.; Hu, X.-L.; Wang, J.-B.; Zang, Y.; D. James, T.; Li, J.; He, X.-P. Human Serum Albumin-Based Supramolecular Host–Guest Boronate Probe for Enhanced Peroxynitrite Sensing. *Org. Biomol. Chem.* **2023**, *21* (22), 4661–4666. https://doi.org/10.1039/D3OB00637A.
(1883) Wang, J.; Liu, Y.; Dong, C.; Wang, Y.; Shuang, S. Ratiometric Imaging of Peroxynitrite in Live Cells, Locusta Malpighian Tubes and Zebrafish by a Benzothiazole-Based Mitochondria-Targetable Fluorescent Probe. *J. Lumin.* **2023**, *254*, 119504. https://doi.org/10.1016/j.jlumin.2022.119504.
(1884) Wang, W.; Deng, J.-B.; Jin, L.; Guan, B.-O. A Highly Sensitive and Selective Near-Infrared Fluorescent Probe for Detecting Peroxynitrite in Living Cells and Drosophila Brains. *Chemosensors* **2023**, *11* (5), 286. https://doi.org/10.3390/chemosensors11050286.
(1885) Qin, S.; Ran, Y.; He, Y.; Lu, X.; Wang, J.; Zhao, W.; Zhang, J. Near-Infrared Fluorescence Probe for Visualizing Fluctuations of Peroxynitrite in Living Cells and Inflammatory Mouse Models. *Chemosensors* **2023**, *11* (6), 316. https://doi.org/10.3390/chemosensors11060316.

(1886) Wu, X.; Shen, Y.; Tan, S.; Jiang, X.; Chen, Z.; Yu, Q.; Chen, H.; Zhuang, Y.; Zeng, H.; Fu, X.; Zhou, H.; Dou, Z.; Chen, G.; Li, X. Multiscale Imaging of Peroxynitrite in Gliomas with a Blood-Brain Barrier Permeable Probe Reveals Its Potential as a Biomarker and Target for Glioma Treatment. *Biosens. Bioelectron.* **2023**, *236*, 115415. https://doi.org/10.1016/j.bios.2023.115415.
(1887) Lu, G.; Fan, H.; Wang, K.; Tian, G.; Chen, C.; Wang, Y.; Wang, L.; Fan, X. A Novel Fluorescent Probe for the Detection of Peroxynitrite and Its Application in Mice Epileptic Brain Model. *Talanta* **2023**, *267*, 125157. https://doi.org/10.1016/j.talanta.2023.125157.
(1888) Wang, Y.; Zhao, L.; Xie, L.; Pang, M.; Zhang, Y.; Ran, H.; Huang, J.; Wang, J.; Tao, Y.; Lyu, S. Construction of a Robust Turn-on Fluorescence NIR Sensor for Rapid Detection and Imaging of $ONOO^-$ in Inflammatory Models. *Spectrochim. Acta. A. Mol. Biomol. Spectrosc.* **2023**, *295*, 122624. https://doi.org/10.1016/j.saa.2023.122624.
(1889) Wang, X.; Wang, X.; Han, Q. Intelligent Detection Strategy and Bioimaging Application of Dual-Responsive Hg2+ and ONOO− Using near-Infrared Probes. *Anal. Chim. Acta* **2023**, *1266*, 341358. https://doi.org/10.1016/j.aca.2023.341358.
(1890) Huang, Y.; Li, M.; Zan, Q.; Wang, R.; Shuang, S.; Dong, C. Mitochondria-Targeting Multifunctional Fluorescent Probe toward Polarity, Viscosity, and $ONOO^-$ and Cell Imaging. *Anal. Chem.* **2023**, *95* (27), 10155–10162. https://doi.org/10.1021/acs.analchem.2c05733.
(1891) Lei, P.; Li, M.; Dong, C.; Shuang, S. Multifunctional Mitochondria-Targeting Near-Infrared Fluorescent Probe for Viscosity, $ONOO^-$, Mitophagy, and Bioimaging. *ACS Biomater. Sci. Eng.* **2023**, *9* (6), 3581–3589. https://doi.org/10.1021/acsbiomaterials.3c00307.
(1892) Zhu, X.-Z.; Zhang, Z.; Zhao, W.; Dong, R.; Wu, Y.-Y.; Wang, C.-Y. A Turn-On Aie Fluorescent Probe with Large Stokes Shift for Peroxynitrite Detection and Imaging in Living Cells. Rochester, NY March 27, 2023. https://doi.org/10.2139/ssrn.4402092.
(1893) Deng, Y.; Shi, X.; Hu, X.; Xu, L.; Liu, X.; Gao, G.; Wang, R.; Liang, G. A Chemiluminescent Probe for Imaging Peroxynitrite in Inflammatory Cells and Tissues. *Anal. Chem.* **2023**, *95* (16), 6496–6500. https://doi.org/10.1021/acs.analchem.3c01124.
(1894) Shen, Y.; Li, M.; Yang, M.; Zhang, Y.; Li, H.; Zhang, X. A Specific AIE and ESIPT Fluorescent Probe for Peroxynitrite Detection and Imaging in Living Cells. *Spectrochim. Acta. A. Mol. Biomol. Spectrosc.* **2019**, *222*, 117230. https://doi.org/10.1016/j.saa.2019.117230.
(1895) Luo, X.; Cheng, Z.; Wang, R.; Yu, F. Indication of Dynamic Peroxynitrite Fluctuations in the Rat Epilepsy Model with a Near-Infrared Two-Photon Fluorescent Probe. *Anal. Chem.* **2021**, *93* (4), 2490–2499. https://doi.org/10.1021/acs.analchem.0c04529.
(1896) Gu, J.; Liu, Y.; Shen, J.; Cao, Y.; Zhang, L.; Lu, Y.-D.; Wang, B.-Z.; Zhu, H.-L. A Three-Channel Fluorescent Probe for Selective Detection of $ONOO^-$ and Its Application to Cell Imaging. *Talanta* **2022**, *244*, 123401. https://doi.org/10.1016/j.talanta.2022.123401.
(1897) Lu, Z.; Dong, C.; Wang, Y.; Liu, Q.; Wei, H.; Zhao, B.; Xu, X.; Dong, B.; Fan, C. A Near-Infrared Fluorescent Probe with Remarkably Large Stokes Shift for Specifical Imaging of Peroxynitrite Fluctuations in Hela Cells. *Bioorganic Chem.* **2023**, *141*, 106866. https://doi.org/10.1016/j.bioorg.2023.106866.
(1898) Yu, F.; Li, P.; Wang, B.; Han, K. Reversible Near-Infrared Fluorescent Probe Introducing Tellurium to Mimetic Glutathione Peroxidase for Monitoring the Redox Cycles between Peroxynitrite and Glutathione in Vivo. *J. Am. Chem. Soc.* **2013**, *135* (20), 7674–7680. https://doi.org/10.1021/ja401360a.
(1899) Ding, Z.; Wang, C.; Feng, G.; Zhang, X. Energy-Transfer Metal–Organic Nanoprobe for Ratiometric Sensing with Dual Response to Peroxynitrite and Hypochlorite. *ACS Omega* **2018**, *3* (8), 9400–9406. https://doi.org/10.1021/acsomega.8b01489.
(1900) Xin, F.; Zhao, J.; Shu, W.; Zhang, X.; Luo, X.; Tian, Y.; Xing, M.; Wang, H.; Peng, Y.; Tian, Y. A Thiocarbonate-Caged Fluorescent Probe for Specific Visualization of Peroxynitrite in

Living Cells and Zebrafish. *Analyst* **2021**, *146* (24), 7627–7634. https://doi.org/10.1039/D1AN00971K.
(1901) Lin, K.-K.; Wu, S.-C.; Hsu, K.-M.; Hung, C.-H.; Liaw, W.-F.; Wang, Y.-M. A N-(2-Aminophenyl)-5-(Dimethylamino)-1-Naphthalenesulfonic Amide (Ds-DAB) Based Fluorescent Chemosensor for Peroxynitrite. *Org. Lett.* **2013**, *15* (16), 4242–4245. https://doi.org/10.1021/ol401932p.
(1902) Peng, T.; Chen, X.; Gao, L.; Zhang, T.; Wang, W.; Shen, J.; Yang, D. A Rationally Designed Rhodamine-Based Fluorescent Probe for Molecular Imaging of Peroxynitrite in Live Cells and Tissues. *Chem. Sci.* **2016**, *7* (8), 5407–5413. https://doi.org/10.1039/C6SC00012F.
(1903) Zhao, C.; An, J.; Zhou, L.; Fei, Q.; Wang, F.; Tan, J.; Shi, B.; Wang, R.; Guo, Z.; Zhu, W.-H. Transforming the Recognition Site of 4-Hydroxyaniline into 4-Methoxyaniline Grafted onto a BODIPY Core Switches the Selective Detection of Peroxynitrite to Hypochlorous Acid. *Chem. Commun.* **2016**, *52* (10), 2075–2078. https://doi.org/10.1039/C5CC08936K.
(1904) Li, J.; Lim, C. S.; Kim, G.; Kim, H. M.; Yoon, J. Highly Selective and Sensitive Two-Photon Fluorescence Probe for Endogenous Peroxynitrite Detection and Its Applications in Living Cells and Tissues. *Anal. Chem.* **2017**, *89* (16), 8496–8500. https://doi.org/10.1021/acs.analchem.7b02059.
(1905) Li, X.; Hou, J.; Peng, C.; Chen, L.; Liu, W.; Liu, Y. A 1,8-Naphthalimide-Based Fluorescent Probe for Selective and Sensitive Detection of Peroxynitrite and Its Applications in Living Cell Imaging. *RSC Adv.* **2017**, *7* (54), 34287–34292. https://doi.org/10.1039/C7RA04317A.
(1906) Zhu, B.; Wang, Z.; Zhao, Z.; Shu, W.; Zhang, M.; Wu, L.; Liu, C.; Duan, Q.; Jia, P. A Simple Highly Selective and Sensitive Hydroquinone-Based Two-Photon Fluorescent Probe for Imaging Peroxynitrite in Live Cells. *Sens. Actuators B Chem.* **2018**, *262*, 380–385. https://doi.org/10.1016/j.snb.2018.01.203.
(1907) Zhu, M.; Zhou, H.; Ji, D.; Li, G.; Wang, F.; Song, D.; Deng, B.; Li, C.; Qiao, R. A Near-Infrared Fluorescence Probe for Ultrafast and Selective Detection of Peroxynitrite with Large Stokes Shift in Inflamed Mouse Models |. *Dyes Pigments* **2019**, *168*, 77–83. https://doi.org/10.1016/j.dyepig.2019.04.046.
(1908) Tang, J.; Li, Q.; Guo, Z.; Zhu, W. A Fast-Response and Highly Specific Si-Rhodamine Probe for Endogenous Peroxynitrite Detection in Living Cells. *Org. Biomol. Chem.* **2019**, *17* (7), 1875–1880. https://doi.org/10.1039/C8OB01598H.
(1909) Li, Y.; Wu, Y.; Chen, L.; Zeng, H.; Chen, X.; Lun, W.; Fan, X.; Wong, W.-Y. A Time-Resolved near-Infrared Phosphorescent Iridium(III) Complex for Fast and Highly Specific Peroxynitrite Detection and Bioimaging Applications. *J. Mater. Chem. B* **2019**, *7* (47), 7612–7618. https://doi.org/10.1039/C9TB01673B.
(1910) Liu, X.; Gu, F.; Zhou, X.; Zhou, W.; Zhang, S.; Cui, L.; Guo, T. A Naphthalimide-Based Turn-on Fluorescence Probe for Peroxynitrite Detection and Imaging in Living Cells. *RSC Adv.* **2020**, *10* (63), 38281–38286. https://doi.org/10.1039/D0RA06564A.
(1911)Wu, W.; Zhang, C.; Rees, T. W.; Liao, X.; Yan, X.; Chen, Y.; Ji, L.; Chao, H. Lysosome-Targeting Iridium(III) Probe with Near-Infrared Emission for the Visualization of NO/$O_2^{\bullet-}$ Crosstalk via In Vivo Peroxynitrite Imaging. *Anal. Chem.* **2020**, *92* (8), 6003–6009. https://doi.org/10.1021/acs.analchem.0c00259.
(1912) Rane, D.; Carlson, E. J.; Yin, Y.; Peterson, B. R. Chapter One - Fluorescent Detection of Peroxynitrite during Antibody-Dependent Cellular Phagocytosis. In *Methods in Enzymology*; Chenoweth, D. M., Ed.; Chemical Tools for Imaging, Manipulating, and Tracking Biological Systems: Diverse Methods Based on Optical Imaging and Fluorescence; Academic Press, 2020; Vol. 640, pp 1–35. https://doi.org/10.1016/bs.mie.2020.04.001.
(1913) Cheng, J.; Li, D.; Sun, M.; Wang, Y.; Xu, Q.-Q.; Liang, X.-G.; Lu, Y.-B.; Hu, Y.; Han, F.; Li, X. Physicochemical-Property Guided Design of a Highly Sensitive Probe to Image

Nitrosative Stress in the Pathology of Stroke. *Chem. Sci.* **2020**, *11* (1), 281–289. https://doi.org/10.1039/C9SC03798E.
(1914) Yan, M.; Fang, H.; Wang, X.; Xu, J.; Zhang, C.; Xu, L.; Li, L. A Two-Photon Fluorescent Probe for Visualizing Endoplasmic Reticulum Peroxynitrite in Parkinson's Disease Models. *Sens. Actuators B Chem.* **2021**, *328*, 129003. https://doi.org/10.1016/j.snb.2020.129003.
(1915) Sheng, W.; Wang, K.; Gao, N.; Wang, L.; Wang, R.; Zhang, X.; Chen, X.; Zhang, Y.; Zhu, B.; Liu, K. A Novel P-Dimethylaminophenylether-Based Fluorescent Probe for the Detection of Native ONOO− in Cells and Zebrafish. *Analyst* **2021**, *146* (17), 5264–5270. https://doi.org/10.1039/D1AN00608H.
(1916) Wang, F.; Jiang, X.; Xiang, H.; Wang, N.; Zhang, Y.; Yao, X.; Wang, P.; Pan, H.; Yu, L.; Cheng, Y.; Hu, Y.; Lin, W.; Li, X. An Inherently Kidney-Targeting near-Infrared Fluorophore Based Probe for Early Detection of Acute Kidney Injury. *Biosens. Bioelectron.* **2021**, *172*, 112756. https://doi.org/10.1016/j.bios.2020.112756.
(1917) Cui, Y.; Han, S.; Zhang, J.; Wang, X. A Ratiometric Fluorescent Nanoprobe for Ultrafast Imaging of Peroxynitrite in Living Cells. *J. Biol. Inorg. Chem.* **2022**, *27* (6), 595–603. https://doi.org/10.1007/s00775-022-01954-3.
(1918) Wang, P.; Yu, L.; Gong, J.; Xiong, J.; Zi, S.; Xie, H.; Zhang, F.; Mao, Z.; Liu, Z.; Kim, J. S. An Activity-Based Fluorescent Probe for Imaging Fluctuations of Peroxynitrite ($ONOO^-$) in the Alzheimer's Disease Brain. *Angew. Chem. Int. Ed.* **2022**, *61* (36), e202206894. https://doi.org/10.1002/anie.202206894.
(1919) Xie, X.; Liu, Y.; Liu, G.; Zhao, Y.; Bian, J.; Li, Y.; Zhang, J.; Wang, X.; Tang, B. Photocontrollable Fluorescence Imaging of Mitochondrial Peroxynitrite during Ferroptosis with High Fidelity. *Anal. Chem.* **2022**, *94* (28), 10213–10220. https://doi.org/10.1021/acs.analchem.2c01758.
(1920) Zhan, Z.; Chai, L.; Yang, H.; Dai, Y.; Wei, Z.; Wang, D.; Lv, Y. Endoplasmic Reticulum Peroxynitrite Fluctuations in Hypoxia-Induced Endothelial Injury and Sepsis with a Two-Photon Fluorescence Probe. *Anal. Chem.* **2023**, *95* (13), 5585–5593. https://doi.org/10.1021/acs.analchem.2c05040.
(1921) Wu, D.; Ryu, J.-C.; Chung, Y. W.; Lee, D.; Ryu, J.-H.; Yoon, J.-H.; Yoon, J. A Far-Red-Emitting Fluorescence Probe for Sensitive and Selective Detection of Peroxynitrite in Live Cells and Tissues. *Anal. Chem.* **2017**, *89* (20), 10924–10931. https://doi.org/10.1021/acs.analchem.7b02707.
(1922) Liu, D.; Feng, S.; Feng, G. A Rapid Responsive Colorimetric and Near-Infrared Fluorescent Turn-on Probe for Imaging Exogenous and Endogenous Peroxynitrite in Living Cells. *Sens. Actuators B Chem.* **2018**, *269*, 15–21. https://doi.org/10.1016/j.snb.2018.04.152.
(1923) Feng, S.; Liu, D.; Feng, G. A Dual-Channel Probe with Green and near-Infrared Fluorescence Changes for in Vitro and in Vivo Detection of Peroxynitrite. *Anal. Chim. Acta* **2019**, *1054*, 137–144. https://doi.org/10.1016/j.aca.2018.12.021.
(1924) Liu, C.; Zhang, X.; Li, Z.; Chen, Y.; Zhuang, Z.; Jia, P.; Zhu, H.; Yu, Y.; Zhu, B.; Sheng, W. Novel Dimethylhydrazine-Derived Spirolactam Fluorescent Chemodosimeter for Tracing Basal Peroxynitrite in Live Cells and Zebrafish. *J. Agric. Food Chem.* **2019**, *67* (22), 6407–6413. https://doi.org/10.1021/acs.jafc.9b01298.
(1925) Zhang, X.; Chen, Y.; Liu, C.; Zhuang, Z.; Li, Z.; Jia, P.; Zhu, H.; Yu, Y.; Zhu, B.; Sheng, W. A Novel Hexahydropyridazin-Modified Rhodamine Fluorescent Probe for Tracing Endogenous/Exogenous Peroxynitrite in Live Cells and Zebrafish. *Dyes Pigments* **2019**, *170*, 107573. https://doi.org/10.1016/j.dyepig.2019.107573.
(1926) Feng, W.; Feng, G. A Lysosome-Targetable Fluorescent Probe for Imaging $ONOO^-$ in Living Cells and Animals. *Dyes Pigments* **2019**, *164*, 174–181. https://doi.org/10.1016/j.dyepig.2019.01.028.

(1927) Sun, S.-G.; Ding, H.; Yuan, G.; Zhou, L. An Efficient TP-FRET-Based Lysosome-Targetable Fluorescent Probe for Imaging Peroxynitrite with Two Well-Resolved Emission Channels in Living Cells, Tissues and Zebrafish. *Anal. Chim. Acta* **2020**, *1100*, 200–207. https://doi.org/10.1016/j.aca.2019.11.065.
(1928) Ding, H.; Peng, L.; Yuan, G.; Zhou, L. Design, Synthesis and Bioimaging Application of a Novel Two-Photon Xanthene Fluorescence Probe for Ratiometric Visualization of Endogenous Peroxynitrite in Living Cells and Zebrafish. *Dyes Pigments* **2020**, *176*, 108232. https://doi.org/10.1016/j.dyepig.2020.108232.
(1929) Sun, Y.; Dong, B.; Lu, Y.; Song, W.; Mehmood, A. H.; Lin, W. A Sensitive and Selective Fluorescent Probe for the Detection of Endogenous Peroxynitrite ($ONOO^-$) in Living Cells. *Anal. Methods* **2020**, *12* (22), 2841–2845. https://doi.org/10.1039/D0AY00012D.
(1930) Jia, P.; Zhuang, Z.; Liu, C.; Wang, Z.; Duan, Q.; Li, Z.; Zhu, H.; Zhang, F.; Sheng, W.; Zhu, B. Development of a Ratiometric Fluorescent Probe with a Large Emission Shift for Imaging $ONOO^-$ in Live Cells and Zebrafish. *Dyes Pigments* **2020**, *173*, 107942. https://doi.org/10.1016/j.dyepig.2019.107942.
(1931) Wu, Y.; Zhang, X.; Lu, X.; Chen, Y.; Ju, J.; Wu, H.; Zhu, B.; Huang, S. An SMVT-Targeting and Peroxynitrite-Activating Fluorescent Probe for Head and Neck Cancer Imaging and Peroxynitrite Detection. *Sens. Actuators B Chem.* **2021**, *348*, 130677. https://doi.org/10.1016/j.snb.2021.130677.
(1932) Tang, J.; Yang, X.; Zhao, F.; Zhang, D.; Mo, S.; Ye, Y. Visualizing Peroxynitrite Fluxes and Protective Effect of Endogenous Hydrogen Sulfide during Carbonyl Stress in Endothelial Cell. *Sens. Actuators B Chem.* **2021**, *330*, 129283. https://doi.org/10.1016/j.snb.2020.129283.
(1933) Zhang, X.-F.; Shen, L.; Wang, S.; Chen, Q.; Cao, X.-Q.; Shen, S.-L.; Li, X. A New Xanthene-Based Platform for Developing NIR Fluorogenic Probes for in Vivo Bioimaging. *Chem. Eng. J.* **2023**, *472*, 145065. https://doi.org/10.1016/j.cej.2023.145065.
(1934) Pan, Y.; Yang, Q.; Xu, H.; Yuan, Z.; Xu, H. Screening and Optimization of a Water-Soluble near-Infrared Fluorescent Probe for Drug-Induced Liver Injury Monitoring. *Anal. Chim. Acta* **2023**, *1276*, 341654. https://doi.org/10.1016/j.aca.2023.341654.
(1935) Zhang, Q.; Zhu, Z.; Zheng, Y.; Cheng, J.; Zhang, N.; Long, Y.-T.; Zheng, J.; Qian, X.; Yang, Y. A Three-Channel Fluorescent Probe That Distinguishes Peroxynitrite from Hypochlorite. *J. Am. Chem. Soc.* **2012**, *134* (45), 18479–18482. https://doi.org/10.1021/ja305046u.
(1936) Yan, J.-L.; Liu, S.-S.; Wu, W.; Zhao, X.-L.; Fan, Y.; Wang, Y.; Xu, Z.-H. Dihydro-Benzo[4,5]Imidazo[1,2-c]Quinazoline-Based Probe with Aggregation-Induced Ratiometric Emission for the Ratiometric Fluorescent Detection of Peroxynitrite in Living Cells and Zebrafish. *Anal. Methods* **2023**. https://doi.org/10.1039/D3AY01416A.
(1937) Kim, S.; Ko, C. W.; Lim, T.; Yoo, S.; Ham, H. J.; Kang, S.-Y.; Kang, S.; Cho, S. K.; Han, M. S. A Hydrazone-Based Turn-on Fluorescent Probe for Peroxynitrite Detection and Live-Cell Imaging. *Dyes Pigments* **2019**, *171*, 107762. https://doi.org/10.1016/j.dyepig.2019.107762.
(1938) Wang, C.; Shu, W.; Chen, Q.; Yang, C.; Su, S.; Gao, M.; Zhang, R.; Jing, J.; Zhang, X. A Simple Dual-Response Fluorescent Probe for Imaging of Viscosity and $ONOO^-$ through Different Fluorescence Signals in Living Cells and Zebrafish. *Spectrochim. Acta. A. Mol. Biomol. Spectrosc.* **2021**, *260*, 119990. https://doi.org/10.1016/j.saa.2021.119990.
(1939) Wu, J.; Lin, Y.; Yu, Y.; Li, Y.; Ye, T.; Zhou, H.; Li, L.; Wang, J. A Highly Selective and Sensitive Fluorescence Probe Based on Rhodol for Imaging of Endogenous Peroxynitrite in Living Cells. *Dyes Pigments* **2022**, *206*, 110597. https://doi.org/10.1016/j.dyepig.2022.110597.
(1940) Liang, C.; Shu, W.; Han, R.; Kang, H.; Zhang, X.; Jing, J.; Zhang, R.; Zhang, X. A Xanthene-Based Fluorescent Probe for Detection of Peroxynitrite in Living Cells and Zebrafish. *Spectrochim. Acta. A. Mol. Biomol. Spectrosc.* **2022**, *277*, 121264. https://doi.org/10.1016/j.saa.2022.121264.

(1941) Huang, J.-C.; Li, D.-J.; Diao, J.-C.; Hou, J.; Yuan, J.-L.; Zou, G.-L. A Novel Fluorescent Method for Determination of Peroxynitrite Using Folic Acid as a Probe. *Talanta* **2007**, *72* (4), 1283–1287. https://doi.org/10.1016/j.talanta.2007.01.033.
(1942) Sun, X.; Lacina, K.; Ramsamy, E. C.; Flower, S. E.; Fossey, J. S.; Qian, X.; Anslyn, E. V.; Bull, S. D.; James, T. D. Reaction-Based Indicator Displacement Assay (RIA) for the Selective Colorimetric and Fluorometric Detection of Peroxynitrite. *Chem. Sci.* **2015**, *6* (5), 2963–2967. https://doi.org/10.1039/C4SC03983A.
(1943) Wu, J.; Yang, Y.; Zhang, L.; Wang, H.; Yang, M.; Yuan, J. A Visible-Light-Excited Eu^{3+} Complex-Based Luminescent Probe for Highly Sensitive Time-Gated Luminescence Imaging Detection of Intracellular Peroxynitrite. *J. Mater. Chem. B* **2017**, *5* (12), 2322–2329. https://doi.org/10.1039/C7TB00345E.
(1944) Wu, J.; Liu, H.; Yang, Y.; Wang, H.; Yang, M. A β-Diketonate−europium(III) Complex-Based Time-Gated Luminescence Probe for Selective Visualization of Peroxynitrite in Living Cells. *Opt. Mater.* **2018**, *77*, 170–177. https://doi.org/10.1016/j.optmat.2018.01.032.
(1945) Lu, G.; Guo, Y.; Zhuo, J.; Li, X.; Chi, H.; Zhang, Z. A General Strategy for Through-Bond Energy Transfer Fluorescence Probes Combining Intramolecular Charge Transfer: A Silyl Ether System for Endogenous Peroxynitrite Sensing. *Chem. – Eur. J.* **2019**, *25* (71), 16350–16357. https://doi.org/10.1002/chem.201903880.
(1946) Li, M.; Huang, Y.; Song, S.; Shuang, S.; Wang, R.; Dong, C. Sensitive Monitoring Mitochondrial Peroxynitrite Based on a New Reaction Site and Cell Imaging by Anthracycline-Based Red Emitting Fluorescence Probe. *Dyes Pigments* **2021**, *195*, 109727. https://doi.org/10.1016/j.dyepig.2021.109727.
(1947) Zuo, Y.; Wang, X.; Lin, W. Four-Armed Functional Siloxane Enables Ratiometric Unconventional Fluorescence for the Detection of $ONOO^-$. *Sens. Actuators B Chem.* **2021**, *331*, 129462. https://doi.org/10.1016/j.snb.2021.129462.
(1948) Wu, W.; Liao, X.; Chen, Y.; Ji, L.; Chao, H. Mitochondria-Targeting and Reversible Near-Infrared Emissive Iridium(III) Probe for in Vivo $ONOO^-$/GSH Redox Cycles Monitoring. *Anal. Chem.* **2021**, *93* (22), 8062–8070. https://doi.org/10.1021/acs.analchem.1c01409.
(1949) Zhang, C.; Zhang, X.; Shen, Y.; Zhou, Z. A Mitochondrion Targetable Dimethylphosphorothionate-Based Far-Red and Colorimetric Fluorescent Probe with Large Stokes Shift for Monitoring Peroxynitrite in Living Cells. *Anal. Methods* **2023**, *15* (2), 196–202. https://doi.org/10.1039/D2AY01614A.